LA-13290-C
Conference

Seventh International Conference on Time-Resolved Vibrational Spectroscopy

Proceedings of the Conference
Santa Fe, New Mexico, USA

June 11–16, 1995

Los Alamos
NATIONAL LABORATORY

Los Alamos National Laboratory is operated by the University of California for the United States Department of Energy under contract W-7405-ENG-36.

Cover illustration by Ward Zaelke, Group CIC-1

ABSTRACT

The International Conference on Time-Resolved Vibrational Spectroscopy (TRVS) is widely recognized as the major international forum for the discussion of advances in this rapidly growing field. The 1995 conference was the seventh in a series that began at Lake Placid, New York, 1982, with subsequent conferences in Bayreuth, West Germany, 1985; Amersfoort, The Netherlands, 1987; Princeton, New Jersey, 1989; Tokyo, Japan, 1991; and Berlin, FRG, 1993. Santa Fe, New Mexico (USA), was the site of the Seventh International Conference on Time-Resolved Vibrational Spectroscopy, held from June 11 to 16, 1995. TRVS-7 was attended by 157 participants from 16 countries and 85 institutions, and research ranging across the full breadth of the field of time-resolved vibrational spectroscopy was presented. Advances in both experimental capabilities for time-resolved vibrational measurements and in theoretical descriptions of time-resolved vibrational methods continue to occur, and several sessions of the conference were devoted to discussion of these advances and the associated new directions in TRVS. Continuing the interdisciplinary tradition of the TRVS meetings, applications of time-resolved vibrational methods to problems in physics, biology, materials science and chemistry comprised a large portion of the papers presented at the conference.

LA-13290-C
Conference

UC-901 and UC-910
Issued: April 1997

Seventh International Conference on Time-Resolved Vibrational Spectroscopy

Proceedings of the Conference
Santa Fe, New Mexico, USA

June 11–16, 1995

Compiled by
R. Brian Dyer
Mary Ann D. Martinez
Andrew Shreve
William H. Woodruff

Los Alamos
NATIONAL LABORATORY
Los Alamos, New Mexico 87545

INTERNATIONAL ORGANIZING COMMITTEE

Andreas Albrecht, USA
George Atkinson, USA
Mostafa El-Sayed, USA
Ch. Flytzanis, France
Hiro-o Hamaguchi, Japan
R.E. Hester, England
Robin Hochstrasser, USA
Teizo Kitagawa, Japan
Yasushi Koyama, Japan
Takayoshi Kobayashi, Japan
J.A. Koningstein, Canada
Albrecht Lau, Germany
Alfred Laubereau, Germany
Jean-Louis Martin, France
Shaul Mukamel, USA
Anne Myers, USA
Friedrich Siebert, Germany
Thomas Spiro, USA
M. Stockburger, Germany
Hiroako Takahashi, Japan
Mitsuo Tasumi, Japan
H.P. Tronnsdorff, France
Douwe Wiersma, The Netherlands
Robert Wilbrandt, Denmark
William H. Woodruff, USA
Lawrence Ziegler, USA

LOCAL ORGANIZING COMMITTEE

R. Brian Dyer, Los Alamos National Laboratory
Mark Ondrias, University of New Mexico
Andrew Shreve, Los Alamos National Laboratory
Basil Swanson, Los Alamos National Laboratory
William Woodruff, Los Alamos National Laboratory

CONFERENCE SPONSORS

Los Alamos National Laboratory
The United States Department of Energy
The University of New Mexico
Environmental Research Institute of Michigan
Coherent, Inc.

CONTENTS

PREFACE

The last decade has seen revolutionary advances in the study of molecular dynamics. These advances include the ability to produce and manipulate short lived species, theoretical understanding and prediction of dynamical processes, and experimental probes of the temporal evolution of molecular structure using time-resolved vibrational spectroscopies. Advances in laser technology, nonlinear optical techniques, pulse shaping methods, multichannel detection, and Fourier transform methods have greatly improved the time resolution, sensitivity and applicability of traditional Raman and infrared spectroscopies and led to the development of new and powerful coherent vibrational techniques. The impact of these approaches is reflected in the extremely wide range of applications involving chemical and biochemical reactions, fundamental photophysics, chemical reaction dynamics in the gas and condensed phases, and solid-state, surface and interfacial phenomena.

The International Conference on Time-Resolved Vibrational Spectroscopy is widely recognized as the major international forum for the discussion of advances in this rapidly growing field. The 1995 conference was the seventh in a series that began at Lake Placid, New York, 1982, with subsequent conferences in Bayreuth, West Germany, 1985; Amersfoort, The Netherlands, 1987; Princeton, New Jersey, 1989; Tokyo, Japan, 1991; and Berlin, FRG, 1993. Santa Fe, New Mexico (USA), was the site of the Seventh International Conference on Time-Resolved Vibrational Spectroscopy (TRVS), held from June 11 to 16, 1995, and was sponsored by Los Alamos National Laboratory, the U. S. Department of Energy, and the University of New Mexico. TRVS-7 was attended by 157 participants, and research ranging across the full breadth of the field of time-resolved vibrational spectroscopy was presented. Advances in both experimental capabilities for time-resolved vibrational measurements and in theoretical descriptions of time-resolved vibrational methods continue to occur, and several sessions of the conference were devoted to discussion of these advances and the associated new directions in TRVS. Continuing the interdisciplinary tradition of the TRVS meetings, applications of time-resolved vibrational methods to problems in physics, biology, materials science and chemistry comprised a large portion of the papers presented at the conference.

TRVS-7 was made possible by financial support from a number of sponsors, and the sponsorship of Los Alamos National Laboratory, the United States Department of Energy, the University of New Mexico, the Environmental Research Institute of Michigan (ERIM), and Coherent, Inc. is gratefully acknowledged. Without the support of these organizations, the scientific interactions and presentations represented in these proceedings could not have occurred.

The TRVS conferences are guided by an international organizing committee, and the members of that committee are thanked for their advice and encouragement. Finally, the other members of the local organizing committee, R. Brian Dyer, Andrew P. Shreve, Basil I. Swanson and Mark Ondrias, and the conference administrators, MaryAnn D. Martinez, Jean Stark and Graciela P. Martinez, are acknowledged for their invaluable contributions to the organization and operation of TRVS-7.

William H. Woodruff

KEYNOTE ADDRESS

Photodissociation Dynamics of Solvated Small Molecules

N. Pugliano, A. Z. Szarka, S. Gnanakaran, and Robin M. Hochstrasser
Department of Chemistry, 231 S. 34th Street,
University of Pennsylvania, Philadelphia, Pennsylvania 19104

Introduction

The study of the dynamics of elementary chemical reactions in solutions presents a number of challenges. In contrast with the situation for isolated molecules, there are not yet available predictive theories for chemical reactions in solution although there is considerable theoretical activity. Some remarkable differences between solution and gas phase reaction parameters were already noted for hydrogen abstraction reactions.[1,2] The photodissociation of simple triatomic molecules into atom-diatom products provide excellent prototypes by which ultrafast reaction dynamics in solutions can be explored. Our work focuses on the photodissociation of mercuric iodide in alcohol solutions, and the data can be compared with that of the isolated molecule. The presence of solvent gives rise to energy transfer to and from the solvent modes, and plays a dominant role in the energy release mechanisms as the reaction proceeds toward thermal equilibrium. Solvent induced modifications of the potential energy surfaces may also be influential in altering reactive trajectories, as well as the product state partitioning of energy. These frictional effects can be partly addressed by monitoring the details of both the population and coherence relaxation associated with the vibrational and electronic levels involved. Dissociating HgI_2 is particularly useful in this regard since the reaction can be impulsively triggered[3] and is known in the gas phase[4] to generate products that are in highly nonequilibrium coherent states. Such a situation permits an evaluation of the solvent effects on the reaction coordinate and the subsequent product state vibrational dynamics.

Experimental

Our laser system is based on the Nd:YAG amplification of a CPM laser. It is capable of delivering 40 fs pump pulses at 320 nm. These are used to initiate the reaction. A sub-50 fs continuously tunable (380 nm - 800 nm) probe is used to monitor the ensuing vibrational dynamics by means of transient absorption spectroscopy of HgI. The probe beam polarization can be varied relative to that of the pump enabling measurements of the anisotropy.

Transition State Dynamics

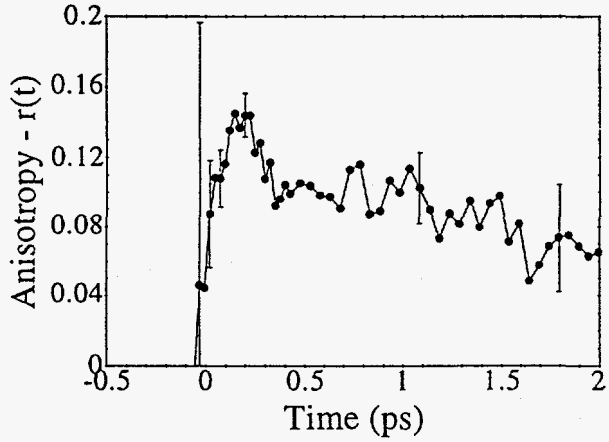

Figure 1. Anisotropy of HgI2 sample.

The transition state dynamics are observed by measuring the time dependent anisotropy of the pumped sample as the reaction proceeds. When the anisotropy of a chemical reaction is followed in the impulsive limit, the electronic and nuclear alignment properties along the reaction coordinate may be interrogated. A representative data set, illustrating the anisotropy decay r(t), of the pumped HgI_2 sample is shown in Figure 1. The data are sensitive to the off resonant pumping of solvent. The excitation of a doubly degenerate state with a femtosecond pump pulse can create a coherent superposition state of the Π_X and Π_Y components. The largest possible initial value of r(0) is therefore 0.7 for the situation in which the system is pumped through a $^1\Sigma_g \rightarrow {}^1\Pi_u$ excitation, and probed through a $^1\Pi_u \rightarrow {}^1\Sigma_g$ transition.[5] If the pumped transitions were $\Sigma_g^+ \rightarrow$

Π_u, but the probing step involved a Π_u -> Π_g transition of HgI_2, the early time anisotropy would be -0.2. Furthermore, it is expected that there is a Σ_g^+ -> Σ_u^+ of HgI_2 in the near UV. Probing this via a Σ_u^+ -> Π_g transition would also result in an initial anisotropy of -0.2. Clearly it is expected that the early time anisotropy depends on the precise wavelength of excitation when there are overlapping states. A number of processes can reduce the anisotropy for the Σ_g^+ -> Π_u -> Σ_g^+ case from 0.7 to 0.4 or even 0.1. This would occur if the states were significantly split, say by solvent interactions, or if the electronic dephasing of the level pair were very rapid. The bending motion could also contribute in principal, but this is very slow for the case of HgI_2. The value can also be reduced if there are a range of static linear and bent structures existing in the solution. The result for 320 nm excitation shown in the Figure 1suggests that the HgI_2 transition state region is indeed probed during the first 50 - 150 fs after which HgI molecules, arising from both the Σ_u^+ and Π_u channels are probed at 440 nm. The anisotropy signature of the transition is completely gone by 200 fs. The subsequent 500 fs decay of the remaining anisotropy is tentatively assigned to arise from the combination of the equilibrium inertial motion and rotational diffusion of the diatomic HgI. This timescale is approximately 3 times faster than the hydrodynamic slip limit. It is unlikely that the fast anisotropy decay time of ca. 50 fs arises from inertial motion. A rotational temperature of 5000K would be needed to account for this anisotropy loss mechanism, whereas a thermal rotational energy distribution is expected for this reaction.

Vibrational Coherence of HgI Products

The ground state vibrational frequencies of HgI_2 for the symmetric stretch, the degenerate bend and the asymmetric stretch are ν_1=156 cm^{-1}, ν_2=33 cm^{-1} and ν_3=237 cm^{-1}, respectively. The vibrational periods associated with each of these frequencies are T_1 = 214 fs, T_2 = 1010 fs and T_3 = 141 fs. The fundamental frequency of the $X^2\Sigma^+$ state of HgI is 125 cm^{-1} and this corresponds to a period of T = 267 fs. Wavepacket dynamics have been observed throughout the spectral range from 380 nm - 560 nm. Two representative magic angle signals of HgI_2 photolysis in ethanol are shown in Figure 2 for probe wavelengths of 400 nm and 540 nm. Each of the transients were fit to a phenomenological molecular response function of the form

$$R(t) = \sum_{i=1}^{2} \{A_i \exp[k_i t]\} + B\exp[k_B t]\cos(2\pi\omega c_0 + \phi) \qquad (1)$$

which was convoluted with an instrument function. The decay constant k_B represents the apparent dephasing of the oscillations, ω is the oscillation frequency and ϕ is the phase factor. The data at each probe wavelength fit to a value of ϕ = 2.8 radians. It is apparent from Figure 2 that the two transients exhibit distinct oscillation frequencies, modulation depths and decay rates. The wavelength dependence of the fitted beat frequencies and dephasing rates are shown in Figure 3.

The solvated HgI_2 wavepacket[6] generated by the pump pulse, impulsively evolves from the point of the Franck-Condon excited region of the transition state to fully dissociated fragments through a set of dissociative continuum states. The probing of these states is evidenced by the initial absorption spike found in the data of Figure 1 and 2. This spike is interpreted as arising from the two photon absorption of the parent as it dissociates to fragments on a sub 200 fs timescale. The spectral carrier of the oscillations are assigned to HgI by comparing the fitted frequencies of Figure 3 to the vibrational frequencies of the isolated X state of HgI. The similarity between these frequencies indicates that the solvated X state is similar to that of the

isolated molecule. In describing the free HgI dynamics, the dissociated HgI superposition state can be constructed from the primitive HgI vibrational basis. This broad distribution of N coherently prepared HgI eigenstates defines the wavepacket, and each set of N(N-1)/2 level pairs begin to oscillate at their unique Bohr frequencies specified by the anharmonic HgI potential.

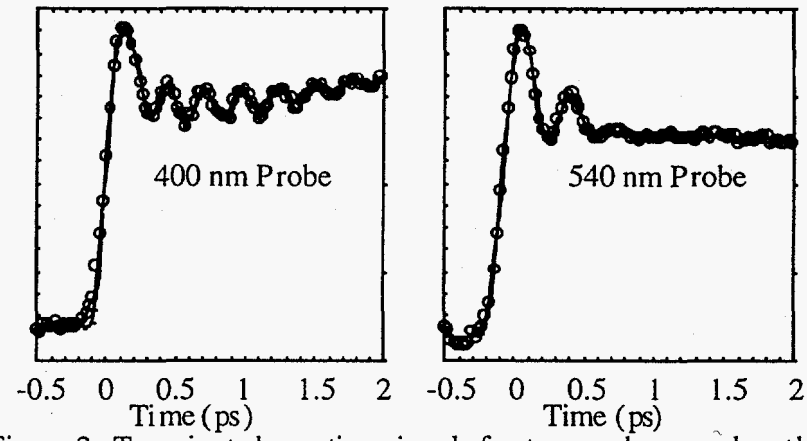

Figure 2. Transient absorption signals for two probe wavelengths.

Spectral analysis of the wavepacket is accomplished by filtering out specific sets of eigenstates with the finite bandwidth of the femtosecond probe. Probing the X state with short wavelengths predominantly samples low lying vibrational levels of HgI, whereas long wavelength probes sample high lying level pairs. This gives rise to the observed wavelength dependence on the oscillation frequency and relaxation dynamics, because the fitted frequencies are related to the mean level pair sampled by a particular probe laser. According to the conventional models for dephasing, the relaxation rates responsible for phase dissipation in the ensemble should increase with the HgI vibrational quantum number. This is realized by plotting the dephasing rate dependence on the probe wavelength in Figure 3. This verifies that level pairs lying high in the HgI anharmonic potential dephase much faster than those low in the well. The decay of the oscillations also contains contributions from the free vibrational HgI Hamiltonian. Because each of the N level pairs dephase at different rates the average energy <E(t)> of the eigenstates composing the wavepacket decrease with time, and this represents the relaxation of the initial phase of the molecular system.

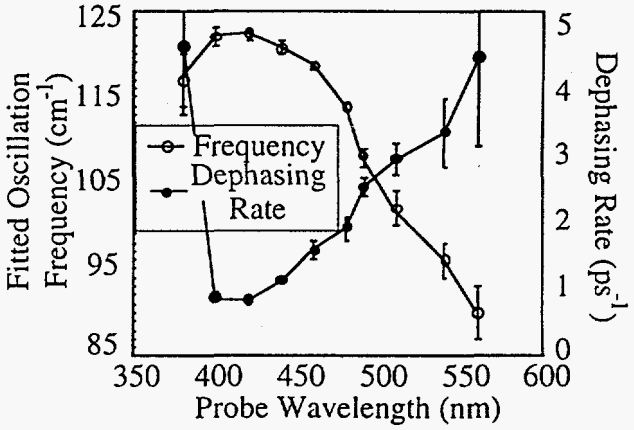

Figure 3. Wavelength dependence on k_B and ϕ.

If the wavepacket were initially launched on the X state of HgI, the fitted value of ϕ corresponds to ca. 90% of a vibrational half cycle of the HgI fundamental vibrational frequency. Hence, we propose that the HgI wavepacket is first probed when it reaches the attractive portion of its potential surface. Probing at one half of a cycle should yield a phase factor of π but our data consistently fit to a value of $\phi = 0.9\pi$. This difference is interpreted as being due to the transition state dynamics in the reacting parent. The HgI_2 proceeds along the reaction coordinate by way of its stretching motions to generate a wavepacket of stretched product fragments. This is consistent with the fact that an HgI bond in the parent measures 2.61 Å, whereas the equilibrated internuclear separation of the HgI fragment is 2.8 Å. Hence, the region of the HgI_2 potential energy surface from which the wavepacket is launched correlates to a compressed HgI product molecule, and the repulsive forces of the transition state produce an expanding HgI. The mean

time taken for an HgI bond to stretch into the region that can be intercepted by the probe as a product species is ca. 0.45 of one (free) HgI vibrational period. This implies that the transition state of I-Hg-I supports an effective vibrational frequency of ca. 140 cm^{-1}. As the wavepacket proceeds out of the exit channel, the attractive side of the HgI X state is probed on successive cycles.

In Figure 4 the HgI_2 transient in ethanol solution is shown for a probe wavelength of 420 nm to illustrate the character of the signal at longer times. The time evolution of the longer time signals are indicative of vibrational relaxation of vibrationally hot HgI.[7] Master equations were utilized to determine characteristic timescales which reproduce the experimental data. The anharmonicity of the HgI solute and a density of solvent states described by the *power spectrum of neat ethanol* were fully included to describe the vibrational population dynamics. The master equation was based on the assumption that the solute transfers its energy via V-> V coupling with the solvent modes. Simulated molecular responses are shown in Figure 4 for v" =1 -> 0 relaxation times of 2, 3 and 4 ps. All of the wavelength dependent data were reproduced best with the 3 ps value. All of the state-to-state relaxation rates for any level pair of the anharmonic

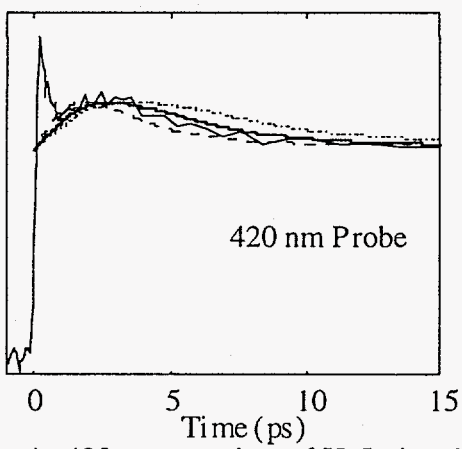

Figure 4. 420 nm transient of HgI_2 in ethanol.

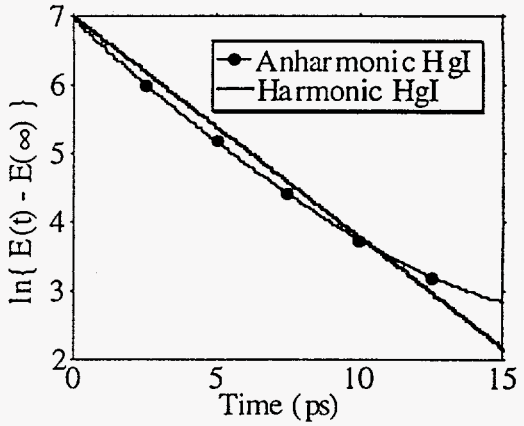

Figure 5. Vibrational energy relaxation of HgI in ethanol.

HgI ground state were calculated with the model. The influence of the anharmonicity to the energy relaxation is illustrated by the nonexponential decay of the total energy out of the HgI system shown in Figure 5. This plot is compared with the energy relaxation out of a harmonic HgI, possessing a fundamental frequency of 125 cm^{-1}. The simulations of the data also provided an estimate of the initial excess energy of the HgI produced by the photodissociation. The best fits were accomplished when the population distribution was centered at v" = 10. This corresponds to a total excess energy of ca. 1050 cm^{-1}. The fast timescales are comparable to vibrational relaxation dynamics for molecular ions in polar solutions, indicating that the forces on the vibrational coordinate are large.

Classical molecular dynamics simulations were used to calculate the vibrational relaxation of HgI. The simulations yielded the classical force-force autocorrelation function for HgI in ethanol. This function is defined by the familiar Landau-Teller expression for T_1 as,[8]

$$\frac{1}{T_1} = \frac{\zeta_{cl}(\omega)}{\mu} \qquad (2)$$

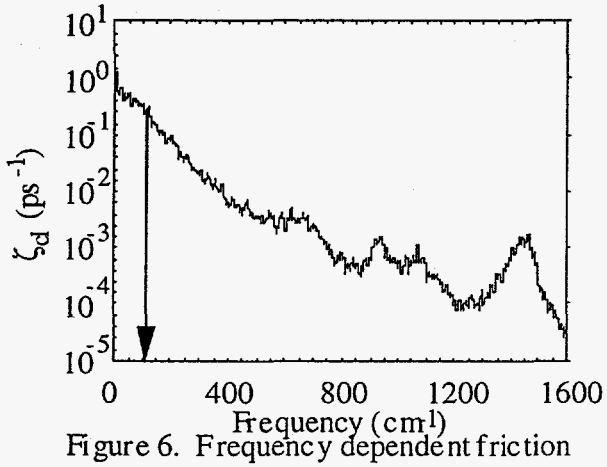

Figure 6. Frequency dependent friction of HgI in ethanol.

in which T_1 is the fundamental relaxation time, μ is the reduced mass and $\zeta_{cl}(\omega)$ is the frequency dependent friction. The simulation consisted of a HgI diatom and 255 ethanol molecules with periodic boundary conditions. The charge distribution for HgI was obtained via ab-initio calculations. The solvated potential of mean force was calculated and was found to be ca. 7% deeper than that of the gas phase. This is consistent with the fact that the measured oscillation frequencies presented in Figure 3 are similar to those of the isolated molecule. All the molecular dynamics simulations were carried out using CHARMM,[9] in which the HgI bond was constrained to its gas phase equilibrium value using SHAKE. The calculated force-force spectrum is shown in Figure 6. At the gas phase frequency the calculated T_1 time is ca. 5 ps. This is in good agreement with the time determined by fitting the experimental data with master equations. Anharmonicity is not present in the simulation and the validity of this is presently under consideration. The simulations indicate that the interactions causing HgI to vibrationally relax are short range in nature, and are dominated by the local rotational and librational modes of the solvent. These modes give rise to the large amplitude of the low frequency region of the spectrum (<200 cm-1) of Figure 6. The peaks in the 650 cm^{-1}, 1000 cm^{-1} and 1450 cm^{-1} spectral regions correspond to the internal modes of ethanol. The solvent remained at equilibrium with the solute for all simulation times. Since the HgI vibrational frequency is comparable to the orientational time of the solvent, a nonequilibrium simulation may be required. This is due to the fact that the ethanol molecules do not have enough time to follow the HgI vibration adiabatically and an additional solvent coordinate is needed. It is also possible that solvent may not able to handle the rapid dissipation of vibrational energy and the energy may flow back into HgI.

Conclusion

This contribution has summarized our current understanding of the photodissociation and relaxation dynamics of HgI_2 in alcohol solutions. Measurements on the early time anisotropy, the wavepacket dynamics and the vibrational relaxation of the fragments have been examined both experimentally and through simulation.

Acknowledgements

This research was supported by grants from NSF and NIH.

References

[1]D. Raftery, E. Gooding, A. Romanovsky and R. M. Hochstrasser, J. Chem. Phy. **101**, 8572 (1994).

[2]D. Raftery, R. J. Sension and R. M. Hochstrasser, in " Activated Barrier Crossing; Applications in Physics, Chemistry and Biology", G. R. Fleming and P. Hänggi (World Scientific Publishing Co., River Edge, NJ, 1993).

[3]N. Pugliano, D. K. Palit, A. Z. Szarka and R. M. Hochstrasser, J. Chem. Phys. **99**, 7273 (1993).

[4]M. Gruebele, G. Roberts, and A. H. Zewail, Phil. Trans. R.Soc. Lond. A 332, 223 (1990), and references within..

[5]K. Wynne and R. M. Hochstrasser, Chemical Physics **171**, 179 (1993).

[6]N. Pugliano, A. Z. Szarka, D. K. Palit and R. M. Hochstrasser, Ultrafast Phenomena IX (eds. G. Mourou, A. H. Zewail P. F. Barbara, and W. H. Knox) Springer Series in Chemical Physics, **60**, 501 (1994).

[7]Nick Pugliano, Arpad Z. Szarka, S. Gnanakaran, M. Treichel and Robin M. Hochstrasser, J. Chem. Phys. (in press).

[8]J. Owrutsky, D. Raftery and R. M. Hochstrasser, Ann. Rev. Phys. Chem. **45**, 519(1994).

[9]B. R. Brooks, R. E. Bruccoleri, B. D. Olafson, D. J. States, S. Swaminathan, M. Karplus, J. Comp. Chem. **4**, 187 (1983).

INVITED PAPERS

Probing the Dynamics of Ligand Motion in Myoglobin with Femtosecond IR Spectroscopy

Timothy A. Jackson, Manho Lim, and Philip A. Anfinrud
Department of Chemistry, Harvard University

INTRODUCTION

Myoglobin (Mb), a heme protein that reversibly binds small ligands has long served as a model system for understanding the relations between protein structure, dynamics, and function. A detailed understanding of this protein requires knowledge of the time-dependent orientation and position of the ligand following dissociation from the heme. To obtain this information under physiologically relevant conditions, we have developed a time-resolved IR spectrometer that achieves < 200 fs time resolution and a level of sensitivity approaching that of conventional FTIR spectrometers. Using this instrument we have determined the orientation of CO bound to and dissociated from Mb, and the dynamics for ligand trapping and escape. These results provide stringent tests for molecular dynamics simulations and provide new insight into the functional role of protein structure.

TIME-RESOLVED IR SPECTROMETER

The time-resolved spectrometer used to record polarized IR absorption spectra is shown in Figure 1. Spectra at times shorter than a few ns were obtained by photolyzing MbCO with an optically delayed 100 fs duration 590 nm optical pulse. Spectra at times beyond a few ns were obtained by photolyzing the sample with an electronically delayed 4 ns duration 527 nm optical pulse. The polarization direction of the

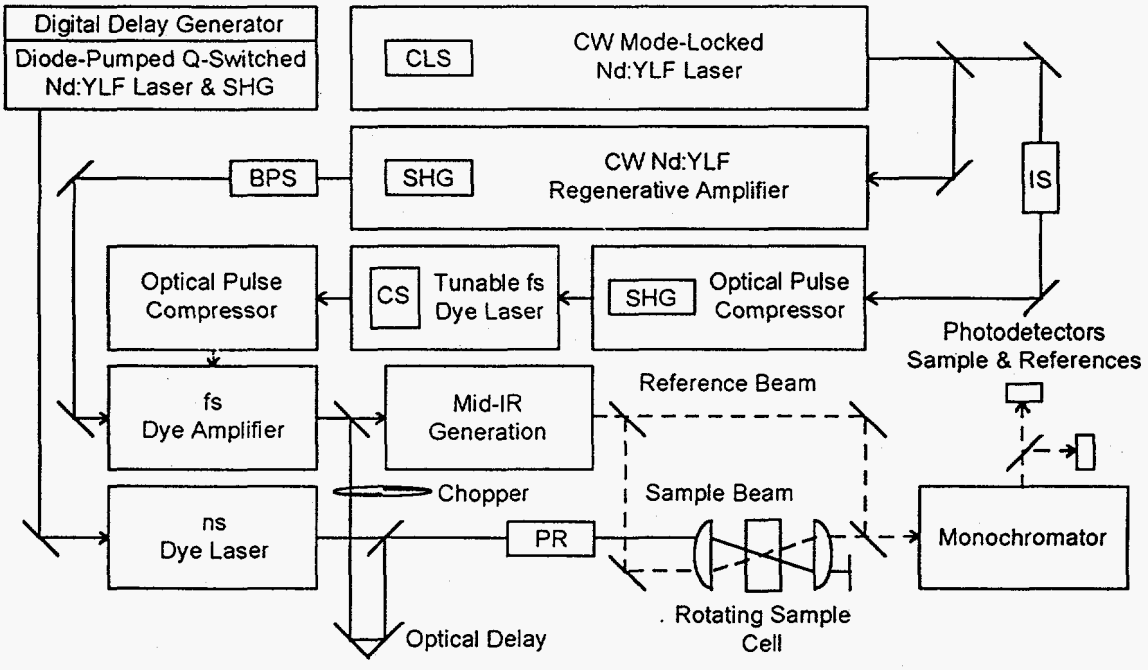

Figure 1. Schematic diagram of the time-resolved IR spectrometer. CLS, cavity length stabilizer; SHG, second harmonic generator; IS, intensity stabilizer; BPS, beam pointing stabilizer; CS, coherent seeder; PR, polarization rotator.

photolysis pulse was controlled electronically by a liquid crystal polarization rotator. The photolyzed sample was probed with a linearly polarized 200 fs duration broadband IR probe pulse whose transmitted intensity was spectrally resolved with an IR monochromator ($3cm^{-1}$ bandpass) and detected with a liquid-nitrogen-cooled InSb photodetector. The photodetector signal was normalized with respect to a reference signal to obtain the transmittance of the sample at the wavelength selected by the monochromator. A synchronous light chopper blocked every other pump pulse, thereby interleaving the pumped and unpumped sample transmittances. The photolysis-induced change of the sample absorbance ΔA was computed from sample transmittances measured with and without the photolysis pulse. The 1.2 – 1.5 kHz repetition frequency of the laser system permitted extensive signal averaging and contributed to the high quality time-resolved spectra reported here. The ≈ 13 mM MbCO solution was loaded into a 100 μm path length IR cell equipped with CaF_2 windows. The cell was mounted in a refrigerated enclosure, chilled to 10 °C, and rotated sufficiently fast so that each photolysis pulse illuminated a fresh volume within the sample.

TRANSIENT IR SPECTRA OF PHOTOLYZED MbCO

We showed earlier that CO photodissociated from Mb becomes trapped in a protein docking site where its orientation is constrained [1]. Here, we determine the proximity of this site relative to the heme iron by probing the sub-picosecond evolution of the CO vibrational spectrum. In addition, using polarized IR spectroscopy, we show that the orientation of "docked" CO is approximately orthogonal to the bound orientation. Finally, by measuring the spectral evolution of CO photodissociated from MbCO from 200 fs out to several μs, we determine the time scale for ligand transport from the docking site to the solvent.

Ultrafast trapping of dissociated CO

The ultrafast spectral evolution of CO following photolysis of MbCO is shown in Figure 2. The 200 fs spectrum reveals two overlapping features. These features separate at longer times and correspond to the *B* states identified by Frauenfelder and coworkers [2]. The two *B* states evidently arise from two different dissociation trajectories. Their integrated absorbance grows in time, long after the photolysis is complete, due to cooling of the protein surrounding the CO. The spectrum at 0.32 ps is quite similar to the spectrum observed at longer times, demonstrating that the dissociated CO becomes trapped in the docking site within ~ 0.5 ps. This suggests that the docking site must be located no more than a few Å from the heme iron, and likely corresponds to the location of unbound CO determined from low temperature x-ray structures of photolyzed MbCO [3,4]. Interestingly, the geminate rebinding yield of CO dissociated from Mb in water at room temperature is less than 1.5%, in spite of the close proximity of CO to the iron.

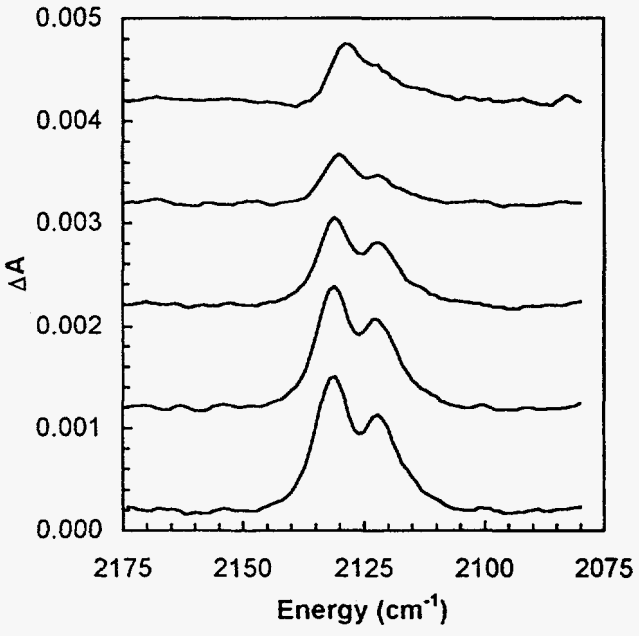

Figure 2. Femtosecond time-resolved mid-IR absorption spectra of photolyzed $Mb^{12}CO$ at 0.20 ps, 0.32 ps, 1.00 ps, 3.16 ps, and 10.0 ps (top to bottom). The background and hot band contributions to the time-resolved spectra have been removed.

Orientation of bound and dissociated CO

The technique of photoselection spectroscopy has been used to determine the orientation of CO bound to and dissociated from Mb. This determination is possible because the spectroscopic transitions for both heme and CO are polarized along specific directions in the molecular frame. When a solution of MbCO is illuminated with linearly polarized light, hemes oriented along the polarization direction absorb light preferentially. The ligands bound to these "photoselected" hemes are dissociated with high quantum efficiency, leading to a loss of bound CO and the production of CO located near but not bound to the heme iron. If the CO is oriented at a particular angle θ relative to the heme plane normal, the ratio of its IR absorbance polarized perpendicular and parallel to the photolysis polarization $\Delta A^{\perp}/\Delta A^{\parallel}$ is a simple analytic function of θ [5]:

$$\frac{\Delta A^{\perp}}{\Delta A^{\parallel}} = \frac{4 - \sin^2\theta}{2 + 2\sin^2\theta}.$$

If the CO orientation was static and along the heme normal, the ratio, $R = \Delta A^{\perp}/\Delta A^{\parallel}$, would assume the theoretical maximum of 2. If the CO orientation was static and oriented in the plane of the heme, the ratio would assume the theoretical minimum of 0.75. At ambient temperature the CO orientation fluctuates about its equilibrium position so its orientation must be described by an orientational distribution function. Because of this motion, the maximum ratio that can be measured experimentally is smaller than 2, and the minimum is larger than 0.75.

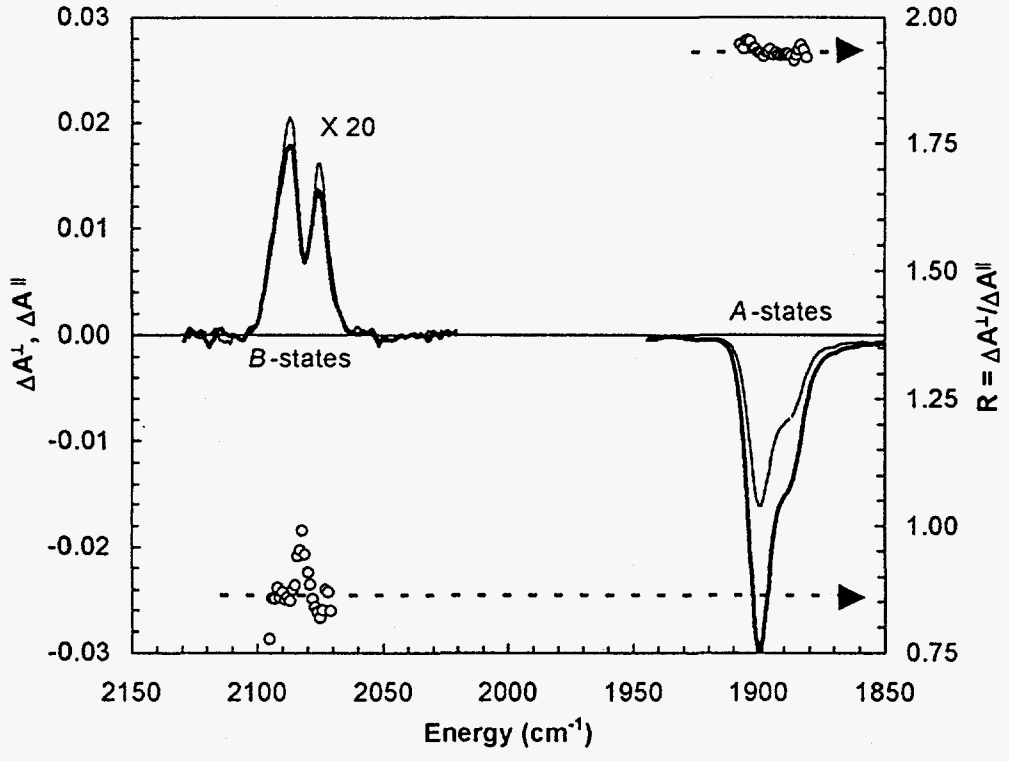

Figure 3. Polarized IR absorbance spectra and their ratio measured 100 ps after photolysis of $Mb^{13}CO$. The left axis labels correspond to the photolysis-induced absorbance changes, $\Delta A^{\perp}$ (thick lines) and $\Delta A^{\parallel}$ (thin lines); the right axis label corresponds to their ratio, $R = \Delta A^{\perp}/\Delta A^{\parallel}$ (open circles).

In low temperature glasses where the protein orientation is frozen and ligand rebinding is slow, the polarized IR spectra can be measured with conventional IR spectrometers [6]. In solution, where rotational tumbling of the protein randomizes the orientation of the photoselected hemes, the measurement must be made on a time scale that is short compared to the rotational diffusion time, which is 8 ns for Mb in H_2O at 288K [7]. Consequently, a structural determination in solution requires ps time resolution.

Time-resolved polarized IR absorption spectra of photolyzed MbCO are shown in Figure 3. The ratio, $R = \Delta A^{\perp}/\Delta A^{\parallel}$, is plotted where the absorbance exceeds ~ 25% of its maximum and has been corrected for fractional photolysis. The validity of this correction, calculated numerically for fractional photolysis of an optically thick sample, has been verified experimentally. The ratio for bound CO is near the theoretical maximum of 2, indicating that bound CO is oriented close to the heme normal. This is in contrast to the high resolution crystal structure of MbCO which shows CO bent 39° away from the heme normal [8]. Based upon our solution structure, the dogma of a bent Fe–C–O must be abandoned.

Upon dissociation from the heme iron, CO assumes an orientation nearly orthogonal to that for bound CO, and is approximately in the plane of the heme [9]. The two *B*-state features have a similar orientation relative to the heme normal, suggesting that they correspond to CO oriented oppositely within the same docking site. The barrier to interconversion between these two orientations is modest, permitting end-to-end rotation on a ps time scale [1].

Dynamics of ligand escape

The ns spectral evolution of photolyzed MbCO is shown in Figure 4. At 10 ns, the spectrum is virtually identical to that observed at 100 ps, demonstrating that the CO remains trapped in the heme pocket docking site for many ns.

At long times, the spectrum reveals a single broad feature, denoted an *S* state, which corresponds to CO in the solvent. At intermediate times, an additional feature centered between the two *B* states is observed. This feature, which we denote a *C* state, grows concomitant with the disappearance of the *B* states, after which it also disappears. Evidently, this feature corresponds to CO transiently trapped in another internal cavity of the protein. Kinetic analysis of the spectral evolution suggests that this new state is accessed reversibly on a time scale similar to that for escape from the *B* state into the surrounding solvent.

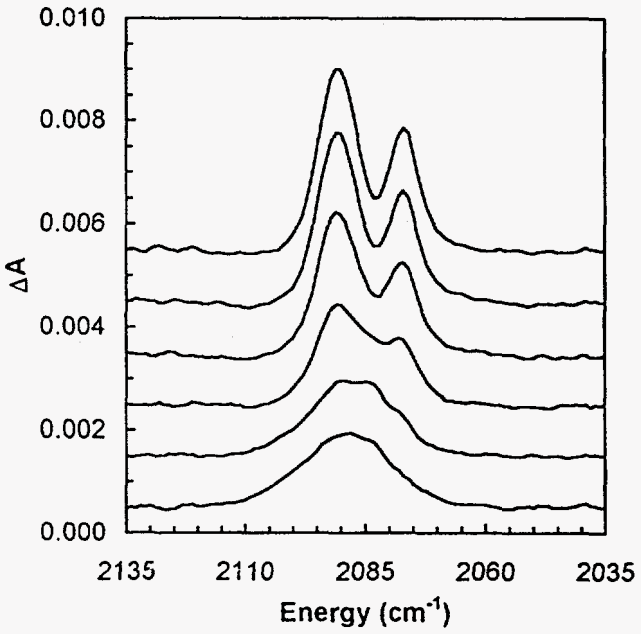

Figure 4. Nanosecond time-resolved mid-IR absorption spectra of photolyzed $Mb^{13}CO$ at 10.0 ns, 31.6 ns, 100 ns, 316 ns, 1.00 μs, and 3.16 μs (top to bottom).

The integrated CO absorbance decreases modestly and monotonically as the CO escapes into the surrounding solvent. Interestingly, the spectral evolution can be modeled by a linear combination of *B*, *C*, and S states at all times. This suggests that transport between these states is fast compared to the residence time within each state. Evidently, Mb provides facile paths for shuttling ligands between the docking site and the surrounding solvent, the bottleneck for which is escape from the docking site.

SUMMARY AND CONCLUSIONS

Using ultrafast time-resolved IR spectroscopy, we have found that CO photodissociated from Mb becomes trapped in a nearby docking site within ~0.5 ps. This site constrains the orientation of CO to lie nominally in the plane of the heme, a direction nearly orthogonal to that for bound CO. The orientational and spatial constraints imposed on the ligand by the surrounding residues slows dramatically the rate of CO binding from the docking site, thereby inhibiting geminate rebinding of CO. The CO departs from the heme pocket on a time scale of a few hundred ns, escaping with a quantum efficiency of ~98.5% in water at ambient temperature. Before escaping, the CO may shuttle reversibly to another internal cavity of the protein. The bottleneck for diffusional escape from the docking site into the surrounding solvent is escape from the *B* state. Consequently, the residues that circumscribe the heme pocket likely dominate the kinetics for ligand binding and escape. The role of these residues is under investigation using mutants of Mb.

The spectrometer developed to acquire ultrafast time-resolved IR spectra provides a unique combination of sensitivity, time resolution, spectral resolution, and temporal range. This experimental approach offers great promise for investigating incisively a broad range of photo-physical, -chemical, and -biological phenomena.

Acknowledgements

This work was supported in part by NIH Grant No. DK45306, the NSF-NYI Program, the Beckman Foundation, and the Mitsubishi Kasei Corporation.

References

1. M. Lim, T. A. Jackson and P. A. Anfinrud, J. Chem. Phys., 102 (1995) 4355.
2. J. O. Alben, D. Beece, S. F. Bowne, W. Doster, L. Eisenstein, H. Frauenfelder, D. Good, J. D. McDonald, M. C. Marden, P. P. Mo, L. Reinisch, A. H. Reynolds, E. Shyamsunder and K. T. Yue, Proc. Natl. Acad. Sci. U. S. A., 79 (1982) 3744.
3. T. Y. Teng, V. Srayer and K. Moffat, Nature Struct. Biol., 1 (1994) 701.
4. I. Schlichting, J. Berendzen, G. N. Phillips, Jr. and R. M. Sweet, Nature, 371 (1994) 808.
5. J. N. Moore, P. A. Hansen and R. M. Hochstrasser, Proc. Natl. Acad. Sci. U. S. A., 85 (1988) 5062.
6. P. Ormos, D. Braunstein, H. Frauenfelder, M. K. Hong, S. L. Lin, T. B. Sauke and R. D. Young, Proc. Natl. Acad. Sci. U. S. A., 85 (1988) 8492.
7. J. Albani and B. Alpert, Chem. Phys. Lett., 131 (1986) 147.
8. J. Kuriyan, S. Wilz, M. Karplus and G. A. Petsko, J. Mol. Biol., 192 (1986) 133.
9. M. Lim, T. A. Jackson and P. A. Anfinrud, Science, (accepted 19 May 1995).

Picosecond Time-Resolved Coherent Anti-Stokes Raman Spectroscopy: Studies in the Room Temperature Bacteriorhodopsin and Rhodopsin Photo-Reactions

G.H. Atkinson, L. Ujj, A. Popp, J. Delaney[†], Frank Jäger, and R. Ligon

Department of Chemistry and Optical Sciences Center, University of Arizona, Tucson, AZ. USA

The molecular mechanism(s) by which energy is stored and transduced within the photosynthetic trans-membrane proteins rhodopsin (Rh) and bacteriorhodopsin (BR) have been subjected to intense study for more than two decades [1-3]. The molecular transformations within the respective photo-reactions are thought to provide insight into how light energy absorbed by the retinal chromophore can be efficiently stored within the protein and how the initial molecular events transduce energy uptake into biochemical function (e.g., G-protein binding at the surface of the protein). The Rh and BR photo-reactions, of course, represent fundamentally important biochemical systems which either directly or indirectly are related to visual processes in vertebrates.

As with many complex chemical and biochemical reactions, energy storage/transduction in proteins involve structural changes not only in the chromophore through which light absorption occurs, but also encompass contributions from the surrounding environment. In the case of Rh and BR, interactions between the retinal chromophore and its protein environment may prove to be the most important elements in what is clearly a complex series of molecular events that stretch in time from femtoseconds to seconds.

Transient absorption spectroscopy involving electronic transitions provided the earliest characterizations of such photo-reactions [1-3]. Primarily monitoring the changes in electronic energy, these transient absorption data have been central to revealing the existence of the kinetic intermediates comprising each photo-reaction and characterizing the time scales over which each transformation occurs. The need to elucidate the structural changes associated with each transformation within a photo-reaction, however, is the central issue upon which time-resolved vibrational spectroscopy can be brought to bear.

Understanding of the vibrational structure of stable species from which each photo-reaction begins is the natural starting point for structural studies. Structural information has been obtained from a variety of methodologies including NMR, chemical extraction, neutron and X-ray diffraction as well as vibrational spectroscopies (e.g., FTIR and resonance Raman (RR)) [4-8]. Characterizing the structures of transient intermediates within these photo-reactions is experimentally more challenging given the femtosecond to millisecond time scales involved.

Much of the initial vibrational data available for BR and Rh intermediates have been measured on BR and Rh samples at low (e.g., 77K) temperatures [4,9,10]. Different BR and Rh intermediates are thought to be trapped (stabilized) at specific temperatures. Low-temperature vibrational data have provided valuable insight into many aspects of the Rh and BR photo-reaction and indeed until recently, provided the only practical method for examining the photochemically-irreversible room-temperature Rh photo-reaction. There remains, however, a concern that temperature-dependent effects exist within these photo-reactions which might alter important structurally-related processes affecting the energy storage/transduction mechanisms, especially with respect to the role(s) of the

protein environment. In addition, a wide range of artificial retinal Rh and BR pigments containing chemically-, isotopically-, and/or structurally-modified retinal chromophores cannot, in general, be examined due to the limited signal to noise ratios available from the vibrational measurements and the small sample sizes.

Picosecond time-resolved vibrational data derived from RR scattering opened the structural characterization of intermediates in the room-temperature BR photocycle to study. Indeed, the first structural data of the early room-temperature intermediates (i.e., K, L, and M) are derived from time-resolved RR scattering.

Experimental methodologies based on spontaneous RR scattering, however, limit the quality of the data (S/N) and therefore restrict both the detail with which structural changes can be determined and the type and size of BR samples which can be studied. In the case of the Rh photoreaction, time-resolved RR cannot be used extensively to measure the vibrational spectra of intermediates due to the irreversibility of the photoreaction itself. The development and application of picosecond time-resolved coherent (anti-Stokes) Raman scattering (PTR/CARS) to the photo-reactions of the trans-membrane proteins containing retinal has been used recently to successfully overcome these limitations [11-15]. The work described here is directly related to PTR/CARS measurements that are utilized to examine the structures of intermediates in the room-temperature BR and Rh photo-reactions.

There are several experimental advantages to PTR/CARS which should be noted:

1. Vibrational data are generated on coherent beams exiting the sample which makes separating the CARS signal only a matter of blocking the interfering pump beams (ω_1 and ω_s).
2. Interference from fluorescence is essentially eliminated.
3. Polarization information can be obtained by quantitatively controlling the polarization properties of the excitation (ω_1 and ω_s) beams. Polarization can also be used to selectively suppress CARS signals from one component of a reactive mixture relative to other components. For example, the CARS signal from Rh^{RT} can be experimentally suppressed while measuring the PTR/CARS signal from the $batho^{RT}$.

There are also several experimental challenges including:

1. The non-resonant background CARS signal from the solvent, and potentially from the protein (opsin), must be considered. In the cases of BR and Rh, the major contribution is found from the non-resonant water signal which can be quantitatively incorporated into the data analysis. No significant non-resonant components from the proteins are observed in either BR or Rh.
2. To record spectrally broad PTR/CARS signal with each pair of ω_1 and ω_s pulses, one laser (ω_s) must be operated with a broad (300-400 cm^{-1}) bandwidth. The generation of picosecond (<10 ps) pulses with such a broad spectral bandpass requires careful optimization of the laser parameters.

Finally, the quantitative analysis of PTR/CARS data requires a non-linear optical formulation utilizing third-order susceptibility ($\chi^{(3)}$) relationships. The methodology underlying the quantitative application of $\chi^{(3)}$ analysis to BR and Rh has been described in detail elsewhere [11-13].

To date, PTR/CARS techniques have been used to examine a wide range of questions involving transient species in the room temperature BR and Rh photo-reactions including (i) the vibrational structure of the K-590 intermediate (thought to have a 13-*cis* retinal chromophores) formed during the room-temperature BR photocycle [16], (ii) vibrational spectra of room-temperature K-590 containing an isotopically-substituted retinal (^{13}C at both C_{14} and C_{15}) [17], and (iii) CARS spectra of the blue membrane of BR [18] which contains two isomeric forms of retinal in its ground-state. Results from these studies are presented elsewhere in this publication.

PTR/CARS techniques have also made it experimentally feasible to measure the vibrational spectra of intermediates (e.g., batho) in the room-temperature Rh photo-reaction [14,15]. The separation of the retinal chromophore from its protein that occurs following meta-rhodopsin formation has previously prevented the detection of vibrational spectra from Rh intermediates at **room-temperature.** The Rh sample simply disappears upon irradiation. The excellent S/N and picosecond (5 ps) time-resolution available in these PTR/CARS measurements removes this experimental barrier by acquiring high quality vibrational data rapidly from intermediates prior to sample degradation.

These CARS data can be compared to vibrational data (RR) recorded from low temperature Rh samples where irradiation is thought to produce a specific intermediate (e.g., batho) that becomes trapped. One element in these comparisons is the presence of temperature dependent changes in the vibrational spectrum of Rh. This information, of course, is the beginning point in any analysis and interpretation of PTR/CARS data from transient Rh intermediates. Attention is focussed here on the temperature-dependent vibrational changes appearing in Rh.

Table 1: Comparison of the vibrational data of low (77K) and room-temperature rhodopsin. Band origin positions (Ω) obtained by fitting C=C stretch region of the PR/CARS spectrs of Rh at room temperature to a $\chi^{(3)}$ relationship. Values of Ω and Rh^{RT} measured by PR/CARS and intensity maxima positions of Rh^{LT} amd Rh^{RT} measured by RR spectroscopy as well as probing wavelengths (nm), are presented to facilitate comparisons.

Resonance Raman					PR/CARS
Rh^{LT}	Rh^{RT}				Rh^{RT}
488[6]	600[19]	590[20]	488[21]	458-647[22]	565
Band maxima [cm^{-1}]					Ω [cm^{-1}]
	1450		1435	1432/1442	(1443)
1549	1545	1545	1546	1549	1545
1582	1580		1580	1581	1577
1599/1609	1605	1595	1607	1609	1602
1636		1633	1635		1627
1657	1660	1655	1658	1659	1653

Specifically, the C=C stretching band of Rh is examined in this paper. The picosecond resonance CARS (PR/CARS) of the stable Rh is presented in Fig. 1 together with its $\chi^{(3)}$ fit. The major band maximum (C=C stretch) appears at 1545-cm^{-1}. This is 4-cm^{-1} lower in frequency than the 1549-cm^{-1} position reported from 77K RR data [6]. The presence of such a temperature-dependence has been reported previously from RR studies [19-22]. The excellent agreement between the RR and PR/CARS results confirms not only the precision of the experimental PR/CARS data, but also the accuracy of the $\chi^{(3)}$ fit. More importantly, the high S/N of the PR/CARS data reveals several other vibrational bands assignable to Rh in the C=C stretching region not consistently reported previously. In other cases, the positions, bandwidths, and relative amplitudes of vibrational features previously reported can be more quantitatively determined. These comparisons are presented in Table 1.

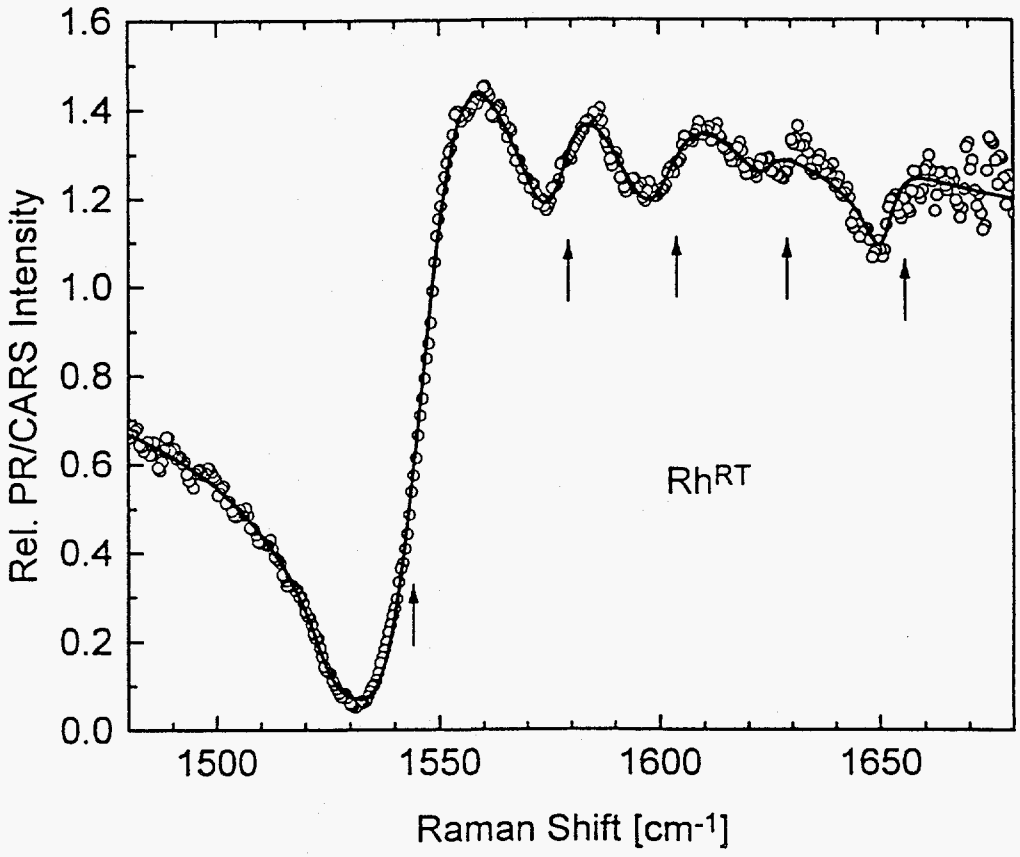

Fig. 1: PR/CARS data with $\chi^{(3)}$ from room-temperature Rh (unfilled circles) with $\chi^{(3)}$ fit (solid line). Vertical arrows mark positions of major bands (see Table 1).

The confirmation of the temperature-dependent C=C stretching frequency in Rh also provides the background information needed to reveal the temperature-dependent changes in batho [15]. The 13-cm^{-1} increase between the C=C band maxima of Rh and batho observed at 77K is **not** found at room temperature. Rather a 2-3 cm^{-1} decrease upon batho formation is found [15]. There are also several

other lower intensity bands that can be observed in greater detail here than previously and which independently exhibit changes upon batho formation [15]. A schematic representation of the C=C stretching frequencies of the Rh and batho, at 77K and room temperature, is presented in Fig. 2.

The capability of observing complete vibrational spectra from intermediates in the room temperature Rh photo-reaction is based on the excellent S/N in the PR/CARS and PTR/CARS data.

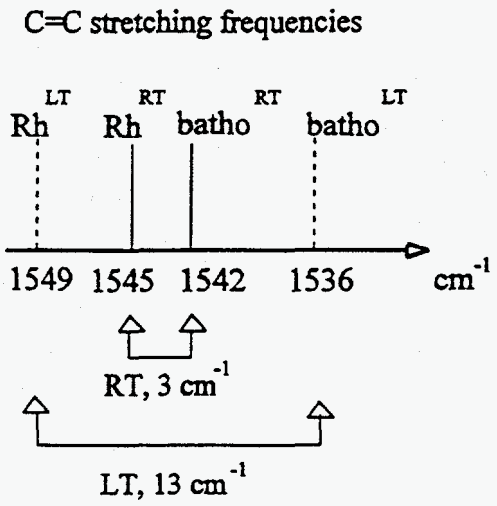

Fig. 2: Schematic representation of the positions of C=C bands positions for Rh^{RT} and Rh^{LT}.

[1]Department of Biology and Chemistry, Johns Hopkins Medical Center, Baltimore, MD, USA

References

1. Birge, R.R. (1990) *Biochim Biophys. Acta* 1016 293.
2. Nathans, J. (1992) *Biochemistry* 31 4923.
3. Lewis, J.W. and Kliger, D.S. (1992) *J. Bioenerg. Biomembr.* 24 201.
4. DeGrip, W.J., Gray, D., Gillespie, J., Bovee, P.H.M., van den Berg, E.M.M., Lugtenburg, J., and Rothschild, K.J. (1988) *Photochem. Photobiol.* 48 497.
5. Ganter, U.M., Gärtner, W., and Siebert, F. (1988) *Biochemistry* 27 7480.
6. Deng, H. and Callender, R.C. (1987) *Biochemistry* 27 7480.
7. Smith, S.O., Courtin, J., deGroot, H., Gebhard, R., and Lugtenburg, J. (1991) *Biochemistry* 30 7409.
8. Rath, P., Decaluwe, L.L.J., Boveegeurts, P.H.M., DeGrip, W.J., and Rothschild, K.J. (1993) *Biochemistry*, 32 10277.
9. Eyring, G. and Mathies, R. (1979) *Proc. Natl. Acad. Sci. USA* 76 33.
10. Bagley, K.A., Balogh-Nair, V., Croteau, A.A., Dollinger, G., Ebrey, T.G., Eisenstein, L., Hong, M.K., Nakanishi, K., and Vittitow, J. (1985) *Biochemistry* 24 6055.
11. Ujj, L. and Atkinson, G.H. (1994) *Israeli J. of Chem.* 33 207.
12. Ujj, L., Volodin, R.L., Popp, A., Delaney, J.K., and Atkinson, G.H. (1994) *Chem. Phys.* 182 291.
13. Ujj, L., Popp, A., and Atkinson, G.H. (1994) *Chem. Phys.* 188 221.
14. Popp, A., Ujj, L., and Atkinson, G.H. (1995) *Biophys. J.* (in press)
15. Popp, A., Ujj, L., and Atkinson, G.H. (1995) *Proc. Natl. Acad. Sci. USA* (in press).
16. Ujj, L., Popp, A., Jäger, F., and Atkinson, G.H. (in this publication)
17. Jäger, F., Ujj, L. and Atkinson, G.H. (in this publication)
18. Ligon, R., Popp, A., and Atkinson, G.H. (in this publication)
19. Mathies, R, Oseroff, R.A., and Stryer, L. *Proc. Natl. Acad. Sci. USA* 73 (1976), 1.
20. Marcus, M.A. and Lewis, A. *Photochem. Photobiol.* 29 (1979) 699.
21. Palings, I., Pardoen, J.A., van den Berg, E., Winkel, C., Lugtenburg, J., and Mathies, R.A. *Biochemistry* 26 (1987) 2544.
22. Loppnow, G.R., and Mathies, R.A. *Biophys. J.* 54 (1988) 35.

Vibrational Photon Echoes in Liquids and Glasses

M. D. Fayer
Department of Chemistry
Stanford University, Stanford, CA 94305

INTRODUCTION

Lineshapes in condensed phases contain all of the details of the interactions of a normal mode with its environment. These interactions include the important microscopic dynamics, intermolecular couplings, and time scales of solvent evolution that modulate the energy of a transition, in addition to essentially static structural perturbations. An infrared absorption spectrum or Raman spectrum gives frequency-domain information on the interactions that couple to the states involved in the transition. Lineshape analysis of vibrational transitions has long been recognized as a powerful tool for extracting information on molecular dynamics in condensed phases. The difficulty with determining the microscopic dynamics from a spectrum arises because linear spectroscopic techniques have no method for separating the various contributions to the vibrational lineshape. The IR absorption or Raman spectrum represents a convolution of the various dynamic and static contributions to the observed lineshape. To completely understand a vibrational lineshape, a series of experiments is required to characterize each of its static and dynamic components. Techniques such as the infrared photon echo [1-3] and Raman echo [4-7] can determine the homogeneous vibrational lineshape which contains the important microscopic dynamics although this lineshape is masked by inhomogenous broadening.

Here the temperature-dependent vibrational dynamics of the triply degenerate T_{1u} CO stretching mode (~1980 cm^{-1}) of tungsten hexacarbonyl ($W(CO)_6$) in the molecular glass-forming liquids 2-methyltetrahydrofuran (2-MTHF), 2-methylpentane (2-MP), and dibutylphthalate (DBP) are briefly described [8]. The contributions to the vibrational lineshape from different dynamic processes are delineated by combining the results of photon echo measurements of the homogeneous lineshape [2] with pump-probe measurements of the lifetime and reorientational dynamics [9]. This combination of measurements allows the decomposition of the total homogeneous vibrational lineshape into the individual components of pure-dephasing (T_2^*), population relaxation (T_1), and orientational relaxation. The results demonstrate that each of these can contribute significantly, but to varying degrees at different temperatures.

INFRARED VIBRATIONAL PHOTON ECHO EXPERIMENTS

The picosecond infrared vibrational photon echo experiment is a time domain nonlinear experiment that can extract the homogeneous vibrational lineshape even when the inhomogeneous linewidth is thousands of times wider than the homogeneous width. The echo is a two pulse sequence. The two resonant IR excitation pulses generate a polarization in the

sample that gives rise to a third pulse of light, which is the photon echo. A measurement of the echo intensity vs. τ, the delay time between the excitation pulses, is called an echo decay. The Fourier transform of the echo decay is the homogeneous lineshape [10]. If the echo decay is an exponential, the lineshape is a Lorentzian with a width $1/\pi T_2$ determined by the exponential decay constant. The vibrational photon echo makes the vibrational homogeneous lineshape an experimental observable.

The description of the third-order nonlinear polarization that governs infrared photon echo experiments in terms of the dynamics of lifetime, pure dephasing, and orientational diffusion has been presented [8]. For the case that the relaxation processes that contribute to the lineshape are separable, the photon echo signal decays exponentially as

$$I(\tau)/I(0) = \exp\left[-4\tau\left(1/T_2^{*} + 1/2T_1 + 2D_{or}\right)\right] = \exp[-4\tau/T_2] \qquad (1)$$

where D_{or} is the orientational diffusion constant, and $2D_{or}$ is contribution to the echo decay from orientational relaxation [8].

The experiments were performed using infrared pulses at ~5 μm generated by the Stanford superconducting-accelerator-pumped free electron laser (FEL). The FEL produces Gaussian pulses that are transform limited with pulse duration that is adjustable between 0.7 ps and 2 ps. The FEL emits a 2 ms macropulse at a 10 Hz repetition rate. Each macropulse consists of the ps micropulses at a repetition rate of 11.8 MHz (84 ns). The micropulse energy at the input to experimental optics is ~0.5 μJ. The two pulses used for photon echo experiments and pump probe experiments were focused in the sample to 220 μm diameter. The signal was measured with a HgCdTe detector. The photon echo signal and a intensity reference signal were sampled by two gated integrators and digitized for collection by computer. Careful studies of power dependence and repetition rate dependence of the data were performed. It was determined that there were no heating or other unwanted effects when data was taken with pulse energies of ~15 nJ for the first pulse and ~80 nJ for the second pulse and the effective repetition rate of 1 kHz (50 kHz during each macropulse). Solutions of $W(CO)_6$ in the glass-forming liquids were made to give a peak optical density of 0.8. These solutions correspond to mole fractions of $\leq 10^{-4}$. The temperatures of the samples were controlled to ±0.2 K using a closed-cycled He refrigerator.

RESULTS AND DISCUSSION

Figure 1a displays photon echo data for $W(CO)_6$ in 2-MP taken in the low temperature glass at 10 K [8]. The inset shows a log plot of the data. The decay is exponential, indicating that the homogeneous line is a Lorentzian. At this temperature, the absorption linewidth is 10.5 cm^{-1} (310 GHz). In contrast, T_2 = 240 ps, yielding a homogenous linewidth of 1.3 GHz. Thus the absorption line is massively inhomogeneously broadened. Figure 1b displays data taken using 0.7 ps pulses in the solvent DBP [3]. With this pulse duration, the bandwidth of the excitation pulses exceeds the vibrational anharmonicity; population can be excited to higher vibrational levels. Thus, short pulse excitation creates a three level coherence involving v = 0, 1 and 2. The expected photon echo signal can be described for an unequally spaced three-level system using a semiclassical perturbative treatment of the third-order nonlinear polarizability in the Bloch limit.

The decay is consistent with the expected decay of a three level vibrational coherence. The decay is modulated at a 2.3 ps frequency, corresponding to a vibrational anharmonic splitting, $\Delta = 14.7\ cm^{-1} \pm 0.3\ cm^{-1}$ [3]. This splitting is in accord with the value of $15\ cm^{-1} \pm 1\ cm^{-1}$ subsequently obtained by Heilweil and co-workers from observation of the $v = 1 \rightarrow 2$ and $v = 2 \rightarrow 3$ transitions using transient infrared absorption [11]. The echo decay data also provide the homogeneous dephasing times for the two transitions involved in the multilevel coherence [3].

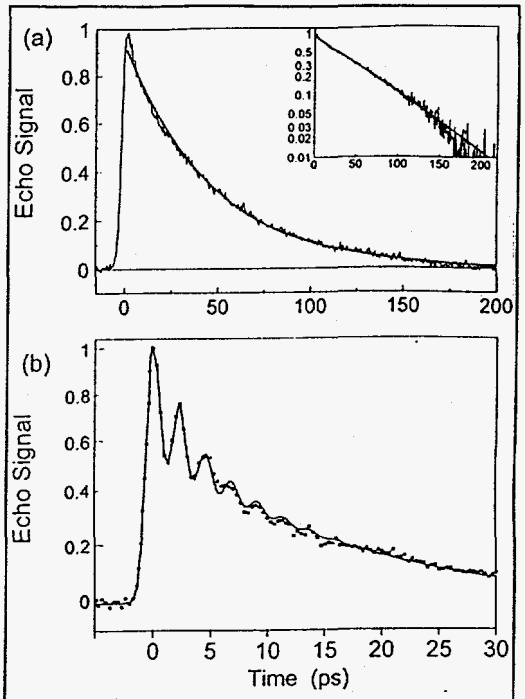

Figure 1 - **(a)** Photon echo decay data in 2-methylpentane glass at 10 K. **(b)** Vibrational photon echo decay gives the homogeneous dephasing of the three level coherence with beating at the anharmonic vibrational frequency splitting.

The temperature dependences of the homogeneous vibrational linewidths in the three glasses at low temperatures are compared using a reduced variable plot [8] in fig. 2a. Such normalization allows comparison of the functional form of the temperature dependences, independent of differences in T_g and coupling strengths of the transition dipole to the bath. Figure 2a shows that the temperature dependences of the homogeneous linewidths are identical in the three glasses and are well described by a power law of the form

$$\Gamma(T) = \Gamma_0 + A\,T^{\alpha} \qquad (2)$$

The offset at 0 K, Γ_0, represents the linewidth due to the low temperature vibrational lifetime. A fit to eq. 2 for all temperatures below the glass transition is shown in fig. 2a, and yields an exponent of $\alpha = 2.1 \pm 0.2$ and $\Gamma_0/\Gamma(T_g) = 0.24 \pm 0.02$. At temperatures above $\sim 1.2T_g$, the linewidths of the three liquids diverge from one another. Because of its high glass transition temperature, DBP allows the largest temperature range over which to observe the power law. The data are presented in two ways in fig. 2b. The solid circles are the data and the line through them is a fit to eq. 2. To show more clearly the power law temperature dependence, the open circles are the data with the low temperature linewidth, Γ_0 (corresponding to a vibrational lifetime, $T_1(0\ K) = 33$ ps) subtracted out. The line through the data is T^2. It can be seen that the power law describes the data essentially perfectly over a change of linewidth of ~500 from 10 K to 200 K. This would be consistent with dephasing caused by Raman (two quantum) phonon scattering.

In 2-MTHF and in 2-MP below 150 K, the echo decays yield a homogeneous linewidth that is much narrower than the width of the absorption spectrum. These results demonstrate that the vibrational lines of these system are inhomogeneously broadened in the glass and supercooled liquid. In 2-MP the $W(CO)_6$ T_{1u} line becomes homogeneously broadened at 250 K and above [8]. However, in DBP the line is substantially inhomogeneous at all temperatures. The homogeneous linewidth at 300 K is $\sim 1\ cm^{-1}$, while the absorption spectrum linewidth is $26\ cm^{-1}$.

This is the first conclusive evidence for intrinsic inhomogeneous broadening of a vibrational line in a room temperature liquid. Thus, even in room temperature liquids, it is not safe to assume that dynamics can be obtained by taking a vibrational spectrum and analyzing it assuming it is homogeneously broadened.

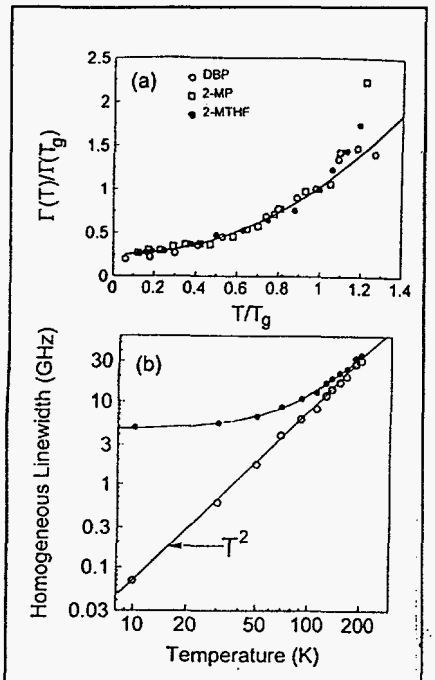

Figure 2 - **(a)** Comparison of the homogeneous linewidth in three organic glasses. **(b)** Homogeneous linewidth in DBP, solid circles, and the corresponding data with the lifetime removed, open circles.

Using the pump-probe measurements of the orientational diffusion constant D_{or} and the population relaxation time T_1 [8,9], the contribution due to pure dephasing can be determined from the homogeneous linewidth. Figure 3 displays the decomposition of the temperature dependence of the homogeneous linewidth in the 2-MP solvent into its three dynamic components [8]. At low temperatures, the lifetime is the dominate contribution. At high temperatures, pure dephasing is the dominate contribution. Only at intermediate temperatures does orientational relaxation make a substantial contribution. The linewidth contribution from lifetime broadening remains significant until ~50 K. Above 50 K, the contributions to the linewidth from pure dephasing and orientational relaxation dominate. Orientational relaxation does not dominate in any temperature range, but makes its largest percentage contribution around 100 K. By 100 K, the pure dephasing is a substantially larger contribution than either the lifetime or the orientational relaxation. Above ~150 K, pure dephasing is the overwhelmingly dominate component of the homogeneous linewidth.

In fig. 3 it is seen that there is a rapid increase in pure dephasing beginning slightly above the glass transition temperature. This implies that an additional mechanism for pure dephasing turns on, and it is linked to the glass-to-liquid transition. The onset of dynamic processes near the glass transition is often described with a Vogel-Tammann-Fulcher (VTF) equation [12]. If the VTF equation applies to pure dephasing near and above the glass transition, then the full temperature dependence would be the sum of the low temperature power law plus a VTF term. To test this idea, the temperature-dependence of pure dephasing was fit to

$$\Gamma^*(T) = A_1 T^{\alpha} + A_2 \exp\left(-B/\left(T - T_0^*\right)\right) \qquad (3)$$

for all temperatures below 300 K, and is shown as the line through the pure dephasing data in fig. 3.

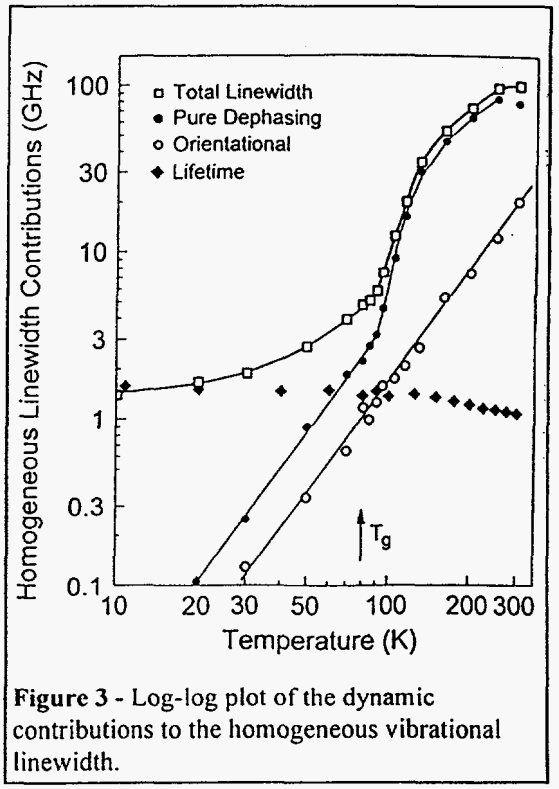

Figure 3 - Log-log plot of the dynamic contributions to the homogeneous vibrational linewidth.

The fit describes the entire temperature dependence exceedingly well and yields a reference temperature of $T_0^* = 80$ K. This reference temperature matches the laboratory glass transition temperature T_g. We can thus infer that the onset of the dynamics that cause the rapid increase in homogeneous dephasing in 2-MP is closely linked with the onset of structural processes near the laboratory glass transition temperature.

The development of picosecond vibrational photon echo experiments to examine condensed matter systems represents a significant extension of the field of vibrational spectroscopy. Echo experiments and other IR vibrational four wave mixing experiments such as stimulated echoes and transient grating experiments that we have recently performed, will provide important tools to greatly increase our understanding of the vibrational dynamics and intermolecular interactions in condensed matter systems.

Acknowledgments

The authors thank Professor Alan Schwettman and Professor Todd Smith of the Department of Physics, Stanford University and their groups for the opportunity to use the Stanford Free Electron Laser. This work was supported by the National Science Foundation (DMR93-22504), the Office of Naval Research (N00014-92-J-1227), the Medical Free Electron Laser Program (N00014-91-C-0170), and the Air Force Office of Scientific Research (F49620-94-1-0141).

References

(1) D. Zimdars, A. Tokmakoff, S. Chen, S. R. Greenfield, and M. D. Fayer, Phys. Rev. Lett., 70 (1993) 2718.
(2) A. Tokmakoff, D. Zimdars, B. Sauter, R. S. Francis, A. S. Kwok, and M. D. Fayer, J. Chem. Phys., 101 (1994), 1741.
(3) A. Tokmakoff, A. S. Kwok, R. S. Urdahl, R. S. Francis, and M. D. Fayer, Chem. Phys. Lett., 234 (1995) 289.
(4) D. Vanden Bout, L. J. Muller, and M. Berg, Phys. Rev. Lett., 67 (1991), 3700.
(5) D. Vanden Bout, L. J. Muller, and M. Berg, J. Chem. Phys., 99 (1993) 810.
(6) R. Inaba, K. Tominaga, N, Tasumi, K. A. Nelson, and K. Yoshihara, Chem. Phys. Lett. 211 (1993) 183.
(7) D. Vanden Bout, J. E. Freitas, and M. Berg, Chem. Phys. Lett., 229 (1994) 87.
(8) A. Tokmakoff, and M. D. Fayer, J. Chem. Phys., (1995) accepted.
(9) A. Tokmakoff, R. S. Urdahl, D. Zimdars, A. S. Kwok, R. S. Francis, and M. D. Fayer, J. Chem. Phys., 102 (1995) 3919.
(10) T. C. Farrar, and D. E. Becker, Pulse and Fourier Transform NM (Academic Press, New York, 1971).
(11) S. M. Arrivo, T. P. Dougherty, W. T. Grubbs, and E. J. Heilweil, Chem. Phys. Lett., 235 (1995) 247.
(12) C. A. Angell, J. Phys. Chem. Solids, 49 (1988) 863.

Phase-Modulation Infrared Spectroscopy of Photoexcitation in Conjugated Polymers

Yukio Furukawa, Nami Yokonuma, and Mitsuo Tasumi
Department of Chemistry, School of Science, The University of Tokyo, Bunkyo-ku, Tokyo 113, Japan

INTRODUCTION

A group of organic polymers with conjugated π-electrons, *i.e.*, polyacetylene, polythiophene, poly(*p*-phenylene), *etc.*, are called conjugated polymers or conducting polymers. These polymers have attracted much attention of scientists in various fields, because of their potential application as well as the novel physics and chemistry inherent in these materials [1, 2]. These polymers have conjugated C=C bonds in their ground-state structures. Excited states in these polymers are expressed by elementary excitations in solid-state physics. Solitons, polarons, bipolarons, excitons, *etc.*, are proposed as excitations in these systems [1, 2]. They are quasi-particles with structural changes over several repeating units in a polymer chain. In chemical terminology, polarons, bipolarons, and charged solitons correspond to radical ions, divalent ions, and ions localized in a polymer chain, respectively. The conjugated polymers show photoinduced infrared absorptions, which are associated with photoconduction. These photoinduced absorptions are attributed to charged excitations [1, 3, 4]. The structures and dynamics of polarons, bipolarons, and charged solitons can be elucidated by time-resolved and transient infrared spectroscopy. In this paper, we will report photoexcitation dynamics of *trans*-polyacetylene, polythiophene, and poly(2,5-thienylenevinylene) by phase-modulation infrared spectroscopy [5], which is a frequency-domain method for studying dynamics of a system.

THEORETICAL BACKGROUND

The intensity of the pump laser light $L(t)$ for photoexcitation is sinusoidally modulated as

$$L(t) = a + b\sin\omega t \qquad (1)$$

where a represents a constant term, b an amplitude, and ω an angular frequency, which is equal to $2\pi f$ where f is the frequency of modulation. The absorbance change of an infrared band at $\tilde{\nu}$,

$\Delta A(\tilde{\nu}, \omega, t)$, induced by the pump laser light is expressed as

$$\Delta A(\tilde{\nu}, \omega, t) = \Delta A(\tilde{\nu}, \omega)' \sin\{\omega t - \phi(\tilde{\nu}, \omega)\} + \Delta A(\tilde{\nu})'' \quad (2)$$

$$= \Delta A(\tilde{\nu}, \omega)^{ip} \sin \omega t - \Delta A(\tilde{\nu}, \omega)^{q} \cos \omega t + \Delta A(\tilde{\nu})'' \quad (3)$$

in which

$$\Delta A(\tilde{\nu}, \omega)' = \sqrt{\left\{\Delta A(\tilde{\nu}, \omega)^{ip}\right\}^2 + \left\{\Delta A(\tilde{\nu}, \omega)^{q}\right\}^2} \quad (4)$$

$$\phi(\tilde{\nu}, \omega) = \arctan \frac{\Delta A(\tilde{\nu}, \omega)^{q}}{\Delta A(\tilde{\nu}, \omega)^{ip}} \quad (5)$$

The photoinduced infrared absorption consists of two terms in Eq. 2. The first term is the time-dependent ac modulation. This term vibrates sinusoidally with the same angular frequency as the external stimulus; the amplitude is $\Delta A(\tilde{\nu}, \omega)'$ and the phase is delayed by $\phi(\tilde{\nu}, \omega)$ relative to the stimulus because of the finite lifetime of the photogenerated species. This ac term can be divided into the in-phase and 90° out-of-phase (quadrature) terms, as shown in Eq. 3. The in-phase and quadrature components are related to the amplitude (magnitude) and the phase delay in Eqs. 4 and 5. The magnitude and the phase delay (or in-phase and quadrature components) expressed as a function of the modulation frequency are the response in the frequency domain. The frequency-domain response is related to the decay function in the time domain by Fourier transformation [5]. The second term of Eq. 2 represents the time-independent dc component, corresponding to the static infrared difference spectrum.

EXPERIMENTAL

The details of the infrared spectrophotometer used for phase-modulation measurements were described in the previous paper [5]. Our system mainly consists of an Argon ion laser, an acousto-optic modulator, a function generator, a lock-in amplifier (EG&G PARC 5209), and a Fourier transform infrared (FT-IR) spectrophotometer (JEOL JIR-5500) with a HgCdTe detector. The speed of the moving mirror of the FT-IR spectrometer is 0.01 cm s^{-1}. The upper limit of the wavenumber range of infrared light is set at about 1650 cm^{-1} by an optical filter. Thus, an unmodulated interferogram involves frequencies lower than 33 Hz. By use of our experimental setup, dynamics in the micro- to millisecond region can be studied in the spectral range between 4000 and 750 cm^{-1}.

The absorbance changes corresponding to the ac and dc terms are given, respectively, as

$$\Delta A(\tilde{\nu}, \omega)' = \log \frac{B(\tilde{\nu})}{B(\tilde{\nu}) + \Delta B(\tilde{\nu}, \omega)' / k} \approx -\frac{0.434 \Delta B(\tilde{\nu}, \omega)'}{k B(\tilde{\nu})} \qquad (6)$$

$$\Delta A(\tilde{\nu})'' = \log \frac{B(\tilde{\nu})}{B(\tilde{\nu}) + \Delta B(\tilde{\nu})''} \qquad (7)$$

where $B(\tilde{\nu})$ denotes the intensity spectrum with laser light off, $\Delta B(\tilde{\nu}, \omega)'$ the photoinduced intensity spectrum arising from the ac term, k the amplification factor of the lock-in amplifier, and $\Delta B(\tilde{\nu})''$ the photoinduced intensity spectrum arising from the dc term. Since the photoinduced absorbance changes are very small (less than 10^{-3}), the induced absorbance from the ac term is approximately proportional to the photoinduced intensity, as shown in Eq. 6.

RESULTS AND DISCUSSION

The photoinduced infrared spectra of polythiophene arising from the ac term with the 1 kHz modulation at 78 K are shown in Fig. 1. The phase angles of Figs. 1a and 1b are – 40° and 50°, respectively. The ϕ = – 40° spectrum is essentially the same as not only the photoinduced infrared spectrum arising from the dc term (not shown) but also the spectrum obtained by difference FT-IR method [6]. Figure 1 shows that the phase delays of the photoinduced bands

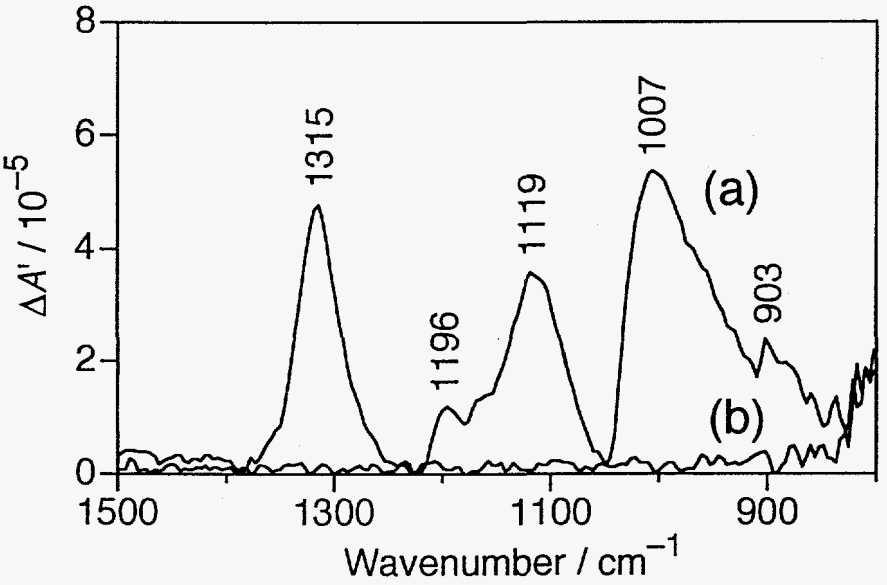

Figure 1: Photoinduced infrared absorption spectra of polythiophene arising from the ac term. Phase angle, (a) – 40° and (b) 50°; modulation frequency, 1 kHz; pump laser light, 514.5 nm, 86 mW/cm^2; temperature, 78 K.

observed at 1315, 1196, 1119, 1007, and 903 cm^{-1} are 40°. Thus, all the photoinduced bands show the same temporal behavior. The magnitude and the phase delay of the 1315 cm^{-1}-band are plotted against the modulation frequencies between 0.4 and 25 kHz in Fig. 2a and 2b, respectively. The magnitude decreases with increasing frequency approximately in proportion to $f^{-0.6}$, whereas a unimolecular decay should show the f^{-1} dependence [5]. Thus, the decay kinetics of photogenerated species is not unimolecular, but is more complicated. *Trans*-polyacetylene and poly(2,5-thienylenevinylene) show the $f^{-0.65}$ and $f^{-0.6}$ dependence, respectively. The lifetime of photogenerated species can be roughly estimated from the phase delay by use of an equation derived from an exponential decay function [5]. The calculated lifetime ranges between 41 and 250 μs for the 0.4–25 kHz modulation frequencies. This result also indicates that the decay kinetics is not unimolecular.

According to ultrafast time-resolved electronic absorption studies of conjugated polymers [7–10], excitations are generated, diffuse along a polymer chain, recombine geminately, or recombine with structural defects on the subpico- and picosecond time scales. Isolated charged excitations, which escape from recombination, are formed within one microsecond [8]. Charged excitations existing in the micro- to millisecond region are considered to be charged solitons for *trans*-polyacetylene [11] and bipolarons for polythiophene [12] and poly(2,5-thienylenevinylene) [13]. Isolated charged excitations can hop between adjacent polymer chains and also move along a polymer chain. If a charged excitation encounters an oppositely charged excitation in this process, they will recombine geminately. Since this diffusion-recombination process is very

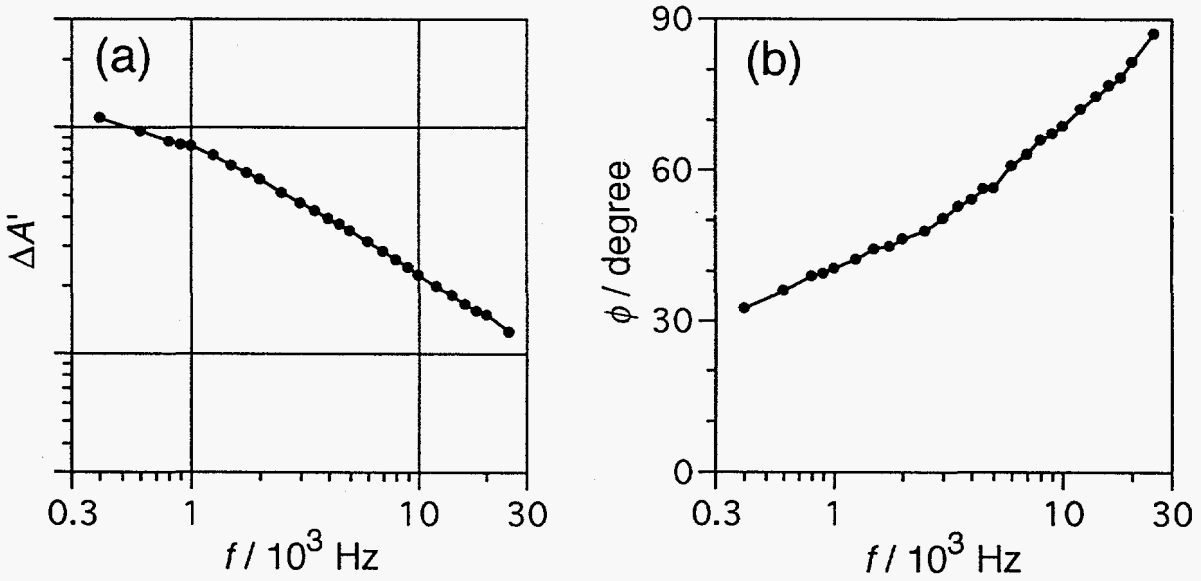

Figure 2: The modulation-frequency dependence of the magnitude (a) and the phase delay (b) of the photoinduced 1315-cm^{-1} band. Pump laser light, 514.5 nm, 86 mW/cm^2; temperature 78 K

fast (picosecond time scale), hopping of charged excitations between polymer chains is probably a rate-determining step in the micro- to millisecond kinetics. The pump-power dependence of photoinduced difference FT-IR spectra suggests bimolecular recombination kinetics [10, 11]. The observed $f^{-\alpha}$ (α = 0.6, 0.65) dependence possibly reflects bimolecular recombination kinetics in polymers with various conjugation-length distributions, defects, and solid structures.

In conclusion, phase-modulation infrared spectroscopy is useful in studying recombination dynamics of photogenerated charged excitations on the micro- to millisecond time scale.

Acknowledgment

This work was supported in part by a grant from the Nissan Science Foundation.

References

1. A. J. Heeger, S. Kivelson, J. R. Schrieffer, and W.-P. Su, *Rev. Mod. Phys., 60* (1988) 781.
2. *Conjugated Conducting Polymers*, Ed. H. Kiess, *Springer Ser. Solid-State Sci., 102,* (Springer-Verlag, Berlin, 1992).
3. R. H. Friend, D. D. C. Bradley, and P. D. Townsend, *J. Phys. D, 20* (1987) 1367.
4. Z. V. Vardeny, *Chem. Phys., 177* (1993) 743.
5. Y. Furukawa, *Appl. Spectrosc., 47,* (1993) 1405.
6. H. E. Schaffer and A. J. Heeger, *Solid State Commun., 59* (1986) 415.
7. C. V. Shank, R. Yen, R. L. Fork, J. Orenstein, and G. L. Baker, *Phys. Rev. Lett., 49* (1982) 1660.
8. L. Rothberg, T. M. Jedju, S. Etemad, and G. L. Baker, *Phys. Rev. B, 36* (1987) 7529.
9. G. S. Kanner, X. Wei, B. C. Hess, L. R. Chen, and Z. V. Vardeny, *Phys. Rev. Lett., 69* (1992) 538.
10. S. D. Halle, M. Yoshizawa, H. Murata, T. Tsutsui, S. Saito, and T. Kobayashi, *Synth. Met., 49* (1992) 429.
11. G. B. Blanchet, C. R. Fincher, T. C. Chung, and A. J. Heeger, *Phys. Rev. Lett., 50* (1983) 1938.
12. Z. Vardeny, E. Ehrenfreund, O. Brafman, M. Nowak, H. Schaffer, A. J. Heeger, and F. Wudl, *Phys. Rev. Lett., 56* (1986) 671.
13. A. J. Brassett, N. F. Colaneri, D. D. C. Bradley, H. Murata, S. Tokito, T. Tsutsui, and S. Saito, *Phys. Rev. B, 41* (1990) 10586.

Hydrogen-Bond and Vibrational Up-Pumping Dynamics Studied by Broadband Transient Infrared Spectroscopy

S. M. Arrivo, T. P. Dougherty[#%], W. T. Grubbs[*%] and E. J. Heilweil

B268/221 Molecular Physics Division, NIST, Gaithersburg, MD 20899
[#]Dept. of Chemistry and Physics, Beaver College, Glenside, PA 19038
[*]NIST and Dept. of Chemistry, Stetson University, DeLand, FL 32720
[%]NIST/NRC Postdoctoral Research Associate

Abstract

Broadband transient infrared (IR) methods are used to study vibrational up-pumping and relaxation dynamics of the CO-stretch T_{1u} mode v=1-3 overtone states of $W(CO)_6$ in n-hexane (ca. 15 cm^{-1} anharmonic shifts, T_1 = 140±20 (errors ±1σ), 75±25, and 30±15 ps for v=1-3, respectively). Results from two-color experiments on dilute, room temperature tertiary solutions of pyrrole:base:CCl_4, methanol:base:CCl_4, and $(CH_3CH_2)_3SiOH$:base:CCl_4 show that the T_1 vibrational relaxation time of the complex NH- or OH-stretch correlates strongly with basicity and is unaffected by base deuteration. There is little evidence for complex IR-induced dissociation. Studies of "free" monomeric acid T_1 lifetimes as a function of base concentration yield acid-dependent bimolecular rate constants that are independent of base. These rates approach the diffusion limit, indicating complexation may occur at times comparable to a binary encounter but depend on acid structural properties.

INTRODUCTION

The generation of femtosecond, tunable mid-IR pulses have enabled investigations of molecular vibrational energy transfer, reaction mechanisms and rates, and structurally sensitive biochemical processes in complex condensed-phase media. More sophisticated studies of microscopic chemical and physical processes will potentially emerge by using transient IR techniques including fast read-out, large format (>256x256) IR focal plane arrays in the 3-11 micron region and Fourier Transform IR methods. In this vein, we are developing multichannel detection methods with high signal-to-noise and data acquisition rates to obtain high quality broadband (<300 cm^{-1} FWHM) IR transient spectra.

In this paper, we review results obtained from studies of population up-pumping and overtone relaxation in the T_{1u} CO-stretch vibrational manifold of a solution-phase metal-hexacarbonyl species. More recently, we have examined organic systems with emphasis on understanding the vibrational dynamics of dilute hydrogen-bonded 1:1 complexes in inert solvents at room temperature. These studies reveal that proton donor NH- and OH-stretch relaxation rates are enhanced by localized interactions and correlate with basicity. Measuring "free" NH- and OH-stretch lifetimes in solution enable extraction of acid-base bimolecular encounter rates which are found to be independent of base composition.

EXPERIMENTAL

Broadband infrared techniques used at NIST include generation of ultrashort pump and broadband IR probe pulses (≥150 fs) by difference frequency downconversion in $LiIO_3$ crystals [1]. Transient difference spectra are obtained in about 7 minutes (at 20 Hz) by averaging normalized single-shot probe and reference tracks. These visible spectral tracks are obtained by $LiIO_3$ upconversion of two IR probe pulses after the sample and detected with a spectrograph/multichannel CCD combination [1]. After determining spectral band positions and shifts, two-color lifetime measurements (multiple runs) are obtained by standard "narrow-band" pump-probe methods using 1 cm^2 single element InSb detectors.

Room temperature samples were flowed through a stainless steel 0.1 cm pathlength cell containing 0.3 cm thick CaF_2 windows. IR pump energies were typically <10 μJ focussed to a 100 μm diameter spot size. Probe pulse polarization was set to the magic angle (54.7 degrees) to eliminate rotational anisotropy. Dilute samples of $W(CO)_6$ in n-hexane (ca. $2x10^{-4}$ mole/dm^3) and binary and tertiary solutions of pyrrole, methanol, triethylsilanol with various bases (e.g., acetonitrile, pyridine, tetrahydrofuran, acetone) in room temperature CCl_4 and $CHCl_3$ solvents were prepared without purification. $CHCl_3$ and acetonitrile were dried over-night by contact with molecular sieves.

VIBRATIONAL UP-PUMPING AND RELAXATION RATES OF $W(CO)_6$ [2,3]

$W(CO)_6$ up-pumping and T_{1u} CO-stretch vibrational fundamental and overtone relaxation dynamics were obtained with 2 ps IR pump pulses at three frequencies: the high frequency side (1990 cm^{-1}), pump and central absorption frequency coincident (1983 cm^{-1}), and to the low frequency side (1968 cm^{-1}) of the absorption. Representative difference spectra taken after IR pumping (0.75 μJ) of $W(CO)_6$ are shown in Figure 1. Each pumping condition produces different population distributions (spectra monitor the *difference* in population between two states) and the subsequent relaxation kinetics in each case are obtained as a function of delay time (t_d) for the various vibrational levels prepared within the CO-stretching manifold. Time-dependent spectra (not shown) for $t_d>0$ indicate that population cascades down the T_{1u} manifold. By directly monitoring the absorption decay kinetics for the highest populated level (dependent on pump conditions) and by multilevel kinetic modelling, T_1 population lifetimes 140±20, 75±25, and 30±15 ps for v=1-3, respectively, are obtained. Evidence for a 10-20 ps T_{1u} to E_g intermode energy transfer lifetime was also extracted from early-time decay components [3].

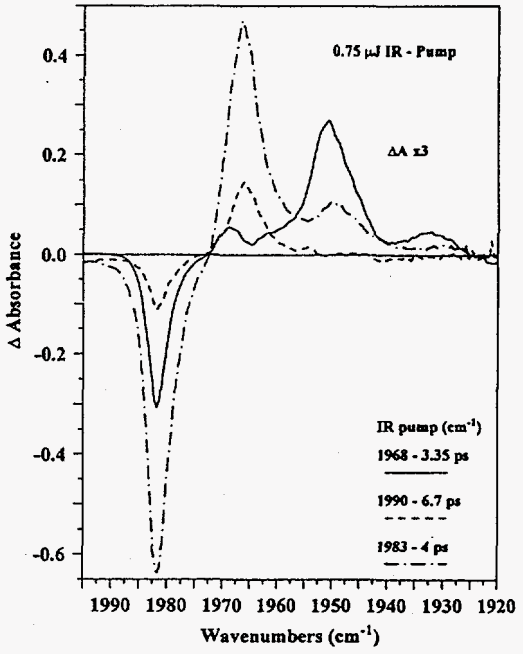

Figure 1 Transient difference spectra for $W(CO)_6/C_6H_{14}$ at indicated pump frequencies

The salient features of this study are: (1) pump frequency and power dictate the population distribution of the v=1-3 vibrational overtone states; (2) the anharmonic frequency shifts (ca. 15 cm^{-1}) of the $W(CO)_6$ in n-hexane overtones *are directly observed* via transient IR broadband spectroscopy [1,2]; (3) experimental overtone state lifetimes are extracted directly from the data and can be compared to theoretical prediction; and (4) a 10-20 ps intermode coupling time of the T_{1u} to E_g manifolds is evident in the level decay data [2,3]. Further work to investigate the effects of using shorter (ca. 100 fs) chirped IR pump pulses to "control" the level population of even higher CO-stretch overtones in this system is in progress [4].

VIBRATIONAL DYNAMICS OF HYDROGEN-BONDED 1:1 COMPLEXES [5]

Investigations of dilute 1:1 proton-donor:proton-acceptor (base) complexes in inert, room temperature CCl_4 solution can directly identify mode-specific energy transfer processes, hydrogen-bond dissociation/reformation rates, and effects of base and solvent vibrational structure on the dynamics. These studies compliment earlier work where concentrated alcohol [6] and water [7] hydrogen-bonded oligomers were examined.

Pyrrole:Base:CCl_4 Complexes [5]

Vibrational energy relaxation rates of the NH-stretch (v=1) vibration of $4.2x10^{-2}$ mole/dm^3 pyrrole (C_4H_5N) in room temperature CCl_4 (T_1=49±3 ps) and in various 1:1 pyrrole:base/CCl_4 complexes (see Table I) is found to depend monotonically with basicity and H-bond strength (proportional to frequency shift). The NH-stretch T_1 lifetime can reduced by more than one order of magnitude upon complexation.

Intramolecular energy transfer appears to be the dominant relaxation pathway in these systems. Since pyrrole complexed to a variety of bases with specific proton-accepting strengths and internal vibrational modes were examined, it appears that the NH-stretch relaxation rate is governed by "localized" hydrogen-bond mode interactions [8]. This conclusion is supported by base deuteration experiments (see below). Despite attempts to observe "free" pyrrole via complex dissociation after NH-stretch excitation (the H-bond dissociation energy is approximately 1200-1700 cm^{-1} or 3-5 kcal/mole, much below the 3400 cm^{-1} excitation energy), only indirect evidence for a minor pathway (<2% of excited complexes) for pump-induced complex dissociation was observed through incomplete baseline recovery or multi-exponential NH-stretch parent bleach transients.

Methanol and Triethylsilanol 1:1 Complexes

Similar measurements were conducted to obtain the internal OH-stretch (v=1) relaxation lifetime for methanol and triethylsilanol complexed with bases in room temperature CCl_4 solutions. Transient absorption (v=1-2) kinetics confirmed that the OH(v=1) lifetime for dilute $(Et)_3SiOH/CCl_4$ was 185±15 ps [9] while the lifetime for methanol (T_1≈15 ps) was obtained previously [9]. Measurements on OH-containing acid:base complexes exhibit reduced OH(v=1) T_1 with basicity (see pyrrole:base results): (1) $(Et)_3SiOH$ complexes with acetonitrile, acetone, and THF yielded T_1=30±5, 12±5, and 4±2 ps, respectively, while (2) methanol complexes with acetonitrile, THF, and pyridine gave T_1≈6.5±2, 6.5±3, and ≤4 ps.

Table I: Frequencies, bandwidths, shifts, basicities, and T_1 lifetimes for hydrogen-bonded solutions at 298 K.

System[a]	ν(NH) (cm^{-1})	$\Delta\nu$(NH) (cm^{-1})[b]	$\Delta\nu_{HB}$ (cm^{-1})[c]	Basicity ($x10^3$ cm^{-1})[d]	T_1 (ps)[e]
"free" pyrrole in CCl_4	3495	11.6	---	0.09	49±3
pyrrole:benzene	3456	36.0	39	0.10	25±2
pyrrole:ethyl acetate in CCl_4	3416	79.1	79	0.48	8.7±1
pyrrole:acetonitrile in CCl_4	3411	90.0	84	0.33	13±2
pyrrole (neat)	3403	77.9	92	0.33	13±2
pyrrole:acetone in CCl_4	3400	114.9	95	0.48	7.3±1
pyrrole:diethylether	3352	78.4	143	0.49	4.3±.5
pyrrole:THF in CCl_4	3346	100.9	150	0.55	4.5±.4
pyrrole:pyridine in CCl_4	3251	143.0	244	0.64	1.5±.4

[a] $4.2x10^{-2}$ moles/dm^3 pyrrole and 1.9 moles/dm^3 base. [b]Full width at half maximum. [c]Shifts measured relative to "free" pyrrole NH-stretch in CCl_4. [d]Kamlet-Taft parameters [10]. [e]Reported lifetimes ($\pm1\sigma$) extracted from transient bleaching and double resonance decays.

Dilute CCl_4 complexes of $(Et)_3SiOH$ with perdeuterated acetonitrile and acetone were examined to determine whether CH-stretch and bend modes participate in the OH-stretch relaxation mechanism. Within experimental uncertainty, substitution of deuterated bases for protonated species studied above exhibited no change in OH(v=1) relaxation of the complexes. Again, these results suggest that the enhancement of NH- and OH-stretch relaxation in acid-base complexes is dominated by a "local mode" coupling mechanism. These observations merit modelling by molecular dynamics or other simulation methods.

Bimolecular H-bond Interactions Studied by "Free" Triethylsilanol Vibrational Relaxation

Pump-probe measurements of the OH-stretch (v=1) lifetime were performed for "free," uncomplexed $(Et)_3SiOH$ present in dilute, room temperature, tertiary $(Et)_3SiOH$:base:CCl_4 hydrogen-bonded solutions (base = acetonitrile, tetrahydrofuran, and pyridine). The intrinsic $(Et)_3SiOH$ OH-stretch T_1 vibrational population lifetime (185±15 ps) is reduced by bimolecular $(Et)_3SiOH$:base hydrogen-bonding encounters but unaffected by hexane or benzene collisions (>1 mole/dm^3). The base concentration dependence of the "free" OH-stretch vibrational deactivation rate was analyzed by a Stern-Volmer kinetic model and a least-squares fit to all $(Et)_3SiOH$:base data yielded a single rate constant k_{BM} = 1.2±0.2 x 10^{10} dm^3 $mole^{-1}$ s^{-1} (Figure 2). This value agrees with estimates for the bimolecular diffusion limit. k_{BM} was the same for all $(Et)_3SiOH$:base interactions studied, suggesting that the bimolecular OH-stretch deactivation mechanism is relatively insensitive to the proton-accepting strength of the base. However, a similar analysis for pyrrole:acetonitrile solutions yielded k_{BM} = 2.5±0.2x10^{10} dm^3 $mole^{-1}$ s^{-1} [5]. The different values for k_{BM} extracted for

$(Et)_3SiOH$ vs. pyrrole under equimolar concentrations of base suggest that steric or acid structural factors may be involved in the acid-base encounters which lead to hydrogen-bond formation. Studies are underway to extract mechanisms and hydrogen-bond association/dissociation rates from bimolecular, "free" acid and acid:base vibrational decay experiments.

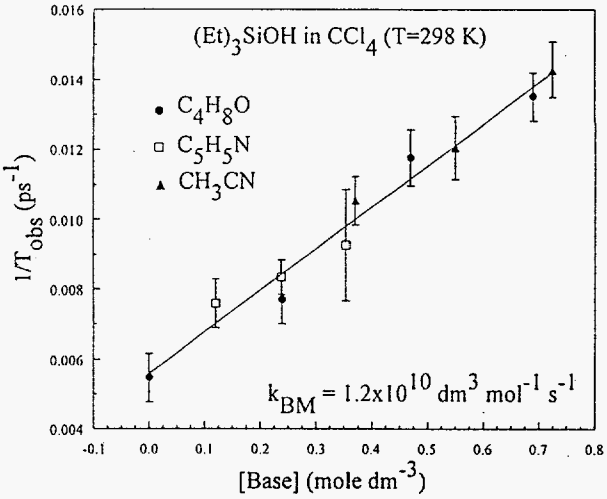

Figure 2 Stern-Volmer plot of $(Et)_3SiOH$ relaxation vs. [base] yielding bimolecular rate

N-METHYLACETAMIDE (NMA) NH-STRETCH VIBRATIONAL RELAXATION

We also performed NH-stretch (v=1) population relaxation measurements for NMA in room temperature, dried CCl_4 and $CHCl_3$ solutions. For concentrations where minimal self-association occurs ($5\text{-}10\times10^{-2}$ mole/dm^3), v=1-2 transient absorption decays were obtained at 3332 cm^{-1} after excitation of the NMA NH-stretch at 3467 cm^{-1} with picosecond IR pulses. Numerous measurements for NMA in both solvents yielded the same NH-stretch relaxation lifetime of 13±2 ps. Studies of NMA 1:1 complexes with water and bases or model short-chain amino-acids are underway to elucidate H-bonding dynamics in small model protein systems.

Acknowledgments

This work was supported by NIST Scientific and Technical Research and Services (STRS) funding and a budget initiative entitled "Atomic Scale Structure and Manipulation."

References

1. T.P. Dougherty and E.J. Heilweil, Optics Letters, **19**(2) (1994) 129.
2. S.M. Arrivo, T.P. Dougherty, W.T. Grubbs and E.J. Heilweil, Chem. Phys. Lett., **235** (1995) 247.
3. A. Tokmakoff, A.S. Kwok, R.S. Urdahl, R.S. Francis, M.D. Fayer, Chem. Phys. Lett., **234** (1995) 289 and references therein.
4. J.S. Melinger, S.R. Gandhi, A. Hariharan, D. Goswami and W.S. Warren, J. Chem. Phys., 101 (1994) 6439.
5. W.T. Grubbs, T. P. Dougherty and E.J. Heilweil, J. Phys. Chem., **99** (1995) 10716.
6. H. Graener, G. Seifert and A. Laubereau, Phys. Rev. Lett., **66** (1991) 2092.
7. H. Graener, T.Q. Ye and A. Laubereau, J. Chem. Phys., **91** (1989) 1043.
8. E.J. Heilweil, Chem. Phys. Lett., **129** (1986) 48.
9. E.J. Heilweil, M.P. Casassa, R.R. Cavanagh, J. Stephenson, J. Chem. Phys., **85** (1986) 5004.
10. O.W. Kolling, Anal. Chem., **54** (1982) 260.

Time-Resolved Resonance Raman Study on Mechanism of Dioxygen Reduction by Cytochrome c Oxidase

Teizo Kitagawa,* Takashi Ogura, Shun Hirota, Denis A. Proshlyakov, Kyoko Shinzawa-Itoh,% Shinya Yoshikawa,% and Evan H. Appelman,#

Institute for Molecular Science, Okazaki National Research Institutes, Myodaiji, Okazaki, 444 Japan, %Department of Life Science, Faculty of Science, Himeji Institute of Technology, 1479-1 Kanaji, Kamigoricho, Akogun, Hyogo 678-12, and #Chemistry Division, Argonne National Laboratory, Argonne, Illinois, 60439 U.S.A.

*Author to whom correspondence should be addressed. Phone:81-564-55-7340, Fax:81-564-55-4639, E-mail:TEIZO@IMS.AC.JP

Introduction

Cytochrome c oxidase (CcO) is the terminal enzyme of the respiratory chain of aerobic organisms and catalyzes the reduction of dioxygen to water. The electron transfer to dioxygen is coupled with vectorial proton translocation across mitochondrial inner membrane [1]. CcO has two heme A groups (Fe_a and Fe_{a3}) and two copper centers (Cu_A and Cu_B) as redox active metal centers. It is known that the Fe_{a3}-Cu_B binuclear center serves as a catalytic site for dioxygen reduction, while the Fe_a and Cu_A centers receive electrons from cytochrome c and transfer them to the catalytic site. Extensive efforts have been made to elucidate the reaction mechanism of this enzyme by using time-resolved absorption [2], cryogenic absorption [3], EPR [4], and resonance Raman (RR) spectroscopy [5]. Time-resolved RR spectroscopy is uniquely powerful for elucidation of the reaction mechanism of CcO, since only this technique is able to detect the vibrations of dioxygen and its reductive intermediates bound to the catalytic site during the enzymic turnover. Indeed, this technique has explored structures of reaction intermediates of various heme proteins [6]. Here we present evidences for the heterolytic cleavage of the O-O bond at the Fe_{a3}-Cu_B site and also for the presence of an electron transfer step which is potentially regulated by a proton transfer.

Results and Discussion

Figure 1 shows the time-resolved RR difference spectra of CcO ($^{16}O_2$ derivatives minus $^{18}O_2$ derivatives) for its reaction in H_2O at the delay time (Δt) from 0.1 to 5.4 ms after the initiation of the reaction. To accumulate these spectra, an Artificial Cardiovascular System for Enzymic Reactions [7a] with some further improvement was used; the lung for O_2 was replaced with a water-jacketed type, to which temperature controlled water at -10°C containing 20% (V/V) ethyleneglycol was circulated. It was demonstrated previously [7a] that the difference peaks at 571/544 cm^{-1} for $^{16}O_2/^{18}O_2$ in spectrum A arose from the dioxygen adduct with

end-on geometry. We pointed out the presence of two sets of difference patterns around 800 cm^{-1} for the subsequent intermediates [7a], although they have not been resolved in other studies [8]. Here we confirm the presence of two bands at 804/764 and 785/750 cm^{-1} together with the low frequency bands at 356/342 cm^{-1} in spectra B (Δt=0.27 ms) and C (Δt=0.54 ms). The order of their appearance is much clearer in Fig. 1 than in the previous study [7a]. Spectrum D, which exhibits only the 785/750 cm^{-1} pair near 800 cm^{-1}, indicates that the 804/764 cm^{-1} pair is followed by the 785/750 cm^{-1} pair, similar to that for the reaction of oxidized CcO with H_2O_2 [9b]. The 450/425 cm^{-1} pair, which arise from the final species with the Fe^{III}-OH heme [7b,8a] at Δt=2.7 ms (spectrum D), disappears at Δt=5.4 ms (spectrum E) due to exchanges of the bound hydroxyl anion with bulk water. The RR spectra in Fig. 1 verify that the 356/342 cm^{-1} pair do not belong to the species which yields the 785/750 cm^{-1} pair. The relative intensities of the 804/764 cm^{-1} bands to the 356/342 cm^{-1} bands were varied in repeated experiments, suggesting that these pairs arise from different species.

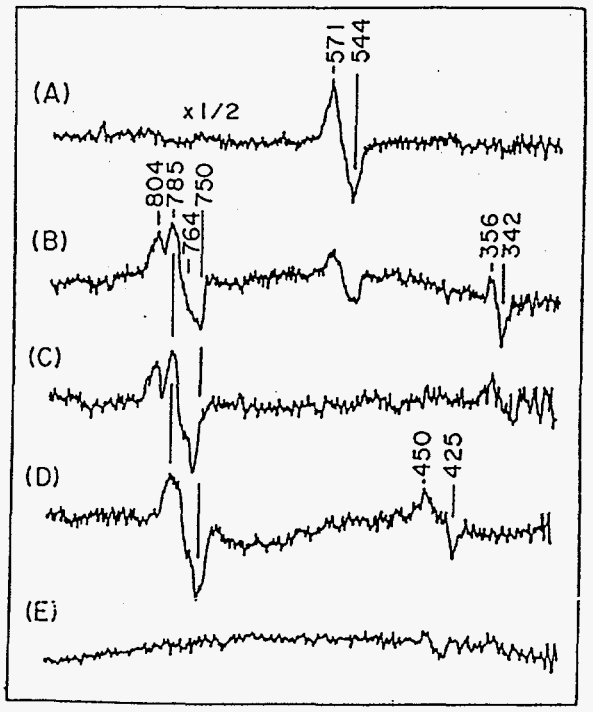

Figure 1. Time-resolved resonance Raman difference spectra of reaction intermediates of cytochrome c oxidase in H_2O. The Raman difference spectra obtained by subtracting the spectrum of $^{18}O_2$ derivatives from the spectrum of $^{16}O_2$ derivatives at each delay time are depicted. Delay time after initiation of the reaction is 0.1 (A), 0.27 (B), 0.54 (C), 2.7 (D) and 5.4 ms (E). Sample conditions; cytochrome c oxidase, 50 μM; ascorbate, 100 mM; cytochrome c, 50 μM; buffer, pottasium phosphate, 50 mM, pH 7.4, ethyleneglycol, 20 %(V/V). The initial O_2 concentration was estimated to be 350 μM. Sample temperature was 3°C at the flow cell. Excitation, 423 nm.

Figure 2 depicts similar difference spectra observed for the D_2O solution. Spectrum A (Δt=0.1 ms) gives the Fe^{III}-O_2 stretching mode at 571/544 cm^{-1} similar to Figure 1A. On the contrary to the case of the H_2O solution, however, a single band was observed at 804/765 cm^{-1} at Δt=0.54 (B) and 2.7 ms (C) in addition to the low frequency bands. Therefore, we previously described [7a] that the 785/750 cm^{-1} pair in the H_2O solution were shifted to 796/766 cm^{-1} in D_2O, giving rise to an overlapping band centered around 800 cm^{-1}. However, it turned out from this experiment that the lifetime of the 804/765 cm^{-1} species is so different between in H_2O and D_2O

that the 785/750 cm^{-1} species was not generated at Δt=2.7 ms in D_2O when it was generated in H_2O. Spectra D (Δt=6.5 ms) and E (Δt=11 ms) for the D_2O solution demonstrated the appearance of the 785/750 cm^{-1} species much later than in the case of H_2O solutions. This strongly suggests that the change from the 804/765 cm^{-1} species to the 785/750 cm^{-1} species is coupled with proton translocation and therefore its rate becomes slow (~1/5) in D_2O. The subsequent appearance of the 443/417 cm^{-1} bands, which arise from the Fe^{III}-OD stretching, is consistent with the results of Fig. 1. The experiments for Δt=0.1-0.5 ms for D_2O solutions (data not shown), which yielded the 804/764 and 356/342 cm^{-1} bands in a manner similar to spectrum B, definitely denied the suggestion [8b] that the 356/342 cm^{-1} bands appeared prior to the 804/764 cm^{-1} bands.

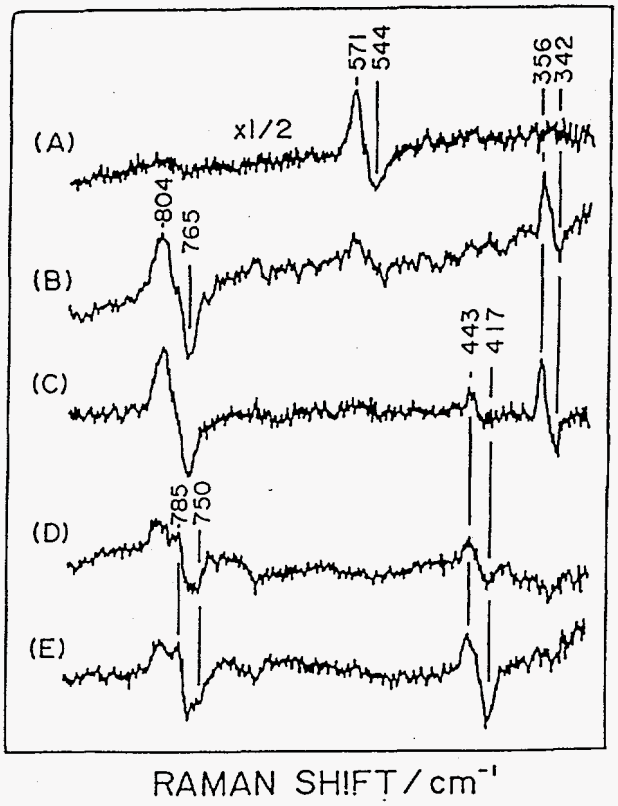

Figure 2. Time-resolved resonance Raman difference spectra of reaction intermediates of cytochrome c oxidase in D_2O. Delay time is 0.1 (A), 0.54 (B), 2.7 (C), 6.5 (D), and 11 ms (E). Other conditions are the same as those for Fig. 1.

Figure 3 shows the RR spectra measured selectively for the "607 nm" form generated in the reaction of oxidized CcO with hydrogen peroxide at ambient temperature [9a]. The "607 nm" form is the primary intermediate in this reaction and has been assigned to a peroxy intermediate [2b]. The RR spectra of the "607 nm" form derived from $H_2{}^{16}O_2$ (A), $H_2{}^{18}O_2$ (B), and $H_2{}^{16}O^{18}O$ (C) and their differences, D=A-B and E=C-(A+B)/2, demonstrate that the band of spectrum A at 803 cm^{-1} is shifted to 769 cm^{-1} in spectrum B, while the other two bands at 823 and 753 cm^{-1} remain unshifted. When $H_2{}^{16}O^{18}O$ was used, bands were seen at 803 and 769 cm^{-1}, but their peak intensities relative to the 753 cm^{-1} band were reduced almost to half of those in spectra A and B. If this band were associated with O^--O^- stretching mode of a putative peroxy structure, the ^{16}O-^{18}O stretching frequency should appear between those of $^{16}O^{16}O$ and $^{18}O^{18}O$. Difference spectrum E indicates no residuals between 769 and 803 cm^{-1}, demonstrating uniquely that the 803/769 cm^{-1} bands arise from Fe=O stretching mode. The absence of a band at intermediate frequency is incompatible with either a Fe^{III}-O_2^{2-} stretching with side-on geometry or an O^--O^- stretching.

These observations and the new facts that the frequency of 785/750 cm^{-1} remains unchanged in D_2O and that the 804/765 cm^{-1}

species appears prior to the 785/750 cm^{-1} species forced us to retract our previous assignments of them to the $Fe^{IV}=O$ and $Fe^{III}OOH$ species. The 804/765 cm^{-1} species belongs to the $Fe^{V}=O$ oxidation state of heme and thus the heterolytic cleavage of the O-O bond. The $Fe^{V}=O$ oxidation state of hemeproteins involves a possibility of $Fe^{IV}=O$ porphyrin π cation radical like compound I of horseradish peroxidase (HRP) or an amino acid cation radical with an $Fe^{IV}=O$ heme like compound ES of cytochrome c peroxidase (CcP). However, the former possibility is ruled out since the Soret absorption of the 804/765 cm^{-1} species is of ordinary intensity, while the latter possibility is less likely as ionization of a protein moiety would not so sensitively change the $Fe_{a3}{}^{IV}=O$ stretching ($\nu_{Fe=O}$) frequency. On the other hand, the electron withdrawing substituent of heme A may lower the HOMO level of the porphyrin and as a result it becomes likely that an electron is taken out from a metal orbital upon oxidation.

Consequently, it is most likely to assign the $Fe_{a3}{}^{V}=O$ heme for the peroxy state rather than the putative FeOOCu or FeOOH structure suggested previously. The frequency and the size of isotopic frequency shifts of the 785/750 cm^{-1} species are quite reasonable to assign it to the ferryloxo compound like compound II of HRP [10]. The 356/342 cm^{-1} pair are assignable to a His-$Fe^{V}=O$ bending vibration, assuming that this species gives the $Fe^{V}=O$ stretching mode near 800 cm^{-1} overlapped to the 804 cm^{-1} band. The His-$Fe^{V}=O$ bending vibration is degenerate and Raman inactive for the upright structure of an Fe=O heme with C_{4v} symmetry, but becomes Raman active for a distorted structure. Based on these assumptions, we propose scheme I for the pathway of dioxygen reduction. One of the characteristics of this scheme is that the O-O bond of the dioxygen adduct undergoes a heterolytic cleavage, yielding the $Fe_{a3}{}^{V}=O$ heme. Another assignment

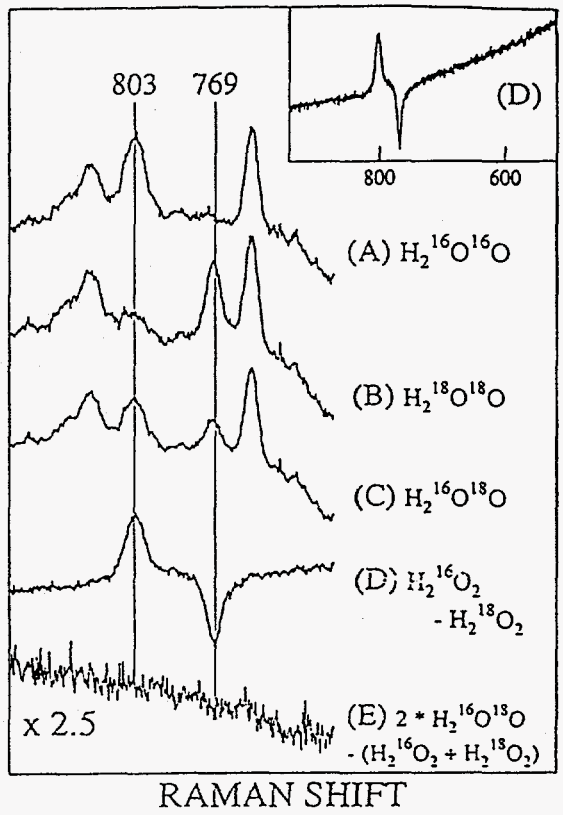

Figure 3. Resonance Raman spectra in the 800 cm^{-1} region of the "607 nm" form generated in the reaction of oxidized CcO with hydrogen peroxide. Hydrogen peroxide used are $H_2{}^{16}O_2$ (A), $H_2{}^{18}O_2$ (B), and $H_2{}^{16}O^{18}O$ (C). Spectra D and E show difference spectra, D = A - B; E = C - (A+B)/2. The inset shows the full frequency range of spectrum D measured. Experimental conditions were: flow cell, 0.6 x 0.6 mm^2; slit width, 4.2 cm^{-1}, laser 607 nm, 100 mW at the sample; total accumulation time, 78,78, 156 min for spectra A, B and C, respectively, and 160 min for the resting enzyme; CcO, 50 μM, pH 7.45.

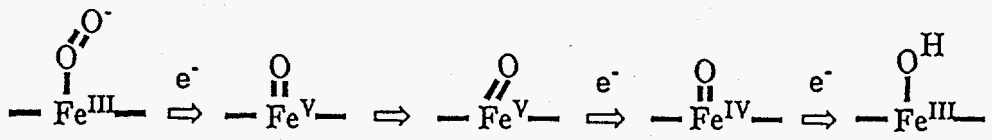

$^{16}O_2/^{18}O_2$	571/544 cm^{-1}	804/764	(ca. 800/760) 356/342	785/750	450/425

Scheme I. Reaction Mechanism of Dioxygen

that the 356/342 cm^{-1} pair arise from the Fe-O stretching of Fe^{III}-O-O-H species located at upstream side of the Fe^{V}=O, cannot be completely excluded, although less likely from the present observations. These results would open a new page in understanding the mechanism of dioxygen reduction by CcO and its coupling with proton pumping.

References

1. G.T. Babcock and M. Wikstrom, Nature 356, (1992) 301.
2. a) Q. H. Gibson and C. Greenwood, Biochem. J. 86, (1963) 541. b) Y. Orii, Ann. N.Y. Acad. Sci. 550, (1988) 105. c) M. Oliveberg, P. Brzezinski, and B. G. Malmstrom, Biochim. Biophys. Acta 977, (1989) 322.
3. a) B. Chance, C. Saronio, and J. S. Leigh, Jr. J. Biol. Chem. 250, (1975) 9226. b) G. M. Clore, L. E. Andreasson, B. Karlsson, R. Aasa, and B. G. Malmstrom, Biochem. J. 185, (1980) 139.
4. a) O. Hansson, B. Karlsson, R. Aasa, T. Vanngard, and B. G. Malmstrom, EMBO J. 1, (1982) 1295. b) S. N. Witt and S. Chan, J. Biol. Chem. 262, (1987) 1446.
5. a) S. Han, Y.-c. Chin, and. D. L. Rousseau, Proc. Natl. Acad. Sci. U.S.A. 87, (1990) 8408. b) C. Varotsis, W. H. Woodruff, and G. T. Babcock, J. Am. Chem Soc. 111, (1989) 6439; ibid, 112, (1990) 1297. c) T. Ogura, S. Takahashi, K. Shinzawa-Itoh, S. Yoshikawa, and T. Kitagawa, J. Am. Chem. Soc. 112, (1990) 5630.
6. T. Kitagawa and T. Ogura, in Advances in Spectroscopy, Ed. R. J. H. Clark and R. E. Hester (John Wiley & Sons, Chichester, 1993) Vol.21, Chap. 3.
7. a) T. Ogura, S. Takahashi, S. Hirota, K. Shinzawa-Itoh, S. Yoshikawa, E. H. Appelman, and T. Kitagawa, J. Am. Chem. Soc. 115, (1993) 8527. b) T. Ogura, S. Takahashi, K. Shinzawa-Itoh, S. Yoshikawa, and T. Kitagawa, Bull. Chem. Soc. Jpn. 64, (1991) 2901.
8. a) S. Han, Y. -c. Ching, and D. L. Rousseau, Nature 348, (1990) 89. b) C. Varotsis, Y. Zhang, E. H. Appelman, and G. T. Babcock, Proc. Natl. Acad. Sci. U.S. A. 90, (1993) 237.
9. a) D. A. Proshlyakov, T. Ogura, K. Shinzawa-Itoh, S. Yoshikawa, E. H. Appelman, and T. Kitagawa., J. Biol. Chem. 269, (1994) 29385; b) D. A. Proshlyakov, T. Ogura, K. Shinzawa-Itoh, S. Yoshikawa, and T. Kitagawa, submitted.
10. T. Kitagawa and Y. Mizutani, Coord. Chem. Rev. 135, (1994) 685.

Presence of Penta- and Hexa-Coordinated States in T_1 and Cation-Radical Bacteriochlorophyll *a*, and Generation of Cation Radical by Photo-Excitation of the Aggregated Forms as Revealed by Transient Raman and Transient Absorption Spectroscopies

Yasushi Koyama[1]*, Leenawaty Limantara[1], Ei-ichi Nishizawa[1],
Yasuhito Misono[2] and Koichi Itoh[2]
[1]*Faculty of Science, Kwansei Gakuin University, Uegahara, Nishinomiya 662, Japan*
[2]*Department of Chemistry, School of Science and Engineering, Waseda University, Shinjuku-ku, Tokyo 169, Japan*

1. INTRODUCTION

Bacteriochlorophyll *a* (BChl *a*) plays different roles in bacterial photosynthesis: The singlet-excited (S_1) state is generated by absorption of a photon in the light-harvesting complex (LHC), and the singlet energy is transferred to another BChl *a* in the LHC and eventually to the special-pair BChl *a* in the reaction center (RC). Upon excitation of the special pair (P_M-P_L), charge separation takes place, and the ejected electron is transferred to the bacteriopheophytin *a* (BPhe *a*) in the L-branch (H_L), mediated by the accessory BChl *a* in the L-branch (B_L). Then, bacteriochlorophyll *a* cation radical (BChl $a^{+\cdot}$) is generated in the special pair. Under the reducing conditions, the reverse electron-transfer reaction causes charge recombination in the special pair; the energy of the resultant triplet (T_1) state is transferred to the carotenoid through the other accessory BChl *a* (B_M), and then it is dissipated by the carotenoid. Chemically the same BChl *a* molecule plays different roles depending on the binding site in the LHC and in the RC (e.g. P_M, P_L, B_M and B_L), and the different excited states of neutral BChl *a* as well as the ground (D_0) state of BChl $a^{+\cdot}$ carry out the physiological functions in the primary processes of photosynthesis. The ground-state, excited-state and redox-state properties of each BChl *a* in the pigment-protein complexes must be delicately controlled through intermolecular interactions with the neighboring pigment(s) and with the apo-peptide(s).

As one of the most important intermolecular interactions, we have focused our attention to the states of coordination, and addressed the following two specific questions: (A) In the S_0 state of neutral BChl *a*, the coordination states are classified into the penta-coordinated and the hexa-coordinated states. Does this classification apply also to the T_1 state of BChl *a* and the D_0 state of BChl $a^{+\cdot}$? (B) In the RC, BChl $a^{+\cdot}$ can be generated by photo-excitation, although BPhe *a* (H_L) does not seem to be a strong oxidant (electron acceptor). Is the generation of BChl $a^{+\cdot}$ by photo-excitation (without adding strong oxidant) a general property of an aggregated form? If the answer is yes, can BChl $a^{+\cdot}$ be generated in the LHC as well? Application of resonance Raman and electronic absorption spectroscopies to the bacteriochlorophyll molecules in various solutions and those bound to the LHC has provided us with the answers to these questions.

2. TRANSIENT RAMAN SPECTROSCOPY OF BChl *a* IN SOLUTIONS

Cotton et al. [1] and Lutz [2] assigned the strongest Raman line of S_0 BChl *a* to the C_a - C_m stretching. Donohoe et al. [3] showed that the stretchings of all the C_a - C_m bonds in the bacteriochlorine skeleton mix one another to form an a_g-type normal vibration giving rise to the highest Raman intensity. This mode is called 'the ring-breathing mode'. We call the ring-breathing frequencies in the S_0 and T_1 states of BChl *a* ν_r and ν_r", respectively (ν_r' is saved for the S_1 state), and that in the D_0 state of BChl $a^{+\cdot}$ $\nu_r{}^+$. The assignments of the ν_r and ν_r" Raman lines have been confirmed by ^{15}N-substitution [1,4].

Table 1. The ring-breathing frequencies in the S_0 (ν_r) and T_1 (ν_r'') states of BChl *a* and in the D_0 state of BChl $a^{+\bullet}$. Solvent parameters are also shown.

Solvent	ν and the coordination states[a]			transient	solvent parameters		
	ν_r	ν_r''	ν_r^+	(ν_r^+)	DN[b]	β[c]	π*[c]
(a) acetonitrile	1606 V	1590 V					
(b) propionitrile	1611 V		1597 V		16.1	0.37	0.71
(c) 1-butyronitrile	1609 V		1596 V		16.6		0.71
(d) acetone	1608 V	1588 V	1598 V		17.0	0.48	0.71
(e) 2-butanone	1610 V	1586 V	1595 V			0.48	0.67
(f) 3-pentanone	1610 V	1590 V	1596 V			0.45	0.72
(g) 2-octanone	1608 V	1589 V	1599 V				
(h) diethyl ether	1607 V	1591 V					
(i) propyl ether	1608 V	1591 V					
(j) methylene chloride	1609 V		1599 V	(1597 V)	0.0	0.00	0.82
(k) carbon tetrachloride	1605 V			(1599 V)			
(l) 2-propanol	1608 V	1585 V	1588 VI			0.95	0.48
(m) methanol	1596 VI		1584 VI		20.0	0.62	0.60
(n) ethanol	1599 VI		1585 VI		19.0	0.77	0.54
(o) 1-propanol	1598 VI		1584 VI		18.0		0.52
(p) 1-butanol	1597 VI	1580 VI	1588 VI			0.88	0.47
(q) 1-hexanol	1594 VI	1578 VI					
(r) 1-decanol	1596 VI	1579 VI					
(s) pyridine	1594 VI	1581 VI					
(t) tetrahydrofuran	1595 VI	1580 VI	1586 VI		20.0	0.55	0.58
LH1	1608 V			(1597 V)			
LH2	1607 V			(1596 V)			

[a]V, the penta-coordinated state and VI, the hexa-coordinated state.
[b]Donor number and [c]Taft parameters.

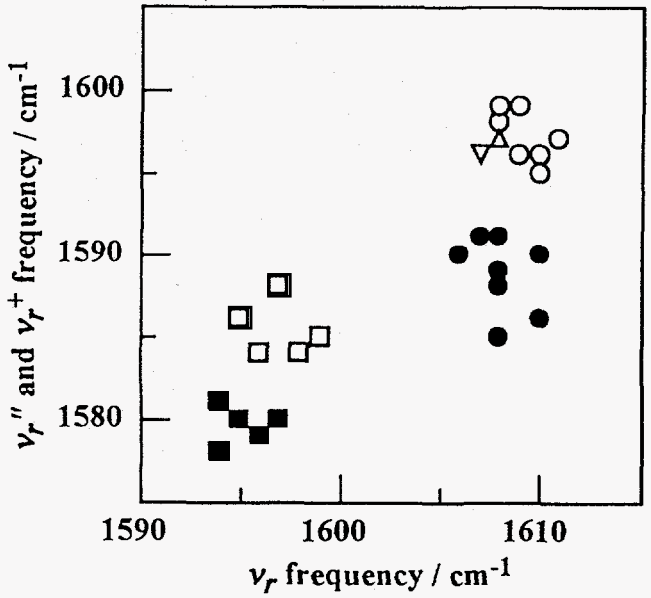

Figure 1. The correlation between the ring-breathing frequency of S_0 BChl *a* (ν_r) and that of T_1 BChl *a* (ν_r'') in the penta- (●) and the hexa- (■) coordinated states, and the correlation between the ring-breathing frequency of S_0 BChl *a* (ν_r) and that of D_0 BChl $a^{+\cdot}$ (ν_r^+) in the penta- (○) and the hexa- (□) coordinated states. The ring-breathing frequencies of the transients generated in the LH1 (△) and LH2 (▽) light-harvesting complexes from *R. sphaeroides* R26 and R26.1, respectively, are also shown.

Callahan and Cotton [5] established the classification of the coordination states of BChl *a* in terms of ν_r; it was 1609 cm^{-1} in the penta-coordinated state and 1595 cm^{-1} in the hexa-coordinated state. By the use of the same set of solvents, we found that it is in the regions of 1606 - 1612 and 1593 - 1598 cm^{-1} in the penta- and hexa-coordinated states, respectively [6]. No clear difference in frequency was found between the penta-coordinated aggregates and the penta-coordinated monomers. This classification of the coordination states in terms of ν_r generally agrees with that in terms of the wavelength of the Q_x absorption [5-7]. Some solvents gave two split ν_r Raman lines, indicating a mixture of both coordination states; those solvents are excluded from discussion here in this paper. Table 1 lists the ν_r values as well as the classification of the coordination states for the present set of solvents .

We measured the Raman spectra of a transient species of BChl *a* in 16 different solvents by the use of one-color, pump-and-probe method using 420 nm, 5 ns pulses [6]. We found that the ring-breathing frequencies of the transients could be classified into three different regions depending on the kind of solvents: (1) The 1578 - 1581 cm^{-1} region for solvents forming hexa-coordinated monomers (in the S_0 state); (2) the 1585 - 1591 cm^{-1} region for solvents forming penta-coordinated monomers; and (3) the 1597 - 1599 cm^{-1} region for solvents forming penta-coordinated aggregates (carbon tetrachloride and methylene chloride). We classified the transient species into three different categories in terms of the above ring-breathing frequencies; (1) the T_1 species in the hexa-coordinated monomers, (2) the T_1 species in the penta-coordinated monomers, and (3) 'the T_1 species in the penta-coordinated aggregates'. Figure 1 shows the relation between the ν_r and ν_r" values for both classes (1) and (2); these classes can be clearly correlated to the penta-coordinated state (closed circles) and the hexa-coordinated state (closed squares). Thus, a positive answer to question A is obtained; the classification of the coordinated states does apply to monomeric T_1 species. However, the ring-breathing frequencies of the transient in class (3) agreed with that of the cation radical (ν_r^+), and therefore, 'the T_1 species in the penta-coordinated aggregates' could be actually BChl $a^{+\cdot}$. Since Raman spectral pattern of T_1 BChl *a* and D_0 BChl $a^{+\cdot}$ are similar to one the other, a definitive conclusion had to wait for the results of electronic absorption spectroscopy of the three classes.

3. TRANSIENT ABSORPTION SPECTROSCOPY OF BChl *a* IN SOLUTIONS

We recorded transient absorption spectra 200 ns after excitation in the same set of solutions [8]. Typical triplet absorption spectra were obtained for the solutions forming the penta- and hexa-coordinated monomers; the $T_n \leftarrow T_1$ absorption bands depended on the state of coordination. The results supported the above assignments of class (1) and class (2) to the hexa-coordinated and penta-coordinated monomers. Further, the effect of hydrogen bonding was clearly seen.

In carbon tetrachloride, a solvent facilitating the formation of higher BChl *a* aggregates, D_0 BChl $a^{+\cdot}$, instead of T_1 BChl *a*, was generated. In methylene chloride forming lower aggregates, generation of T_1 BChl *a* and subsequent transformation into D_0 BChl $a^{+\cdot}$ were observed. These results prove that BChl $a^{+\cdot}$ can be generated simply by photo-excitation of the BChl *a* aggregates *without* adding any electron acceptor (oxidant). Actually, this is the answer to question B. No indication of the generation of bacteriochlorophyll *a* anion radical (BChl $a^{-\cdot}$) was seen; the ejected electron may be shared among the BChl *a* molecules in the aggregate. The results strongly support the idea that we were actually observing not T_1 BChl *a* but D_0 BChl $a^{+\cdot}$ in the transient Raman spectroscopy of the aggregates (*vide supra*). Since higher aggregates tend to be formed at higher BChl *a* concentrations, and since the concentration used in the transient Raman measurements (3×10^{-3} M) is one order of magnitude higher than that used in the transient absorption measurements (3×10^{-4} M), it is likely that BChl $a^{+\cdot}$ was generated in both carbon tetrachloride and methylene chloride within the pulse duration of 5ns (*vide supra*).

4. RAMAN SPECTROSCOPY OF ELECTROCHEMICALLY-FORMED BChl $a^{+\cdot}$ IN SOLUTIONS

We recorded the Raman and electronic absorption spectra of BChl $a^{+\cdot}$ in 14 different solvents [9,10]. Formation of BChl $a^{+\cdot}$ was confirmed by electronic absorption spectroscopy. Table 1 lists the ν_r^+ values; the ν_r^+ value was in the 1584 - 1588 cm^{-1} region in the hexa-coordinated state, while it was in the 1594 - 1599 cm^{-1} region in the penta-coordinated state. Figure 1 shows the relation between the ν_r and ν_r^+ values for solvents forming the penta-coordinated state (open circles) and the hexa-coordinated state (open squares). The states of coordination in BChl $a^{+\cdot}$ are clearly classified into the penta- and hexa-coordinated states, and they are retained even after one-electron oxidation. This is another answer to question A; the classification of the coordination states does hold in the D_0 state of BChl $a^{+\cdot}$. One exception is the case of 2-propanol, where transformation from the penta- to the hexa-coordinated state seems to take place upon conversion from BChl *a* to BChl $a^{+\cdot}$. A key electronic-absorption band for BChl $a^{+\cdot}$ was found in the region of 545 - 575 nm. It appeared in the 546 - 554 nm region in the penta-coordinated state and in the 557 - 562 nm region in the hexa-coordinated state. It appeared at 562 nm in 2-propanol showing that BChl $a^{+\cdot}$ was in the hexa-coordinated state in this solvent. Thus, the states of coordination classified by ν_r^+ are in complete agreement with those classified by λ^+. No clear difference was found either in ν_r^+ or in λ^+ between the penta-coordinated monomers and the penta-coordinated aggregates.

5. SOLVENT PARAMETERS DETERMINING THE RELATIVE STABILITY OF THE COORDINATION STATES, AND THE TRANSIENT SPECIES OF BChl *a* GENERATED BY PHOTO-EXCITATION IN THE LIGHT-HARVESTING COMPLEXES

Table 1 lists the donor number [11], DN, and the Taft parameters [12], β and π^*, which are expected to determine the relative stability of the penta- and hexa-coordinated states. The DN value scales the electron-donating power of the solvent. It is seen, in the D_0 state of BChl $a^{+\cdot}$, that the penta-coordinated state is formed in solvents with DN $\leq$ 17, and that the hexa-coordinated state is formed in solvents with DN $\geq$ 18. One of the Taft parameters, β, also measures the electron-donating power of the solvent. It is seen that the penta-coordinated state is formed in solvents with $\beta < 0.5$, and that the hexa-coordinated state is formed in solvents with $\beta > 0.5$. Obviously, those solvents having higher electron-donating power tend to form the hexa-coordinated state.

The value of another Taft parameter, π^*, scales dielectric stabilization of a dipole by the solvent system. It is seen that the penta-coordinated state is formed in solvents with $\pi^* > 0.65$, and that hexa-coordinated state is formed in solvents with $\pi^* < 0.65$. In the penta-coordinated state, an axial dipole is expected to be formed between the central magnesium atom of the BChl $a^{+\cdot}$ and the nitrogen or oxygen atom of the solvent. In the hexa-coordinated state, on the other hand, a pair of axial dipoles with the same magnitudes and with the opposite directions are expected to cancel out with each other. Therefore, the penta-coordinated state can be characterized by a strong axial polarization, while the hexa-coordinated state can be characterized by a zero axial polarization. Thus, stronger dielectric stabilization by the solvent system (higher π^* value of the solvent) must push the equilibrium from the hexa-coordinated state toward the penta-coordinated state.

The above control of the two states of coordination through the electron-donating power of the solvent and the dielectric stabilization by the solvent system seems to explain the transformation in 2-propanol from the penta- to hexa-coordinated state upon one-electron oxidation. The high value of β (0.95) and the low value of π^* (0.48) indicate that this solvent tends to form the hexa-coordinated state of BChl $a^{+\cdot}$ rather than the penta-coordinated state. The

formation of the hexa-coordinated state must be prohibited in neutral BChl *a* by a strong steric hindrance due to the particular structure of this secondary alcohol. The strong ligating power caused by the positive charge on the magnesium atom in BChl $a^{+\cdot}$ must overcome this steric hindrance, and trigger the formation of the hexa-coordinated state.

A pair of light-harvesting complexes, i.e. LH1 and LH2, were isolated from *Rhodobacter sphaeroides* R26 and R26.1 by the use of detergents, sucrose monocholate and lithium dodecyl sulfate, respectively. Transient Raman spectra of the LHCs were recorded by the one-color pump-and-probe method using 420 nm, 5 ns pulses [6,13]. The ring-breathing frequencies of the transients were 1597 and 1596 cm^{-1} for the LH1 and LH2 complexes, respectively (Table 1). The relations of these values with the ν_r values in the S_0 state are shown in Figure 1 (see the triangles). Application of the rules of the ring-breathing frequencies among ν_r, ν_r" and ν_r^+ found in the *in vitro* solutions (Figure 1) leads us to the conclusion that the transient species generated by photo-excitation in these LHCs are BChl $a^{+\cdot}$. Recent X-ray crystallography of an LH2 complex from *Rhodopseudomonas acidophila* 10050 showed that the B800 - 850 BChl molecules form a circular (infinite) aggregate [14]. If generation of BChl $a^{+\cdot}$ is a general property of BChl *a* aggregates as found *in vitro*, it is likely that the BChl *a* molecules in the penta-coordinated aggregate in the LHC generate BChl $a^{+\cdot}$. The ν_r and ν_r^+ frequencies for the LHCs indicate that both S_0 BChl *a* and D_0 BChl $a^{+\cdot}$ are in the penta-coordinated state. A transient (difference) absorption spectrum of chromatophores from *R. sphaeroides* R-26 [15] seems to support this conclusion. However, the final conclusion must wait for more detailed investigation by transient, electronic absorption and EPR spectroscopies.

References

1. T. M. Cotton, K. D. Parks and R. P. Van Duyne, J. Am. Chem. Soc., 102 (1980) 6399.
2. M. Lutz, in Advances in Infrared and Raman Spectroscopy, Ed. R. J. H. Clark and R. E. Hester (John Wiley & Sons, Chichester, 1984) 211.
3. R. J. Donohoe, H. A. Frank and D. F. Bocian, Photochem. Photobiol., 48 (1988) 531.
4. L. Limantara, Y. Koyama, I. Katheder and H. Scheer, Chem. Phys. Letters, 227 (1994) 617.
5. P. M. Callahan and T. M. Cotton, J. Am. Chem. Soc., 109 (1987) 7001.
6. E. Nishizawa, L. Limantara, N. Nanjou, H. Nagae, T. Kakuno and Y. Koyama, Photochem. Photobiol., 59 (1994) 229.
7. T. A. Evans and J. J. Katz, Biochem. Biophys. Acta., 396 (1975) 414.
8. E. Nishizawa, H. Nagae and Y. Koyama, J. Phys. Chem., 98 (1994) 12086.
9. Y. Misono, E. Nishizawa, L. Limantara, Y. Koyama and K. Itoh, Chem. Phys. Letters, 236 (1995) 413.
10. Y. Misono, L. Limantara, Y. Koyama and K. Itoh, to be published.
11. V. Gutmann, in Donor-Acceptor Approach to Molecular Interactions (Plenum Press, New York, 1978) 20.
12. M. J. Kamlet, J.-L. M. Abboud, M. A. Abraham and R. W. Taft, J. Org. Chem. 48 (1983) 2877.
13. L. Limantara, T. Kakuno, T. Yagura, Y. Okabe, R. J. Cogdell and Y. Koyama, to be published.
14. G. McDermott, S. M. Prince, A. A. Freer, A. M. Hawthornthwaite-Lawless, M. Z. Papiz, R. J. Cogdell and N. W. Isaacs, Nature, 374 (1995) 517.
15. T. G. Monger, R. J. Cogdell and W. W. Parson, Biochem. Biophys. Acta., 449 (1976) 136.

Vibrational and Electronic Dynamics of Dyes Measured by Incoherent Light

A. Kummrow, A. Lau

Max-Born-Institut für Nichtlineare Optik und Kurzzeitspektroskopie,

Rudower Chaussee 6, D-12474 Berlin, Germany

1.INTRODUCTION

Monitoring dephasing processes on a femtosecond time scale is an important probe of and dynamic properties of condensed matter, e.g. dye molecules in solution. This paper deals with dephasing of vibrational and electronic transitions in all-*trans*-β-carotene molecules in different solvents using special methods of incoherent light scattering. Incoherent light means laser pulses, the bandwidth of which is much greater than the corresponding time duration (non-transform limited). Though nowadays femtosecond pulses are available, their production as well as their handling are still costly. In recent years new methods have been developed, which can give similar results using nanosecond broadband laser radiation [1]. In all these methods, sub-structure pulses of short time duration inherent in broadband radiations are used to coherently excite and probe a molecular transition. The time duration of these subpulses are determined by the bandwidth of the applied laser radiation. We shall discuss results obtained with corresponding methods delivering dephasing times of vibrations (*interferometric coherent anti-Stokes Raman scattering*, ICARS) and dephasing times of electronic transitions (*forced light scattering*, FLS).

2. EXPERIMENTAL SETUP

In our experiments we used one narrowband and one broadband laser, both of which are pumped by a Nd:YAG laser delivering nanosecond pulses with a repetition rate of maximal 10 Hz. The radiation of the broadband laser was split into two twin parts in an interferometer with a variable delay line. Afterwards, all three beams were focused by a lens in a folded boxcars geometry into the sample, taking into account the phasematching condition. A pinhole served for spatial filtering the ICARS, and a monochromator for a monochromatic detection of the broadband ICARS signal. Due to other phasematching conditions the FLS signal leaves the sample in a different direction. In Fig. 1 the applied phasematching condition and the corresponding spectral feature for ICARS are depicted schematically. The ICARS signal is detected with a photomultiplier, the FLS signal with a photodiode. For comparison scanning CARS spectra were detected too. Details are published elsewhere [2]. We used two different excitation conditions, in which the broadband laser radiation was either in the wing of the absorption band or in its first maximum. The narrowband laser radiation was in both cases in the long wavelength wing. β-carotene solutions were filled into 200 μm cuvettes with 100 μm thick glass windows using concentrations of 10^{-4} to $3\ 10^{-4}$ in 1-dodecanol and in cyclohexane, respectively.

All-*trans*-β-carotene (Fluka, purum) is a highly reactive compound. We therefore considered the absorption spectrum before and after measurements. Even for solutions exposed for a longer time we detected only a decrease of the well known absorption. New absorption bands do not

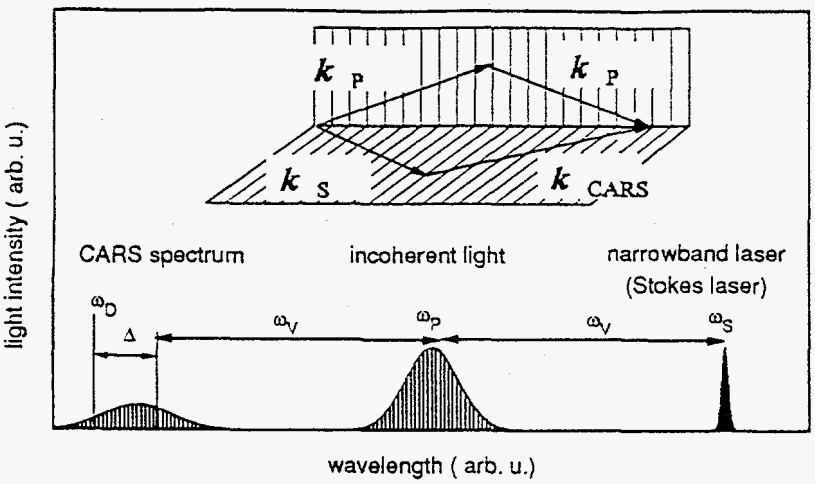

Fig. 1:
Spectral features of ICARS using incoherent light and the applied phase-matching diagram.

occur in the visible region, which could have been designed to decomposition products. So we can conclude, that the signals in our experiments are due to all-*trans*-β-carotene.

3. INTERFEROMETRIC CARS

We report on new ICARS results of all-*trans*-β-carotene under electronic resonance conditions. To interpret the resonance ICARS data, we developed appropriate formulae, using the correspondence between resonance CARS and ICARS. Ordering the terms in ICARS as leading in resonance CARS to a constant background [3]

$$A = (\chi^0_{nr} + cb')^2 + (cb'')^2 \tag{1}$$

(with χ^0_{nr} the non-Raman-resonant solvent susceptibility and b' and b'' the non-Raman resonant contribution of β-carotene), to a Lorentzian line shape

$$B = 2[cR(\chi^0_{nr} + cb') + c^2 Jb''] \tag{2}$$

(with the pure Raman-resonant susceptibilities (R+iJ)), and to a dispersion like line shape,

$$C_1 = 2\gamma[c^2 Rb'' - cJ(\chi^0_{nr} + cb')] \tag{3}$$

$$C_2 = c^2(R^2 + J^2)$$

we can describe the ICARS by [3]

$$I_{I\text{-}CARS}(\tau) = I_0 + I_A(\tau) + I_B(\tau) + I_C(\tau) \tag{4}$$

The first term is a constant, the second term decays with a time constant corresponding to the coherence time determined by the width of the broadband laser Γ (in our case ~40 fs). The two last terms give the T_2-time and the frequency of the vibration we are interested in. The connection of the 'detuning oscillation frequency' Δ and the molecular vibration frequency ω_v is given by $\Delta = 2\omega_v - (\omega_D - \omega_s)$. The two terms read:

$$I_B(\tau) \propto B \times \Delta_\Gamma^2(\Delta_1^2+\Delta_\Gamma^2)^{-1}(\Delta_2^2+\Delta_\Gamma^2)^{-1}\exp(-2|\tau|/T_2)\sin(\Delta|\tau|) \quad (5)$$

and

$$I_C(\tau) \propto (C_1+C_2)\times\Delta_\Gamma^2(\Delta_1^2+\Delta_\Gamma^2)^{-1}\ (\Delta_2^2+\Delta_\Gamma^2)^{-1}\exp(-2|\tau|/T_2) \times\left((2\gamma)^{-1}\cos(\Delta\tau)+\Delta^{-1}\sin(\Delta|\tau|)\right) \quad (6)$$

The Δ_i are frequencies connected with the frequencies of the lasers and the position of the monochromator slit [4].

For the C=C in phase chain vibration of all-*trans*-β-carotene at 1522 cm^{-1}, we found a dephasing time of 600 fs in agreement with the value published [5]. For the chain vibration at 1153 cm^{-1}, we found 900 fs if the simultaneously excitation of at least 3 vibrations is not taken into consideration, again in good agreement with the published data [6]. Taken into account the corresponding simultaneous excitation we obtained 660 fs.

In dependence of the excitation intensity and the resonance conditions the ICARS features changed unexpectedly. In the C=C vibrational region high laser intensities seem to introduce a strong decrease of the T_2-time for preresonance conditions. A closer analysis show, that instead of two new lines, which have not been reported before, together with a decreased concentration have to be taken into account. Then the T_2-time stays unchanged at 600 fs. These observations are confirmed by scanning CARS measurements we carried out under equal conditions. We could fit the CARS and ICARS data with the same molecular parameters using Lorentzian line shapes for the CARS spectra and exponential decay curves for the ICARS features. This is a hint of homogeneous lineshapes for the vibrational spectra.

An other striking observation is a dip at delay time zero for some ICARS interferograms instead

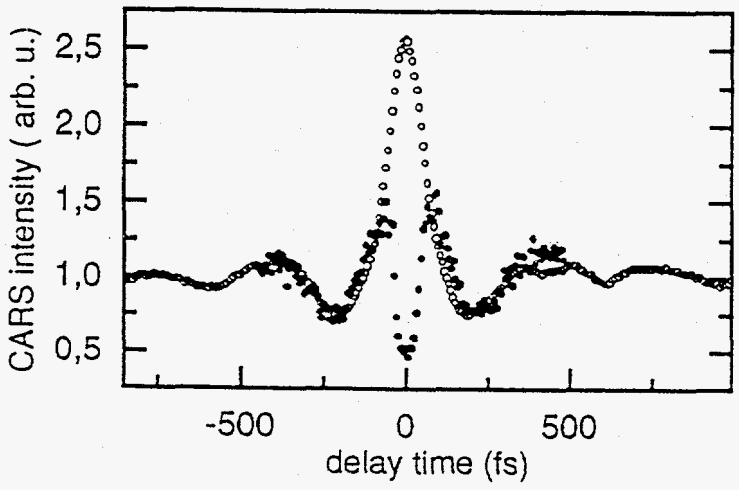

Fig. 2:
ICARS intensity as function of delay time between the two pump pulses for the 1522 cm^{-1} mode of β-carotene dissolved in cyclohexane with (closed circle) and without competition to FLS and degenerated four wave mixing (open circle).

of a peak. We can explain this feature by a strong competition between ICARS and degenereated four wave mixing and FLS respectively in this time region depending on concentration and laser intensities (Fig 2).

4. FORCED LIGHT SCATTERING

We applied a special DFWM technique, Forced Light Scattering, to measure dephasing times of β-carotene. In this technique, in addition to the two beams generating the phase grating, a third light beam out of the absorption is used for probing the time decrease of the grating. This method offers usually a much higher dynamic measuring range than DFWM. For thin samples the intensity of the diffracted signal of the probe beam is given by [7]

$$I_{FLS}(t) = T\left(\frac{\pi d}{2\lambda_S}\right)^2 I_S(t) n_\Delta^2(t) \tag{7}$$

T is the transmission of the sample, d its thickness; λ_S is the wavelength and J_S the intensity of the probe beam. n_Δ^2 (t) is the change of the refractive index in the phase grating, induced by the pump beams. Presuming for the statistical light a stationary Gaussian process one finds [7]

$$I_{FLS} \propto (f(\tau))^2 = \text{const.} + \frac{64\pi^6\mu^4\rho_0^2 T_1^2}{h^4}\left|\int_{-\infty}^{\infty} ds D(s-\tau)\exp(-g(|s|))\right|^2 \tag{8}$$

D is given by the autocorrelation function of the broadband laser radiation and $g(|s|)$ is the response function to be measured. In a simple case the experimental curve can be described by a Kubo function with Δ_K the modulation strength and τ_C the correlation time

$$g_K(t) = (\Delta_K \tau_C)^2 [t/\tau_C - 1 + \exp(-t/\tau_C)] \tag{9}$$

We measured the FLS curves for two different resonance conditions in accordance to the frequency of the broadband laser radiation and the absorption of β-carotene. The curves are depicted in Fig. 3. For λ_p = 512 nm the curves could even been fitted by a simple Gaussian function. For λ_p = 477 nm a Kubo function was used for the fit neglecting the oscillations on the wing of the curves. The latter are due to coherent excitations of vibrations. After deconvolution of the decay curves with the autocorrelation function we found for λ_p = 512 nm a linewidth of 62 THz and for λ_p = 477 nm from the Kubo model Δ_K = 50 THz and a correlation time of 37 fs

The dephasing occurs on a time scale which is comparable to the autocorrelation time of the broadband laser radiation. The latter time can be calculated for a Gaussian intensity distribution of the pump laser by

$$\tau_{auto} = 0.62\ \lambda_p^2 / (c_0 * \Delta\lambda_p), \tag{10}$$

leading to 40 fs. For an excitation in the first maximum of the absorption we are therefore in the intermediate region of the fast and slow modulation limit of the Kubo model. The different values of the dephasing in dependence on the resonance conditions are connected with the physical causes which are responsible for the long wavelength's wing of the absorption spectrum. As was discussed by [8] the modulation strength is dependent on the Franck-Condon factors (which could be different in different spectral positions) and the temperature, which could also be

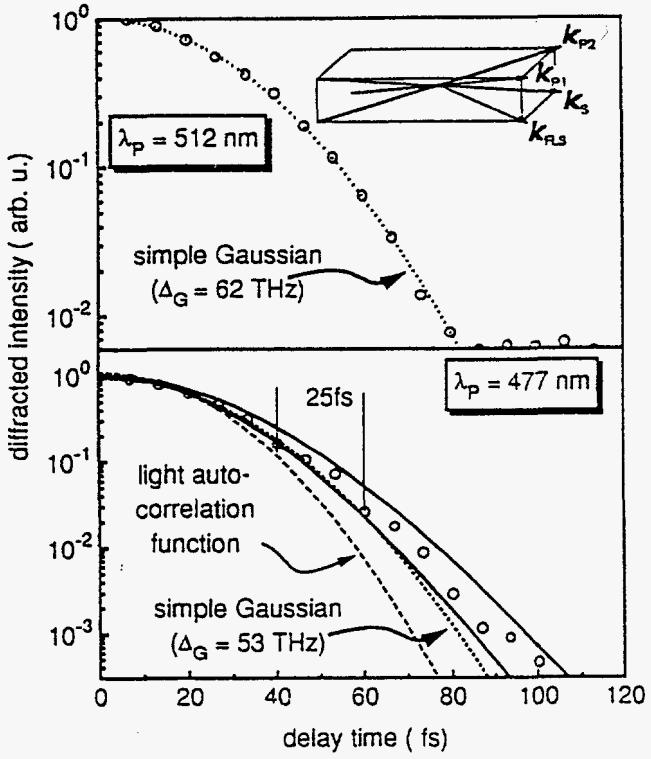

Fig. 3:
Diffracted intensity as function of delay time for FLS. Upper diagram: Excitation below the 0-0-transition of β-carotene with a simple Gaussian fit curve (wavevector matching diagram shown as inset). Lower diagram: excitation between the 0-0 and the 0-1 transition, fitted with a Kubo like decay curve. The oscillations on the wing are due to coherent vibrational excitations. The outer solid line corresponds to fit parameters: Δ_K = 52 THz and τ_C= 39 fs, the inner one to Δ_K = 48 THz and τ_C= 36 fs.

different due to different hot sub-ensembles of the molecules or to different heating of the laser radiations in both spectral regions.

Acknowledgment

We thank Mrs. R. Goleschny and H.-J Ludewig for technical assistance, Dr. M. Pfeiffer for helpful discussions. This work was supported by Deutsche Forschungsgemeinschaft.

References

[1] T. Yajima, N. Morita and Y. Ishida, Phys. Rev. A 30 (1984) 2525.
M. A. Dugan, and A. C. Albrecht, Phys. Rev. A 43 (1991) 3877 and 3922.
T. S. Yang, R. Zhang and A. B. Meyers, J. Chem. Phys. 100 (1994) 8573.
[2] A. Lau, A. Kummrow, M. Pfeiffer and S. Woggon, J. Raman Spectr. 25 (1994) 607.
[3] A. Kummrow, A. Lau and H.-G. Ludewig, SPIE Vol. 2370: Laser Appl. in Life Sciences (1994) 207
[4] S. A. Schaertel, A. C. Albrecht A. Lau and A. Kummrow, Appl. Phys. B 59 (1994) 377.
[5] H. Okamoto, H. Hayashi, K. Yoshihara and M. Tasumi, Chem. Phys. Lett. 182 (1991) 96.
[6] H. Okamoto and K. Yoshihara,J. Opt. Soc. Am. B7 (1990) 1702.
[7] A. Kummrow, S. Woggon and A. Lau, Phys. Rev. A 50 (1994) 4264
[8] Y. J. Yan and S. Mukamel, J. Chem. Phys. 89, (1988) 5160.

Femtosecond THz Spectroscopy

Stephen E. Ralph

Emory University, Department of Physics
Atlanta, GA 30328

ABSTRACT

A new Far infrared generation and spectroscopy technique is described. Terahertz (THz) beams composed of 200 femtosecond duration pulses of far infrared radiation are generated via the induced dipole of photogenerated charge within a strong electric field in semiconductors. This generation mechanism provides the basis for a new transmission spectroscopy technique called Time Domain Spectroscopy. We describe the generation techniques and the spectroscopic system which we have shown is capable of providing time resolved spectra from $5cm^{-1}$ to $200cm^{-1}$ with 200fs resolution.

INTRODUCTION

Recently a new technique of generating short pulses of Far Infrared Radiation (FIR) has been the subject of intense study[1]. This FIR radiation has been studied in an effort to understand the fundamental physics of the generation mechanism[2-4] and to make use of this new source in a time resolved Far Infrared spectroscopic tool[5-12]. In the most straight forward implementation, the generation mechanism consists of creating a transient electric dipole via the excitation of semiconductors using laser pulses of femtosecond duration. The resulting emission consists of a burst of FIR radiation with a temporal duration close to that of the excitation pulse and a continuum spectral content spanning the Terahertz (THz) frequencies (λ=40 -> 1000μm). Importantly, there are no other comparable sources of short pulse Far Infrared radiation. The emission characteristics have been used to study fundamental transport properties of photoexcited carriers in semiconductors. However, the potential of this new source as part of a sensitive spectroscopic tool is just beginning to be explored.

The work presented here involves the study of the temporal dynamics of the photoinduced conductivity in semiconductors. Thus, we first outline the theoretical descriptions of this interaction followed by a description of the FIR system. We conclude with a description of some recent time resolved spectroscopic measurements of the photoinduced conductivity in the semiconductor $In_{0.53}$ $Ga_{0.47}$ As (InGaAs).

THEORETICAL FRAMEWORK

The interaction between the electromagnetic wave and the material can be described by the frequency and time dependent dielectric response function $\varepsilon(\omega,t)$. The dielectric response function of many bulk semiconductors can be represented as a sum of three contributions, I) interband transitions including intersubband transitions, ii) free carrier effects resulting from electrons(holes) in the conduction(valence) and iii) the contribution of the fixed ions of the lattice in the form of phonons. For organic molecules transitions between distinct vibrational and rotational states must be considered.

For the semiconductor studies presented here, we will require only free carrier effects since the photon energy of the FIR pulses in not sufficient to cause interband excitations in our materials and intersubband states do not exist in our bulk like samples. Additionally, the phonon energies are sufficiently large that we do not need to consider them. The complete dielectric response function is then

$$\varepsilon(\omega)=\varepsilon_{\infty}+\frac{i\sigma}{\omega\varepsilon_{o}} \tag{1}$$

where σ is the complex conductivity. The conductivity of (1) is completely general and completely describes the material. Materials parameters including the mobility μ and carrier density, N can be determined via an appropriate model of the conductivity. Using the Drude theory, the conductivity is expressed in terms of the plasma frequency $\omega_p=\sqrt{Ne^2/\varepsilon_o m^*}$ and is given by

$$\sigma(\omega)=\iota\varepsilon_{o} w_{p}^{2}/(\omega+i\Gamma_{\varepsilon}) \tag{2}$$

where Γ_ε is the carrier scattering rate, m is the effective mass of the carrier and the other terms have their usual meaning. The carrier mobility is determined via the relation $\mu= q/m^*\Gamma$.

The Terahertz spectroscopic system thus interacts preferentially with mobile charge species and is a direct measure of the sample conductivity. The time resolved capability of the new pulsed FIR source allows the determination of both $\sigma(\omega,t)$ and, assuming and appropriate model of conduction, N(t) and $\mu(t)$.

FIR INTERFEROMETER

The interferometer is shown in Fig. 1 which depicts two pulsed FIR sources. These sources are comprised of metal electrodes defined on Semi-Insulating Gallium Arsenide substrates[13]. The FIR pulses are generated by creating carriers within the large electric field developed between the externally biased electrodes. The transient photocurrent gives rise to the freely propagating FIR radiated field. It should be noted that direct optical rectification of the incident optical pulse may also contribute to the radiated signal[12]. The strength of this contribution is proportional to the nonlinear optical susceptibility χ^2 in GaAs. Due to the large trap enhanced electric field[3] in our biased sources, the generated FIR results mostly from the macroscopic current transport.

The interferometer is scanned by adjusting the relative delay between the two laser excitations sources. The beams are combined using a silicon beam splitter and the interferogram is obtained by measuring the total power incident on a liquid helium cooled bolometer[8,15,16]. The interferometric technique eliminates the bandwidth limiting effects of photoconductive receivers. The power spectrum of the FIR beam is obtained via the Fourier transform of the interferogram. Figure 2 depicts a typical ~300fs FWHM interferogram and the corresponding power spectrum. The power spectrum shown in Fig 2b has a peak power near 1.5THz ($50cm^{-1}$) and useful power extends beyond 4 THz ($133cm^{-1}$). We have previously shown useful power extending beyond 6 THz (200cm-1).

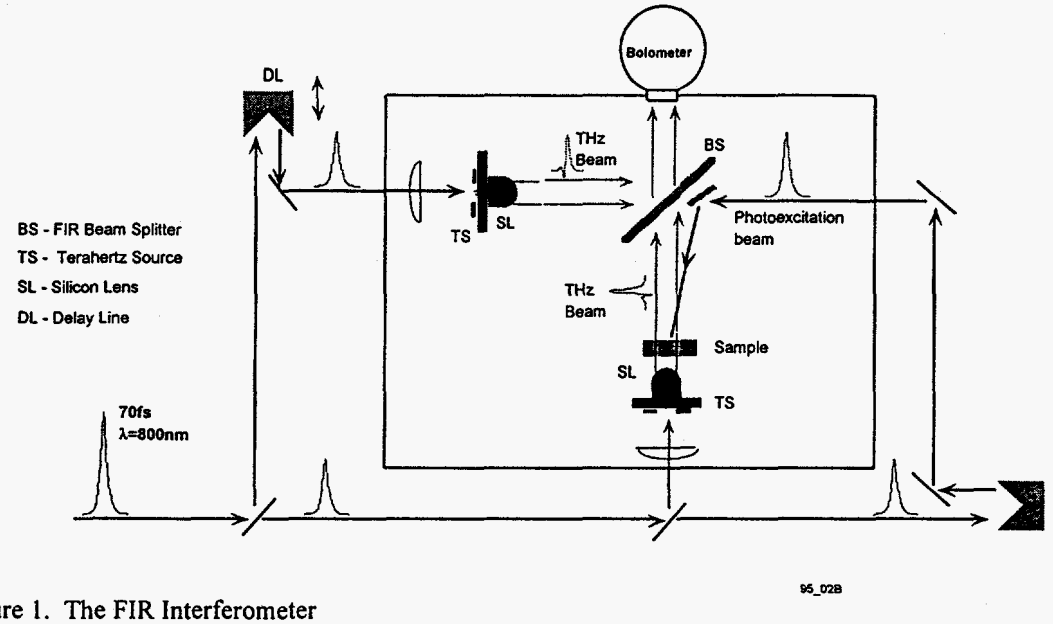

Figure 1. The FIR Interferometer

With the sample inserted into one arm of the interferometer, the system shown in figure 1 can be used to acquire data in two ways. First, using only source 1, the transmission of the sample following photoexcitation is measured by scanning the relative delay between the photoexcitation pulse and the arrival of the FIR probe pulse at the sample. This technique measures the spectrally integrated FIR transmission of the sample. This technique may have advantages over conventional FTIR spectrometers due to the available power at low wavenumbers. The second measurement takes advantage of the interferometer capability by fixing the relative delay between the photoexcitation and the arrival of the FIR pulse at the sample. The interferogram of the transmitted FIR pulse is then obtained by scanning the relative delay of source 2. In this fashion, a sequence of interferograms is taken, each corresponding to a different delay between the photoexcitation source and the probe FIR pulse of source 1. Thus, following photoexcitation, the complex conductivity $\sigma(\omega,t)$ can be determined.

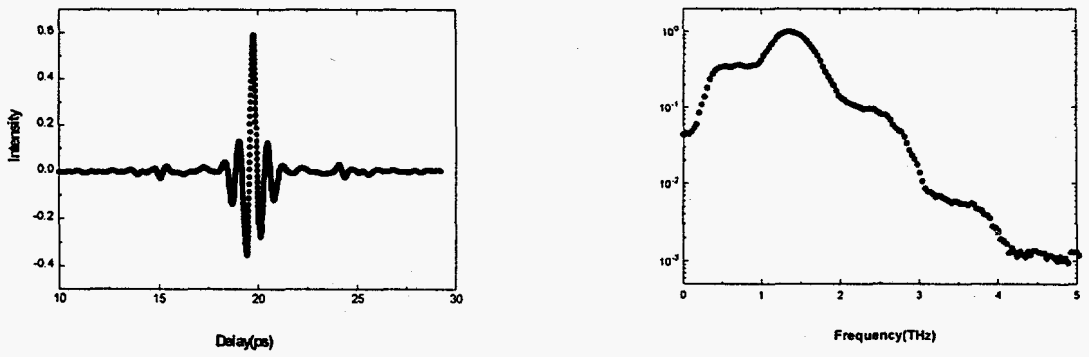

Figure 2 Temporal and Spectral Response of the Dual Source Interferometer. a) Temporal response indicating 200fs resolution, b) Spectral response of Figure 2a.

Figure 3 shows the typical spectrally integrated transient transmission change observed for the compound semiconductor Indium Gallium Arsenide (InGaAs). For the purpose of explaining these results, the band structure of InGaAs can be described by two distinct conduction bands separated by ~0.5eV and characterized by different effective masses. Hence, carriers in the different bands exhibit dramatically different conductivites. In particular, the higher lying conduction band (L-band) has a conductivity which is more than one order of magnitude less than that of the lowest lying conduction band(Γ-band). If carriers are photoexcited with sufficient energy to occupy the upper conduction band, the initial conductivity will correspond to that achieved by carriers in that band alone. As carriers cool to the lower lying conduction band the conductivity will increase. The temporal change in conductivity thus represents the temporal dynamics of carriers scattering out of the upper band and cooling to the bottom of the lower conduction band. In Fig. 3 $-\Delta T$ is plotted for photoexcitations at two photon energies, 1.4eV and 0.8eV. Increasing signal strength corresponds to increasing sample conductivity. As shown in Figure 3 the conductivity reaches the maximum value within 1ps for the 0.8eV excitation yet the increasing conductivity for 1.4eV excitation exhibits a 2.8ps rise time. This represents the scattering rate from L to Γ and the subsequent cooling to the bottom of Γ.

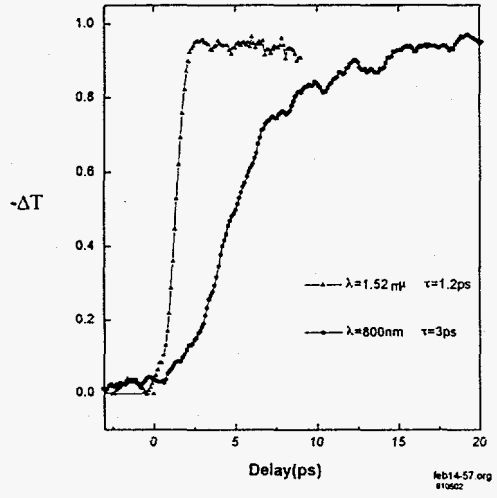

Figure 3 Transient FIR transmission of InGaAs semiconductor for different photoexcitation wavelengths.

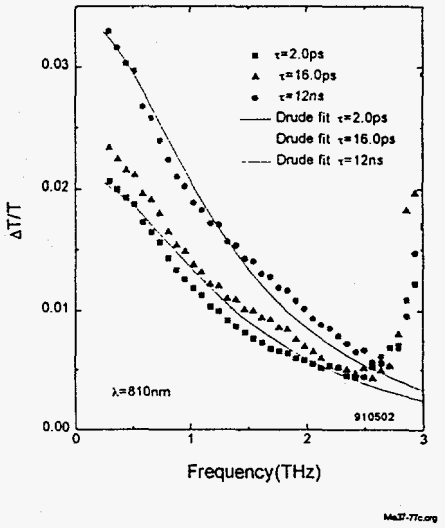

Figure 4 Spectrally resolved transient transmission of the InGaAs following photoexcitation at 810nm.

Figure 4 depicts the spectrally resolved data of Figure 3 for 3 different delays following photoexcitation. Note that the transmission change is in the range of a few percent. The solid curves are the best fit predictions based on the Drude model. From this model we can extract the carrier density in Γ as a function of time delay following g photoexcitation.

SUMMARY

A new time resolved FIR spectroscopic technique which relies on a new method of short pulse FIR generation has been demonstrated. The ultrafast pulses of FIR are generated via the induced dipole of photogenerated charge within semiconductors. The capability of this technique can be summarized as follows:

- Trap enhanced Field effect dramatically increases anode field and THz generation efficiency
- Interferometric techniques eliminate bandwidth limits of photoconductive receivers
- Power observed to 8 THz (266cm^{-1})
- Resolution <1cm-1 (0.1meV)
- Polarization> 100:1 dynamic range
- Real time iterative tuning
- Static spectroscopy demonstrated to 6 THz
- Time resolved spectroscopy demonstrated to 3 THz

ACKNOWLEDGEMENTS

This work was conducted with the efforts of Yue Chen and M. Hargis of Emory University Department of Physics and J. Woodall and D. McInturff of Purdue University, Dept. of Electrical Engineering, West Layfayette, IN

REFERENCES

1. S. E. Ralph, S. Perkowitz, D. Grischkowsky and N. Katzenellenbogen, J.Opt.Soc. Am. B, Vol 11 (1994)., and other papers in this special Terahertz issue.
2. D. H. Auston et. al Appl. Phys. Lett. Vol. **45**, 284 (1984).
3. S. E. Ralph and D. Grishkowsky, Appl. Phys. Lett. Vol. **59**, 1972 (1991).
4. H. Roskos, M. Nuss, J. Shah, Karl Leo, D. A. B. Miller, A.M. Fox, S. Schmitt-Rink and K. Kohler, Phys. Rev. Lett. 68, 2216 (1992).
5. B.I. Greene, P. N. Saeta, D.R. Dykaar, S. Schmitt-Rink and S. L. Chuang , IEEE J Quantum Elect Vol. 28, 2302 (1992).
6. S. E. Ralph and D. Grischkowsky, in Photoinduced spacecharge effects in semiconductors: Electro-optics, photoconductivity and the photorefractive effect, Ed by D. D. Nolte N. M. Haegel and K. W. Goossen, Mat. Res. Soc. Symp. Proc. Vol. 261. p89 (1992).
7. R. H. M. Groeneveld and D. Grischkowsky, J.Opt.Soc. Am. B, Vol 11, 2502, (1994)
8. S. E. Ralph and D. Grishkowsky, Appl. Phys. Lett. Vol. **60**, 1070 (1992).
9. P.R. Smith, D.H. Auston, and M.C. Nuss, IEEE J. Quantum Elect. Vol. 24, 255 (1988).
10. Y. Pastol, G. Arjavalingam, J-M. Halbout, and G.V. Kopcsay, Electron. Lett. Vol.24, 1318 (1988).
11. M. van Exter, Ch. Fattinger and D. Grischkowsky, Appl. Phys. Lett., Vol.55, 337 (1989).
12. X.-C. Zhang, B.B. Hu, J.T. Darrow, and D.H. Auston, Appl. Phys. Lett., Vol.56, 1011 (1990).
13. N. Katzenellenbogen and D. Grischkowsky, Appl. Phys. Lett., Vol. 58, 222 (1991).
14. D.R. Dykaar, B.I. Greene, J.F. Federici, A.F.J. Levi, L.N. Pfeiffer, and R.F. Kopf, Appl. Phys. Lett., Vol. **59**, 262 (1991).
15. B.I. Greene, J.F. Federici, D.R. Dykaar, R.R. Jones and P.H. Bucksbaum, Appl. Phys. Lett., Vol. 59, 893 (1991).
16. D. Grischkowsky, Soren Keiding, Martin van Exter and Ch. Fattinger, J.Opt.Soc.Am.B, Vol.7, 2006 (1990).

Protein Dynamics and Proton Transfer Steps in Bacteriorhodopsin Studied by Time-Resolved Infrared Difference Spectroscopy

O. Weidlich, B. Schalt, F. Siebert
N. Friedman, M. Sheves

Institut für Biophysik und Strahlenbiologie, Albert-Ludwigs-Universität
Albertstr. 23, D-79104 Freiburg, Germany
Department of Organic Chemistry, The Weizmann Institute of Science
76100 Rehovot, Israel

Considerable progress has been made in elucidating the structure and mechanism of the light-driven proton pump bacteriorhodopsin (BR) (for review see [1] and references therein). The light-sensitive part is the chromophore all-*trans* retinal bound via a protonated Schiff base to lysine 216. Static and time-resolved infrared spectroscopy has especially contributed to our understanding by identifying groups of the protein involved in proton translocation [2-5]. From these and other functional investigations strong evidence has bee provided that it is the Schiff base proton which is being pumped. An essential step is Schiff base deprotonation which is finally caused by the light-triggered 13-*trans* -> 13-*cis* isomerization of the chromophore [6,7]. Furthermore, it has been established that the Schiff base proton is transferred to Asp85, and that Schiff base reprotopnation occurs via deprotonation of Asp96. At least two additional groups have been postulated to be involved, one at the cytoplasmic, the other at the external side. The importance of water molecules has been firmly established [8-10]. Also protein conformational changes seem to play an essential role. However, it is not clear how the retinal isomerization triggers these important events in the protein. In the related system, the visual pigment rhodopsin, we have found that removal of the methyl group at position 9 of the ployene chain of the retinal alters completely the photoreaction [11]. The deprotonation of the Schiff base is blocked, which inhibits the formation of the active state. Therefore, it appears interesting to investigate the potential role of the retinal methyl groups in the proton pumping mechanism of bacteriorhodopsin.

By reconstituting bacteriorhodopsin with retinal lacking the 13-methyl group, evidence has been provided that this group is important to favour the generation of the light-adapted all-*trans* configuration of the chromophore: if this group is removed, 90 % of the chromophore in this pigment is, even after light-adaptation, in the inactive 13-*cis*,15-*syn* geometry. The remaining 10 % represent, however, a correctly functioning proton pump [12,13]. Therefore we have investigated the influence of the 9-methyl group on the properties, function and photocycle of bacteriorhodopsin. In earlier experiments normal pumping activity has been reported [12,14].

Time-resolved UV-vis investigations have shown that the flash induced signals are very small: as compared to native BR the formation of L in 9-demethyl BR is reduced by a factor of 5, and that of M by an additional factor of three. A further reduction is observed if the laser pulse is shortened from 20 ns to 5 ns. A very long-lived intermediate is generated with a decay time constant increased by over a factor of 100 as compared to the overall cycling time of native BR.

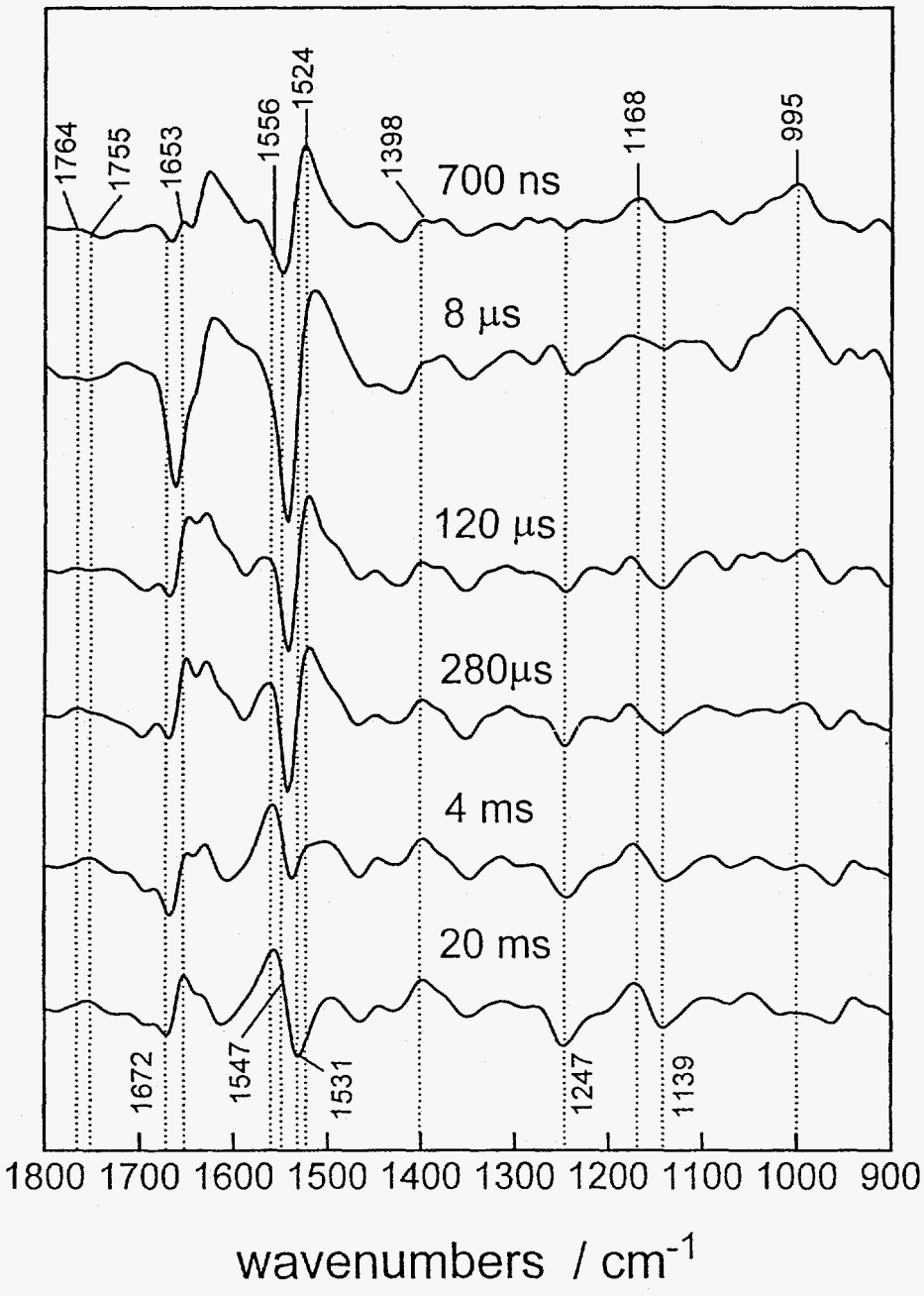

Fig. 1 Time-resolved step-scan FTIR difference spectra of 9-demethyl bacteriorhodopsin, measured at 40 °C, in order to shorten the cycling time. Spectra are labelled with the time elapsed after the flash.

The decay of M, however, appears not to be drastically altered. These first results demonstrate that the 9-methyl group influences the early and later parts of the photoreaction. Low-temperature static infrared difference spectra have revealed that already at 80 K the KL intermediate is produced (for native BR this transition occurs only at 135 K [15-17]). The formation of L is normal, but its decay is slowed down since it can still be observed at 213 K. Time-resolved step-scan FT-IR investigations [17,18] are difficult to perform with this system, since the slow cycling time and the small yield of photoreaction cause a poor signal/noise ratio in the spectra. Therefore, experiments have been performed at 8 cm^{-1} resolution, and the results are shown in Fig. 1. In order to shorten the cycling time, the temperature was raised to 40 °C. The presence of positive bands at 1524 and 995 cm^{-1} in the 700 ns spectrum demonstrate the formation of a red-shifted KL intermediate. The small positive band at 1764 cm^{-1} in the 0.28 ms spectrum shows that M is formed, although with low yield. The later spectra, which last for very long time, are chracteristic of the N intermediate (at this temperature, the photocycle of native BR would last only 1 ms). A pecularity is the ethylenic mode at around 1520 cm^{-1} in the spectra measured between 8 and 280 µs. UV-vis experiments performed with a completely light-adapted sample have shown that it cannot be due to a long-lived KL intermediate. Controls have indicated that it must be ascribed to the red-shifted photoproduct of the 13-*cis*,15-*syn* species present in the sample. This demonstrates that, in contrast to native BR, the slow repetition rate of the laser (0.3 Hz) used for the step-scan measurements was not capable of keeping the sample in the light-adapted state over the long measuring time of over 3 h. Thus, the 9-methyl group influences the efficiency of light-adaptation.

For investigation of the later part of the photocycle we used the time-resolved rapid-scan FTIR technique [7,19], a Xe-flash lamp providing the sample excitation. This caused a large improvement in the quality of the spectra. The results are shown in Fig. 2 for measurements performed at -5 °C. In the first spectrum (6-17 ms) the positive band at 1762 cm^{-1} shows that M is still present (this band is caused by protonation of Asp85), but the amplitude is very low. The positive band at 1163 cm^{-1} indicates the early formation of N. This is in agreement with the negative band at 1741 cm^{-1}, being caused by deprotonation of Asp96 which reprotonates the Schiff base. In the next spectrum, the amplitude of this negative band is somewhat reduced, and the amide-I bands (1620-1700 cm^{-1}) are changed. The amide-I bands now exhibit the typical features of N [20]. This demonstrates that these conformational changes mirrored by the amide-I bands cannot be a prerequisite for Schiff base reprotonation, as has been proposed recently [20,21]. This spectrum, and the following one show that during the life-time of N Asp96 becomes reprotonated. This is in contrast to native BR, where Asp96 becomes reprotonated only with the formation of O. Due to the long life-time of N, no O can be detected. The prolonged life-time is propably caused by an increase in activation entropy, due to the greater flexibility of the chromophore. Since the fingerprint band in the last spectrum have increased and the positive band at 1762 cm^{-1} has decayed, one can conclude that the small amount of M deduced from the first two spectra has decayed to N. The first spectrum, and time-resolved UV-vis measurements indicate that the M-N transition must be, as compared to native BR, very fast. Preliminary experiments with the mutant Trp182Phe, and a recent publication [22], indicate that the 9-methyl group interacts sterically with Trp182. However, this interaction allone cannot explain all the observed effects on the photocycle.

The results clearly demonstrate that removal of the 9-methyl group strongly affects the photocycle and the function of BR. The reduced yield of photoexcitation and the greatly

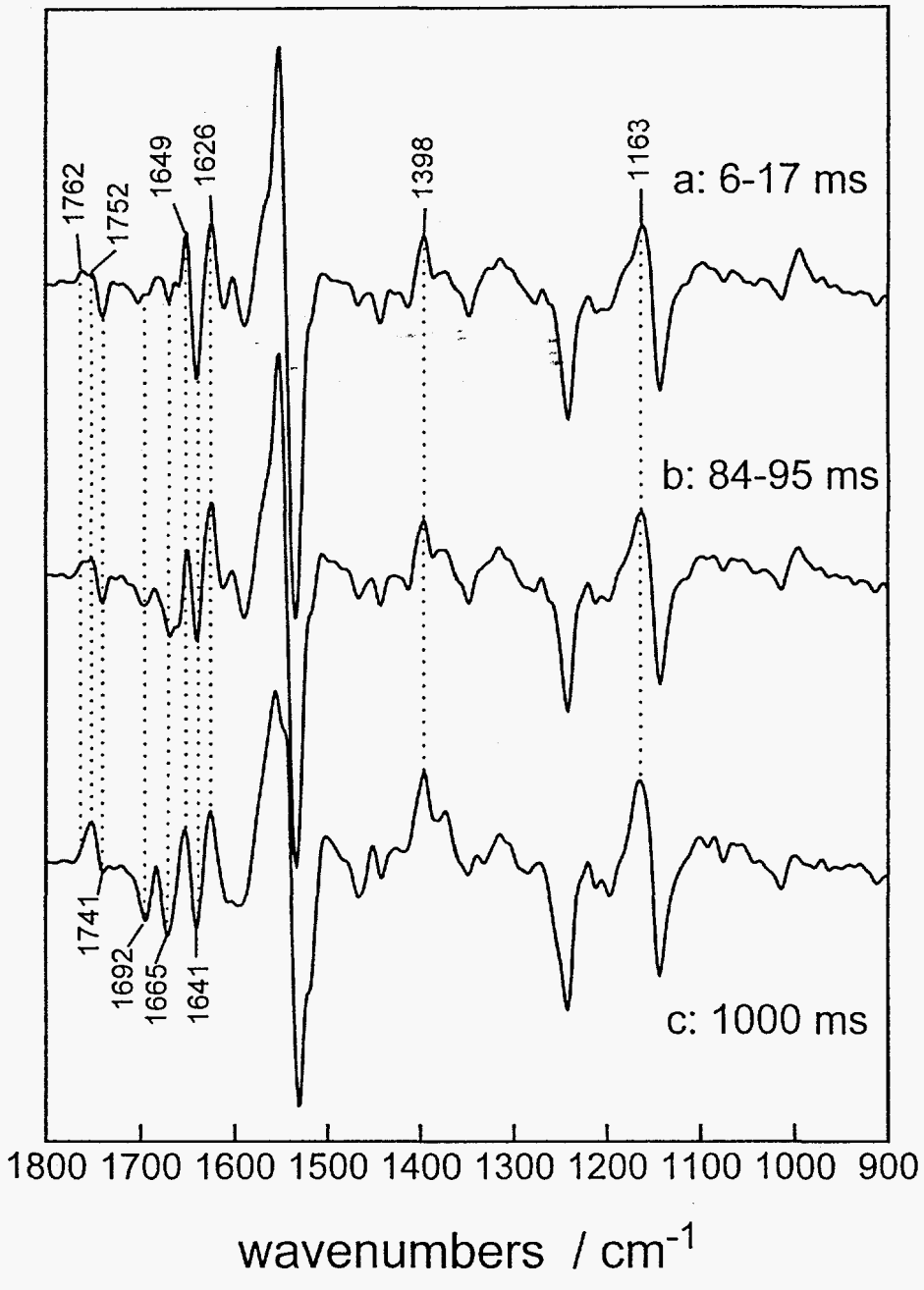

Fig. 2 Time-resolved rapid-scan FTIR difference spectra of 9-demethyl bacteriorhodopsin, measured at -5 °C. The spectra are labelled with the time range elapsed after the flash.

prolonged life-time of N render the pump considerably less effective. Time-resolved infrared measurements have been helpful in identifying the molecular consequences of removing the 9-methyl group. Thus, it appears that the methyl group of the chromophore in retinal proteins are of upmost importance for an efficient coupling of chromophore isomerization and functionally important protein conformational changes.

Acknowledgement

Work supported by the Deutsche Forschungsgemeinschaft, Az Si 278/6-3.

References

1. J.K. Lanyi, Biochim. Biophys. Acta, 1183 (1993) 241.
2. F. Siebert, in Biomolecular Spectroscopy Part A, Ed. R.J.H. Clark, R.E. Hester (John Wiley & Sons: Chichester, 1993) 1.
3. K. Gerwert, Curr. Opin. Struct. Biol. 3 (1993) 769.
4. M.S. Braiman, K.J. Rothschild, Ann.Rev.Biophys.Biophys.Chem. 17 (1988) 541.
5. K.J. Rothschild, J. Bioenerg. Biomembr. 24 (1992) 147.
6. C. Longstaff, R.R. Rando, Biochemistry, 26 (1987) 6107.
7. R. Kräutle, W. Gärtner, U.M. Ganter, C. Longstaff, R.R. Rando, and F. Siebert, Biochemistry, 29 (1990) 3915.
8. G. Papadopoulos, N.A. Dencher, G. Zaccai, and G. Büldt, J. Mol. Biol. 214 (1990) 15.
9. A. Maeda, J. Sasaki, Y. Shichida, and T. Yoshizawa, Biochemistry, 31 (1992) 462.
10. A. Maeda, J. Sasaki, Y. Yamazaki, R. Needleman, and J.K. Lanyi, Biochemistry, 33 (1994) 1713.
11. U.M. Ganter, E.D. Schmid, D. Perez-Sala, R.R. Rando, and F. Siebert, Biochemistry, 28 (1989) 5954.
12. W. Gärtner, P. Towner, H. Hopf, and D. Oesterhelt, Biochemistry, 22 (1983) 2637.
13. K. Fendler, W. Gärtner, D. Oesterhelt, and E. Bamberg, Biochim. Biophys. Acta, 893 (1987) 60.
14. M.A. Marcus, A. Lewis, E. Racker, and H. Crespi, Biochem. Biophys. Res. Commun. 78 (1977) 669.
15. K.J. Rothschild, P. Roepe, and J. Gillespie, Biochim. Biophys. Acta, 808 (1985) 140.
16. J. Sasaki, A. Maeda, C. Kato, and H. Hamaguchi, Biochemistry, 32 (1993) 867.
17. O. Weidlich, F. Siebert, Appl. Spectrosc. 47 (1993) 1394.
18. W. Ulmann, A. Becker, C. Taran, and F. Siebert, Appl. Spectrosc. 45 (1991) 390.
19. K. Fahmy, O. Weidlich, M. Engelhard, J. Tittor, D. Oesterhelt, and F. Siebert, Photochem. Photobiol. 56 (1992) 1073.
20. J.M. Pfefferlé, A. Maeda, J. Sasaki, and T. Yoshizawa, Biochemistry, 30 (1991) 6548.
21. J. Sasaki, Y. Shichida, J.K. Lanyi, and A. Maeda, J. Biol. Chem. 267 (1992) 20782.
22. Y. Yamazaki, J. Sasaki, M. Hatanaka, H. Kandori, A. Maeda, R. Needleman, T. Shinada, K. Yoshihara, L.S. Brown, and J.K. Lanyi, Biochemistry, 34 (1995) 577.

Effects of Vibrations in Chemical Dynamics: High-Frequency Vibrational and Low-Frequency Solvent Dynamical Effects on Intermolecular Electron Transfer

Keitaro Yoshihara, Haridas Pal, Hideaki Shirota, Yutaka Nagasawa and Keisuke Tomianga

Institute for Molecular Science, Myodaiji, Okazaki 444, JAPAN

INTRODUCTION

For the past decade critical comparison between theory [1-5] and experiments [6-13] has been giving important insight into the dynamical aspects of electron transfer (ET) in solution. Contemporary theories on ET which consider finite response of solvent polarization relaxation have predicted that the barrierless ET recations are controlled by the solvent fluctuations and the ET rates cannot exceed the inverse of the solvation time [2,5]. This theoretical prediction has been tested for several ET systems in polar solvents [14-16].

More recent attention in ET studies has been focused on the understanding of the role of internal degrees of freedom in the reaction [3-5,17]. The work is partly motivated by the observation of ET with reaction rates much larger than the solvation rates, which cannot be rationalized by the solvent-cotrolled ET theories and suggests the important contribution of the vibrational modes in ET [6-13].

In this work we report our recent work on substituent and deuterium isotope effects on ultrafast intermolecular ET with highlighting the role of vibrational modes in the reaction [5-13]. The observed reaction kinetics can be succesfully explained in terms of a new theoretial model which incorporates both solvation and vibrational dynamics as well as vibrational excitation in the ET process [3-6].

THEORETICAL BACKGROUND

Recently Barbara and coworkers observed photoinduced intramolecular ET which are much faster than the solvation process [6-8]. We observed photoinduced intermolecular ET between the electronically excited dye molecules and the electron donating solvents where ET occurs much faster than the solvation dynamics [9-13]. In order to explain these ET dynamcis it is necessary to invoke the two dimensional ET model (2D-model) [3,4] along with its extension by incorporating the participation of high-frequency vibrational modes [5,6]. The extended 2D-model includes two vibrational degrees of freedom: a quatized high frequency mode (ν_h) of the product which acts as the accepting mode in the ET and a classical low frequency mode (nuclear coordinate, q) which serves to drive ET in the absence of solvent fluctuation. A third degree of freedom corresopnds to an overdamped solvent coordinate, X. ET occurs with a rate which is dependent on the position along the X coordinate. A conceptual picture for the extended

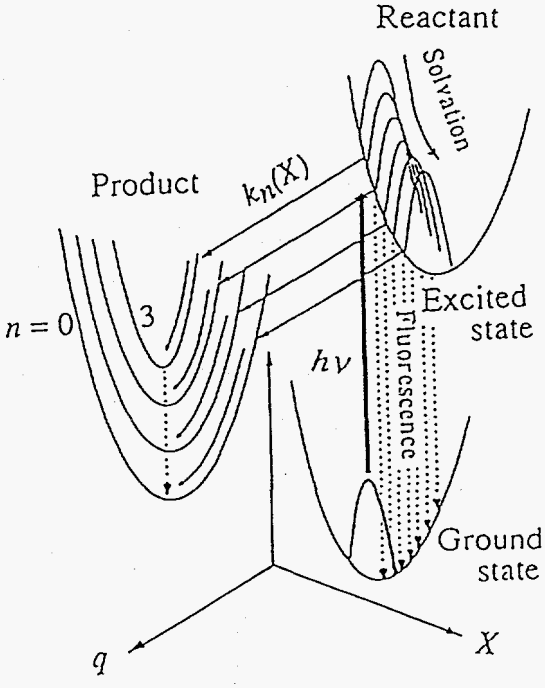

Figure 1: A conceptual picture of the 2D-model. Solvation occurs on the solvation coordinate (X) and ET occurs on the nuclear coordinate (q) with the participation of the high frequency vibrational mode (n).

2D-model is shown in Figure 1. The motion of the population along X can beexpressed by the diffusion-reaction equation [3,4],

$$\frac{\partial p(X,t)}{\partial t} = D\frac{\partial}{\partial X}\left[\frac{\partial}{\partial X} + \frac{1}{k_B T}\frac{dV(X)}{dX}\right] p(X,t) - \sum_n k_n(X)\, p(X,t) \qquad (1)$$

where D is the solvent polarization diffusion coefficient, $V(X)$ is the free energy of the reactant, $p(X,t)$ is the classical probability distribution function at X and t and $k_n(X)$ is the X coordinate dependent reaction rate corresponding to the n-th high frequency vibrational state of the product. The reaction rate $k_n(X)$ is expressed as [6]

$$k_n(X) = \frac{2\pi (V_{el}^{0\to n})^2}{\hbar\sqrt{4\pi\lambda_l k_B T}}\, exp\left(-\frac{(\Delta G_0^{0\to n}(X) + \lambda_l)^2}{4\lambda_l k_B T}\right) \qquad (2)$$

Here λ_l is the reorganization energy of the classical low frequency vibrational mode. $(V_{el}^{0\to n})$ is the effective electronic matrix element considering the Franck-Condon overlap between the ground vibronic state of the reactant and n-th vibronic state of the product and is expressed as,

$$(V_{el}^{0\to n})^2 = V_{el}^2 \left|\langle 0|n\rangle\right|^2 = V_{el}^2 \{(S^n/n!)\, exp(-S)\} \qquad (3)$$

where $S = \lambda_h/h\nu_h$, is the electron-vibrational coupling strength and λ_h and ν_h are the reorganization energy and frequency respectively of the quantized high frequency mode. $\Delta G_0^{0\to n}(X)$ is the effective energy gap between the ground vibrational state of the reactant and n-th vibrational state of the product and is solvent coordinate dependent as,

$$\Delta G_0^{0\to n}(X) = \lambda_S + \Delta G_0 - 2\lambda_S X + nh\nu. \qquad (4)$$

Here it is assumed that the vibrational relaxation of the internal degrees of freedom in the reactant and product is very fast on the ET time scale.

SUBSTITUENT EFFECTS

We have studied intermolecular ET from aniline (AN), N-alkyl anilines and N,N-dialkyl anilines to a number of excited (S_1) cumarin dyes by femotosecond fluorescence up-conversion technique [10,11]. The fluorescence decays of 4-CF_3, 7-amino coumarins in AN and DMA (N,N-dimethyl aniline) are shown in Fig. 2. In these series of measurements, there are several interesting observations. (1) For most of the cases the ET is faster than the diffusive solvation process.(2) Most of them shows non-exponential fluorescence decay. The results of analysis are tentatively made with a double exponential function. (3) The ET rate drastically depends on the substituent groups of the coumarin. Thus as the alkyl chain in the 7-amino group is extended the reaction becomes slower and when it forms a hexagonal ring with the benzene moiety the reaction becomes the slowest. (4) The ET rate also drastically depends on the substituents at the amino group of the electron donor. Thus for N-alkyl and N,N-dialkyl anilines the ET rates are much larger than those in AN.

We first focus our attention on the effect of substitutions at the 7-position of the 4-CF_3,7-amino coumarins. The differences in substitutions can cause a change in the energy gap (ΔG_0) between the reactant and product states. It can also cause a change in the frequencies of the vibrational

modes involved in the ET process. Extending the alkyl chain may also restrict the flexibility of the 7-amino group and thus reducing the ET rates. We mainly attribute the substituent effects to the difference in ΔG_0 and perform the simulation based on the extended 2D-model keeping other ET parameters fixed. ΔG_0 was estimated from the steady-state spectroscopic and cyclic voltammetric measurements. It is to be mentioned that simulation reproduces very nicely the experimental trend of the ET rates with energy gap [12].

Usually coumarin dyes change their electric dipole moments drastically upon photo-excitation. Therefore, the initially prepared state in the reactant is away from thermally equilibrated one in the S_1 state (see fig.1). The fate of this reactant state is either to perform solvation on the X coordinate or to react along the q coordinate, depending on the ET rate. We can expect competition between the ET dynamics and solvation process if both processes occur in the same time scale. In the case of the fast reacting systems (large $-\Delta G_0$), the initially prepared state in the X coordinate is close to or in the region where the effectively reacting vibrational channels are located; the reaction quickly takes place through these channels without much solvation. By reducing $-\Delta G_0$, the initial population in the X coordinate is away from the effective vibrational channels and should react through less effective channels or perform solvation to reach more effective channels. In this case the reaction occurs relatively slowly compared to the case of the large $-\Delta G_0$.

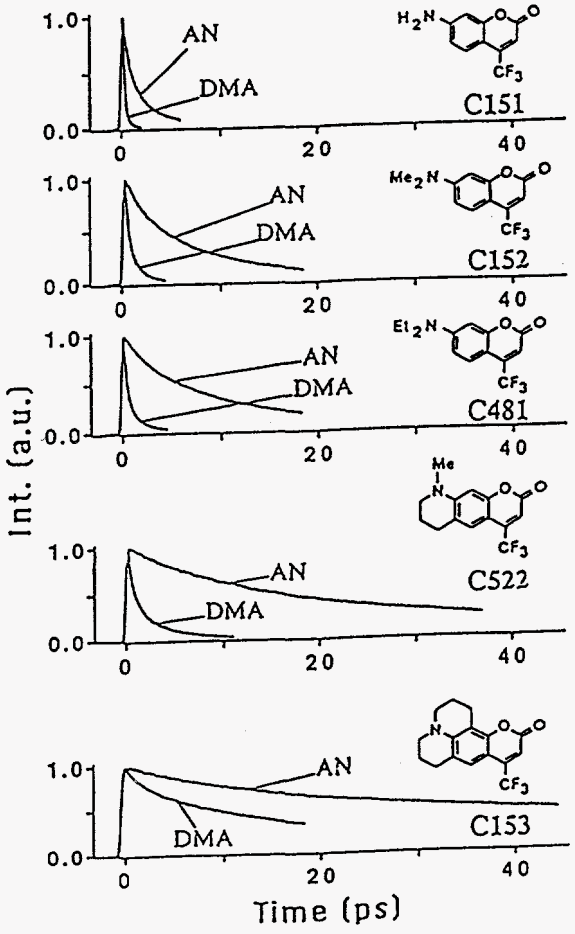

Figure 2: Fluorescence decays of 4-CF_3 coumarins in AN and DMA. The effect of substituents of both the acceptor (coumarins) and the donor (AN and DMA) is indicated.

We now focus our attention on the effect of substitutions at the amino group of the electron donors. As the NH_2 group hydrogens of AN is substituted by alkyl groups the ET rate becomes drastically faster. The effect becomes very drastic on substituting the first amino hydrogen of AN by alkyl group. The effect of substitution of the second hydrogen is not that strong. Among the N,N-dialkyl anilines as the chain length of the alkyl group is increased the ET rate becomes substantially reduced. Thus ET rate gradually reduces as we go from N,N-dimethyl to N,N-diethyl to N,N-dipropyl aniline. In the case of N-alkyl anilines the effect of the alkyl chain length on the ET rate is not much. Thus the ET rates for N-methyl, N-ethyl and N-propyl anilines are almost in the same range. These results are tentatively explained from the following considerations. The +I effect of the alkyl groups makes the amine stronger electron donor and thus faster the ET rate. The other opposing effect probably comes from the high fequency mode involved in the ET process, which is most expectedly associated to the amino group of the electron donor. The higher mass of the N-alkyl groups reduces the frequency of this high frequency mode and consequently reduces the ET rate. It is possible that in case of N,N-dialkyl anilines the effect of high frequency mode predominates over the +I effect and thus makes ET rates slower with increasing the alkyl chain length. For N-alkyl anilines the two opposing effects may be compensating each other to make ET

rates almost independent of the alkyl chain length. It may also be possible that for N-alkyl anilines the bulkiness of the alkyl groups can have a retarding effect to the ET rate. The studies are in progress to characterise the origin of the donor substitution effects on the ET dynamics.

DEUTERIUM ISOTOPE EFFECTS

We have investigated deuterium isotope effect in the ET dynamics for the present systems using deuterated donors, such as, AN-d2 ($C_6H_5ND_2$), AN-d7 ($C_6D_5ND_2$) and DMA-d6 ($C_6H_5N(CD_3)_2$) and also deuterated acceptors such as C151-d2 (7-amino group is deuterated) and C152-d6 (7-amino methyl group is deuterated). The intention of these studies was to have a better understanding of the mechanistic details of the ultrafast ET processes in the present systems. Deuterium isotope effect on the ET dynamics have also been demonstrated to give information regarding the contribution of the tunnelling effects through high frequency quantum modes [18] and also the effect arising from the solvent structures which are altered on deuteration [19].

Using AN-d2 and AN-d7 as the electron donors we observe quite substantial amount of isotope effect on the ET rates for all the coumarin dyes. With both the deuterated solvent donors the ET rates are slowed down at the same extent in comparison to those in normal AN. Thus it appears that the isotope effect in these two solvents is mainly associated with the NH_2 group of AN. Fig.3 shows some of the fluorescence decays observed in AN-d7 and compares these with the corresponding ones observed in normal AN.

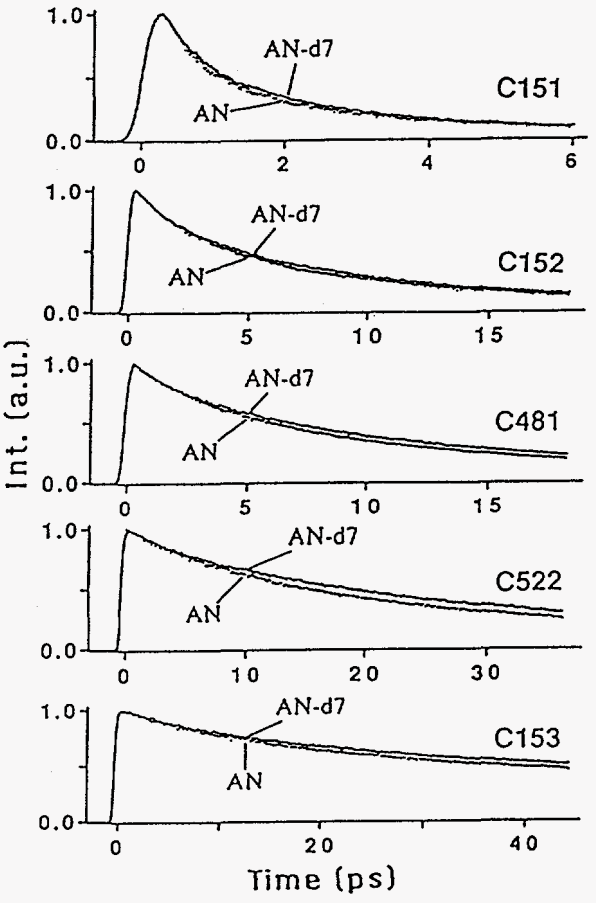

Figure 3: Fluorescence decays of 4-CF_3 coumarins in AN and AN-d7. Isotope effect on the ET dynamics is indicated.

Though with deuterated AN the ET rates become clearly slower, there is no isotope effect when we use DMA-d6 as the electron donor. Similarly using deuterated acceptors (C151-d2 and C151-d6) we do not observe any isotope effect in the ET dynamics. Thus the isotope effect is typical for AN and must be related to the free NH_2 group. It is very much expected that some high frequency vibrational mode of the amino group of the donor (AN and DMA) could be coupled to the ET process.The frequency of this mode is expected to get lowered on isotopic substitution and this in turn should reduce the ET rate. Since with DMA-d6 there is no isotope effect in the ET dynamics, it is not very clear about the isotope effect on this high frequency mode. Probably the effect of the high frequency mode towards the observed isotope effect is not very high.The other origin of the isotope effect in the ET dynamics could come from the solvent structure. Since AN is an intermolecularly hydrogen bonded solvent and since deuteration of such solvents makes these hydrogen bonds more stronger [20], it is expected that the solvent structures around the reactant and product could be different in normal and deuterated AN [18]. Such differences can reduce the reaction exothermicity ($-\Delta G_0$ less) for the present systems and thus can make the ET process slower in the deuterated solvent [19]. We measure the reduction potential of a coumarin dye (C153) in AN-d7

by cyclic voltammetry and is seen to be about 10mV more negative than that in normal AN. Thus it appears that the alteration of the solvent structures around the reactant and product largely contribute to the deuterium isotope effect in the present systems. It is also likely that a small contribution to the observed isotope effect can come from the zero point energy. Since we do not observe any isotope effect with DMA-d6, it indicates that the effect of zero point energy could be very small for the present system. Other support for this is that the oxidation potential of AN and AN-d7 in acetonitrile is measured (by cyclic voltammetry) to be the same within experimental error.

We have also investigated the deuterium isotope effect using N-alkyl anilines where the NH hydrogen was deuterated. For all the deuterated N-alkyl anilines we observe isotope effect in the ET dynamics just similar to those observed with deuterated AN. Thus it is very evident that the isotope effect is directly associated to the NH hydrogens and strongly related to the hydrogen bonded structures in these solvents.

References

1. R. A. Marcus and N. Sutin, Biochim. Biophys. Acta, 811 (1985) 265.
2. L. D. Zusman, Chem. Phys., 49, 295 (1980).
3. N. Agmon and J.J. Hopfield. J. Chem. Phys., 78 (1983) 6947.
4. H. Sumi and R. A. Marcus, J. Chem. Phys., 84 (1986) 4894 .
5. J. Jortner and M. Bixon, J. Chem. Phys., 88 (1988) 167.
6. G. C. Walker, E. Akesson, A. E. Johnson, N. E. Levinger, and P. F. Barbara, J. Phys. Chem., 96 (1992) 3728.
7. P. J. Reid and P.F. Barbara, J. Phys. Chem., 99 (1995) 3554.
8. K. Tominaga, D. A. V. Kliner, A. E. Johnson, N. E. Levinger, and P. F. Barbara, J. Chem. Phys., 98 (1993) 1228.
9. T. Kobayashi, Y. Takagi, H. Kandori, K. Kemnitz and K. Yoshihara, Chem. Phy. Lett., 180 (1991) 416.
10. Y. Nagasawa, A. P. Yartsev, K. Tominaga, A. E. Johnson, and K. Yoshihara, J. Am. Chem. Soc., 115 (1993) 7922.
11. Y. Nagasawa, A. P. Yartsev, K. Tominaga, A. E. Johnson, K. Yoshihara, J. Chem. Phys., 101 (1994) 5717.
12. Y. Nagasawa, A. P. Yartsev, K. Tominaga, P. B. Bisht, A. E. Johnson, and K. Yoshihara, J. Phys. Chem., 99 (1995) 653.
13. K. Yoshihara, K. Tominaga and Y. Nagasawa, Bull. Chem. Soc. Jpn., 68 (1995) 696.
14. E. M. Kosower and D. Huppert, Annu. Rev. Phys. Chem., 37 (1986) 127.
15. P. F. Barbara and W. Jarzeba, Adv. Photochem., 15 (1990) 1.
16. T. J. Kang, W. Jarzeba, P. F. Barbara, and T. Fonseca, Chem. Phys., 149 (1990) 81.
17. M. Bixon and J. Jortner, Chem. Phys., 176 (1993) 467.
18. E. Buhks, M. Bixon and J. Jortner, J. Phys. Chem., 85 (1981) 3763.
19. M. J. Weaver and S. M. Nettles, Inor. Chem., 19 (1980) 1641.
20. G. Nemethy and H.A. Scheraga, J. Chem. Phys., 41 (1964) 680.

CONTRIBUTED PAPERS

Photoexcitations in Electroluminescent Conducting Polymers: Time-Resolved Absorption, Luminescence, and Infrared Spectroscopy of Pyridine Based Polymers

James W. Blatchford,[a] Scott W. Jessen,[a] Liang-Bih Lin,[b] Jiin-Jou Lih,[b] Darren D. Gebler,[a] Yunzhang Wang,[a] Terry L. Gustafson,[b] and Arthur J. Epstein[a,b]
[a]Department of Physics and [b]Department of Chemistry, The Ohio State University, Columbus, OH 43210

Hsing-Lin Wang, Timothy M. Swager, and Alan G. MacDiarmid
Department of Chemistry, University of Pennsylvania, Philadelphia, PA 19104-6323

Tetsuro Yuzawa, Tahei Tahara, Shoichi Yamaguchi, and Hiro-o Hamaguchi
Kanagawa Academy of Science and Technology, KSP East 301, 3-2-1 Sakato, Kawasaki 213, Japan

The recent demonstration of electroluminescence in the conjugated polymers poly(*p*-phenylene vinylene) (PPV) [1] and poly(*p*-phenylene) (PPP) [2], and the subsequent promise of commercially viable polymer light-emitting devices (LEDs), has resulted in substantial research effort, both toward understanding the underlying photophysics of such systems and also toward the development of improved materials for LED applications. As an active layer for LEDs, both PPV and PPP have substantial shortcomings: both polymers are insoluble and, in general, must be thermally converted from a spun precursor film [3]. Also, PPV films have been shown to be susceptible to oxygen degradation via carbonyl formation [4,5]. We summarize here results for an analogous class of conjugated polymers based on pyridine, in particular poly(*p*-pyridyl vinylene) (PPyV) and poly(*p*-pyridine) (PPy). The electron-deficient nature of these polymers may render them less susceptible to oxidation, as well as improve their transport properties. In addition, the incorporation of a nitrogen heteroatom into the conjugated backbone of these polymers renders them soluble, and therefore processible, in weakly acidic solvents such as *m*-cresol or formic acid (HCOOH). In the following, we present the results of extensive optical studies on both PPy and PPyV, encompassing techniques such as cw and time-resolved fluorimetry, femtosecond to millisecond photoinduced absorption, and nanosecond to millisecond photoinduced infrared activity. We have taken advantage of the solubility of these polymers and studied them in both solution and solid forms. The results indicate that Coulombically bound excitons are the primary photoexcitations in both systems. Furthermore, an enhancement of intersystem crossing due to the influence of the nitrogen nonbonding orbitals allows detailed study of the physics of triplet excitons in these systems.

EXPERIMENTAL

The syntheses of PPy and PPyV are reported elsewhere [6,7]. Samples were obtained in powder form and were mixed with KBr for experiments. Solution samples were obtained by dissolving the polymer in HCOOH. Film samples were obtained by spinning or dropping the solution onto quartz or glass substrates. The femtosecond photoinduced absorption (fs PA) measurements were performed using 3.2 eV excitation from a doubled Ti:Sapphire oscillator/amplifier [8]. The picosecond PA and

photoluminescence (PL) measurements utilized 2.8 eV or 4.2 eV excitation from a synchronously pumped dye laser system [9]. The ps PA measurement utilized a second synchronously pumped dye laser, and the ps PL was detected via time-correlated single photon counting. The nanosecond photoinduced infrared (ns IR) measurements [10] were performed using 3.5 eV radiation from a tripled Nd:YAG laser. The millisecond PA and photoinduced IR measurements were performed under excitation from a cw argon-ion laser [11]. The cw measurements were performed on conventional spectrometers.

RESULTS

Figure 1 displays the PL and absorbance spectra of PPy and PPyV in both solution (solid lines) and powder (dashed lines) forms. The absorption spectra of both polymers in solution lack vibronic structure, indicative of strong inhomogeneous broadening, possibly due to a distribution of chain lengths. The solution PL spectra show somewhat more vibronic structure, especially for PPy. The excitation spectra for the PL (not shown) is strongly peaked at the energy of maximum emission in both polymers, indicating that lattice relaxation around the excited state is minimal in solution.

The absorption spectra for powder samples show somewhat greater broadening than the solution spectra, indicative of further disorder in powders. For both polymers, the powder PL spectrum shows a slight redshift with respect to the solution PL spectrum. In PPyV, this phenomenon may simply be due to reabsorption of the emission by the sample. For PPy, an additional Stokes shift due to lattice relaxation or excimer formation may be present [12].

The ps PA spectrum of PPyV at 'zero' time delay is shown in Fig. 2 for powder (circles), solution (solid line) and film forms (x) of PPyV. The solution data are the results of broadband fs PA measurements, integrated over the first 10 ps of time delay. For reference, the powder PL and absorption spectra are also reproduced in the Figure. A strong PA signal is seen which peaks at 1.5 eV. The solution PA becomes negative above 2.2 eV due to stimulated emission, crossing over to photoinduced bleaching of the absorption edge at higher energies.

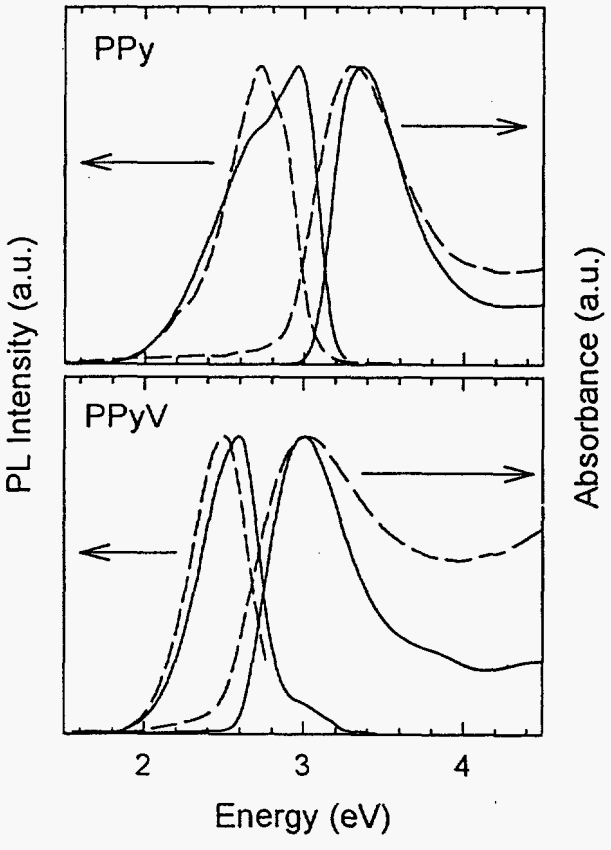

Figure 1: Absorption and PL spectra of PPy and PPyV in solution (solid lines) and powder (dashed lines) forms.

In solution, the time dynamics of the PL and PA are identical, indicating that

both the PA and PL are due to the same excited state [9]. Moreover, the powder and solution PA have the same time dynamics for delays <700 ps, indicating that the same state is produced in solution and powder. In powder samples, an additional long-lived component to the PA appears, peaking at ~1 ns [9]. This long-lived component has a substantially different spectral signature than that of the 0 ps PA in PPyV powders. In fact, the 1 ns PA spectrum more closely resembles the PA spectrum at millisecond time scales. Preliminary results indicate similar behavior in PPy samples. More extensive studies on PPy are in progress.

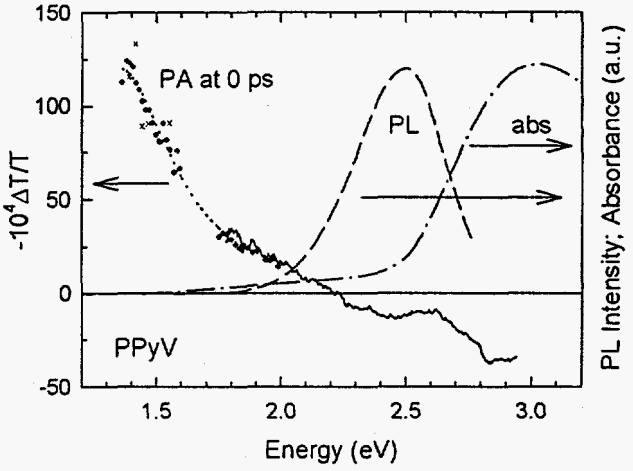

Figure 2: ps PA spectrum at zero delay for PPyV powder (circles) and film (x); fs PA spectrum of PPyV solution (solid line), integrated to 10 ps. Powder PL and absorbance spectra are shown for reference.

Figure 3 shows the ms PA spectrum for both PPy (solid line) and PPyV (dashed line) powder samples. Both show a large PA response, which peaks at ~1.8 eV. The 1.8 eV peak is linear in laser intensity in both polymers [11]. PPyV powders show a second small PA peak at ~0.8 eV, indicated by the arrow in the Figure. This peak has a sublinear intensity dependence and a different frequency dependence from the 1.8 eV peak. The 0.8 eV peak is much more prominent in PPyV films samples.

Figure 4 displays the ns and ms photoinduced IR absorption spectra for both PPy and PPyV powder samples. The ground-state absorption spectra for both polymers are shown for reference. The ms IR signal of PPyV has a uniform intensity and frequency dependence, and has been shown to correlate with the 0.8 eV feature in the electronic spectrum of the ms PA (Fig. 3) [11]. For PPyV, the ns and ms spectra are identical to within experimental error, indicating the same charged species is present at both ns and ms time scales. In addition to photoinduced IR absorption, the PPyV powder samples show significant depletion of the 1470 cm^{-1} ground state mode. Additionally, no strong C-N stretching modes are seen, possibly indicating that the photoinduced charged

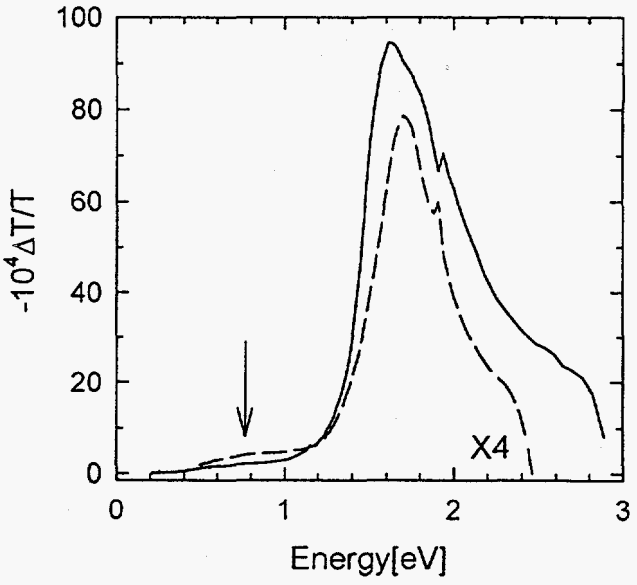

Figure 3: ms PA spectra of PPy (solid line) and PPyV (dashed line).

species resides on the olefin bridge between the pyridine rings.

In contrast, in PPy powders the ms IR spectrum has no observable associated electronic absorption. Furthermore, the ns and ms IR spectra of PPy are clearly different. No ground state depletion is seen in the ns spectrum, indicating a strong dipole moment for the charged species. A strong mode appears in the ns spectrum at 1270 cm^{-1}, in the C-N stretch region, suggesting the presence of a charged defect which is strongly localized on a pyridine ring in PPy. This mode also appears in the ms spectrum, but with a reduction in intensity relative to the other spectral peaks.

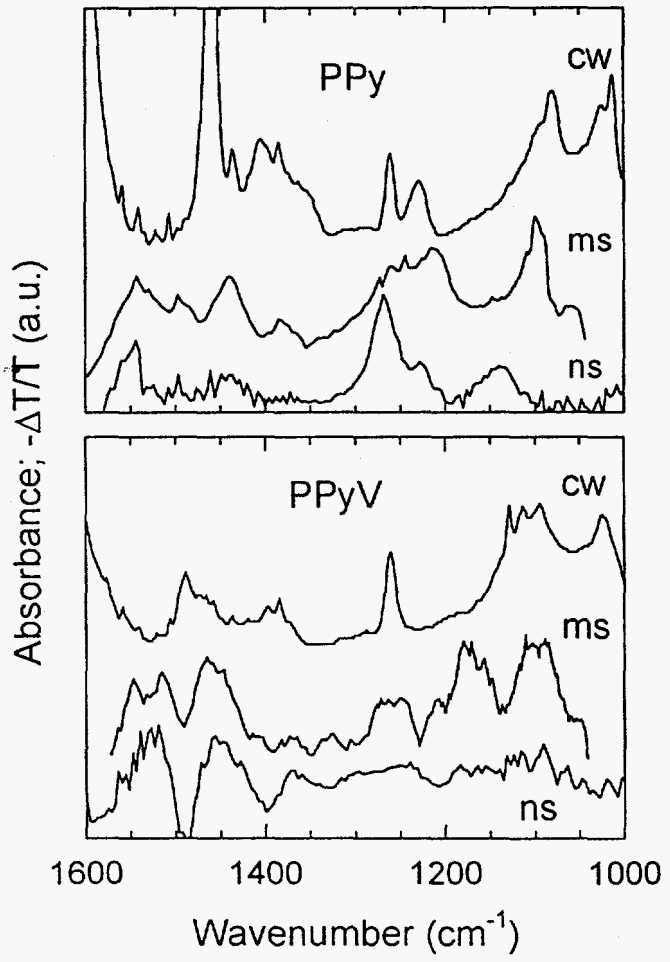

Figure 4: ns and ms photoinduced IR activity of PPy and PPyV powder samples. The ns data have been integrated to 2 μs delay. The ground state IR absorption spectrum for each polymer is shown for reference (cw).

DISCUSSION

The lack of a significant Stokes shift between the PL and excitation spectra of PPy and PPyV in solution indicates that in both polymers the emission is from a state with little accompanying lattice relaxation, which we assume is a singlet exciton [9]. A lack of concentration dependence for both the PL and PA in solution indicates that the exciton is confined to a single polymer chain. The agreement between the PA and PL decays for PPyV in solution indicates that the singlet exciton has a substantial PA signature in this polymer system. The similarity between the PL spectra in powders and films for both polymers suggests that the singlet exciton is also responsible for the emission in powder samples. Concentration quenching via excimer formation therefore does not seem to be the limiting factor in the luminescence efficiency of the powder samples. This conclusion is bolstered by the agreement between the solution and powder PA at early times (<700 ps). We therefore conclude that intrachain singlet excitons are the primary photoexcitations in both powder and solution forms of these polymers.

In powder samples, an additional long-lived state is seen, indicated by the tail of the powder PA in Fig. 3, which evolves very slowly after 1 ns delay. We have demonstrated [9] that the spectral signature of this long-lived species matches that seen on millisecond time scales. Both the ps and ms signals have a linear intensity dependence, suggesting their association with triplet excitons. We

have further demonstrated that the rise of the long-lived component is correlated with the decay of the singlet exciton, indicating that the triplet excitons are created via direct intersystem crossing from the singlet manifold. We suggest that this intersystem crossing is facilitated by the presence of nonbonding electrons, as $(n,\pi^*)^1 \rightarrow (\pi,\pi^*)^3$ transitions are allowed to first order in the spin orbit interaction [13]. While quantum chemical calculations on long oligomers of PPy and PPyV indicate that the lowest (n,π^*) states of these polymers are well above the lowest (π,π^*) states in planar forms of the polymer, deviations from planarity may serve to mix the characters of the (n,π^*) and (π,π^*) states, leading to enhanced triplet production. Such nonplanarity is probably more prominent in the powder form of PPyV, leading to the observation of a triplet component to the powder PA which is not present in the solution PA. Furthermore, the PPy polymer should be forced to nonplanarity by steric interactions, leading to the extremely large triplet-triplet signal seen in the ms PA.

The presence of photoinduced IR modes with associated electronic transitions in PPyV suggests the presence of polaron or bipolaron excitations. The dominance of the excitonic signals in the PA of the powder samples on all time scales suggests that the polarons are not directly photogenerated, but rather result from a small number of excitons which undergo thermal or disorder-induced dissociation. This conclusion is bolstered by the increased generation of polarons in film samples, which spectroscopically appear to be more disordered than the powder samples.

The present results are particularly encouraging with respect to the fabrication of blue light emitting devices. We note that both dc [14] and ac [15] devices have been successfully fabricated using PPy.

Acknowledgments

This research was supported by the Office of Naval Research, the OSU Center for Materials Research, and Kanagawa Academy of Science and Technology.

References

1. J.H. Burroughes *et al.*, *Nature* 347 (1990) 347.
2. G. Grem, G. Leditzky, B. Ullrich and G. Leising, *Synth. Met.* 51 (1992) 383.
3. D.D.C. Bradley, *J. Phys.* D 20 (1987) 1389.
4. M. Yan *et al.*, *Phys. Rev. Lett.* 73 (1994) 744.
5. F. Papadimitrakopoulos *et al.*, *Chem. Mater.* 6 (1994) 1563.
6. T. Yamamoto, T. Ito and K. Kubota, *Chem. Lett.* (1988) 153.
7. M.J. Marsella and T.M. Swager, *Polym. Preprints* 33 (1992) 1196.
8. S. Yamaguchi and H. Hamaguchi, *Chem. Phys. Lett.* 227 (1994) 255.
9. J.W. Blatchford *et al.*, in preparation.
10. T. Yuzawa, C. Kato, M.W. George and H. Hamaguchi, *Appl. Spectrosc.* 48 (1994) 684.
11. S.W. Jessen *et al.*, in preparation.
12. L.B. Lin *et al.*, in preparation.
13. M.A. El-Sayed, *J. Chem. Phys.* 38 (1963) 2834.
14. D.D. Gebler *et al.*, *J. Appl. Phys.*, in press.
15. Y.Z. Wang *et al.*, submitted.

Exciton Self-trapping of Low-dimensional Aggregates of Carbocyanine Dyes

Valey Kamalov[1,2)#] and Keitaro Yoshihara[1)]

[1)]Institute for Molecular Science, Myodaiji, Okazaki, 444 Japan
[2)]Institute of Chemical Physics, Russian Academy of Sciences, Kosygin Street, 4 Moscow 117977 Russia

ABSTRACT

We measured the temperature dependence of emission quantum yields and lifetimes of carbocyanine J-aggregates. Both radiative and nonradiative rate constants are found to be temperature dependent. Radiative lifetime is found to linearly increase as temperature rises and explained by low dimensionality of J-aggregate. Nonradiative relaxation of exciton was observed. We suggest exciton self-trapping determines the nonradiative decay.

INTRODUCTION

It is known since 1930's that dyes form aggregates show a red shifted sharp absorption band compare to the monomer absorption [1]. Recently both dephasing time and emission decay of aggregate in glass was measured at low temperature [2]. A progress in technology of producing small size structures of semiconductor (at the nanometer scale) stimulated a number of authors on the exciton behavior in the low dimensional systems such as quantum wells and quantum wires [3,4]. We discuss on the dimensionality of J-aggregate based on the temperature dependence of the radiative lifetime with a theory developed for Frenkel exciton in this low dimensional semiconductor structures.

The second key result is the observation of subnanosecond dynamics of emission spectra of J-aggregates at low temperature. We explain it as due to nonradiative relaxation of a free exciton to a self-trapped state.

EXPERIMENTAL and RESULTS

Second harmonic of the femtosecond solid state forsterite laser [5] at 607 nm (band center) was used to excite J-aggregate. Two-dimensional data acquisition system based on the streak-camera was used and it had a 40 ps response function (FWHM). Excitation pulse passed through the interference filter for spectral narrowing shown in fig.1 together with the exciton emission at 4K. Exciton emission of J-aggregate of carbocyanine dye in the film of polyvinyl alchohol (PVA) (preparation described in [6]) has a sharp peak at 654 nm with 35 ps lifetime. Absorption and time-resolved emission were recorded in the

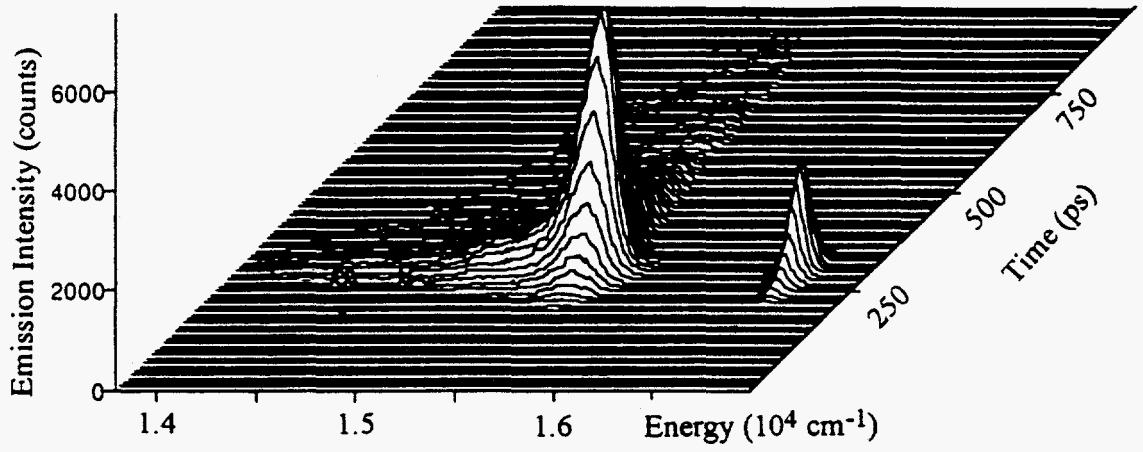

Figure 1: Exciton emission in J-aggregates of carbocyanine dye at low temperature (4K) together with the excitation pulse (second harmonic of forsterite laser at 607 nm).

temperature range of 4-150K to obtain the temperature dependence of emission quantum yields and lifetimes. Excitation intensity was always kept below 10^3 W/cm^2 to prevent possible contribution of two-exciton effects [7].

Radiative Decay

The temperature dependence of radiative lifetime (τ) is plotted in fig.2. It was calculated according to $\tau(T) = \tau_{em}(T) / \Phi(T)$, both emission lifetime (τ_{em}) and quantum yield (Φ) are temperature dependent.

It was realized by Feldmann et al. [3] that the exciton radiative decay time has a temperature dependence $\tau(T)$ which also depends on the dimensionality of the sample. Because of the k-conservation rule, the exciton with large center-of-mass wave vector $k>k_0$ cannot decay radiatively, where k_0 is the wave vector of light with the same energy as the exciton [8]. The effect of the thermalization is characterized by the following parameter $\zeta(T)$, which expresses the fraction of excitons with $k<k_0$. By assuming Maxwell-Boltzmann distribution for excitons [3], $\zeta(T)$ is given by

$$\zeta(T) = \int_0^{\Delta} D(E)e^{-E/k_BT}dE \,/\, \int_0^{\infty} D(E)e^{-E/k_BT}dE \qquad (1)$$

where D(E) denotes the density of states (DOS) of excitons, and $\Delta = \hbar^2k_0^2/2M$ the maximum kinetic energy of excitons which can decay radiatively. The values of $M = 15m_e$ (m_e is the free electron mass; estimation assuming exciton bandwidth of 4V = 0.6 eV [6]) and the photon energy of the observed emission $h\nu$ = 2.1 eV for J-aggregates give $\Delta = 0.6\,\mu$eV. Substituting DOS for 1-dimensional and 2-dimensional systems ($\sim 1/\sqrt{E}$ and constant, respectively), and assuming $T>>\Delta/k_B$, we obtain

$$\zeta_{1D}(T) = \sqrt{4\Delta/\pi k_B T} \quad (2)$$

$$\zeta_{2D}(T) = \Delta/k_B T \quad (3)$$

The average radiative lifetime $\tau(T)$ is then given by

$$\tau_{1D}(T) = \tau_o \zeta_{1D}(T)^{-1} = \tau_o \sqrt{\pi k_B T/4\Delta} \quad (4)$$

$$\tau_{2D}(T) = \tau_o \zeta_{2D}(T)^{-1} = \tau_o k_B T / \Delta \quad (5)$$

where τ_o is the intrinsic radiative lifetime of the exciton at $k \sim 0$. Therefore, for a two-dimensional system, the assumption of a thermal distribution of excitons with the requirement that only excitons with small value of center-of-mass wavevector can recombine radiatively leads to $\tau(T) \sim T$ [3]. Similar consideration for one-dimensional semiconductors (quantum wires) gives $\tau(T) \sim T^{1/2}$, which have recently been confirmed experimentally [4]. The solid line in fig. 2 is the best fit of radiative lifetime of J-aggregate assuming its linear dependence on the temperature. This contradicts with the model of one-dimensional chain usually used for J-aggregates, which should give square route temperature dependence. Several reasons can be considered. First the theory developed for low-dimensional semiconductors should be modified in the case of J-aggregate. Second, one-dimensional chains of J-aggregates can be packed in the crystal parallel to each other so that the effective interaction between them takes place. J-aggregate observed by atomic force microscope contained multi-chain woven or parallel located chains [9].

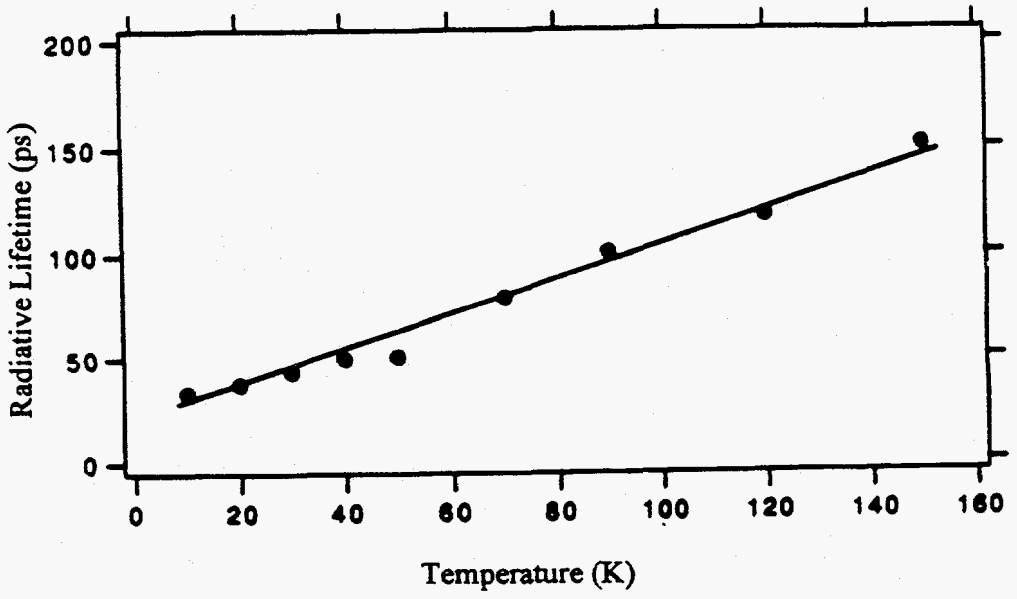

Figure 2: Temperature dependence of radiative lifetime.

Nonradiative Decay

We observed red shift and broadening of emission spectra of carbocyanine dye J-aggregates at low temperature. Fig.3 shows normalized time-resolved spectra of those at 4K. That are exciton emission shown in fig.1 cut at different time delay (100 ps between the spectra) after the excitation pulse. Emission maximum shifted from 654 nm to 659 nm. The characteristic time of the spectral transformation at 4K is about 330 ps. This data allows us to suppose that not only radiative decay of excited state of J-aggregate exists at 4K but there is also a nonradiative decay. The mechanism of nonradiative decay can be the relaxation of a free exciton to a self-trapped state. According to the shift of the maximum of time-resolved spectra the self-trapped exciton state is located 100 cm^{-1} below the bottom of the free exciton state. The free exciton emission quantum yield at 4K can be estimated as 0.9.

The characteristic time of spectral dynamics depends on the temperature. We observed spectral dynamics became faster with the temperature rise. That allows us to suppose that there is an activation barrier between the bottom of the free exciton state and self-trapped state. The corresponding diagram of energy levels is shown in fig.4. At low temperature the transformation of free exciton to self-trapped state through the barrier could be due to exciton tunnelling [10].

The mechanism of self-trapping was studied based on the temperature dependence and will be reported later. Briefly, it can be described as a phonon-assisted tunnelling through the potential barrier at the temperature range 20-60K, and passing over an energy barrier at T > 60K.

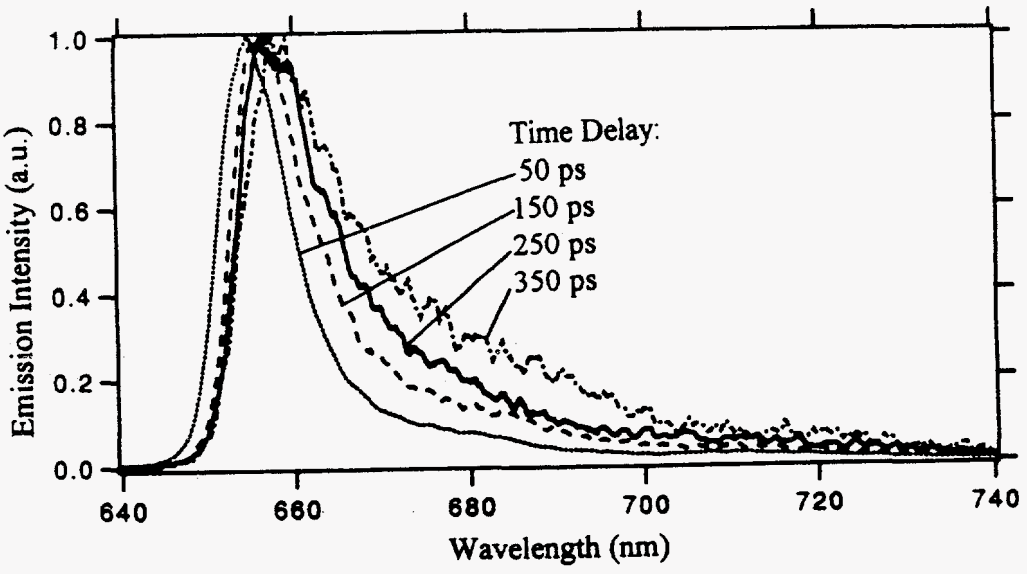

Figure 3: Temporal evolution of emission spectra at low temperature (4K). Time delay 100 ps between spectra.

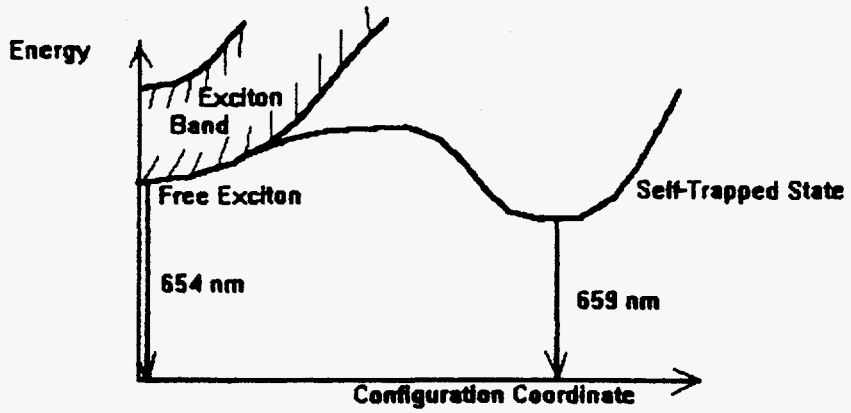

Figure 4: Transformation of a free exciton to the self-trapped state.

CONCLUSION

Temperature dependence of carbocyanine J-aggregate emission was studied. Radiative lifetime was found to linearly increase with temperature. This contradicts with the model of one-dimensional chain of J-aggregates usually used for J-aggregates. Low temperature dynamics of emission spectra of J-aggregates was observed. Relaxation of a free exciton to a self-trapped state is proposed responsible for this dynamics.

Acknowledgements

We appreciate Prof.E.I.Rashba and Prof.M.A.El-Sayed for discussions, Dr.T.Tani for providing a dye powder, Dr.I.A.Struganova and Dr.E.V.Slobodchikov for help in experiments. The research described in this publication was made possible in part by Grant NEF300 from the International Science Foundation and Russian Goverment.

References

#)Present address: V.F.Kamalov, Department of Chemistry, Georgia Institute of Technology, Atlanta, Georgia 30332 USA; e.mail: *Valey.Kamalov@chemistry.gatech.edu*

1. E.E. Jelley, Nature (London), 138 (1936) 1009.
2. S. De Boer, D.A. Wiersma, Chem.Phys.Lett., 165 (1990) 45.
3. J. Feldmann, G. Peter, E.O. Gobel, P. Dawson, K. Moore, C. Foxon, R.J. Elliot, Phys.Rev.Lett., 59 (1987) 2337.
4. H. Akiyama, S. Koshiba, T. Someya, K. Wada, H. Noge, Y. Nakamura, T. Inoshita, A. Shimizu, H. Sasaki, Phys.Rev.Lett., 72 (1994) 924.
5. V.F. Kamalov, A.P. Lifanov, B.I. Minkov, E.V. Slobodchikov, Quant.Electr., 1995.
6. V.F. Kamalov, I.A. Struganova, K. Yoshihara, J.Phys.Chem., to be published.
7. V.F. Kamalov, I.A. Struganova, Y. Koyama, K. Yoshihara, Chem.Phys.Lett. 226 (1994) 132.
8. V.M. Agranovich, Theory of Excitons (Nauka: Moscow, 1968).
9. P.L. Barbara, Private Communication.
10. A.S. Ioselevich, E.I. Rashba, in Quantum Tunnelling in Condensed Media, ed. Yu. Kagan and A.I. Leggett (Elsevier: Amsterdam, 1992) 347.

Sub-microsecond Dispersive Time-resolved Infrared Study on Preliminary Process of Electric-Field-Induced Reorientation of a Ferroelectric Liquid Crystal, 5-(2-Fluoroalkoxy)-2-(4-*n*-alkylphenyl)-pyrimidine

Norihisa Katayama[1)], Takashi Sato[2)], Yukihiro Ozaki[2)],
Katsuyuki Murashiro[3)], Makoto Kikuchi[3)], Shinichi Saito[3)], Dietrich Demus[3)],
Tetsuro Yuzawa[4)], and Hiro-o Hamaguchi[4)]
[1)]*Department of Chemistry, School of Science, Kitasato University,*
[2)]*Department of Chemistry, School of Science, Kwansei Gakuin University,*
[3)]*Research Center, Chisso Petrochemical Corporation,*
[4)]*Molecular Spectroscopy Laboratory, The Kanagawa Academy of Science and Technology,*

ABSTRACT

This paper demonstrates the potential of sub-microsecond dispersive time-resolved infrared spectroscopy in exploring preliminary process of electric field-induced reorientation of ferroelectric liquid crystals (FLCs). A 5-(2-fluorooctyloxy)-2-(4-hexylphenyl)-pyrimidine, which shows the inversion of the spontaneous polarization, is taken up as the example. The observed absorbance change for bands arising from both rigid core and flexible hydrocarbon chains indicates that the FLC molecule reorients from a stationary state with a slight delay (less than 1 μs) just after the upswing of the electric field, while counter-reorientation en route to the reorientation occurs with rather longer delay time after the reverse of the electric field. The delay time for the counter-reorientation is unrelated to the length of the pulse induced. This fact suggests that the theoretical consideration can be applied to dynamics in the preliminary process of the reorientation and that the delay for the counter-reorientation can be interpreted in terms of a rotation of a macroscopic rigid rod. The present study also indicates that the whole FLC molecule reorients simultaneously as a rigid rod in both the preliminary and the counter-reorientation process.

INTRODUCTION

New type of electrooptic device, *i.e.*, surface stabilized ferroelectric liquid crystal (FLC) display, consisting of FLC molecules in a thin LC cell has been developed in these 15 years[1]. The FLC materials in the chiral smectic C phase are potentially useful as the electrically active media in a wide variety of applications, such as displays and light-valves[1-3]. However, the orientation behavior of FLCs is so complicated compared with that of nematic LC, that various approaches must be employed to explore it. In recent years, infrared studies on FLCs by means of several types of time-resolved FT-IR methods have aroused keen interest because the temporal responses of individual infrared bands provide solid information about the detailed reorientation dynamics of FLCs[4-8]. We have used an asynchronous time-resolved FT-IR technique to investigate the electric-field-induced reorientation of FLCs[5,8]. This technique is useful for infrared studies of time-dependent phenomena in the microsecond range. In our previous study on the C* phase of 5-(2-fluorooctyloxy)-2-(4-octylphenyl)-pyrimidine, (8BPyO8(2F)*), in which

was found an inversion of the spontaneous polarization (Ps) with temperature change[9], we obtained the following conclusions[8]: (1) The FLC molecule reorients reversely between positive and negative Ps. (2) The change in the magnitude of the voltage applied has little influence on the rate of reorientation in the region of the positive Ps, while the rate in the region of the negative Ps strongly depends upon the voltage.

In parallel with time-resolved FT-IR techniques, an ac-coupled dispersive time-resolved infrared technique has been developed[10]. This technique is particularly suitable for measurements of response curves of individual absorption bands, so that the time-resolution as high as 50 ns has been achieved with the minimum detectable change $\Delta A/A \sim 10^{-6}$ in the region 4000 to 700 cm^{-1} [11]. This technique has been applied to the studies of the electric-field-induced reorientation of nematic LCs[12,13]. The multiplexing ability of the dispersive system in the time domain was demonstrated very clearly in these studies, in which many temporal response curves of individual absorption bands were measured under a variety of conditions for the applied electric field[12,13].

In the present study we apply the dispersive time-resolved infrared spectroscopy to a FLC, 5-(2-fluorooctyloxy)-2-(4-hexylphenyl)-pyrimidine (6BPyO8(2F)*; Figure 1) which also shows an inversion of the Ps with temperature change (Fig. 1) [14]. The purpose of the present study is to explore further the mechanism of the electric-field-induced reorientation of the FLC in the sub-microsecond time scale.

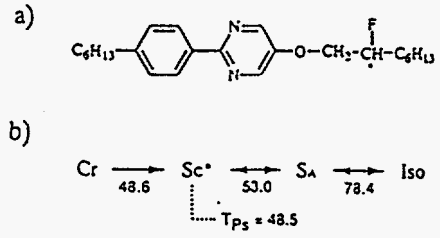

Figure 1. Chemical structure (a) and phase transitions (b) of 6BPyO8(2F)*. This compound shows a Ps inversion at 48.5 °C.

EXPERIMENTAL

A sample cell of 6BPyO8(2F)* was assembled by using BaF_2 windows covered with a thin layer of transparent conductive material (ITO) [5]. A poly(vinyl alcohol) (PVA) film was deposited on the surface of the windows and was rubbed in one direction in order to induce the homogeneous orientation of the sample along the rubbing direction. The cell thickness was controlled to be 3.2 μm. The cell was put into a temperature-control unit consisting of an Omron E5T thermocontroller and a Peltier element. To obtain a good domain, the cell was gradually cooled down (1 $Kmin^{-1}$) from the isotropic phase. The alignment of the FLC molecules was checked by microscopic polarized infrared measurement with a JIR-6500 (Jeol) FT-IR spectrometer. A wire-grid polarizer was placed in front of the LC cell to obtain polarized infrared light; the axis of the polarizer was set parallel to the rubbing direction.

A rectangular pulse wave with a voltage of ± 5.0 V from a function generator (Kenwood FG-273) was applied to the cell. Pulse widths of 5.0, 10.0, 20.0, and 300 μs with repetitions of every

230, 470, 920, and 3000 μs, respectively, were employed for the measurements.

Time-resolved infrared spectra (difference spectra) were recorded on an ac-coupled dispersive time-resolved infrared spectrometer previously reported[10,11,15]. The time resolution in both rise and decay signals of an absorbance change is in the sub-microsecond range. A digital sampling oscilloscope (Tektronix, 2430A) was employed for the measurement of the time response of a certain infrared band at a fixed wavenumber. The axis of the polarizer was set suitable direction for the measurements.

RESULTS AND DISCUSSION

Prior to measurements with short pulse wave, the behavior of reorientation with ordinary electric field was investigated. The electric field with the pulse width of 300 μs and repetition of 3 ms was used for this purpose, and the temperature was changed in the range of 40 to 60 °C. In Figure 2 is shown the temperature dependence of the absorbance change for a band at 1440 cm^{-1} assignable to a ring-stretching mode of the phenylpyrimidine group[8]. This band, the strongest one in the difference spectra of the FLC molecule[8], is very suitable to probe dynamics of its core part. To the best of our knowledge, the decay curves shown in Fig. 2 are the best in terms of a signal-to-noise ratio among all the time-resolved infrared studies of FLCs reported previously[5,7,8,16]. This is by virtue of using the ac-coupled dispersive technique.

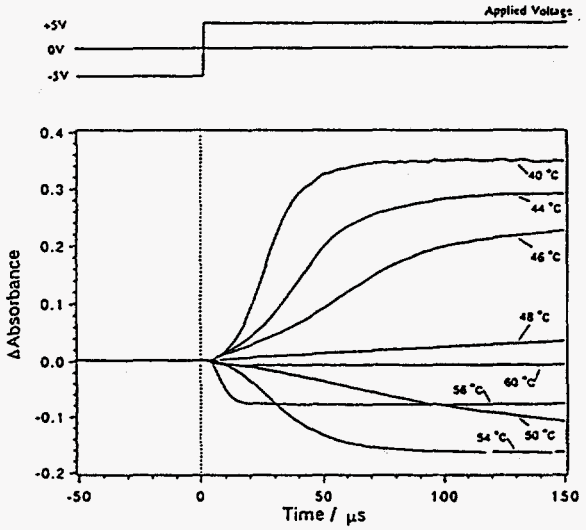

Figure 2. Temperature dependence of the absorbance change for the band at 1440 cm^{-1} in the long-delay time scale. The pulse width and repetition of the electric field were 300 μs and 3 ms, respectively.

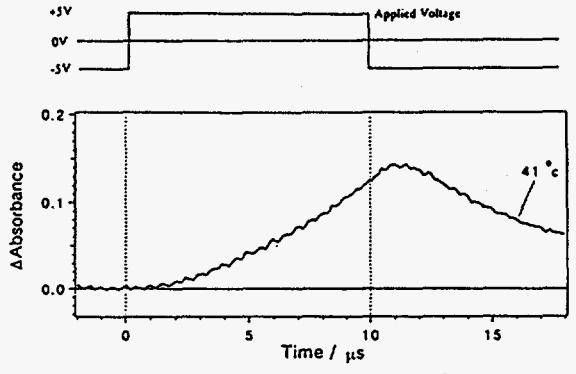

Figure 3. Absorbance change of the 1440 cm^{-1} band at 41 °C. The pulse width and repetition of the electric field were 10.0 and 470 μs, respectively.

With the temperature change, the absorbance decay inverts its polarity; in the lower temperature range the delta absorbance is positive, while in the higher temperature range it is negative. These results for the temperature changes of the rate and extent of reorientation well agree with the measurements of the Ps, response time, and tilted angle reported previously[9].

Figure 3 shows the absorbance decay for the same band in the preliminary process at 41 °C. The pulse width and repetition rate of the electric field were 10.0 and 470 μs, respectively. The

reorientation from the stationary state starts with a slight delay (less than 1 μs) after the leading edge of the positive electric field pulse, while the counter-reorientation occurs with a delay of more than 1 μs after the reverse of the electric field. This result shows that the FLC molecule is very sensitive to the electric field in the stationary state while it needs a rather longer time scale for the counter-reorientation.

Figure 4 compares the absorbance change of the band between 5.0 and 10.0 μs of pulse width measured at 46 °C. The delay of the counter-reorientation is about 1.7 μs in both pulse width, indicating that the pulse width has little influence on the delay time of the counter-reorientation. The angular velocity (the velocity of rotation to a molecule) of the reorientation is almost constant during those time delays. The results obtained in this study indicate that the theoretical consideration [17] can also be applied to dynamics in the preliminary process of the reorientation. The presence of a time delay in the counter reorientation can be interpreted as the consequence of an action of the moment of inertia.

Figure 5 illustrates the absorbance change for a band at 2928 cm^{-1} due to a CH_2 antisymmetric stretching mode. This band was so weak in the time-resolved difference spectra that an electric field with the pulse width of 20.0 μs and repetition of 920 μs was employed. The delay time for the counter-reorientation is *ca.* 1.5 μs, very close to those of the bands arising from the core part. Contrary to the expectation that the hydrocarbon chains have some conformational flexibility and little sensitivity to the electric field, the present result indicates that the whole FLC molecule reorients simultaneously as a rigid rod even in the case of counter-reorientation process, at least within the time resolution of this study. It is also suggested that the same mechanism of the interaction between FLC molecule and electric field is applicable to both the normal and counter-reorientation, although the hydrocarbon chains must receive a force working against their own internal force from the core part.

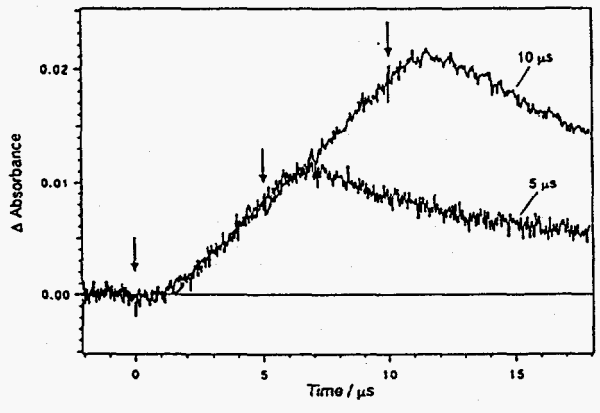

Figure 4. Comparison of absorbance change of the 1440 cm^{-1} band between 5.0 and 10.0 μs pulse width measured at 46 °C.

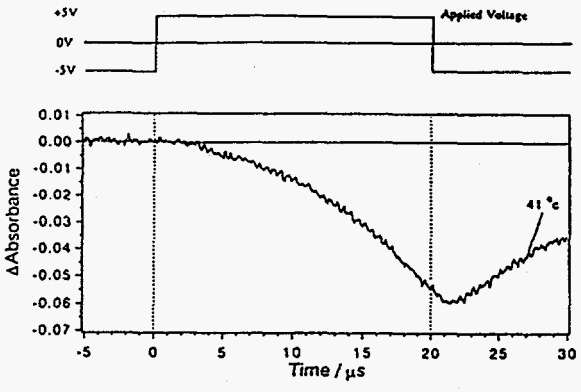

Figure 5. Absorption change of the 2928 cm^{-1} band from the hydrocarbon chains. The pulse width of 20.0 μs and repetition of 230 μs were employed.

CONCLUSION

The present study has demonstrated that the ac-coupled dispersive time-resolved infrared technique is very useful in probing dynamics of the FLC molecule induced by the pulsed electric field. The same experiment, if undertaken with an FT-IR apparatus, would have been prohibitively difficult. The conclusions reached from the present study are summarized as follows: (1) The FLC molecule reorients from the stationary state with a slight delay (less than 1 μs) after the leading edge of the positive electric field pulse, whereas its counter-reorientation takes place with a delay of more than 1 μs after the reversal of the electric field. (2) The whole FLC molecule reorients simultaneously as a rigid rod even in the case of counter-reorientation process, and the same mechanism of the reorientation seems to be applicable to both the preliminary and counter-reorientation. (3) The delays in preliminary and counter-reorientation processes can be interpreted in terms of a rotation of a macroscopic rigid rod having a moment of inertia.

References

1. J.W. Goodby, R. Blinc, N.A. Clark, S.T. Lagerwall, M.A. Osipov, S.A. Pikin, T. Sakurai, K. Yoshino, and B. Zeks, in *Ferroelectric Liquid Crystals: Principles, Properties and Applications;* (Gordon and Breach Science Publishers, Philadelphia, 1991).
2. R.B. Meyer, L. Liebert, L. Strzelecki, and P. Keller, *J. Phys. Lett.*, **36** (1975) 69.
3. H. Tachibana, T. Nakamura, M. Matsumoto, H. Komizu, E. Manda, H. Niino, A. Yabe, and Y. Kawabata, *J. Am. Chem. Soc.*, **111** (1989) 3080.
4. K. Masutani, H. Sugisawa, A. Yokota, Y. Furukawa, and M. Tasumi, *Appl. Spectrosc.*, **46** (1992) 560.
5. M.A. Czarnecki, N. Katayama, Y. Ozaki, M. Satoh, K. Yoshio, T. Watanabe, and T. Yanagi, *Appl. Spectrosc.*, **47** (1993) 1382.
6. T. Nakano, T. Yokoyama, and H. Toriumi, *Appl. Spectrosc.*, **47** (1993) 1354.
7. A. Yasuda, K. Nito, and E. Matsui, *Liq. Crystals*, **14** (1993) 1725.
8. N. Katayama, M.A. Czarnecki, Y. Ozaki, K. Murashiro, M. Kikuchi, S. Saito, and D. Demus, *Ferroelectrics*, **147** (1993) 441.
9. S. Saito, K. Murashiro, M. Kikuchi, T. Inukai, D. Demus, M. Neundorf, and S. Diele, *Ferroelectrics*, **147** (1993) 367.
10. K. Iwata and H. Hamaguchi, *Appl. Spectrosc.*, **44** (1990) 1431.
11. T. Yuzawa, C. Kato, M.W. George, and H. Hamaguchi, *Appl. Spectrosc.*, **48** (1994) 684.
12. T.I. Urano and H. Hamaguchi, *Chem. Phys. Lett.*, **195** (1992) 287.
13. T.I. Urano and H. Hamaguchi, *Appl. Spectrosc.*, **47** (1993) 2108.
14. N. Katayama, T. Sato, Y. Ozaki, K. Murashiro, M. Kikuchi, S. Saito, D. Demus, T. Yuzawa, H. Hamaguchi, *Appl. Spectrosc.*, **49** (1995), in press.
15. C. Kato, K. Iwata, and H. Hamaguchi, *Bunko-Kenkyu*, **40** (1991) 255.
16. K. Masutani, A. Yokota, Y. Furukawa, M. Tasumi, and A. Yoshizawa, *Appl. Spectrosc.*, **47** (1993) 1370.
17. N.A. Clark, M.A. Handschy, and S.T. Lagerwall, *Mol. Cryst. Liq. Cryst.*, **94** (1983) 213.

Photon Echoes as Collective Resonances in Multidimensional Vibrational Spectroscopy of Liquids

Vadim Khidekel, Vladimir Chernyak, and Shaul Mukamel
Department of Chemistry, University of Rochester, Rochester, NY 14627

I. INTRODUCTION

Multidimensional vibrational spectroscopy is a powerful tool for studying the dynamics of molecular and atomic liquids. An ideal time-domain technique that can be successfully carried out with very short pulses is the photon echo observed in high-order Raman or infrared measurements [1–6]. In off-resonant fifth-order Raman experiments the system interacts with two pairs of pulses, and a fifth pulse ($\mathbf{k}_f\omega_f$) generates the signal with the wavevector $\mathbf{k}_s = \pm(\mathbf{k}_1 - \mathbf{k}_1') \pm (\mathbf{k}_2 - \mathbf{k}_2') \pm \mathbf{k}_f$ (Fig. 1). The process is described by the fifth-order[1] response function $S^{(5)}$.

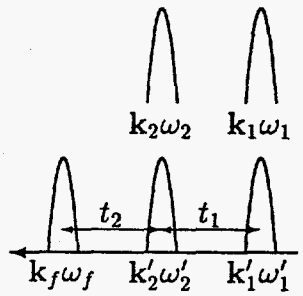

Fig. 1

A close connection between high-order photon echoes in the time domain and collective resonances in the frequency domain was established [7,8]. We compare below two models of a multilevel system with different types of broadening, which produce similar photon echo signals. We first study the effect of static and dynamic correlations in a multilevel system coupled to Brownian oscillator bath. We then consider a model in which the transition frequencies are equal; this corresponds to a harmonic oscillator with a continuous distribution of frequencies, and present numerical simulations of the echo signal. Finally, we analyze the frequency-domain susceptibility of a multilevel system and show how multiphoton resonances appear when the broadening of different levels is correlated. In the time domain these resonances show up as photon echo signals.

II. DYNAMIC CORRELATIONS IN THE BROWNIAN OSCILLATOR MODEL

We study the fifth-order echo signal in a multilevel system (Fig. 2) coupled the Brownian oscillator bath and analyze its dependence on the static and dynamic correlation of the frequencies ω_{ab} and ω_{bc}. We assume short pulses, and the signal is given by $|S^{(5)}(t_1,t_2)|^2$. We consider below only the terms that contribute to the photon echo signal (diagrams in Fig. 3(b)) and denote the contribution of these terms to the fifth-order response by $S^{(5)}_{\rm PE}$. We then have

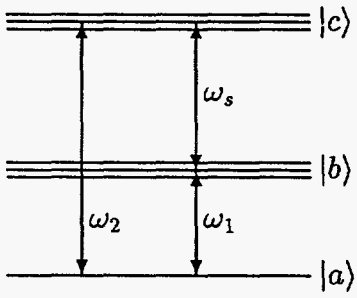

Fig. 2

[1]As far as nuclear dynamics is concerned, the technique has only two time intervals and this response function is equivalent to $S^{(2)}$. Similar resonant infrared results will be described by $S^{(2)}$.

$$S^{(5)}_{\rm PE}(t_1,t_2) = \langle\langle V_{cb}|\mathcal{G}_{bc}(t_2)\mathcal{V}_{bc,ba}\mathcal{G}_{ba}(t_1)\mathcal{V}_{ba,aa}|\rho_g\rangle\rangle + c.c.$$

Here $\mathcal{V}$ is the Liouville-space operator, V being the electronic polarizability, acting on an ordinary operator A through the commutator: $\mathcal{V}A = [V,A]$, and $\mathcal{G}(\tau)$ is the Liouville-space Green function for the system without the radiation field, $\mathcal{G}(\tau) = \theta(\tau)\exp\left(-\frac{i}{\hbar}\mathcal{L}\tau\right)$, $\mathcal{L} \equiv [H,A]$. The coupling to the bath results in fluctuations of the transition frequencies $\omega_{\nu\nu'}$ around $\omega^0_{\nu\nu'}$: $\omega_{ba} = \omega^0_{ba} + \delta\omega_{ba}(t)$, $\omega_{cb} = \omega^0_{cb} + \delta\omega_{cb}(t)$. Then the response function is

$$S^{(5)}_{\rm PE}(t_1,t_2) \propto e^{-i\omega^0_{ba}t_1 + i\omega^0_{cb}t_2}\left\langle \exp\left\{ -i\int_0^{t_1}\delta\omega_{ba}(\tau)\,d\tau + i\int_{t_1}^{t_1+t_2}\delta\omega_{cb}(\tau')\,d\tau'\right\}\right\rangle + c.c.$$

We can calculate the average by expanding the exponent in powers of $\delta\omega$ up to second order; this is known as the second-order cumulant expansion [6].

$$S^{(5)}_{\rm PE}(t_1,t_2) \propto \cos(\omega^0_{ba}t_1 - \omega^0_{cb}t_2)\exp\Big[- g_1(t_1) - g_2(t_2) + g_3(t_1+t_2) - g_3(t_1) - g_3(t_2)\Big], \quad (1)$$

with the line broadening functions

$$\begin{aligned} g_1(t) &\equiv \int_0^t d\tau \int_0^\tau d\tau' \langle \delta\omega_{ba}(\tau)\delta\omega_{ba}(\tau')\rangle, \\ g_2(t) &\equiv \int_0^t d\tau \int_0^\tau d\tau' \langle \delta\omega_{cb}(\tau)\delta\omega_{cb}(\tau')\rangle, \\ g_3(t) &\equiv \int_0^t d\tau \int_0^\tau d\tau' \langle \delta\omega_{ba}(\tau)\delta\omega_{cb}(\tau')\rangle. \end{aligned}$$

We next assume that $g_1(t) = g_2(t) \equiv g(t)$ and $g_3(t) = (1-\zeta)g(t)$, where the parameter ζ represents the correlation between the fluctuations $\delta\omega_{ba}$ and $\delta\omega_{cb}$. $\zeta = 1$ or 0 correspond to uncorrelated or fully correlated fluctuations, respectively. We further adopt the overdamped Brownian oscillator model for the correlation function of level fluctuations

$$\langle \delta\omega_{ba}(t)\delta\omega_{ba}(0)\rangle = \Delta^2 e^{-\Lambda t}.$$

where Δ is the magnitude and Λ^{-1} is the timescale of the fluctuations. In the static limit $\Lambda \ll \Delta$ we get $g(t) \approx \frac{\Delta^2 t^2}{2}$, and upon substituting in (1), we obtain

$$S^{(5)}_{\rm PE}(t_1,t_2) \propto \cos(\omega^0_{ba}t_1 - \omega^0_{cb}t_2)\exp\left\{ -\frac{\Delta^2(t_1-t_2)^2}{2} - \Delta^2\zeta t_1 t_2\right\}. \quad (2)$$

We get an echo signal at $t_1 = t_2$ if the levels are fully correlated ($\zeta = 0$). The temporal width of the echo signal is $\sim \Delta^{-1}$. Thus, the stronger the coupling strenght Δ, the sharper is the echo. In the case of partial correlation $\zeta \neq 0$ the echo (as it appears, for example in Fig. 3(a)) becomes less pronounced, and at $\zeta = 1$ the echo disappears completely.

As the dynamics of fluctuations becomes important (that is, Λ is comparable to or larger than Δ), the echo will be eroded as well; No echo is observed in the motional narrowing (homogeneous) limit $\Lambda \gg \Delta$ where $g(t) \approx \Gamma t$ with $\Gamma \equiv \Delta^2/\Lambda$ and

$$S^{(5)}_{\rm PE}(t_1,t_2) \sim \cos(\omega^0_{ba}t_1 - \omega^0_{cb}t_2)\exp\{-\Gamma(t_1+t_2)\}.$$

III. CONTINUOUS DISTRIBUTION OF HARMONIC OSCILLATORS

We now consider the case of fully correlated levels with $\omega_{ba} = \omega_{cb}$. This system is harmonic [1,9]. We use the Hamiltonian $H = H_0 - E(\mathbf{r},t)V$, where $H_0 = \hbar\omega_0(a^\dagger a + 1/2)$. We also need to specify how the electronic polarizability V depends on nuclear coordinates. With $V(q) = \alpha q$ the response is linear, and all $S^{(n)}(t_n,\ldots,t_1)$ vanish for $n > 1$. We assume $V(q) = V_0 e^{\alpha q}$.

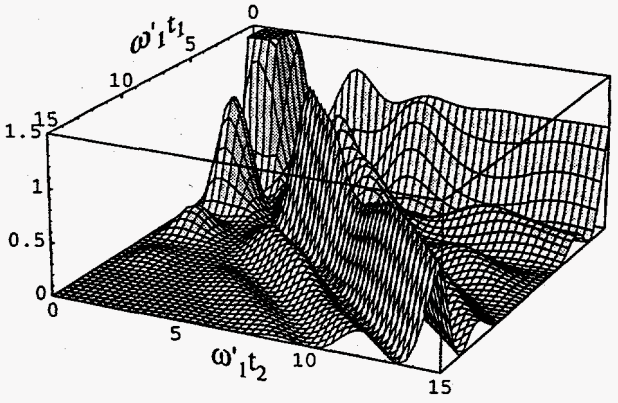

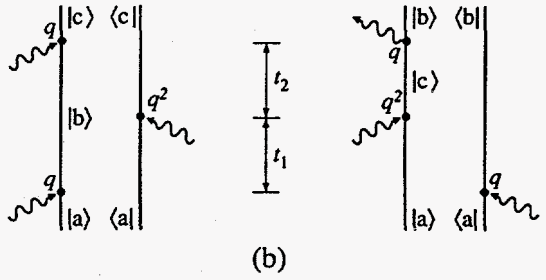

Fig. 3

We now consider the nonlinear response to lowest order in α. For $S^{(5)}$ this is $\sim \alpha^4$. The reason is very simple: there are three interactions with the field, and in the lowest-order nonlinear response we should take one q^2 and two q interactions. This corresponds to expanding the electronic polarizability in the form $V(q) = \alpha q + \frac{1}{2}\alpha^2 q^2$. As a result of each interaction of the q type the system moves either one level up or one level down, whereas the q^2 interaction either moves the system by two levels or does not change its state at all. For the fifth-order response we then have,

$$S^{(5)}(t_2,t_1;\omega_0) = \frac{V_0^3\alpha^4}{m^2\omega_0^2}\Big\{\cos[\omega_0 t_1] - \cos[\omega_0(t_1+t_2)] + \cos[\omega_0(t_1+2t_2)] - \cos[\omega_0(t_1-t_2)]\Big\}. \quad (3)$$

To introduce inhomogeneous broadening, we assume that the oscillator frequency ω_0 is distributed around some central frequency ω_1 with half-width γ:

$$f(\omega_0) = \frac{1}{2\pi}\frac{\omega_0\gamma}{(\omega_1^2-\omega_0^2)^2+\omega_0^2\gamma^2}. \quad (4)$$

The response is then calculated by averaging (3) over the distribution function (4). Hereafter we consider only the last term in (3) that produces the echo signal. In the underdamped limit $\omega_1 \gg \gamma/2$ we obtain

$$S^{(5)}_{\rm PE}(t_2,t_1) = \frac{V_0^3\alpha^4}{4m^2(\omega_1')^2}\cos[\omega_1'(t_1-t_2)]e^{-\gamma|t_1-t_2|}. \quad (5)$$

This resembles Eq. (2). Since (5) is written for a harmonic oscillator, for which $\omega^0_{ba} = \omega^0_{cb}$, the quantum beats, which show up in (2), disappear. Also, the levels of an oscillator are fully correlated, therefore the parameter ζ is zero. Finally, the difference in the echo profile vs $t_1 - t_2$ (Gaussian in (2) and exponential in (5)) reflects the different models used:

the former assumes Gaussian distributions of frequencies, whereas here the distribution is (4), and the parameter γ in (5) plays the role of Δ in (2).

In Fig. 3(a) we show the squared absolute value of the response function (5) as a function of t_1 and t_2 for $\gamma = \omega_1/2$. It is clearly seen that for $t_1 = t_2$ the response does not vanish for long times, resulting in the photon echo signal. The corresponding double-sided Feynman diagrams are given in Fig. 3(b).

IV. COLLECTIVE RESONANCES IN THE FREQUENCY DOMAIN

In this section we analyze the frequency-domain susceptibility of a multilevel system and show how partial correlation in the broadening leads to new multiphoton resonances. In the time domain these resonances show up as photon echo signals. The fifth-order susceptibility of a three-level system is [6]

$$\chi^{(5)}(-\omega_s;-\omega_1,\omega_2) = \frac{1}{\hbar^2}\rho_0 \sum_{\text{perm}} \sum_{a,b,c} P(a) V_{ab} V_{bc} V_{ca} \times \Big\{ I_{ab}(\omega_1) I_{ac}(\omega_1+\omega_2) + I_{ca}(\omega_1) I_{ba}(\omega_1+\omega_2) - I_{ab}(\omega_1) I_{ca}(\omega_2) \Big\} \quad (6)$$

Where $I_{\nu\nu'}(\omega) \equiv (\omega - \omega_{\nu\nu'} + i\Gamma_{\nu\nu'})^{-1}$ are the (frequency-domain) lineshape functions and the levels $|a\rangle$, $|b\rangle$, $|c\rangle$, are shown in Fig. 2. We are interested only in the last term, which gives rise to the desired resonance. In that case,

$$\chi^{(5)}(-\omega_s;-\omega_1,\omega_2) \propto \sum_{\text{perm}} I_{ab}(\omega_1) I_{ca}(\omega_2) = \frac{1}{\omega_1 - \omega_{ba} + i\Gamma} \cdot \frac{1}{\omega_2 - \omega_{ca} - i\Gamma} + c.c'.,$$

where $c.c'.$ denotes complex conjugation with simultaneous changing the signs of ω_1 and ω_2. We now assume that ω_{ba} and ω_{cb} are inhomogeneously broadened with a joint distribution $S(\omega_{ba},\omega_{cb})$:

$$S(\omega_{ba},\omega_{cb}) = N S(\omega_{ba}) S(\omega_{cb}) \frac{\eta}{(\omega_{cb} - \omega_{ba} - \Omega)^2 + \eta^2}.$$

where N is a normalization factor and Ω represents an anharmonicity. This distribution represents partial correlation. In the limit of noncorrelated levels ($\eta \to \infty$) it factorizes as $S(\omega_{ba})S(\omega_{cb})$. In the other extreme of fully correlated levels ($\eta \to 0$), we have $S(\omega_{ba},\omega_{cb}) \sim S(\omega_{ba})S(\omega_{cb})\delta(\omega_{cb} - \omega_{ba} - \Omega)$. Then,

$$\langle \chi^{(5)}(-\omega_s;-\omega_1,\omega_2) \rangle \propto \frac{1}{4\pi^2} \int d\omega_{ba} d\omega_{cb} S(\omega_{ba}) S(\omega_{cb}) \times \frac{\eta}{(\omega_{cb} - \omega_{ba} - \Omega)^2 + \eta^2} \cdot \frac{1}{\omega_1 - \omega_{ba} + i\Gamma} \cdot \frac{1}{\omega_2 - \omega_{ca} - i\Gamma} + c.c'. \quad (7)$$

Assuming that the distributions $S(\omega)$ are much broader than the homogeneous width Γ and the correlation parameter η, we have

$$\langle \chi^{(5)}(-\omega_s;-\omega_1,\omega_2) \rangle \propto S(\omega_1) S(\omega_2) \frac{1}{\omega_2 - 2\omega_1 - \Omega - i\varkappa} + c.c'., \qquad \varkappa \equiv \eta + 3\Gamma. \quad (8)$$

We thus obtained a new resonance with width $\varkappa$. If the two levels were fully correlated, that is, $\eta = 0$, the width would be determined by homogeneous broadening. We next show how this resonance corresponds to the photon echo in the time domain. The time-domain response function is related to the susceptibility as

$$\mathcal{S}^{(5)}_{\rm PE}(t_1,t_2) = \frac{1}{2\pi}\int d\omega_1 d\omega_2 \langle \chi^{(5)}(-\omega_s;-\omega_1,\omega_2)\rangle \exp\{-i\omega_1(t_1+t_2)+i\omega_2 t_1\}. \tag{9}$$

Substituting (8) to (9), we get

$$\mathcal{S}^{(5)}_{\rm PE}(t_1,t_2) \propto e^{i\Omega t_2}e^{-\varkappa t_2}\int d\omega_1 S(\omega_1)S(2\omega_1+\Omega)e^{i\omega_1(t_2-t_1)} + c.c. \tag{10}$$

Assuming a Gaussian distribution, $S(\omega_1) = \exp\{-(\omega_1-\omega_1^0)^2/2\Delta^2\}$. we have,

$$\mathcal{S}^{(5)}_{\rm PE}(t_1,t_2) \propto \cos[\Omega t_2 + \omega_1^0(t_2-t_1)]\exp\left\{-\frac{\Delta^2(t_2-t_1)^2}{2} - \varkappa t_2\right\}. \tag{11}$$

This is similar to the response function (2), derived in Sec. II with the correlation parameter $\varkappa$ playing the role of $\Delta^2\zeta$ in (2).

For a Lorentzian distribution $S(\omega_1) = \gamma/[(\omega_1^2-\omega_1^0)^2+\gamma^2]$ we obtain

$$\mathcal{S}^{(5)}_{\rm PE}(t_1,t_2) \propto \cos[\Omega t_2 + \omega_1^0(t_2-t_1)]e^{-\varkappa t_2-\gamma|t_1-t_2|}. \tag{12}$$

This recovers the echo signal derived in Sec. III (Eq. (5)).

ACKNOWLEDGMENTS

The support of the National Science Foundation and the Air Force Office of Scientific Research is gratefully acknowledged.

REFERENCES

[1] Y. Tanimura and S. Mukamel, J. Chem. Phys, **99**, 9496 (1993).
[2] K. Tominaga and K. Yoshihara, Phys. Rev. Lett. (in press).
[3] T. Joo, Y. Jia, and G. Fleming, J. Chem. Phys, **102**, 4063 (1995).
[4] A. Tokmakoff, A.S. Kwok, R.S. Urdahl, R.S. Francis, and M.D. Fayer, Chem. Phys. Lett, **234**, 289 (1995).
[5] M.S. Pshenichnikov, K. Duppen, and D.A. Wiersma, Phys. Rev. Lett, **74**, 674 (1995); D. Thorn Leeson and D.A. Wiersma, Phys. Rev. Lett, **74**, 2138 (1995)
[6] S. Mukamel, *Principles of Nonlinear Optical Spectroscopy* (Oxford, New York, 1995).
[7] V. Chernyak and S. Mukamel, Phys. Rev. Lett, **74**, 4895 (1995).
[8] V. Chernyak, N. Wang, and S. Mukamel, Phys. Reports (in press).
[9] V. Khidekel and S. Mukamel, Chem. Phys. Lett. (in press).

Photodissociated Cytochrome *bo* Oxidase: A Time-Resolved Raman Study of the Fe-His Stretching Mode

Constantinos Varotsis,* Douglas H. Kreszowski,# Gerald T. Babcock,# Anne Puustinen,§ and Mårten Wikström§

* Department of Chemistry, University of Crete 71409 Iraklion, Crete, Greece, #Department of Chemistry and LASER Laboratory, Michigan State University, East Lansing, Michigan 48824, §Helsinki Bioenergetics Group, Institute of Biomedical Sciences, Department of Medical Chemistry, P.O. BOX 8, 000014 University of Helsinki, Helsinki, Finland

Cytochrome *bo* is a terminal ubiquinol oxidase in the aerobic respiratory chain of *Escherichia coli.*[1-2] This membrane protein catalyzes the four-electron reduction of molecular oxygen to water, and couples the two-electron oxidation of ubiquinol-8 oxidation with dioxygen reduction to translocate protons across the energy-transducing cytoplasmic membrane. The *bo*-type cytochrome oxidase contains a low-spin heme B, a high spin heme O and an EPR silent copper which is antiferromagnetically coupled with the high spin heme-iron in the oxidized state of the enzyme.[3] Site-directed mutagenesis experiments have been carried out for the cytochrome *bo* complex to clarify the coordination of amino acid residues to cytochrome *o* and Cu_B.[12-18] The current view places four conserved histidines at the oxygen-activating heme-copper binuclear center: His 284,-333, and-334, are assigned as Cu_B ligands while His 419 is assigned as the proximal ligand of cytochrom *o*. Recently, in a report on the Raman spectrum of cytochrome *bo*, the mode observed at 208 cm^{-1} showed an isotopic shift of 1 cm^{-1} upon substitution of ^{56}Fe with ^{54}Fe and accordingly, was assigned to the $\nu(Fe^{2+}$-His) of the wild-type ferrous cytochrome *o*.[4] Direct detection of cytochrome *o* and Cu_B/bound ligand vibrations is necessary to test the proposed proton pump mechanism as well as to provide detailed information on the pathways and control of electron transfer. Ultimately, this should lead to an understanding of how protein structure controls and regulates the binuclear site properties, and also how these heme-protein interactions change when oxygen is bound or photodissociated.

In the work presented here, we have used time-resolved resonance Raman spectroscopy to study the structure and relaxation pathway from the CO-bound to the CO-free state of cytochrome *o*. The questions to be answered are whether the relaxation of the proximal site, and the rebinding rate of the CO to the distal site of cytochrome o differ from that of cytochrome *a*3. Recently, the dynamics of CO binding were measured for wild-type and mutant cytochrome *bo*. Woodruff and co-workers [5] showed that the equilibration of Cu_B-CO with CO in solution occurs with a rate constant of 500 s^{-1} which is very slow compared to that observed in *aa3* oxidase. From this, they concluded that Cu_B severely limits the approach of ligands to the heme active site. In our own work, the photolytic transient species of cytochrome o, when compared to the equilibrium unligated species, exhibit frequency changes in the 208 cm^{-1} vibrational mode. The 208 cm^{-1} mode in the transient photoproduct produced by CO photolysis appears at 212 cm^{-1} and its behavior is similar to that observed for the Fe^{2+}-His vibration of cytochrome *a*3.[6] The Fe^{2+}-His vibration of cytochrome *a3* occurs at 221 cm^{-1} in the transient photoproduct, and is upshifted by 6 cm^{-1} relative to its frequency in the equilibrium reduced, deoxy form of the enzyme. The frequency of the 208 cm^{-1} mode in the deoxy form of cytochrome *bo* as well as its frequency upshift in the transient photoproduct (212 cm^{-1}), suggest that this mode arises from the out of plane Fe^{2+}-His in agreement with the assignment of Tsubaki et al.[5] The Fe^{2+}-His stretching mode is lower relative to that observed in cytochrome *a3*, however, from which we conclude that the iron-histidine bond in cytochrome *o* is weakly H-bonded.

Time-resolved resonance Raman spectra of cytochrome *bo* at various delay times (t_d=10ns-1.2ms) subsequent to carbon monoxide photolysis in the 200-450 cm^{-1} region exhibits modes at 208, 268 307, 349, 372, and 416 cm^{-1}. The only change upon photodissociation occurs in the 208 cm^{-1} mode. Interestingly, the cytochrome *o* porphyrin π^* electron density sensitive mode, ν_4 displays no frequency shifts in the photolytic transients relative to the equilibrium species. The behavior of the ν_4 in cytochrome *o* transient is similar to that observed in cytochrome *a3* transient, but in contrast to the correlated shifts in ν_4 and $\nu(Fe^{2+}$-His) exhibited by Hb photolytic transients. The 208cm^{-1} mode in the fully reduced enzyme moves to 212 cm^{-1} in the photodissociated enzyme. Similar transient Fe-Ligand (L=His) behavior was originally noted for the Hb.CO and CO-bound mammalian cytochrome c oxidase. The only change that occur in the evolution from the photoproduct to the transient spectra is the Fe^{2+}-His mode which display small intensity and/or position alterations. The appearence of the 208 cm^{-1} peak in the 2-μs spectrum, suggests partial relaxation of the Fe^{2+}-His mode in the first 2 μs subsequent to CO photolysis. Although, the inherent line width of ν(Fe-His) precludes the direct observation of two distnct Fe-His modes, the 10 and 30 μs spectra show rexation of the Fe-His mode. The continous evolution of the ν(Fe-His) over the 10 ns-1.2 ms time scale is the most quantified aspect of hemopocket relaxation and ligand rebinding. At times longer than 100

μs, the overall effect of ligand rebinding is the continous upshift of the frequency of the Fe^{2+}-His mode. At times longer than 200 μs, the presence of the 212 cm^{-1} indicates rebinding of CO to the photolyzed cytochrome *o*. This results from the CO photolysis by the probe 416 nm beam, producing the 10 ns spectrum. Since we are photolyzing all of the cytochrome *o* with the pump beam, the appearance of the 212 cm^{-1} peak indicates ligand rebinding to the previously photolyzed cytochrome *o*.

The observation of a single mode at 208 cm^{-1} indicates a conserved proximal enviroment in cytochrome *o* similar to that observed in cytochrome *aa*3. A split iron-histidine stretching mode, however, has been assigned in the Raman spectra of *Thermus thermophilus ba*3, *Bacillus subtilis aa*3 oxidases, and in cytochrome-c peroxidase. In these enymes, the two stretching modes are proposed to arise from two different heme-protein conformations that effect the iron-histidine bond strength. Table I summarizes several of these frequencies; The 208 cm^{-1} mode is similar to, but slightly lower than that observed for several histidine-coordinated Fe heme proteins, which indicates that its bonding to the iron atom of the heme are unique among the histidine-coordinated heme proteins that have been studied to date. The frequency of the Fe^{2+}-His stretching band of cytochrome *o* is 6 cm^{-1} lower than that observed in cytochrome *a*3 which indicates that significant differences in the Fe-His bonding and/or interaction occur in the cytochrome *c* and quinol oxidase family of enzymes. A plausible explanation for the weak Fe-His bond in cytochrome *o* as compared to the corresponding bond in cytochrome *a*3 is the hydrogen-bond strength of the Histidine N_δ proton. Studies on heme model compounds (Table I) have shown that the $\nu(Fe^{2+}$-His) ranges from 200 cm^{-1} for those complexes in which there is no hydrogen bond acceptor, to ~ 220 cm^{-1} when there is a hydrogen-bond acceptor, to ~233 cm^{-1} when the hydrogen is removed resulting in the imidazolate form of the complex.

The angle of the histidine relative to the heme nitrogens is a second factor that may influence the strength of the iron-histidine bond. In the case of *Bacillus subtilis aa*3 oxidase, the two iron-histidine modes observed at 194 and 214 cm^{-1} might be due to rotamers of the imidazole ring plane relative to the heme N-Fe-N axis. An analogous situation is thought to occur in *ba*3 oxidase, and in the T state of Hb where a strained Fe-His conformation weakens the iron-histidine bond.

Lemon et al.[5]and Woodruff[7] determined the coordination dynamics of the binuclear site of cytochrome *bo* and found that the equilibration of Cu_B-CO with CO in solution which occurs with a rate constant of 500 s^{-1} is very slow compared to the $7x10^5$ s^{-1} observed for *aa*3 oxidase. From this they concluded that Cu_B severely limits the approach of ligands to the heme active site. Our data indicate that the rate of CO rebinding in cytochrome *bo* is considerable faster than that observed in cytochrome *aa3* which suggests significant differences in the distal pockets of these enzymes. If the flow/flash approach is to work effectively, several conditions

must be met.[8] One of these is that the photodissociated CO must leave the binuclear active site quickly following photolysis, and the heme pocket must relax rapidly, relative to the O_2-binding reaction. Svensson and Nilsson,[9] and more recently Orii et al.[10] applied the flow/flash approach, and reported that cytochrome *bo* reacts with O_2 with a maximal rate constant of $5.1 \times 10^4\ s^{-1}$ (12 μs) which is slower than the $1.6 \times 10^5\ s^{-1}$ (3.8 μs) reported for cytochrome *aa*3. Moreover, Svensson and Nilsson concluded that the mechanism for oxygen reduction in cytochrome *bo* is analogous to that suggested for cytochrome *aa*3. The fast rate of CO rebinding data reported here, however, in conjunction with the 1.4 ms Cu_B/CO dissociation rate constant suggest perturbation in the cytochrome *bo*/dioxygen reaction.

The frequency difference between the $\nu(Fe^{2+}$-His) frequencies in cytochrome *bo* and cytochrome *aa*3 indicate that the proximal site of cytochrome *o*, while similar, is not identical to cytochrome *a*3. The small frequency differences between the Fe^{2+}-His modes in the deoxy and transient photoproduct in cytochrome *bo* and cytochrome *aa*3, and the absence of any correlation, as opposed to hemoglobin, between $\nu(Fe^{2+}$-His) and ν_4 do indicate, that similar proximal hemepocket relaxation mechanisms occur in the bacterial and mammalian enzymes. The rate of CO rebinding in these two enzymes, however, is quite different.

Table I: Iron-Histidine (Imidazole) Stretching Frequencies (cm^{-1}) for some Proteins and Model Compounds[a]

Complexes	ν(Fe(II)-His)	References
Myoglobin	210-220	11, 12
Hemoglobin	203-224	11, 12
cytochrome c oxidase(*aa*3)	214	13, 14
cytochrome *aa*3-600	194/214	15
cytochrome *ba*3	193/209	16
HRP	243	12
CcP	227/249	17
Cytochrome *bo*	206	4, this work
Fe(PPDME)(2MeIm)/CH_2Cl_2	200	12
Fe(PPDME)(2MeIm)/DMF	205	12
Fe(PP)(2MeIm)/H_2O	219	12
Fe(PPDME)($2MeIm^-$)/Me_2SO	233	12

[a]Abbreviations: HRP, horseradish peroxidase; CcP, cytochrome c peroxidase; PP, protoporphyrin; DMF, dimethyl ester; 2MeIm, 2-methylimidazole; DMF, dimethylformamide.

REFERENCES

1. Anraku, Y.; Gennis, R. B. *Trends Biochem. Sci.* **1987**, *12*, 262-266.
2. Puustinen, A.; Wikström, M. *Proc. Natl. Acad. Sci. U.S.A.* **1991**, *88*, 6122-6129.
3. Wu, W.; Chang, C. K.; Varotsis, C.; Babcock, G. T.; Puustinen, A.; Wikström, M. *J. Am. Chem. Soc.* **1992**, *114*,1182-1187.
4. Tsubaki, M.; Mogi, T.; Hori, H.; Hirota, S.; Ogura, T.; Kitagawa, T.; Anraku, Y. *J. Biol. Chem.* **1994**, 49, 30861-30868.
5. Lemon, D. D.; Calhoun, M. W.; Gennis, R. B.; Woodruff, W. H. *Biochemistry* **1993**, *32*, 11953-11956.
6 Findsen, E. W.; Centeno, J.; Babcock, G. T.; Ondrias, M. R. *J. Am. Chem. Soc.* **1987**, *109*, 5367-5373.
7. Woodruff, W. H. *J. Bionerg. Biomembr.* **1993**, *25*, 2, 177-188.
8. Babcock, G. T.; Varotsis, C. *J. Bioenerg. Biomemb.* **1993**, *25*, 71-80.
9. Svensson, S.; Nilsson, T. *Biochemistry* **1993**, *32*, 5442-5447.
10. Orii, Y.; Mogi, T., Sato-Watanabe, M.; Hirano,T.; Anraku, Y. *Biochemistry* **1995**, *34*, 1127-1132.
11. Rousseau, D. L.; Friedman, J. M. in *Biological Applications of Raman Spectroscopy* **1988**, Vol. 3. (Spiro, T. eds.), Wiley, New York, 133-215.
12. Kitagawa, T. in *Biological Applications of Raman Spectroscopy* **1988**, Vol. 3, (Spiro, T. eds.),Wiley, New York, 97-131.
13. Ogura, T.; Hon-nami, K.; Oshima, T.; Yoshikawa, S.; Kitagawa, T. *J. Am. Chem. Soc.* **1983**, *105*, 7781-7783.
14. Salmeen, I.; Rimai, L.; Babcock, G. T. *Biochemistry* **1978**, *17*, 800-806.
15. Lauraeus, M.; Wikström, M.; Varotsis, C.; Tecklenberg, M. J.; Babcock, G. T.; *Biochemistry* **1992**, *31*, 10054-10060.
16. Oertling, W. A.; Surerus, K. K.; Einarsdottir, O.; Fee, J. A.; Dyer, R. B.; Woodruff, W. H.*Biochemistry* **1994**, *33*, 3128-3141.
17. Smulevich, G.; Mauro, J. M.; Fishel, L. A.; English, A. M.; Kraut, J.; Spiro, G.T. *Biochemistry* **1988**, *27*, 5477-5485.

Wavepacket Dynamical Studies On Trans-azobenzene

N. Biswas and S. Umapathy*
Department of Inorganic and Physical Chemistry,
Indian Institute of Science, Bangalore-560012, India.

INTRODUCTION

Azobenzene isomerization has been a challenging academic problem since the first report by G. S. Hartley [1]. Unlike stilbene, where the dynamics of isomerization has been well understood [2], the mechanism of isomerization in azobenzene is still unclear [3]. A study of substituent effects on isomerization of trans-azobenzene (TAB) by Rau *et al* [3, 4] has indicated that the mechanism of isomerization critically depends on excitation wavelength. They proposed that on visible excitation ($n \rightarrow \pi^*$ transition), the isomerization pathway was through inversion , whereas, the mechanism would follow rotation pathway for UV excitation ($\pi \rightarrow \pi^*$ transition) [3]. In solution, it has been proved that TAB contains a centre of symmetry [5, 6], but it is not yet established whether the molecule is planar (C_{2h}) or, slightly distorted from planarity (C_i) [7]. The electronic absorption spectrum of TAB in CCl_4 consists of a weak band at $\sim$ 440 nm ($\epsilon \approx 500$ M^{-1} cm^{-1}) which is assigned to a symmetry forbidden ($A_g \leftarrow A_g$) transition, assuming C_i symmetry. In fact, the ($A_g \leftarrow A_g$) absorption intensity of TAB has been observed to be unusually large for a forbidden transition and has been explained to originate from vibronic coupling with allowed ($A_u \leftarrow A_g$) transition through the isomerization (rotation or inversion) coordinate.

Resonance Raman (RR) spectroscopy is an ideal tool to understand the excited state displacements for a given vibrational mode on excitation [8]. A study of the Raman excitation profiles (REPs) of various vibrational modes observed under resonance would provide information on the architectural changes associated with the given excitation. In particular, a comparison of the theoretically simulated REP with that of the experiment would provide vital clues regarding the dynamics associated with that specific vibrational mode [8, 9]. In the case of TAB, a study of the REPs of the various vibrational modes under both UV and VIS excitations is expected not only to lead to structural evidence for the isomerization pathway but also to provide valuable insight into the origin of Raman intensities.

In this paper, simulation of REPs under VIS excitation has been carried out using Heller's time-dependent wavepacket formalism [10 - 12]. This time-dependent theory of Raman scattering has an advantage, in that knowledge of all the eigenstates in the excited electronic surface is not required. Further, Heller's approach provides a more transparent physical picture of the dynamics. A comparison of the simulated REPs with the experimental ones by Okamoto *et al* [13] show that only five modes fit well whereas the other five modes hardly fit in the blue region of the spectrum [14]. In order to get a good fit for the latter, interference effect [15] of the ($A_u \leftarrow A_g$) transition with that of the resonant electronic ($A_g \leftarrow A_g$) transition has been incorporated in our simulation.

THEORY:

In the time-dependent theory of Raman scattering pioneered by Heller *et al* [10 - 12], the resonance Raman amplitude for the transition from the initial state |i> to the final state |f> (where both the vibrational eigenstates |i> and |f> correspond to the electronic ground state) is expressed as a half Fourier transform of the correlation function <f|i(t)>,

$$\alpha_{i\rightarrow f}(E_L) = \frac{i}{\hbar}\int_0^\infty M^2 < f|i(t) > exp[i(E_L + E_i)t/\hbar - \Gamma t/\hbar]dt \qquad (1)$$

where E_L is the energy of incident photon, $\hbar = h/2\pi$ (h being Planck's constant), M the electronic transition dipole moment, E_i the zero-point energy of ground electronic state, Γ the homogeneous broadening, and |i(t)> the evolving wave packet at various intervals of time under the influence of the excited state Hamiltonian (H_{ex}). Thus,

$$|i(t) >= exp(-iH_{ex}t/\hbar)|i > \qquad (2)$$

For the simulations carried out in this work, it is assumed that all potential surfaces are harmonic except the torsional mode which is considered to be linear and dissociative in the excited electronic state, normal coordinates are not mixed in the excited state, transition dipole moments are constant and frequencies for all the vibrational modes are same in both the ground and excited electronic states. Propagation of the wavepacket on excited electronic surface has been carried out using the time-dependent quantum-mechanical (TDQM) method involving a grid technique [16 - 18]. In the present study, an initial wave function |i> at t = 0 is specified on a chosen spatial grid of 2048 points with grid spacing of 0.1 dimensionless units. A fourth order differencing (FOD) scheme has been used for the time evolution. FOD method is much faster and equally efficient [19, 20] as the normally used second order differencing (SOD) scheme [17, 21 - 23]. In this paper, the time evolution involves a total of 8192 steps with each step (Δt) corresponding to 0.01 fs.

A multi-mode calculation has been carried out for TAB. Multi-mode Raman correlation function is given by the product of correlation function, $<f_k|i_k(t)>$ for the Raman active mode (k) and autocorrelation function, $<i_j|i_j(t)>$ for other vibrational modes (j).

$$< f|i(t) >_M = < f_k|i_k(t) > \prod_{j=1,j\neq k}^{N-1} < i_j|i_j(t) > \qquad (3)$$

where, N is total number of vibrational modes. The polarizability ($\alpha_{i\rightarrow f}$) for the multi-modes can be obtained by substituting the values of $<f|i(t)>_M$ in eq. (1).

The simulated REPs obtained by considering only a single excited electronic state does not fit well with the experimental results for five Raman active vibrational

modes. Hence, the interference effect from the higher lying ($A_u \leftarrow A_g$) transition has been introduced in our calculations. This transition has a higher transition dipole moment than the resonant electronic state. Thus, assuming a two state model, i.e if we consider the presence of an interfering state along with the resonant state, the expression for polarizability ($\alpha_{i\rightarrow f}$) is as follows [15]:

$$\alpha_{i\rightarrow f}(E_L) = \frac{i}{\hbar}\int_0^\infty (M_R^2 O_R + M_I^2 O_I) exp[i(E_L + E_i)t/\hbar - \Gamma t/\hbar]dt \qquad (4)$$

where, M_R and M_I are the transition dipole moments and O_R and O_I are the Raman correlation functions for the resonant and interfering excited electronic states. Since $\alpha_{i\rightarrow f}$ is proportional to the square of transition dipole moment, the transition having larger dipole moment is expected to influence the resonance REPs considerably.

RESULTS AND DISCUSSION

The REPs of all Raman active vibrational modes of TAB in resonance with ($n-\pi^*$) transition have been simulated. Only for five modes, *viz.*, 1592, 1491, 1470, 939 and 912 cm^{-1}, do the simulated curves fit well with experiment, whereas for the other five modes, *viz.*, 1439, 1312, 1181, 1142 and 1000 cm^{-1}, experimental REPs show a decrease in Raman intensity (de-enhancement) which did not fit well with the simulated curves [14]. In order to account for the de-enhancement, an interference effect of $A_u \leftarrow A_g$ transition has been introduced in our simulation. The experimental REPs and the simulated ones with and without interference for all Raman active modes of TAB are shown in Fig. 1.

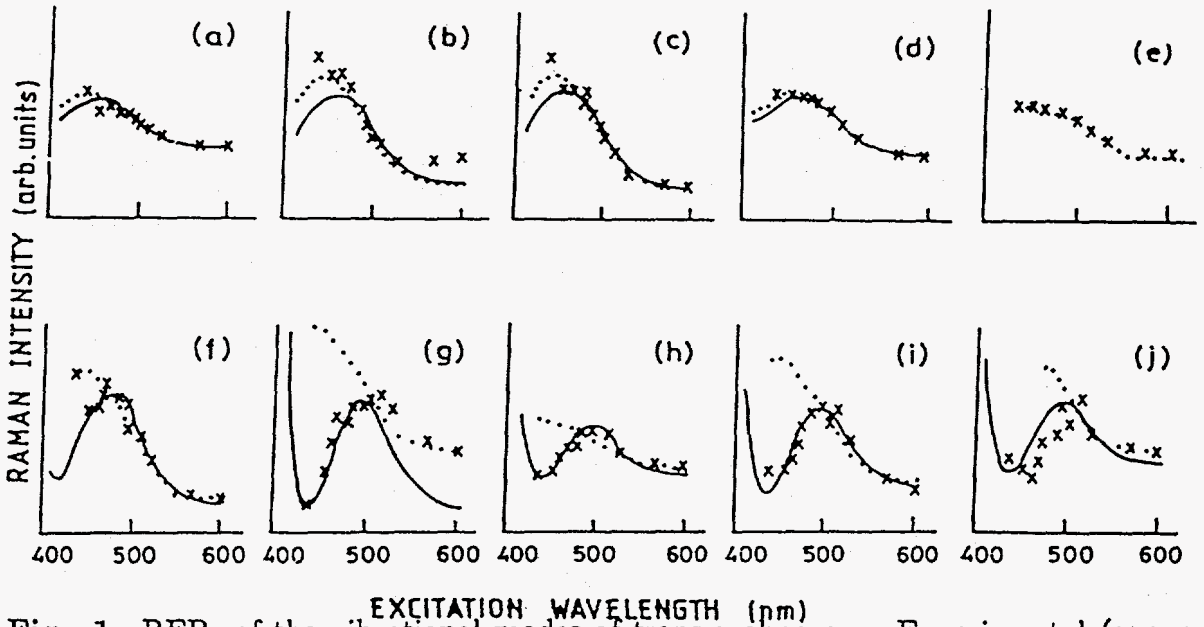

Fig. 1. REPs of the vibrational modes of trans-azobenzene: Experimental ($\times \times \times$) and Simulated (..... without interference and —— with interference) for (a) 1592, (b) 1491, (c) 1470, (d) 939, (e) 912, (f) 1439, (g) 1312, (h) 1181, (i) 1142 and (j) 1000 cm^{-1}.

It is evident from Fig. 1. that incorporation of the interference of ($A_u \leftarrow A_g$) transition in our calculation resulted in very good fit for all the vibrational modes of TAB with the experimental REPs. Thus, we conclude that the origin of the decrease in Raman intensity near the maximum of the VIS absorption band (resonance de-enhancement [15]) for some vibrational modes is due to the interference from higher lying excited electronic state. The values of zero-zero energy (E_{00}), homogeneous broadening (Γ), slope of the torsional potential (β) and transition dipole moment for the resonant electronic state are 20470 cm^{-1}, 50 cm^{-1}, 980 cm^{-1} and 0.8 $\AA$. The resonance Raman frequencies (ω cm^{-1}), dimensionless displacements (Δ) and the description of vibrations for the resonant electronic state are given in Table 1. Similarly, values of E_{00}, Γ and M for the interfering electronic state is 27710 cm^{-1}, 50 cm^{-1} and 2.52 $\AA$ respectively. Details of the de-enhancement results have been discussed elsewhere [24].

A comparison of the displacement values for the important vibrational modes of cis- and trans-stilbene and that of TAB under VIS excitation provides valuable clues regarding the isomerization dynamics. The vibrational modes 1439 and 1142 cm^{-1} assigned to (N=N) and (C-N) stretchings respectively have the largest displacements and correspondingly the highest intensities. However, when we compare the case of cis- (trans-) stilbene, where isomerization occurs via rotation, the most intense Raman bands, 1629 (1638 for trans) and 1600 (1599 for trans) cm^{-1} correspond to inter ring (ethylenic) C=C stretch and ring stretch, respectively [8, 9]. Therefore, in the case of TAB, if rotation along N=N axis occurs, it is reasonable to expect large displacements for both (N=N) stretch at 1439 cm^{-1} and the ring stretch mode at 1491 cm^{-1}. Contrary to this expectation, comparable displacement has been observed for 1439 and 1142 cm^{-1} ($\Delta_{1439} = 0.95$ & $\Delta_{1142} = 1.03$) and a smaller displacement ($\Delta_{1491} = 0.67$) for the ring stretch mode at 1491 cm^{-1} in TAB. This suggests that inversion is the most likely route of isomerization and not rotation.

Table 1. Description of vibrational modes of trans-azobenzene, their Raman frequencies (cm^{-1}) and respective displacements (Δ).

DESCRIPTION OF VIBRATIONAL MODES	FREQUENCY (in cm^{-1})	DIMENSIONLESS DISPLACEMENT $\lvert\Delta\rvert$
H oop wag	939	0.47
ring def	1000	0.60
C-N str	1142	1.03
ring H rock	1181	0.67
C-C-H ben	1312	0.28
N=N str	1439	0.95
Ring C-C str, N=N str	1470	0.76
Ring str	1491	0.67
Ring str	1592	0.49

def : deformation, oop : out of plane, ben : bending, str : stretching.
linear dissociative mode: $\omega = 912$ cm^{-1} and $\beta = 980$ cm^{-1}.

Acknowledgements

We would like to acknowledge financial assistance from the Jawaharlal Nehru Centre for Advanced Scientific Research, Bangalore and the Department of Science and Technology and the Council of Scientific and Industrial Research, Government of India.

References

[1] G. S. Hartley, *Nature*, 140 (1937) 281.

[2] R. J. Sension, S. T. Repinec, A. Z. Szarka and R. N. Hochstrasser, *J. Chem. Phys.*, 98 (1993) 6291.

[3] H. Rau, in " *Photochromism : molecules and systems* " , eds. H. Durr and H. Bouas-Lauran (Amsterdam: Elsevier, 1990) p. 165.

[4] H. Rau and S. Yu-Quan, *J. Photochem. Photobiol. A : Chemistry*, 42 (1988) 321.

[5] G. S. Hartley and R. J. W. Le Fevre, *J. Chem. Soc.*, (1939) 531.

[6] D. J. W. Bullock, C. W. N. Cumper and A. I. Vogel, *J. Chem. Soc.*, (1965) 5316.

[7] B. Tellerer, H. H. Hacker and J. Brandmuller, *Ind. J. Pure and App. Phys.*, 9 (1971) 903.

[8] A. B. Myers and R. A. Mathies, in " *Biological Applications of Raman Spectroscopy* " , ed. T. G. Spiro, Vol. 2 (John Wiley and sons: Inc. New York, 1987) p. 1.

[9] A. B. Myers and R. A. Mathies, *J. Chem. Phys.*, 81 (1984) 1552.

[10] S.-Y. Lee and E. J. Heller, *J. Chem. Phys.*, 71 (1979) 4777.

[11] E. J. Heller, R. L. Sundberg and D. J. Tannor, *J. Phys. Chem.*, 86 (1982) 1822.

[12] D. J. Tannor and E. J. Heller, *J. Chem. Phys.*, 77 (1982) 202.

[13] H. Okamoto, H. Hamaguchi and M. Tasumi, *Chem. Phys. Lett.*, 130 (1986) 185.

[14] N. Biswas and S. Umapathy, *Chem. Phys. Lett.*, 236 (1995) 24.

[15] K-S. K. Shin and J. I. Zink, *J. Am. Chem. Soc.*, 112 (1990) 7148.

[16] N. Biswas, S. Umapathy, C. Kalyanaraman and N. Sathyamurthy, *Proc. Indian Acad. Sci. (Chem. Sci.)*, submitted.

[17] R. Kosloff, *J. Phys. Chem.*, 92 (1988) 2087.

[18] S. O. Williams and D. G. Imre, *J. Phys. Chem.*, 92 (1988) 3363.

[19] U. Manthe and H. Köppel, *J. Chem. Phys.*, 93 (1990) 345.

[20] U. Manthe and H. Köppel, *J. Chem. Phys.*, 93 (1990) 1658.

[21] D. Kosloff and R. Kosloff, *J. Comput. Phys.*, 52 (1983) 35.

[22] R. Kosloff and D. Kosloff, *J. Chem. Phys.*, 79 (1983) 1823.

[23] V. Mohan and N. Sathyamurthy, *Comput. Phys. Rept.*, 7 (1988) 215.

[24] N. Biswas and S. Umapathy, manuscript in preparation.

Femtosecond IR Spectroscopy of Optically Excited Molecules

Chengfei Wang, Brian Mohney, Boris Akhremitchev, and Gilbert C. Walker
Department of Chemistry, University of Pittsburgh, Pittsburgh, PA 15260

Just as static vibrational infrared spectroscopy is a principal means to determine the structure and environment of chemical species, via the measurement of frequencies, force constants and bandwidths, so should ultrafast time resolved infrared vibrational spectroscopy provide that same information. Recent developments make possible the characterization of short-lived IR chromophores: the environmental fluctuations they experience, the kinetics of their state populations, and their orientational motions. The physical and analytical optics necessary for this spectroscopy are the focus of this report. We first explain the experimental procedure by which we generate 100fs tunable visible and infrared pulses, and then describe optial pump-infrared probe measurements on neat liquids, and dye-solvent mixtures.

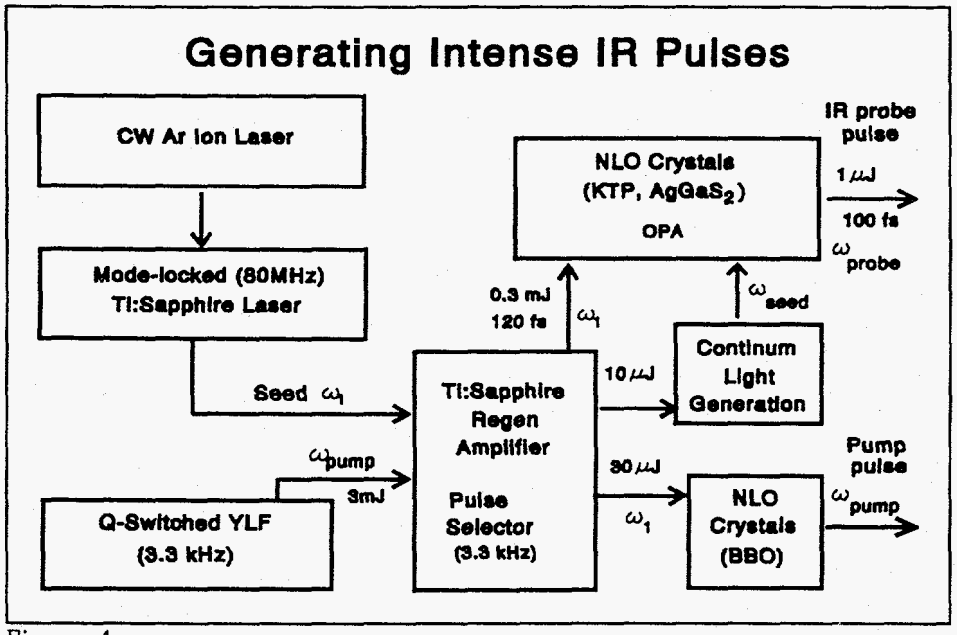

Figure 1.

Experimental:

An all solid state laser system has been constructed for the generation of pulses throughout the visible and infrared. The Ti:sapphire system is show in Figure 1. A cw Ar+ ion laser producing 4W on all lines (Coherent Innova 310) is used to pump a self-mode-locked Ti:sapphire oscillator built approximately after the design of Asaki et al [1]. The mode-locked oscillator produces 30fs, 2nJ, 800nm pulses at 80MHz. The pulses are amplified using the chirped pulse amplification method of Mourou and coworkers [2]. We use a combination of faraday rotator, thin film polarizers, and double-passed single (1800gr/mm) grating pulse stretcher to inject 50ps pulses into a Ti:sapphire regenerative amplifier. The frequency profile of the pulse injected into the amplifier is controlled by a mask within the stretcher. The pulse selection is performed using a pockels cell. The pulse stretching is necessary to prevent damage of the amplifier optics from an intense, ultrashort pulse. The regenerative amplifier is composed of two end mirrors (rc = 0.5m), a broadband thin film polarizer (Alpine Optics), a pockels cell (Medox), and a Ti:sapphire crystal. The crystal is 20mm long and doped to absorb 80% of the 3mJ pump light. The pump light comes from an intracavity-doubled Q-switched Nd:YLF laser (Quantronix 527) whose 527nm pulses are ca

300ns at 3.3kHz. After amplification to 300μJ, the pulses are recompressed in a double-pass single grating compressor to 100fs at a cost of 30% of the pulse energy.

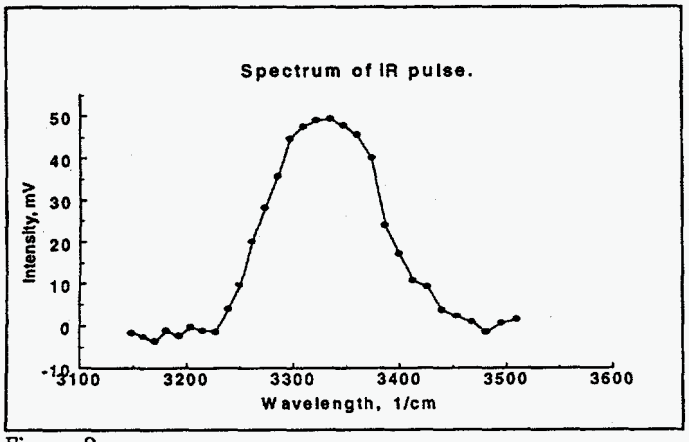

Figure 2

The generation of tunable pulses is accomplished by non-linear optics. A fraction (10μJ) of the compressor output is used to generate a white light continuum in a 4mm sapphire optical flat. Continuum adequate for probe pulses is generated from 400nm-2000nm. However, since we are interested in infrared light generation, we select a frequency fraction of that continuum, e.g., 1100nm, and use it as a photon seed source in an optical parametric amplifier (OPA). The OPA consists of a non-linear optical crystal, e.g., KTP, $AgGaS_2$, or GaSe, that has focused into it an appropriately delayed, powerful (100μJ) 800nm pulse, addition to the seed NIR pulse. The NIR photons serve to seed the OPA, and 0.1-1μJ IR pulses can be generated in a single amplification stage. Tuning the crystal angle provides phase matching at the desired frequency. See Figure 2 for an example of the frequency profile of an 100fs IR pulse generated in KTP.

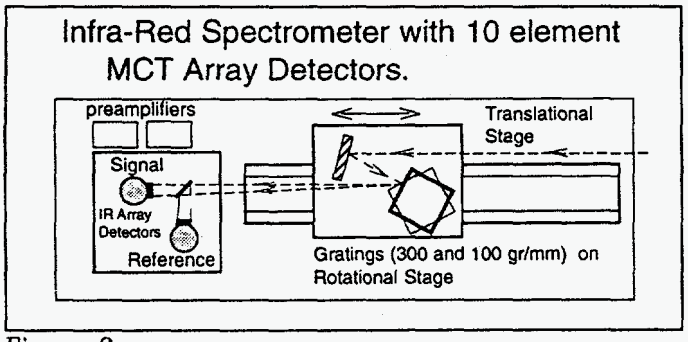

Figure 3

We report two kinds of infrared detection. First, a pair of HgCdTe detectors, one for the infrared reference channel, and the second for an IR signal channel. The electrical signals are collected using gated integration and hold (Stanford SRS250), 12 bit A/D conversion (Keithley DAS20) and processed by a personal computer. The sensitivity of this detection scheme proved to be quite good: typically better than 1mOD in 1 sec data collection/processing at a given infrared frequency and pump/probe delay.

However, as will be obvious from the discussion below, the advantages of multi-frequency detection using IR arrays are numerous, and we have rapidly replaced the two detector scheme with a twin 10 element HgCdTe array scheme [3]. We have similar sensitivity, and the ability to rapidly capture patches of the IR spectrum with varying frequency resolution, see Figure 3.

Due to the complexity of material responses that can contribute to the observed transient absorption signal, we first show the transient spectra obtained for a 400nm pump IR probe of neat dimethylformamide, see Figure 4. The most obvious feature of this figure is an oscillating wave around time zero. This feature is due to frequency-chirping of the probe pulse as a function of delay between the pump and probe pulses. This is a phase modulation of the probe pulse induced by the pump pulse acting through the sample [4,5]. The phase delay may be calculated from the following phenomenological relation.

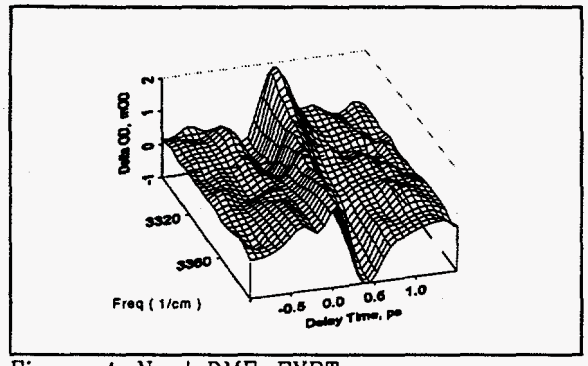

Figure 4. Neat DMF, EXPT.

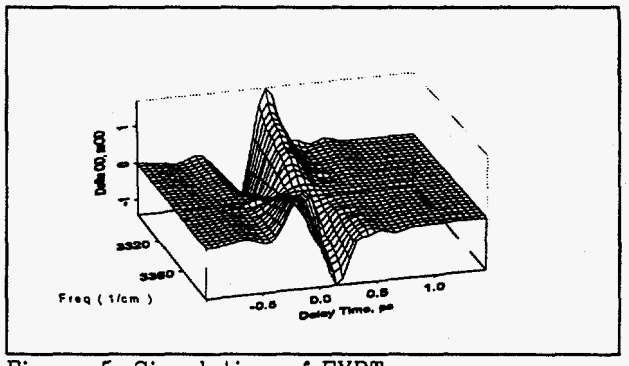

Figure 5. Simulation of EXPT.

$$\Delta\Phi(t) = \alpha I(t) + \beta\Theta(t)\,[\Sigma_i r_i(t)] \qquad (1)$$

In this expression the first term represents the electronic response, with a normalized pump intensity I(t). The second term represents the nuclear response from orientational relaxation, where $\Theta(t)$ is a normalized step function and $\Sigma_i r_i(t)$ represents intra-and inter-nuclear contributions to the signal. Figure 5 shows a transient OD spectrum calculated via time derivative of the phase delay induced by the pump beam convoluted with the probe pulse profile. The consequence of this phase modulation is a shift of the probe pulse to lower frequency at small negative times, and a shift to higher frequency at small positive times. Because this response derives from dispersion and not loss, integration of the spectral response over frequency will result in a net zero signal. Figure 6 shows the result of such manipulation of data for a similar experiment in dichloromethane from Figure 6, integrated from 3357cm^{-1} to 3280cm^{-1} . Note that the signal is not uniformly zero, but a small bleaching component remains around zero time.

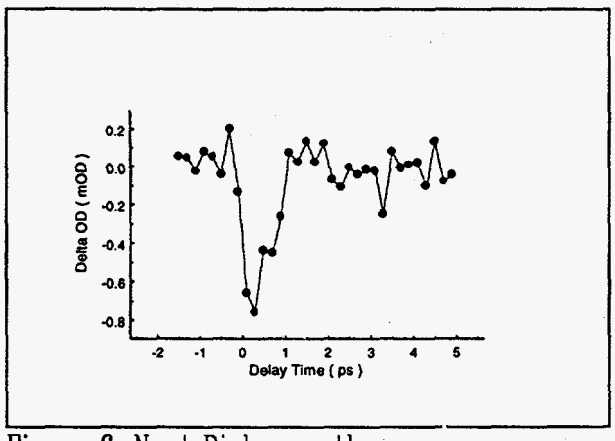

Figure 6. Neat Dicloromethane.

It might be argued that this component could result from a lens, not included in the above expression, whose influence and focal length depends on the displacement of the sample from the focus of the probe light. However, we keep the probe focus at the sample, and in our geometry the signal from such a lens would result in a transient absorption contribution to our net signal, not a bleach as is seen in Figure 6. Similarly, induced birefringence, which could arise if the angle between pump and probe polarization vectors were not 0 or 90°, would lead to an absorption, not a bleach.

Instead, we consider the electric field of the pump pulse and its ability to shift the vibrational transition frequencies of the solvent vibrations. The probing light frequency in this experiment is on the wing of the CH stretch absorption of CH_2Cl_2. Following second order perturbation theory we estimate that the pump pulse will induce a ~0.2-2cm^{-1} down-shift of the CH stretch band [6]. For our sample this effect would result in a decrease in absorption of ca 2-

20mOD over this frequency region, which is larger than we observe but of the right sign.

Solvation Dynamics:

These measurements are oriented toward a more detailed understanding of solution dynamics, in particular the effects of a perturbing solute on the surrounding solvent's vibrational spectrum. These measurements should be take in the context of a large body of work that identifies role of polar solvents (or proteins) to stabilize charge shifts [7]. Recent theoretical studies [8] suggest that in small molecule solvent-solute systems the majority of stabilization energy and the fastest response comes from molecules in the first solvation shell.

We report the transient absorption of a dimethyl formamide solution at 3340cm^{-1} following optical excitation of dissolved coumarin 183 at 400nm. This dye molecule exhibits a larger dipole moment in the excited electronic state than in the ground state. It belongs to a class of dyes which have been used to study the dynamic solvent effect by monitoring the time dependent shift of the frequency maximum of the coumarin fluorescence emission spectrum, which reveals the developing solvent polarization.

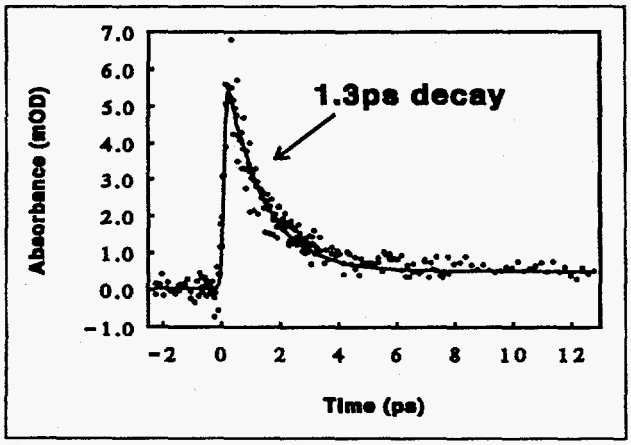

Figure 7. C183 in DMF

Here we focus instead on the effect of the dye on the time resolved solvent spectrum [9]. The spectrum has been measured in the vicinity of the dimethyl formamide carbonyl overtone absorption, the OH stretch of the ground state coumarin, and trace water. The transient absorption signal is fit with a convolution of the pump pulse with two decaying exponentials. The characteristic decay times are 1.3ps and a much longer time constant (which we associate with the excited electronic state lifetime). The shorter time compares well with the 1.4ps solvation time for dimethyl formamide estimated by the time-dependent fluorescence Stokes shift method using related coumarin molecules [7].

Acknowledgements

This research was supported by the CRDF Fund of The University of Pittsburgh, the Petroleum Research Fund, and 3M Company.

References:

1. M. T. Asaki, C. P. Huang, . Garvey, J. Zhou, H. C. Kapteyn, M. M. Murnane, *Opt. Lett.* 1993, **18**, 977.
2. J. Squier, F. Salin, G. Mourou, *Opt. Lett.* 1991, **16**, 324.
3. P. Hamm, S. Wiemann, M. Zurek, ad W. Zinth *Opt. Lett.* 1994, **19**, 1642.
4. E. Tokunaga, A. Terasaki, and T. Kobayashi *Phys. Rev. A*, 1993, **47**, R4581. D. McMorrow, W. T. Lotshaw, G. A. Kenney-Wallace, *IEEE J. Quant. Electr.*, 1988, **24**, 443.
5. T. Lian, Y. Kohldenko, B. Locke, and R. M. Hochstrasser *J. Phys. Chem.*, 1995, **9**, 7272.
6. M. Joffre, D. Pulin, A. Migus, and A. Antoinetti *J. Mod. Opt.*, 1988, **12**, 1951.
7. W. Jarzeba, G. C. Walker, A. E. Johnson, and P. F. Barbara *Chem. Phys.* 1991, **152**, 57., and references therein.
8. M. Maroncelli, V. Kumar, A. Papazyan *J. Phys. Chem.* 1993, **97**, 13.
9. T. Lian, Y. Kholodenko, and R. M. Hochstrasser *J. Phys. Chem.* 1995, **99**, 2546.

Spectral Diffusion of Molecular Vibrations on a Picosecond Timescale

Marco J.P. Brugmans[1], Huib J. Bakker[1], Mischa Bonn[1,2], Aart W. Kleyn[1], Rutger A. van Santen[2], and Ad Lagendijk[1]

[1] *FOM-Institute for Atomic and Molecular Physics, Kruislaan 407, 1098 SJ Amsterdam, The Netherlands*

[2] *Schuit Institute of Catalysis, Eindhoven University of Technology, P.O. Box 513, 5600 MB Eindhoven, The Netherlands*

Abstract

With two-color picosecond infrared laser pulses the dynamics of O–H stretch vibrations in zeolites are investigated. We find that vibrational stretch excitations hop among O–H sites which have an inhomogeneous distribution of absorption frequencies. This site-to-site transfer is caused by dipole-dipole coupling of the O–H oscillators and leads to diffusion of the vibrational excitations both in place and in frequency.

The dynamics of chemical reactions on a molecular scale[1] can nowadays be studied thanks to the availability of ultrashort laser pulses. High-intensity infrared pulses can be used to reveal directly vibrational excited-state lifetimes and energy pathways of vibrational energy. We investigate the vibrational dynamics of the industrially important catalysts zeolites[2]. The catalytically active sites in the zeolitic lattice are the acidic O–H groups, which are found near Al-atoms in the porous alumino-silicate structure. Besides the industrial interest to understand the catalytic reactions on a molecular scale, zeolites appear to be good model systems to study relaxation processes of molecular vibrations encaptured in a solid lattice[3, 4, 5].

The proton-loaded zeolites were obtained by heating in vacuo (at least 1 h at 723 K) fully exchanged zeolite Y with a Si/Al ratio of 2.8. The conventional infrared spectrum of zeolite Y around the O–H stretch vibration frequency is depicted in Fig. 1. Two separate absorption bands are observed. We concentrate on O–H oscillators with vibrational frequencies in the high frequency (HF) absorption band at 3637 cm^{-1}.

At room temperature, all the O–H vibrations are initially in the $v = 0$ vibrational ground state. In our two-pulse experiment, a first, intense ($\sim$ 100 μJ) picosecond (27 ps) infrared pump pulse is tuned to the fundamental absorption band. Due to the anharmonicity of the vibration, the pump pulse is only resonant with the first transition and excites a significant fraction ($\sim$ 10 %) of the O–H oscillators to the first excited vibrational level, $v = 1$. The transient level populations are monitored by the transmission of a second, weak ($\sim$ 1 μJ) picosecond probe which is independently tunable in wavelength[6]. By varying the delay of the probe pulse with respect to the pump pulse, the transmission changes induced by the saturating pump pulse are measured in a time-resolved way. Excited state population lifetimes can be inferred from the return to the equilibrium value of the probe transmission. Pump induced changes in the absorption spectrum can be recorded by fixing the delay between the pulses and tuning the frequency of the probe pulse.

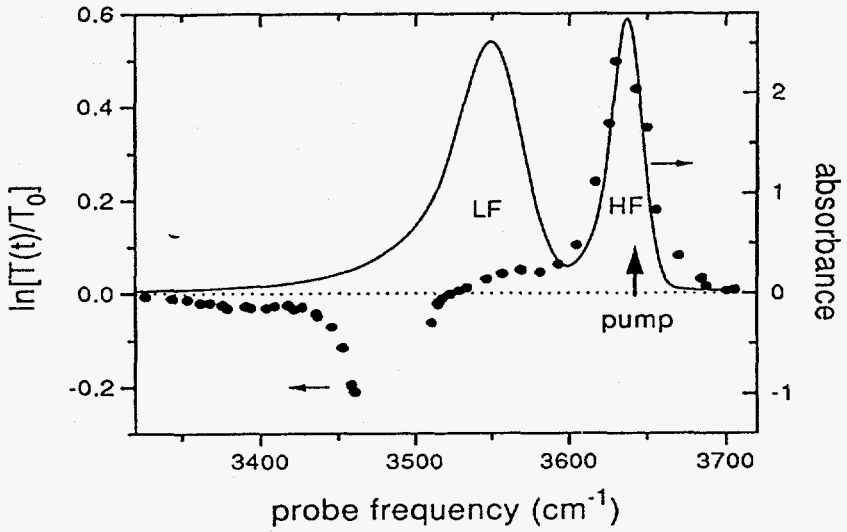

Figure 1: *Transient transmission spectrum (dots, left axis) 32 ps after excitation the HF O–H absorption by a pump pulse at 3639 cm^{-1} (big arrow). The conventional absorption spectrum is depicted as the solid line (right axis). Due to water absorption in the non-linear crystals used for generation of the laser pulses, no light can be generated in the in the region 3465 to 3510 cm^{-1}*

The pump induced changes of the absorption spectrum 32 ps after excitation of the HF O–H oscillators by the pump pulse are shown in Fig. 1. The probe transmission around the excitation frequency is increased (the absorption is bleached) because a significant fraction of the population is excited and thus the population difference between $v = 0$ and $v = 1$ is decreased. As long as the $v = 1$ level is populated, absorption from $v = 1$ to $v = 2$ occurs and consequently the transmission of a probe pulse at the $v_{1\rightarrow 2}$ transition frequency is decreased. This induced 'hot-band' absorption between first and second excited levels is found around 3475 cm^{-1}, in agreement with the value for the anharmonicity determined by overtone spectroscopy[7].

Due to the random distribution of Al-atoms in the zeolite lattice the absorption bands are expected to be inhomogeneously broadened, which means that they are composed of *distributions* of vibrational frequencies. Excitation of a subset of oscillators within such an inhomogeneous band would result in a transient spectral hole in the band (see e.g. Ref. [8]). This is not observed in Fig. 1, because our laser pulses at the O–H frequency have a too large spectral width (Full Width at Half Maximum (FWHM) = 35 cm^{-1}) to excite a subset of oscillators within the HF band. At the O–D frequency however, the linewidth of our pulses is much smaller (8 cm^{-1} FWHM at the HF O–D absorption frequency of 2683 cm^{-1}, see also Ref. [5]). Transient absorption spectra at the O–D frequency were measured for samples in which part of the O–H hydroxyls were replaced by O–D oscillators. Indeed, for the transient spectrum of the HF O–D band it is found that the bleaching has a narrower linewidth (FWHM = 13 cm^{-1}) than the width of the unexcited fundamental absorption band as measured by the probe pulse only (FWHM = 19 cm^{-1})[9]. This means that a transient spectral hole is burnt, proving the inhomogeneity of the infrared absorption bands in zeolites. From a deconvolution of the laser spectrum and the bleached spectrum at the HF O–D band, the homogeneous linewidth is estimated to be 5 cm^{-1}[9].

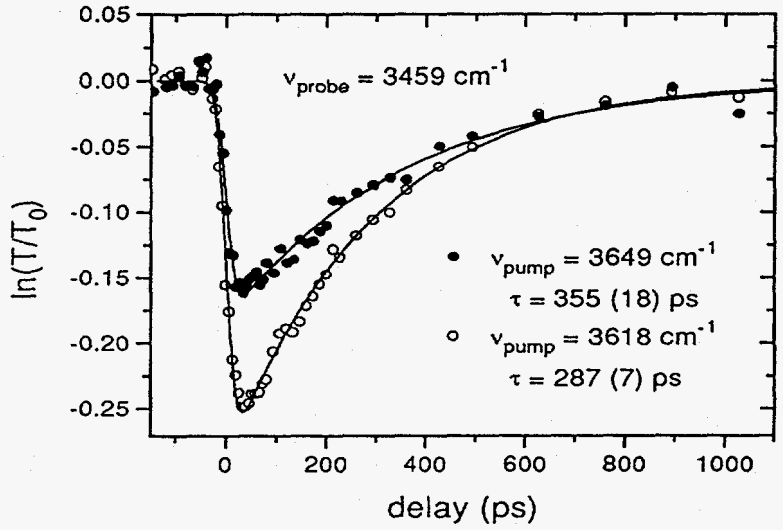

Figure 2: *Relative transmission change* $\ln[T(t)/T_0]$ *of a probe pulse at the red side of the hot band as a function of the delay with the pump pulse, for two values of the center frequency of the pump. The lifetimes* τ *corresponding to single exponential decay of the transmission changes (with the standard deviations) are depicted in the graph. The relatively long lifetimes are in agreement with previous saturation experiments on similar sytems [16]).*

The population *dynamics* of the O–H vibration can be studied by measuring the probe transmission as a function of the delay time with respect to the pump pulse. To monitor the population dynamics of the $v = 1$ excited level, the probe frequency is fixed at 3459 cm^{-1}, at the red (low frequency) side of the $v_{1\rightarrow 2}$ hot band (see Fig. 1). At this frequency the laser linewidth is reduced to 12 cm^{-1} FWHM, due to water absorption in the region 3465 to 3510 cm^{-1} in the $LiNbO_3$ crystals in which the infrared pulses are generated. In this way the $v = 1$ excited level population is monitored for the subset of the O–H oscillators which have the lowest frequencies within the distribution of different vibrational frequencies in the (inhomogeneously broadened) HF absorption band. In Fig. 2, the transient $v = 1$ excited level population is shown for two excitation frequencies. The lifetime of the transient absorption is found to be different for different excitation frequencies. This is unexpected, since the same subset of oscillators, with a definite intrinsic population lifetime T_1, is probed in these experiments. The transient absorption lifetimes for several values of the center frequency of the pump are plotted in Fig. 3. The transient absorption probed at the red side of the hot band clearly lives longer after excitation at the blue side than after excitation at the red side of the absorption band.

Although in all experiments the same subset of oscillators is probed, the increasing lifetime τ for the transient absorption with increasing pump frequency could in principle be due to different population lifetimes T_1 for oscillators at different frequencies. For different pump frequencies the distribution of the excitations varies over the set of frequencies within the probe bandwidth, and a strong dependence of T_1 on frequency would result in a pump-frequency dependent transient absorption lifetime. A simple calculation shows that to explain the data of Fig. 3, the T_1 lifetimes should increase by more than a factor of two with frequency in the HF absorption band. In one-color bleaching experiments, in which the laser frequency was tuned over the absorption band, such a depencence has not been

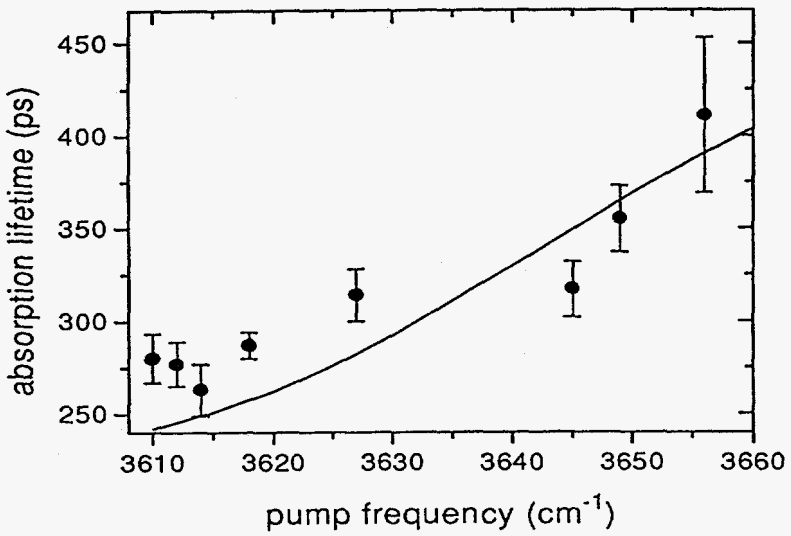

Figure 3: *Transient absorption lifetime for a probe pulse with frequency fixed at the red side of the $v_{1\rightarrow 2}$ hot band (at 3459 cm^{-1}), as a function of the central frequency of the exciting pump pulse. The probe pulse monitors the population in the excited $v = 1$ level for a subset of oscillators with fundamental absorption frequencies around 3621 cm^{-1} (= 3459 cm^{-1} + anharmonicity, obtained from Fig.1).*

found[4, 10]. Furthermore, such a distribution of T_1 lifetimes would result in a one-color bleaching lifetime which is larger than the transient absorption lifetime probed at the red side of the hot band. However, the exponential bleaching lifetime for the probe frequency equal to the pump frequency is found to be significantly shorter (250 $\pm$ 12 ps).

The observed dependence of the transient absorption lifetime on pump frequency is evidence for spectral diffusion of the O–H excitations on a picosecond timescale. The lifetime of the induced hot-band absorption, reflecting the excited population of the subset of probed oscillators, is determined by two effects: (i) vibrational relaxation of the O–H stretch vibrations and (ii) spectral diffusion of the excitations out of or into the probe bandwidth. For the pump frequency *resonant* with the frequency of the probed oscillators, at the red side of the absorption band, excitations are transferred to oscillators with other frequencies, which are not probed. Spectral diffusion then acts as a depopulation channel for the excited level of the probed oscillators, additional to vibrational relaxation, and consequently the transient absorption lifetime is shortened. In the case of slight *off-resonant* excitation, at the blue side of the absorption band, excitations are transferred from oscillators at the pump frequency to the probed oscillators at the red side. In this way the $v = 1$ excited level of the probed oscillators is being populated *after* excitation by the pump pulse and consequently the observed transient absorption lives longer than expected from the vibrational relaxation time T_1 alone.

The spectral diffusion can be explained by direct energy transfer of the O–H stretch vibrational quanta between O–H sites with slightly different frequencies. Dipole-dipole interactions can lead to this site-to-site energy transfer of excitations. This is the so called Förster transfer[11], which is well known for electronic systems[12], and has recently also been observed for vibrations on a surface[13, 14]. As long as the homogeneous absorption lines of the oscillators spectrally overlap, the excitation can be transferred among O–H

groups with slightly different frequencies. The small energy mismatch is compensated by the phonons which cause the homogeneous broadening.

Because the dipole-dipole excitation transfer time between two oscillators is inversely proportional to the distance to the sixth power, Förster transfer is expected to depend strongly on the concentration. Indeed, it was found in previous one-color experiments that with decreasing proton concentration the transient bleaching lifetime increases[4]. Using the structural information known for the fausjasite structure of zeolite Y[15] and the homogeneous linewidth of the oscillators, which is inferred from the O–D hole-burning experiments, we have calculated the Förster transfer rate of a vibrational excitation between two O–H oscillators[9]. In fully exchanged zeolites the distances between the O–H groups can be as short as 3 $\AA$ [15]. The effect of diffusion of the excitations on the transient probe transmission is calculated taking all possible oscillator sites within the lattice into account. This calculation is represented by solid line in Fig. 3.

In conclusion, we have observed spectral diffusion of vibrational excitations among the inhomogeneous distribution of O–H sites in a zeolite. This is explained by direct site-to-site transfer of the excitations due to dipole-dipole coupling of the oscillators (Förster transfer), which takes place on the same timescale as vibrational relaxation.

Acknowledgments

The work described in this paper is part of the research program of the Stichting Fundamenteel Onderzoek van de Materie (Foundation for Fundamental Research on Matter) and was made possible by financial support from the Nederlandse Organisatie voor Wetenschappelijk Onderzoek (Netherlands Organization for the Advancement of Research).

References

[1] I.W.M. Smith, *Nature* **358** (1992) 279, and references therein.
[2] J.M. Thomas, *Sci. Am.* **266** (April 1992) 82.
[3] J. Kubota, M. Furuki, Y. Goto, J. Kondo, A. Wada, K. Domen, and C. Hirose, *Chem. Phys. Lett.* **204** (1993) 273.
[4] M.J.P. Brugmans, A.W. Kleyn, A. Lagendijk, W.P.J.H. Jacobs, R.A. van Santen, *Chem. Phys. Lett.* **217** (1994) 117.
[5] M. Bonn, M.J.P. Brugmans, A.W. Kleyn, R.A. van Santen, *J. Chem. Phys.* **102** (1995) 2181.
[6] H. Graener, R. Dohlus, A. Laubereau, *Chem. Phys. Lett.* **140** (1987) 306.
[7] L.M. Kustov, V.Y. Borovkov, V.B. Kazansky, *J. Catal.* **72** (1981) 149.
[8] H. Graener, T.Q. Ye, A. Laubereau, *Phys. Rev. B* **41** (1990) 2597; H. Graener, T. Lösch, A. Laubereau, *J. Chem. Phys.* **93** (1990) 5365.
[9] M.J.P. Brugmans, H.J. Bakker, and A. Lagendijk, submitted for publication.
[10] M. Bonn, M.J.P. Brugmans, A.W. Kleyn, R.A. van Santen, and Ad Lagendijk, in *Studies in Surface Science and Catalysis*, Ed. J. Weitkamp, H.G. Karge, H. Pfeifer, and W. Hölderich, (Elsevier, Amsterdam, 1994) Vol. 84, p. 493.
[11] Th. Förster, *Discussions Faraday Soc.* **27** (1959) 7; Th. Förster, in *Modern Quantum Chemistry*, Ed. O. Sininoğlu, (Academic Press, New York, 1965), Part III, p. 93.
[12] J.M. Drake, J. Klafter, P. Levitz, *Science* **251** (1991) 1574, and references therein.
[13] M. Morin, P. Jakob, N.J. Levinos, Y.J. Chabal, A.L. Harris, *J. Chem. Phys.* **96** (1992), 6203.
[14] K. Kuhnke, M. Morin, N.J. Levinos, Y.J. Chabal, and A.L. Harris, *J. Chem. Phys.* **99**, (1993) 6114.
[15] M. Czjzek, H. Jobic, A.N. Fitch, and T. Vogt, *J. Phys. Chem.* **96** (1992) 1535.
[16] E.J. Heilweil, M.P. Casassa, R.R. Cavanagh, J.C. Stephenson, *Annu. Rev. Phys. Chem.* **40** (1989) 143.

Pressure Dependent Photon Echo Measurements of the Dynamics of Local Phonons and Tunneling Two Level Systems in Mixed Molecular Crystals and Glasses

Bruce J. Baer, Otto Berg, and Eric L. Chronister*
Department of Chemistry, University of California, Riverside, CA 92521.

INTRODUCTION

The local phonon dynamics in mixed molecular crystals can be investigated by measuring pressure induced changes in the frequency of the local phonons. In addition, since inhomogeneous broadening at high pressure obscures sharp features in the phonon side band spectrum, photon echo measurements are used in the present study for determining the effect of pressure on pseudolocal phonon dynamics.

Recent experiments have shown that pressure induced (0-20 kbar) changes in local phonon frequencies can give rise to dramatic changes in the electronic dynamics of chromophore guest molecules in both crystalline [1,2] and amorphous hosts [3,4,5]. The intramolecular vibronic relaxation rates of molecular crystals are also found to be very pressure dependent due to both pressure induced shifts in bulk phonon frequencies as well as changes in the magnitude of the anharmonic mode couplings.

The unique temperature dependent homogeneous linewidths observed for organic chromophores in polymer glasses has fueled a number of low temperature (<5K) optical dephasing studies by both photon echo[6,7] and hole burning measurements [8,9]. For the most part, the anomalous temperature dependent properties observed in glasses at very low temperature (i.e. < 3 K) have been attributed to the existence of tunneling two-level systems (TLS) [7,8,10,11], whereas scattering from optical phonons become important at higher temperatures [12]. Although a void space model has been suggested [13], a physical description of the TLS remains elusive.

The temperature dependent homogeneous pure dephasing rate of impurity chromophores in many organic and inorganic glasses can be characterized by the equation,

$$\frac{1}{T_2^*} = aT^{\alpha} + \frac{be^{-\hbar\omega/kT}}{1-e^{-\hbar\omega/kT}} \qquad (1)$$

where the first term on the right represents coupling of the impurity excited state to the TLS and the second term represents coupling to optical phonons of the glass of energy $\hbar\omega$. Homogeneous linewidths calculated from TLS models indicate that at low temperature (i.e. T < 4K) the pure homogeneous linewidth (or dephasing rate) should show a power law increase with temperature, where α is a characteristic of the host glass with typical values in the range 1.3 to 1.4 for organic glasses. The temperature dependent exponent α is often related to the TLS density of states $\rho=\rho_0 E^{\mu}$, where E is the tunnel state splitting, and where $\alpha = 1+\mu$.[14]

EXPERIMENTAL

The details of the high pressure techniques[15], laser system[16] and optical measurements have been described previously [17]. The second harmonic output of a mode-locked Q-switched Nd:YAG laser was used to pump a cavity dumped, tunable, dye laser with pulse energies of 10μJ, pulsewidth of 30ps, at a repetition rate of 800 Hz. The laser pulses were attenuated to about 0.1

μJ, focused to 50μm, and spatially overlapped in the sample. The photon echo emission was spectrally filtered with a monochromator, detected with a cooled photomultiplier (Hamamatsu R955P) and a lock-in amplifier, digitized and averaged over several scans, and analyzed on a personal computer.

Pressures were measured by the shift of the R_1 Ruby line as well as by the shift in the pentacene absorption frequency.[15] Temperatures between 4.3 K and 10 K were obtained using a temperature controlled (Lake Shore, Model 330) helium flow cryostat (Janis, STVP-100) while temperatures in the range 1.2 to 2.1 K were obtained using an optical liquid helium dewar.

RESULTS AND DISCUSSION

The Effect of Pressure on Pseudolocal Phonon Energies in Mixed Crystals

A useful phenomenological expression for evaluating temperature dependent photon echo measurements of electronic dephasing in mixed crystals is given by [18],

$$T_2^*(T) = T_2^*(\infty)\exp\left(\frac{\Delta E}{kT}\right) \qquad (2)$$

where T_2^* is the pure dephasing time (i.e. $(T_2)^{-1} = (2T_1)^{-1} + (T_2^*)^{-1}$), and ΔE is often correlated with the pseudolocal phonon energy $h\nu_i$, and the prefactor $T_2^*(\infty)$ reduces to the pseudolocal phonon lifetime τ^* in the slow exchange limit. Thus, the observed pressure induced *decrease* in the homogeneous decay rate is due to an increase in the pseudolocal phonon frequency ν_i.

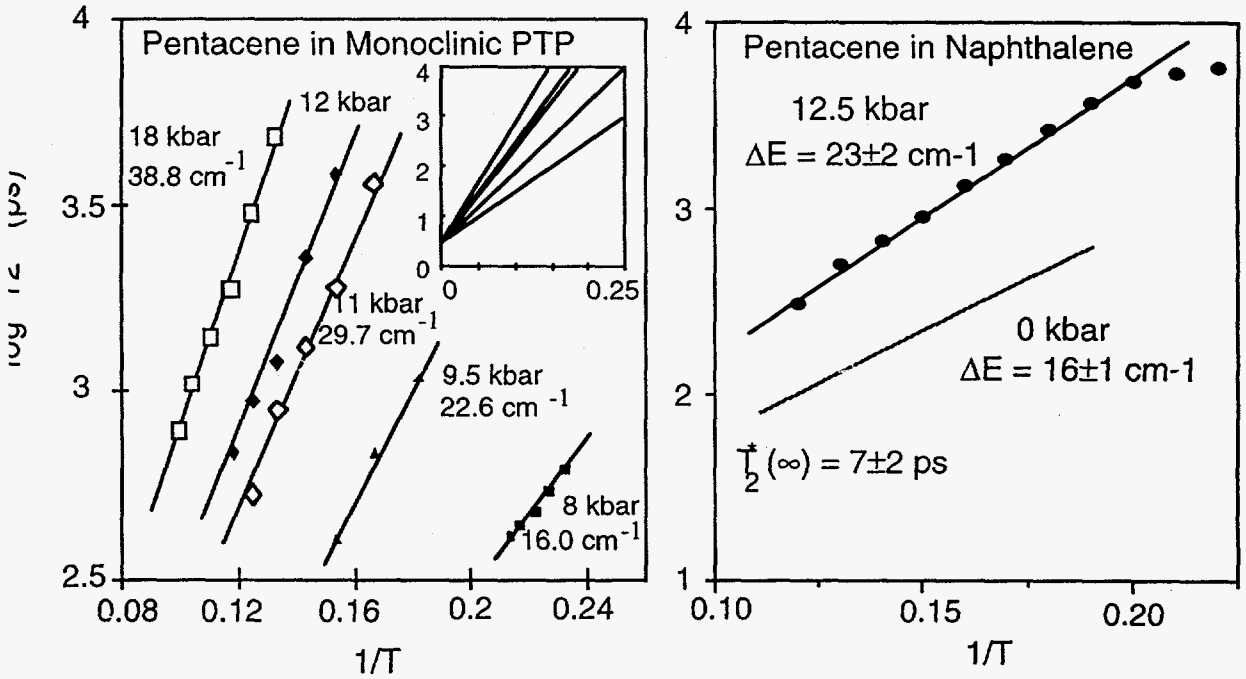

Figure 1. Arrhenius plots of the pure dephasing time (T_2^*) at variable pressure. a) Pentacene in monoclinic p-terphenyl. b) Pentacene in naphthalene. The slope ΔE is characteristic of the pseudolocal phonon frequency. The high temperature intercepts $T_2^*(\infty)$ are pressure independent.

The pressure induced shifts in pseudolocal phonon frequencies ν_i arise due to anharmonic intermolecular interactions which can be described by a Grüneisen model,

$$\frac{\nu_i(p)}{\nu_i(o)} = \left(\frac{V_o}{V_p}\right)^{\gamma_i} \tag{3}$$

where $\nu_i(p)$ is the mode frequency at pressure p, V_p is the molar volume at pressure p, and γ_i is the mode Grüneisen parameter. Thus, pressure can alter the thermal occupation of pseudolocal phonons by raising their energy relative to kT, resulting in dramatic pressure induced changes in optical dephasing.[1,2,19]

Temperature dependent photon echo measurements can be used to investigate the effect of pressure on the pseudolocal phonon energy (characterized by ΔE), which in turn can be used to obtain a mode Gruneisen parameter γ_i for the pseudolocal phonon. For pentacene in monoclinic p-terphenyl γ_i is found to be large and very pressure dependent, ranging from a value of $\gamma_i = 28$ at 9 kbar to a value of $\gamma_i = 2.5$ above 18 kbar. Not shown in this paper are the results for a triclinic p-terphenyl host in which γ_i for the pseudolocal phonon is found to be negative. These very large and anomalous results can be attributed to a polymorphic phase transition of the p-terphenyl lattice at a pressure near 6 kbar.

The relatively pressure independent $T_2^*(\infty)$ values observed for pentacene in both monoclinic p-terphenyl and naphthalene host crystals are somewhat surprising since one might expect large shifts in phonon energies to affect the phonon relaxation rates.

The Effect of High Pressure on Optical Dephasing in Organic Polymers

High pressure (0-30 kbars) has been used to investigate the density dependence of the temperature dependent optical dephasing of rhodamine 101 (Rh101) in polymethyl methacrylate (PMMA). Photon Echo measurements have been performed on Rh101 doped PMMA at temperatures between 1.2 and 2.1 K at pressure up to 30 kbar. At 30 kbar the 20% volume compression resulted in little change in either the magnitude or the temperature dependence of the optical dephasing rate, i.e. a relatively pressure independent homogeneous linewidth $\Gamma = 110\text{MHz}\cdot T^{1.35}$ is observed.

A pressure increase of 30 kbar from ambient results in a volume reduction of about 20% [20], corresponding to a 7% reduction in the tunneling distance, d, sketched in Figure 2. In addition, the effect of pressure on the TLS barrier heights can be approximated using the polymer glass transition temperature T_g as a qualitative measure of the relative tunneling barrier heights. For PMMA the glass transition temperature at ambient pressure is $T_g(0\text{kbar})=105^\circ\text{C}$ and increases by 23 K/kbar from 0 to 3 kbar [21]. Even a conservative extrapolation to 30 kbar yields a two fold increase in the glass transition temperature. Such an increase in the glass transition temperature corresponds to a considerable increase in the *average* of the barrier height distribution.

If the *form* of the TLS density of states is not dramatically changed by compression, then the temperature dependent power law in eq (1) should remain relatively unchanged, however, one would expect a change in the absolute magnitude of the dephasing rate. Thus, it is surprising that the temperature dependent optical dephasing of rhodamine 101 in PMMA is not significantly altered over the pressure range 0 - 30 kbar, as shown in Figure 2. Without a fortuitous cancellation of pressure induced tunneling effects, i.e. unchanged tunneling rates due to the opposing effects of increased barrier heights and decreased tunneling distances at high pressure, it is still not clear why pressure had so little affect on the observed optical dephasing rate.

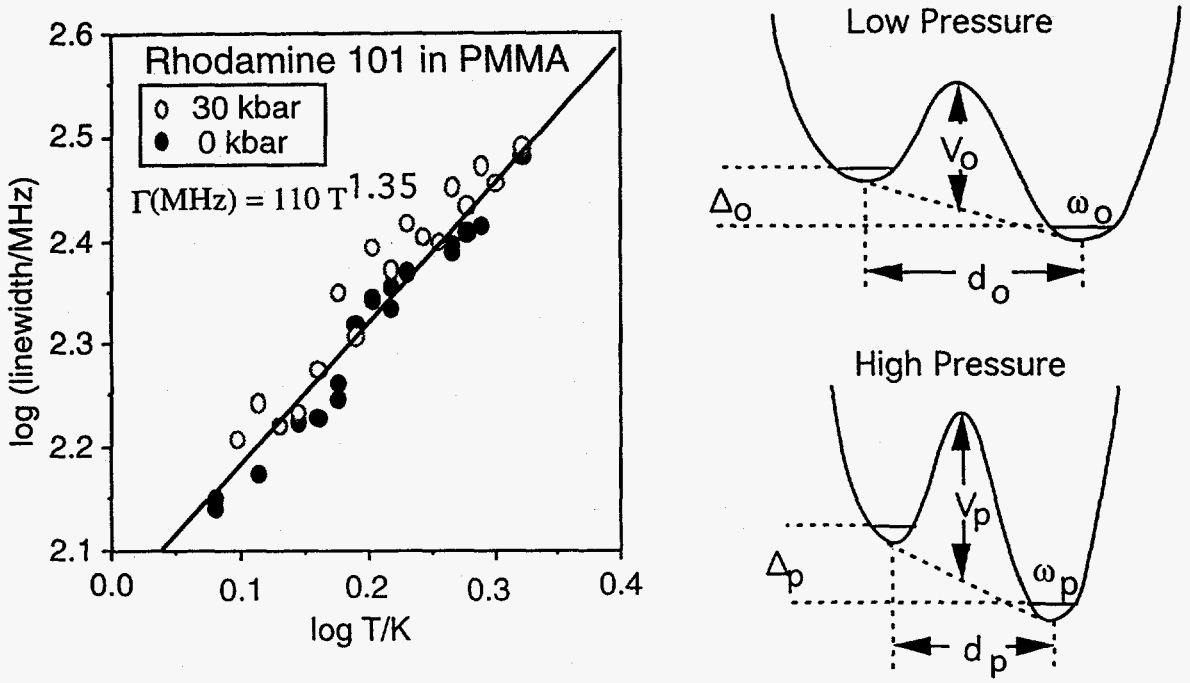

Figure 2. a) Log-log plot of the temperature dependent homogeneous linewidth at ambient pressure and at a pressure of 30 kbar. The data is nearly pressure independent and is a fit to the equation $\Gamma = 110 \cdot T^{1.35}$ MHz. b) A sketch of changes in the TLS potential energy diagram under compression. Δ is the asymmetry, V the barrier height, and d the spatial separation between the potential minima.

CONCLUSION

Although dramatic pressure induced changes in vibrational relaxation and optical dephasing are observed in crystalline systems, the low temperature optical dephasing of an impurity in an amorphous polymer host is found to be nearly pressure independent. Whereas pressure induced line narrowing in mixed crystalline systems results from a dramatic increase in pseudolocal phonon frequencies at high pressure, temperature dependent photon echo measurements in amorphous PMMA are relatively insensitive to a pressure induced volume decrease of 20%. By examining the effect of density on a wider range of amorphous systems we expect to gain a better physical picture of the TLS's used to describe the anomalous temperature dependent homogeneous linewidths in glassy systems.

Acknowledgments

We acknowledge the National Science Foundation (CHE-9400542) for financial support.

References

1. B. J. Baer and E. L. Chronister, J. Phys. Chem., 99 (1995) 7324.
2. R. A. Crowell and E. L. Chronister, Chem. Phys. Lett., 216 (1993) 293.

3. H. C. Meijers and D. A. Wiersma, J. Chem. Phys., 101 (1994) 6927.
4. A. Ellervee, R. Jaanisco, J. Kikas, A. Laisaar, A. Suisalu and V. Shcherbakov, Chem. Phys. Lett., 176 (1991) 472
5. A. Ellervee, V. V. Hizhnyakov, J. Kikas, A. Laisaar, and A. Suisalu, J. Lumin., 53 (1992) 223
6. H. C. Meijers and D. A. Wiersma, Phys. Rev. Lett., 68 (1992) 381.
7. L. R. Narasimhan, Y. S. Bai, M. A. Dugan and M. D. Fayer, Chem. Phys. Lett., 176 (1991) 335.
8. L. R. Narasimhan, K. A. Littau, D. W. Pack, Y. S. Bai, A. Elschner and M. D. Fayer, Chem. Rev., 90 (1990) 439.
9. D. W. Pack, L. R. Narasimhan and M. D. Fayer, J. Chem. Phys., 92 (1990) 4125.
10. H. Fidder, S. De Boer and D. A. Wiersma, Chem. Phys., 139 (1989) 317.
11. W.A. Phillips, Ed., Amorphous Solids: low-temperature properties (Springler-Verlag, Berlin 1981).
12. A. Elschner, L. R. Narasimhan and M. D. Fayer, Chem. Phys. Lett., 171 (1990) 19.
13. M. H. Cohen and G. S. Grest, Phys. Rev. Lett., 45 (1980) 1271; and Solid State Commun., 39 (1981) 143.
14. R. Jankowiak, J.M. Hayes, and G.J. Small, Chem. Rev., 93 (1993) 1471.
15. B.J. Baer, E.L. Chronister, Chem. Phys., 185 (1994) 385.
16. R.A. Crowell, E.L. Chronister, J. Phys. Chem., 96 (1992) 9660.
17. B.J. Baer, E.L. Chronister, J. Chem. Phys., 100 (1994) 23.
18. W.H. Hesselink, D.A. Wiersma, J. Chem. Phys., 73 (1980) 648.
19. B. J. Baer and E. L. Chronister, J. High Press. Res., 12 (1994) 101.
20. P.W. Bridgeman, Proc. Amer. Acad. Arts. Sci., 76 (1948) 71.
21. C. Price, Polymer, 16 (1975) 585.

Optical and Vibrational Coherence in Bacteriochlorophyll a

D.C. Arnett, T-S. Yang and N. F. Scherer
Department of Chemistry, University of Pennsylvania,
Philadelphia, PA 19104-6323

The dynamic nature of a liquid medium causes structural changes to occur on timescales corresponding to the Fourier transform of the far-infrared or Raleigh-wing spectrum of the material. Experiments that are performed on such short timescales are capable of directly capturing the solvent effect on or response to chemical processes. [1] The nonlinear response function description of third-order polarization, $P^{(3)}(t_1,t_2,t_3)$, spectroscopy [2] shows that chromophore optical dephasing is described by the correlation function of the chromophore electronic frequency modulation; this, in turn, depends upon the magnitude of the chromophore transition dipole-bath coupling and the spectral range of bath fluctuations. A comparison of the solvent spectral density obtained from optical Kerr effect studies and the evolution of optical coherence of cyanine dyes has shown that similar bath dynamics are reflected in both measurements. [3]

Optical coherence methods, especially photon echo techniques, have recently been applied to the study of chromophore dephasing in solution.[4-8] These include 2-pulse (2PE), 3-pulse (3PE) and time gated photon echos (TG-PE) that allow variations of coherence and/or population time delays. The TG-PE approach even allows for establishing the temporal profile of the third-order polarization [5b,7] rather than the time-integrated polarization. [3,4,5a,6] Time-gated photon echo signals [7] are obtained via sum-frequency generation of the polarization with a separate gate pulse at time t_{3g} for various values of t_{12} and t_{23} making this a 4-dimensional measurement. Combinations of these different measurements along with nonlinear response function analysis [2,8] can be used to establish the low and high-frequency bath (i.e. solvent) fluctuations that cause evolution of the energy gap correlation function and optical dephasing.

This paper presents the the 3-pulse photon echo response of Bacteriochlorophyll$_a$ (BChla) monomers in pyridine and THF solutions. These measurements reflect the evolution of optical and vibrational coherence of the system along time axes t_{12} and t_{23}, respectively. In particular, optical dephasing is probed by scanning the time delay between the first two pulses (t_{12}), vibrational dephasing is probed while scanning the second delay (t_{23}), and spectral diffusion is detected via the time shift of the photon echo response (scanning t_{12} for various values of t_{23}).

The optical source for the results presented here is a home-built cavity-dumped Kerr lens mode-locked Ti:Sapphire laser of a unique design producing 13fs duration gaussian pulses with 90-100nm spectral bandwidth and 40nJ energies. The sample is contained in a 0.5 mm path length spinning cell and the echo signal is detected in the $k_s=k_3+k_2-k_1$ direction. The system temporal response and the experimental zero-of-time are determined from the nonresonant scattering response of the pure solvent which is detected in the same direction as the resonant photon echo from BChla. The samples included both THF and pyridine solutions of BChla (Sigma, Rb. Sphaeroides). These solvents serve to hexa-coordinate the central Mg atom thereby producing monomeric BChla solutions.

Figure 1 shows the $|P^{(3)}(0,0,t_3)|^2$ "pump-probe scattering" or transient grating response of BChla in THF. **Vibrational coherences** are impulsively driven and detected in the nonlinear optical response; the Fourier absolute magnitude spectrum is shown in the inset. The vibrational frequencies observed in the figure (185, 210, 340, 480, 560, 730, 790, 890, and 1180 cm^{-1}) are in very good agreement with line positions obtained from cw-Raman measurements. [10,11] The time constants for vibrational dephasing are determined to be about 1 ps by singular value decomposition analysis. The vibrational dephasing reflects the force autocorrelation function of the bath projected onto the vibrational modes. Clearly, the timescale for vibrational dephasing is much shorter than the relaxation of the population contribution to the photo-bleach/stimulated emission [12] signal (i.e. dc-offset). Similar results are obtained in pyridine solution. Intense low frequency modes between 100 cm^{-1} and 300 cm^{-1} reported for BChla in the photosynthetic reaction center[11] are weak in the present data. This finding is, however, consistent with the lack of vibrational coherence excitation of BChla in solution obtained with 50 fs pulse excitation and probing. [12]

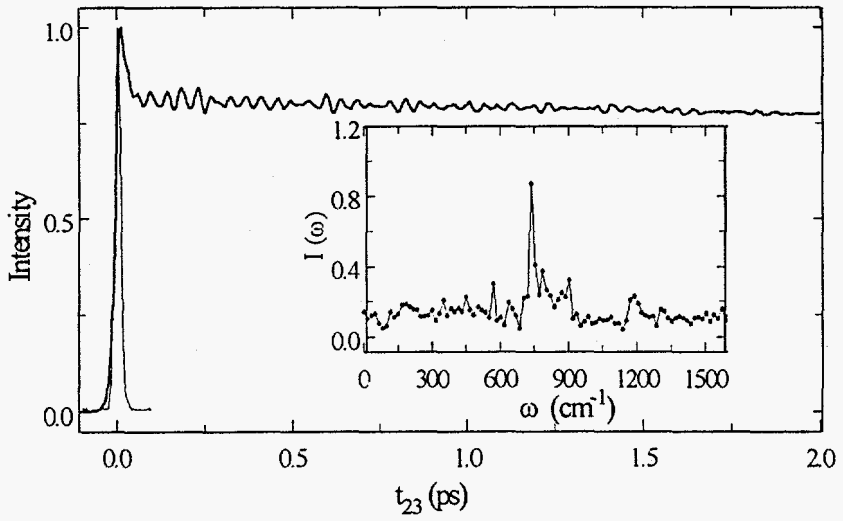

Figure 1. Modulus square four wave mixing response of BChla in THF measured in a Boxcar geometry. Inset: Fourier transform of the time domain data deconvoluted for the finite laser pulse duration. The display is of the absolute magnitude of the FT data, i.e. square-root of the power spectrum. A biexponential decay fit to the time domain data has been subtracted before Fourier transformation.

The $|P^{(3)}(t_1,t_2=t_3)|^2$ **optical coherence** response of BChla in THF is shown in Fig. 2. The echo shape is asymmetric with a significant time-shift (10-12 fs) from the zero-of-time point. The echo shift indicates that the solvent response is not in the homogeneous limit but has an inhomogeneous contribution.[13,14] The prompt decay of the echo signal indicates that homogeneous relaxation is, however, significant; the chromophore coherence decays on a series of timescales reflecting the spectrum of and coupling to the solvent fluctuations. The timescale for **spectral diffusion** is inferred from the evolution of the echo time-shift for increasing t_{23} time delays, $|P^{(3)}(t_1,t_2<t_3)|^2$. These results are shown in figure 3a. The evolution of the optical coherence response in pyridine and THF solutions both show fast and slow contributions to the chromophore spectral diffusion.

Numerical simulations incorporating the solvent polarizability spectral density and the multi-mode aspect of the chromophore response, i.e. intra-chromophore vibrational modes, are capable of faithfully capturing the dynamical responses recorded above. The simulations, using

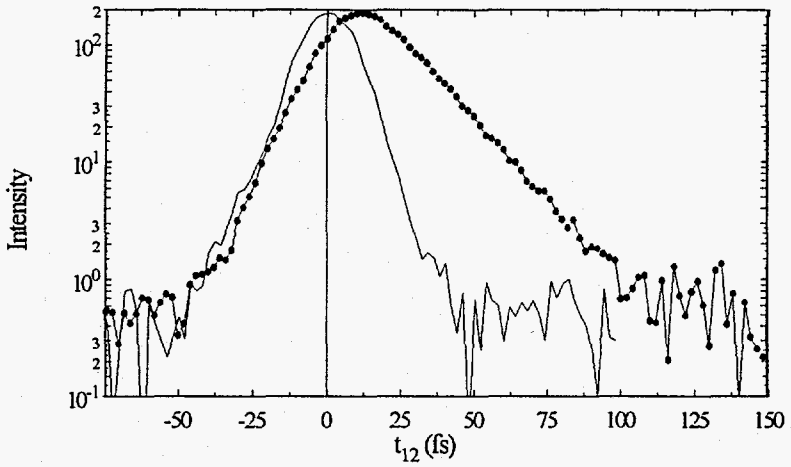

Figure 2. Photon echo response of BChla in pyridine. Solid line + dots: Bchla photon echo signal, line only: pure-solvent (pyridine) 3-beam scattering response. The nonresonant Pyridine response from the pure solvent is at least 5 times smaller than the resonant BChla signal, but is normalized in this representation to show the instrument temporal resolution.

mode displacements from resonance Raman spectra, test both the utility of the pure solvent polarizability response for analysis of short time dynamics as well as the long-time spectral diffusion response. The nonlinear response function simulation peak-shift results are superimposed on the experimental. Good agreement is obtained for early t_{23} time delays up to about 100 fs. The two curves then diverge from each other. The simulation using the measured solvent spectral density does not contain sufficient low frequency amplitude to match the slow change of the experimental peak shift over 5 ps delay (t_{23}). This finding is in agreement with the recent work of Fleming and coworkers on the 3-pulse photon echos of HITCI in ethylene glycol where low frequency terms had to be added to the from a single Brownian oscillator spectral density to reproduce the longer t_{23} spectral diffusion dynamics.[14]

The low frequency spectral density not reflected in the OKE susceptibility/spectral density used here may result from the direct solvent-solute interaction and restricted solvent motions at the solute "interface". These slow solvent bath fluctuations are "inhomogeneous" (static) broadening contributions to the photon echo signal at early t_{23} time delays as shown in fig. 1 (t_{23}=0). Alternatively, other low frequency modes of the chromophore that exhibit an overdamped response may also contribute to the "bath" spectral density. When t_{23} is increased more chromophore intramolecular fluctuations (vibrational coherences) and the lower frequency bath fluctuations contribute to the ernegy gap correlation function. Broadening or bath contributions that were previously static become dynamic and contribute to the "homogeneous" dephasing behavior of the optical coherence.

Figure 3b shows the 3-pulse photon echo peak shift obtained at 9 fs intervals in t_{23}. Here, the peak shift exhibits oscillations over a 1 ps (or more) t_{23} delay. The solid curve through these points is a LPSVD analysis [15] of the time-shift data exhibiting sinusoidal components of 730 and 463 cm^{-1} frequency that are in agreement with the vibrational coherence features seen in the pump-probe scattering data shown in fig. 2. We conclude that chromophore vibrational coherences contribute to the temporal shift of the echo signal and therefore also to the optical coherence dephasing.

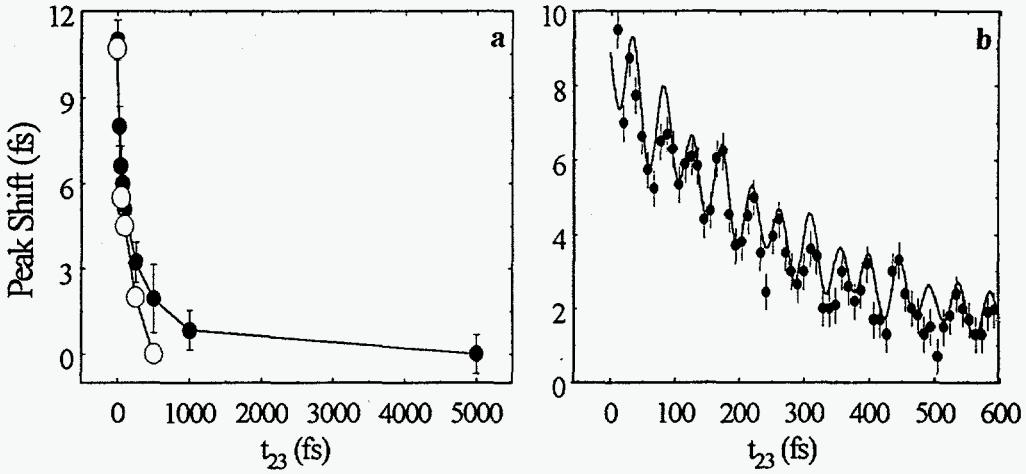

Figure 3. (a) Spectral diffusion dynamics of BChla monomers in pyridine. The solid points and error bars show the experimental echo maxima as a function of t_{23} delay time. The points represent the simulated results based on the solvent polarizability spectral density and multi-mode chromophore response. (b) Spectral diffusion dynamics of BChla monomers in THF observed as a function of t_{23} delay. The experimental echo maxima are shown as points with error bars for t_{23} time steps of 9 fs. The line through the points is a LPSVD fit containing 2 oscillatory components of 730 and 463 cm^{-1}.

Figure 4 shows a comparison between the experimental photon echo signal at t_{23} = 100 fs and the multi-mode spectral density nonlinear response function simulation of the echo signal. The agreement between experiment and simulation is excellent. This result supports the idea that incorporation of seven intra-chromophore modes observed in resonance Raman measurements [11] and displacements [16] along with the measured solvent spectral density well reflects the high frequency fluctuations that contribute to the decay of BChla optical coherence in liquids.

The experimental results presented here indicate that BChla is a useful probe of bath fluctuations in solution and will presumably also serve well in this capacity in the more "glassy" environment inside of proteins. BChla is an important chromophore that is involved in energy and electron transfer processes in photosynthesis. [17, 18] The present results indicate that the vibrational and optical dephasing responses obtained *in vitro* will be helpful in establishing the spectrum of bath fluctuations[19] and the coupling of the chromophore vibrational[20] and electronic coordinates to the protein bath in light harvesting antennas and photosynthetic reaction centers.

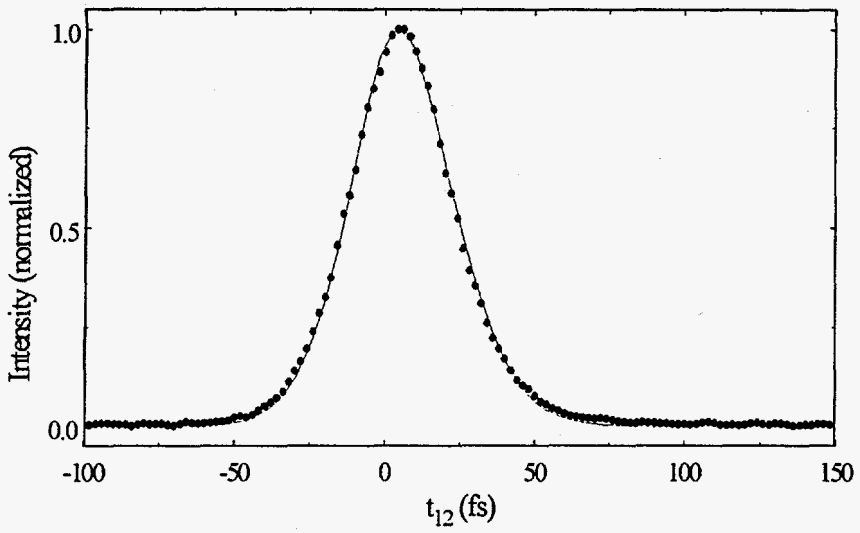

Figure 4. Comparison of 3-pulse photon echo response of BChla in pyridine and simulation using the solvent spectral density approach. The dots are experimental data points for t_{23}=100 fs, while the solid line is the calculated signal for the same t_{23} delay.

References

1. M. Cho, S.J. Rosenthal, N.F. Scherer, L.D. Ziegler and G.R. Fleming, *J. Chem. Phys.*, **96**, 5033 (1992).
2. Y.J. Yan and S. Mukamel, Phys. Rev. A, **41**, 6485 (1990); *J. Chem. Phys.*, **94**, 179 (1991).
3. P. Vöhringer, D.C. Arnett, R.A. Westervelt, M.J. Feldstein and N. F. Scherer, *J. Chem. Phys.*, **102**, 4027 (1995);
4. J-Y Bigot, M. T. Portello, R. W. Schoenlein, C. J. Bardeen, A. Migus and C. V. Shank. *Phys. Rev. Lett.* **66**, 1138 (1991); (b) C. J. Bardeeen, and C. V. Shank. *Chem. Phys. Lett.* **226**, 310 (1994).
5. (a) E. T. J. Nibbering, D. A. Wiresma, and K. Duppen. *Phys. Rev. Lett.* **66**, 2464 (1991). (b) M. S. Pshenichnikov, K. Duppen, and D. A. Wiersma, *Phys. Rev. Lett.* 74 674 (1995).
6. T. Joo, and A. C. Albrecht. Chem. Phys., **176** 233 (1993).
7. P. Vöhringer, D.C. Arnett, T-S. Yang and N. F. Scherer, *Chem. Phys. Lett.*, **237**, 387 (1995).
8. T. Joo, Y. Jia, and G. R. Fleming, *J. Chem. Phys.* **102**, *10*, 4063 (1995).
9. T-S. Yang, P. Vöhringer, D. C. Arnett, and N. F. Scherer. *J. Chem. Phys.* in press (1995).
10. T.M. Cotton and R.P. van Duyne, *J. Am. Chem. Soc.*, **103**, 6020 (1981).
11. N. J. Cherepy, A. P. Shreve, L. F. Moore, S. Franzeu, S. G. Boxer, and R. A. Mathies. *J. Chem. Phys.* **98**, *23*, 6023 (1994).
12. S. Savikhin and W.S. Struve, *Biophys. J.*, **67**, 2002 (1994).
13. N.E. Shemetulskis and R.F. Loring, *J. Chem. Phys.*, **89**, 1217 (1992).
14. M. Cho and G.R. Fleming, *J. Chem. Phys.*, **98**, 2848 (1993).
15. P. Vöhringer, R. Westervelt, T-S. Yang, D. C. Arnett, M. J. Feldstein, and N. F. Scherer, *J. Raman Spec.* July (1995).
16. H. C. Chang, G. H. Small, and R. Jankowiak, *Chem. Phys.* **194**, 323 (1995).
17. J.M. Olson, *Biochimica et Biophysica Acta,* **594**, 33 (1980).
18. G. R. Fleming and van Grondelek, *Physics Today,* **47**, 48, February (1994).
19. J. N. Gehlen, M. Marchi, and D. Chandler, *Science*, **263**, 499 (1994).
20. M. H. Vos, F. Rappaport, J-C. Lambry, J. Breton, and J-L. Martin, *Nature,* **363**, 320 (1993).

Raman Echo Studies of Vibrational Dephasing in Liquids and Glasses

Mark Berg, David Vanden Bout and John Freitas
Department of Chemistry and Biochemistry, University of South Carolina, Columbia, SC 29208

INTRODUCTION

The intrinsic line width of a vibrational transition in a condensed phase is a direct reflection of the interaction of the vibrational mode with the surrounding matrix. Many different types of interaction which can potentially affect vibrations have been identified theoretically.[1, 2] New time-resolved spectroscopic methods such as the Raman echo are providing more detail on these interactions and also reexamining standard assumptions about the relative importance of different interactions.

Of special interest are isotropic Raman transitions, which are not broadened by molecular rotation as many IR transitions are. Measurements of vibrational lifetimes (T_1) show that they are typically several picoseconds or longer, too slow to account for most of the observed line widths.[3] The consensus has developed that pure dephasing is responsible for most isotropic Raman line widths.[1,2] In this case, the lineshape is given by the Fourier transform of a single-time correlation function of the frequency shifts induced in the vibrator by the environment $\delta\omega(t)$,

$$C_{FID}(\tau) = \left\langle \exp\left[-i\int_0^{\tau} \delta\omega(t)\, dt \right] \right\rangle . \tag{1}$$

This function is measured by transforming the Raman lineshape, or more recently, by a time-domain experiment, the Raman free induction decay (RFID).[1,2] Also known as time-resolved CARS, the RFID experiment starts with a coherent excitation of the vibration by stimulated Raman scattering between a pair of subpicosecond pulses. After a delay time τ, the degree of coherence remaining is measured by coherent Raman scattering from a third pulse.

Although this measurement contains a great deal of information, it also has an inherent ambiguity.[4] The size of the integral is determined by both Δ, the rms amplitude of $\delta\omega(t)$, and τ_ω, the time scale over which $\delta\omega(t)$ varies. In the limit of slow perturbations, $\tau_\omega >> 1/\Delta$, the decay of $C_{FID}(t)$ is determined by Δ and the associated line is inhomogeneously broadened. In the limit of fast perturbations, $\tau_\omega << 1/\Delta$, the decay rate of $C_{FID}(t)$ is determined by $\Delta^2\tau_\omega$, and the associated line is homogeneously broadened. In liquids, potential sources of perturbation span both limits and the intermediate region in between. Thus the properties of $\delta\omega(t)$ cannot be uniquely determined from $C_{FID}(t)$ alone.

The Raman echo experiment removes this ambiguity. The Raman echo is a five-pulse experiment exploiting a higher order nonlinearity than the Raman FID, and has only recently been observed in liquids.[5-9] It measures a two-time correlation function,[4]

$$C_{RE}(\tau_1,\tau_2) = \left\langle \exp\left(i\int_{\tau_1}^{\tau_1+\tau_2} \delta\omega(t)\, dt - i\int_0^{\tau_1} \delta\omega(t)\, dt \right) \right\rangle . \tag{2}$$

An example of a measurements of this function is shown in Fig. 1.

As in the RFID, the vibration is initially excited via stimulated Raman by a pair of pulses. Dephasing occurs for a time τ_1, after which a second pulse pair reverses the phase of the coherent vibration. If $\delta\omega(t)$ has not changed much during τ_1, the dephasing will be reversed, and the coherence will increase. In contrast, if all memory of $\delta\omega(t)$ is lost during τ_1, the coherence will simply continue to decay as it does in the RFID. The size of the coherence at a time τ_2 is

monitored by coherent anti-Stokes scattering from a fifth pulse. By comparing the decay of the coherence during τ_2 with the RFID, the time scale of $\delta\omega(t)$ is unambiguously determined.

In this paper, we report Raman echo measurements on the symmetric methyl stretching vibration in different environments. Although the vibrator is essentially the same in all cases, the dephasing dynamics change substantially in different environments.

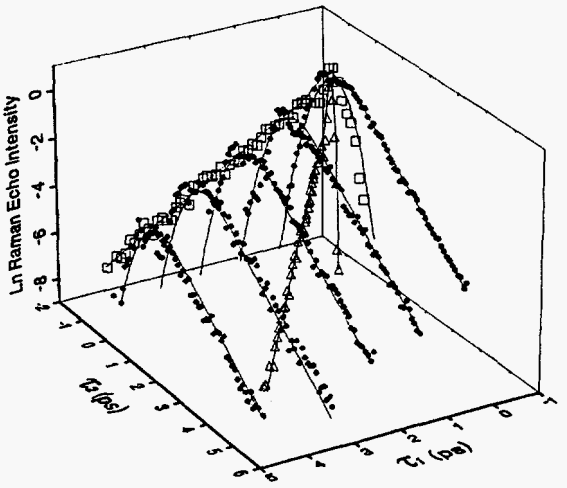

Fig. 1. The full two dimensional $C_{RE}(t)$ function measured for the sym. methyl str. of CH_3CN. The decay in τ_2 is the same as the RFID decay (curves) regardless of τ_1, indicating that $\delta\omega(t)$ decays rapidly, i.e. the Raman line is homogeneously broadened. If $\delta\omega(t)$ varied more slowly, the rephasing effects of the second excitation would raise the Raman echo points above the RFID curves, especially for larger values of τ_1 and τ_2.

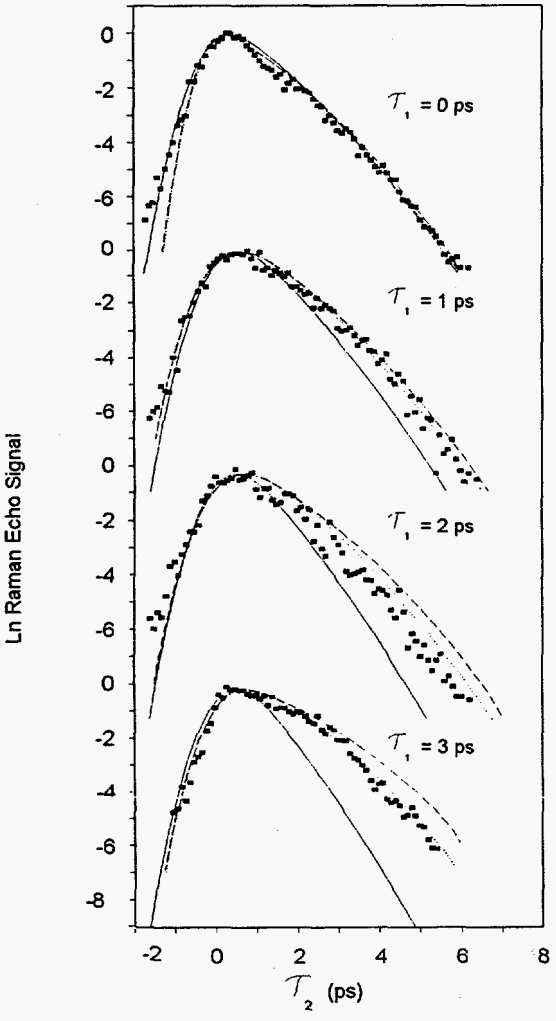

Fig. 2. Raman echo data on the sym. methyl str. of $CH_3I/CDCl_3$ (points) compared to models for purely homogeneous broadening (solid), partial static inhomogeneous broadening (dashed), and partial inhomogeneous broadening with spectral diffusion (dotted).

INHOMOGENEOUS BROADENING AND SPECTRAL DIFFUSION

An example of inhomogeneous broadening is the sym. methyl str. in a 1:1 mixture of $CH_3I/CDCl_3$. Raman echo data from this system are shown in Fig. 2. Under all circumstances, the Raman echo decay in τ_2 for $\tau_1 = 0$ should match the RFID (solid curve). However, as τ_1 increases, the Raman echo decay becomes progressively slower relative to the RFID. This effect results from the rephasing of an inhomogeneous component of the line broadening. However, the rephasing is incomplete, indicating that there is also a homogeneous component present.

The inhomogeneous component arises from concentration fluctuations, as originally suggested by Döge, et al.[10] In the local region around each methyl group, the ratio of CH_3I to $CDCl_3$ molecules may fluctuate significantly from the bulk average. The frequency of the symmetric stretch is a linear function of the concentration, as shown by concentration-dependent Raman experiments. The result is an inhomogeneous contribution to the line shape.

Concentration fluctuations were modeled very simply by assuming random mixing among

N neighboring molecules, each of which affects the vibrational frequency equally. The model was required to fit not only the Raman echo data, but also the RFID data and concentration-dependent Raman lineshape measurements. The results are shown in Fig. 2 as dashed curves. The model is qualitatively correct in predicting a slower decay in τ_2 as τ_1 increases, but overestimates the magnitude of the rephasing. A major deficiency of this model is that it assumes the inhomogeneity is static, whereas the local composition may change by diffusion within the 9 ps covered by the experiment. This effect would cause spectral diffusion within the inhomogeneous band. Without including spectral diffusion, a quantitative fit to all the available data is not possible.

An improved model including spectral diffusion is shown as dotted curves in Fig. 2. Quantitative agreement is found for a spectral diffusion time of ~5 ps. This time is consistent with diffusion over a distance of one molecular diameter, and suggests that the "local" environment is actually the first solvation shell. The fit value of $N = 5.4$ is also consistent with the number of molecules expected in the first solvation sphere and confirms that only the nearest neighbor molecules have a significant effect on the frequency of the vibrator. As originally argued by Schweizer and Chandler,[11] an interaction modulated by diffusion and extending approximately one molecular diameter is characteristic of interaction through the attractive portion of the intermolecular potential, as opposed to the repulsive wall.

SOLVENT-INDUCED INTRAMOLECULAR VIBRATIONAL REDISTRIBUTION

As shown in Fig. 1, the sym. methyl stretch in neat acetonitrile, where concentration fluctuations are absent, has no inhomogeneous broadening. However, the same mode in ethanol initially appears to be a strong candidate for showing inhomogeneous broadening in a neat liquid. Its line width is more than twice as large as acetonitrile's (18 cm^{-1} vs. 6.5 cm^{-1}), suggesting a new effect is present in ethanol. The extra line width is not due to a fast T_1. The population relaxation time for this mode has been measured as 20 ps, far too slow to affect the line width.[3]

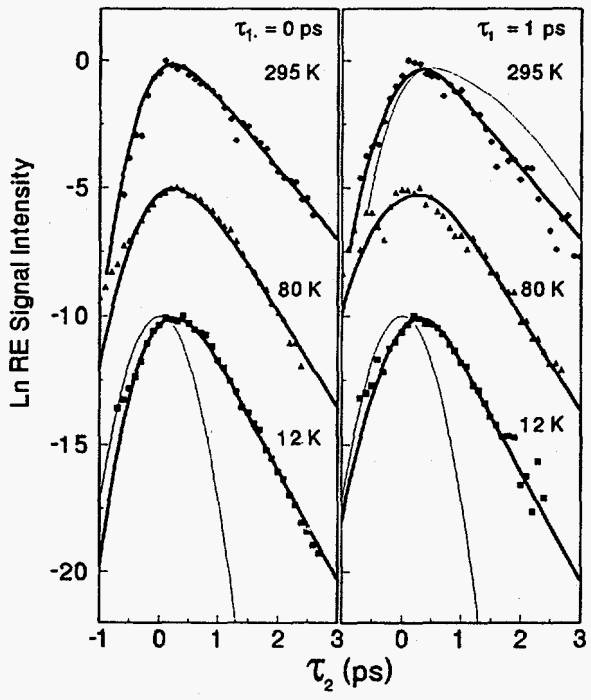

Fig. 3. Raman echo data on ethanol-1,1-d_2 at room temperature, just below the glass transition and at low temperature. Neither line narrowing nor inhomogeneous broadening are found at low temperature. The light curve at 298 K is the prediction if the additional line width relative to acetonitrile were due to inhomogeneous broadening. The instrument response is shown as the light curves at 12 K.

All theories of homogeneous pure dephasing predict a significant slowing of the dephasing when the temperature is reduced.[1, 2] Figure 3 shows Raman echo measurements on ethanol-1,1-d_2 over a wide temperature range. The deuteration prevents interaction of the methyl stretch with the methylene stretches. The curves on the left, taken at $\tau_1 = 0$, are equivalent to RFID measurements, and are simply the Fourier transform of the line shape. When the temperature is lowered below the glass transition, the dephasing rate does not slow down. The temperature was lowered even further to 12 K, a factor of 25 times lower absolute temperature than room temperature. The dephasing rate does not slow and even speeds up slightly. These results are inconsistent with homogeneous pure dephasing, but are consistent with inhomogeneous broadening.

Despite all these factors suggesting inhomogeneous broadening is important in ethanol, the Raman echo results show it is not. On the right side of Fig. 3, the Raman echo

measurements are compared to predictions for a homogeneously broadened line. For comparison, the curve expected if the additional broadening relative to acetonitrile is entirely due to inhomogeneous broadening is shown. Inhomogeneous broadening cannot account for the additional line width in ethanol.

Resonant intermolecular transfer of energy is another mechanism which can cause line broadening and still remain active at very low temperatures. However, this mechanism is turned off by isotopic dilution. Figure 4 shows a RFID measurement of ethanol diluted in its fully deuterated equivalent. A nonresonant "coherence" peak dominates the early times, but the phase decay seen at later times is the same as it is in the undiluted sample. Resonant energy transfer is not responsible for the line broadening in ethanol.

The combined results of all these experiments have eliminated all the standard mechanisms for line broadening. We suggest that solvent-assisted intramolecular vibrational redistribution (SIVR) is responsible. There are several vibrational levels associated with the methyl group which are within kT of the symmetric stretch at room temperature (asym. stretch and CH bend overtones). Energy can be reversibly transferred within this group of modes, using the energy of the solvent thermal bath to make up for the small energy mismatches. Because the energy exchange is reversible, it is not the T_1 measured in standard experiments. The measured 20 ps T_1 time represents the irreversible loss of energy to lower energy modes subsequent to the rapid SIVR.

Although SIVR has not been previously proposed as an important line broadening mechanism, there is strong evidence that SIVR occurs in methyl groups. Energy has been detected in the nearby modes within 10 ps of exciting the sym. stretch.[3] For SIVR to account for the wide line in ethanol, it must be a very rapid process. If SIVR is the dominant cause of the line width in ethanol, the SIVR time is estimated to be 225-365 fs.

Under the SIVR hypothesis, the increased dephasing rate in ethanol can be attributed to its hydrogen bonding network. The hydrogen bonding greatly increases the density of high frequency intermolecular modes. These modes are required to provide the thermal energy needed for SIVR, and their presence should increase the dephasing rate.

Acknowledgments

We thank Prof. Richard McPhail and Dr. Xun Pan for providing us with Raman lineshape measurements on the $CH_3I/CDCl_3$ system. This material is based upon work supported by the National Science Foundation under Grant Nos. CHE-9115838 and CHE-94239935. MB is a Presidential Young Investigator and a Sloan Research Fellow.

References

1. D.W. Oxtoby, Adv. Chem. Phys., 40 (1979) 1.
2. J. Chesnoy and G.M. Gale, Adv. Chem. Phys., 70 pt.2 (1988) 297.
3. A. Seilmeier and W. Kaiser, in Ultrashort Laser Pulses and Applications, Ed. W. Kaiser, Topics in Appl. Phys., 60 (Springer-Verlag: New York, 1988) 279.
4. R.F. Loring and S. Mukamel, J. Chem. Phys., 83 (1985) 2116.
5. D. Vanden Bout, L.J. Muller and M. Berg, Phys. Rev. Lett., 67 (1991) 3700.

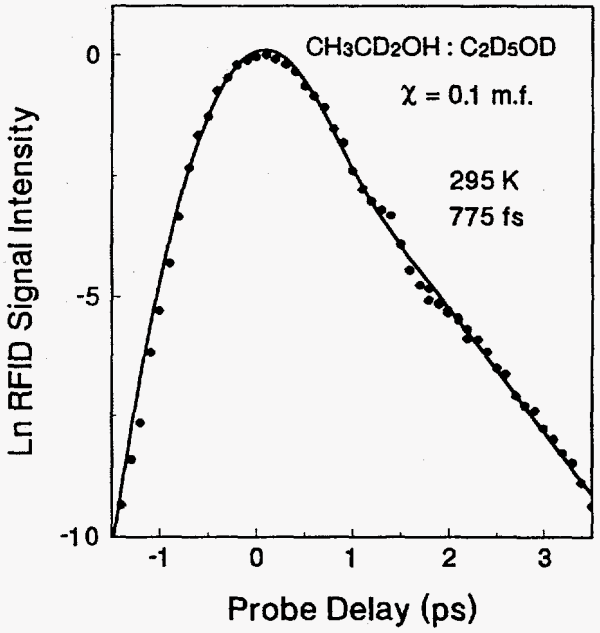

Fig. 4. Raman free induction decay for a 10% solution of ethanol-1,1-d_2 in ethanol-d_6 at room temperature. The decay time is almost identical to that of a 100% solution, showing that resonant intermolecular energy transfer is unimportant and cannot account for the lack of line narrowing at low temperature.

6. L.J. Muller, D. Vanden Bout and M. Berg, J. Chem. Phys., 99 (1993) 810.
7. R. Inaba, K. Tominaga, M. Tasumi, K.A. Nelson and K. Yoshihara, Chem. Phys. Lett., 221, (1993) 183.
8. D. Vanden Bout, J.E. Freitas and M. Berg, Chem. Phys. Lett., 229 (1994) 87.
9. D. Vanden Bout and M. Berg, J. Raman. Spectrosc., in press.
10. G. Döge, R. Arndt, H. Buhl and G. Betterman, Z. Naturforsch. Teil A, 35 (1980) 468.
11. K.S. Schweizer and D. Chandler, J. Chem. Phys., 76 (1982) 2296.

Probing Intermolecular Dynamics in Liquids by Time-resolved Optical-Heterodyne Detected Raman-Induced Kerr Effect Spectroscopy (OHD-RIKES)

Peijun Cong, Hans P. Deuel, and John D. Simon
Department of Chemistry and Biochemistry and Institute for Nonlinear Science
University of California at San Diego, La Jolla, California 92093-0341, U. S. A.

Femtosecond time-resolved OHD-RIKES has emerged as a powerful technique in studying intermolecular dynamics in liquids in the last few years [1 - 8]. In this paper some of the recent advances in elucidating a detailed picture of intermolecular interactions in solvents from our laboratory are highlighted [6 - 8]. These include (a) the effect of molecular symmetry on the inter- vs. intramolecular contributions to the OHD-RIKES signal, (b) isotope substitution effects on the strength and line shape of collective intermolecular vibrations in non-associative liquids, and (c) the aromatic-aromatic interactions in various substituted benzenes.

First, the effects of molecular symmetry on the OHD-RIKES response are discussed [6]. Figure 1 displays the OKE data of four nitriles taken with 30 fs transform-limited pulses. As the series progresses from acetonitrile to *t*-butyl nitrile, the molecular shape evolves from being approximately cylindrical to nearly spherical. There are two prominent trends in the OKE data for these four molecules. First, the subpicosecond decay component that is pronounced in acetonitrile (the shoulder feature at ~100 fs delay time) becomes less dominant with increased molecular size. For the case of *t*-butyl nitrile, the shoulder feature is apparently absent. Secondly, the oscillatory quantum beat feature that is present in acetonitrile increases its prominence and becomes the dominant component in *t*-butyl nitrile. The subpicosecond decay feature is due to intermolecular motions such as libration. The quantum beat feature is caused by intramolecular low-frequency coherent vibrational motions. Thus this set of time-domain data clearly establishes the qualitative correlation between the shape of the molecule and the relative weight of intra- and inter-molecular contributions to the OKE signal.

To obtain more quantitative information about the inter- and intra-molecular contributions, this time-domain set of data is converted to frequency domain spectra by a well-established Fourier-transform deconvolution procedure.[6] The results are show in Figure 2. In this figure, the inter- and intra-molecular contributions are clearly separated. The intermolecular contributions are reflected by a broad spectral feature in the 0 to 150 cm^{-1} region and the intramolecular components are converted from persisting oscillations in the time domain to isolated peaks in the frequency domain. The quantum beat feature in the time-domain data of

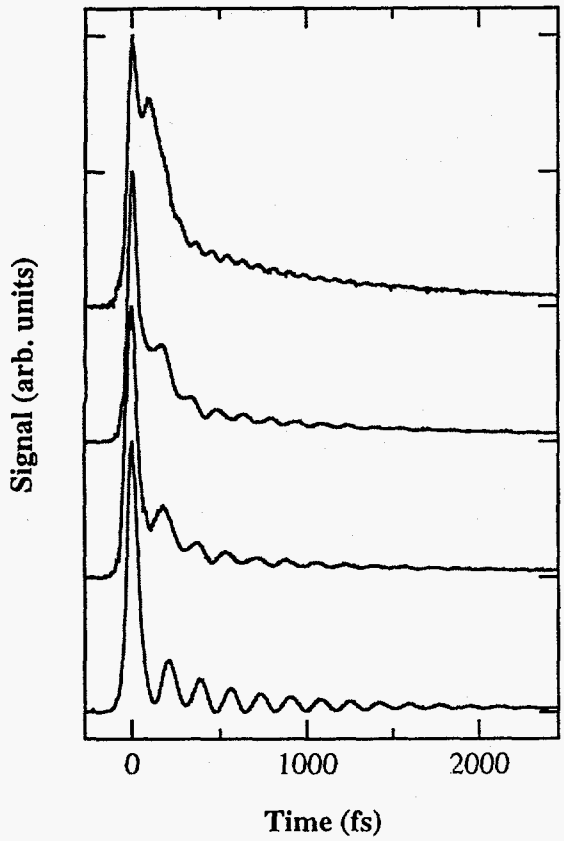

Figure 1. Time-domain OHD-RIKES data of nitriles. From top to bottom: CH_3CN, CH_3CH_2CN, $(CH_3)_2CHCN$, and $(CH_3)_3CCN$.

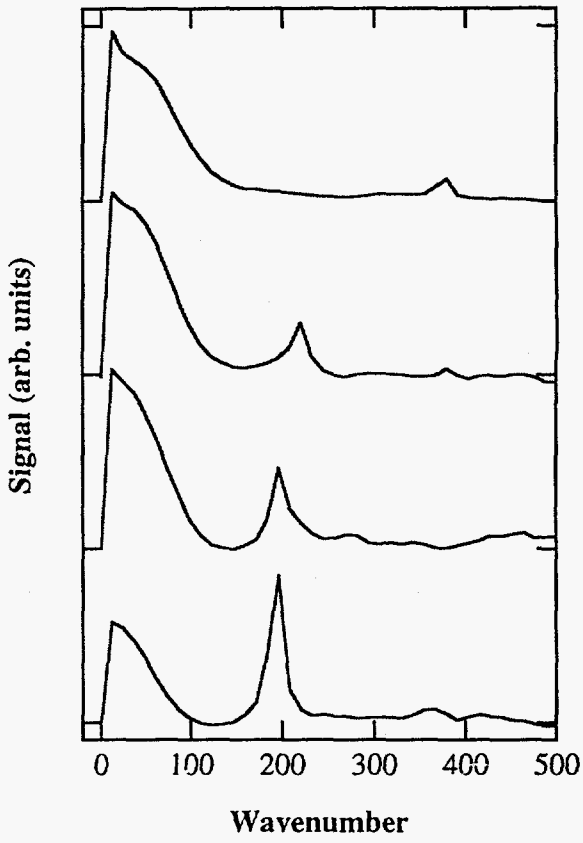

Figure 2. Frequency-domain OHD-RIKES data of nitriles. From top to bottom: CH_3CN, CH_3CH_2CN, $(CH_3)_2CHCN$, and $(CH_3)_3CCN$.

acetonitrile corresponding to the band at ~370 cm^{-1} in the frequency-domain spectrum is due to the C-CN bending mode. The relative intensity of this band to that of the intermolecular spectral density grows in importance with methylation of CH_3CN and becomes the most dominant feature in *t*-butyl nitrile.

In other words, the intermolecular contribution to the OKE signal decreases in relative weight down the series. To understand this trend, we need to consider the origin of the optical Kerr effect. The intermolecular part of OHD-RIKES signal is caused by *anisotropic* intermolecular interactions and is equivalent to depolarized Raman spectrum in the frequency domain. Given this connection, this trend can be explained by the symmetry of the nitrile molecules. Going down the series of molecules from acetonitrile to *t*-butyl nitrile, the molecules become more and more symmetric in shape, and the intermolecular interactions become more and more isotropic accordingly. This decrease of anisotropy in intermolecular interactions is reflected in the declining anisotropy in the permanent polarizability ellipsoids from acetonitrile to

t-butyl-nitrile and results in the decrease of intermolecular contributions to the overall optical Kerr effect signal.

To further understand the nature of the OKE signal and isolate the influence of potential energy and the effect of molecular mass, we studied three pairs of solvents, CCl_3H/CCl_3D, CH_3CN/CD_3CN, and C_6H_6/C_6D_6 [7]. In these undeuterated/deuterated solvents, the intermolecular potential is not varied and any changes in the intermolecular spectral density must be due to mass. It is observed throughout these non-associative liquids that the shape and strength of the spectral densities are not significantly influenced by isotope substitution, as one would expect. However, upon deuteration a small but persistent shift in the maximum of the librational spectrum is detected [9]. The location of this maximum can be characterized by a simple linear relationship: $\upsilon_{max} \propto B^{1/2}$, where B is the rotational constant around the most Raman active axis, i.e., $\upsilon_{max}(H)/\upsilon_{max}(D) = (B(H)/B(D))^{1/2}$. These observations seem to indicate the nature of the librational (short-time) motions is dictated by the moment of inertia of the individual molecules, at least in these nonpolar or weakly polar liquids that lack specific intermolecular interactions such as hydrogen bonding.

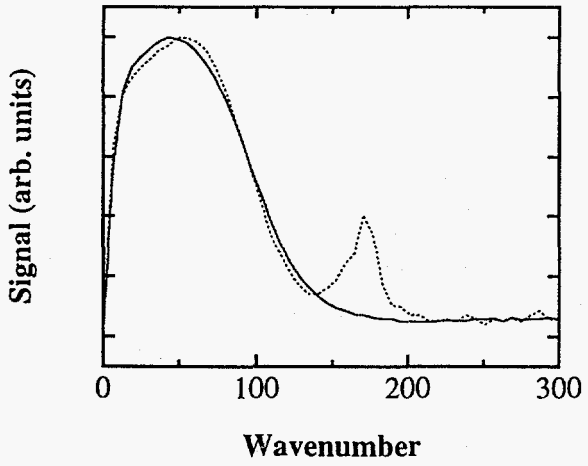

Figure 3. Comparison of the librational spectral desnities of benzene (solid line) and benzonitrile (dotted line).

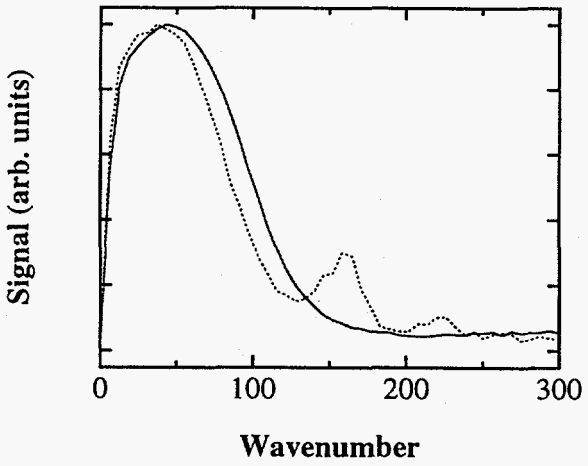

Figure 4. Comparison of the librational spectral desnities of benzene (solid line) and o-methyl-benzonitrile (dotted line).

The combined effects of potential energy surface and molecular mass are studied systematically in benzene and benzene derivatives [8]. Figure 3 shows a comparison of the librational spectral densities of benzene and benzonitrile. Benzene is nonpolar while benzonitrile is strongly polar with a dipole moment of ~4 D. This difference is reflected in the bulk properties of these two liquids, such as viscosity and vaporization enthalpy. The reorientational times for these two molecules are also quite different; benzene has a single time constant of 2.4

ps, benzonitrile on the other hand has to be described by at least two time constant, one at 3.8 ps, the other one at 22.2 ps. Despite all the differences, the librational spectral densities as shown in Figure 3 are remarkably similar. This experimental observation can be explained by considering the important modes of rotational motions that contribute to the OKE signal in both liquids. Because the symmetry of benzene is D_{6h}, there is only one rotation that is important to OKE, the tumbling end-to-end motion. For benzonitrile which has a lower degree of symmetry, the degeneracy is broken. There are two important rotations that contribution to the OKE. Both occur around in-plane axes, one contains the CN bond, the other is perpendicular to it. For the one that contains the CN bond, the moment of inertia and the anisotropic polarizability are not very different from benzene, so the resulting spectral density should be similar to that of benzene. For the one that is perpendicular to the CN axis, the anisotropic polarizability is increased, which favors a broader spectrum. However, the moment of inertia is decreased which narrows the spectrum. These compensating factors result in an overall spectral density that does not differ much from that of benzene. When the ortho position of benzonitrile is further substituted with a methyl group, the only effect should be to increase the moments of inertia for both rotations (CH_3 is not a very polarizable group as compared to the CN group or the benzene ring). Thus the net effect of this substitution should be a narrower spectrum. Figure 4 confirms this prediction.

As a final point, we have recently compared the time-domain OHD-RIKES data for benzene with that obtained from the frequency-domain spectroscopic technique of stimulated Raman gain [10]. Both techniques measure a signal that is proportional to Im $\chi^{(3)}_{1221}(\omega)$, so an exact agreement between the data from both techniques is expected. We see that the agreement is exact for energies greater than 20 cm^{-1}. However, the OHD-RIKES data underestimates the intensity in the region < 20 cm^{-1}. This results from the limited time scan of the experiment and signals that caution must be exercised in extracting long time relaxational time constants from the time-domain data.

In summary, we have demonstrated that time-resolved OHD-RIKES is a powerful technique in elucidating the details of anisotropic intermolecular interactions in liquids. With a judicious choice of molecules, the effects due to potential energy surfaces (anisotropic polarizability) and mass (moments of inertia) can be isolated and studied in a controlled fashion.

Acknowledgment

This work is supported by the National Science Foundation and the MFEL Program administrated by the Office of Naval Research. We thank Professor C. Y. She for stimulating discussions regarding the connection of frequency-domain Raman gain and time-domain OHD-RIKES data.

References:

1. D. McMorrow, W. T. Lotshaw, and G. A. Kenney-Wallace, IEEE J. Quantum Electron. **QE-24** (1988), 443.
2. D. McMorrow and W. T. Lotshaw, J. Phys. Chem. **95** (1991), 10395.
3. M. Cho, M. Du, N. F. Scherer, G. R. Fleming, and S. Mukamel, J. Chem. Phys. **99** (1993), 2410 .
4. Y. J. Chang and E. W. Castner Jr., J. Chem. Phys. **99** (1993), 113.
5. E. W. Castner Jr., Y. J. Chang, Y. C. Chu, and G. E. Walrafen, J. Chem. Phys. **102** (1995), 653.
6. H. P. Deuel, P. Cong, and J. D. Simon, J. Phys. Chem. **98** (1994), 12600.
7. H. P. Deuel, Ph.D. Thesis (1995), University of California at San Diego.
8. P. Cong, H. P. Deuel, and J. D. Simon, Chem. Phys. Lett. (1995) in press.
9. The librational part of the intermolecular spectral density is defined here as the overall spectral density *minus* the diffusive reorientational part. It should be noted that this definition of librational spectral density contains contributions from both intermediate and higher frequency regimes and is more general than some previous usages of this term. The procedure for extracting the librational spectral density from OHD-RIKES data is given in D. McMorrow and W. T. Lotshaw, Chem. Phys. Lett. **201** (1993), 369.
10. P. Cong, J. D. Simon, and C. Y. She, J. Chem. Phys. submitted.

Multiple-pulse femtosecond waveform generation and spectroscopy

Marc M. Wefers, Hitoshi Kawashima, and Keith A. Nelson
Department of Chemistry
Massachusetts Institute of Technology
Cambridge, MA 02139

INTRODUCTION

Optical control over the coherent behavior of molecules and materials has recently drawn considerable attention [1-2]. This field expands the context of spectroscopy to emphasize not only observation of but also control over sample dynamics. The control objective may range from excitation of selected electronic and/or vibrational coherences to guidance of molecules or condensed materials along selected reaction or rearrangement pathways. A substantial theoretical literature exists on systematic strategies to drive an initial quantum state into a prescribed one through use of tailored radiation fields [3-4]. Experiments have been few, but have demonstrated promise in control over electronic and vibrational degrees of freedom in crystal lattices [5,6], multiple quantum wells [7], atoms [8,9], and molecules [10,11].

Many current efforts are motivated by recent advancements in ultrafast optical pulse shaping technology. The majority of pulse shaping efforts have involved linear filtering of spatially separated frequency components as pioneered by Weiner and Heritage [12]. A grating and lens are used to image the spectrum of an ultrashort pulse onto a spatially varying mask which can attenuate and/or retard (phase-shift) different frequency components. A subsequent lens and grating are used to combine the spectrally filtered components, producing a "shaped" waveform in the time domain. Originally, the mask patterns were etched microlithographically onto glass substrates. Using such a mask for spectral phase filtering, timed sequences of femtosecond pulses were used for selective amplification of lattice vibrations in molecular and ionic crystals through non-resonsant impulsive stimulated Raman scattering (ISRS) [5,6]. Recently it was demonstrated that liquid crystal (LC) spatial light modulators (SLMs) or acousto-optic modulators (AOM) could be used as programmable masks [13-15]. This opened the door to computer-controlled optical waveform generation with wide-ranging spectroscopic possibilities.

AUTOMATED OPTICAL WAVEFORM GENERATION

We have designed a pulse shaping apparatus based on two LC SLMs integrated into a single unit [16], with which user-specified waveforms with complex time-dependent amplitude and phase profiles have been produced. Waveforms with controlled time-dependent polarization profiles can also be produced. In our opinion, this apparatus has yielded the greatest versatility and fidelity among pulse shaping efforts to date. Figure 1 shows cross-correlation measurements of various shaped waveforms. Figure 1a illustrates an 800-fs optical square pulse. Figures 1b and 1d illustrate multiple-pulse waveforms in which the timings, optical phases, and amplitudes of the different pulses are specified. Figure 1c illustrates a phase-related two-pulse sequence in which a controlled 'chirp' (the rate of change of the instantaneous carrier frequency) has been imposed on the pulses. In figures 1c and 1d the dashed curves give the intensity profiles of the desired waveforms. High fidelity multiple-pulse waveforms with as many as ten pulses have been produced (figure 1d). The temporal resolution of individual features of in the shaped waveform is limited by the available bandwidth in the input pulse which in our case corresponds to a 70-

fs pulse from a titanium-sapphire laser. The temporal range of the shaped wavefrom depends on a number of factors including the number of pixels (128) on the mask and diffraction effects, producing in our case a time window of about 3-4 ps. The waveforms can be generated in an automated and computer-controlled fashion so that a spectrosopic observable can be monitored as excitation waveform parameters are scanned.

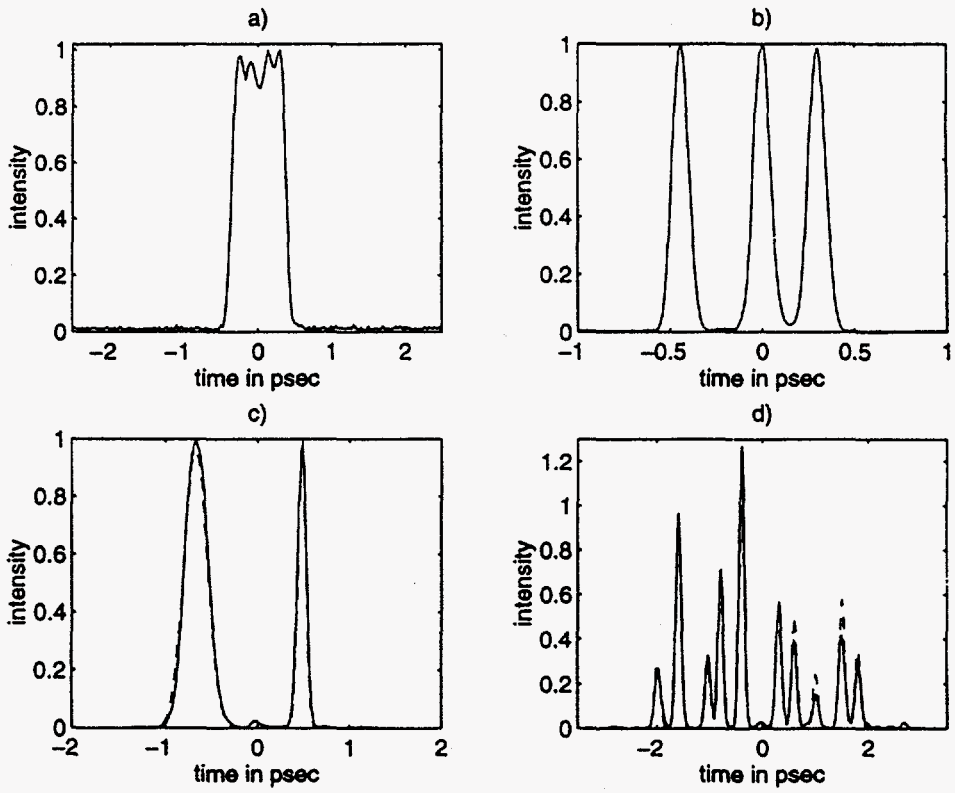

Figure 1. Cross-correlation measurements of shaped waveforms produced by the pulse-shaping apparatus.

AUTOMATED CONTROL OF ELECTRONIC COHERENCES

An initial demonstration of automated, multiple-pulse femtosecond spectroscopy was provided by experiments in which electronic coherences in atomic potassium vapor were controlled [17]. Transitions at 769 nm and 766.5 nm between the $4^2S_{1/2}$ ground state and the spin-orbit split $4^2P_{1/2}$ and $4^2P_{3/2}$ excited states were induced by a 70-fs pulse whose spectrum spanned the two resonances and was centered between them. The two resulting electronic coherences begin in phase, gradually go out of phase, and then go back in phase after one "beat" period given by the inverse of the frequency splitting. A second pulse interacts with the two coherences produced by the first, adding either constructively or destructively to each depending on its optical delay and phase relative to the first pulse. With two phase-related pulses, complete control over the relative amplitudes and phases of the two coherences in the potassium three-level system can be achieved. This was a 2-dimensional experiment in which both the optical delay and phase were scanned. For systems with more than two excited-state levels, such as vibrational levels on an excited electronic state manifold, pulse sequences consisting of more pulses would be necessary to achieve complete control over the multiple coherences. In potassium, more pulses permit

control over not only the final dual-coherence state but of the pathway along which it is reached. Three excitation pulses were used to demonstrate the possibilities. This is a 4-D experiment in which the total fluorescence out of both levels was measured with the two relative optical delays and the two relative optical phases were varied. The data were recorded in a fully automated manner, with the fluorescence monitored as the specified waveform parameters were scanned under computer control.

CONTROL OVER VIBRATIONAL TRAJECTORY

Earlier experiments with multiple-pulse sequences demonstrated control over lattice vibrational amplitudes [5]. Here we demonstrate that for degenerate vibrational modes, the orientation as well as the amplitude of the lattice displacements can be controlled through the use of multiple-pulse sequences with controlled polarization. The simplest demonstration, presented here, involves just two excitation pulses whose phases need not be related, so advanced pulse-shaping apparatus is not necessary. Two equal-energy, linearly polarized 70-fs pulses whose polarizations differ by 45 degrees were used to independently and impulsively excite orthogonal modes (denoted Q_1 and Q_2) of the Raman-active, degenerate E-symmetry 128 cm^{-1} vibration in crystalline α-quartz. The degenerate vibrational modes will undergo oscillation along a trajectory that depends on the delay between the two pulses. For example, if there is no delay, then oscillatory motion along the Q_1+Q_2 direction is induced. In this case the amplitude but not the vector direction of the displacement varies. On the other hand, if the delay is equal to one-fourth the vibrational period, then after the second pulse the magnitude of the vibrational displacement remains constant but its orientation rotates, i.e. the degenerate mode undergoes either clockwise or counterclockwise psuedorotation [18] depending on which pulse is first.

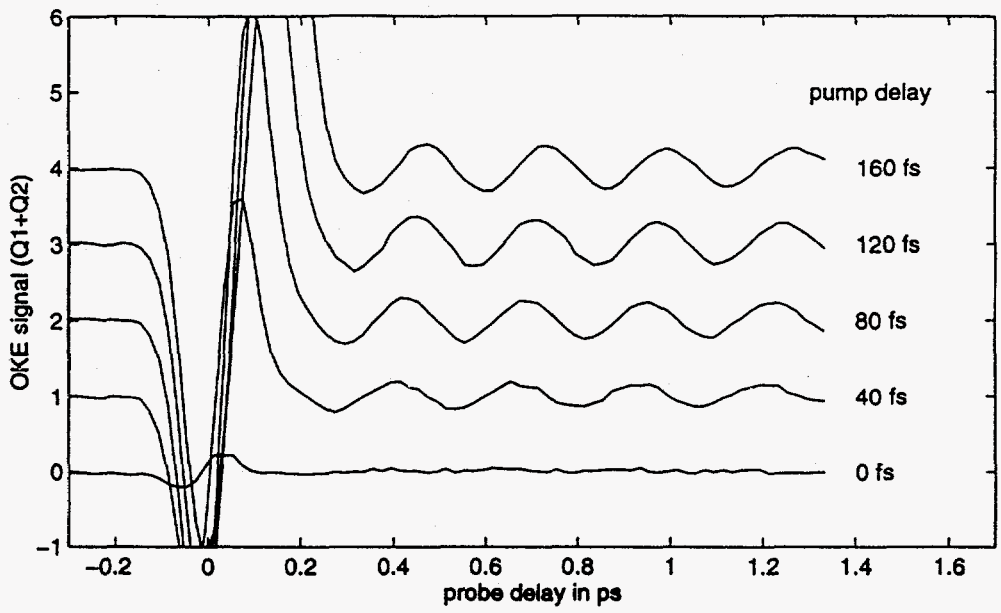

Figure 2. The OKE siganl from crystalline α-quartz with excitation pulses polarized at 45° and 90°, and a probe pulse polarized at 67.5°.

Experiments were carried out by spatially overlapping three nearly collinear pulses (produced from partial reflectors) along the c crystallographic axis of the uniaxial quartz

sample. The first two pulses excited the vibrational motion, and the resulting time-dependent birefringence gave rise to polarization rotation of the third, variably-delay pulse which was measured as a heterodyned optical Kerr effect (OKE) signal. For a fixed delay between the excitation pulses, the time-dependent OKE signal was monitored with the probe pulse linearly polarized at two different incident polarizations that differed by 45 degrees. The resulting data yielded projections of the induced polarizability tensor onto orthogonal axes so that the orientation of the pseudorotational signal could be determined uniquely. Figure 2 shows the transient birefringence induced by two excitation pulses with polarizations at 90° and 45°, monitored by a probe pulse with incident 67.5° polarization at which Q_1+Q_2 displacement is measured. The data show strong signals due to the purely electronic responses of the sample to the two excitation pulses, followed by coherent lattice vibrational oscillations and decay. As the delay between the excitation pulses is varied the amplitude and phase of the lattice vibrational response is changed. Similar data were collected with the incident probe pulse polarized at 112.5°, with which Q_1-Q_2 displacement was measured.

Figure 3 shows the reconstructed trajectories of the degenerate vibrations for different delays between the excitation pulses. Only the parts of the response subsequent to the instantaneous electronic responses are used to reconstruct the trajectories. The points are separated by 20 fs. The ellipticity and helicity of the trajectories are controlled entirely by the delay between the excitation pulses.

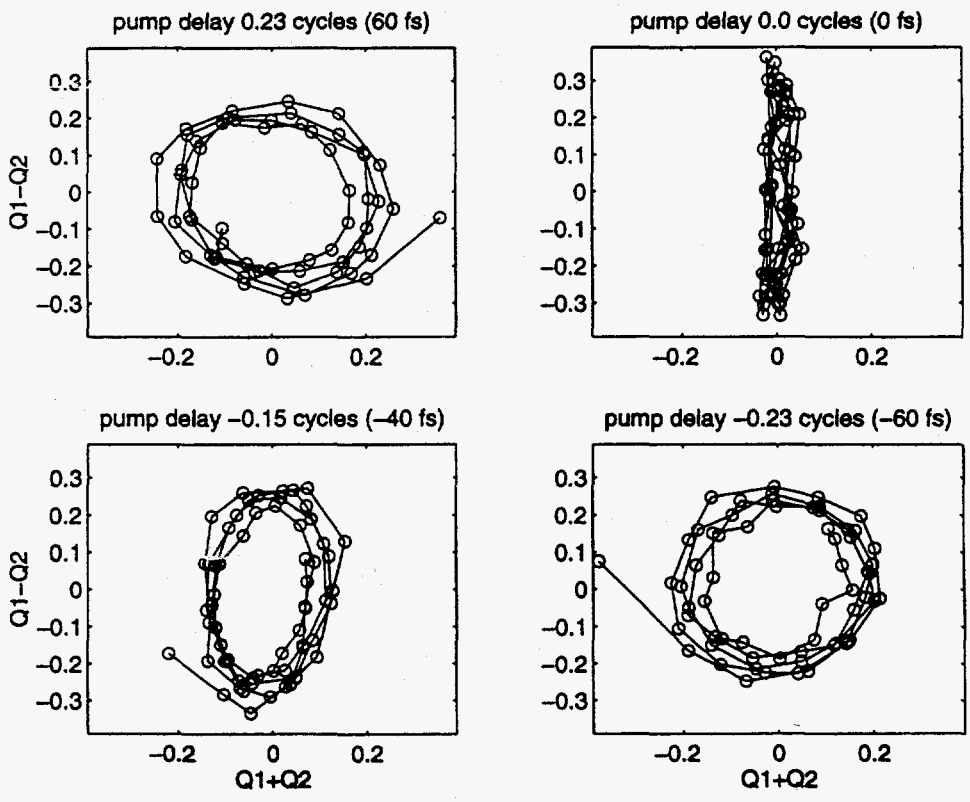

Figure 3. Reconstructed trajectories of the vibrational motion of the 128 cm^{-1} degenerate E-symmetry mode of crystalline α-quartz.

PROSPECTS

The generation of shaped optical waveforms and their application to control over electronic coherences and the orientation of vibrational coherences has been demonstrated. Future prospects include more ambitious control objectives such as domain switching in ferroelectric crystals [19-21]. Generation of shaped terahertz radiation from shaped optical waveforms and their application to control over vibrational and orientational molecular and lattice responses is also being explored.

Acknowledgements

This work was supported in part by ONR grant N00014-92-1503 and NSF CHE-9404548 M. M. W. is supported by a graduate fellowship from the Canadian Natural Science and Engineering Research Council.

References

1. W. S. Warren, H. Rabitz, M. Dahleh, Science **259**, 1581 (1993)
2. P. Brumer, M. Shapiro, Annu. Rev. Phys. Chem. **43**, 257 (1992)
3. S. Shi, A. Woody, H. Rabitz, J. Chem. Phys. **88**, 6870 (1988)
4. D. J. Tannor, R. Kosloff, S. A. Rice, J. Chem. Phys. **85**, 5805 (1986)
5. A. M. Weiner, D. E. Leaird, G. P. Wiederrecht, K. A. Nelson, Science **247**, 1317 (1990)
6. G. P. Wiederrecht, T. P. Dougherty, L. Dhar, K. A. Nelson, A. M. Weiner, D. E. Leaird, Ferroelectrics **144**, 1 (1993)
7. P. C. M. Planken, I. Brener, M. C. Nuss, M. S. C. Luo, S. L. Chuang, Phys. Rev. **B48**, 4903 (1993)
8. P. H. Bucksbaum, D. W. Schumacher, D. Pinkos, J. H. Hoogenraad, J. L. Krause, K. R. Wilson, in Ultrafast Phenomena IX, ed. G. A. Mourou, A. H. Zewail, P. F. Barbara, W. H. Knox, Berlin: Springer-Verlag (1995)
9. J. T. Fourkas, W. L. Wilson, G. Wackerle, A. E. Frost, M. D. Fayer, J. Opt. Soc. Am. B. **6**, 1905 (1989)
10. N. F. Scherer, A. J. Ruggiero, M. Du., G. R. Fleming, J. Chem. Phys. **93**, 856 (1990)
11. B. Kohler, J. L. Krause, R. M. Whitnell, K. R. Wilson, V. V. Vakovlev, Y. J. Yan, in Ultrafast Phenomena IX, ed. G. A. Mourou, A. H. Zewail, P. F. Barbara, W. H. Knox, Berlin: Springer-Verlag (1995)
12. A. M. Weiner, J. P. Heritage, E. M. Kirschner, J. Opt. Soc. Am. B. **5**, 1563 (1988)
13. A. M. Weiner, D. E. Leaird, J. S. Patel, J. R. Wullert, Opt. Lett. **15**, 326 (1990)
14. M. M. Wefers, K. A. Nelson, Opt. Lett. **18**, 2032 (1993)
15. C. W. Hillegas, J. X. Tull, D. Goswami, D. Strickland, W. S. Warren, Opt. Lett. **19**, 737 (1994)
16. M. M. Wefers, K. A. Nelson, Opt. Lett. **20**, 1049 (1995)
17. M. M. Wefers, H. Kawashima, K. A. Nelson, J. Chem. Phys. **102**, 9133 (1995).
18. J. A. Cina, V. Romero-Rochin, J. Chem. Phys. **93**, 3844 (1990)
19. Y. X. Yan, E. B. Gamble, K. A. Nelson, J. Chem. Phys. **83**, 5391 (1985)
20. S. Fahy, R. Merlin, Phys. Rev. Lett. **73**, 1122 (1994)
21. K. A. Nelson, pp 47-49 in Ultrafast Phenomena IX, ed. G. A. Mourou, A. H. Zewail, P. F. Barbara, W. H. Knox, Berlin: Springer-Verlag (1995)

Infrared Spectroscopy of Excited States

J J Turner, M W George and F P A Johnson
Department of Chemistry, University of Nottingham, Nottingham, NG7 2RD, UK

INTRODUCTION

The excited states of transition metal complexes have been studied by a variety of techniques, including absorption/emission spectroscopy, excitation spectroscopy and resonance Raman spectroscopy (of the ground state). These techniques might be called "indirect" since they do not interrogate the excited state directly. "Direct" interrogation techniques have traditionally included excited state absorption spectroscopy and time-resolved resonance Raman (TR^3) spectroscopy. With the development of fast time-resolved infrared (TRIR) spectroscopy, it has become possible to study the excited states of transition metal complexes, particularly *via* ν(CO) and ν(CN) vibrations which are usually intense [1]. Moreover these vibrations are largely uncoupled from other vibrations and provide a sensitive measure of structure and electron distribution. Thus in the photochemistry of transition metal carbonyls, represented schematically by:

$$\underset{P}{M(CO)_x} \xrightarrow{h\nu} \underset{E}{[M(CO)_x]^*} \rightarrow \underset{I}{M(CO)_{x-1}} + CO \xrightarrow{L} \underset{F}{M(CO)_{x-1}L}$$

it has become possible to examine the ν(CO) IR spectra of parent P, excited state E, intermediate I, and final product F [2].

EXCITED STATE INFRARED STUDIES

Complexes involving the $Re(CO)_3$ Group

The first coordination compound whose excited state was probed by TRIR was $ClRe(CO)_3(4,4'\text{-bipyridyl})_2$ [3], selected because previous spectroscopic studies had demonstrated that the lowest excited state was very stable and long-lived (~ 2μs) at room temperature. In addition since this excited state is metal-to-ligand-charge-transfer (MLCT), because of back-bonding the ν(CO) bands in the excited state should be sensitive to the change in the effective oxidation state of the Re (I to II). As expected the ν(CO) bands showed a shift to high frequency on going from ground to excited state [3,4]; details are given in the Table. Similar shifts have been observed for the shorter-lived $ClRe(CO)_3$(2,2'-bipyridyl) [5] and $[Re(CO)_3$(2,2'-bipyridyl)(4-Etpyr)$]^+$ [6] (see Table). The shift in ν(CO) frequencies, and more specifically the change in energy-factored force constants, should be a reflection of the electron density, and hence C-O back bonding at the metal centre. Recent work has demonstrated this. In $[Re(CO)_3(dppz)(PPh_3)]^+$ (dppz = dipyrido[3,2-a:2'2'-c]phenazine) [7], the excited state

state shows a slight (~8 cm^{-1}) **downward** shift in ν(CO) frequencies (seeTable) explained as due to the lowest excited state being dppz-$^3\pi\pi^*$ based, with the more extensive π^* orbitals of the dppz ligand being more effective at donating electron density back to the metal. Similarly the lowest excited state of $Re(CO)_3(^iPr\text{-}DAB)(benzyl)$ (^iPr-DAB = N,N'-di*iso*-propyl-1,4-diaza-butadiene, $^iPr\text{-}N{=}CH\text{-}CH{=}N\text{-}^iPr$) is believed [8] to be $\sigma\pi^*$ (ie electron transfer from the Re-benzyl bond to ^iPr-DAB ligand); in support of this the ν(CO) bands in the excited state are hardly shifted from the ground state [9] (see Table), thus confirming that there is very *little* change in electron density at the Re centre.

Table Frequency shifts (cm^{-1}) of ν(CO) bands of some $Re(CO)_3$ complexes from ground to excited states

Complex	shift[a]	mean shift
$ClRe(CO)_3(4,4'\text{-bipyridyl})_2$	30, 65, 66	54
$ClRe(CO)_3(2,2'\text{-bipyridyl})$	40, 66, 58	55
$[Re(CO)_3(2,2'\text{-bipyridyl})(4\text{-Etpyr})]^+$	39, 84, 57	60
$[Re(CO)_3(dppz)(PPh_3)]^+$		~-8
$Re(CO)_3(^iPr\text{-}DAB)(benzyl)$		~0

---

[a]a'(1), a", a'(2) respectively

Complexes involving the $W(CO)_5$ Group

This sensitivity of ν(CO) to electron distribution is also exhibited by some $W(CO)_5L$ compounds. When L is 4-CNpyridine or 4-acetylpyridine, the lowest excited state is MLCT [10], and the ν(CO) bands shift up in frequency [2] as expected; decomposition *via* loss of L occurs because the ligand-field (LF) state responsible for this decomposition is only modestly higher than the MLCT state and is in thermal equilibrium with it. When L is pyridine or piperidine it is well known that the lowest excited state is LF [10], and this is reflected in the high quantum yield for ejection of pyridine or piperidine. Resonance Raman measurements on the ground state of $W(CO)_5$(pyridine) have been used, *via* the Heller treatment, to calculate the distortions in the LF state [11]: W-N, W-C_{ax} W-C_{eq} bond lengths increase by 0.18, 0.12 and 0.04 Å respectively.

Although the change in C-O bond lengths was not calculated it was suggested that since the W-N and W-C bonds increase in length, the C-O bonds should decrease and hence the ν(CO) frequencies should increase [12]. These complexes (L = pyridine or piperidine) show no emission at room temperature and hence are presumably very short-lived. However there is emission in 77K glasses with a lifetime of ~0.8 to 2 μs, depending on the glass [10]. TRIR experiments on the two complexes in a methylcyclohexane/isopentane glass at ~77K show that the ν(CO) frequencies **decrease** on excitation [13]. On the face of it this contradicts the rR data, but as

pointed out by Zink, the Heller method gives the magnitude but **not** the sign of the bond length change.

With $(OC)_5W(B)W(CO)_5$, where B is a bridging ligand such as pyrazine or 4,4'-bipyridyl, the lowest excited state is believed to involve W-->B charge transfer; this has been confirmed by TR^3 on the excited state of the 4,4'-bpy complex, which shows that 4,4'-bpy becomes negatively charged, ie $(4,4'\text{-bpy})^-$ [14]. There is thus the question as to whether, on the infrared timescale, the excited state is localised or delocalised (ie schematically W^+B^-W or $W^{+1/2}B^-W^{+1/2}$). Figure 1 shows the high frequency ν(CO) region of $(OC)_5W(4,4'\text{-bpy})W(CO)_5$ [15]. Loss of parent ν(CO) band at 2073 cm^{-1} - assigned to the in-phase totally symmetric C-O stretch of the $W(CO)_5$ group - is accompanied by the generation of two new ν(CO) bands, one to high and one to low frequency of the ground state band.

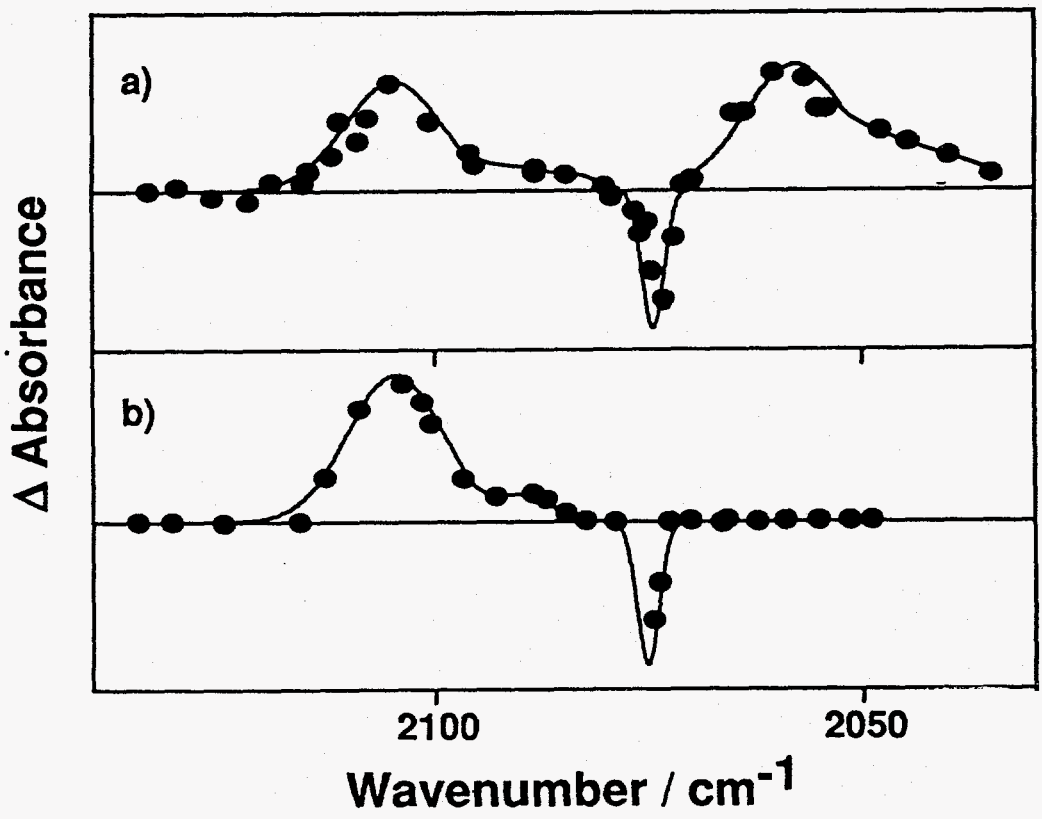

Figure 1 (a) TRIR spectrum at ~85 ns after photolytic flash (355 nm, 40 mJ) of $(OC)_5W(4,4'\text{-bipyridyl})W(CO)_5$ in CH_2Cl_2 (~3.5 x 10^{-3} mol dm^{-3}); (b) TRIR spectrum at ~65 ns after flash of $(OC)_5W(4,4'\text{-bipyridyl})$ in CH_2Cl_2 (~2 x 10^{-3} mol dm^{-3}). In both (a) and (b) data points plotted downwards signify loss of parent and data points plotted upwards signify generation of excited state. Reproduced with permission from reference [15]. The weak feature in (b) at ~2088 cm^{-1} is due to the generation of a small amount of solvated $W(CO)_5$.

The implication is that the lowest excited state is localised, the higher frequency band corresponding to $[(OC)_5W^+][4,4'\text{-bpy}^-]$ and the lower frequency band to $[4,4'\text{-bpy}^-][W(CO)_5]$. The alternative explanation is that we are looking at a species $W^{+1/2}B^-W^{+1/2}$, the two bands arising from the in-phase and out-of-phase components caused by vibrational coupling across the bridge. This latter explanation can be rejected because the two bands are approximately the same intensity. A further argument for localisation comes from the ν(CO) spectrum of the excited state of $W(CO)_5$(4,4'-bpy), also shown in figure 1. In the MLCT excited state this complex must be schematically W^+L^-; the high frequecy ν(CO) band is in the same position as the band assigned to the $[(OC)_5W^+]$ unit in $[(OC)_5W(4,4'\text{-bpy})W(CO)_5]^*$. Infrared spectroelectrochemical measurements [16] on the reduced form of $(OC)_5W(4,4'\text{-bpy})W(CO)_5$, ie $(OC)_5W(4,4'\text{-bpy}^-)W(CO)_5$, provide ν(CO) shifts to low frequency comparable to those experienced by the $[4,4'\text{-bpy}^-][W(CO)_5]$ unit in $[(OC)_5W(4,4'\text{-bpy})W(CO)_5]^*$. Thus the demonstration of localisation in the MLCT excited state is complete. Similarly, localised charge distributions have been deduced from the ν(CN) TRIR of the excited state of $[(NC)(2,2'\text{-bpy})_2Ru\text{-}CN\text{-}Ru(2,2'\text{-bpy})_2(CN)]^+$ [17]. The search is now on for species of the type $(OC)_xMBM(CO)_x$ that display **d**elocalisation in the MLCT excited state.

Infrared Rigidochromism

The TRIR experiments [13] on $W(CO)_5$(pyridine) in a glass at 77K prompts the question as to whether the fluid --> glass transition has an effect on the shift in ν(CO) bands on going from ground to excited state. Fluorescence measurements show that emission bands from LF excited states hardly alter on phase change . However emission bands of MLCT states show a considerable shift to high energy on freezing - the "rigidochromic" effect - ie the MLCT state is pushed to higher energy [18]. It has been proposed [18,19] that this effect arises because the increase in viscosity on freezing means the solvent molecules are less able to accommodate the asymmetric charge distribution in the MLCT excited state From analysis of the spectral emission one would expect the frequencies of the acceptor vibrational modes to increase on freezing [19]. Preliminary experiments [20] on $ClRe(CO)_3$(bpy) in butyronitrile show, surprisingly, that the ν(CO) bands shift **less** on excitation in the glass than in the fluid. It is not yet clear why this should be so; clearly further studies on the effects of solvent freezing on vibrational spectra of excited states is a topic worth pursuing.

ACKNOWLEDGMENTS

Work in Nottingham has been supported by SERC, EEC, Perkin-Elmer Ltd, the Paul Fund of the Royal Society and Mütek GmbH. We are grateful to Dr. J. R Schoonover and Dr J. J. McGarvey for pre-publication information.

REFERENCES

1. J. J. Turner, M. W. George, F. P. A. Johnson and J. R. Westwell, Coord. Chem. Rev., 125 (1993) 101.
2. P. Glyn, F. P. A. Johnson, M. W. George, A. J. Lees and J. J. Turner, Inorg. Chem., 30 (1991) 3543; F. P. A Johnson, M. W. George and J. J. Turner, Inorg. Chem., 32 (1993) 4226.
3. P. Glyn, M. W. George, P. M. Hodges and J. J. Turner, J. Chem. Soc., Chem. Commun., (1989) 1655.
4. D. R. Gamelin, M. W. George, P. Glyn, F-W. Grevels, F. P. A. Johnson, W. Klotzbücher, S. L. Morrison, G. Russell, K. Schaffner and J. J. Turner, Inorg. Chem., 33 (1994) 3246.
5. M. W. George, F. P. A. Johnson, J. R. Westwell, P. M. Hodges and J. J. Turner, J. Chem. Soc.,Dalton Trans., (1993) 2977.
6. J. R. Schoonover, K. C. Gordon, R. Argazzi, W. H. Woodruff, K. A. Peterson, C. A. Bignozzi, R. B. Dyer and T. J. Meyer, J. Am. Chem. Soc., 115 (1993) 10996.
7. J. R. Schoonover, R. B. Dyer, W. D. Bates, G. F. Strouse, P. Chen and T. J. Meyer, J. Phys. Chem., in press.
8. D. J. Stufkens, Comments Inorg. Chem., 13 (1992) 359.
9. B. D. Rossenaar, M. W. George, F. P. A. Johnson, D. J. Stufkens, J. J. Turner and A. Vlcek, Jr., J. Am. Chem. Soc., submitted for publication.
10. M. S. Wrighton, H. B. Abrahamson and D. L. Morse, J. Am. Chem. Soc., 98 (1976) 4105.
11. L. Tutt and J. I. Zink, J. Am. Chem. Soc., 108 (1986) 5830; K-S. Shin and J. I. Zink, Inorg. Chem., 28 (1989) 4385.
12. For a relationship involving C-O bond lengths and energy-factored C-O force constants see: S. L. Morrison and J. J. Turner, J. Mol. Struct., 317 (1994) 39.
13. F. P. A. Johnson, M. W. George, S. L. Morrison and J. J. Turner, J. Chem. Soc., Chem. Commun., (1995) 391.
14. R. A. McNicholl, J. J. McGarvey, A. H. R. Al-Obaidi, S. E. J. Bell, P. M. Jayaweera and C. G. Coates, J. Phys. Chem., in press.
15. M. W. George, J. J. Turner and J. R. Westwell, J. Chem. Soc.,Dalton Trans., (1994) 2217.
16. M. W. George, F. P. A. Johnson, J. J. Turner and J. R. Westwell, J. Chem. Soc., Dalton Trans., in press.
17. C. A. Bignozzi, R. Argazzi, J. R. Schoonover, K. C. Gordon, R. B. Dyer and F. Scandola, Inorg. Chem., 31 (1992) 5260.
18. M. S. Wrighton and D. L. Morse, J. Am. Chem. Soc., 96 (1974) 998.
19. R. S. Lumpkin and T. J. Meyer, J. Phys. Chem., 90 (1986) 5307; E. Danielson, R. S. Lumpkin and T. J. Meyer, J. Phys. Chem., 91 (1987) 1305.
20. I. Clark, M. W. George, F. P. A. Johnson and J. J. Turner, J. Phys. Chem., submitted for publication.

Resonance Raman Investigation of Heterocyclic Aromatic Compounds Showing Photoinduced Intramolecular Proton Transfer

M. Pfeiffer, K. Lenz, A. Lau, T. Elsaesser
Max Born Institut für Nichtlineare Optik und Kurzzeitspektroskopie
D-12589 Berlin - Germany

Ultrafast intramolecular proton transfer occurring after photoexcitation represents one of the most elementary changes of the nuclear configuration of aromatic molecules. In this contribution, we investigate vibronic effects related to the proton transfer mechanism with the help of resonance Raman spectroscopy for a group of 3 conjugated isoelectronic organic molecules differing by the presence of heteroatoms. In the electronic ground state, the molecules exist in the enol form, whereas after electronic excitation a keto geometry is formed on a time scale of 100 to 200 fs. In the case of TINUVIN, this reaction product is deactivated by internal conversion within 150 fs and undergoes a back-reaction to the enol geometry on a 600 fs time scale. This fast reaction cyle creates enol molecules with a highly excited vibrational system. The resonance Raman study presented here gives direct information on the vibronic structure of the enol S_0-S_1 absorption band and - thus - allows a quantitative simulation of the spectra of hot molecules. Furthermore, the results give insight into the initial phase of the excited state reaction. The data are analyzed by numerical calculations which model the spectroscopic results and are based on the time-correlator representation for the processes of absorption and Raman scattering.

1. THE THEORETICAL METHOD OF SPECTRA ANALYSIS

Electronic absorption bands

The numerical analysis of the spectroscopic results is performed with help of the time-correlator technique [1]. The molecular absorption is expressed by

$$\sigma_{absorption}(\omega) = \frac{1}{\pi} Re \int_0^\infty dt \exp(-i\Delta t + gt) \qquad (1)$$

Here, $\Delta=\omega_{00}-\omega$ denotes the frequency separation from the purely electronic transition at ω_{00}. The linear damping and the electron-phonon coupling are described by the lineshape function

$$g(t) = -\Gamma t + \sum_{j=1}^{\infty} z_j^2 [(n_j + 1)(e^{-i\omega_j t} - 1) + n_j (e^{i\omega_j t} - 1)] \qquad (2)$$

assuming a thermal population of the vibrational modes: $n_j(T) = \dfrac{1}{\exp \dfrac{\hbar \omega_j}{kT} - 1}$

Contributions of bath modes and the weakly coupled internal modes can be extracted from the sum expression and put together in the short time limit into a Gaussian-damping term. The present calculations are performed with the effective line shape function

$$g_{fit}(t) = -\Gamma t - \beta t^2 + z^2 \sum_{j=1}^{N_a} \xi_j^2 [(n_j + 1)(e^{-i\omega_j t} - 1) + n_j (e^{i\omega_j t} - 1)] \qquad (3)$$

The relative amplitudes with which the internal modes strongly coupled to the electronic transition ξ_j^2 take part are determined experimentally from the relative intensities of the strongest resonance Raman lines. Numerical fit of the enol-absorption spectrum at room temperature gives the respective values for the parameters Γ, β, ω_{00} and the scaling factor z^2.

Resonance Raman Intensities

In time correlator representation, the intensity of spontaneous Raman spectra is given by

$$I_{Raman}(\omega) = \omega^4 B \sum_{p=-\infty}^{\infty} C_p \delta(\omega - \omega_{excit} + p\omega_{vib}) \qquad (4)$$

Here, the weightening factors C_p give the strength of the p^{th} overtone related to fundamental C_1. In the low temperature limit the following relation holds for $p \geq 0$

$$C_p^{T=>0} = \frac{z_1^{2p}}{p!} \left| \int dt [e^{-i\omega_1 t} - 1]^p \exp\left[-(i\Delta + \Gamma)t - \beta t^2 + \Sigma z_j^2 (e^{-i\omega_j t} - 1) \right] \right|^2 \qquad (5)$$

In case p=1 this formula expresses Albrecht's transform model, relating the Raman excitation profile for the fundamental ω_1 to the molecular first order susceptibility

$$I_{Raman}^{\omega_1}(\omega) \propto \xi_1^2 \left| \chi^{(1)}(\omega - \omega_1) - \chi^{(1)}(\omega) \right|^2 \text{ with } \xi_1^2 = \frac{z_1^2}{z^2} \qquad (6)$$

Eq. (6) is used to determine the relative origin shift parameters from experimental resonance Raman intensities deriving the $\chi^{(1)}$-function from the measured dispersion of the absorption.

Combination band intensities are calculated by

$$C_{p1p2}^{T=>0} = \frac{z_1^{2p_1}}{p_1!} \frac{z_1^{2p_2}}{p_2!} * \left| \int_0^{\infty} dt [e^{-i\omega_1 t} - 1]^{p_1} [e^{-i\omega_2 t} - 1]^{p_2} \exp\left[-(i\Delta + \Gamma)t - \beta t^2 + \Sigma z_j^2 (e^{-i\omega_j t} - 1) \right] \right|^2 \qquad (7)$$

2. THE INVESTIGATED MOLECULES

The structure of the investigated molecules in their enol and keto-forms are shown in Fig. 1

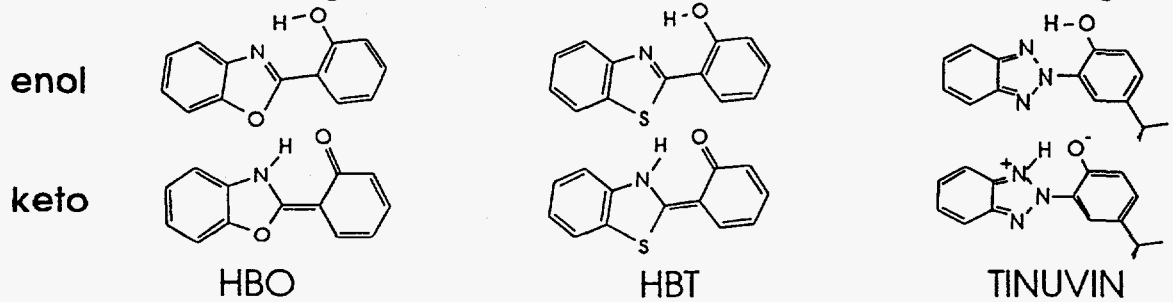

Fig. 1 Structure of the investigated molecules

The vibronic character of the enol S_0-S_1 spectra is analysed by investigation of the intensity distribution in the resonance Raman spectrum for this transition. The resonance Raman spectra of the enol-form for the 3 molecules are given in Fig. 2. For the 15 strongest Raman modes the electron-phonon coupling strengths ($\sim\xi_i^2$) was determined applying eq. (6). Normal coordinate analysis reveals the character of the nuclear redistribution belonging to these modes. It is important to notice that even relatively weak low frequency Raman modes may show very strong electron-phonon coupling [2].

Applying the origin shifts for the 15 vibrational modes with the strongest electron-phonon coupling a fit of the absorption profiles for the molecules at room temperature was performed on the basis of eq. (1) and (3) rendering the parameters given in Table 1 for the TINUVIN and the HBT. The correspondence of measured and calculated absorption profiles for TINUVIN is shown in Fig. 3 (left side). By this fit the following characteristica for the vibronic transition are obtained: the position of the 00-transition frequency, the scaling factor for the absolute Franck Condon parameters and the values for the actual damping parameters. From the measured slope of the long wavelength absorption edge follows prevailing Gaussian damping

$$(\Delta_G = 2\sqrt{\beta \ln 2} >> \Gamma).$$

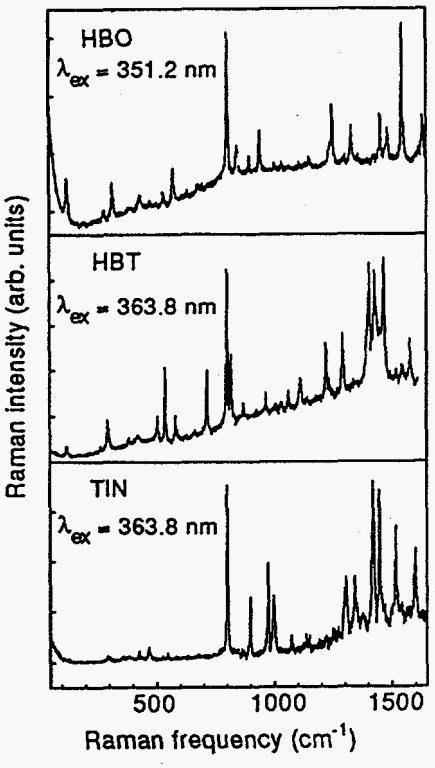

Fig. 2 Resonance Raman spectra of the enol-form for the 3 investigated molecules Concentration: 10^{-3} mole/ in cyclohexane

Table 1
Parameters characterizing the electronic transition as derived from numericals fit of the absorbance

	$\Gamma/2\pi c$ [cm^{-1}]	β[1/fs^2]	$\omega_{00}/2\pi c$ [cm^{-1}]
TIN	<50	1,5 10^{-5}	27260
HBT	100	1,4 10^{-5}	28340

3. THE VIBRATIONAL COOLING PROCESS

The parameters for the origin shift and those of Table 1 which are obtained under steady state conditions allow the quantitative analysis of the cooling process which the molecules undergo at the end of the proton transfer cyclus. Returned from the keto state the molecules find themselves with the large amount of vibrational excess energy resulting from the initial photo excitation (~ 4 eV per molecule). Applying tunable sub-ps probe pulses, transient changes of the absorption band of enol-TINUVIN for up to 50 ps delay time were measured. At 7 ps after photoexcitation the S_0-S_1 absorption shows a strong enhancement of the low-energy absorption tail and a reduced extinction around the maximum (Fig. 3, right side).

The transient spectra were analyzed on the basis of the model outlined above, introducing an elevated vibrational temperature, i.e. assuming a fully thermalized vibrational system. Such simulations are in quantitative agreement with the experimental results for delay times longer than

about 5 ps. The time evolution of vibrational temperature as derived from this simulation is shown in Fig. 4. We conclude from the quantitative agreement of data and theory that the vibrational manifold of TINUVIN is well described by a thermal distribution on a time scale longer than 5 ps. At earlier times, there are some discrepancies pointing to nonthermal distributions.

The hot TIN molecules cool down by inelastic collisions with the surrounding solvent. At early times after excitation, the rate of energy flow from the TIN molecules to the first solvent shell is considerably higher than that out of the first shell, leading to a strong heating of the solvent

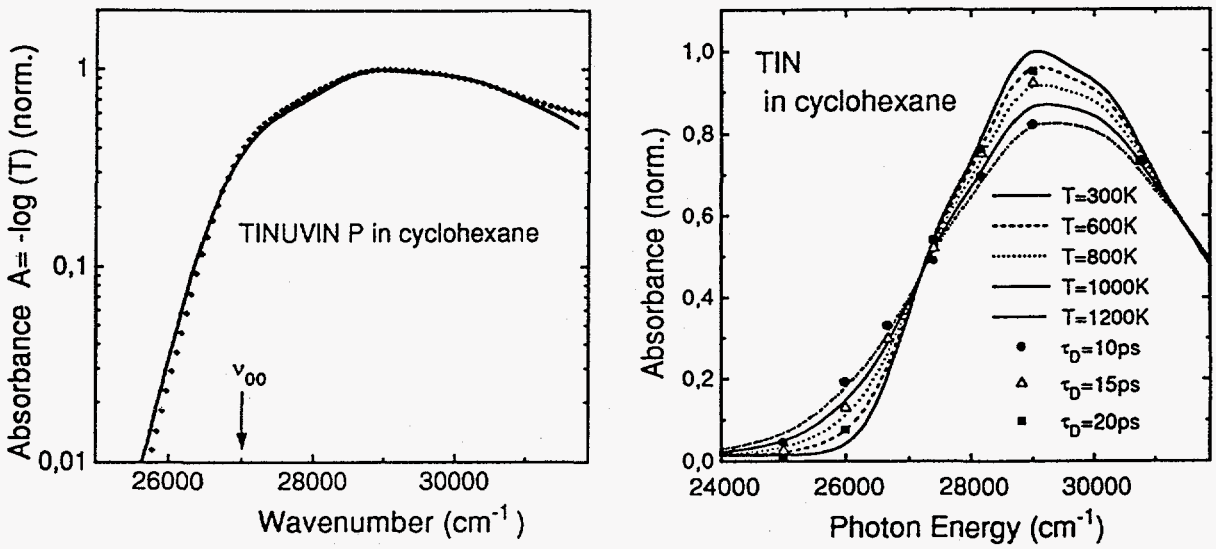

Fig. 3 Results for TIN: numerical fit of the absorbance at room temperature (left figure); fit curves to determine the time development of temperature of internal vibrational modes at the end of the proton transfer cycle (right figure)

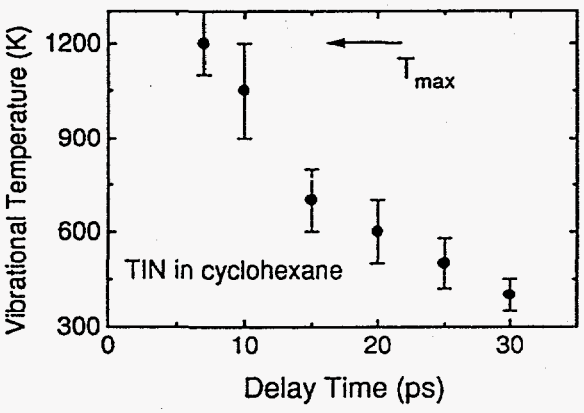

Fig. 4 Vibrational temperature of TIN derived from the trans-sient absorption

molecules neighbouring the solute. A quantitative simulation of the energy transfer process gives cooling times of several tens of picoseconds[4].

4.ANALYSIS OF THE COMBINATION BAND SPECTRUM

In the Raman combination band range there is a characteristic intensity anomaly if the exciting laser frequency falls beyond the 00-frequency. For TINUVIN-p enol and HBT beginning above several strong Raman fundamentals there are built each a ladder of combination tones by the 469 (TIN) resp. 293 cm^{-1} (HBT) modes. The second step in the ladder, i.e. the combination band with two quants of the low frequency mode is the most intense one. According to eq. 7 this can be explained by an enhanced effective origin shift value at higher phonon excitation for the low frequency mode. This and the observed anharmonic lowering of the mode frequency points to a widening and flattening of the corresponding oscillator potential. These effects are bound to

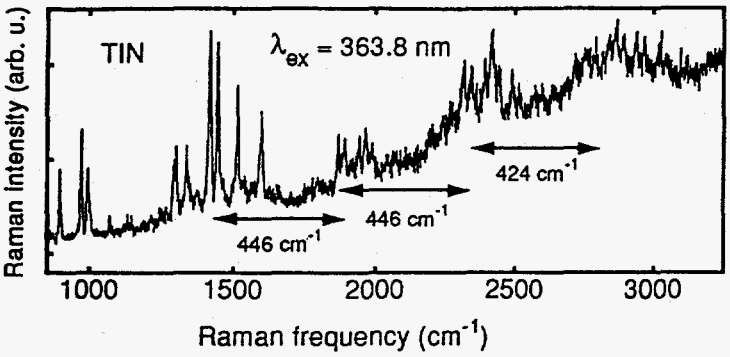

Fig.5 Combination tone spectrum for the TIN in the frequency range beyond 1600 cm^{-1}

just one low frequency mode suggesting that this mode is directly related to the beginning of the proton transfer process.

5. CONCLUSIONS

1. Applying the normal mode-spectrum of the Raman active enol-vibrations the time de- velopment of the enol absorption spectrum at the end of the proton transfer cycle can be well fitted with help of the time correlator model. The fit shows, that from a time of about 5 ps after excitation the vibrational excess energy is thermalized. To describe the observed width of the absorption band and its change in time, the vibrational energy exchange with the solvent and its heating in the picosecond regime must be taken into consideration.

2. Combining the results from the Raman measurements in the combination band range with the femtosecond measurements of transient absorption for the investigated molecules [5], it can be concluded that proton transfer starts on a barriereless reaction pathway deriving from an in-plane low frequency vibrational mode determined by a bending of the C-O-H-group against the triazole ring.

3. As to the 3 different isoelectronic species, there are no differences with respect to the character of the proton transfer mechanism. The time scale in the mode initiating the transfer depends strongly on the mass in the modified triazol group.

References

1. J. B. Page, in Light Scattering in Solids VI, Ed. M. Cardona and G. Güntherodt (Springer-Verlag, Berlin, Heidelberg, New York, London, Paris, Tokyo,1991) p.17
2. K. Lenz, M. Pfeiffer, A. Lau and T. Elsaesser, Chemical Physics Letters, 229 (1994)340
3. M. Pfeiffer, K. Lenz, A. Lau and T. Elsaesser, Journal of Raman Spectroscopy, 26 (1995) in press
4. U. Sukowski, A. Seilmeier, T. Elsaesser and S. F. Fischer, Journal Chemical Physics, 93 (1990) 4094
5. C. Chudoba, S. Lutgen, T. Jentzsch, E. Riedle, M. Woerner and T. Elsaesser, Chemical Physics Letters, (1995), in press

Time-resolved Infrared Spectroscopy in Supercritical Fluids

Michael W. George, Xue-Zhong Sun and Martyn Poliakoff
Department of Chemistry, University of Nottingham, University Park, Nottingham NG7 2RD, UK.

Supercritical Fluids (SCFs) are curious hybrids of gases and liquids which offer intriguing possibilities for transient vibrational spectroscopy. A Fluid is said to be "supercritical" when its temperature and pressure exceed the temperature and pressure at the critical point (T_c and P_c). Many gases have P_c and T_c which are easily accessible, eg CO_2 (74 atm, 31 °C), Xe (58 atm, 17 °C), Kr (54 atm, -64 °C) and Ar (48 atm, -122 °C). SCFs are unique solvents since their properties (viscosity, dielectric constant, diffusivity) vary with density which is a strong function of temperature and pressure [1]. Supercritical Fluids possess features which have made them the subject of wide ranging research from chromatography and extraction to reaction chemistry [2].

Supercritical fluids may affect reactions in a variety of ways: increased diffusion rates, increased reactant solubilities and elimination of mass transfer bottle necks, facilitated separation, catalyst life extension, pressure effects on the rate constant, changes in selectivity and effect of local density [3]. Interest in transient spectroscopic studies in SCFs has experienced an explosive growth in recent years particularly because of many intriguing results obtained near the critical point, e.g. triplet-triplet annihilation in benzophenone [4] and pyrene excimer formation [5] which have been attributed to "clustering" of solute and solvent molecules. We have developed ns-Time-resolved Infrared Spectroscopy (TRIR) [6], a combination of UV flash photolysis with fast IR detection, to generate vibrational data as an aid to understanding the fundamental properties of these fluids [7]. We have also used SCFs to investigate the interaction of weakly coordinating ligands (eg Xe and CO_2) with metal centres.

Photolysis of $W(CO)_6$ in supercritical Ar (scAr), Kr (scKr), Xe (scXe) and CO_2 ($scCO_2$)

A general scheme summarising the photoreactivity of metal carbonyls in solution is shown below.

$$M(CO)_x \xrightarrow{h\nu} [M(CO)_{x-1}] + CO \xrightarrow{<1ps} M(CO)_{x-1}\text{-Solvent} \xrightarrow{L} M(CO)_{x-1}L$$

Photoejection of CO is followed by rapid coordination of a solvent molecule and it is this solvated complex that reacts subsequently with any ligand L. If L is a weakly coordinating ligand such as Xe or CO_2, it is impossible to study its interaction with the metal centre in conventional solvents because the solvent will coordinate more strongly.

Photolysis of $W(CO)_6$ in scAr, scKr or scXe generates, for the first time, organometallic noble gas compounds in solution *at room temperature*. The stability of these complexes is, as expected, Ar < Kr < Xe. The wavenumber of the e ν(CO) IR absorption band of $W(CO)_5L$ is very sensitive to the nature of L (Ar 1972, Kr 1969 and Xe 1964 cm^{-1}). Photolysis of $W(CO)_6$ in scKr doped with a small amount of Xe generates $W(CO)_5Xe$ (ν(CO) = 1964 and 1940 cm^{-1}) and this experiment confirms the coordination of Xe to the metal center. The addition of Xe to scKr also lengthens the lifetime of $W(CO)_5L$ from 350 ns to 1300 ns, a lifetime close to the value obtained in pure scXe, which further supports the interpretation that Xe preferentially binds to the metal center. The coordination of Kr to W is confirmed by a similar experiment in scAr. Doping scAr with a small amount of Kr shifts the e ν(CO) absorption of $W(CO)_5L$ from 1972 to 1969 cm^{-1} together with a lengthening the lifetime of $W(CO)_5L$ from 125 to 280 ns.

Figure 1 also shows that $W(CO)_5(CO_2)$ can be generated by photolysis of $W(CO)_6$ in $scCO_2$. We illustrate one of the unique properties of supercritical fluids with $W(CO)_5(CO_2)$ because its decay is expected to occur by a dissociative mechanism. If $W(CO)_5(CO_2)$ does decay by a dissociative mechanism, then its lifetime should be proportional to the concentration of CO_2. The density, and hence, the concentration of a supercritical fluid can be varied by changing the pressure of the fluid. Figure 2(a) shows how the density of CO_2 varies with pressure at 32, 37 and 50 °C. Figure 2(b) shows that the lifetime of $W(CO)_5(CO_2)$ is proportional to the density of CO_2 and indicates that the decay of $W(CO)_5(CO_2)$ occurs mainly by a dissociative mechanism. Although this does not prove that there is no associative contribution to the decay

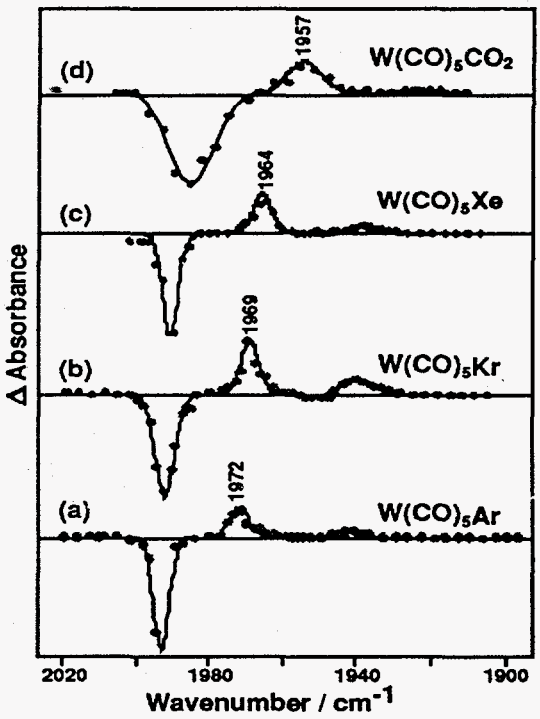

Figure 1 TRIR spectra obtained 100 ns following photolysis (355 nm) $W(CO)_6$ in (a) scAr, (b) scKr, (c) scXe and (d) $scCO_2$. The spectra show the generation of (a) $W(CO)_5Ar$, (b) $W(CO)_5Kr$, (c) $W(CO)_5Xe$ and (d) $W(CO)_5CO_2$.

mechanism, we have performed additional experiments where we have varied the concentration of CO in solution but kept the ratio CO : CO_2 constant. These experiments show that there is no significant associative contribution to the decay mechanism.

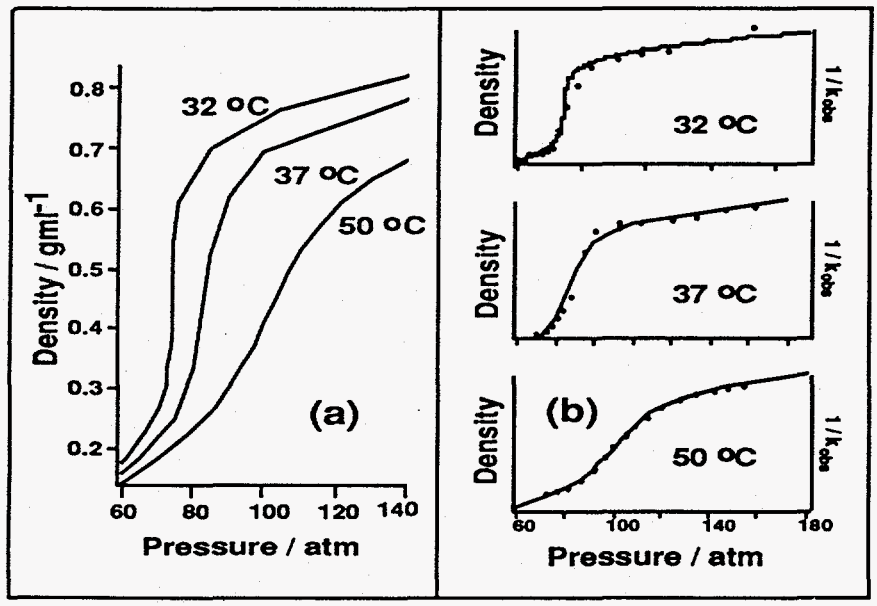

Figure 2 shows (a) the variation in density of CO_2 with pressure at 32 ^{0}C, 37 ^{0}C and 50 ^{0}C; (b) the variation in lifetime of $W(CO)_5(CO_2)$ with pressure (circles - experimental data and solid line - CO_2 density data from Figure 2(a))

Photolysis of $[CpMo(CO)_3]_2$ in $scCO_2$

The photochemistry of $[CpMo(CO)_3]_2$ in n-heptane has recently been studied by TRIR [8]. Only *trans*-$[CpMo(CO)_3]_2$ is detectable in n-heptane and the visible photochemistry is summarised by in scheme 1 [8].

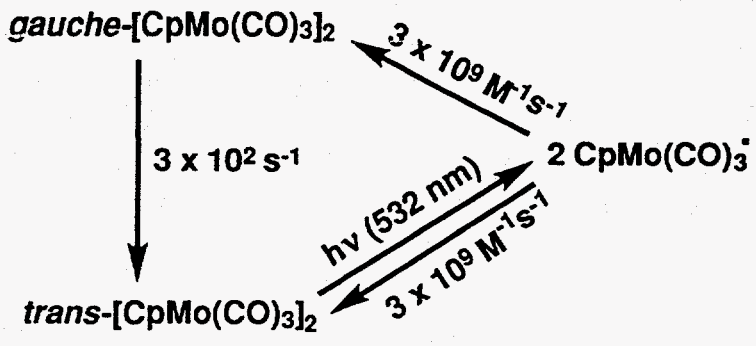

Scheme 1 showing the visible photochemistry of $[CpMo(CO)_3]_2$

Visible (532 nm) irradiation of *trans*-$[CpMo(CO)_3]_2$ in $scCO_2$ appears be very similar to the results obtained in n-heptane solution, in that visible irradiation results in formation of $CpMo(CO)_3\cdot$ radicals via cleavage of the Mo-Mo bond and these radicals decay to form both *trans* and *gauche* $[CpMo(CO)_3]_2$.

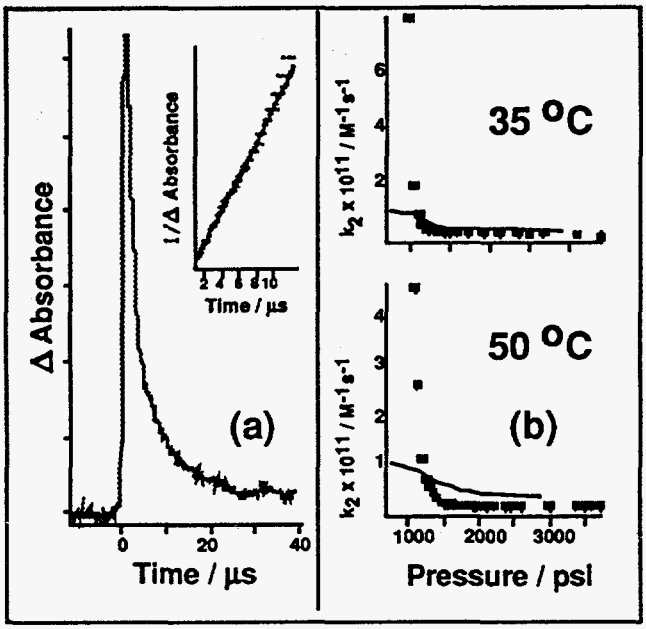

Figure 3 Showing (a) the TRIR decay trace of $CpMo(CO)_3$ radical (2011 cm^{-1}) obtained following photolysis (355 nm) of $[CpMo(CO)_3]_2$ in $scCO_2$ (37 °C, 1870 psi) and (b) pressure dependence of radical recombination rate (k_2); solid line represents calculated diffusion controlled rate constant.

The decay of $CpMo(CO)_3\cdot$ radicals follows 2nd order kinetics (Figure 3(a)) and the value of k_2 is close to diffusion control in $scCO_2$ at pressure far removed from the critical point. The variation of k_2 for recombination of $CpMo(CO)_3\cdot$ radicals with respect to pressure is shown in Figure 3(b). It can be seen that, at both 35 and 50 °C, k_2 increases as the pressure is decreased to approach P_c and the value of k_2 is significantly greater than the expected diffusion controlled rate. We attribute this, like other workers, to an increased local density of solvent molecules. Cage effects in supercritical fluids have been the subject of considerable interest [9] and the $[CpMo(CO)_3]_2$ allows the effect of the solvent cage on recombination of $CpMo(CO)_3\cdot$ radicals to be investigated. Formation of *gauche*-$[CpMo(CO)_3]_2$, in n-heptane solution, was found to occur via two different processes; a rapid (detector limited) rise followed by a slower growth as the $CpMo(CO)_3\cdot$ radicals decayed [8]. This two stage formation of *gauche*-$[CpMo(CO)_3]_2$ was attributed to in-cage and out-of-cage recombination of $CpMo(CO)_3\cdot$ radicals. The formation of *gauche*-

$[CpMo(CO)_3]_2$ in $scCO_2$ was found to have no detectable "rapid" rise and the *gauche*-$[CpMo(CO)_3]_2$ formation follows the decay of the $CpMo(CO)_3\cdot$ radicals. Thus it appears that the solvent cage around the $CpMo(CO)_3\cdot$ radicals has no significant influence on the recombination over the pressure range used in this study. Solvent cages in supercritical fluids are expected to exist only for a few ps [10] and the lack of a pronounced cage effect on the recombination $CpMo(CO)_3\cdot$ radicals is interpreted to mean that the recombination of radicals within the solvent cage occurs on a timescale longer than the transient existence of the cage.

We have shown that TRIR is a powerful tool for elucidating reaction kinetics in supercritical fluids and we believe that transient vibrational data will play an important part in the understanding of the intermolecular solute-fluid and solute-solute interactions in supercritical fluids.

Acknowledgements

We thank Professor J. J. Turner and Dr. S. M. Howdle for many helpful discussions. We thank EPSRC, the Royal Society & the Royal Academy of Engineering for support. X-Z S thanks the Royal Society for a K.C. Wong Foundation Fellowship.

References

[1] For a recent review of Spectroscopy in SCF solution, see M. Poliakoff, S, G. Kazarian and S. M. Howdle Angew. Chem. Int. Ed. Engl. in press

[2] M. A. McHugh and V J. Krukonics, Supercritical Fluid Extraction: princeples and practice (Butterworth-Heinemann: Boston 1994).

[3] J. F. Brennecke ACS Symposium Series 514 (1993) 201.

[4] C. B.Roberts, J. Zhang, J. F. Brennecke, J. E. Chateauneuf, J. Phys. Chem. 97 (1993) 5618.

[5]. J. Zagrobelny and F. V. Bright,. J. Am. Chem. Soc. 97 (1993) 701 and references therein.

[6] M. Poliakoff, M. W. George and J. J. Turner,. Analyst 119 (1994) 551.

[7]. M. Poliakoff,S. M. Howdle, M. Jobling and M. W. George, 2nd Int. Symp. Supercrit. Fluids:Boston, USA (1991) 189; S. G. Kazarian, M. J. Clarke, M. W. George, M. Poliakoff, R. B. Gupta and K. P. Johnston 3rd Int. Symp. Supercrit. Fluids: Strasbourg, France (1994) 349.

[8] J. Peters, M. W. George and J. J. Turner, Organometallics 14 (1995) 1503.

[9] K. E. O'Shea, J. R. Combes, M. A. Fox and K. P. Johnson, Photochem. and Photobiology 54 (1991) 571.

[10] I. B. Petsche and P. G. Debenedetti, J. Phys. Chem. 91 (1991) 7075.

Vibrational Relaxation of Carbonmonoxide in Myoglobin Mutants and Model Heme Compounds

Kristen A. Peterson[†], Steven G. Boxer[#], Sean Decatur[#], Dana D.Dlott[‡], M. D. Fayer[#], J. R. Hill[‡], Chris W. Rella[§], Michael M. Rosenblatt[‡], Kenneth S. Suslick[‡], and Christopher J. Zeigler[‡]

[†]Department of Chemistry and Biochemistry, New Mexico State Unviersity, Las Cruces NM 88003
[#]Department of Chemistry, Stanford University, Stanford CA 94305
[‡]School of Chemical Sciences, University of Illinois at Urbana-Champaign, Urbana IL 61801
[§]Hansen Experimental Physics Laboratory, Stanford University, Stanford CA 94305

INTRODUCTION:

Last year we reported experimental measurements of vibrational lifetimes (T_1) for carbon monoxide (CO) bound to myoglobin as a function of protein conformational substate and temperature [1]. An infrared vibrational ground state recovery technique was used to monitor the rate of loss of vibrational excitation in the carbonyl stretching mode. The results of those experiments, along with the results of Orwutsky *et. al* [2] for hemoglobin and for protoheme in solution at ambient temperature, allowed us make some suggestions as to the mechanism of ligand vibrational relaxation in heme proteins. We concluded that the vibrational relaxation rate can be affected by ligand-protein interactions and suggested that this may be a result of changes in metal-ligand backbonding induced by electrostatic interactions between the protein and CO ligand. In addition, the lack of a temperature dependence for T_1 in the 10 - 300 K range showed that the predominant relaxation mechanism does not involve direct coupling from the CO stretch to modes with frequency ≤ 500 cm^{-1} such as the continuum of protein or solvent instantaneous normal modes [1,3].

In order to investigate these issues more fully, we have conducted two further studies, T_1 measurements for CO bound to (a) a series of metalloporphyrins, where only the metal is changed, and (b) a series of myoglobin mutants. These new studies provide a greater understanding of the vibrational relaxation mechanism by allowing the separation of effects due to changes in mass, metal-ligand interactions and ligand-protein interactions. On the basis of the metalloporphyrin study, we conclude that the CO vibrational fundamental is coupled to porphyrin ring modes through the π molecular orbitals. The change in axial ligand vibrational relaxation observed when the metal is changed from Fe to Ru or Os arises from corresponding changes in the π orbital structure (backbonding) and not from changes in mass. We find that the vibrational relaxation rate in heme proteins is sensitive to mutations in the binding pocket. The VR rates in the mutant myoglobins can also be understood in terms of changes in the electronic interactions between CO and iron, which affects the coupling to the porphyrin modes. In this case, interactions between CO and specific protein residues affect the degree of backbonding from the metal ion.

The measurements are made by a single frequency mid-infrared pump-probe technique using the Stanford Free-electron Laser [1]. Population in the first excited vibrational level of the CO stretch is created with an infrared pump pulse of ~1.5 ps fwhm and ~200 nJ tuned to the $V=1 \leftarrow 0$ transition. Recovery of the vibrational ground state is monitored at the same frequency by a delayed probe pulse of ~ 20 nJ. The continuous tunability, excellent wavelength stability, high energy (up to 1 μJ/pulse) and short duration of the pulses from the Stanford Free-electron Laser make it an excellent source for vibrational dynamics studies of this type.

RESULTS AND DISCUSSION:

Vibrational Relaxation in Metalloporphyrin Model Compounds:

Vibrational lifetimes were measured for CO bound to a series of d^6-metalloporphyrin complexes, M-coproporphyrinate I tetraisopropyl ester (CO) (pyridine), where M = Fe, Ru, Os. Sample preparation and synthesis were according published procedures [4,5]. The results are given in Table 1 and shown graphically in Figure 1A. The vibrational relaxation rate correlates inversely with vibrational frequency. These results and their interpretation are discussed more fully elsewhere [4], the conclusions are given in summary here.

Table 1: Vibrational lifetimes of the carbonyl stretch of M-coproporphyrinate I tetraisopropyl ester (CO) (pyridine) in CH_2Cl_2 solution at ambient temperature.

Metal M	carbonyl frequency (cm^{-1})	Vibrational lifetime (ps)
Fe	1963	42 ± 2
Ru	1935	23 ± 2
Os	1902	11 ± 2

In this metalloporphyrin series, the CO stretch frequency shifts to lower frequency as the mass of the metal ion increases, but also as the principal quantum number for the metal outer shell electrons increases. In order to understand the relationship between the CO frequency and the VR rate, two mechanisms were considered; (1) through σ-bond anharmonic coupling between the CO and metal ion and (2) anharmonic coupling between the ligand and porphyrin modes via the π orbitals [4]. The through σ-bond mechanism involves coupling between the carbonyl stretch and modes involving movement of the metal ion such as the Fe-(CO) stretching (ca. 575 cm^{-1}) and Fe-C-O bending (ca. 510 cm^{-1}) motions which can then transfer mechanical motion of the CO to vibrations of the porphyrin. Quantum mechanical models which are essentially an anharmonic triatomic molecule M-A-B coupled to a harmonic bath predict that the VR rate of AB should decrease as the mass of M increases [6,7]. However, in the metalloporphyrin series, the exact opposite behavior is observed. Our results rule out this model for the predominant mechanism of ligand vibrational relaxation in metalloporphyrins. It is also possible that changes in the intramolecular potential functions occur with substitution at M that effect the VR pathway. A study of the lifetimes of OH stretching vibrations in alcohols and silanols showed that a change from C-OH to Si-OH leads to a significant decrease in the VR rate [8]. Although those results follow the trend predicted by the mass effect, the data were interpreted in terms of differences in the nearest neighbor mode frequencies which change the order of the relaxation pathway. However, resonance Raman studies on a number of metalloporphyrin complexes show that when ν_{CO} shifts by 20 cm^{-1}, the Fe-(CO) stretching and bending modes shift by 5 cm^{-1} or less[9]. These shifts do not seem large enough to explain the metalloporphyrin results by a consideration of nearest neighbor σ-bond coupling alone. Furthermore, isotopic substitution of ^{13}CO for ^{12}CO in myoglobin (*vida infra*) shifts ν_{CO} more than when Ru is replaced by Os, yet the VR rate does not change (figure 1B).

It is well known that the frequency shifts for CO bound to d^6-metalloporphyrins are largely determined by the magnitude of backbonding from the metal's d_π-orbitals to the carbonyl's π^* antibonding orbital. More backbonding leads to a decreased CO stretching frequency and an increased M-(CO) stretching frequency [9]. In the Fe - Os series, the increasing size and polarizability of the metal d-orbitals result in greater backbonding for the heavier metal. We have proposed that the observed correlation between CO vibrational lifetime and frequency is actually a

correlation between CO vibrational lifetime and π-system electronic structure [4]. This mechanism involves long ranged anharmonic coupling between the carbonyl stretch and the porphyrin vibrational modes via the ligand π- and metal dπ-orbitals and is consistent with the recent suggestion of Orwutsky *et. al* [2] that the rapid relaxation in carbonmonoxy heme compounds, as compared to metal carbonyls, arises from fluctuating partial charges on the metal and ligand during vibrational motion which couples to the porphyrin via the π-system. Because the coupling between carbonyl and porphyrin involves delocalized π-orbitals, the range of interaction is greater than for nearest neighbor through σ-bond mechanisms. As backbonding increases, coupling of the CO to the porphyrin ring modes increases, leading to an increase in VR rate for the axial ligand. This through π-bond model would predict that other factors which change the π-electronic structure of the metalloporphyrin-CO complex will affect VR. For example, the electronic structure of the porphyrin can be significantly affected by the nature of the substituents on the porphyrin perimeter. Changes in the local electric field or polarity of the environment around the axial ligand can also change the degree of backbonding and should affect the VR rate for the ligand similarly to that observed for backbonding changes due to metal substitution.

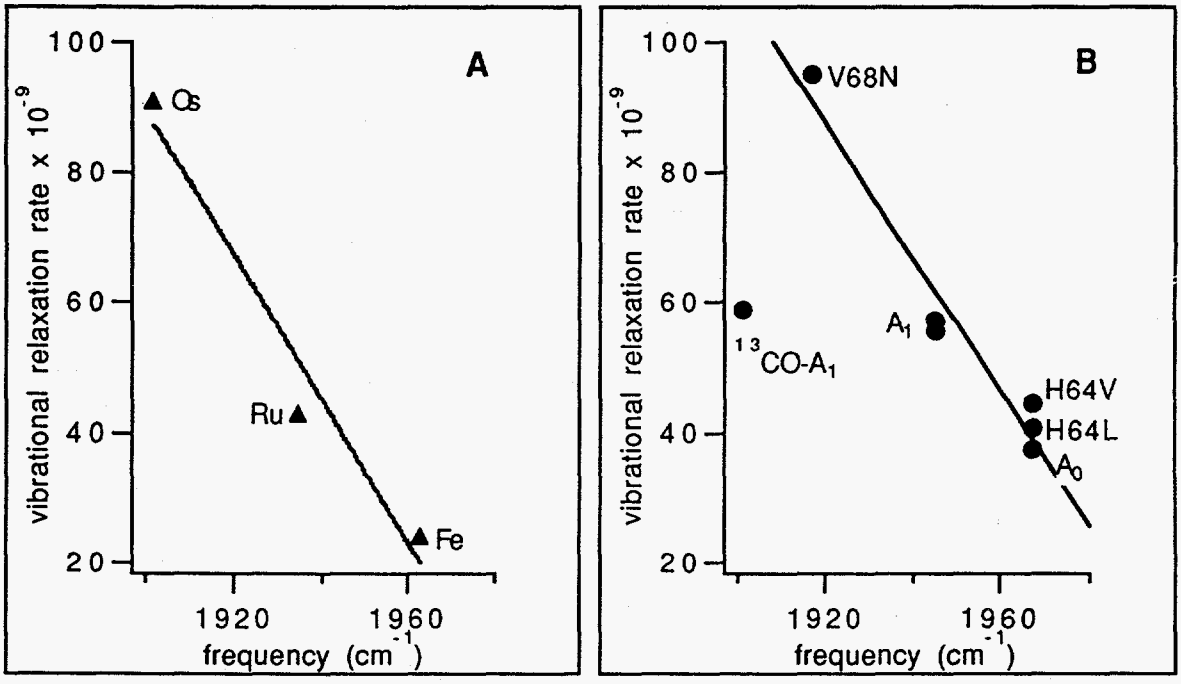

Figure 1: Vibrational relaxation rates versus carbonyl stretching frequency for (A) a series of model heme compounds with differing metal ions and (B) myoglobin and myoglobin with distal pocket mutations. The lines are linear regression fits with the exclusion of the ^{13}CO-A1 point and illustrate the similarity in change of VR rate with frequency for the two series.

Effects of Binding Pocket Mutation in Myoglobin:

In order to investigate the origin of the difference in CO vibrational lifetimes for different myoglobin conformational substates, we decided to study the effects of changing ligand-protein interactions through binding pocket mutations. It has been observed that point mutations in the binding pocket can significantly shift the CO vibrational frequency and that the iron to carbon stretch frequency decreases as the CO frequency increases [9,10]. These shifts have been interpreted in terms of metal to ligand backbonding changes induced by changes in electrostatic fields and/or chemical interactions such as hydrogen bonding between the CO and protein residues.[9,10].

Table 2: Vibrational lifetimes of carbonyl stretch for carbonmonoxy myoglobin and myoglobin mutants at ambient temperature.

Myoglobin*	carbonyl frequency (cm^{-1})	vibrational lifetime (ps)
H64V	1967	24.5 ± 2
H64L	1967	22.5 ± 2
†wildtype, A_0 band in poly(vinyl alcohol)	1967	26.6 ± 1
†wildtype, A_1 band in poly(vinyl alcohol)	1945	18.2 ± 1
†wildtype, A_1 band	1945	17.4 ± 1
V68N	1917	10.5 ± 2
wildtype, ^{13}CO	1901	17 ± 2

* All samples are in glycerol/H20 (60:40) at pH 7 and with ^{12}CO except where noted.
† From reference 1.

We have measured T_1 for the stretching fundamental of CO bound to myoglobins with single residue mutations in the distal pocket. Preparation and characterization of the mutants is described in reference 11. IR samples were prepared as previously [1]. Two mutations of the distal histadine were examined; H64L and H64V where the histadine is replaced by leucine and valine respectively. In the case of H64V, both sperm whale and human myoglobin mutants were prepared. Human myoglobin mutant V68N, valine to asparagine, was also investigated. (The reader is referred to [10,11] for structural details of these mutants.) In addition, we measured the CO vibrational lifetime for isotopic ^{13}CO bound to wildtype human myoglobin. The results of these measurements are summarized in Table 2 along with the results for wildtype sperm whale myoglobin A_0 and A_1 CO bands reported previously [1]. No differences in VR between sperm whale and human wildtype myoglobin or between sperm whale and human H64V were observed, therefore we report only one combined value for each distal residue configuration.

Figure 1B shows these results graphically, with the CO vibrational relaxation rate plotted as a function of CO frequency. With the exception of the isotopic CO sample, there is an inverse correlation between CO vibrational relaxation rate and frequency. In the case of isotopic CO, the frequency shift is caused by a change in reduced mass of the ligand, but the electronic structure of the complex is not changed. Despite the large shift in frequency, the VR rate does not change when ^{13}CO is substituted for ^{12}CO in wildtype myoglobin. These results are consistent with the through π-bond coupling model described above.

The results for the mutant myoglobins can also be explained by the through π-bond coupling model when polar interactions with the protein residues in the binding pocket are considered. For H64V and H64L the polar distal histadine is replaced by nonpolar valine and leucine respectively. A decrease in positive polarity around the oxygen atom of CO would destabilize a partial negative charge on oxygen and reduce backbonding[9,10]. This is reflected in the shift of ν_{CO} to higher frequency and a decrease in the CO VR rate. ν_{CO} for these mutants is the same as for the A_0 conformational substate in wildtype myoglobin, and the vibrational lifetime is similar. It has been proposed that the A_1 and A_0 substates differ in the conformation of the distal histadine which results in differing polar interactions with bound CO [9,10]. In the case of V68N, a nonpolar valine residue is replaced by asparagine. The NH_2 group of the side chain of asparagine can hydrogen bond to CO, stabilizing backbonding [10,12]. This results in a decrease in ν_{CO} and an

increased VR rate. Electrostatic and chemical interactions between the protein residues and distal ligand affect the electronic structure of the ligand-heme complex. These changes in π-bonding are reflected in the CO frequencies and the vibrational dynamics.

SUMMARY:

The rate of CO vibrational relaxation in a series of model carbonmonoxy heme compounds is seen to increase with the extent of backbonding from the metal's d_π-orbitals to CO. These results cannot be explained by through σ-bond models in which the carbonyl stretching motions is coupled to the bath of porphyrin modes via mechanical displacements of the central metal ion. Instead we propose a through π-bond mechanism which involves longer ranged anharmonic coupling between the CO and porphyrin ligands through the delocalized π-electron orbitals. According to this model, changes in the structure of the complex or in its environment which affect the π-electron distribution will affect the ligand vibrational dynamics. Such an effect is observed in myoglobin when mutations in the binding pocket of the protein change the electrostatic fields near the bound CO. The electric fields arising from the protein residues substantially influence the mechanical coupling and dynamics at the active site as reflected in the CO vibrational lifetimes. These effects, which are not seen in molecular mechanics simulations which seek to model protein structure and function, may have profound implications in understanding protein-ligand interactions and binding site chemistry.

Acknowledgment:

This research was supported by the Office of Naval Research, Biology Division by contract N00014-1-0259 (DDD and JRH) and by the ONR Medical Free Electron Laser Program, contract N00014-91-C0170. MDF acknowledges additional support from NSF Grant DMR-90-22675. KS, MR, and CZ wish to acknowledge support from NIH Grant PHS 5R01-HL-25934. We thank Professors Alan Schwettman and Todd Smith and their research groups for making it possible to perform these experiments at the Stanford Free Electron Laser Center.

References:

1. J. R. Hill, A. Tokmakoff, K. A. Peterson, B. Sauter, D. Zimdars, D. D. Dlott and M. D. Fayer, J. Phys. Chem., 98 (1004) 11213.
2. J. C. Owrutsky, M. Li, J. P. Culver, M. J. Sarisky, A. G.Yodh and R. M. Hochstrasser, Springer Proc. Physics (Time-Resolved Vibrational Spectroscopy VI) 1993; J. C. Owrutsky, M. Li, B. Locke and R. M. Hochstrasser, J. Phys. Chem., 99 (1995) 4842.
3. V. M. Kenkre, A. Tokmakoff and M. D. Fayer, J. Chem. Phys., 101 (1994) 10618.
4. J. R. Hill, D. D. Dlott, M. D. Fayer, K. A. Peterson, C. W. Rella, M. M. Rosenblatt, K. S. Suslick and C. J. Zeigler, Chem. Phys Lett. (submitted).
5. M. Barley, J. Y. Becker, G. Domazetis, D. Dolphin and B. R. James, Can. J. Chem., 61 (1987) 2389; C. M. Che, C. K. Poon, W. C. Chung and H. B. Gray, Inorg. Chem., 24 (1985) 1277. A. D. Adler, F. R. Longo, F. Kampas, and J. Kim, Inorg. Nucl. Chem., 32 (1970) 2443.
6. I. Benjamin and W. P. Reinhardt, J. Chem. Phys., 90 (1989) 7535.
7. K. N. Swamy and W. L. Hase J. Chem. Phys 82 (1985) 123.
8. E. J. Heilweil, M. P. Casassa, R. R. Cavanagh and J. C. Stephenson, J. Chem. Phys., 85 (1986) 5004.
9. X. Y. Li and T. G. Spiro, J. Am. Chem. Soc., 110 (1988) 6024.; G. B. Ray, X. Y. Li, J. A. Ibers, J. L. Sessler and T. G. Spiro, J. Am Chem Soc., 116 (1994) 162.
10. B. A. Springer, S. G. Sligar, J. S. Olson and G. N. Phillips Jr., Chem. Rev., 94 (1994) 699
11. S. Balasubramnian, D.G. Lambright and S.G. Boxer, Proc. Natl. Acad. Sci. USA, 90 (1993) 4718.
12. S. M. Decatur and S. G. Boxer, Biochem. Biophys. Res. Commun. 1995 (in press).

Defining the Allosteric Pathway in Hemoglobin: Time-Resolved UV and Visible Resonance Raman Spectroscopy of Kinetic Intermediates

Vasanthi Jayaraman and Thomas G. Spiro
Department of Chemistry, Princeton University, Princeton, NJ 08544.
Kenton R. Rodgers
Department of Chemistry, North Dakota State University, Fargo, ND-58105.
Ishita Mukerji
Department of Biochemistry and Molecular Biology, Wesleyan University, CT-06457.

ABSTRACT

The allosteric transition of hemoglobin [Hb] has been monitored by time-resolved resonance Raman spectroscopy in the nanosecond to microsecond interval following HbCO photolysis. Excitation at 230 nm provides enhancement of tyrosine and tryptophan vibrational modes, which probe different regions of the protein: the $\alpha_1\beta_2$ subunit interface, where most of the alterations in quaternary contacts occur, and also A-E helix contacts on the distal side of the heme binding pockets. Complementary experiments with 436 nm excitation provide enhancement of heme vibrational modes, which monitor relaxation of the porphyrin ring and of the Fe-histidine bond, as well as the time course of CO recombination. The kinetic data from all of these probes can be fit to a set of four exponential processes, whose time constants are in good agreement with those reported previously on the basis of optical absorption transients. Spectra of the four intermediates are extracted from the transient data, and are used to construct a structural model for the allosteric transition in Hb.

INTRODUCTION

Allostery, the process by which proteins change their shape upon binding small molecules or ions, drives numerous biological functions, from muscle contraction, to nerve conduction, to the efficient transport of oxygen in the blood (1). Hemoglobin [Hb] offers the best hope for providing insight into the allosteric transition, because so much is known about the connection between its structure and function. The allosteric transition can be studied directly by kinetic methods. Transient absorption spectroscopy has provided rate constants for several kinetic steps subsequent to the photo-dissociation of HbCO (2,3). The Fe-CO bond breaks on the sub-picosecond time scale (7), and the resulting deoxy-heme undergoes small but measurable absorptivity changes with time constants of about 0.05, 0.7 and 20 μs (4). At the same time, recombination is observed on the nanosecond time-scale, in a first-order geminate phase [rebinding from within the protein] (5), and on the millisecond time-scale in a second-order phase [rebinding from solution] (3). We have now characterized the protein intermediates subsequent to ligand dissociation, using time-resolved resonance Raman [RR] spectroscopy (6-9) to monitor structural evolution at the heme and at aromatic residues that are located at strategic positions in the protein.

TR^3 KINETICS

UVRR spectra with 230 nm excitation contain bands arising from ring modes of tyrosine [Y] and tryptophan [W] residues (6). Time-resolved UVRR difference spectra, obtained by subtracting the spectrum of HbCO from that of the photoproduct generated by a 419 nm photolysis pulse preceding the 230 nm probe pulse evolve toward the static difference spectrum of deoxyHb on the microsecond time-scale . The time course of these changes was analyzed by

fitting the integrated areas of the most prominent bands in the parent spectra to a sequence of four successive exponential processes. The same time constants were obtained from Y and W peaks [Table 1], and they agreed within experimental error with those determined by Hofrichter et al. (3) from the heme optical absorption transients at pH 7.4.

Table 1: Relaxation time constants (μs) from RR intensity variations

pH	τ_1	τ_2	τ_3	τ_4
5.8	0.01 ± 0.01	0.25 ± 0.05	10 ± 1	125 ± 100
7.4	0.02 ± 0.01	0.50 ± 0.10	17 ± 2	500 ± 500
7.4*	0.05 ± 0.01	0.71 ± 0.14	19 ± 3	1500 ± 300
8.8	0.03 ± 0.01	0.66 ± 0.12	50 ± 5	1500 ± 500

*Determined from optical absorption transient spectra by Hofrichter et a. (1983).[3]

These time constants define a set of intermediates, B-F, in the photocycle of HbCO [labeled A]. Because the kinetic steps are well separated, the intermediates reach high population levels [except F], permitting reliable extraction of their spectra from the transient data, using populations calculated from the kinetic equations. Difference UVRR spectra [Figure 1] were calculated for each intermediate by subtracting the HbCO spectrum; the figure contains no entry for the immediate photoproduct, B, because its spectrum does not differ from HbCO. The spectra of C [20 ns] , D [0.5 μs] and E [20 μs] are essentially the same at all three pH values, despite the differences in time course. Because of low population, the spectrum of F [1 ms] could not be determined at pH 8.8, and the calculated spectra at pH 7.4 and 5.8 are noisy. They are nevertheless distinctive, and differ between the two pH values.

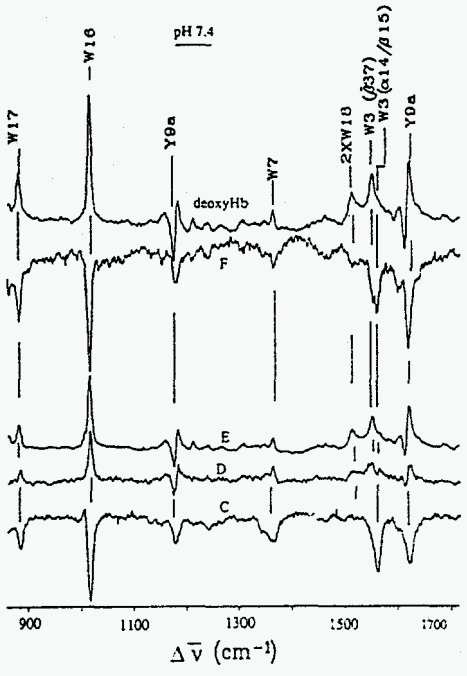

Figure 1: UVRR difference spectra of the intermediates C-F extracted from the transient spectra with the kinetic model. The static difference spectrum of deoxyHb vs HbCO is shown at the top for comparison.

Excitation at 436 nm, near resonance with the heme Soret band, enhances vibrational modes of the porphyrin ring and of the Fe-ligand bonds (10, 11). The frequencies of the ring stretching modes ν_2, ν_3 and ν_4, shift down upon photolysis, due to the porphyrin core expansion in the high-spin photoproduct (7). Subsequently, these frequencies shift up slightly, as the Fe atom attains its full out-of-plane displacement (7), and the HbCO features return to about half their original intensity, due to geminate recombination. Both processes were found to be coincident with the first UVRR relaxation, 20 ns.

The geminate recombination is also seen in the recovery of the 507 cm^{-1} Fe-CO stretching band, but the Fe-histidine stretch of the deoxy-heme photoproduct, ~220 cm^{-1}, relaxes over the whole time course of the experiments. From the kinetic analysis, its frequency was determined to be 228, 224, 222 and 216 cm^{-1} in the intermediates B, C, D, and E.

HEMOGLOBIN REACTION COORDINATE

The definition of a series of intermediates, and the determination of their RR spectra permit a number of inferences about the nature of the allosteric reaction coordinate, which are diagrammed in Figure 2.

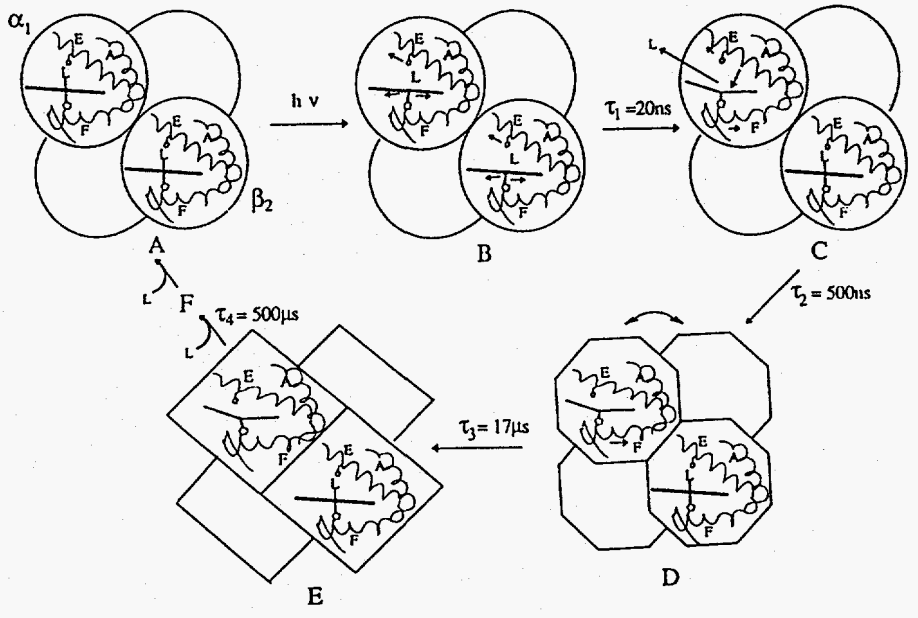

Figure 2: Cartoon of the Hb reaction coordinate starting with the photolysis of ligated (L=CO) Hb tetramers, A, and proceeding through the intermediates B-F to complete the photocycle. Arrows in the tetramer indicate motion proposed from the time resolved UVRR and Visible RR spectra. The time constants are from the pH 7.4 UVRR kinetics.

The first intermediate, B. is the geminate state, in which the Fe-CO bond is broken, and the CO is believed to take up a well-defined position in the heme pocket, as evidenced by a narrow C-O stretching IR band in the B state (12). In recent x-ray crystal structures of MbCO photolyzed at 4 K, the CO is seen lying over one of the pyrrole rings of the heme (13, 14). The Fe atom is displaced from the heme plane, in this structure, but only by about 80 % of the displacement seen in deoxyMb (13), in agreement with the 75 % estimate derived from the 2 cm^{-1} downshifts of ν_2 and ν_3 relative to deoxyHb (7). This displacement is restrained by the proximal histidine, which is attached to the F helix. The elevated frequency of the Fe-His frequency, 228 cm^{-1}, in the B intermediate is evidence of stress on the F helix. The UVRR spectrum is the same in B as it is in A, indicating that there are no large-scale protein motions at this early stage of the reaction coordinate.

In the transition to C [20 ns], the CO in half the chains recombines with the heme, but escapes from the other half. Structural change in the deoxy chains is evident in both the visible and UVRR spectra. The porphyrin core size marker frequencies have relaxed to their deoxyHb values, signaling full out-of-plane displacement of the Fe atom. The Fe-His frequency has decreased from 228 to 224 cm^{-1}, only slightly higher than the value expected for a relaxed deoxy-heme structure (15). We infer that most of the deoxy-chain energy has spread to the surrounding protein at this stage. The UVRR spectrum [Figure 1] suggests that some of this energy is now stored in a displacement of the E helix, which lines the distal side of the heme pocket. E helix motion is implicated because the W3 difference band of C is at the position expected for the interior tryptophan residues, $\alpha 14$ and $\beta 15$, and the intensity loss indicates a weakening of their H-bonds via increased separation of the A and E helices (16). E helix displacement towards the heme impels geminate recombination in half the chains, and CO escape from the heme pocket in the remaining half.

The difference UVRR spectrum of D (0.5 μs) reproduces all the features of the deoxyHb difference spectrum, but with much lower amplitude. It has previously been assumed that the quaternary rearrangement of the subunits takes place in the final kinetic phase of the protein, the ~ 20 μs phase leading to the species we have labeled E. The present evidence, however, implicates C→D as the quaternary transition. It is impossible for the quaternary contacts to begin to form until the subunits are close to being in the correct positions. However, the Fe-His stretching frequency is 222 cm^{-1}, a typical value for a relaxed deoxy-heme (15). We infer that D retains an R-like tertiary structure even after having undergone the subunit rearrangement that leads to the T state.

The D→ E transition produces T-like properties. The Fe-His band is at the same low frequency, 216 cm^{-1}, as in deoxyHb (15) and the slow CO binding rate is similar to that of deoxyHb (3). The difference UVRR spectrum has all the features of the deoxyHb spectrum, and is substantially stronger than the spectrum of D, but it is weaker [60 %] than that of deoxyHb. It has the same amplitude as has been found for the asymmetrically diligated cyanometHb hybrids, in which the cyanomet hemes are in the $\alpha_1\beta_1$ [or equivalently $\alpha_2\beta_2$] dimer (17). This species represents a third cooperativity state, T', because its dimer/tetramer assembly free energy is intermediate between those of deoxyHb and of the symmetrically diligated hybrids (18). The T' state is inferred to have a deformed $\alpha_1\beta_2$ interface, with weakened Trp $\beta 37$ and Tyr $\alpha 42$ H-bonds (17). Because of geminate recombination, E contains two ligated hemes, and we infer that both CO's are on the same dimer, producing the T' state.

Second-order recombination with CO returns the Hb photoproduct to HbCO, but an additional intermediate, F, is formed en route, as revealed by changes in the UVRR spectra. At pH 7.4, the spectrum of F is the same as that of C, i.e. it is an R_{deoxy} spectrum, with negative peaks. Since E already has two CO ligands, we infer that F is a triligated species and is in the R state; the UVRR signal is provided by the one remaining deoxy chain. Consistent with this interpretation, the spectrum is the same as that obtained for triligated cyanometHb hybrids (17). At pH 5.8, the calculated spectrum of F is quite noisy, but although a negative difference band is still seen for W16, a positive W3 signal is found, at the Trp $\alpha 14$ and $\beta 15$ position. The latter feature was also seen in the difference spectrum of fluorometHb with and without IHP (19). Since the signal is opposite to that found in the R_{deoxy} spectrum, it was suggested to result from a strengthening of the Trp $\alpha 14$ and $\beta 15$ H-bonds in ligated chains within the T state. It is likely that CO recombination at low pH produces triligated molecules that remain in the T' state, and that give rise to a positive W3 band.

With the exception of F, the UVRR difference spectra of all the intermediates are independent of pH, but the time constants increase with increasing pH. The speeding up of the reaction as the pH is lowered implicates the same interactions that are responsible for the well-known stabilization of the T state at low pH (1).

Acknowledgments

We thank Prof. Gary Ackers for helpful discussions. This work was supported by NIH grant GM 25158.

References

1. M. F. Perutz, *Mechanisms of Cooperativity and Allosteric Regulation in Proteins* (Cambridge University Press, Cambridge, 1990).

2. C. Sawicki and Q. H. Gibson, J. Biol. Chem., 251 (1976) 1533.

3. J. Hofrichter, J. H. Sommer, E. R. Henry and W. A. Eaton, Proc Natl Acad. Sci. U.S.A., 80 (1983) 2235.

4. J. L. Martin, A. Migus, C. Poyart, Y. LeCarpentier, R. Astier, and A. Antonetti, Proc. Natl. Acad. Sci. U.S.A., 80 (1983) 173.

5. J. M. Friedman and K. B. Lyons, Nature, 284 (1980) 570.

6. K. R. Rodgers, C. Su, S. Subramaniam and T. G. Spiro, J. Am. Chem. Soc., 114 (1992) 3697.

7. S. Dasgupta and T. G. Spiro, Biochemistry, 25 (1986) 5941.

8. T. W. Scott, and J. M. Friedman, J. Am. Chem. Soc. 106 (1984) 5677.

9. S. Kaminaka, T. Ogura, and T. Kitagawa, J. Am. Chem. Soc., 112 (1990) 23.

10. D. L. Rousseau and J. M. Friedman, *Biological Applications of Raman Spectroscopy* (John Wiley & Sons, New York, 1987) vol.3, 133.

11. T. G. Spiro and X. Y. Li, *Biological Applications of Raman Spectroscopy* (Wiley, New York, 1987) Vol.3, 1.

12. B. Locke, T. Lian, and R. M. Hochstrasser, Chem. Phys., 158 (1991)409.

13. I. Schlichting, J. Berendzen, G. N. Phillips and R. M. Sweet, Nature, 371 (1994) 808.

14. T. Y. Teng, V. Srajer and K. Moffat., Nature Structural Biology, 1 (1994) 701.

15. J. M. Friedman, T. W. Scott, R. A. Stepnoski, M. Ikeda-Saito and T. Yonetani, J. Biol. Chem., 258 (1983) 10564.

16. K. R. Rodgers and T. G. Spiro, Science, 265 (1994) 1697.

17. V. Jayaraman and T. G. Spiro, Biochemistry, 34 (1994) 4511-4515.

18. G. K. Ackers, M. L. Doyle, D. Myers and M. A. Daugherty, Science, 255 (1992) 54.

19. V. Jayaraman, K. R. Rodgers, I. Mukerji and T. G. Spiro, Biochemistry, 32 (1993) 4547.

Femtosecond Time Resolved Infrared Laser Study of the J - K Transition of Bacteriorhodopsin

Rolf Diller*†, Sudipta Maiti#, Gilbert C. Walker‖, Benjamin R. Cowen§, Robert Pippenger§, Roberto A. Bogomolni§ and Robin M. Hochstrasser§;
Reiner Dziewior* and Dietmar Stehlik*

*†to whom correspondence should be sent, Institut für Experimentalphysik, Freie Universität Berlin, Arnimallee 14, D-14195 Berlin, Germany, e-mail: diller@omega.physik.fu-berlin.de, phone: +49 30 838-6232(-6081 fax); #Present address: Department of Applied and Engineering Physics, F-15, Clark Hall, Cornell University, Ithaca, NY 14853-2501; ‖Present address: Department of Chemistry, University of Pittsburgh, Pittsburgh, Pennsylvania 15260; §Department of Chemistry, University of California, Santa Cruz, California 95064; §Department of Chemistry, University of Pennsylvania, Philadelphia, Pennsylvania 19104.

INTRODUCTION

We are interested in the ultrafast vibrational response of proteins after photoexcitation of an attached chromophore (for a review see [1]). The application of highly time resolved infrared spectroscopy to the bacteriorhodopsin (BR) photocycle, as already demonstrated in our earlier work [2], has now been extended to the sub picosecond time regime [3]. The light driven photocycle of the membrane bound protein BR generates an electrochemical potential across the cell membrane of halobacteria. The primary all-trans to 13-cis photoisomerization of the lysine bound retinal cofactor is followed by a series of thermal relaxations involving the protein and the chromophore. Thereby, a proton gradient is generated across the cell membrane. The photocycle is completed after a few milliseconds under ambient conditions. The first reaction states, including the light adapted BR_{570}, the photoexcited state BR*, the isomerized state J and its decay into the K - intermediate are subject of this study.

MATERIALS AND METHODS

Purple membrane from Halobacterium Halobium ET 1001 [4] was prepared as thin humidified film in order to reduce the IR absorption by water. By moving the sample, the excited and probed sample volume was replaced between two laser shots by fully regenerated, light adapted BR_{570}. Short light pulses from a kHz Titanium Sapphire laser system provided for a spectral continuum generated in a water cell and for weak, delayed pulses, used to optically gate the continuous wave IR probe carbon monoxide (CO) laser beam. The pump pulses, centered at 540 nm, were directly extracted from the continuum and chopped at half the system repetition rate. The upconverted light pulses were detected using a photomultiplier and processed by lock-in techniques. The overall instrument response had a FWHM of about 400 fs. The experiments were performed at room temperature.

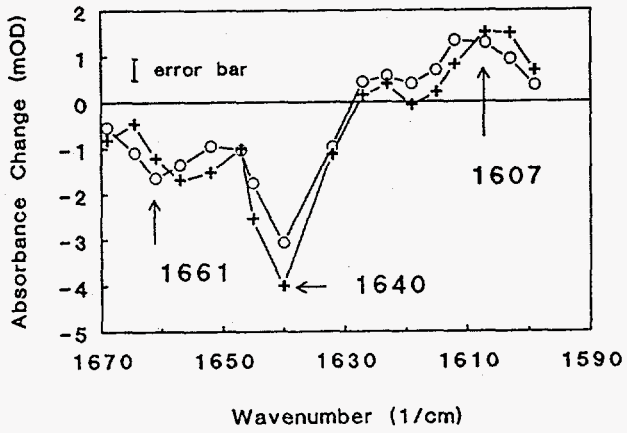

Figure 1: IR difference spectra of BR, taken at 1.5 ps (+) and 9 ps (o) after photoexcitation at 540 nm.

RESULTS AND DISCUSSION

Difference spectra

Fig. 1 shows IR difference spectra (pumped - unpumped absorbance) in the region between 1600 and 1670 cm^{-1}, taken at 1.5 and 9 ps after photoexcitation, respectively. The negative band at 1640 cm^{-1} is assigned to the C=NH stretch vibration of the all trans BR_{570} chromophore which is bleached under isomerization and shifts to about 1610 cm^{-1}, leading to an increased absorbance at the latter wavelength. The weak signal at ca. 1660 cm^{-1} lies in the center of the amide-I protein absorption. Since no chromophoric vibrational modes in this region are known, the signal most likely is due to a non chromophoric mode, e. g. a peptide stretch or the bending mode of a protein bound water molecule. Between 1.5 and 9 ps the bands at 1661 and 1607 cm^{-1} shift ca. 5 cm^{-1} to higher energies and the strong bleach at 1640 cm^{-1} recovers partially. Since the J-K transition takes between 3 and 4 ps (cf. Kinetics), the spectrum at 1.5 ps is dominated by the J - state, whereas the spectrum at 9 ps represents the K - state. The small differences between the spectra indicate that, compared to the preceeding isomerization, only small conformational changes take place during the J-K transition. This is in line with [5,6], where it was suggested that the J-K transition is dominated by vibrational cooling and torsional relaxation of the chromophore.

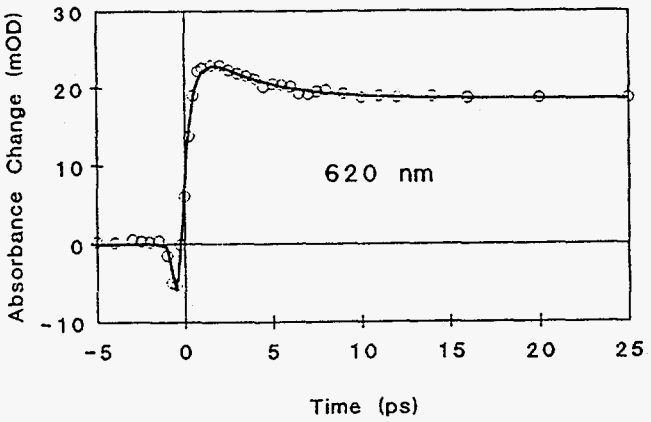

Figure 2: Kinetics of the BR photocycle, taken at 620 nm.

Kinetics

Kinetics were taken at 1640, 1607 and 1661 cm^{-1}. In order to compare the vibrational dynamics with the electronic dynamics under identical experimental conditions, kinetics were taken at 620 nm (Fig. 2). At this wavelength BR_{570}, J and K absorb. The kinetics fit well the sequential of intermediates BR $\rightarrow$ J $\rightarrow$ K, convoluted with the system response, assuming a time constantant of 500 fs for J - formation. The fit yields a time constant of 3.4 $\pm$ 0.5 ps for the slow component, i. e. the J-K transition. This is in agreement with literature data [7,8].

The kinetics taken in the IR show a fast component and a slower, weaker component in accordance with the difference spectra. For a complete quantitative interpretation, dephasing processes of the related vibrational transitions have to be taken into account. The dephasing times of the vibrational transitions involved in this experiment lie between 0.5 and 2 ps, corresponding to linewidths between 20 and 5 cm^{-1}, and hence are longer than the experimental system response. For example, if an infrared absorber (a vibrational transition) is instantaneously created (by the pump pulse) at the probe wavelength, it takes the dephasing time T_2 for the IR intensity behind the sample to decrease to its final steady state value. However, if an absorber is instanteneously removed from the probe wavelength, the IR probe intensity will increase equally fast. For a detailed account of the coherent response formalism see [9,10]. The kinetics are interpreted as follows.

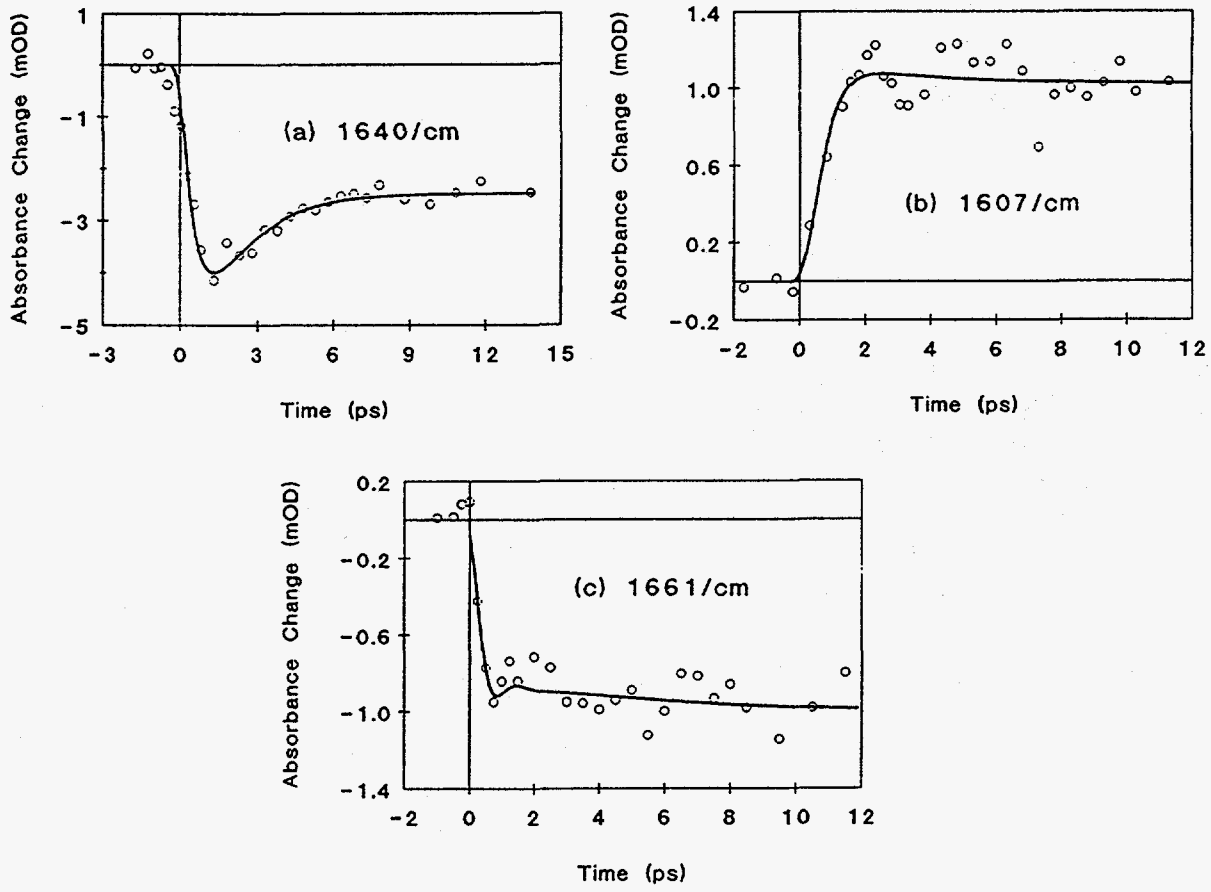

Figure 3: IR kinetics of BR, taken at 1640 cm^{-1} (a), 1607 cm^{-1} (b) and 1661 cm^{-1} (c).

The bleach at 1640 cm^{-1} appears with a time constant of 0.6 - 1.0 ps, i.e. much slower than the depletion of the BR_{570} electronic ground state. This is explained by a transfer of the probe induced, macroscopic IR polarization from the ground to the excited electronic state S_1. The observed bleach occurs with the S_1 decay. The partial recovery of the bleach occurs within 1.4 - 2.4 ps, i.e. significantly faster than the J-K transition. It is related to that fraction of excited BR molecules which return to S_0 of BR_{570}, i. e. does not follow the photocycle reaction pathway to J, K, etc.. S_1 decay and the vibrational cooling process determine the ground state recovery. Using this model, values of 0.50 - 0.55 were obtained for the J - formation quantum yield Φ_J. Literature values for the BR photocycle quantum yield range from $\Phi = 0.25$ [11] to $\Phi = 0.67$ [12].

The rise of the signal at 1607 cm^{-1} represents the J - formation. Its appearance within 0.9 - 1.2 ps is determined by the population kinetics of J - formation (0.5 - 0.7 ps) and the dephasing time (0.8 ps) of the vibrational transition corresponding to a bandwidth of ca. 13 cm^{-1}. The kinetics in the ps regime (J - K transition) were fitted to a small amplitude decay with a fixed time constant of 3.4 (from the kinetics at 620 nm).

The bleach at 1661 cm^{-1} shows a much faster response than that at 1640 cm^{-1}. An upper limit of 0.5 ps can be given. The slow component was again set to 3.4 ps. Taking into account the non-chromophoric origin of this band, the fast rise of the signal suggests a perturbation of amide-I carbonyls in the vicinty of the chromophore concomitantly to photoexcitation or J - formation. The perturbation could be purely coulombic or steric. It is estimated that a reasonable change in the electric field of $4*10^4$ V/cm could induce the observed bleach if a sufficiently large number of peptide carbonyls is affected. Other explanations for the origin of this bleach include the interaction of the positively charged Schiff's base with a water molecule as suggested in [13,14] and the isomerization induced strain on a peptide group, e.g. that of Lys216.

CONCLUSIONS

Femtosecond time resolved infrared spectroscopy was used to monitor the vibrational dynamics of the BR photocycle. The intermediate states J and K can be distinguished by their BR_{570} difference spectra between 1670 and 1600 cm^{-1}. Kinetics, taken at 1640 and 1607 cm^{-1} show rise times determined by the dephasing times of the vibrational modes. The partial decrease of the bleach signal at 1640 cm^{-1} is interpreted as a recovery of the vibrationally cooled BR_{570} electronic ground state and provides a new method to measure the photocycle quantum yield. The development of the bleach at 1661 cm^{-1} occurred faster than 500 fs, suggesting an almost instantaneous response of non chromophoric origin to the electronic excitation. In order to extend the range of probe wavenumbers we (Freie Universität Berlin) built a liquid nitrogen cooled CO laser [15] and implemented it into a fs laser system. This laser covers the spectral region from 1230 to 2130 cm^{-1} and from 2380 to 3850 cm^{-1} (overtone regime).

Acknowledgements

This work was supported by NIH and NSF. R. Diller gratefully acknowledges a fellowship from the Deutsche Forschungsgemeinschaft. R. Diller, R. Dziewior and D. Stehlik thank Prof. W. Urban and his coworkers (Universität Bonn) for their support regarding the CO laser.

References

1. B. Locke, R. Diller and R. M. Hochstrasser, in Advances in Spectroscopy, Vol. 21, Ed. R. J. H. Clark and R. E. Hester (John Wiley and Sons, Chichester, 1993) p. 1.
2. R. Diller, M. Iannone, B. R. Cowen, S. Maiti, R. A. Bogomolni and R. M. Hochstrasser, Biochemistry 31 (1992) 5567.
3. R. Diller, S. Maiti, G. C. Walker, B. R. Cowen, R. Pippenger, R. A. Bogomolni and R. M. Hochstrasser, Chemical Physics Letters , in press.
4. D. Oesterhelt and W. Stoeckenius, Methods. Enzymol. 31 (1974) 667.
5. H. -J. Polland, M. A. Franz, W. Zinth, W. Kaiser, E. Kölling and D. Oesterhelt, Biophys. J. 49 (1986) 651.
6. S. J. Doig, P. J. Reid and R. A. Mathies, J. Phys. Chem. 95 (1991) 6372.
7. J. Dobler, W. Zinth, W. Kaiser and D. Oesterhelt, Chem. Phys. Lett. 144 (1988) 215.
8. J. W. Petrich, J. Breton, J. L. Martin and A. Antonetti, Chem. Phys. Lett. 137 (1987) 369.
9. R. M. Hochstrasser, in Monographs on Chemistry in the 21 st Century Series, IUPAC, Ed. M. A. El-Sayed (Blackwell, Oxford, 1994).
10. K. Wynne and R. M. Hochstrasser, Chem. Phys. 193 (1995) 211.
11. C. R. Goldschmidt, O. Kalisky, T. Rosenfeld and M. Ottolenghi, Biophys. J. 17 (1977) 179.
12. G. Schneider, R. Diller and M. Stockburger, Chem. Phys. 131 (1989) 17.
13. A. Maeda, J. Sasaki, Y. Shichida and T. Yoshizawa, Biochemistry 31 (1992) 462.
14. P. Hildebrandt and M. Stockburger, Biochemistry 23 (1984) 5539.
15. W. Urban, in Frontiers of Laser Spectroscopy of Gases, (Ed. A. C. P. Alves et al. (Kluwer Academic Publishers, 1988) p. 9 ff.

Femtosecond Infrared Spectroscopy on Reaction Centers of *Rb. Sphaeroides*

Klaas Wynne, Gilad Haran, Gavin D. Reid, Chris C. Moser, Gilbert C. Walker, Sudipta Maiti, P. Leslie Dutton and Robin M. Hochstrasser

Department of Chemistry and Johnson Foundation, University of Pennsylvania, Philadelphia, PA19104-6323, USA

INTRODUCTION

In the past few years we have performed a series of experiments that employ infrared (IR) light to probe the dynamics of the photosynthetic bacterial reaction center (RC) on an ultrafast timescale. The reasons these studies were undertaken are twofold: First studies in the mid- and far-IR can reveal the dynamics of vibrational modes, both on cofactors as well as in the protein, responding to the electron transfer reactions. In the second place near- and mid-IR pulses can probe transient absorption and emission changes due to the transient population of electronic states of the cofactors. In addition, since the visible transient absorption spectrum is congested, new states or transients may be observed by studying the near-IR.

In this paper we will present some of the theory of ultrafast visible-pump IR-probe spectroscopy, outlining the differences between using a continuous-wave (CW) IR probe in combination with a short visible gate pulse versus using an ultrashort IR probe pulse. This theory is employed to understand recent experimental studies on the RC in the range 1700-2000 cm^{-1}. A brief description will be given of our efforts to generate femtosecond tunable pulses in the near- and mid-IR. Finally two sets of experiments on electronic states of the RC will be discussed: an investigation of energy transfer from the accessory bacteriochlorophyll (B) to the special pair (P) and observations of low lying electronically excited states of the special pair.

VISIBLE-PUMP / IR-PROBE SPECTROSCOPY

Two approaches are currently in use for visible-pump IR-probe spectroscopy: CW probing and pulsed probing. In both cases a sample is excited with an ultrashort visible pulse. In CW-probing the transient changes in sample absorbance are probed by a CW IR field and the transients are recorded on top of the CW IR beam. These transients on top of the CW beam can be read out by sending this beam with a visible gate pulse of variable delay into a nonlinear upconversion crystal and detecting the generated sum-frequency radiation. In pulsed-probing a short IR pulse detects the change of sample absorbance and either the total probe transmission is registered or the probe-pulse is sent into a monochromator to select a frequency band of the probe spectrum to be detected [1].

Electronic transitions in condensed phases typically have absorption bands with a full width at half maximum (FWHM) of 100-1000 cm^{-1} and therefore a corresponding dephasing time

of $T_2 = 2 - 100$ fs. Vibrational transitions, on the other hand, have absorption bands with a FWHM of 5-20 cm^{-1} and therefore a dephasing time of $T_2 > 0.5$ ps. Since the time resolution in current visible-pump IR-probe experiments is on the order of 40-400 fs, coherent transients will occur at short delay times. Since these coherent transients appear on a time scale that may be similar to the kinetics of the studied system, they have to be fully understood in order to extract the dynamics from the data. Here we will give a very brief summary of our theoretical results [1] regarding coherent transients in the IR. In the case that the IR-probe monitors the transient bleaching of a ground state absorption, the bleaching signal will rise instantaneously if it is probed by a CW-probe. However, if a pulsed probe is used, the bleaching signal will rise with the dephasing time of the ground state vibrational transition. If the IR-probe monitors a transient absorption (for example a vibrational mode that has a changed frequency or an enhanced transition strength in an excited electronic state) the signal will rise instantaneously if a pulsed IR-probe is used whereas the signal with a CW-probe will rise with the dephasing time of the excited-state vibrational transition. A much more detailed description of the theory of visible-pump IR-probe spectroscopy is given in Ref. 1.

FEMTOSECOND EXPERIMENTS ON VIBRATIONAL TRANSITIONS IN THE RC

Our experiments in the range 1700-2000 cm^{-1} were published last year [2], therefore we will only give a brief summary of the main results. Samples of *Rb. Sphaeroides R-26* were excited at 870 nm by a Ti:sapphire based regenerative amplification system, using pulses of ~200 nJ and a width of approximately 350 fs. The transient absorbance changes were monitored by the output of a CW CO-laser which was upconverted after the sample in a $AgGaS_2$ crystal by an 870 nm gate pulse. An overall increase of absorbance after excitation was noted in the range of IR frequencies used; There is no sign of large scale protein relaxation in the signals, that is, all the IR transients follow the well known electron transfer kinetics (3 ps or 200 ps); There may be a small signal due to protein relaxation at 1665 cm^{-1} possibly due to a Stark effect enhanced transition strength of amide I carbonyls; Anisotropy measurements indicate that a transient absorption at 1702 cm^{-1} is due to P_M^+; It seems that the excited state surface of P^* is very similar to surface of P. At 1682 cm^{-1} a transient bleaching is observed that shows a slow (3 ps) and not an instantaneous rise as expected (see above). This will occur if the 9-keto C=O vibrations are very similar in P and P^* (frequency shifted by less than the linewidth of ~9 cm^{-1}) and the bleach at 1682 cm^{-1} only develops after P^* decays into P^+H^- or P^+B^-. There may be a signal due to the formation of the intermediate state P^+B^-. The data at 1665 cm^{-1} shows a rise of the absorbance consistent with the formation of P^+B^-. However, given the current signal-to-noise ratio in the experiment, the transient is equally consistent with a model involving only P^*. Future studies that carefully compare the signals with CW- and pulsed-probing can be expected to resolve this issue.

RECENT DEVELOPMENTS IN THE GENERATION OF ULTRASHORT IR PULSES

After developing new ultrashort pulse, dispersion compensated, Ti:sapphire regenerative amplifiers [3], these new light sources were employed to generate tunable femtosecond pulses in the near- and mid-IR through parametric generation and amplification. In a scheme similar to that

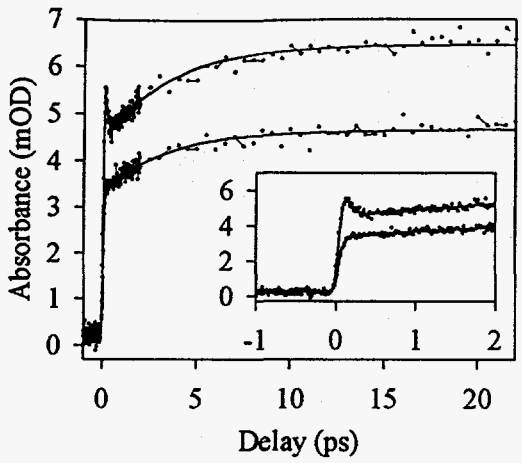

Figure 1. *Transient absorption signal observed at 1.2 μm after pumping RCs of* Rb. Sphaeroides R-26 *at 800 nm*

published recently [4] the nonlinear material BBO was used to generate pulses tunable from 1.2 to 2.4 μm with a pulse width ranging from 48 to 120 fs. KTP was used to improve the tuning range to 1 to 4.3 μm with a pulse width on the order of 100 fs. GaSe crystals are now being used successfully to extend the tuning range into the mid-IR (5-20 μm).

ELECTRONIC TRANSITIONS

The ultrashort near-IR pulses generated through parametric processes were employed to study various electronic transitions in the RC [5]. The bands due to the electronic transitions are wide, have correspondingly short dephasing times and therefore coherent effects at short delay times will be absent. Below results will be presented on energy transfer from B^* to P^* and on the observation of excited electronic states of P^* and P^+H^-.

Results Pumping the Reaction Center at 800 nm

In the following experiments samples of the RC of *Rb. Sphaeroides R-26* are excited at 800 nm with 100 nJ pulses and therefore it may be expected that Förster energy transfer from excited B to the special pair takes place. The experiments are done with two different Ti:sapphire regenerative amplifier laser systems, both with approximately 30-40 fs time resolution and employing BBO and KTP parametric devices, respectively, for generating IR. Also white light continuum generation in sapphire is used to create near-IR pulses. Initial experiments at 1.2 μm (see ***Figure 1***) show a rise of P^+H^- transient absorption as seen previously in experiments where the RC sample was excited at 610 nm [6]. In addition a fast transient is observable at short times that decays with 120 fs. In monomeric bacteriochlorophyll-a in acetone solution one can observe a transient absorption at 1.2 μm as well which, however, decays on a nanosecond timescale. The transient in the RC thus appears to reflect the rate of energy transfer from B* to P*. Also the rise of the stimulated emission from P^* at 950 nm was measured (see ***Figure 2***); the rise is single exponential and has a characteristic time of 120 fs.

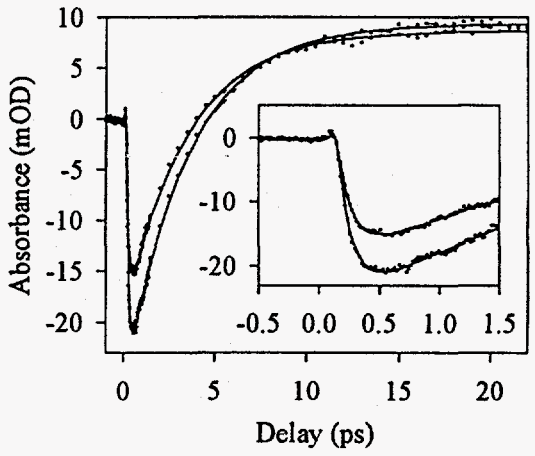

Figure 2. *Transient gain observed at 950 nm. The inset shows the same signal at short delay times.*

The fast 120 fs decay observed at 1.2 μm could be energy transfer or "internal

conversion" from B^* to P^* or electron transfer from B^* to P^+B^- or from B^* to B^+H^-. There are several reasons to assign this transient to relaxation from B^* to P^*. First of all the rise of the gain signal at 950 nm is on an identical time scale as the decay observed at 1.2 μm. Furthermore a rise of the P^+H^- signal with the "regular" 3.4 ps is observed and a signal from P* is observed at 950 nm that decays with 3.4 ps. There are reasons, however, to expect that P^* and B^* are strongly mixed. For example it can be calculated that the theoretical Förster energy transfer time can be as fast as 25 fs. It is therefore possible that the 120 fs decay is due to an internal conversion process rather than Förster-like energy transfer. These issues will be discussed in more detail in a forthcoming publication [7].

Electronic Transitions in P^*

The RC has approximate C_2 symmetry which allows one to construct stationary states and estimate transition dipoles. Calculations of the excited state (P^*) absorption were performed, based on the electronic structure calculations of Warshel and Fischer [8-10] and as described before in Ref. 11 Essentially excitonic states are constructed from individual chlorophyll excitations as: $|P_Y^{+/-}\rangle \approx |P_M^*P_L\rangle \pm |P_MP_L^*\rangle$ and charge resonance states as: $|CT^{+/-}\rangle \approx |P_M^+P_L^-\rangle \pm |P_M^-P_L^+\rangle$. The actual mixing coefficients are obtained from the electronic structure calculations. Using the experimental transition and permanent dipole moments of bacteriochlorophyll-a, it is predicted that transitions from P_Y^- to higher lying states that have mainly $CT^{+/-}$ character, should be observed in the near-IR.

The experiments were performed with the same ultrafast laser setups and on the same type of RC samples as described in the preceding section. In the region 1.4-2.2 μm an instrument limited rise is followed by a decay with 3.4 ps to a constant background. The constant background can be assigned to absorption from P^+H^- on the basis of a previous study of the RCs of *Rb. Sphaeroides* [12]. Around 4 μm another band due to P^* can be observed; The long time signal is due to the 2600 cm^{-1} band of P^+H^- (hole exchange transition). The first P^* band is centered at 5000 cm^{-1} with a transition dipole moment of approximately 8 D. The second band is centered at 2400 cm^{-1} with a transition dipole moment of 6 D (See ***Figure 3***). The latter band can be assigned to the $P_Y^+ \leftarrow P_Y^-$ transition based on anisotropy measurements.

The result that the $P_Y^+ \leftarrow P_Y^-$ transition is at 2400 cm^{-1} may appear inconsistent with previous hole burning results [13] which indicate that the $P_Y^+ \leftarrow P_Y^-$ transition is at 1300 cm^{-1}. It should be noted, however, that the electronic absorption may extend *further into the IR* and that the band observed at 2400 cm^{-1} may be a Herzberg-Teller transition based on a vibration of ca. 1100 cm^{-1}. Although the transition from the ground state to P_Y^+ may have a strong 0-0 component, the $P_Y^+ \leftarrow P_Y^-$ transition may have a weak origin due to both the frequency dependence of the absorption coefficient and that it may be mainly vibrationally induced.

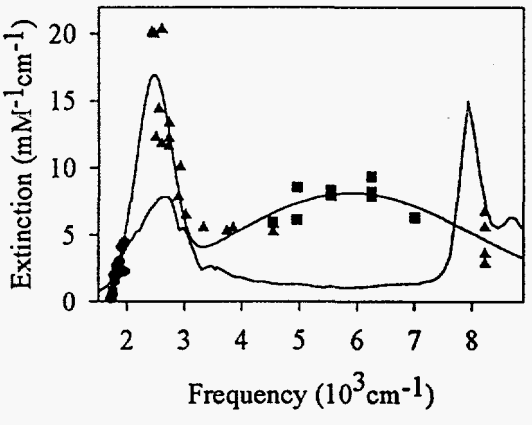

Figure 3. *Spectrum of the transient absorption from P^* and P^+H^- observed in the RC.*

CONCLUSIONS

In summary, ultrafast vibrational and electronic spectroscopy has been performed on the RC and energy transfer from B^* to P^*, or internal conversion between states of similar origin, was measured to occur in 120 fs. In addition new excited electronic states of the accessory bacteriochlorophyll and the special pair have been observed. A summary of the excited electronic states that have been observed in our experiments is shown in ***Figure 4***.

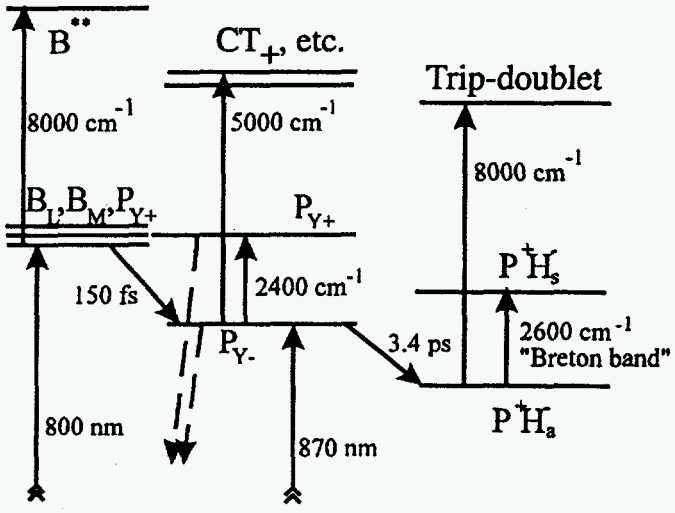

Figure 4. *Level scheme for the RC*

Acknowledgment

This research was supported by grants from the NSF and NIH.

References

1 K. Wynne, R.M. Hochstrasser, Chem. Phys. **193** (1995) 211-236.

2 S. Maiti, G.C. Walker, B.R. Cowen, R. Pippenger, C.C. Moser, P.L. Dutton, R.M. Hochstrasser, Proc. Natl. Acad. Sci. USA **91** (1994) 10360-10364.

3 K. Wynne, G.D. Reid, R.M. Hochstrasser, Opt. Lett. **19** (1994) 895-897.

4 V.V. Yakovlev, B. Kohler, K.R. Wilson, Opt. Lett. **19** (1994) 2000-2002.

5 G.C. Walker, S. Maiti, G.D. Reid, K. Wynne, C.C. Moser, R.S. Pippenger, B.R. Cowen, P.L. Dutton, R.M. Hochstrasser, in *Ultrafast Phenomena IX*, Eds. P.F. Barbara, W.H. Knox, G.A. Mourou, A.H. Zewail (Springer, Berlin, 1994), pp.439-440.

6 N.W. Woodbury , M. Becker, D. Middendorf, W.W. Parson, Biochemistry **24** (1985) 7516-7521.

7 G. Haran, K. Wynne, C.C. Moser, P.L. Dutton, R.M. Hochstrasser, in preparation.

8 W.W. Parson, A. Warshel, J. Am. Chem. Soc. **109** (1987) 6152-6163.

9 P.O.J. Scherer, S.F. Fischer, Chem. Phys. **131** (1989) 115-127.

10 P.O.J. Scherer, S.F. Fischer, in: *Chlorophylls*, Ed. H. Scheer, (CRC Press, Boca Raton, 1991).

11 G.C. Walker, S. Maiti, B.R. Cowen, C.C. Moser, P.L. Dutton, R.M. Hochstrasser, J. Phys. Chem. **98** (1994) 5778-5783.

12 J. Breton, E. Nabedryk, W.W. Parson, Biochem. **31** (1992) 7503-7510.

13 D. Tang, S.G. Johnson, R. Jankowiak, J.M. Hayes, G.J. Small, D.M. Tiede, Jerusalem Symp. Quantum Chem. and Biochem. **22** (1990) 99-120.

Four-Wave Mixing with Noisy Light: Classification by Time Correlators

D. Ulness and A. C. Albrecht
Department of Chemistry, Cornell University, Ithaca, New York

In a pioneering paper Morita and Yajima in 1983 [1] discussed how the inherently short auto-correlation time, τ_c, of noisy light can lead to femtosecond-scale time resolution using nanosecond scale light pulses. Several groups have since pursued this interesting subject in the context of 4WM spectroscopies - details can be found in the most recent work from the laboratories of Hartmann [2a], Kobayashi [2b], Apanesevich [2c], Lau [2d], Myers [2e], and our own [2f]. The usual theory of a given cw spectroscopy must be suitably averaged over the phase and amplitude noise of the light [1]. Typically a noisy source (such as a commercial Nd:YAG pumped dye laser with grating at zeroth order) is split into identical twin beams we call 2 and 2' which enter a Michaelson interferometer that delays beam 2' by a delay, τ over 2. Two general classes of nearly degenerate incoherent (I) 4WM experiments are encountered in which the phase matching condition produces a uniquely directed signal field (the fourth field). In the simplest experiment the twin noisy beams are assigned unique k-vectors, $\vec{k}_2$ and $\vec{k}_{2'}$ and supply the three fields needed to generate the signal field along $\vec{k}_s = 2\vec{k}_2 - \vec{k}_{2'}$ (or $\vec{k}_s = 2\vec{k}_{2'} - \vec{k}_2$) - the field from one beam acting twice and *with the same phase*. The new fourth wave derived from the *out-of-phase* action of fields from <u>one</u> of the beams is best seen in a "box" configuration where beam 2, say, is split and assigned two k-vectors, $\vec{k}_2$ and $\vec{k}_2'$, to produce a new signal along $\vec{k}_s = \vec{k}_2 - \vec{k}_2' + \vec{k}_{2'}$. We nickname these as *two-beam* $I^{(3)}$4WM and *three-beam* $I^{(3)}$4WM respectively (though the latter includes the former), the noisy (incoherent) fields acting three times in each case. The second major class of nearly degenerate "I"4WM spectroscopies is $I^{(2)}$4WM in which the noisy fields only act twice, being joined by a third field, field 1 (possibly of a different color), from a "monochromatic" source that has zero cross correlation with the noisy source. Naturally in a "box" configuration, ($\vec{k}_2 \neq \vec{k}_{2'} \neq \vec{k}_1$) one encounters two subclasses - one where the twin noisy fields act *in-phase* ($\vec{k}_s = \vec{k}_2 + \vec{k}_{2'} - \vec{k}_1$), one where they act *out-of-phase* ($\vec{k}_s = \vec{k}_2 - \vec{k}_{2'} + \vec{k}_1$).

In any configuration ultrafast dynamic properties of the material can be probed (though on an accumulated basis) and in the conventional Bloch two-level language (vibrational or electronic) one can acquire the dephasing time, the lifetime, and even the inhomogeneity, just as one does in true real-time femtosecond experiments. The important distinction is that in real-time studies that

are free of accumulation effects (spectral diffusion being one), one can dissect chromophore-bath interactions with particular ("non-exponential") insight. On the other hand, spectrally resolved *in-phase* $I^{(2)}$4WM has been found to yield a new class of damped Rabi detuning oscillations (RDO) which represent a highly precise down-conversion of the Bohr frequency of the two-level system damped by the dephasing rate constant. Furthermore a new dephasing induced extra resonance is seen exactly at the zero of the RDO. It is induced only by the nonzero slit-width of the monochromator. Bandwidth due to the chromophore/bath coupling (material dephasing) is completely suppressed [2f].

Other striking general properties of the I4WM spectroscopies have appeared which are directly tied to the nature of the time correlators involved when averaging over the phase and amplitude noise of the incoherent light. The signal field is normally quadrature detected. This means that the signal is derived from the modulus squared of the sum of chromophore-derived fourth fields at the detector. The cross terms fully dominate so that the quadrature signal is drawn from fourth fields derived from two separate chromophores (summed over all pairs). This is called the "bichromophore" model. We assign field intervention times t_1, t_2, t_3, to produce the polarization (and fourth wave) on one chromophore and intervention times s_1, s_2, s_3, to produce the (*conjugate*) polarization (and the *conjugate* fourth wave) on the other chromophore (of any pair). In general if noisy fields are involved at every one of the six steps (as in $I^{(3)}$4WM) the noise average produces a six-point time correlator of the complex envelope function, p, of the noisy light. With complex circular Gaussian statistics and the consequent moment theorem, the six-point correlator breaks into a sum of six distinct terms each being a product of three pair correlators. Any pair correlator requires that the envelope function (p) at one time be paired with its conjugate (p*) at the other. This implies that pair correlators only survive across times when two noisy fields act *conjugately* - namely *out-of-phase*. Otherwise a given pair correlator would vanish. Any one such triplet of pair correlators can be summarized in diagrammatic form. For example consider the *τ-dependent* triplet correlator :

$$<p^*(t_2-\tau)p(t_1)><p^*(s_2)p(s_1-\tau)><p^*(s_3)p(t_3)>\rightarrow$$

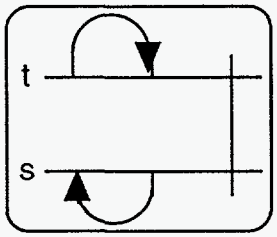

and, next, the *τ-independent* triplet correlator (time increases left-to-right):

$$<p^*(t_2-\tau)p(s_1-\tau)><p^*(s_2)p(t_1)><p^*(s_3)p(t_3)>\rightarrow$$

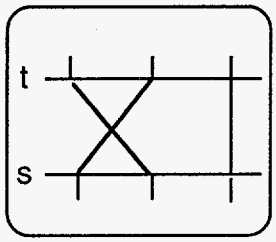

The lines (or arrows) connect the time intervals of the pair correlators. Whenever a given time interval is τ-dependent an arrow-head appears, and points to field 2'.

Consider the electronic two-level problem, lifetime, T_1, dephasing time, T_2 where only the *two* triply resonant Liouville pathways (D_1 and D_2 on the t-line) are included in the polarization. In the *two-beam* $I^{(3)}$4WM four six point correlators appear as a result of the noise average (< >): $I \equiv <D_1\ D_1^*>$, $II \equiv <D_1\ D_2^*>$, $III \equiv <D_2\ D_1^*>$, and $IV \equiv <D_2\ D_2^*>$ each leading to 6 triplets of pair correlators (24 total). (The *three-beam* $I^{(3)}$4WM will have 96 triplets). Analytic results have been obtained for the 16 τ-dependent ("arrowed") diagrams (see Fig. 1) of the 24. Here some qualitative insight into any correlator diagram, analytically justified elsewhere [3], is summarized. Thus the 8 τ-*independent* diagrams (of the 24) - not shown in Fig. 1 - are "lined" and contain only *inter-chromophore* pair correlators, just as in the second diagram above. This forces a tight synchronization of the three events on the t-line and on the s-line which greatly weakens the signal. The arrowed diagram above - and all 16 in Fig. 1(a) - contain two *intra-chromophore* pair correlators (arrows) and only one *inter-chromophore* pair correlator (line). These generally represent a 'very' strong contribution to the *two-beam* $I^{(3)}$4WM - though with a range of strength. In general each time the *inter-chromophore* line touches t_1, or s_1, or is embraced by an arrow, there is a weakening of the signal. Of these features Group B has none, Groups A and D have one, and Group C has two. The greater T_1 is than T_2, the stronger is the signal (principally from B - see Table) and the greater the distinction by group. Roughly speaking the weak onesided C-decay measures T_1, the strong B-decay measures T_2. Furthermore since all "arrowed" diagrams vanish for $\tau \rightarrow \infty$, and become purely "lined" diagrams at $\tau = 0$, one can comment about the "peak-to-background" ratio in <u>some</u> of the I4WM spectroscopies. For *in-phase* $I^{(2)}$4WM the lined diagrams derived from the arrowed ones at $\tau = 0$ match <u>one-to-one</u> those of the τ-independent diagrams (background terms). A 2:1 ratio is thus predicted (and observed). (In *three-beam* $I^{(3)}$4WM we predict a (nearly) 4:1 ratio.) In *two-beam* $I^{(3)}$4WM and *out-of-phase* $I^{(2)}$4WM no such simple reduction appears. Instead the "peak-to-background" contrast can become very large, going approximately as T_1/T_2.

(a)

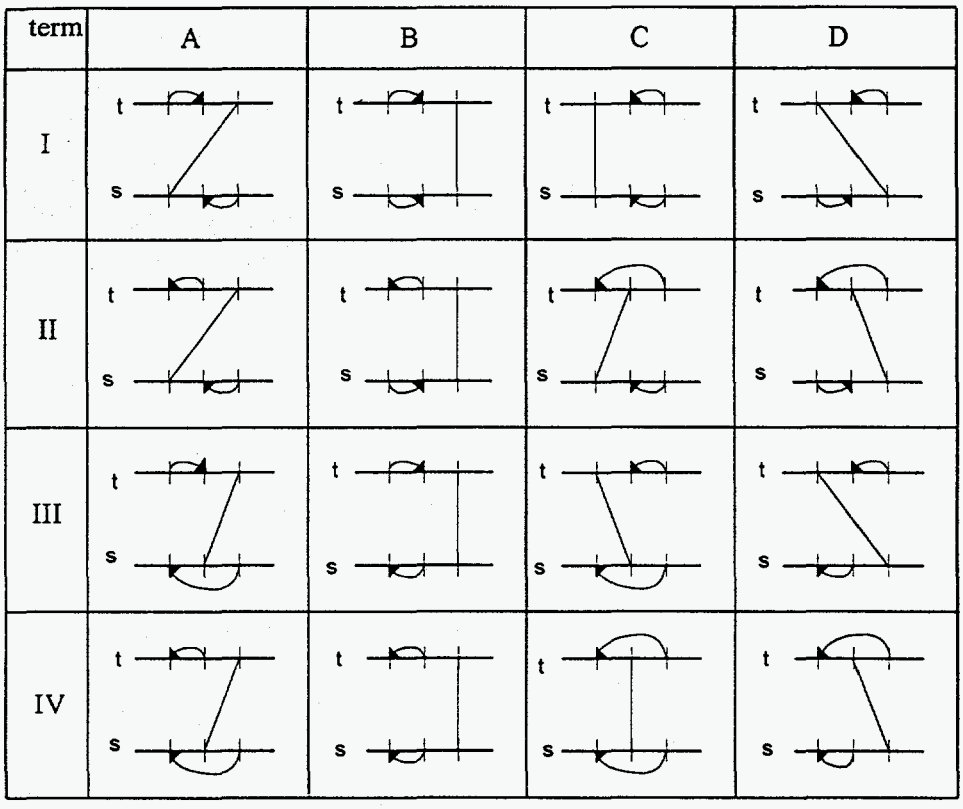

(b)

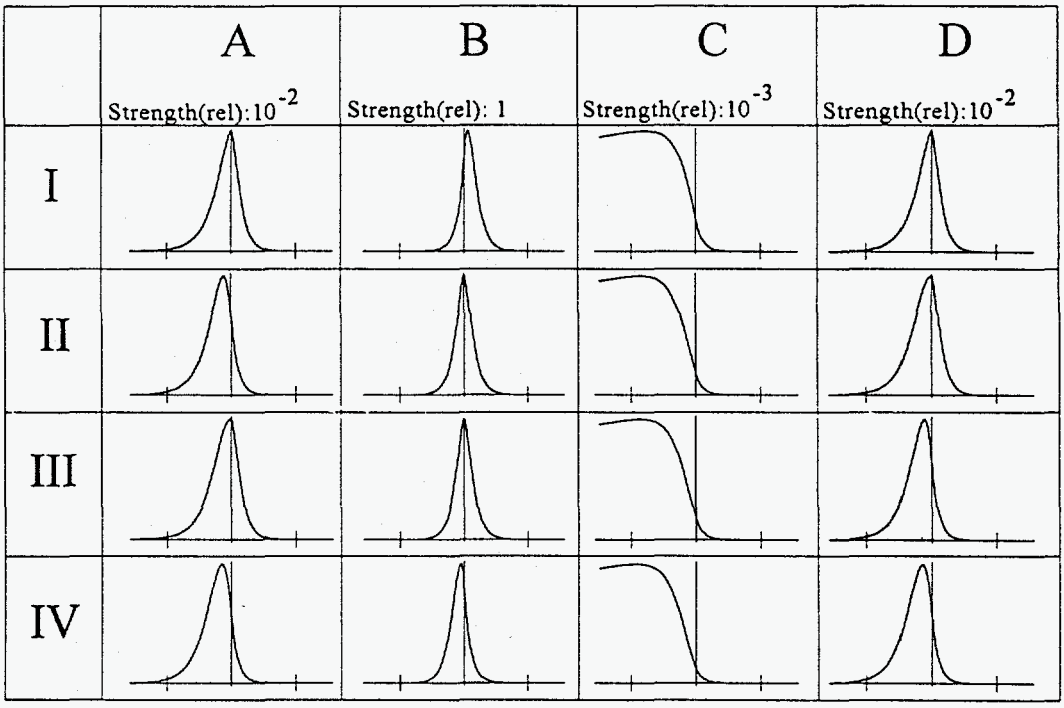

Fig.1:The sixteen τ-dependent triplets of pair correlators in two-beam $I^{(3)}4WM$ grouped (A,B,C,D) by relative strength. (a) the correlator diagrams; (b) the corresponding analytic results with peak strength (rel); abscissa: tick marks at $\tau = \pm$ 500 fs. Parameters in row 2 of Table.

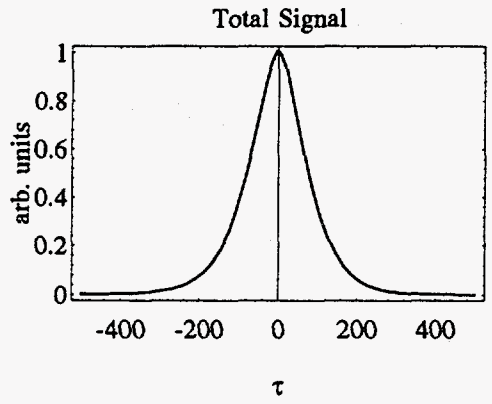

Fig. 2: Total *two-beam* $I^{(3)}$4WM signal (rel) - the sum of the sixteen signal components shown in Fig. 1(a). τ in fs.

Table: $I^{(3)}$4WM signal strength (rel) for several material and light parameters.

τ_c (fs)	T_2 (fs)	T_1 (ps)	A	B	C	D
100	300	10	1	10^2	10^{-1}	1
100	50	10	10^{-2}	1	10^{-3}	10^{-2}
100	1	10	10^{-9}	10^{-7}	10^{-10}	10^{-9}
1	200	0.6	10^{-7}	10^{-7}	10^{-7}	10^{-7}
1	200	10^4	10^{-2}	10^2	10^{-7}	10^{-2}

In general the total signal dramatically decreases with decreasing dephasing time (compare rows 1 to 3) and decreasing lifetime (compare row 5 to row 4). Furthermore the triplet correlators of Group B dominate (except for the shortest T_1 - row 4) - dramatically so with increasing lifetime (compare especially row 4 to row 5).

Acknowledgements

Support under NSF Grant CHE-9311959 is gratefully acknowledged.

References

1. N. Morita and T. Yajima, Phys. Rev A, 30 (1983) 2525.

2. a) Y. Zhang, F. Moshary, and S. R. Hartmann, in press. b) T. Kobayashi, Adv. in Chem. Phys., LXXXV (1994) 55. c) P. A. Apanesevich, V. P. Kozich, A. I. Vodschitz, and B. L. Kontsevoy, Springer Proceedings in Physics V63, Eds. G. Marowsky and V. V. Smirnov (Springer: Berlin, 1992) 148. d) A. Kummrow, S. Woggon and A. Lau, Phys. Rev. A, 50 (1994) 4264. e) T.-S. Yang, R. Zhang, and A. B. Myers, J. Chem. Phys., 100 (1994) 8573. f) A. C. Albrecht, S. P. Smith, D. Tan, S. A. Schaertel, and D. DeMott, Laser Physics, 5 (1995) 1.

3. D. Ulness and A. C. Albrecht, to be published.

Theory of Vibrational Echo Phenomena in Harmonic and Weakly Anharmonic Oscillators

John T. Fourkas

Eugene F. Merkert Chemistry Center, Boston College, Chestnut Hill, MA 02167

INTRODUCTION

Understanding the dynamics of molecular vibrations in liquids is a problem of long-standing interest. Time-resolved nonlinear spectroscopies have been particularly useful in this regard, especially techniques such as Coherent Anti-Stokes Raman Scattering (CARS) for intramolecular modes [1] and the optical Kerr effect (OKE) for intermolecular modes [2]. Both of these spectroscopies are formally nonlinear in the vibrational mode of interest [3], and therefore cannot readily distinguish between homogeneous and inhomogeneous broadening of vibrational lines. With recent advances both in ultrafast laser technology [4] and in experimental techniques [5, 6, 7], it has become possible to perform experiments that are vibrationally nonlinear, and can therefore provide important new insights into vibrational dynamics.

Ultrafast laser pulses can have a bandwidth that is on the order of the anharmonicity of many molecular vibrational modes. When this is the case, wave-mixing pathways among excited vibrational states can contribute to the signal in nonlinear-optical techniques such as the photon echo (PE) [8]. Furthermore, the excited states of low-frequency vibrational modes can have appreciable equilibrium populations at room temperature. These two phenomena can combine to produce nonlinear-optical signals that are dramatically different from those observed from electronic transitions (which can often be modelled as two-level systems). Here we investigate theoretically the PE behavior of harmonic and weakly anharmonic oscillators for which $\hbar\omega \gg k_B T$. We show that quantum interferences due to wave-mixing pathways that involve transitions between excited vibrational states strongly influence the photon echo signal, and can provide a considerable amount of information about vibrational dynamics in liquids.

THEORY

In a PE experiment, a resonant ultrafast laser pulse of wave vector $\mathbf{k}_1$ creates vibrational coherences between oscillator energy levels $|0\rangle$ and $|1\rangle$ that evolve at frequency $\omega_{10} = (E_1 - E_0)\hbar$. The molecular coherences dephase due to population relaxation, pure dephasing, spectral diffusion, and any inhomogeneity in the distribution of vibrational frequencies $G(\omega)$. Time τ later, a second resonant laser pulse with wave vector $\mathbf{k}_2$ is applied. This pulse acts reverses the phase of the coherent superposition of each molecule (i.e., the coherences now evolve at frequency ω_{01}). The effects of inhomogeneity thus disappear at time τ after the second pulse, and the molecules coherently radiate a signal with wave vector $2\mathbf{k}_2 - \mathbf{k}_1$. The dependence of the signal on τ gives direct information about the rates of the various

other dephasing mechanisms.

We treat the vibrational PE using semiclassical perturbation theory [9], as described in detail elsewhere [10]. At lowest (third) order, pulse 1 interacts with the sample once and pulse 2 interacts twice. The contributions of each fully-resonant path through Liouville space are summed, and the resultant third-order polarization ($\mathcal{P}^{(3)}$) is multiplied by its complex conjugate and integrated over all possible interaction times. Since our goal is to examine the effects of excited vibrational states on the echo signal, we make several simplifying assumptions: the laser pulses are taken to be temporal delta functions with finite bandwidth and all dephasing is taken phenomenologically to be exponential.

There are two pathways through Liouville space that contribute to the signal in a two-level system (2LS) at positive delay times [11], representing the two possible orderings of the interactions of the second pulse. In a harmonic or weakly anharmonic oscillator, an extra pathway is available in which the second pulse creates a coherence between levels $|2\rangle$ and $|1\rangle$ instead of levels $|1\rangle$ and $|0\rangle$. The contribution of this pathway to $\mathcal{P}^{(3)}$ is of opposite sign to the contributions of the two normal pathways. Furthermore, due to the properties of the harmonic oscillator transition matrix elements, the magnitude of this term is equal to the sum of the magnitudes of the other two terms. This extra pathway thus creates the possibility of a complete destructive interference of the signal [6].

In a 2LS, there are no Liouville-space pathways that contribute to the signal at negative delay times, although there are two extra pathways that can contribute at zero delay time (leading to a "coherence spike"). The addition of the second excited state of the harmonic oscillator opens a third pathway at zero delay time, which again has the potential to completely cancel the 2LS terms. In addition, two non-echo-like pathways are available at negative delay times, in which pulse 2 creates a coherence between $|2\rangle$ and $|0\rangle$ and pulse 1 converts this to a coherence between $|1\rangle$ and $|0\rangle$. As we shall show, the contributions of these pathways are strongly influenced by the degree of inhomogeneous broadening.

THE HARMONIC OSCILLATOR

In the limit of broad inhomogeneity, the extra pathways at negative and zero delay times contribute negligibly to the signal. In this case a simple analytic expression is found for the signal $S(\tau)$:

$$S(\tau) \propto \exp\left(-2\Gamma_{10}\tau\right)\left[\exp\left(-\Gamma_{10}\tau\right) - \exp\left(-\Gamma_{21}\tau\right)\right]^2 \ , \qquad (1)$$

where Γ_{10} is the dephasing rate between $|1\rangle$ and $|0\rangle$ and Γ_{21} is the rate between $|2\rangle$ and $|1\rangle$. If $\Gamma_{10} = \Gamma_{21}$, the cancellation among the pathways through Liouville space is complete at all times, and there is no signal. Generally $\Gamma_{10} \neq \Gamma_{21}$, in which case the signal predicted in this equation is strikingly different from that of a 2LS. The signal is zero at $\tau = 0$, then builds in with a time constant characteristic of the faster of the two dephasing times and decays with a time constant characteristic of the slower of the dephasing times. The echo thus provides direct information about the dynamics of the lowest three quantum states of the vibrational mode.

The echo signal is exceptionally sensitive to the degree of inhomogeneity in the vibrational line shape. To illustrate this, Fig. 1 shows a series of echo decays with varying amounts of inhomogeneous broadening (where $G(\omega)$ is assumed to be a normalized Gaussian centered about frequency ω_o and with a standard deviation σ, conditions for which an analytic expression for the signal can be obtained). The signal has been calculated for positive and

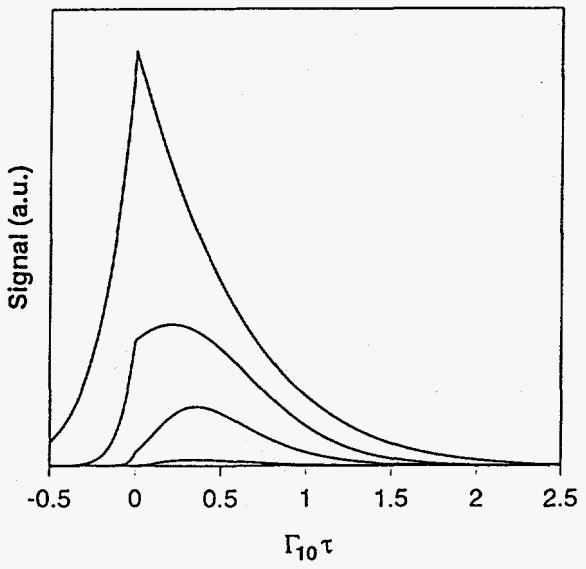

Figure 1: Harmonic oscillator echo signal. $\Gamma_{21} = 3\Gamma_{10}$ for all plots. From top to bottom: $\sigma/\Gamma_{10} = 0.6,\ 2,\ 6,\ 60.$

negative delay times, but the $\tau = 0$ spike, which is large for small σ, has been suppressed for clarity.

Several effects are obvious in these echo decays. First, since the oscillators remain in phase longer when there is less inhomogeneity, the signal strength increases. Second, the shape of the decay changes greatly with the inhomogeneity. For broad inhomogeneity, the behavior of Eq. 1 is reproduced. With decreasing inhomogeneity, signal appears at zero and negative delay times. The smooth peak of the signal moves to shorter delay times, eventually becoming a sharp peak centered at zero delay time in the limit of narrow inhomogeneity. In this limit, the echo decay becomes as asymmetric double-sided exponentially, with the faster time constant at negative delay times.

THE WEAKLY ANHARMONIC OSCILLATOR

We now turn to the case of the weakly anharmonic oscillator. Levels $|1\rangle$ and $|2\rangle$ of the oscillator are assumed to by separated by energy $\hbar\omega_{21} = \hbar\omega_{10}(1-\Delta)$. The bandwidth of the laser is assumed to be great enough that both the $|0\rangle \rightarrow |1\rangle$ and $|1\rangle \rightarrow |2\rangle$ transitions are well within the pulse spectrum, but narrow enough that no transitions are driven in which the change in vibrational quantum number is greater than one. Both Δ and the width of the inhomogeneous distribution are assumed to be small enough that $\Delta\omega_{10}$ is much less than the inverse of the longest delay time for which signal is observed, such that $\Delta\omega_{10}$ can be taken to be independent of ω_{10}.

The same Liouville-space pathways apply to this system as applied to the harmonic oscillator. However, the positive-delay pathway that involves transitions between $|1\rangle$ and $|2\rangle$ evolves at frequency $\omega_{10}(1-\Delta)$ between the second laser pulse and the rephasing, whereas the other two pathways evolve at frequency ω_{10} during this period. As a result, these

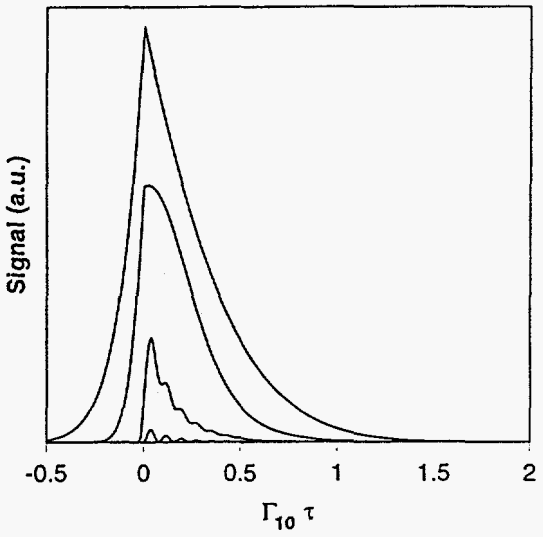

Figure 2: Anharmonic oscillator echo signal. $\Gamma_{21} = 3.5\Gamma_{10}$ and $\Delta\omega_{10} = 40\Gamma_{10}$ for all plots. From top to bottom: $\sigma/\Gamma_{10} = 1.2,\ 4,\ 28,\ 40$.

contributions to $\mathcal{P}^{(3)}$ beat with each other at frequency $\Delta\omega_{10}$, causing a large oscillation in the echo decay. This offers a direct experimental method for measuring the magnitude of the anharmonicity in the vibrational mode, as has recently been demonstrated [12]. In the limit of broad inhomogeneity, there is once again no signal at zero or negative delay times. The positive delay signal is given by the expression

$$S(\tau) \propto \exp\left(-4\Gamma_{10}\tau\right) - 2\exp\left[-\left(3\Gamma_{10} + \Gamma_{21}\right)\tau\right]\cos\left(\Delta\omega_{10}\tau\right) + \exp\left[-2\left(\Gamma_{10} + \Gamma_{21}\right)\tau\right] \ . \quad (2)$$

The signal does not go to zero at the minima of the oscillations. The envelope of the signal minima $S_{\min}(\tau)$ corresponds to Eq. 1. The envelope of the maxima of the oscillations is given by the relation

$$S_{\max}(\tau) \propto \exp\left(-2\Gamma_{10}\tau\right)\left[\exp\left(-\Gamma_{10}\tau\right) + \exp\left(-\Gamma_{21}\tau\right)\right]^2 \ . \quad (3)$$

The lower envelope of the decay thus has its maximum at the same delay time as the harmonic-oscillator echo signal, while the upper envelope of the decay decays monotonically, and its maximum is at the peak of the first beat (when $\tau = \pi/\Delta\omega_{10}$). These envelopes can be used directly to determine Γ_{10} and Γ_{21}.

As in the case of the harmonic oscillator, the anharmonic oscillator echo signal is strongly sensitive to the amount of inhomogeneity in the vibrational line shape. The anharmonic echo signal for different amounts of Gaussian inhomogeneous broadening is illustrated in Fig. 2, in which the $\tau = 0$ spikes have been suppressed. Once again, as the inhomogeneity is decreased signal appears at negative delay times. The depth of the oscillations is also highly dependent on the inhomogeneous broadening; interestingly, the beats *decrease* in amplitude as the inhomogeneity is decreased. This phenomenon is due to the fact that when the vibrational line has little inhomogeneous broadening, the oscillators can radiate immediately

following the second pulse, rather than having time to rephase and create the beats. The beats therefore disappear once the inhomogeneity is small enough that significant signal has appeared at negative delay times. The echo decay resembles the harmonic oscillator echo decay at small inhomogeneities, and has an identical small-inhomogeneity limit of an asymmetric, double-sided exponential.

CONCLUSIONS

We have performed a simple theoretical analysis of the photon echo signal in harmonic and weakly anharmonic oscillators. The similarity of the ground-state and excited-state absorption frequencies in these systems opens Liouville-space pathways that involved transitions between excited states of the oscillator. The new pathways can interfere destructively with the normal 2LS pathways, which can radically change the behavior of the echo signal. The degree of this interference, in conjunction with new mixing pathways that open at negative delay times, provides unique information on the magnitude of the anharmonicity in the vibrational mode, the dynamics of excited vibrational states, and the amount of inhomogeneity in the vibrational line shape. As the lasers and experimental techniques for performing these nonlinear experiments become more readily available, vibrational echoes will provide a wealth of new information about the dynamics of vibrations in liquids.

Acknowledgements

I thank the Camille and Henry Dreyfus Foundation for a New Faculty Award, and Keith Nelson, Hitoshi Kawashima and Mike Fayer for helpful conversations.

References

[1] D. D. Dlott, Ann. Rev. Phys. Chem., 37 (1986) 157.

[2] R. Righini, Science, 262 (1993) 1386.

[3] R. F. Loring and S. Mukamel, J. Chem. Phys.,83 (1985) 2116.

[4] D. Zimdars, A. Tokmakoff, S. Chen, S. R. Greenfield, M. D. Fayer, T. I. Smith and H. A. Schwettman, Phys. Rev. Lett., 70 (1993) 2718.

[5] D. Vanden Bout, L. Muller and M. Berg, Phys. Rev. Lett., 67 (1991) 3700.

[6] Y. Tanimura and S. Mukamel, J. Chem. Phys., 99 (1993) 9496.

[7] K. Tominaga and K. Yoshihara, Phys. Rev. Lett., 74 (1995) 3061.

[8] D. A. Wiersma, Adv. Chem. Phys., 47 (1981) 421; C. A. Walsh, M. Berg, L. R. Narasimhan, K. A. Littau and M. D. Fayer, Acc. Chem. Res., 20 (1987) 120.

[9] S. Mukamel and R. Loring, J. Opt. Soc. Amer. B, 3 (1986) 595.

[10] J. T. Fourkas, Laser Phys., in press; J. T. Fourkas, H. Kawashima and K. A. Nelson, J. Chem. Phys, submitted.

[11] Y. J. Yan and S. Mukanel, J. Chem. Phys., 94 (1991) 179.

[12] A. Tokmakoff, A. S. Kwok, R. S. Urdahl, R. S. Francis and M. D. Fayer, Chem. Phys. Lett., 234 (1995) 289.

ABSTRACTS FOR POSTERS
CHEMISTRY AND MATERIALS

Ultrafast Time-Resolved Infrared Spectroscopy of a Binuclear Rhenium Polypyridyl Complex

C.J. Arnold, R.B. Girling, K.C. Gordon†, R.E. Hester, J.N. Moore, R.N. Perutz, and T-Q. Ye

Chemistry Department, University of York, Heslington, York YO1 5DD, UK
†Chemistry Department, University of Otago, P.O. Box 56, Dunedin, New Zealand

Time-resolved infrared (TRIR) spectroscopy has been applied recently to the study of excited states in transition metal complexes [1] and nanosecond TRIR spectroscopy has been used successfully to study metal-to-ligand charge transfer (MLCT) states in several systems. These have included both monomeric and dimeric carbonyl complexes and, in the case of the dimeric tungsten system $[(OC)_5W(4,4'\text{-bipy})W(CO)_5]$, the long-lived excited state has been found to have an asymmetric electron distribution of the form $[(OC)_5W^{+1}(4,4'\text{-bipy}^{-1})W^0(CO)_5]$ [2].

In many cases, faster time resolution is required to observe excited states. In this study we have used ultrafast TRIR spectroscopy to probe a short-lived MLCT state of the related binuclear rhenium (I) complex $[Re(I)(CO)_3Cl]_2BL1$ for which the ground state structure is shown below as **1** [3], and thereby to investigate the structure and dynamics of the excited state on the picosecond timescale. Due to the intrinsic asymmetry of the polypyridyl ligand (BL1), the two rhenium atoms experience different environments, and hence it may be expected that the most stable form of the excited state will have an asymmetric (localised) charge distribution.

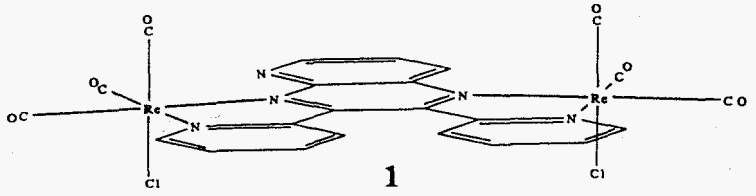

1

The TRIR experiments were performed using the amplified output (200 fs, 50 μJ, 1.05 kHz) of a dye laser operating at 605 nm. A portion of this output (10 μJ) was used to photolyse the sample, and the continuous wave output of either a CO or diode laser was used in conjunction with gated upconversion detection to obtain the TRIR data. The sample (c. 1.75×10^{-3} mol dm^{-3} in dichloromethane) was flowed through a 1 mm pathlength cell.

TRIR spectra of $[Re(CO)_3Cl]_2BL1$ obtained at several delay times after excitation into the MLCT absorption band are presented in Figure 1. The spectra show bleaching of the ground state υ(CO) bands at 1915, 1939 and 2024 cm^{-1}, and a kinetic study showed that these bleached bands recover on a timescale of 100 ps. In addition to the bleaching, photoinduced absorption is evident on both the high and low wavenumber sides of these ground state features. At early times the photoinduced absorption bands are broad, but kinetic studies showed that the bands sharpen up on a timescale of 4 ps and then decay with a lifetime of 100 ps.

The difference spectrum obtained at a time delay of 15 ps may be assigned to the MLCT state of

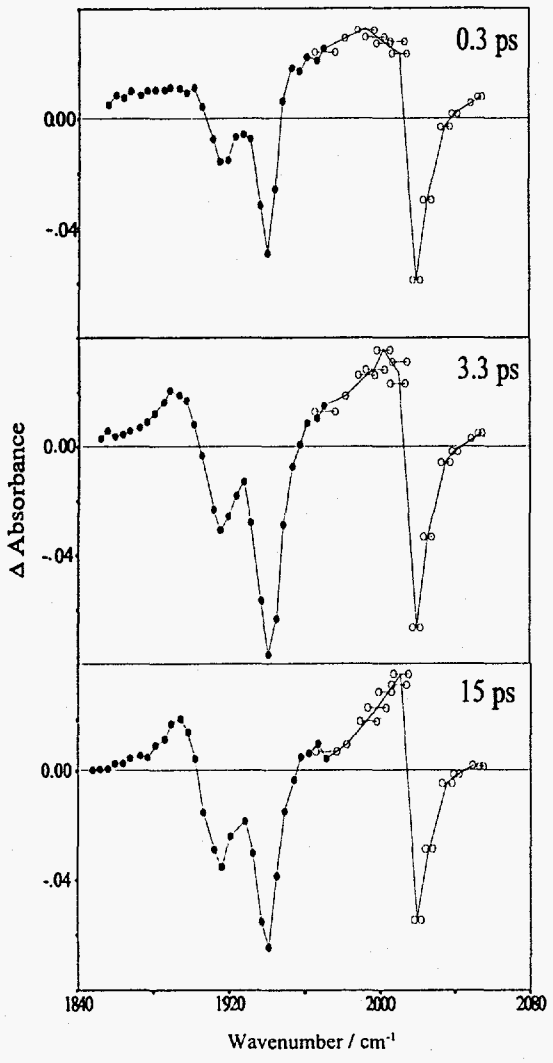

Figure 1: TRIR spectra of BL1 at several delay times after photolysis. (● CO laser data, ○ diode laser data)

1. The subtraction of a scaled ground state spectrum from this TRIR difference spectrum clearly revealed prominent positive bands at 1900, 1925 and 2012 cm^{-1} in the MLCT state, and further analysis using a band-fitting procedure indicated that additional positive features occur in the region 1960-2000 cm^{-1}.

The observation of υ(CO) bands in the spectrum of the MLCT state which are downshifted by 10-20 cm^{-1} from the respective ground state bands is indicative of the increased back-bonding present in a Re(I) centre attached to a reduced polypyridyl ligand; for comparison, the bands of the monomeric Re(I) complex $Re(CO)_3Cl(2, 2'\text{-bipy})$ are reported to show a downshift of c. 30 cm^{-1} on electrochemical reduction [4]. The MLCT state of **1** therefore appears to have the asymmetric form $[Cl(CO)_3Re(I)(BL1^-)Re(II)(CO)_3Cl]$ since a symmetric, delocalised form would be expected to result only in a small upshift of the ground state bands [2].

The υ(CO) bands of the Re(II) centre in this proposed structure would be expected to show an upshift from those of the ground state, and indeed an upshift of the ground state bands at 1915 and 1939 cm^{-1} may give rise to the weak positive features in the 1960-2000 cm^{-1} region of the band-fitted TRIR spectrum. Further TRIR studies in the range to 2100 cm^{-1} are planned to observe the positive feature expected in this region from the upshift of the ground state band at 2024 cm^{-1}.

Acknowledgements

We wish to thank the Engineering and Physical Science Research Council for Research Grant (GR/G41870) and Advanced Fellowship (JNM) support, and also Shell Research Ltd. for EPSRC CASE studentship support (CJA).

References

1. J.J. Turner, M.W. George, F.P.A. Johnson, J.R. Westwell, Coord. Chem. Rev. , 125, (1993) 101.
2. M.W. George, J.J. Turner, J.R. Westwell, J. Chem. Soc. Dalton Trans. (1994) 2217.
3. K. C. Gordon, T. J. Simpson,in Proc. XIV Internat. Conf. Raman Spectrosc. Ed. N-T Yu and X-Y Li (Wiley, 1994) 544.
4. M.W. George, F.P.A. Johnson, J.R. Westwell, P.M. Hodges, J.J. Turner, J. Chem. Soc. Dalton Trans. (1993) 2977.

Femtosecond IR Spectroscopic Study of the Mechanism of C-H Bond Activation by Organometallic Complexes

T. Lian, S. E. Bromberg, H. Yang, G. Proulox, R. G. Bergman, and C. B. Harris
Dept. of Chemistry, Univ. of California, Berkeley, CA 94720, USA

INTRODUCTION

Carbon-hydrogen bonds in alkanes are among the strongest single bonds known. The mechanism for the photochemical activation of C-H bond by transition metal centers has been intensively studied since its first discovery[1,2]. The mechanism for this type of reaction is commonly thought to be[3]

$$\begin{aligned} &CpM(CO)_2 + h\nu \rightarrow CpMCO + CO \\ &CpM(CO) + RH \rightarrow CpMCO(RH) \rightarrow CpMCO(H)(R) \end{aligned} \qquad (1)$$

where M=Ir, Rh, Cp=C_5H_5 or C_5Me_5. CpMCO(RH) is the postulated σ-complex and CpMCO(R)(H) is the final C-H bond activated product.

Although, the intermediate species have not been directly observed in room temperature alkane solutions due to the rapid rate of these reactions, time resolved IR and visible spectroscopic studies in the μs and slower time scale have identified some of the intermediate species involved in low temperature matrix, liquefied rare gases (Kr, Xe) and in the gas phase. Monocarbonyl CpM(CO) and its solvated form have been observed in gas phase[4] and in liquid Kr, Xe[5], while the σ complex intermediate CpMCO(RH) has yet to be detected. Recent femtosecond and picosecond time resolved studies of this system in room temperature alkane solution in the infrared[6] and visible[7], has found that >99% of the initial molecules return to the ground state in 40ps without losing a CO ligand, indicating a <1% yield for the reaction. because of this low quantum yield, the C-H activation reaction has not been observed.

In this paper, we report the first femtosecond time resolved IR spectroscopic study of the C-H bond activation reaction of (HB-Pz_3*)$Rh(CO)_2$ (Pz_3*=3,5-dimethylpyrazolyl) in room temperature n-pentane solution. The relatively high quantum yield for C-H activation[8] of this compound has enabled us to detect the transient intermediate species. A 30 Hz fs IR spectrometer with 200 fs time resolution and 4 cm^{-1} spectral resolution was used in this study, the details of which will be published elsewhere[9] Briefly, the sample is pumped by a UV pulse at 295nm and the subsequent change in the IR absorption is monitored as a function of time and wavelength.

RESULTS AND DISCUSSIONS

Shown in figure 1 are transient difference IR spectra of the sample at -10, 10, 66, and 200ps. Detailed kinetics of the spectral features are also measured up to 1ns. An instrument response limited bleach of the parent molecule symmetric CO stretching band at 2055cm^{-1} is observed which does not recover within 1 ns. The spectrum of the new absorption feature, with a single CO stretching band at ca.1981cm^{-1} that overlaps with the bleach of the parent molecule antisymmetric CO stretching band, narrows in 60 ps and shifts to the higher frequency side in 300 ps. No final C-H activated product, whose absorption centers at 2032 cm^{-1}, is observed within 1ns, although separate experiment with μs time resolution showed that its formation was complete within 1 μs.

We tentatively assign the new transient species to the pentane solvated monocarbonyl

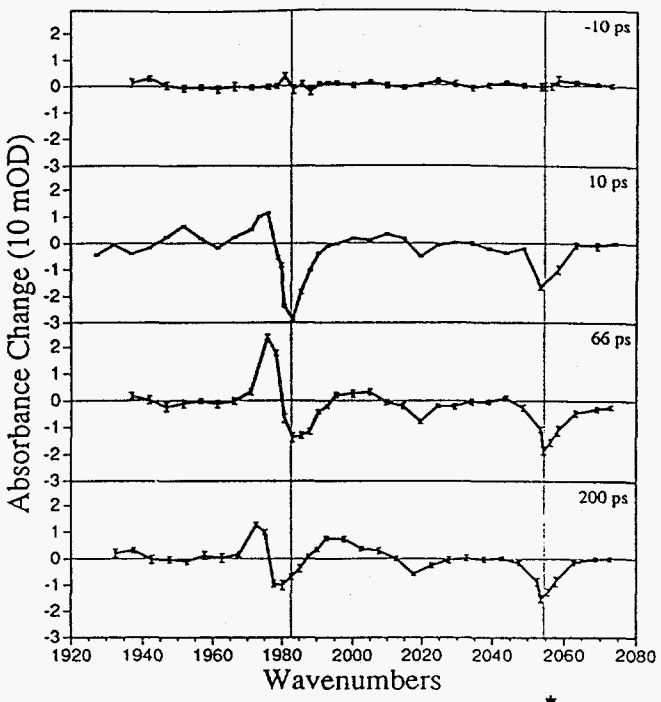

Fig. 1, transient difference IR spectra of [HB-Pz_3*$Rh(CO)_2$] in room temperature n-pentane after 295nm photolysis.

intermediate species (HB-Pz_3*)$Rh(CO)C_5H_{12}$ [A]. Upon absorbing a UV photon, one CO ligand is photodissociated leaving behind a monocarbonyl intermediate [A] that has a CO stretching band at ca. 1981cm^{-1}. The spectral narrowing in the 60 ps time scale is a result of vibrational cooling and initial solvation of the nascent species. In addition, the 300 ps blue shift of the spectrum is attributed to the rearrangement of the pentane molecule to form a more stable solvated complex such as the postulated σ-complex. C-H bond activation occurs between 1ns and 1μs, the barrier of which is estimated to be around 5.5 kcal to 9.7 kcal/mol..

Our experiment represents the first direct observation of the alkane complexed intermediate species[A] in room temperature solution. It demonstrates the ability of fs IR spectroscopy to time resolve the photodissociation, solvation and bond activation steps. Currently, the spectrum after 1ns is being measured to follow the actual C-H bond activation step. Measurements in other solvents are also planned to establish the relation between the properties of the solvents and the rates for both the solvent complex formation and C-H bond activation.

References:

1) A. H. Janowicz, R. G. Bergman, J. Am. Chem. Soc., 104 (1982), 352.
2) J. K. Hoyano, W. A. G. Graham, J. Am. Chem. Soc. , 104(1982), 3723.
3) R. G. Bergman, Science , 223 (1984) , 902.
4) E. P. Wasserman, C. B. Moore, R. G. Bergman, Science, 255 (1992), 315-318
5) B. H. Weiller, E. P. Wasserman, C. B. Moore, R. G. Bergman, J. Am. Chem. Soc., 115(1993), 4326; R. H. Schultz, A. A. Bengali, M. J. Tauber, B. H. Weiler, E. P. Wasserman, K. R. Kyle, C. B. Moore, R. G. Bergman, J. Am. Chem. Soc., 116(1994), 7369.
6) T. P. Dougherty, W. T. Grubbs, E. J. Heilweil, J. Phys. Chem., 98 (1994), 9396.
7) S. E. Bromberg, T. Lian, R. G. Bergman, C. B. Harris, Manuscript in preparation.
8) A. A. Purwoko, A. J. Lees, Inorg. Chem., 132 (1994), 155.
9) T. Lian, S. E. Bromberg, M. Asplund H. Yang and C. B. Harris, manuscript in preparation.

The Photochemistry of Dinuclear Organometallic Compounds: Ground State Resonance Raman and Time-Resolved Infrared Studies of $Mn_2(CO)_{10}$

Terry L. Gustafson, Holly B. Lavender, Marcello Vitale, Frank A. Kvietok, and Bruce E. Bursten
Department of Chemistry, The Ohio State University, 120 West 18th Avenue, Columbus, OH 43210

Tetsuro Yuzawa and Hiro-o Hamaguchi
Molecular Spectroscopy Laboratory, Kanagawa Academy of Science and Technology,
KSP East 301, 3-2-1 Sakato, Kawasaki 213, Japan

Transition metal organometallic complexes exhibit a rich and diverse photochemistry.[1-3] Interest in these complexes arises from their potential as tunable photocatalysts, as controllable photochemical reagents for small-molecule activation, as selective photosensors, and as energy acceptors in photochemical energy storage. However, a detailed understanding of the factors that control the photochemistry of transition metal organometallic complexes has not been achieved. Photochemical studies are consistent with two primary reaction pathways:[1] (1) homolysis into mononuclear radicals and (2) ligand loss to form unsaturated intermediates. Although the two pathways are known, the relative quantum yields for the two reactions depend upon several factors, including the system, the solvent, and the excitation wavelength.[1] The fundamental question we are trying to address is how does a specific electronic excited state configuration provide the appropriate structural distortion to facilitate a particular reaction?

In this work we have obtained the ground state resonance Raman spectra (from 263 to 647 nm) and the time-resolved infrared spectra at two different excitation wavelengths (262 nm and 349 nm) of a prototypical dinuclear organometallic compound, $Mn_2(CO)_{10}$ in cyclohexane. In Figure 1 we show the ground state and transient infrared spectra of $Mn_2(CO)_{10}$ in cyclohexane with 349 nm excitation. The time-resolved spectra are consistent with the presence of at least three photoproducts: the homolysis product, $\cdot Mn(CO)_5$, the primary ligand loss product, $Mn_2(CO)_9$, and a secondary ligand loss product, $Mn_2(CO)_8$.[3] In Figure 2 we compare the dynamics of the bands at 1760 cm^{-1} and 1940 cm^{-1}. The 1760 cm^{-1} band is characteristic of the bridging CO in $Mn_2(CO)_9$ and the 1940 cm^{-1} band is assigned to $Mn_2(CO)_8$.[3] The rise time of the 1940 cm^{-1} band is the same as the decay time of the 1760 cm^{-1} band. It is significant that we are observing the secondary ligand loss product formed directly from $Mn_2(CO)_9$ with only single photon excitation.

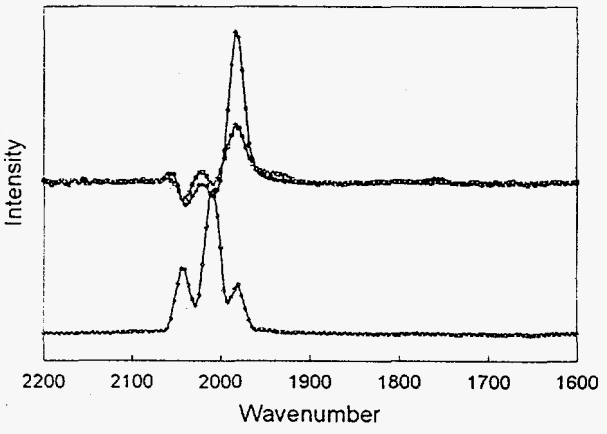

Figure 1: Ground (bottom) and time-resolved (top) infrared spectra of $Mn_2(CO)_{10}$ in cyclohexane obtained with 349 nm excitation.

The ground state resonance Raman spectrum obtained with 351 nm excitation shows a significant increase in the intensities of the e_3

vibrations at 1980 cm^{-1} (equatorial C=O stretch) and 673 cm^{-1} (Mn-C-O bend). There is also an increase in the intensity of the a_1 vibration at 159 cm^{-1} (Mn-Mn stretch), but the increase is not as great as the e_3 vibrations. We have compared our data to Fenske-Hall calculations and to Density Functional calculations of $Mn_2(CO)_{10}$ and $Mn_2(CO)_9$. The calculations predict that the optimum geometry for the ligand loss product is a semi-bridged $Mn_2(CO)_9$. The picture that emerges from this work is that the formation of the ligand loss product with 351 nm excitation occurs by the loss of an equatorial CO, followed by the formation of a semi-bridged $Mn_2(CO)_9$. These results also call into question the original assignment of the electronic state that is at 336 nm. The original assignment was that this is a $\sigma^* - \sigma$ state,[4] but our results are more consistent with the assignment of this state as a $d\pi^* - \sigma$ state. More work remains in order to confirm this assignment.

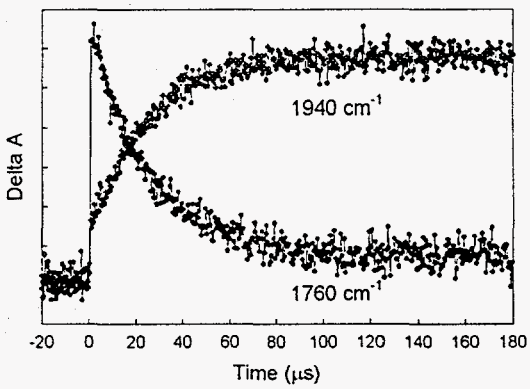

Figure 2: Dynamics of the 1760 and 1940 cm^{-1} bands of $Mn_2(CO)_{10}$ in cyclohexane with 349 nm excitation.

The combination of ground state resonance Raman experiments and time-resolved vibrational spectra provides a powerful tool for probing the structure and dynamics of organometallic photochemistry.

Acknowledgements

We gratefully acknowledge NSF for support of this research via Grant CHE-9208703 (to B.E.B) and Grant CHE-9108384 (to T.L.G. and B.E.B).

References

1. T. J. Meyer and J. V. Caspar, *Chem. Rev.*, 85 (1985) 187.
2. M. Vitale, K. K. Lee, C. F. Hemann, C. R. Hille, T. L. Gustafson, and B. E. Bursten, *J. Am. Chem. Soc.*, 117 (1995) 2286.
3. F. A. Kvietok and B. E. Bursten, *Organometallics*, 14 (1995) 2395.
4. R. A. Levenson and H. B. Gray, *J. Am. Chem. Soc.*, 97 (1975) 6042.

Time-Resolved Resonance Raman Spectroscopy of Excited States of Ruthenium Diimine Complexes.

Sonya Scott and Keith Gordon.
Chemistry Department, University of Otago.

Metal polypyridyl complexes are of interest because of their potential for use in solar energy and supramolecular devices.[1] A number of mixed-ligand ruthenium(II) complexes of the type, $[RuL(bpy)_2]^{2+}$, have been prepared as have copper(I) complexes of the type $[Cu(PPh_3)_2L]^+$. The photophysical properties of these complexes under visible excitation are dominated by their lowest metal-to-ligand charge-transfer (MLCT) excited states. Copper(I) complexes show significant geometric distortion upon photoexcitation to the MLCT state consistent with the fact that the copper(I) is formally oxidised to copper(II). The latter oxidation state prefers a 5 coordinate environment whereas the copper(I) is tetrahedral.[2] The geometric distortions attendant upon ruthenium complexes when photoexcited are much less severe. The ruthenium(II) and ruthenium(III) sites being coordinantively similar. This study examines the properties of ruthenium and copper complexes with a series of geometrically constrained ligands.

We have chosen to use a series of binaphthyridine and biquinoline ligands in which the degree of ligand planarity may be tuned. Figure 1. These ligands can be modified in a number of ways to increase or decrease the extent of conjugation between the two halves of the ligand. Modifications that can be made are as follows: changing the length of the alkyl chain bridging the halves of the ligand; substitution for the alkyl chain of two methyl groups.

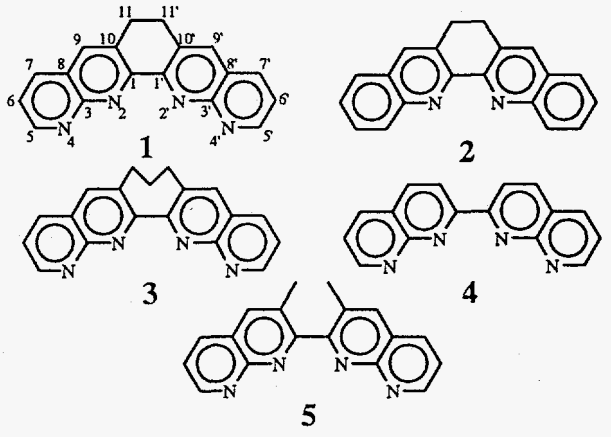

FIGURE 1: Ligands

The longer alkyl chain decreases the degree of planarity in the ligand as do the presence of the methyl substituents at the 10,10' positions. X-ray crystallographic data indicates that for **1** the angle between the naphthyridine units is ca. 14°, as the chain is extended this angle becomes greater.

The MLCT excited states results in the formal oxidation of the metal centre and formal reduction of a ligand moiety. Each of these processes may be achieved by electrochemical means. We have used electronic and Raman spectroelectrochemistry to model the MLCT excited state and then compared these results to the direct measurement of the excited state resonance Raman spectra.

Spectroelectrochemical measurements suggest that for $[Ru(bpy)_2(L)]^{2+}$ where L = **1** through

5 the first reduction is ligand based on the naphthyridine or quinoline ligand. The resonance Raman data for these complexes have many bands that are 2,2'-bipyridyl (bpy) modes. This is evidenced by their frequency coincidence with other ruthenium bpy complexes. Close analysis of the resonance Raman data reveals two bands that are associated with the naphthyridine / quinoline ligand. The first of these, 1483-1494 cm^{-1}, is a torsion angle sensitive and is associated with the 1, 1' linkage. The second, 1359-1383 cm^{-1} seems to be more sensitive to replacement of naphthyridine with quinoline. Figure 2 shows the resonance Raman spectra of $[Ru(bpy)_2(\mathbf{1})]^{2+}$ in the ground and first reduced state. The resonance enhancement of these bpy modes in the ground state spectrum indicates that the absorption at 514.5 nm is made up of two types of MLCT transition; one terminating on a bpy ligand and the other on the naphthyridine ligand. Time-resolved resonance Raman spectra show that the excited states of all complexes are localised on the naphthyridine / quinoline ligands. No bpy^{-} features are observed. Furthermore it appears that the optical electron is localised across the ligand framework in **1**, **2** and **4** but is further localised on one of the naphthyridine moieties in **3** and **5**.

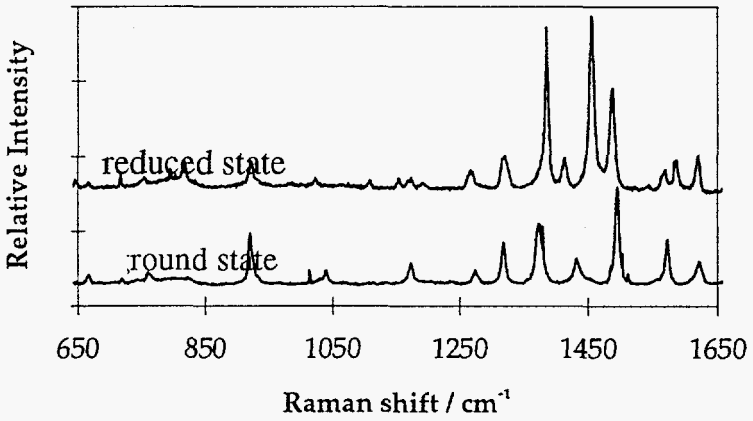

Figure 2: Resonance Raman OTTLE of $[Ru(\mathbf{1})bpy_2]^{2+}$

Acknowledgements:

We would like to thank the University of Otago for a Ph.D. scholarship for Sonya Scott, the New Zealand Lotteries Board for equipment funding, and the University of Otago Division of Sciences and the Royal Society of New Zealand for awards of travel grants.

References:

1 Scandola, F.; Argazzi, R.; Bignozzi, C. A.; Chiorboli, C.; Indelli, M. T.; Rampi, M. A. in Supramolecular Chemistry; Balzani, V.; DeCola, L. (Eds.); (Kluwer Academic Publishers: Netherlands, 1992).

2 McMillin, D. R.; Kirchhoff, J.R.; Goodwin, K. V.; Coord. Chem. Rev., 64, (1985) 83.

Application of Time-Resolved, Step-Scan Fourier Transform Infrared Spectroscopy to Excited-State Electronic Structure in Polypyridyl Complexes of Re(I)

Jon R. Schoonover and R. Brian Dyer
Bioscience and Biotechnology Group
Los Alamos National Laboratory, Los Alamos, NM 87545

Recent advances in transient infrared spectroscopy have provided the means for infrared measurements to be made following laser excitation on short time scales. The infrared technique is particularly valuable in the study of metal complexes containing CO or CN^- because ν(CO) and ν(CN) stretching vibrations have high oscillator strengths and the sensitivities of their energies and bandwidths to electronic and molecular structure are well established. Electronic excitation generally produces significant transient infrared absorption changes which are intense and characteristic of the changes in electron structure between states. For example, in $[(phen)(CO)_3Re(NC)Ru(bpy)_2(CN)]^+$ (phen is 1,10-phenanthroline; bpy is 2,2'-bipyridine) $Re^I(d\pi) \rightarrow phen(\pi^*)$ excitation produces initially a $Re^{II}(phen^{\bullet-})$ metal-to-ligand charge transfer (MLCT) excited state and large shifts in ν(CO) (40 - 80 cm^{-1}) compared to the ground state. Subsequently, rapid, cross-bridge energy transfer occurs ($k_q = 2 \times 10^{11}\ s^{-1}$) to give $[(phen)(CO)_3Re^I(NC)Ru^{III}(bpy)(bpy^{\bullet-})(CN)]^{+*}$ which is accompanied by large shifts of the ν(CN) bands and only a slight shift in ν(CO) compared to the ground state. We demonstrate the use of step-scan transient infrared to the elucidation of the excited-state electronic structure in this dimer and complexes **1** - **3**. There is a complex interplay between MLCT and ligand-based excited states in Re(I) complexes We have explored the question of their excited-state electronic structure by employing a powerful new approach to acquiring time-resolved infrared spectroscopy based on the step-scan Fourier transform technique.

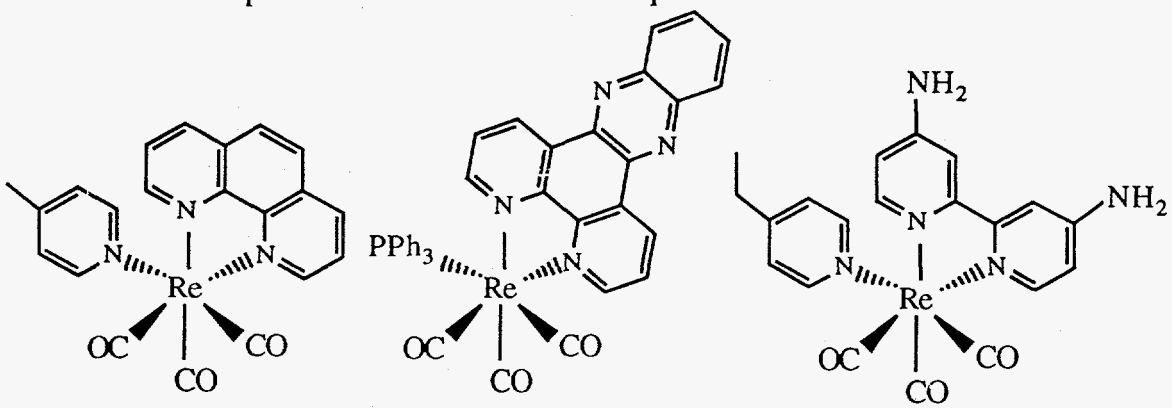

1 **2** **3**

The transient difference spectrum in the ν(CO) region for *fac*-$[Re(phen)(CO)_3(4\text{-}Mepy)]^+$ (**1**, phen is 1,10-phenanthroline; 4-Mepy is 4-methylpyrdine) was acquired 600 ns after 354.7 nm excitation in CH_3CN by using step-scan FTIR. In the spectrum, the

ground state ν(CO) band at 1930 cm^{-1} splits and shifts to higher energy with new bands appearing at 1962 and 2009 cm^{-1}. The ground-state band at 2036 shifts to 2062 cm^{-1}. These shifts are consistent with oxidation of Re(I)to Re(II) and formation of an MLCT excited state.

In the difference spectrum for **2**, *fac*-$[Re(dppz)(CO)_3(PPh_3)]^+$ (dppz is dipyrido[3,2-a:2',2'-c]phenazine; PPh_3 is triphenylphosphine), the three ν(CO) bands shift only slightly in the excited state, and significantly, *the shifts are to lower energy*. Each ν(CO) band in the excited state is shifted on average 8 cm^{-1} to lower energy and broadened by ~2 compared to the ground state.

The relative magnitudes of the shifts in ν(CO) are revealing. The large shifts to higher energy for **1** are expected for an MLCT excited state in which Re(I) is formally oxidized to Re(II). Similar shifts have been observed for the MLCT excited states of other Re(I) complexes. The small shifts for **2** are consistent with a lowest, ligand-localized excited state, presumably $^3\pi\pi^*$(dppz) consistent with room temperature emission from this complex which has the characteristic, resolved vibronic structure and extended excited-state lifetime ($\tau = 42$ μs) of a $^3\pi\pi^*$ excited state.

The power of the step-scan transient IR technique to elucidate electronic structure is also illustrated by measurements on **3**, *fac*-$[Re(4,4'-(NH_2)_2)\text{-bpy})(CO)_3(4\text{-Etpy})]^+$ (4,4'-$(NH_2)_2$)-bpy is 4,4'-diamino-2,2-'bipyridine). In transient UV-visible absorption difference spectra, there is evidence for both a ligand-localized excited state (or states) with a broad absorption feature at 450 nm, and an MLCT excited state with a band appearing at 370 nm. The relative intensities of the two are solvent and temperature dependent. The features of the transient infrared difference spectrum for **3** in CH_3CN that appear can be attributed to an MLCT excited state and at least one additional, ligand-based state. The positive shifts in ν(CO) from the ground state at 1914 and 2025 cm^{-1} to 1979, 2002 and 2064 cm^{-1} are comparable to those observed for **1**. ν(CO) bands are also observed shifted to lower energy at 1881 and 2014 cm^{-1} which are comparable to the shifts observed for the $^3\pi\pi^*$ state of **2**. There is evidence for still a third set of excited-state bands at 1930 and 2031 cm^{-1} suggesting the possibility of a third excited state probably ligand-centered.

These results demonstrate the utility of step-scan FTIR in obtaining transient infrared spectra of transition metal complexes. They provide a new dimension by utilizing oxidation state sensitive CO stretches to distinguish between excited states of different orbital origins. The technique also addresses questions pertaining to internal electronic structure such as backbonding and oxidation state based on the magnitudes of ν(CO) shifts. There is a further advantage that the step-scan technique can be applied throughout the infrared region including bands arising from the polypyridine ligands.

Time Resolved Vibrational Spectroscopy of some Rhenium (I) Polypyridyl Complexes

T.J. Simpson and K.C. Gordon
Chemistry Department,
University of Otago,
P.O. Box 56,
Dunedin,
New Zealand.

INTRODUCTION

Metal polypyridyl complexes are of interest because of their utility in solar energy devices, and as building blocks for photonic molecular devices [1]. Complexes based on $Re(CO)_3Cl$ are of interest because of their potential use in the photocatalytic conversion of CO_2 to CO [2]. Furthermore visible spectroscopy of such Re(I) complexes is less complicated than other d^6 metal systems owing to the lack of visible chromophores from the spectator CO and Cl ligands.

Resonance Raman of the ground and neutral species as well as time resolved resonance Raman (TR^3) spectroscopy were employed to try and understand the lowest energy metal to ligand charge transfer (MLCT) transition. The MLCT excited state can be written as

$$(Re^{I}(CO)_3Cl)L + h\nu \rightarrow (Re^{II}(CO)_3Cl)(L^{\cdot-})$$

i.e. a formal oxidation of the metal centre and reduction of the ligand.

Four complexes were studied, the ligands used were 2,3-di(2-pyridyl)quinoxaline (**dpq**), 2,3-di(2-pyridyl)-5-methylquinoxaline (**BL3**), 6,7-dimethyl-2,3-di(2-pyridyl)quinoxaline (**dmdq**) and 2-(2-pyridyl)quinoxaline (**pqx**). By subtle ligand modification we can tune the properties of the complexes e.g. MLCT energy and vibrational spectra. Consequently we may expect modification of excited state properties.

DISCUSSION AND RESULTS

The electronic absorption spectra of the neutral and reduced species were taken prior to the collection of the vibrational data. From this data and previous work it was concluded that the lowest energy transition was MLCT in nature [3]. In the reduced species this transition is bleached and a new transition at longer wavelengths is observed. This band is assigned as a ligand centered (LC) (π,π^*) or (π^*,π^*) transition. In the vibrational spectra of the reduced complex the $\nu(C\equiv O)$ was seen to bleach, consistent with the electronic transition having no MLCT character.

Localization of the molecular orbitals might be expected for a ligand such as **dpq**, and derivatives, the different types of localization being on the quinoxaline and pyridyl rings. Tentative vibrational assignments have been made on the following basis. From electrochemical data, as a methyl group is added to the quinoxaline ring the potential for

the reduction becomes more negative by about 50 mV per methyl group. This corresponds to a blue shift in the MLCT energy as we go from the **dpq→BL3→dmdq** ligands. An intensity decrease might be anticipated in the quinoxaline based modes on going from **Redpq→Redmdq** in the RR spectra, because of this blue shift in the MLCT energy. This leads to the proposed assignment for 1476 cm^{-1}, 1360 cm^{-1} and 1574 cm^{-1} **Redpq** bands as being quinoxaline based. Further to this, these bands are also seen in the RR spectra of **Repqx**. Similarly the 1215 cm^{-1} and 1603 cm^{-1} bands are assigned as bound pyridyl modes, as they are seen in all complex spectra. The intensities of all the pyridyl bands is significantly less than that of the quinoxaline bands. This suggests that the HOMO maybe localised on the quinoxaline. The band at 1291 cm^{-1} is assigned as a C-C stretch, this is consistent with data obtained for biphenyl systems and only seen as a weak stretch at 1301 cm^{-1} for the **Repqx** system.

The reduced RR spectra for the complexes was taken using a cell described previously [3]. Complete bleaching of the $\nu(C\equiv O)$ was seen in each case and confirms the nature of the transition is no longer MLCT.

Incomplete bleaching of the excited state was evidenced by the intensity of the $\nu(C\equiv O)$. Power dependence studies were undertaken, and features assignable as excited state were seen and showed a non-linear dependence on photon density at the sample. Correlations are seen between the excited state bands and bands associated with the reduced species. This is expected if the electronic excited sate is MLCT in nature. The excited state bands seen in the TR^3 spectra are associated with the quinoxaline ring. The frequency shifts are consistent with a HOMO extending over some part of the substituted quinoxaline ring.

CONCLUSIONS

Tentative analysis of the vibrational spectra of some rhenium(I) polypyridyl has been made. The molecular orbitals are seen to cover the quinoxaline ring, substitution significantly effects the vibrational spectrum. The excited state is seen to be MLCT in character, evidence is observed in the TR^3 and RR of the reduced species.

Acknowledgements

TJS thanks the University of Otago for a postgraduate scholarship. Equipment was funded in part from grants from the New Zealand Lottery board, and from the Division of Sciences, University of Otago.

References

1. F. Scandola, R. Argazzi, C.A. Bignozzi, C. Chiorboli, M. Indelli, M. A. Rampi, in Supramolecular Chemistry, V. Balzani, L. DeCola, (Kluwer Academic Publishers: Netherlands, 1992).

2. J.J. Turner et al., Inorganic Chemistry, 33 (1994) 4712.

3. K.C. Gordon, T.J. Simpson, Inorganic Chemistry, Submitted for publication.

Sensitivity Issues In Step-scan FT-IR Spectrometry

Christopher Manning
Manning Applied Technology
Peter R. Griffiths
Chemistry Department, University of Idaho

INTRODUCTION

Step-scan FT-IR has been accepted as a useful tool for obtaining vibrational spectra of a variety of time-dependent systems, including photoacoustic spectrometry, polymers undergoing dynamic strain, photochemical reactions and electrochemical interfaces. Unfortunately, there has been a significant SNR disadvantage associated with step-scan data collection, relative to the same data collection time with rapid-scan FT-IR. For step-scan signal processing, a lock-in amplifier (LIA) is traditionally used to demodulate the detector signal. We have shown that the analog LIA's generally utilized have insufficient dynamic range to process the detector signal without degrading it. As an alternative, we have demonstrated demodulation by digital signal processing to improve the SNR by an order of magnitude or more.[1]

However, a significant noise disadvantage remains. The key difference between rapid-scan and step-scan FT-IR is the range of effective modulation frequencies. A rapid-scan spectrometer using a TGS detector typically operates with a mirror velocity of 0.15 cm/s, producing modulation frequencies of 5 kHz at the reference laser wavelength, 1.25 kHz at 4000 cm^{-1} and 125 Hz at 400 cm^{-1}. The separation between adjacent spectral elements is then 1.3 Hz, at 4 cm^{-1} resolution. A higher mirror velocity may be used with a cryogenic detector, producing modulation frequencies at the laser wavelength as high as 100 or 125 kHz, and a separation of 25 to 30 Hz between adjacent spectral elements. In contrast, a typical step-scan measurement utilizes a step-rate on the order of 1 fringe per second. The corresponding IR modulation frequencies are 0.25 to 0.025 Hz, from 4000 to 400 cm^{-1}, respectively. This is 5000 times lower in frequency than the rapid-scan measurement, and the spacing between spectral elements is correspondingly smaller, or about 0.24 mHz. It is the close spacing and low modulation frequencies that make step-scan data collection susceptible to multiplicative noise sources.

MULTIPLICATIVE NOISE

For noise sources that simply add to the detector signal, there is no difference in performance between step-scan and rapid-scan operation. However, many of the instabilities present in FT-IR spectrometers have a multiplicative effect, which mixes them with the spectral modulation frequencies to produce noise sidebands on each spectral component. In rapid-scan operation the noise sidebands do not reach to adjacent spectral elements, and are efficiently rejected. In step-scan measurements, the noise components and their sidebands can spread completely across the spectral range.

Many sources of multiplicative noise in FT-IR spectrometers can be identified. The most important one in most step-scan spectrometers is the fluctuation of refractive index of the air in the interferometer. For each degree Celsius by which the temperature of the air in the two arms of the interferometer differs, a path difference error of 88 nm can be generated. To achieve a SNR of 10,000:1 in the mid-IR, the RMS path difference error must be held to less than 1 nm, corresponding to a temperature difference of about 0.01 °C. Other refractive index variations

cause the IR beam image to wander on the detector. Fluctuations in the temperature of a pyroelectric detector vary its responsivity. Even the beamsplitter efficiency varies up to 0.25%/°C. Virtually every instability is related to temperature fluctuation. The most significant source of heat inside most FT-IR spectrometers is the reference laser which typically dissipates 10 watts of waste heat. Since the heat capacity of air is approximately 1 Joule/gram-°C, the waste heat is sufficient to raise the temperature of 1 liter of air by more than 5 °C *per second*, while temperature variations should be held to < 0.01 °C.

EXPERIMENTAL CONFIRMATION

To test the hypothesis that temperature fluctuations and convection are significant noise sources, two sets of measurements were made with a step-scan spectrometer.[2] One set was measured as a control, then the spectrometer was fitted with insulation to minimize temperature variations and convection. For both sets of data six scans were acquired sequentially to 4 cm^{-1} resolution, with a nominal averaging time of 20 minutes per scan. A TGS detector was used with 150 Hz, 2 λ_{HeNe} phase modulation. The spectra were used to compute two series of five 100% lines, which appear in Figures 1 and 2. The traces in Figure 1 exhibit a SNR between 2000 and 3000:1, and are tightly clustered around 100% T, but exhibit noticeable slopes. For the traces in Figure 2, the SNR is improved by approximately 2x to between 5000 and 6000:1, and the slope of the lines is also substantially improved. However, they are no longer clustered

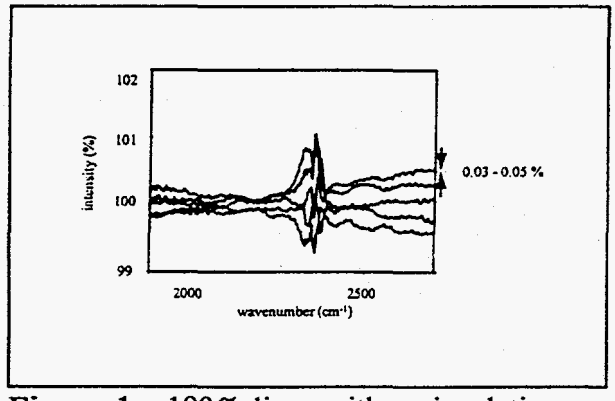

Figure 1 - 100% lines without insulation.

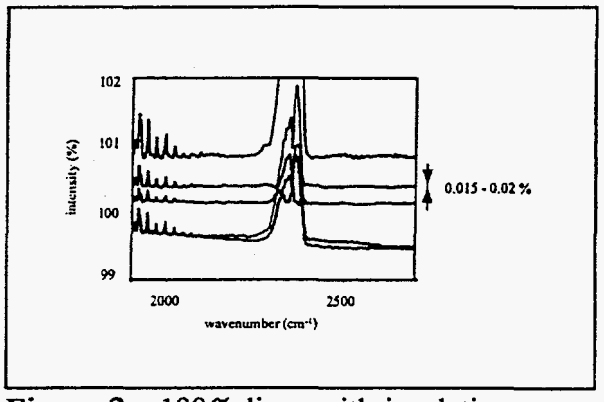

Figure 2 - 100% lines with insulation.

at 100% T. The insulation has caused a slow temperature rise inside the spectrometer which is affecting either or both the pyroelectric detector and beamsplitter efficiencies.

ACKNOWLEDGMENTS

This material is based upon work supported by the National Science Foundation under Grant No. DMI-9413633. The contributions of the University of Idaho, Matt Williamson, Michele Johnson, E. I. Dupont, and Dr. Kevin McNesby are also gratefully acknowledged.

REFERENCES

1. Christopher J. Manning and Peter R. Griffiths, Proceedings of the 5th Symposium on Computer Enhanced Analytical Spectroscopy, Snowbird, Utah, June 23, 1994, in press.

2. Christopher J. Manning and Peter R. Griffiths, Appl. Spectrosc. **47**, 1345 (1993).

A Photoinduced Conformational Change Leads to a Long-lived, High-spin Ni^{II} tetra(*tert*-butyl) Porphyrin Intermediate State

[1]M. C. Simpson, [1]W. Jentzen, [2]M. R. Ondrias, [3]S. Gentemann, [3]M. Drain, [3]D. Holten, [1,2]J. A. Shelnutt

[1] Fuel Sciences Dept., Sandia National Laboratories, Albuquerque, NM 87185-0710.
[2] Department of Chemistry, University of New Mexico, Albuquerque, NM 87131.
[3] Department of Chemistry, Washington University, St. Louis, MO 63130.

Symmetrically substituted metalloporphyrins generally exhibit a variety of static nonplanar distortions that can be described by the lowest frequency out-of-plane normal modes [1]. Of particular importance are the doming (*dom*), ruffling (*ruf*), saddling (*sad*), and waving (*wav*) deformations, each of which typically lead to stable porphyrin conformers. The relative energies of these conformers depend upon metal size, the size, shape and orientation of the substituents, and perturbations from the porphyrin's environment. Photoinduced changes in the metal electronic configuration can thus alter the relative energies of and interconversion rates between these conformers.

We report experimental and theoretical studies of Ni^{II} tetra(*tert*-butyl) porphyrin (NiTtBuP). Time-resolved absorption (TRA) measurements show that absorption of visible photons by NiTtBuP is followed by a rapid (1.2 ps) decay to a low-lying, non-phosphorescent, d-d* state [2]. In contrast to other Ni porphyrins that relax to the ground state in < 500 ps, relaxation of NiTtBuP* occurs on a > 50 ns timescale [2]. In addition, the transient Soret absorbance maximum is blue-shifted relative to that of the ground state. Transient resonance Raman (TRR) spectroscopy has been used to probe the structure of this intermediate (Fig. 1). At low incident laser fluxes ($<10^6$ W/cm^2), the TRR spectrum generated by Soret excitation is dominated by ground state scattering. Structurally sensitive lines such as ν_4 (1355 cm^{-1}) and ν_2 (1534 cm^{-1}) correspond to those measured with CW resonance Raman. As the laser flux is increased, scattering from a d-d* excited transient intermediate appears (ν_4 ~1336 cm^{-1}, ν_2 ~ 1527 cm^{-1}). The relative contributions of the photoconformers to the total spectrum is laser flux dependent (Fig. 1).

Figure 1: Transient Resonance Raman of NiTtBuP vs Incident Laser Flux
High Frequency Region and Curvefitting of the ν_4 Region

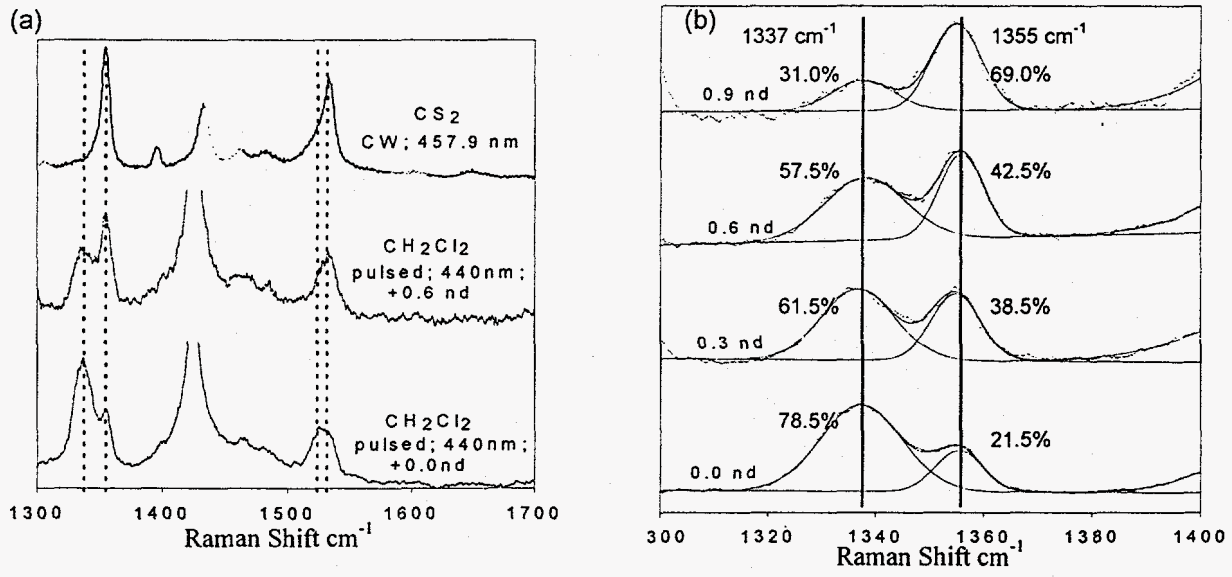

Figure 1: TRR spectra were measured as previously described [3]. Pulsed spectra in (a) and (b): 440 nm, 7ns pulses, 10 Hz. A cylindrical lens focused an expanded beam at the sample. Flux was attenuated with neutral density filters. Curvefitting was done with a program based upon the Levenberg-Marquardt non-linear least squares method [3]. Gaussian band shapes and a linear baseline function were used. The full width at 1/e is 20 cm^{-1} for the 1337 cm^{-1} (intermediate d-d* state) band and 12 cm^{-1} for the 1355 cm^{-1} (ground state) band.

Classical mechanics calculations using a forcefield developed to accurately predict Ni porphyrin equilibrium structures and relative energies [1] suggest an explanation for these results. In the ground state, the ruffled geometry of NiTtBuP is stabilized relative to a domed local minimum structure by > 25 kcal/mol. Upon formation of the d-d* state, the Ni - pyrrole nitrogen equilibrium bond length increases, and as a result the domed form moves to within 7 kcal/mol of the ruffled conformer. Thus the two 'stable' photoconformers observed in the absorbance and TRR studies may correspond to these ruffled and domed structures. The barrier to interconversion from the domed to the ruffled conformations is expected to be high, and to involve rotation of the *tert*-butyl peripheral groups. This postulated interconversion barrier would account for the long lifetime of the intermediate state.

Further evidence in support of this hypothesis is provided by ZINDO/S calculations carried out upon the classical minimum energy geometries. These results predict that if the ruffled ground state NiTtBuP merely undergoes a photoinitiated transition to a d-d* ruffled excited state, both Soret and Q bands should red-shift. In contrast, if the long-lived d-d* excited state is domed, the Soret and Q bands should blue shift. In light of the observed absence of phosphorescence and the blue shift of the Soret band in the TRA studies, the abnormally long excited state lifetime, and the conversion to a d-d* excited species in the TRR spectra, the ZINDO/S evidence supports the presence of a domed, high spin intermediate species. We propose a model that is consistent with our findings (Fig. 2). Further studies are underway to characterize this photo-induced conformational change.

Figure 2: Postulated Kinetic Trapping Model for NiTtBuP

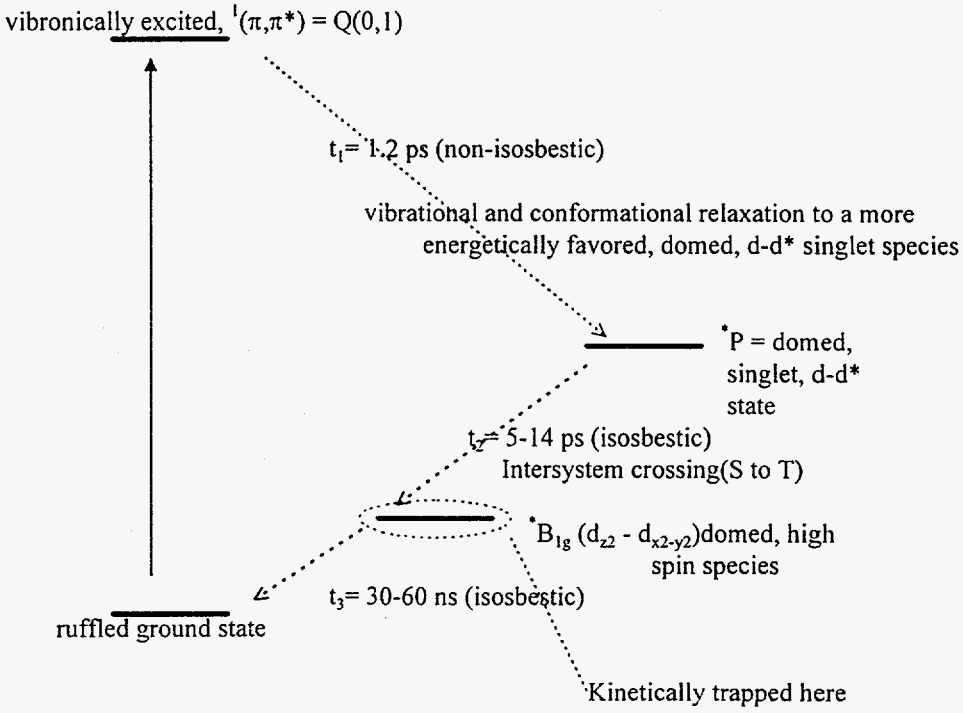

References

1. Jentzen et al., J. Am. Chem Soc., (1995) in press, and references therein.
2. Drain, M. et al., manuscript in preparation.
3. M.C. Simpson, PhD dissertation, U. of New Mexico, (1994).

Acknowledgements

This research was funded by the U.S. D.O.E. Contract DE-AC04-94-AL85000 (JAS), National Institutes of Health (GM33330, to MRO), a D.O.E. Distinguished Postdoctoral Research Fellowship (MCS), and a Postdoctoral Associated Western University Fellowship (WJ). M.C. Simpson was previously M.C. Schneebeck.

Transient Raman Spectroscopic Study on Ruthenium Porphyrins in Various Solvents

Sae Chae Jeoung[1], Dongho Kim[1], Dae Won Cho[2] and Minjoong Yoon[3]
[1]*Spectroscopy Lab., Korea Research Institute of Standards and Science, Taejon 305-606, Korea*
[2]*Department of Chemistry, Seonam University, Namwon 509-170, Korea*
[3]*Department of Chemistry, Chungnam National University, Taejon 305-764, Korea*

Among the various important aspects in the photophysics of Ru(II) porphyrins, the marked influenece of the two axial ligands on the photokinetics has drawn a special attention. The previous studies [1-3] unequivocally demonstrated that CO ligand withdraws π-electron density from the metal d_π-orbitals to lower the energy of $T(\pi,\pi^*)$ through $d_\pi \rightarrow CO(\pi^*)$ back bonding effect. On the other hand, $Ru(II)P(L)_2$ (P = TPP or OEP and L = pyridine, piperidine, or 1-methyl imidazole) has been known to have a metal-to-ring (d,π^*) CT state as the lowest excited-state. Holten et al. [2,3] reported, however, that the dynamics of excited Ru(II)P(CO)(L) have strong temperature dependencies caused by a (d,π^*) CT state thermally accessible from $T(\pi,\pi^*)$.

Figure 1(b) presents the transient Raman spectrum of $Ru(II)TPP(py)_2$ in pyridine obtained by the high-power 416 nm single pulse excitation. In comparison with the spectrum of Figure 1(a) probed by the low-power excitation, an apparent increase in the intensities of the Raman peaks at 1528 and 1364 cm^{-1} was easily noticeable. The excited state Raman spectrum is displayed in Figure 1(c), and yields the transient Raman bands at 1528, 1364 and 1228 cm^{-1}, respectively. No strong enhancement of the ϕ_4 (phenyl) and ν_1 modes indicates that the transient state responsible for the excited state Raman spectrum in Figure 1(c) is not contributed from the $T_1(\pi,\pi^*)$ state of photoexcited $Ru(II)TPP(py)_2$, because the strong enhancement of these two modes are the characteristic changes for the porphyrin ring $T_1(\pi,\pi^*)$ states of Zn(II)TPP, H_2TPP and Cu(II)TPP[4]. The excited state Raman spectrum reveals that the ν_2, which is C_β-C_β stretching mode, is shifted to lower frequency (1528 cm^{-1}) by 15 cm^{-1} relative to that of ground state, and the ν_4, which is C_α-N breathing mode, is shifted to higher frequency (1364 cm^{-1}) by 13 cm^{-1}. The observation that the ν_4 mode is shifted to higher frequency by 13 cm^{-1} relative to the ground state can be easily explained if the electronic transition involved in the photodeactivation process of $Ru(II)TPP(py)_2$ is not the $(d_\pi,\pi^*(ring))$ but a metal-to-pyridine $(d_\pi,\pi^*(py))$ CT excited state.

No noticeable difference was found in the transient Raman spectra of Ru(II)TPP(CO)(py) between in benzene and in THF as shown in Figure 2(b) and 2(c). This indicates that the overall spectral feature of excited state Ru(II)TPP(CO)(py) is almost independent of the ligand nature between in benzene and in THF solvents while their ground electronic absorption spectra are different each other. The transient Raman spectra show that the ν_2 mode is slightly shifted to lower frequency (1541 cm^{-1}) by 2 cm^{-1} relative to the ground state, and the ν_4 mode is shifted to lower frequency (1349 cm^{-1}) by 6 cm^{-1}. It is also interesting that in contrast to $Ru(II)TPP(py)_2$ we observed the opposite shift direction of the ν_4 in the excited state, which suggests that the electron density distribution among the porphyrin ring, central metal Ru(II), and axial ligands should be different from that for $Ru(II)TPP(py)_2$. In the bis(pyridine) adducts, upon photoexcitation some portion of the charge density of the porphyrin ring, which is partially populated from the d_π orbitals, flows into the metal due to the formation of the $(d_\pi,\pi^*(py))$ CT excited state. If the discussion presented in the previous section were also applied to the carbonylated Ru(II) porphyrin, the extra charge density should be ad ded to the porphyrin ring to produce the excited state electronic configuration similar to that of the porphyrin π-anion radical. Among the possible candidates for the charge transfer states such as the (π,d), $(d_\pi,\pi^*(ring))$, $(d_\pi,\pi^*(py))$ and (d,d) transitions, the $(d_\pi,\pi^*(ring))$ transition is the only CT state to exhibit an increase in the electron density of the porphyrin ring relative to the ground state electronic configuration.

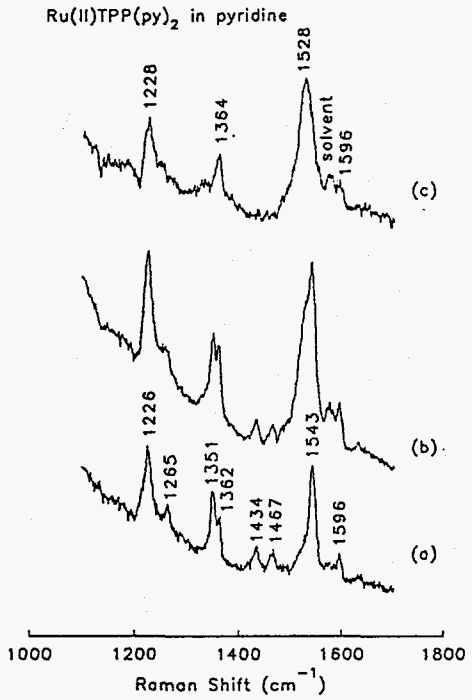

Fig. 1 Transient Raman spectra of $Ru(II)TPP(py)_2$ with 416 nm single pulse excitation; (a) the low power, (b) the high power and (c) difference Raman spectra (b)−(a) with a proper subtraction factor

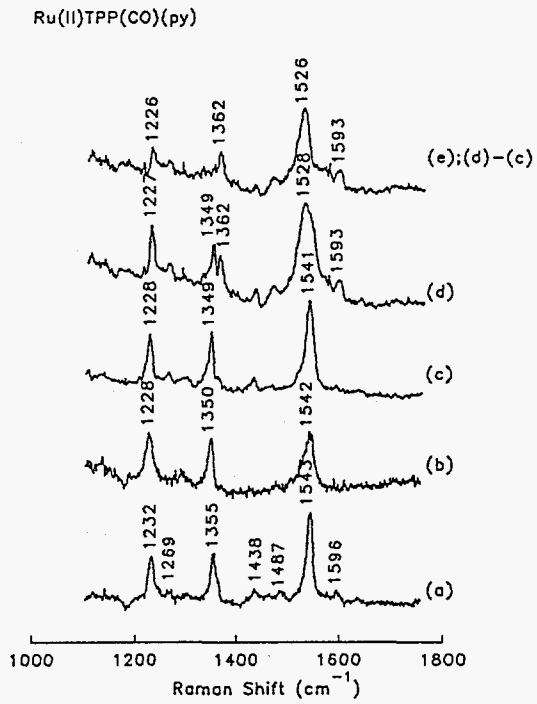

Fig. 2 Transient Raman spectra of Ru(II)TPP(CO)(py) with 416 nm single pulse excitation; (a) the low power, (b) the difference spectrum in benzene, (c) in THF, (d) in pyridine and (e) the difference spectrum (d)−(c).

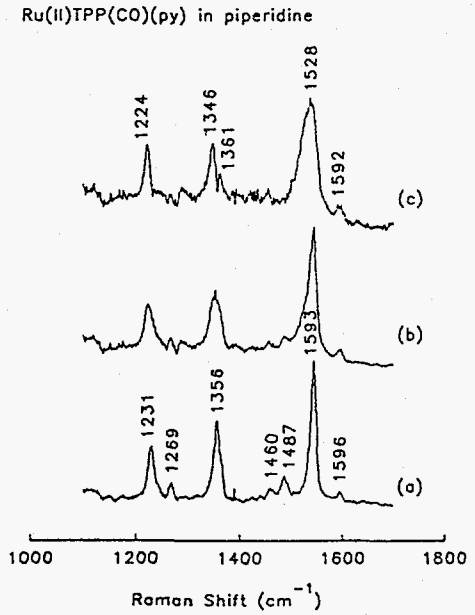

Fig. 3 Transient Raman spectra of Ru(II)TPP(CO)(py) in piperidine solvent with 416 nm single pulse excitation; (a) the low power, (b) the high power and (c) the difference Raman spectrum (b)−(a) with a proper subtraction factor.

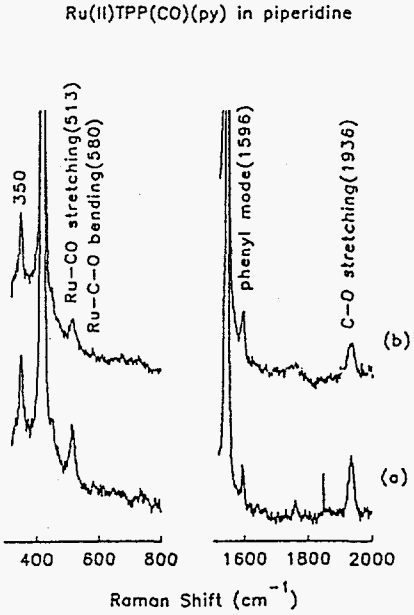

Fig. 4 Raman spectra for Ru(II)TPP(CO)(py) in piperidine solvent observed with the low power (a) and the high power (b). The spectra are normalized to the peak intensities of the phenyl mode and the band at 413 cm^{-1}. The laser powers for the low and high power experiments are ca. < 0.1 mJ and 1 mJ, respectively.

We have also conducted the transient Raman measurements on Ru(II)TPP(CO)(py) in pyridine and presented the results in Figure 2(d). If we notify the emergence of the two comparable peaks at 1349 and 1362 cm^{-1} corresponding to the ν_4 mode, and a much broader band centered at 1528 cm^{-1}, we can easily suggest that the transient Raman spectra in Figure 2(d) are contributed by more than two different excited states. We can tentatively propose that one excited state among the possible transient states of Ru(II)TPP(CO)(py) in pyridine should be the same as the CT state observed in benzene and THF solvents. The subtraction of the transient Raman peaks of Figure 2(c) from the spectra of Figure 2(d) exhibits the difference Raman spectrum (Figure 2(e)), which is essentially similar to that of Figure 1(c) observed from Ru(II)TPP$(py)_2$ in pyridine. These experimental findings indicate that CO molecule of Ru(II)TPP(CO)(py) is at least partially replaced by pyridine in the excited state.

We also observed another interesting aspect of the CT state of bis(pyridine) adducts of Ru(II) porphyrins by comparing the transient Raman spectra of Ru(II)TPP(CO)(py) in piperidine with those in pyridine. The transient peaks at 1362 cm^{-1} observed in pyridine almost disappear in piperidine solvent as shown in Figure 3(c), even though the broadness of the Raman peak at 1528 cm^{-1} remains almost unchanged. The appreciable decrease in the peak intensity at 1362 cm^{-1} suggests that the metal-to-pyridine (d_π,π^*(pyridine)) CT state hardly participate in the deactivation process of photoexcited Ru(II)TPP(CO)(py) in neat piperidine solvent. From the discussion on the nature of the (d_π,π^*(pyridine)) CT state and the photodecarbonylation of Ru(II)TPP(CO)(py) in the strongly ligating solvent, we can propose the following mechanisms. The photodecarbonylation of Ru(II)TPP(CO)(py) in the two solvents, pyridine and piperidine, produces two different types of Ru(II) porphyrins, Ru(II)TPP$(py)_2$ and Ru(II)TPP(py)(pip)↔Ru(II)TPP$(pip)_2$, respectively. Since piperidine solvent does not have the empty π^* orbital which is essential to produce the (d_π,π^*(py)) CT state, Ru(II) porphyrins having two piperidine molecules as axial ligands can not form the metal-to-ligand CT state. This would affect the deactivation process by altering the spin-orbit pathways or opening new decay channels. Indeed, the lifetimes of photoexcited Ru(II)TPP$(py)_2$ (15 ns) and Ru(II)TPP$(pip)_2$ (2 ns) are different each other, supporting the above postulate.

Figure 4 depicts the Raman spectra of Ru(II)TPP(CO)(py) in piperidine with an excitation of one-color 416 nm pulses having different laser powers. In Figure 4(a), three additional bands are observed in the carbonylated Ru(II)P complex at 513, 580 and 1936 cm^{-1} in comparison with Raman spectrum observed for Ru(II)TPP$(py)_2$ (not shown). By analogy with the assignment for Ru(II)OEP(CO)(py) as well as the similar bands for carbonylated iron porphyrins around this frequency region, these Raman bands are assignable to Ru-CO stretching, Ru-C-O bending and C-O stretching mode, respectively. Apparently, the exposure of Ru(II)TPP(CO)(py) to high-power laser pulses in piperidine results in a decrease in the peak intensities at 513, 580 and 1936 cm^{-1}, which are related to the ligated CO. These observations and the above experimental results led us to conclude that CO in Ru(II)TPP(CO)(L) is easily replaced by pyridine and piperidine solvents in the excited state.

This work was supported by MOST and KOSEF through center for molecular science (D. Kim) and the Basic Science Research Institute Program, Ministry of Education (M. Yoon).

[1] D.Kim, Y. O. Su, and T. G. Spiro, *Inorg. Chem.* **25**, 3993 (1986)
[2] L. M. A. Levine and D. Holten, *J. Phys. Chem.* **92**, 714 (1988)
[3] J. Rodriguez, L. McDowell and D. Holten, *Chem. Phys. Lett.* **147**, 235 (1988)
[4] S.C. Jeoung, D. Kim, D. W. Cho and M. Yoon, *J. Phys. Chem.* **99**, 5826 (1995).

Time-Resolved Resonance Raman and Transient Absorption Studies on Water-Soluble Copper(II) Porphyrins

Sae Chae Jeoung[1], Dongho Kim[1], Dae Won Cho[2] and Minjoong Yoon[3]
[1]*Spectroscopy Laboratory, Korea Research Institute of Standards and Science Taejon 305-606, Korea*
[2]*Department of Chemistry, Seonam University, Namwon 509-170, Korea*
[3]*Department of Chemistry, Chungnam National University Taejon 305-764, Korea*

The series of transient Raman studies using high power nanosecond lasers were carried out on the complexes of Cu(II)(TMpy-P4) with a variety of synthetic oligonucleotides as well as calf thymus DNA [1]. These experiments revealed that several factors - (i) the presence of A-T sites in the duplexes, thymin or uracil residues, (ii) the fixation mode of CuP on nucleotide, and (iii) the proper secondary structure of polymer - play an important role in the exciplex formation. This exciplex was suggested to involve a charge transfer (CT) from the donor excited-state copper porphyrin to the acceptor nucleo-bases in poly(dA-dT). The previous Raman spectroscopic investigations suggested that the lowering of vibrational frequencies of Cu(II)(TMpy-P4)-DNA complexes is attributable to a π-radical cation, (CuP^+), which is induced by an intermolecular charge transfer from the highest occupied CuP orbital into the lowest vacant orbital of a thymine residue. On the contrary, the time resolved resonance Raman (TR^3) and excitation profile investigations assigned a short-lived five-coordinated complex of Cu(II)(TMpy-P4) with synthetic nucleotides as a (d,d) excited state [2], of which an effective structural property was required for the formation of the fifth ligand.

In this report, we show that some simple solvents such as H_2O, THF and dioxane are also capable of forming the exciplex, which do not require the consideration of the binding mode and the favorable secondary structure of nucleotides and DNA, which has been suggested to be the most important exclusive factor. In addition, we examine the exciplex nature of water-soluble Cu(II) porphyrins in terms of a photoinduced axial ligation with solvent molecules. Figure 1(B) presents the transient Raman spectrum of Cu(II)TSPP in water obtained by the high-power 416 nm single pulse excitation. In comparison with the spectrum of Figure 1(A) monitored by the low-power excitation, an apparent increase in the intensities of the Raman peaks at 1536 and 1340 cm^{-1} was easily noticeable. The emergence of these new Raman bands indicated that the water solvent, like THF and dioxane in the previous studies on Cu(II)TPP and Cu(II)OEP [3], acts as an axial ligand for photoexcited Cu(II)TSPP, and consequently lowers the energy of the intramolecular charge transfer (π,d) state below the tripmultiplet $^2T/^4T(\pi,\pi^*)$ states, serving as the main deactivation channel of photoexcited Cu(II)TSPP in water. The Raman spectral features for ground state Cu(II)TSPP were subtracted to yield the excited state Raman spectrum using a subtraction factor sufficient enough to avoid any negative feature, and the difference Raman spectrum is displayed in Figure 1(C). This difference spectrum gives the transient Raman bands at 1586, 1549, 1538, 1354, 1340, 1233, 1120, 1093, and 1080 cm^{-1}, respectively. We have attempted to record the transient Raman spectrum with a two-color pump/probe technique with a time delay in order to obtain further information for the transients of Cu(II)TSPP in water; however, it turned out to be a failure. This fact indicates that the overall decay process of photoexcited Cu(II)TSPP in water is faster than our nanosecond laser pulse width (3.5 ns). Indeed, the overall decay having $\sim$100 ps time constant was obtained from the transient absorption experiment of Cu(II)TSPP in water.

We carried out the transient RR spectroscopy on Cu(II)TSPP in the mixed solvent with increasing the extent of dioxane (Figure 2). In the mixed solvent, some new transient Raman bands appeared with the addition of dioxane. The emergence of these new Raman bands can be explained in terms of two factors: (i) the occurrence of five-coordinated Cu(II)TSPP formed by dioxane, and (ii) the excited state dynamics of

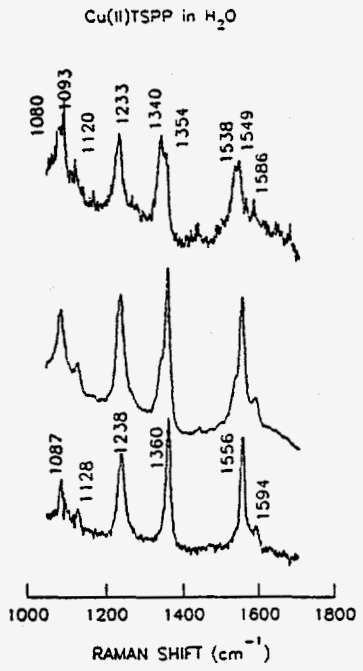

Fig. 1 The nanosecond transient RR spectra of Cu(II)TSPP in H_2O with 416 nm nanosecond pulse excitation: (A) the low power, (B) the high power, and (C) the difference spectrum (B)-(A) with a proper subtraction factor.

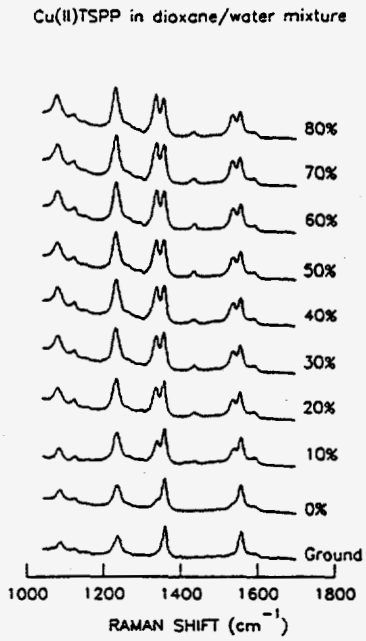

Fig. 2 The nanosecond transient RR spectra of Cu(II)TSPP in dioxane/water mixture solvents with increasing the relative portions of dioxane with an excitation of 416 nm nanosecond pulses under the same experimental conditions.

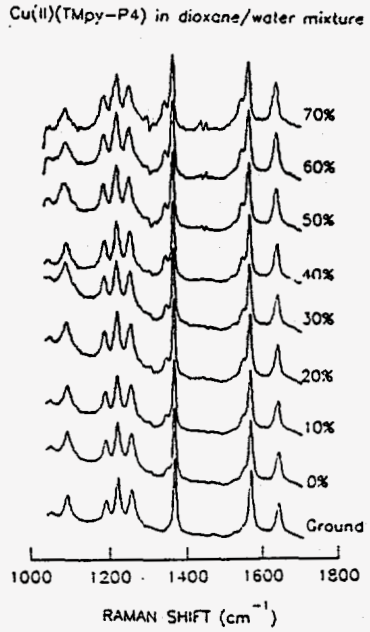

Fig. 3 The nanosecond transient RR spectra of Cu(II)(TMpy-P4) in dioxane/water mixture solvents with increasing the relative portions of dioxane with an excitation of 416 nm nanosecond pulses under the same experimental conditions.

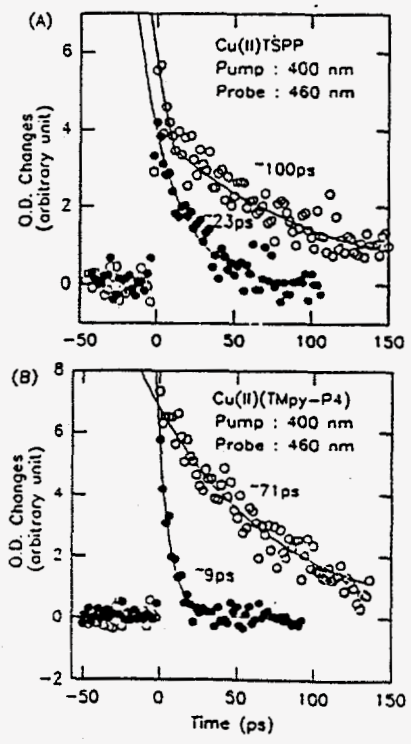

Fig. 4 The transient absorption decay profiles at 460 nm for Cu(II)TSPP (A) and Cu(II)(TMpy-P4) (B) in H_2O (closed circles) and H_2O/dioxane (6:4 in volume, open circles) solvents.

Cu(II)TSPP in the mixed solvent. Although our results presented here cannot distinguish which is predominantly responsible for the appearance of the new Raman bands, the transient absorption spectrum unambiguously showed that the excited state dynamics of Cu(II)TSPP plays an important role. In other words, the Cu(II)TSPP transients formed in dioxane have longer lifetimes than those in water, and consequently account for the appearance of some new bands probed by 3.5 ns laser pulses.

The nanosecond transient RR spectra of Cu(II)(TMpy-P4) in the various composition of solvents were obtained under the identical experimental conditions (laser power and porphyrin concentrations) to avoid any possible experimental artifact resulting from their changes. Figure 3 shows a series of transient Raman spectra as we increased the partial fraction of dioxane. It is interesting to note that the lifetime of excited Cu(II)(TMpy-P4) in dioxane is longer than that in water, which was verified by the kinetic results from the time-resolved transient absorption measurements. This behavior enables us to monitor the transient Raman bands of Cu(II)(TMpy-P4) with the nanosecond pulse excitation increasing the extent of dioxane solvent.

To elucidate the excited state dynamics of Cu(II)TSPP and Cu(II)(TMpy-P4) in various solvents, we performed the picosecond transient absorption measurements by exciting with *ca.* 150 fs optical pulses at 400 nm and probing the absorbance change at 460 nm. The transient absorption changes (Figure 4) for both Cu(II)TSPP and Cu(II)(TMpy-P4) in water displayed the first order kinetics with the lifetimes of 23 ps and 9 ps (closed circles in Figure 4), respectively. On the other hand, for Cu(II)TSPP in water/dioxane mixture (6:4 in volume), the photoexcited transient exhibited a biexponential decay with the lifetimes of ~20 ps (a minor component having about 20 % in amplitude) and 100 ps (80 % in amplitude) (open circles in Figure 4(A)), respectively. The lifetime of the shorter component is similar to that of excited Cu(II)TSPP in water. These observations can be attributed to the five-coordinated complex formation of photoexcited Cu(II)TSPP with water as an axial ligand, which participates in the decay process even under the mixture solvents. The other transient component with the lifetime of 100 ps is contributed by the complex formation of photoexcited Cu(II)TSPP with dioxane. If the formation constants of five-coordinated Cu(II)TSPP complexes with water and dioxane are equal, the major component should be Cu(II)TSPP:water complex because the molar ratio of [dioxane]/[water] is *ca.* 0.13 in the used solution. On the contrary, the major component was turned out to be the dioxane complex. These findings can be explained by the difference in the complex formation constants, i.e., the formation constant of Cu(II)TSPP with dioxane is much larger than that with water. From a quantitative analysis, the former was found to be larger than the latter by a factor of *ca.* 33. A certain clue to the difference in the ratio between Cu(II)TSPP:water and Cu(II)TSPP:dioxane complexes was also seen in the ground state absorption spectra, in which an apparent red shift in the Soret band was observed with the addition of dioxane to the aqueous solution of Cu(II)TSPP.

The time-resolved transient absorption spectroscopy has been carried out on Cu(II)(TMpy-P4) in the water/dioxane mixed solvent (6:4 in volume)(open circles in Figure 4(B)). However, in this case we hardly observed the biexponential decay, of which one is due to the complexation of Cu(II)(TMpy-P4) with water, and the other with dioxane; instead, only a single exponential decay of 71 ps lifetime was detected. Thus, we can attribute the observed decay constant to the complex formation by the interaction of photoexcited Cu(II)(TMpy-P4) with dioxane solvent, because the formation constant of Cu(II)(TMpy-P4) with the dioxane is believed to be larger than that with water.

This work was supported by MOST and KOSEF through Center for Molecular Science (D. Kim) and the Basic Research Insitute Program, Ministry of Education (M. Yoon).

[1] P. Mojzes, L. Chinsky, and P. -Y. Turpin, *J. Phys. Chem.* **97**, 4841 (1993)
[2] S. G. Kruglik, V. A. Galievsky, V. S. Chirvony, P. A. Apanasevich, V. V. Ermolenkov, V. A. Orlovich, L. Chinsky, and P. -Y. Turpin, *J. Phys. Chem.* **99**, 5732 (1995)
[3] S. C. Jeoung, D. Kim, D. W. Cho, and M. Yoon *J. Phys. Chem.* **99**, 5826 (1995)

Time-Resolved Resonance Raman Spectra of Porphyrins: Effects of the Peripheral Substituents and the Metal Size on the Porphyrin Ring-to-aryl Charge Transfer.

Sae Chae Jeoung[1], Dongho Kim[1], Kwang-Hyun Ahn[2], Dae Won Cho[3] and Minjoong Yoon[4]

[1]*Spectroscopy Laboratory, Korea Research Institute of Standards and Science, Taejon 305-606, Korea*

[2]*Department of Chemistry, Kyung Hee University, Yongin 449-701, Korea*

[3]*Department of Chemistry, Seonam University, Namwon 509-170, Korea*

[4]*Department of Chemistry,Chungnam National University, Taejon 305-764, Korea*

Time-resolved resonance Raman (TR^3) spectra of H_2-tetratoluylporphyrin (H_2TTP) and H_2-tetramesityl-porphyrin (H_2TMP) were obtained to investigate the peripheral substituent effect on the structural changes in the excited states. Fig. 1 shows the one-color transient Raman spectra of H_2TTP in THF and, for comparison, the two-color pump/probe TR^3 spectra in CH_3I. In the T_1 state Raman spectrum of H_2TTP, ν_2 was shifted to lower frequency (1539 cm^{-1}) by 12 cm^{-1} relative to the ground state. ν_4 was only weakly enhanced, and showed an up-shift in frequency. The ν_6 mode at 1004 cm^{-1} in the ground state moved to *ca.* 1020 cm^{-1} in the T_1 state. ν_{15} mode at 964 cm^{-1} was shifted to 955 and 956 cm^{-1} in S_1 and T_1 states, respectively. The characteristic features in the T_1 state Raman spectrum of H_2TTP were found in the aryl mode (ϕ_4) enhancement at 1608 cm^{-1} and ν_1 mode, which is C_m-aryl vibration, at 1234 cm^{-1}.

The TR^3 bands of H_2TMP in the S_1 and T_1 states are similar to those for H_2TTP except that ν_4 band shifted to lower frequency in the S_1 state and ν_1 mode to higher frequecy in the T_1 state (Fig. 2). It is noticeable that the enhancement of aryl mode (ϕ_4) of H_2TMP in the excited states is much weaker than that of H_2TTP. The aryl mode enhancement in the T_1 state is due to a charge transfer from porphyrin e_g^* to phenyl π^* orbitals [1]. This charge transfer transition should be coupled to a rotation of the aryl groups into the porphyrin ring plane, presumably because the resulting favorable orbital overlap would increase the transition moment of this charge transfer state. Therefore, the rotation of aryl groups toward coplanarity would be enhanced for more favorable electronic conjugation in the T_1 states of H_2TTP. The aryl mode frequency and intensity changes of H_2TMP, however, are not significant between the ground and T_1 states. This indicates that little electronic interaction exists between mesityl and porphyrin ring in the ground state. This interpretation allows for an assessment of the fact that those two rings are kept nearly orthogonal by the steric repulsion between bulky mesityl group and pyrrole H atoms of porphyrin in the ground and excited triplet states.

The TR^3 spectra of metallo-tetraphenylporphyrins (TPP) such as Zn(II)TPP, Pd(II)TPP, Pt(II)TPP and Rh(III)TPPCl were measured in different solvents to investigate the metal size effects on the porphyrin ring-to-phenyl charge transfer in the excited state. In the cases of Zn(II)TPP, Pd(II)TPP and Pt(II)TPP in THF, B_{1g} and B_{2g} modes in the triplet states becomes intense with the metal size increases (Fig 3, 4). In addition, ν_2, ν_{10}, ν_{27} and ν_{29} modes in the excited state were found to gain their intensities as the metal size increases. These results imply that the distortion and ruffling of porphyrin macrocycle becomes manifest, resulting in the Jahn-Teller (JT) distortion in the triplet state. On the other hand, the phenyl modes at 1600 cm^{-1} do not exhibit a significant enhancement upon excitation as the metal size increases. In contrast to the T_1 state Raman spectra of the four-coordinated porphyrins, the phenyl mode in the TR^3 spectra of five-coordinated heavy-metal complex, Rh(III)TPPCl, is significantly enhanced in THF. In comparison with TR^3 spectra of Rh(III)TPPCl in THF, those in pyridine revealed that the enhancement of the other modes were comparable to the phenyl mode enhancement. In piperidine, the phenyl mode of

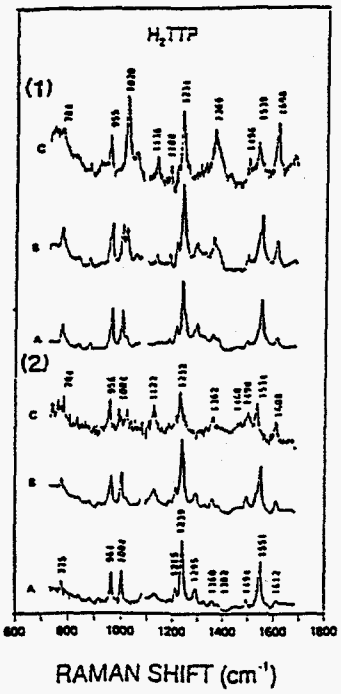

Fig. 1 (1) The nanosecond TR³ spectra of H_2TTP in CH_2I with 532 nm pump and 435 nm probe pulses: (A) probe only, (B) pump and probe (time delay: 7 ns), and (C) difference (B-A). (2) The transient Raman spectra in THF with one-color pulses at 435 nm: (A) the low power, (B) the high power, and (C) the difference spectrum (B-A) with a proper subtraction factor.

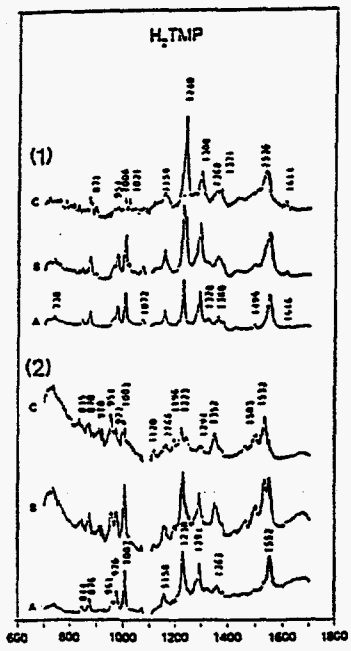

Fig. 2 (1) The nanosecond TR³ spectra of H_2TMP in CH_2I with 532 nm pump and 435 nm probe pulses: (A) probe only, (B) pump and probe (time delay: 7 ns), and (C) difference (B-A). (2) The transient Raman spectra in THF with one-color pulses at 435 nm: (A) the low power, (B) the high power, and (C) the difference spectrum (B-A) with a proper subtraction factor.

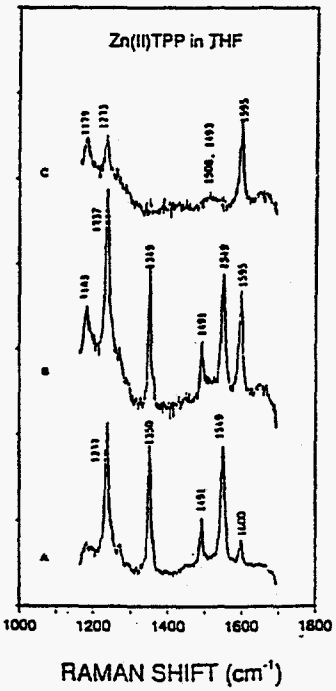

Fig. 3 The nanosecond TR³ spectra of Zn(II)TPP in THF with 565 nm pump and 458 nm probe pulses: (A) probe only, (B) pump and probe (time delay: 7 ns), and (C) difference (B-A) with a proper subtraction factor.

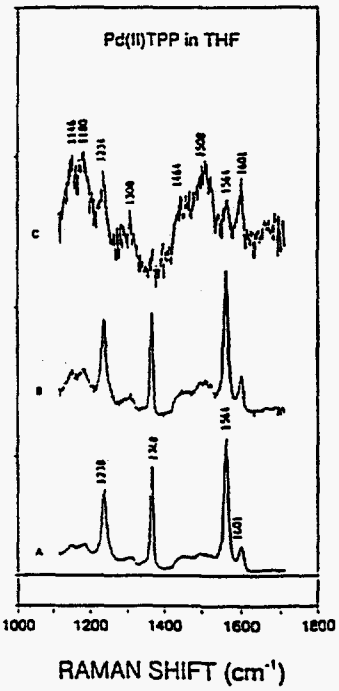

Fig. 4 The nanosecond TR³ spectra of Pd(II)TPP in THF with 532 nm pump and 435 nm probe pulses: (A) probe only, (B) pump and probe (time delay: 1 ns), and (C) difference (B-A) with a proper subtraction factor.

Pd(II)TPP is enhanced in the T_1 state. These results suggest that the structural JT distortion reduce the dihedral angle between phenyl gruops and porphyrin ring, resulting in the inhibition of charge transfer due to a decrease in conjugation between phenyl groups and porphyrin ring.

This work was supported by MOST and KOSEF through center for molecular science (D. Kim), Kyung Hee University (K. -H. Ahn) and the Basic Science Research Institute Program, Ministry of Education (M. Yoon).

[1] R. A. Reed, R. Purrello, K. Prendergast, T. G. Spiro, *J. Phys. Chem.* **95**, 9720 (1991)

Raman Spectral Characteristics of Excited-State Porphyrins Revealed by Pump/Probe Time-Resolved Technique

M. Asano-Someda, S.Sato, K. Aoyagi[§] and T.Kitagawa*
Institute for Molecular Science, Okazaki National Research Institutes, Myodaiji, Okazaki 444, JAPAN
[§]Department of Industrial Chemistry, Fukushima National College of Technology, Taira, Iwaki 970, JAPAN

INTRODUCTION

Copper(II) porphyrins emit phosphorescence but no fluorescence in solution at room temperature in contrast to diamagnetic zinc(II) and magnesium(II) porphyrins. This is because the central metal ion, copper(II) has an unpaired electron in the $3d_\sigma$ orbital and interaction between the unpaired electron and the porphyrin π electrons makes porphyrin T_1 state partially allowed to the porphyrin singlet states. After the excitation to S_1 state, Cu(II) porphyrins relax into triplet manifolds within a few picoseconds and emit luminescence from a $^2T_1$(trip-doublet) state. The lifetimes of the triplet manifolds are reported to be between several tens of nanoseconds and 1 μs.

The emission spectra of meso-substituted Cu(II) porphyrins are independent of the meso-substituents in rigid media. However, in fluid media, the emission spectra depend on substituents of the meso-phenyl groups; some meso-substituted copper porphyrins exhibit considerably red-shifted emission spectra in fluid media compared with those in rigid media[1]. On the basis of the TR^3 spectra of several meso-substituted Cu(II) porphyrins, we discuss a possible relation between the T_1 structure and the red-shift of the emission spectra in addition to the general characteristics of the triplet structures of Cu(II)-porphyrins.

RESULTS AND DISCUSSION

The TR^3 spectra were measured with the pump/probe technique using two pulsed Nd:YAG lasers with 7 ns duration and 10 Hz repetition. Raman scatterings were probed at 450 nm with the delay time after the excitation of 532 nm to the lowest singlet state. Raman spectra were measured in the back-scattering geometry with an intensified photodiode array attached to a triple-polychromator. Measurements were carried out both in benzene and in benzene-d_6 solution[2].

The TR^3 spectra of TPPCu(copper tetraphenyl porphin) for the delay time of 15 ns showed sharp intense band at 1598 cm^{-1} and several other broader bands. The RR spectrum of the triplet state has different feature from that of the ground state and from that of the solvent coordinated (d,d*) excited state[3]. Upon the phenyl deuteration, three bands at 1598(p), 1296(dp) and 1233(p) cm^{-1} were significantly downshifted but not affected by the pyrrole deuteration and thus assigned to phenyl internal ν_{8a}, Cm-phenyl stretching ν_{27} and ν_1 modes, respectively. On the other hand, the bands at 1515(p), 1443(dp) and 1404(p) cm^{-1} showed large downshifts by the pyrrole deuteration and assigned to ν_2 (C_β-C_β), ν_{11} (C_β-C_β) and ν_3 (C_α-C_m) porphyrin skeletal modes, respectively.

Upon excitation to the T_1 state of TPPCu, the ν_2, ν_{11} and ν_3 bands exhibit large downshifts. This is in qualitative agreement with the results observed for TPPZn[4]. The sizes of the frequency shifts for ν_2, ν_{11}, and ν_3 for (TPP)Cu are -49, -57, and -56 cm^{-1}, respectively. If the vibrational modes in the excited states are not greatly altered, the low frequency shifts of these bands would suggest lowering of π bond order of the $C_\beta C_\beta$ bond, and possibly of the $C_\alpha C_m$ bond. With regard

to the C_m-phenyl stretching modes, the out-of-phase mode (ν_{27}) is upshifted by 26 cm^{-1} in the T_1 state while the in-phase (ν_1) band is slightly downshifted (-5 cm^{-1}). Although the two modes are mainly composed of the C_m-phenyl stretchings, they shift in opposite directions because of different symmetry properties (A_{1g} and B_{2g}).

In the TR[3] spectra of TMPCu(copper tetramesitylporphin), which exhibits only a slight red-shift of the emission spectra, the RR spectral pattern is different from that of TPPCu although their band positions are rather alike. The most pronounced peak of T_1 TPPCu is the phenyl ν_{8a} mode, but the corresponding band of T_1 TMPCu at 1610 cm^{-1} is considerably weaker. In the case of the T_1 ($T_{3,4,5OMe}PP$)Cu(copper tetra(3,4,5-trimethoxy)phenylporphin), the ν_{8a} mode at 1600 cm^{-1} is significantly weaker than the case of T_1 TPPCu, although ($T_{3,4,5OMe}PP$)Cu exhibits large amount of the emission red-shift in fluid solution. For all porphyrins examined here, the ν_{8a} frequencies were similar between the S_0 and T_1 states, suggesting that their torsional angles are little altered in the T_1 state. It is rather likely that the torsional angle is altered upon $T_n \leftarrow T_1$ excitation in TPPCu. The deformation of the phenyl group in the T_n state is not related to the emission red-shift.

($T_{F5}PP$)Cu(copper tetrapentafluorophenylporhin) showed no shift of emission spectra and has [$^3(a_{1u}e_g)$] configuration in the lowest excited triplet state, which is different from those of other three cases [$^3(a_{2u}e_g)$]. This copper porphyrin exhibits downshifts of the ν_2 and ν_{11} modes upon excitation to the T_1 state, although it is unexpected from the symmetry property of HOMO and LUMO. However, low frequency shift of ν_2 mode was also observed for the T_1 state of (OEP)Zn in tetrahydrofuran and T_1 (OEP)Cu in benzene, having the [$^3(a_{1u}e_g)$] configuration.

Regarding relation to the emission red-shift, the frequency differences of ν_2 between the T_1 and S_0 states are nearly proportional to the order of the magnitudes of the red-shift; -47 cm^{-1} for ($T_{3,4,5OMe}PP$)Cu ≈ -49 cm^{-1} for TPPCu > -39 cm^{-1} for TMPCu > -34 cm^{-1} for ($T_{F5}PP$)Cu. The upshift of ν_{27} upon excitation to T_1 state is observed in the same order; +28, +26 and +14 cm^{-1} for ($T_{3,4,5OMe}PP$)Cu, TPPCu and TMPCu, respectively. In the case of the ν_1 mode, the shifts increase systematically; -11,-5,-2 and +9 cm^{-1} for ($T_{3,4,5OMe}PP$)Cu, TPPCu, TMPCu and ($T_{F5}PP$)Cu, respectively. Such correlation is not observed for ν_{11} mode. The present results suggest that the strength of the vibrational coupling has some correlation with the size of the red shift of the emission spectra in fluid solution from that in rigid media. Although both the ν_2 and ν_{11} modes mainly involve the $C_\beta C_\beta$ stretching, the difference between ν_2 and ν_{11} lies in appreciable contribution from the $C_\alpha C_m$ stretching coordinate to ν_2. Consequently, it is likely that the compounds which exhibit the larger red-shift in the emission spectra in the fluid medium have a larger coupling term between the C_m-phenyl and C_α-C_m bonds and thus a larger distortion at the methine bridge fragment, including the C_α C_m and C_m-phenyl bonds.

REFERENCES

[1] Asano, M.; Kaizu, Y.; Kobayashi, H. *J.Chem.Phys.* **1988**, 89, 6567. Asano-Someda, M.; Kaizu, Y. *J.Photochem. Photobiol. A(Chem.)*, **1995**, 87, 23.

[2] Asano-Someda, M.; Sato, S.; Aoyagi, K.; Kitagawa, T. *submitted to J.Phys.Chem.*

[3] Kruglik, S.G.; Apanasevich, P.A.; Chirvony, V.S. ; Kvach, V.V.; Orlovich, V.A. *J.Phys.Chem.* **1995**, 99, 2978. de Paula, J.C.; Walters, V.A.; Jackson, B.A. ; Cardozo, K. *J.Phys.Chem.* **1995**, 99, 4373.

[4] Reed, R.A.; Purrello, R.; Prendergast, K.; Spiro, T.G. *J Phys.Chem.* **1991**, 95, 9720. Bell, S.E.J.; Aakeröy, C.B.; Al-Obaidi, A.H.R.; Hegarty, J.N.M.; McGarvey, J.J.; Lefley, C.R.; Moore, J.N., Hester, R.E. *J.Chem.Soc.Faraday Trans.* **1995**, 91, 411.

Resonance Raman Studies on Excited States of Zn(II) Octaethylporphyrin and Zn(II) Methyloctaethylchlorin.

G. Deinum, D.H. Kreszowski, J.P.M. Schelvis, C.K. Chang and G.T. Babcock
Department of Chemistry and the LASER laboratory, Michigan State University, East Lansing, Michigan 48824-1322

Introduction

The primary step of photosynthetic energy transfer involves charge separation in the reaction center. In this process, a chlorophyll complex, after excitation into its lowest excited π,π^* singlet state (S_1) by light absorption or by energy transfer from neighboring pigments, is oxidized. Most critical in this process are the electronic and redox properties of the reaction center chlorophylls, which are modulated by the protein environment and by exciton interactions between different chromophores. We used picosecond time-resolved resonance Raman to obtained more insight into the structure of the chlorphyll model systems Zn(II) Octaethylporphyrin (ZnOEP) and Zn(II) Methyloctaethylchlorin (ZnMeOEC). Of the latter compound, one of the pyrrole rings is reduced.

Experimental

Pulses obtained from synchronously pumped dye lasers at 575 nm (ZnOEP) and 616 nm (ZnMeOEC) with a full width at half maximum of about 5 ps were used to excite the sample dissolved in tetrahydrofuran. A probe pulse at 450 nm was used to obtain the resonance Raman spectra of the transient states. The repetition rate of the lasers was 1.38 MHz. A liquid nitrogen cooled CCD detector and a single grating monochromator were used to measure the Raman spectra.

Results and Discussion

Figure 1a shows the resonance Raman spectra of ZnOEP, obtained without a pump pulse, and with a pump pulse preceding the probe pulse by 500 ps and 27 ns, respectively. The time evolution of the spectra reflects porphyrin in the ground state (S_0), the lowest excited singlet state (S_1) and the lowest triplet state (T_1) states, respectively[1]. The spectra of S_0 and S_1 are dominated by totally symmetric modes as previously reported[2] and show a clear resemblance. Isotopic exchange showed that in both states the mode composition is very similar. It was shown that the shifts of the modes could be explained using Gouterman's four orbital model[2,3]. The small changes indicate that after excitation to S_1 the D_{4h} symmetry is retained. Based on frequency-core size correlations for the ground state, we calculated a core size increase of about 5 % in S_1. Using published results of molecular orbital calculations, we can rationalize part of the observed structural changes. For this it is important to include all four orbitals of Gouterman's model to describe the electronic transition to S_1. These calculations also predict a very small D_{2h} distortion of the macrocycle. The triplet spectrum of ZnOEP shows much broader peaks that also after isotopic exchange could not clearly be related to ground state modes. In the ground state, the full

widths at half maximum of most of the modes are about 15 cm^{-1}. In S_1 the widths increase to about 25 cm^{-1} and in T_1, modes with a width of 40 cm^{-1} are observed. We suggest that these linewidth changes are a reflection of the distortions of the porphyrin macrocycle that take place in the excited states. In the S_1 state, the distortion is only small because of the near degeneracy of the a_{1u} and a_{2u} orbital. Configuration interaction then reduces the macrocycle changes that would take place if the transition to the S_1 state could simply be described by one electron promotion. In the T_1 state, configuration interaction is absent, and much larger changes are observed. Resonance Raman spectra of ZnMeOEC are shown in Figure 1b. Analogous to ZnOEP, the spectra reflect the transient species of ZnMeOEC in S_1 and T_1. However, the spectra of S_0 and S_1 are very different. The spectrum of S_1 is dominated by one polarized mode only. Several of the other modes are due to the peripheral ethyl groups. Isotopic exchange will further clarify the mode composition changes. The triplet spectrum shows the peripheral modes and some core modes.

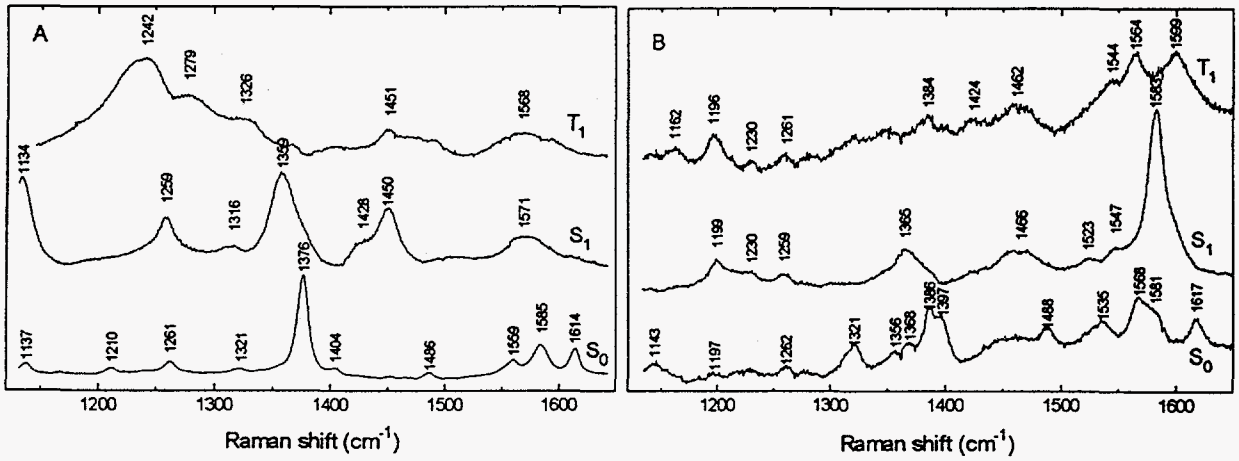

Figure 1: (A) Resonance Raman spectra of ZnOEP in THF obtained at 450 nm of S_0, S_1 and S_2, respectively ; (B) Spectra obtained under the same conditions for ZnMeOEC.

From these data we conclude that reduction of one of the pyrrole rings has a very large influence on the excited state properties. Configuration interaction in the chlorin is smaller because the degeneracy of the e_g orbitals and the near accidental degeneracy of the a_{1u} and a_{2u} orbitals has been lifted. Apparently the energy barriers between the different conformations are larger for ZnMeOEC with fewer dynamic changes of the macrocycle.

Acknowledgments

This work was supported by NIH Grant GM25480.

References

1. J. Rodriguez, C. Kirmaier and D.J. Holten, J. Am. Chem. Soc., 111 (1989) 6500-6506.
2. D.H. Kreszowski, G. Deinum and G.T. Babcock, J. Am. Chem. Soc., 116 (1994) 7463-7464.
3. R.Kumble, G.R. Loppnow, S. Hu, A. Mukherjee, M.A. Thompson and T.G. Spiro, J. Phys. Chem., 99 (1995) 5809-5816.

A Time-resolved Resonance Raman Study of the T_1 State of Free-base Tetraphenylbacteriochlorin

Milton E. Blackwood Jr., Ranjit Kumble, Ching-Yao Lin, Thomas G. Spiro

Department of Chemistry, Princeton University, Princeton, NJ 08544

The T_1 excited State of free-base tetraphenylbacteriochlorin (H_2TPBC) has been studied by nanosecond time-resolved transient absorption spectroscopy (TA) and resonance Raman spectroscopy (TR[3]). The TA spectrum shows a red-shift in the Soret transition as seen for the $^3(\pi,\pi)$ states of other porphyrins and hydroporphyrins. Ground state spectra of natural abundance (NA), *meso*-C-13, phenyl-D_{20}, and pyrrole-D_8 isotopomers of H_2TPBC were acquired with 397 nm excitation from a Nd:YAG laser (Raman-shifted third harmonic in D_2) and are shown in figure 1. Assignments of ground state vibrations were made based on a empirical normal coordinate analysis. Spectra for the first triplet state of H_2TPBC are shown in figure 2 for the same isotopomers. To obtain the difference spectra shown a probe only spectrum (397 nm) was subtracted from a pump/probe spectrum (532 nm pump). The probe pulse was delayed by 25 ns in the spectra shown but experiments at longer delays were performed to insure that singlet state features were not being observed.

Large shifts are seen in vibrational modes associated with skeletal stretching modes in the T_1 spectrum of H_2TPBC. These changes suggest that significant structural distortion is occurring in the T_1 state. Modes associated with $C_\alpha C_m$ bond stretching show different shift patterns; ν_{10} and ν_{28} both upshift while ν_{19} downshifts. Bond order changes expected for the formation of the triplet state show that the $C_\alpha C_m$ bonds adjacent the pyrrole rings contract and those next to the other two pyrrole expand suggesting some mode localization for these bonds in the T_1 state[1]. Also ν_4, a $C_\alpha C_\beta$ and $C_\alpha N$ stretching mode downshifts in the T_1 state consistent with the expected bond order changes.

Isotope shift patterns, though mostly similar, differ somewhat in the T_1 state compared to the ground state. This suggest that the mode composition of H_2TPBC changes in the T_1 state. Also, no enhancement of phenyl substituent vibrations are observed in the T_1 state in contrast to tetraphenylporphyrins (TPPs).

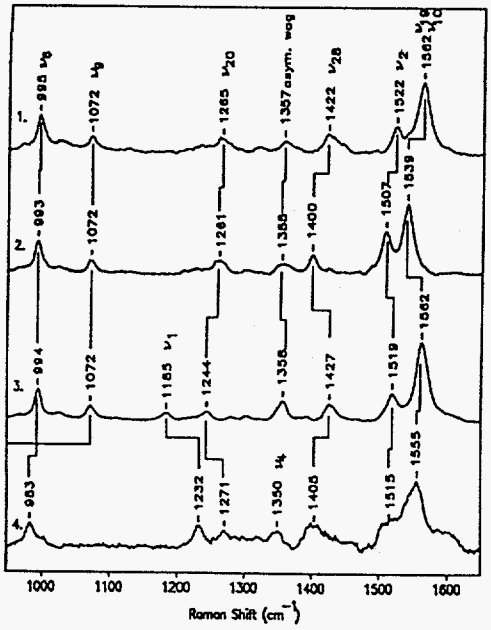

Figure 1: Ground State RR of H2TPBC

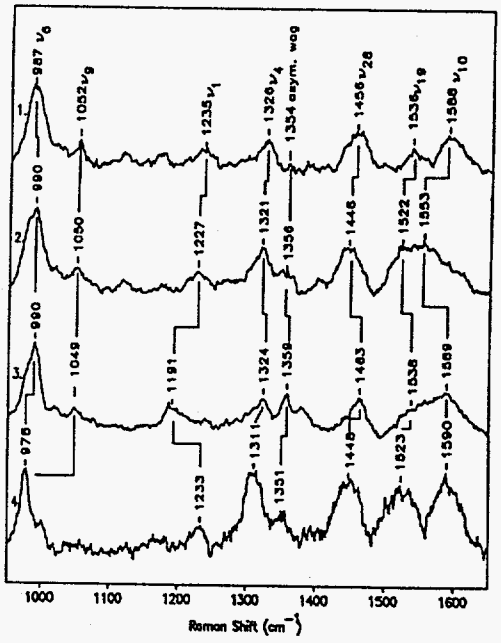

figure 2: RR Spectra of T_1 state of H2TPBC

1. Sekin, H., Kobayashi, H., J. Phys. Chem. 86 (9), 5045-5052

Femtosecond Transient-Absorption Spectroscopy of the Solvated Electron in Alcohols

C. Silva, P. K. Walhout, P. J. Reid, D. Huppert,† and P. F. Barbara
Department of Chemistry, University of Minnesota, Minneapolis, MN 55455, USA
†Permanent Address: Beverly and Raymond Sackler Faculty of Exact Sciences, School of Chemsistry, Tel-Aviv University, Ramat Aviv, Tel Aviv 69978, Israel

We present direct femtosecond near-infrared pump-probe transient experiments on the equilibrated solvated electron in alcohols. Excess electrons are generated with an ultraviolet (UV) pulse by photodetachment from solutes such as iodide or α-naphtholate. After relaxation to the ground-state and equilibration, s-state electrons are promoted to the excited p-states via a pump pulse (780 nm). The subsequent spectral dynamics are probed with a tunable pulse (400 nm - 1100 nm).

The ΔO.D. spectrum of the solvated electron in methanol is presented in Figure 1 at various delays between the pump and probe pulses. Throughout the spectrum, large changes in optical density are observed in a subpicosecond time scale. Additional evolution occurs with a time constant of 8-10 ps. Finally, a permanent bleach is observed at all wavelengths, caused by the reaction of excited-state excess electrons with the solvent.

We have investigated the dynamics of excess electrons in the alcohols methanol, ethanol, propanol, butanol, octanol, and ethylene glycol. In each of these solvents the data displays a fast, ~0.5 ps component, followed by a longer component, which becomes longer in slower relaxing solvents. The time constant of the latter component is roughly proportional to the longitudinal relaxation time in each solvent, and is ascribed to diffusive solvent motion.[1] These results support a previously proposed model in which an excess electron initially promoted to the p-states undergoes rapid internal conversion, followed by ground-state solvation and/or cooling.[2] If this is the case, then although the excited-state lifetime of the excess electron is much shorter than the time scale for diffusive solvation, internal conversion from the excited-state results in energy deposition into these slow relaxing modes.

Transient absorption anisotropy measurements of the solvated electron in ethanol are displayed in Figure 2 probing at 700 nm, 820 nm, and 950 nm. Close comparison of the transients obtained with parallel and orthogonal polarization of the pump beam relative to the probe beam reveals an anisotropic component to the dynamics (Figure 3). At 700 nm the magnitude of the initial bleach is ~17% smaller in the perpendicular transient. At 950 nm, a similar phenomenon is observed: the

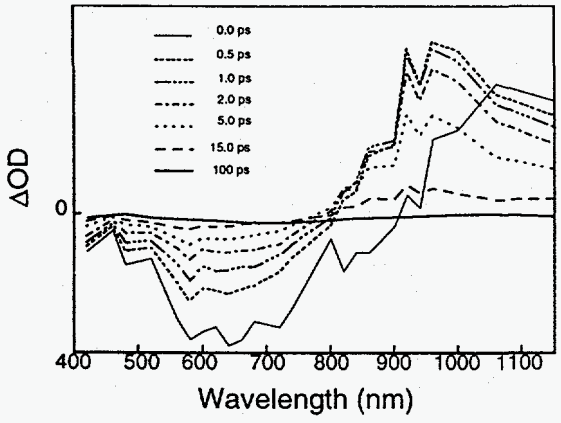

Figure 1. Transient ΔO.D. spectrum of the solvated electron in methanol, showing the spectral evolution after excitation to the p-states and subsequent radiationless transition and equilibration in the ground state. The time delays are given in the figure.

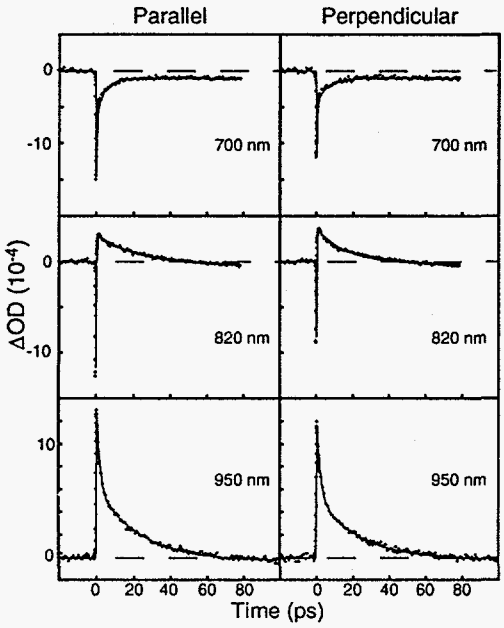

Figure 2. Pump/probe transients of the solvated electron in ethanol with the polarization of the pump parallel (left) and orthogonal (right) to that of the probe. The probe wavelenghts are given in the figure.

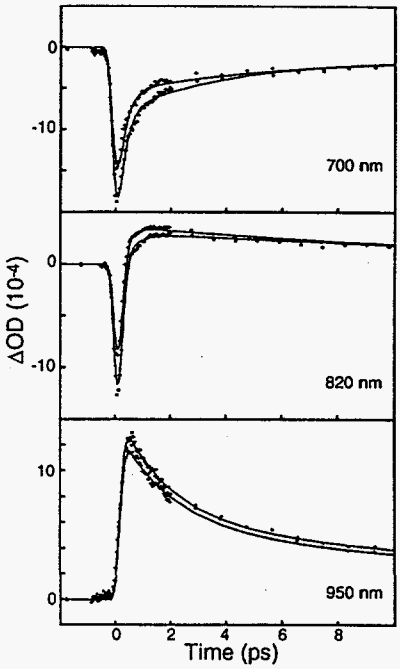

Figure 3. Comparison of the temporal evolution of the pump/probe transients displayed in Figure 2. The parallel transient corresponds to the one with the largest initial bleach or absorption at each wavelength.

initial increased absorption is smaller in the perpendicular transient relative to parallel excitation. Finally, at 820 nm the initial bleach is also greater for parallel excitation. However, as this initial bleach recovers and overshoots to become an increased absorption, the amplitude of the absorptive component is greater for the perpendicular data. This establishes the presence of a negative anisotropy at this wavelength. These observations are qualitatively similar to the results obtained for the solvated electron in water probing at similar regions of the ground-state spectrum.[3]

The presence of an anisotropic component to the dynamics of the solvated electron in ethanol demonstrates that the solvent cavity in which the excess electron resides (which defines the energetics of the orthogonal s-p transitions) is asymmetric (assuming that electronic dephasing is complete).[4] A negative anisotropy at 820 nm suggests the presence of an electronic transition orthogonal to that of the actinic pulse at this wavelength. Overall, these results show that anisotropic solvent fluctuations play an active role in the dynamics of the solvated electron in ethanol.

Acknowledgment

This research was supported by a grant from the Basic Energy Sciences Program of the Department of Energy.

References

1. M. Maroncelli, J. Molec. Liquids, 37 (1993) 1.
2. Y. Kimura, J. C. Alfano, P. K. Walhout, and P. F. Barbara, J. Phys. Chem., 98 (1994) 3450.
3. P. J. Reid, C. Silva, P. K. Walhout, and P. F. Barbara, Chem. Phys. Lett., 228 (1994) 658.
4. K. Wynne and R. M. Hochstrasser, Chem. Phys., 171 (1993) 179.

Ultrafast Measurement of the Electron-Transfer Dynamics in Mixed Valence Metal Dimers

P. J. Reid[1], *C. Silva*[1], *L. Karki*[2], *J. T. Hupp*[2], *and P. F. Barbara*[1]
[1]Department of Chemistry, University of Minnesota, Minneapolis, MN 55455, USA
[2]Department of Chemistry, Northwestern University, Evanston, IL 60208

Recent interest in condensed-phase electron-transfer has focused on the dynamical effect of both nuclear and solvent motion.[1] Mixed valence metal dimers represent an ideal class of compounds in which to develop electron-transfer (ET) theories which incorporate both effects in predicting electron-transfer rates.[2] Here we report the results of femtosecond pump-probe experiments on the back-electron transfer in both Ruthenium-Iron (RuFe) and the Ruthenium-Ruthenium (RuRu) dimers.[3] The chemistry of these compounds (represented by RuRu) is as follows:

$$(NH_3)_5\text{-Ru(III)-NC-Ru(II)-(CN)}_5^- \underset{\text{b-ET}}{\overset{h\nu}{\rightleftharpoons}} (NH_3)_5\text{-Ru(II)-NC-Ru(III)-(CN)}_5^-$$

Photoexcitation initiates the migration of an electron between metal centers with internal conversion from the excited state to the ground state resulting in the back-electron transfer (b-ET). The transient pump-probe signal obtained for RuRu in H_2O with the 20 fs output from a Ti:Sapphire oscillator is presented in Figure 1A. The large, symmetric feature centered at zero time is the coherence coupling signal. This signal follows the instrument response and the ratio of the amplitude of this component to the longer-time features was insensitive to change in the pulse-width suggesting the electronic-coherence decay is extremely rapid (<20 fs).[4] Closer evaluation of the transient (Figure 1B) reveals the presence of a ground-state bleach that evolves into an absorption at later times. Assignment of these components is in accord with our previous analysis.[5]

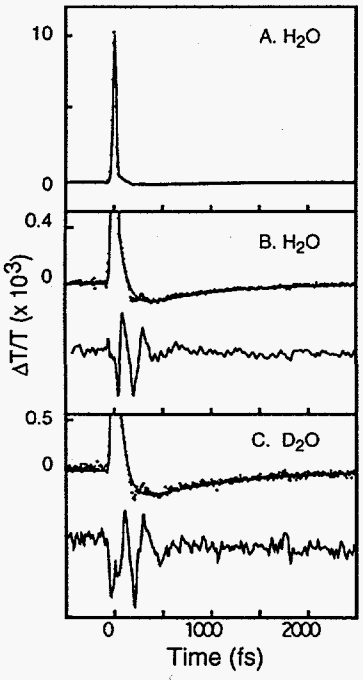

Figure 1. A. Transient absorption of RuRu in H_2O. B.Expansion of A with residual difference between the data and fit at the bottom. C. RuRu in D_2O.

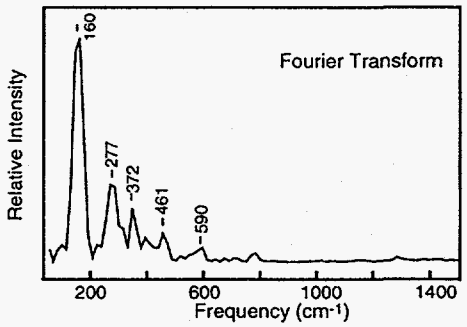

Figure 2. Fourier transform of residual in Fig. 1B.

The ground-state bleach results from photoexcitation with recovery due to internal-conversion from the excited state (i.e. the back-electron transfer). The later-time absorption and decay corresponds to solvation on the ground-state surface following internal conversion to reestablish the pre-excitation equilibrium distribution. Best fit to the data with a biexponential convolved with the instrument response resulted in a b-ET time of 85 ± 10 fs and an absorption decay time of 880 ± 160 fs. Experiments in D_2O (Figure 1C) revealed that the absorption decay time is identical to that in H_2O. However, the b-ET time increases to 122 ± 18 fs. Further experiments were performed which assigned the origin of this deuterium isotope effect to the solvent.[3] Finally, experiments on RuFe in H_2O and D_2O demonstrated that the b-ET transfer time and solvent deuterium isotope effect are almost identical to that of RuRu.[3] These data provide information on the nuclear and solvent motions coupled to the b-ET. The 85-fs b-ET in RuRu coupled with the solvent deuterium isotope effect demonstrate that ultrafast solvent motions are coupled to the b-ET. In particular, the rapidity of the b-ET suggests that the inertial component of the solvation is of mechanistic importance in this electron transfer reaction.[6]

The coherent nuclear response of RuRu is observed in residual difference between the fit and the transient (Figure 1B). Figure 2 presents the Fourier transform of this residual. The frequencies determined from this analysis agree with pervious measurements of the post-resonance Raman spectrum of RuRu demonstrating that this response originates from the solute.[7] This observation combined with the absence of an excited-state absorption in this spectral region indicates that the oscillatory response is due to a displaced ground-state population created by resonant impulsive-stimulated Raman scattering (RISRS). To ascertain the time-scale for vibrational dephasing, the residual was modeled with three components with frequencies corresponding to 170, 280 and 480 cm^{-1} with separate dephasing times. An average vibrational dephasing time of ~300 fs was determined in agreement with the Raman linewidths.[7] If we project a similar vibrational dephasing time in the excited state, the back-electron transfer occurs in a vibrationally coherent fashion consistent with the conclusions of previous time-resolved infrared absorption studies.[8] This result combined with the ultrafast decay of the coherence coupling signal suggests that the electron transfer in RuRu occurs in an electronically incoherent, but vibrationally coherent fashion.

Acknowledgment

This research was supported by the NSF and the donors of The Petroleum Research Fund, administered by The American Chemical Society (PFB) and the DOE (JTH).

References

1. Barbara, P. F.; Walker, G. C.; Smith, T. P. Science, 247 (1992) 975. Maroncelli, M.; MacInnis, J.; leming, G. Science, 256 (1989) 1674.
2. Hush, N. S. Prog. Inorg. Chem., 8 (1967) 391. Walker, G. C.; Akesson, E.; Johnson, A. E.; Levinger, N. E.; Barbara, P. F. J. Phys. Chem., 96 (1992) 3728.
3. Reid, P. J.; Silva, C.; Barbara P.F.; Karki, L.; Hupp, J. T. J. Phys. Chem., 99 (1995) 2609.
4. Cong, P.; Yan, Y. J.; Deuel, H. P.; Simon, J. D. J. Phys. Chem., 100 (1994) 7855.
5. Tominaga, K.; Kliner, D. A. V.; Johnson, A. E.; Levinger, N. E.; Barbara, P. F. J. Chem. Phys., 98, (1993) 1228.
6. Bader, J. S.; Chandler, D. Chem. Phys. Lett., 157 (1989) 501. Maroncelli, M. J. Molec. Liquids, 57 (1993) 1.
7. Doorn, S. K.; Blackbourn, R. L.; Johnson, C. S.; Hupp, J. T. Electrochimica Acta., 36 (1991) 1775.
8. Doorn, S. K.; Dyer, R. B.; Stoutland, P. O.; Woodruff, W. H. J. Am. Chem. Soc., 115 (1993) 6398.

Photo-initiated Electron Transfer Reactions Studied by TR^3 Spectroscopy

A.W.Parker[1] D.Phillips[2], M.Towrie[1], P.Matousek[1], E.Vauthey[3],

[1]Central Laser Facility, Rutherford Appleton Laboratory, Chilton, Didcot, Oxfordshire, OX11 0QX, UK
[2]Department of Chemistry, Imperial College of Science and Technology and Medicine, London, SW7 2AY, UK
[3]Institute of Physical Chemistry, University of Fribourg Pérolles, CH-1700 Fribourg, Switzerland

Electron transfer (et) processes are of paramount importance in chemistry and in nature, and the enhancement of oxidation potentials in electronically excited states of molecules makes excited state electron transfer of especial interest and relevance to a range of diverse fields, ranging from photosynthesis to imaging technologies. To date much experimental work has been devoted to understanding the dynamics of photoinduced et reactions. The et pathway involves the formation of several intermediates, in particular the exciplex and the geminate ion pair. The general mechanism involves interactions between the excited state acceptor/donor and ground state donor/acceptor molecules which eventually leads to solvated free ions or, as is more often the case, the intermediates relax by returning to their initial states. We have successfully applied ns-TR^3 to elucidate the structure of the geminate ion pair and quantified the energetics for the formation of solvated free ions from this species[1,2]. This work studied the geminate ion pair formed within the reaction of triplet anthraquinone (AQ) and 1,2,4-trimethoxybenzene (TMB) in a medium polar solvent (1,1,2,2 tetrachloroethane,TCE);

$$^3AQ + TMB \rightarrow {}^3(AQ\text{--}TMB) \rightarrow {}^3(AQ^{\cdot-}\text{--}TMB^{\cdot+}) \xrightarrow{separation} AQ^{\cdot-} + TMB^{\cdot+}$$

and showed that the ions within the ion pair are **not** solvent separated. The centre-to-centre interionic distance is 7.5 Å and the activation barrier for ion separation is 0.04 eV. This corresponds to the amount of energy required to overcome electrostatic stabilisation and increase the distance between the ion pair to 9.5 Å allowing a solvent molecule to penetrate between the ions. We are now continuing this work by investigating other donor/acceptor geminate ion pairs and moving into the ps time domain. The faster time resolution will not only test out et. theories in the more polar environments but also investigate singlet state et reactivity and intramolecular et reactions. The latter being of particular interest in determining whether or not there are any structural differences in the intermediates produced from excitation of a ground state charge transfer complex and a diffusion encounter complex. Benzophenone (BP) and 1,4-diazabicyclo[2,2,2]octane (DABCO) have been well studied by transient absorption spectroscopy and we present preliminary ns and ps TR^3 results for this system.

Nanosecond TR^3 The following reaction was studied in both acetonitrile and TCE;

$$BP \xrightarrow{h\nu,308nm} {}^1BP \xrightarrow{isc} {}^3BP \xrightarrow{DABCO} {}^3(BP^{\cdot-}\text{--}DABCO^{\cdot+}) \rightarrow BP^{\cdot-} + DABCO^{\cdot+}$$

In acetonitrile no time dependent spectral band shift was observed. However, in TCE, illustrated in Fig. 1, the *c.* 1390 cm^{-1} band does show a slight shift from 1386 cm^{-1}, to 1382 cm^{-1} respectively at 0 and 30 ns pump/probe delay times. It is of particular note that the peak shifts from high to low wavenumbers with increase in time delay as this is what is also observed in the AQ/TMB system. We tentatively assign this band as the CO stretch based on the band intensity, the electron being localised on the carbonyl oxygen and Raman spectra of ^{3}BP.[3] The spectral identification of BP$^{\cdot-}$ was confirmed by obtaining BP$^{\cdot-}$ from the addition of

sodium to a solution of BP in tetrahydrofuran which gave a similar Raman spectrum as that illustrated in Fig 1.

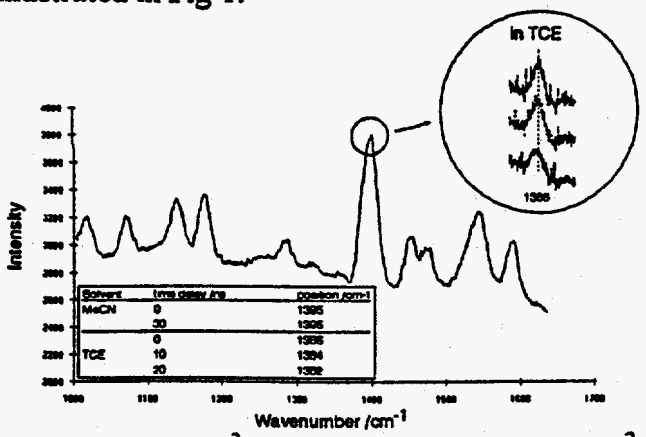

Figure 1: ns-TR^3 spectrum of $BP^{\cdot-}$.; BP ($2x10^{-2}$ M) and DABCO (0.1 M) in acetonitrile. The pump (360 nm) and probe (670 nm) time delay was 0 ns. The spectra were accumulated from 6000 laser shots.

Picosecond TR^3 Fig 2 shows the ps TR^3 spectra obtained from photolysing an acetonitile solution of BP and DABCO. These preliminary results show the Raman spectrum of $BP^{\cdot-}$ to be formed with a grow in time of 140 ps and this indicates that we are observing collisional electron transfer between ^{3}BP and DABCO. If the reaction was occurring from ^{1}BP then we would expect to see a substantial yield of $BP^{\cdot-}$ at times earlier then 50 ps, i.e. the time taken for intersystem crossing to occur from ^{1}BP. This would also be so if the reaction was between a donor/ acceptor complex. Experiments with improved S/N and resolution are necessary to investigate the subtle peak changes already observed using ns time resolution.

CONCLUSIONS

Our initial findings for BP/DABCO indicate that the geminate ion pair is of similar structure to the AQ/TMB system i.e. a loose ion pair (probably not solvent separated), the peak shift indicating a change in $BP^{\cdot-}$ environment as the ion changes from within the geminate ion pair to solvated ions. This conclusion is different from that obtained for BP and dimethylamine (Mataga *et al.*)[4] and BP and DABCO in acetonitrile (Peters *et al.*)[5] who concluded, from ps fluorescence and transient absorption studies that the geminate ion pair is solvent separated. We are confident that we can now apply ps TR^3 to investigate electron transfer reactions and are currently modifying the setup to investigate the BP and DABCO system in TCE where the quantum yield of solvent separated radical ion formation will be much less and require higher sensitivity/resolution.

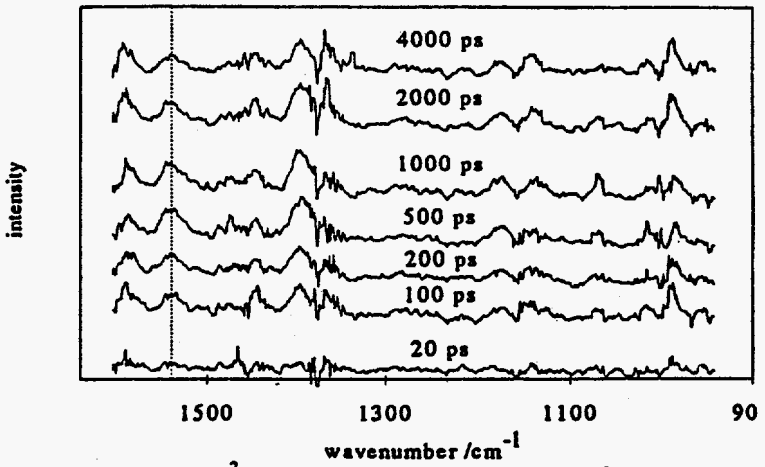

Figure 2: ps TR^3 spectrum of $BP^{\cdot-}$ obtained from photolysing a solution of BP (0.16 M) in the presence of DABCO (0.4 M) in acetonitrile. The pump and probe wavelengths were 328 and 655 nm respectively.

References

1 E. Vauthey, D. Phillips and A. W. Parker, J. Phys. Chem. 96 (1992) 7356.
2 E. Vauthey, A. W. Parker, B. Nohova and D. Phillips, J.Am. Chem. Soc. 116 (1994) 9812.
3 T. Tahara, H. Hamaguchi and M. Tasumi, Chem. Phys. Lett. 152 (1988) 135.
4 H. Miyasaka, K. Morita, K. Kamada and N. Mataga, Bull. Chem. Soc. Japan 63 (1990) 3385.
5 K. S. Peters and J. Lee, J. Phys. Chem. 91 (1993) 3761.

The Role of Conformation in the Ordering of Excited Electronic States: Picosecond Transient Raman Studies of Diphenylbutadiene and Its Structural Analogues

Daniel L. Morris, Jr., and Terry L. Gustafson
Department of Chemistry, The Ohio State University, 120 West 18th Avenue, Columbus, OH 43210

One of the fundamental issues in chemistry is the relationship between chemical structure and chemical reactivity. We are using picosecond transient Raman spectroscopy to probe the way that structure affects chemical reactions in the excited state.[1,2] In particular we are studying the photoisomerization of diphenylbutadiene (DPB) in the first excited electronic state. The photophysics of DPB provides a unique probe of how state ordering and conformation influence chemical reactivity. The two lowest excited states in DPB, the 2^1A_g and 1^1B_u states, are believed to be virtually degenerate. One- and two-photon absorption studies suggest that the 2^1A_g state of DPB is the lowest excited singlet state. However, emission studies of DPB indicate that the lowest excited singlet state is the 1^1B_u state. The photophysics and S_1 lifetime of DPB are dependent on temperature, solvent viscosity, and solvent polarity. On the basis of the solvent and temperature dependence of the transient absorption spectra of DPB and rigid s-*cis* and s-*trans* analogs, Wallace-Williams *et al.* propose that s-*cis* rotamers contribute significantly to the excited state spectra of DPB when excited at the extreme red edge of the ground state absorption band.[3,4] They also demonstrate the absence of anomalous rise time variations across the transient absorption spectrum, indicating that only one electronic state gives rise to the transient absorption spectrum of DPB in solution.

We have recently presented picosecond transient Raman spectra of 1,4-diphenyl-1,3-butadiene (DPB).[1,2] We observe bands that arise from both the 2^1A_g and 1^1B_u states and suggest that we are observing a "mixed state" (*i.e.* a single electronic state that exhibits both 2^1A_g and 1^1B_u character). We also observe unusually broad (>50 cm^{-1}) features in the 1250 and 1650 cm^{-1} regions of the transient Raman spectra. In Figure 1, we plot the S_1 Raman spectra of DPB in the linear alkanes from pentane to dodecane using a 630 nm probe at a 20 ps delay. We observe systematic changes in the relative intensities of the 1250 and 1650 cm^{-1} regions as the solvent is varied from pentane to dodecane. The feature at 1250 cm^{-1} contains several overlapping

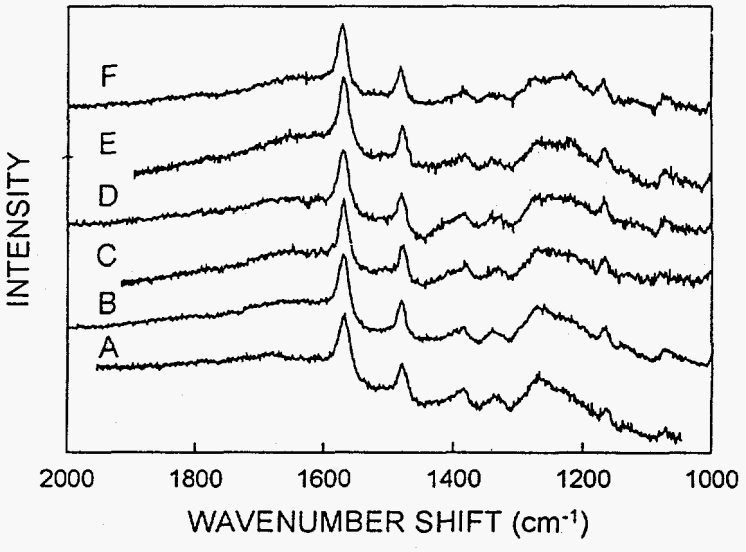

Figure 1: S_1 Raman spectra of DPB in the linear alkanes, (A) Pentane, (B) Hexane, (C) Heptane, (D) Octane, (E) Decane, and (F) Dodecane. Pump: 305 nm; Probe: 630 nm; Delay: 20 ps.

bands. We have fit this feature to a minimum of three Lorentzian bands at ~1238, ~1269, and ~1294 cm^{-1} and assigned them to motions involving the olefin portion of the molecule. We also assigned the 1650 cm^{-1} entity to a $C_o=C_o$ stretch. We suggest that the changes in the relative intensities of the 1250 and 1650 cm^{-1} regions in S_1 DPB as the solvent is varied reflects a viscosity-dependent distribution of s-*trans* conformers that ultimately affects the mixing of the 2^1A_g and 1^1B_u states.

In order to test this interpretation, we have obtained the S_1 Raman spectra of several analogues of DPB, including 1,4-diphenyl-1,3-cyclopentadiene (DPCP), a "stiff" s-*cis* analogue. In Figure 2 we compare the S_1 Raman spectra of DPB and DPCP in hexane at two probe wavelengths at a delay of 20 ps. We note that excitation of DPB at 305 nm only excites ground state s-*trans* conformers. We note the absence of any broad features in the DPCP spectrum and conclude that the broad features in the DPB spectra arise from a distribution of s-*trans* conformers in solution. These results have also been confirmed by examining the spectra of other phenyl substituted and "stiff" DPB analogues, including tetraphenylbutadiene and tetraphenylcyclopentadiene.

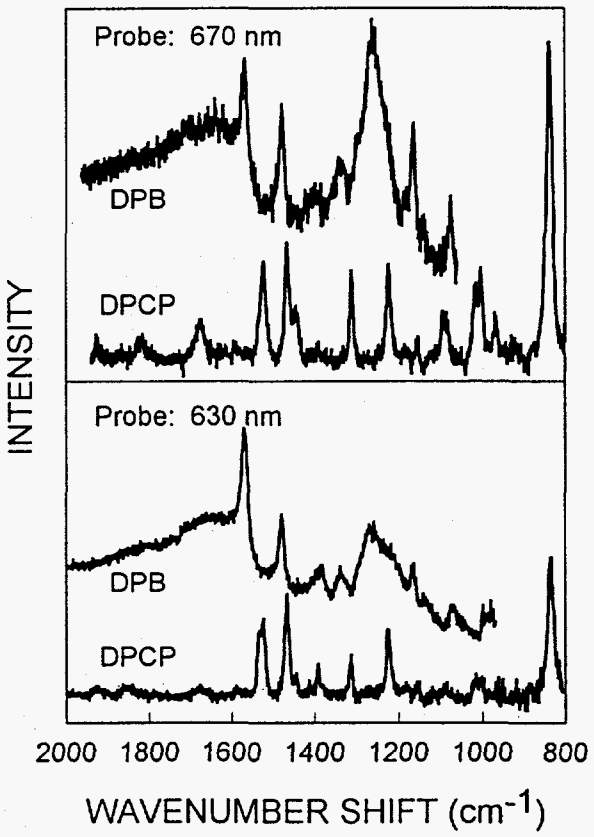

Figure 2: S_1 Raman spectra of DPB and DPCP in hexane. Pump: 305 nm; Delay: 20 ps.

References

1. D. L. Morris, Jr., and T. L. Gustafson, *J. Phys. Chem.*, 98 (1994) 6725.
2. D. L. Morris, Jr., and T. L. Gustafson, *Appl. Phys. B*, 59 (1994) 389.
3. S. E. Wallace-Williams, S. Moller, R. A. Goldbeck, K. M. Hanson, J. W. Lewis, W. A. Yee, and D. S. Kliger, *J. Phys. Chem.*, 97 (1993) 9587.
4. S. E. Wallace-Williams, B. J. Schwartz, S. Moller, R. A. Goldbeck, W. A. Yee, M. A. El-Bayoumi, and D. S. Kliger, *J. Phys. Chem.*, 98, (1994) 60.

Resonance Raman Investigation of the Radical Cation of 1,3–Butadiene

Tamás Keszthelyi, Robert Wilbrandt
Department of Environmental Science and Technology, Risø National Laboratory,
DK–4000 Roskilde, Denmark
Thomas Bally
Institut de Chimie Physique, Université de Fribourg, Pérolles,
Fribourg, Switzerland

INTRODUCTION

Apart from general scientific interest, the properties of radical ions in condensed media are also important in the context of materials science and technology [1,2]. Polyene radical cations have been in the focus of research related to the conductivity of polymers, especially of polyacetylene. Butadiene radical cation, being the smallest member of the family of linear conjugated polyene cations, serves as the prototype of such ions. In the present study we applied the method of radiolytic generation of radical cations in a frozen Freon glass together with resonance Raman spectroscopy to contribute to the characterization of the butadiene radical cation.

EXPERIMENTAL AND THEORETICAL METHODS

Solutions of 1,3–butadiene in the Freon mixture were frozen to form transparent glasses at 77 K, irradiated by ^{60}Co γ–rays and then transferred to a liquid nitrogen cryostat to perform the optical measurements. Resonance Raman spectra were excited at 550 nm in the first absorption band, in resonance with the allowed $1^2A_u \leftarrow 1^2B_g$ electronic transition. Geometry optimizations and the calculation of vibrational frequencies were performed by density functional theory employing unrestricted open-shell wave functions and nonlocal exchange–correlation functionals (UB–LYP level), using the 6-31G* basis.

RESULTS AND DISCUSSION

The Raman spectra of 1,3–butadiene solutions in FM at 77 K prior to γ–irradiation showed several bands due to the matrix material and the neutral ground state of the solute butadiene.

Following γ–irradiation 16 new bands appeared in the Raman spectra of samples of butadiene in the region 200 to 2250 cm^{-1}.

Of the 16 bands observed in the spectrum, 14 could be assigned as fundamentals, overtones and combinations of totally symmetric normal modes of the *s–trans* rotamer. The remaining two bands are identified as fundamentals of the *s–cis* rotamer. This is the first experimental observation of the *s–cis* rotamer of the butadiene radical cation. The assignment was assisted by theoretical calculations of harmonic vibrational frequencies (DFT UB–LYP/6-31G*), which yield excellent agreement with the experimental values.

The spectrum of the *s–trans* rotamer shows the characteristics of Franck–Condon scattering, allowing us to draw some conclusions regarding the distortion of the excited state relative to the ground state potential energy surface. The main geometric distortions accompanying the electronic transition under consideration are identified as C–C–C bending and C=C stretching, while no evidence of out–of–plane deformations has been found.

For the *s–trans* rotamer a SQM force field, based on IR active fundamentals of six isotopomers, is available from the literature [3]. It is, however, expected that inclusion of the Raman active fundamentals observed in the present work in the scaling procedure would improve the resulting force field. Therefore Resonance Raman spectra of three deuterated isotopomers of butadiene radical cation have also been recorded, and these data are currently used in the fitting of a force field based on both infrared and Raman spectra.

Owing to the sensitivity and selectivity provided by the resonance effect, resonance Raman spectroscopy is a very well suited method for the investigation of radical cations, which usually absorb at longer wavelengths then the corresponding neutrals. We have further demonstrated the power of this technique by applying it to the study of the butadiene radical cation.

References

1. Ed.A.Lund, M.Shiotani, Radical ionic systems, properties in condensed phase, (Kluwer Academic Publishers, Dordrecht, 1991).
2. T. Shida, Electronic absorption spectra of radical ions (Elsevier, Amsterdam, 1988).
3. W.Tang, X–L.Zhang and T.Bally, J. Phys. Chem. 97 (1993) 4373.

Anti-Stokes Picosecond Time-Resolved Resonance Raman Spectroscopy in the Study of Singlet Excited *trans*-Stilbene

P.Matousek[1], D.L.A.de Faria[2], R.E.Hester[2], J.N.Moore[2], A.W.Parker[1], W.T.Toner[1], M.Towrie[1]

[1]Central Laser Facility, Rutherford Appleton Laboratory, Chilton, Didcot, Oxfordshire, OX11 0QX, UK

[2]Department of Chemistry, University of York, Heslington, York, YO1 5DD, UK

INTRODUCTION

Mode-specific, solvent-dependent changes in the time-resolved resonance Raman (TR^3) spectrum of photoexcited S_1 *trans*-stilbene, *t*S, occurring on a *c.* 10 ps timescale following photoexcitation, have recently been reported by ourselves and others [1]. We now report measurements of the anti-Stokes (AS) spectrum of S_1 *t*S up to the band arising from the C=C olefinic stretching mode of *t*S at *c.* 1570 cm^{-1}. Further details have been reported elsewhere [2]. An independent observation of AS S_1 *t*S spectra has also been reported by Jean *et al.* [3].

RESULTS AND DISCUSSION

The apparatus has been described earlier [1]. The AS TR^3 spectra of S_1 *t*S in methanol (Fig. 1) shows several bands which are prominent at the early time delay, but which decrease in relative intensity at later times (i.e. 1570, 1240 and 1180 cm^{-1}). The time dependence of

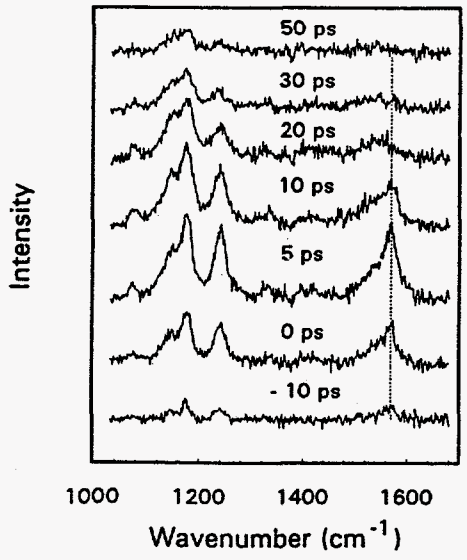

Figure 1: AS TR^3 spectra of photoexcited S_1 *t*S (1 mM) in methanol (16 °C) at different pump/probe time delays. The pump and probe wavelengths were 305 and 610 nm, respectively.

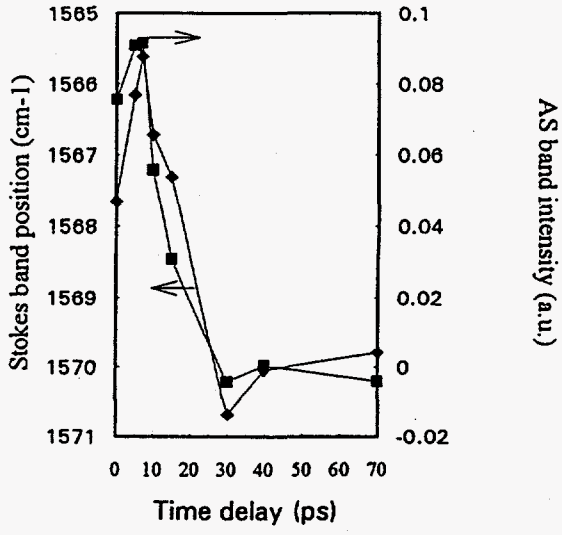

Figure 2: Comparison of the time dependencies reported earlier for the S_1 *t*S Stokes 1570 cm^{-1} band position with the newly observed normalised 1570 cm^{-1} AS band intensity. Pump/probe wavelengths were 295/590 nm; *t*S (1 mM) in n-hexane.

the AS 1570 cm^{-1} band intensity normalised to the integrated area of the *c.* 1530 and *c.* 1570 cm^{-1} Stokes bands is seen to decay with a characteristic timescale of *c.*10 ps and relaxation is virtually complete by 50 ps. This is similar in behaviour to the band position and bandwidth changes observed earlier in the Stokes region (see Fig. 2) [1]. Similar AS spectra were also observed in n-hexane, carbon tetrachloride, acetonitrile, and trichlorotrifluorethane, and with perdeuterated *t*S. Measurements in n-hexane and methanol showed that the AS 1570 cm^{-1} band position is temperature dependent (see Fig. 3).

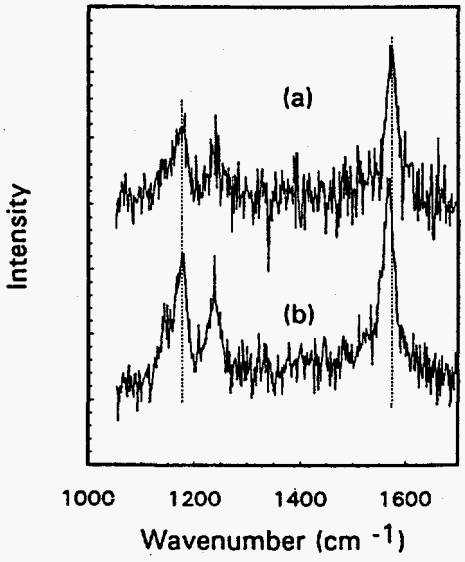

Figure 3: AS TR^3 of S_1 *t*S (1 mM) in n-hexane at 5 ps time delay at temperatures (a) -60 °C and (b) 16 °C showing the position change of the 1570 cm^{-1} band with temperature. The pump and probe wavelengths were 305 and 610 nm, respectively.

The AS spectra indicate the formation of vibrationally excited ($v > 0$) S_1 *t*S at short pump-probe delay times. However, the populations of the excited vibrational levels at early times cannot be deduced directly from the changes in the AS/S intensity ratios between early and late times because the Raman excitation profiles may change during the relaxation process. This may contribute to the anomalous effect demonstrated in Fig. 1, where the 1570 cm^{-1} band is not observed in the AS spectrum at 50 ps but the neighbouring 1530 cm^{-1} band is seen. We estimate the AS/S intensity ratio of the 1530 cm^{-1} band at 50 ps to be at least 150 times greater than that calculated from Boltzmann factors. Whatever its precise origin, the magnitude of the AS signal and its rapid change with time requires a re-examination of the mechanism producing the time-dependent changes in the Stokes spectrum reported earlier [1]. In the case of modes having significant anharmonicity, true band position and bandwidth changes in the Stokes spectrum will result in part from the superposition of time-dependent Stokes $v = 1$ to $v = 2$ hot bands which might reasonably be supposed to have intensities similar to those of the AS $v = 1$ to $v = 0$ bands since both sets of bands arise from population of the $v = 1$ level. A detailed analysis of the 1570 cm^{-1} region of the Stokes spectrum suggests that a part of the time-dependent effects seen previously may arise from this cause [2]. However, another mechanism is required to account for the temperature dependent shift in the position of the 1570 cm^{-1} AS band shown in Fig. 3. This shift is comparable to the temperature-dependent shift in the S_1 Stokes spectrum reported previously [1]. Smaller temperature-dependent shifts have also been observed in ground state spectra of *t*S [4].

References

1. R.E.Hester, P.Matousek, J.N.Moore, A.W.Parker, W.T.Toner, M.Towrie, Chem.Phys.Lett. **208** (1993) 471 and references therein.
2. P.Matousek, A.W.Parker, W.T.Toner, M.Towrie, D.L.Faria, R.E.Hester, J.N.Moore, Chem.Phys.Lett. **237**, (1995) 373.
3. J.Qian, S.L.Schultz, J.M.Jean, Chem.Phys.Lett **233** (1995) 9.
4. W.T.Toner, R.E.Hester, P.Matousek, J.N.Moore, A.W.Parker, M.Towrie, in Time-Resolved Vibrational Spectroscopy VI, Springer Proceedings in Physics 74, Ed. A.Lau, F.Siebert and W.Werncke (Springer-Verlag, New York, 1994) 115.

Resonance Raman Spectra from Non-Stationary States: Picosecond Transient Raman Spectra of *trans*-4,4'-Diphenylstilbene

James D. Leonard, Jr., Lisa A. Huston, and Terry L. Gustafson
Department of Chemistry, The Ohio State University, 120 West 18th Avenue, Columbus, OH 43210

We and others have shown that picosecond transient Raman provides information about solute-solvent interactions [1]. An advantage of time-resolved Raman spectroscopy is that it provides mode-specific information about the probe molecule so that solvent induced structural effects may be observed. Two types of effects are observed in these studies. "Static" effects are manifested as changes in the bandwidth, peak position, and relative intensities of certain bands in different solvents. "Dynamic" effects are changes in bandwidth, peak position, and relative intensity that are observed as the time delay is varied. The transient spectra provide sensitive vibrational markers for these interactions. It is now well established that the dynamical changes in the peak position and bandwidth arise from vibrational relaxation [2]. Dynamical changes in relative intensities, beyond those associated with population relaxation, are observed only in certain molecules. One molecule that exhibits dynamical changes in relative intensities is *trans*-4,4'-diphenylstilbene (DPS) [3]. In order to probe the origin of the relative intensity changes, we have obtained the time-resolved resonance Raman spectra of S_1 DPS at several different pump/probe wavelength combinations.

In Figure 1 we compare the S_1 Raman spectra of DPS in dioxane and methylene chloride pumped at 310 nm and probed at 630 and 660 nm. These spectra have been normalized to the 1185 cm^{-1} as described previously [3]. We note that the relative intensities of several bands are enhanced in the 660 nm spectrum relative to the spectrum acquired with a probe wavelength of 630 nm. We have observed that the peak position shift with delay is independent of probe wavelength, but it does depend on the pump wavelength. This is consistent with the interpretation that peak position change with delay is evidence for vibrational relaxation. Changes in the relative intensities with delay are observed in DPS. We have assigned this to conformational relaxation in the molecule. The relative intensity changes are only slightly dependent on the pump wavelength for certain bands, but are strongly dependent on the probe wavelength. We attribute the

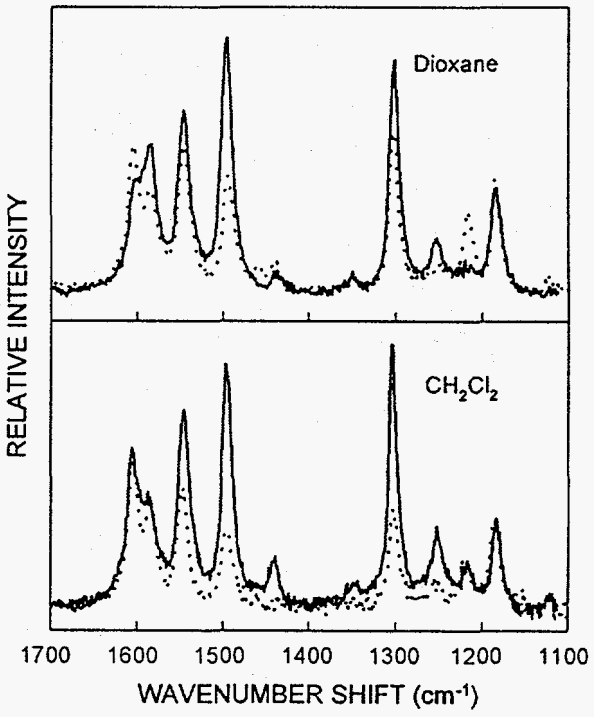

Figure 1: Probe wavelength dependence of the S_1 Raman spectra of DPS. 630 nm probe (dashed line); 660 nm probe (solid line).

change in relative intensities to a change in the Franck-Condon overlap between S_1 and S_n as the nuclear coordinates relax to their optimum geometry in S_1. In other words, the resonance enhancement of the S_1 vibrational bands changes with time as the S_1 potential energy surface evolves with time delay.

In Figure 2, we demonstrate that the dynamics of the intensity changes for the olefin band of DPS is comparable to the vibrational relaxation dynamics when examined with a probe wavelength of 660 nm (Plot A). However, we note that at a probe wavelength of 630 nm the relative intensity dynamics do not follow those of the peak position change (Plot B). The picture that emerges is that there is a connection between the dynamics of the vibrational relaxation and the conformational dynamics that occur on the S_1 potential energy surface. We suggest that modes involved in exchanging vibrational energy with the solvent involve the same nuclear coordinates along which geometric relaxation occurs in S_1 DPS. These are likely the torsional coordinates involving the phenyl-phenyl twist in DPS. These studies demonstrate the power of having independently tunable pump and probe wavelengths for unraveling the dynamical processes in transient Raman spectroscopy.

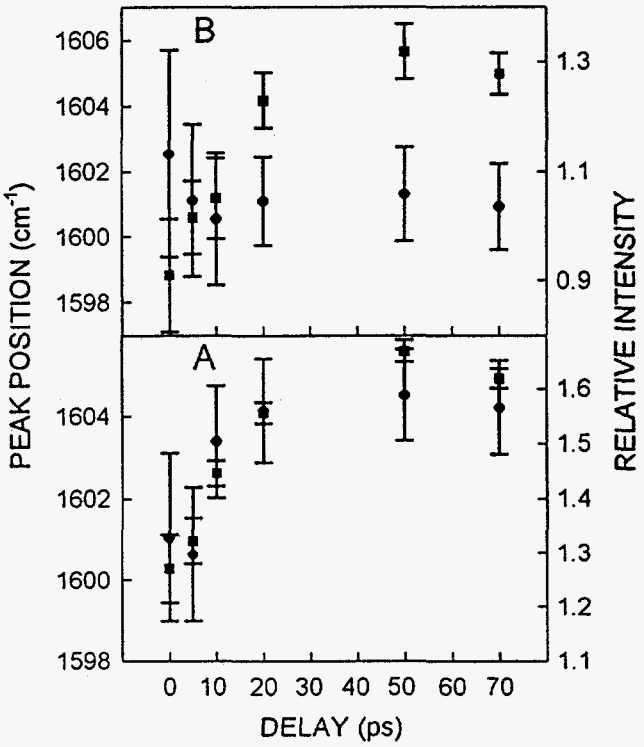

Figure 2: Comparison of the vibrational and conformational relaxation rates for the olefin stretch of S_1 DPS. Peak position shift (■, left axis) and relative peak intensity (●, right axis) versus time delay at probe wavelengths of 660 nm (A) and 630 nm (B). Pump wavelength: 287 nm.

References

1. H. Hamaguchi and T. L. Gustafson, *Annu. Rev. Phys. Chem.*, 45 (1994) 593.
2. K. Iwata and H. Hamaguchi, *J. Mol. Liq.* (1995) in press.
3. R. M. Butler, M. A. Lynn, and T. L. Gustafson, *J. Phys. Chem.*, 97 (1993) 2609.

Jet-Cooled Fluorescence Spectra and Potential Energy Surfaces of Stilbenes and Cyclic Ketones

J. Laane, W.-Y. Chiang, P. Sagear, and J. Zhang
Department of Chemistry, Texas A&M University, College Station, TX 77843-3255 - U.S.A.

The jet-cooled fluorescence excitation spectra (FES) and dispersed fluorescence spectra of *trans*-stilbene[1] (t-S), 4-methoxy-*trans*-stilbene (MOS), and 4,4′-dimethyl-*trans*-stilbene (DMS) have been recorded and analyzed. The high-temperature vapor-phase and liquid phase Raman spectra of these molecules and *cis*-stilbene have also been recorded, and these were critical for making the vibrational assignments. In each case the primary interest was in identifying the low-frequency vibrational modes, with a particular emphasis on the two phenyl torsions and the ethylinic internal rotation. The latter vibration primarily governs the photoisomerization process. For t-S sufficient data were collected to determine the two-dimensional phenyl torsion potential energy surface and the one-dimensional carbon-carbon double bond torsional potential energy function for both the S_0 and $S_1(\pi, \pi^*)$ states. Several computer programs were written in order to rigorously determine both the kinetic energy and potential energy functions. The barriers to simultaneous phenyl rotation are 3100 cm^{-1} for the ground state and 3000 cm^{-1} for the excited state. The data for the C=C torsion are consistent with a *trans* → *cis* barrier of 48.3 kcal/mole for the S_0 state and a *trans* → twist barrier of 2000 to 3500 cm^{-1} for the S_1 state. Figure 1 shows these potential energy surfaces. The depth of the well for the twisted structure in the S_1 state can not be determined from these data but has been estimated (Lit). For the methoxy compound (MOS) the barrier to simultaneous phenyl torsion for both the S_0 and S_1 state is 2860 cm^{-1}. The C=C torsional barrier for MOS in both the S_0 and S_1 states is approximately 10% higher than that of t-S. The spectroscopic studies of DMS are still at a preliminary stage.

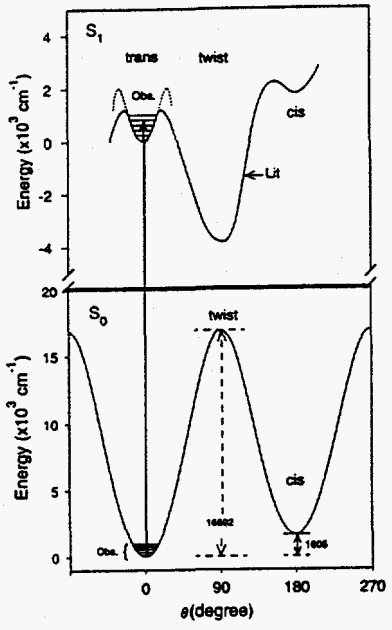

Figure 1. Potential energy functions for the C=C torsion of *trans*-stilbene.

The jet-cooled laser-induced fluorescence excitation spectra of seven cyclic ketones have also been recorded and the carbonyl wagging and out-of-plane ring modes have been analyzed in each case. The barrier to inversion and the wagging angle in the $S_1(n,\pi^*)$ excited state have been found to increase with the ring strain. The molecules studied and their carbonyl inversion barriers are: 2-cyclopentenone[2] (2CP), 0 cm^{-1}; 3-thiacylclopentanone (3TCP), 659 cm^{-1}; cyclopentanone[3,4] (CP), 672 cm^{-1}; bicyclo[3.1.0]hexan-3-one[5] (BCHO), 860 cm^{-1}; 3-cyclopentenone[6] (3CP), 939 cm^{-1}; 3-oxacyclopentanone (3OCP), 1151 cm^{-1}; and cyclobutanone[7] (CB), 2149 cm^{-1}. Figures 2 and 3 show the fluorescence excitation spectrum and carbonyl wagging potential function for the S_1 state, respectively, of 3TCP.

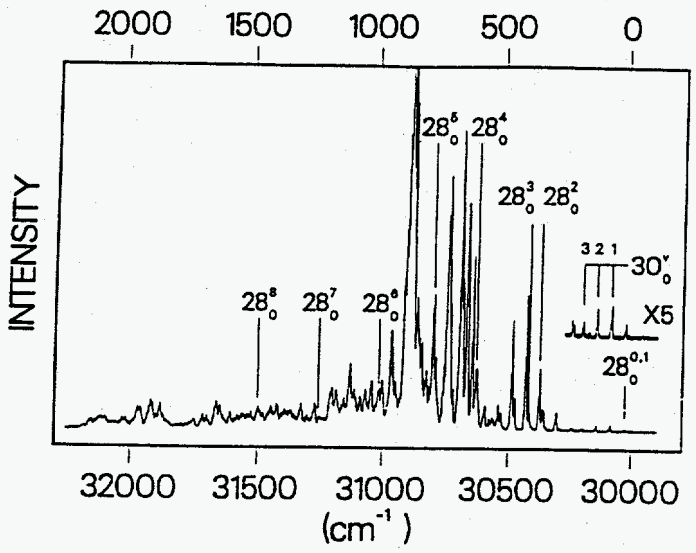

Figure 2. FES of 3TCP

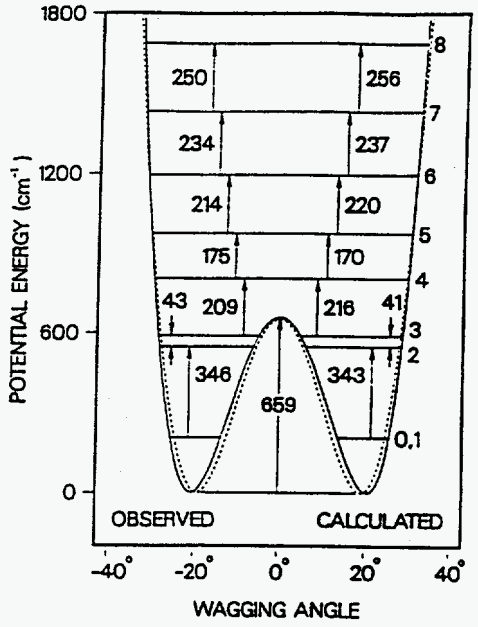

Figure 3. C=O wagging function for the S_1 state

The asymmetry of the potential function for BCHO was found to be surprisingly small. For 2CP the ring-puckering potential energy function becomes more floppy in the S_1 state while for 3CP, BCHO, and CB it becomes considerably stiffer. Two-dimensional potential energy surfaces for the ring-bending and ring-twisting modes of CP in both the S_0 and S_1 states have been determined[4] and found to be fairly similar although in the excited state the energies of the bending saddle points have been substantially lowered.

References

1. W.-Y. Chiang and J. Laane, J. Chem. Phys., **100**, 8755-8767 (1994).
2. C. M. Cheatham and J. Laane, J. Chem. Phys., **94**, 7734-7743 (1991).
3. J. Zhang, W.-Y. Chiang, and J. Laane, J. Chem. Phys., **98**, 6129-6137 (1993).
4. J. Choo and J. Laane, J. Chem. Phys., **101**, 2772-2778 (1994).
5. W.-Y. Chiang and J. Laane, J. Phys. Chem., in press (1995).
6. P. Sagear and J. Laane, J. Chem. Phys., in press (1995).
7. J. Zhang, W.-Y. Chiang, and J. Laane, J. Chem. Phys., **100**, 3455-3462 (1994).

The study of conformations of 1-phenyl- and 2-phenyl-naphtalene in the triplet state by transient absorption and Raman spectroscopies.

R.Bini, S.Corti, P.Foggi, V.Schettino

Dipartimento di Chimica, v. G. Capponi 9 - 50121 Firenze, Italy

G.Buntinx

LASIR, CNRS, USTLFA, bât C5 - 59655 Villeneuve-d'Asq, France

O.Poizat

LMM, CNRS - 94320 Thiais, France

The isomers 1-phenyl-naphthalene (I) and 2-phenyl-naphthalene (II) are known from spectroscopic data (absorption, fluorescence and phosphorescence spectra) and semi-empirical calculations to have different equilibrium geometries in the ground and excited states because of the different steric hindrance experienced by the phenyl ring.[1] Semi-empirical calculations predict that in isomer I the phenyl and the naphthalene planes form an angle of 50° in the ground state and of 30° in the first excited singlet and triplet state. In isomer II the planes form a smaller angle (23°) in the ground state and the molecule becomes almost planar in the S_1 and T_1 states.

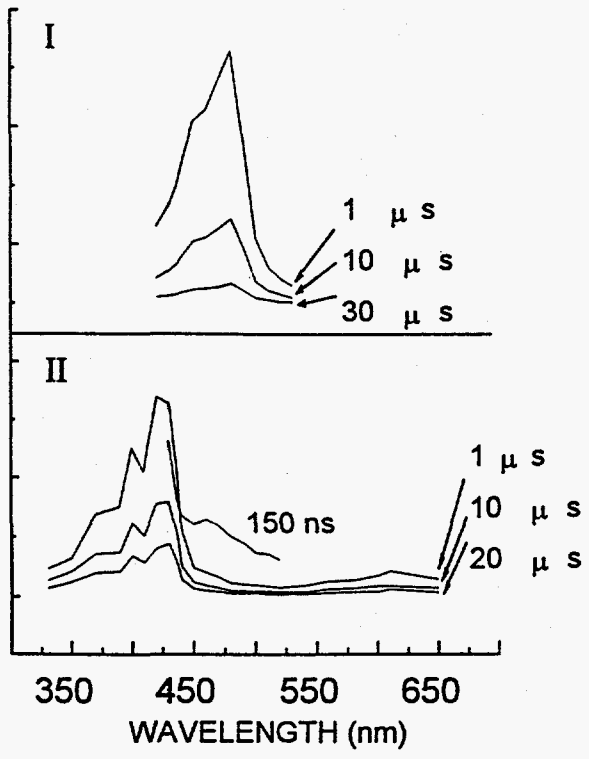

Fig. 1 Transient absorption spectra recorded at different delay times

It can be expected that the different geometries in the T_1 state can cause appreciable differences in the dynamics of the excited states. Therefore a study by transient absorption and transient Raman spectroscopic techniques with nanosecond resolution[2] of the two molecules in various solvents has been undertaken to investigate in more detail the conformation and the relaxation dynamics of the triplet states. In parallel semi-empirical calculations by the QCFF/PI method[3] have been performed in order to estimate the oscillator strength of the $T_n \leftarrow T_1$ transitions and the vibrational frequencies in the T_1 state.

Transient absorption spectra have been recorded in the 350 - 700 nm interval and in the 0-60 μs time range and are shown in Fig. 1. The isomer I shows a structureless absorption band with a maximum around 480 nm while the isomer II shows a more complex spectrum with maxima at 610 nm and 430 nm. This last band shows a well

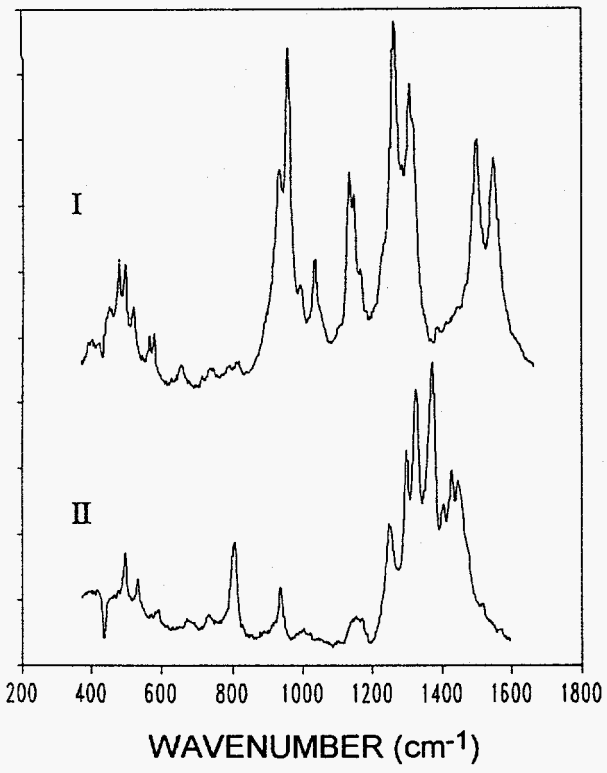

Fig. 2 Transient Raman spectra recorded 1 μs after excitation.

defined progression (see Fig. 1). The dynamics is well reproduced by a double exponential with the first time constant of 4.2 μs for isomer I and 6.8 μs for isomer II. In isomer II it is also possible to observe in the first 200 ns the contribution of the transient absorption from the S_1 state.

Transient Raman spectra have been measured in the 300 - 1800 cm^{-1} range with the probing field in resonance with the main peak of the transient absorption spectra. The transient Raman spectra are shown in Fig. 2. The Raman spectra of the two isomers are similar in the ground state while they show appreciable differences in the T_1 state. The differences in intensity can clearly be ascribed to the resonant character of the spectra in the triplet state. However, the frequency shifts observed for isomer II arise from the different geometry compared to the ground state.

In order to clarify this point we have undertaken some semi-empirical calculations using the QCFF/PI method.[3] The calculations include the evaluation of Franck-Condon factors for the most stable conformation and reproduce satisfactorily the transient absorption spectra of isomer I. The same kind of agreement is obtained for the transient absorption of isomer II from the S_1 state. On the contrary the calculations are unable to reproduce the transient absorption of isomer II from the triplet state. This can be due to the fact that the rotational barrier in the latter case is less pronounced thus making the phenyl rotation almost free. The QCFF/PI method is known to give poor rotational barrier energies. Ab initio calculations are in progress to verify this hypothesis.

Calculations of the ground and T_1 state vibrational frequencies show that modes of isomer II are rather different in the ground and excited state. The Duschinsky matrix contains big off diagonal elements in the region of the 1000 - 2000 cm^{-1} and for the C-H stretching modes. This is in agreement with experiments.

References

[1] K.Gustav, M.Storch, Chem.Phys.Lett. 164 (1988) 237.
[2] G.Buntinx, O.Poizat, P.Valat, V.Witgens, R.Righini, P.Foggi J.Chim.Phys. 90 (1993) 1733.
[3] A.Warshel, M.Karplus J.Am.Chem.Soc. 94 (1972) 5612.

Short-Time Photodissociation Dynamics of Haloiodomethanes from Resonance Raman Spectroscopy

Wai Ming Kwok and David Lee Phillips*
Department of Chemistry, University of Hong Kong
Pokfulam Road, Hong Kong

INTRODUCTION

Iodomethane has long been examined as a prototypical molecule for photodissociation taking place on a repulsive excited electronic state surface.[1-3] While the major features of iodomethane photodissociation in the A-band absorption are fairly well understood, little is known about the photodissociation of closely related molecules like haloiodomethanes. Haloiodomethanes are interesting since one is able to investigate substituent effects on photodissociation dynamics by systematically replacing one hydrogen atom on iodomethane with a halogen molecule. Haloiodomethanes also allow the opportunity to examine weak to strong coupling of two chromophores in a molecule. Using the time-dependent wavepacket approach developed by Heller and co-workers [4] to describe the resonance Raman process, the short-time (~<100 femtoseconds) photodissociation dynamics can be elucidated from interpretation of resonance Raman intensities. We have obtained resonance Raman spectra of chloroiodomethane and diiodomethane in cyclohexane solvent at several excitation wavelengths within the A-band absorption spectra in order to examine the short-time photodissociation dynamics of haloiodomethanes.

RESULTS AND DISCUSSION

Figure 1 shows the resonance Raman spectra excited within their respective A-band absorptions of chloroiodomethane and diiodomethane. These spectra show progressions of fundamentals, overtones, and combination bands of several Frank-Condon active modes for most of the Raman intensity: ν_5 (C-I stretch), ν_4 (C-Cl stretch), ν_3 (CH_2 wag), and ν_2 (CH_2 scissor) for chloroiodomethane and ν_4 (I-C-I bend), ν_3 (I-C-I symmetric stretch), and ν_9 (I-C-I anti-symmetric stretch) for diiodomethane. The time-scale of C-I bond breaking appears to be similar to the vibrational motions of the remaining halomethylene radical so that the short-time photodissociation dynamics of the haloiodomethanes probably cannot be considered psuedodiatomic like iodomethane A-band photodissociation. Simple replacement of one hydrogen atom on methyl iodide with a halogen molecule has a strong substituent effect on the short-time photodissociation dynamics. [5,6] Figure 2 shows a comparison of our 355 nm solution phase diiodomethane resonance Raman spectrum with a 355 nm gas phase spectrum. The gas and solution phase spectra display substantial differences indicating that solvation effects are very important for the short-time photodissociation dynamics. This strong solvation effect on the short-time photodissociation dynamics of diiodomethane is probably due to reduction of symmetry in solution of the two C-I bonds and/or a slower dissociation during

which solvent molecules are not "frozen" during the part of the dissociation to which the resonance Raman scattering is sensitive.[5]

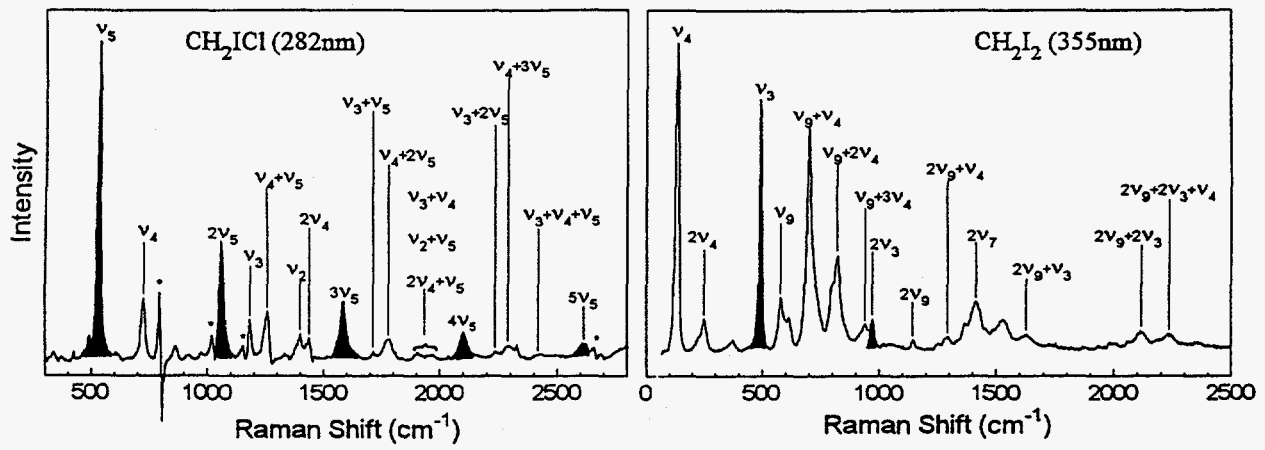

Figure 1: Resonance Raman spectra of chloroiodomethane (282 nm) and diiodomethane (355 nm). The nominal C-I stretch progressions are shaded black. The asterisks mark solvent subtraction artefacts.

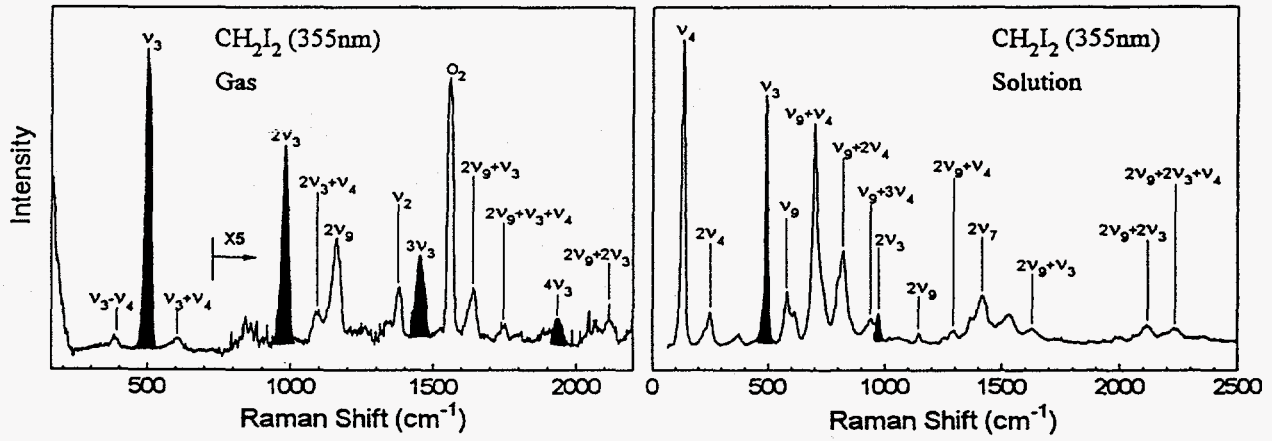

Figure 2: Resonance Raman spectra of gas phase and solution phase diiodomethane with 355 nm excitation. The nominal C-I stretch progressions are shaded black. The asterisks mark solvent subtraction artefacts.

Acknowledgments

This work was supported by grants from the Committee on Research and Conference Grants (CRCG) and the Research Grants Council (RGC) of Hong Kong.

References

1. H. Guo and G. C. Schatz, J. Chem. Phys., 93 (1990) 393.
2. P. G. Wang and L. D. Ziegler, J. Phys. Chem., 97 (1993) 3139.
3. F. Markel and A. B. Myers, J. Chem. Phys., 98 (1993) 21.
4. E. J. Heller, R. L. Sundberg, and D. J. Tannor, J. Phys. Chem., 86 (1982) 1822.
5. W. M. Kwok and D. L. Phillips, Chem. Phys. Lett., 235 (1995) 260.
6. D. L. Phillips and W. M. Kwok, Chem. Phys. Lett., in press.

Hydrogen Transfer Photoreaction of ortho-Nitrobenzylpyridines

Yoshiaki Watanabe and Hiroaki Takahashi
Department of Chemistry, School of Science and Engineering
Waseda University, Tokyo 169, Japan

Benzyl compounds having a nitro group at the ortho-position are known to undergo reversible intramolecular hydrogen transfer of the methylene group by irradiation with UV light. In the case of ortho-nitrobenzylpyridines, such as 2-(2'-nitrobenzyl)pyridine (2,2'-NBP), there are two possible hydrogen accepting sites in a molecule: an oxygen atom of the nitro group and the nitrogen atom of the pyridyl group. The former possibility would generate an aci-nitro acid isomer while the latter an N-H quinoid isomer.

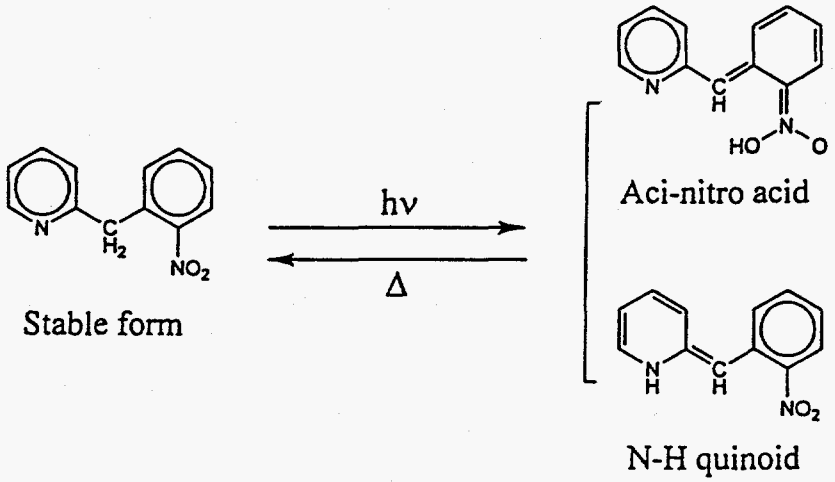

Figure 1: Possible structures of the photolytically produced transient species of 2,2'-NBP.

The purpose of this investigation is to clarify, using nanosecond time-resolved resonance Raman and absorption spectroscopies, which of the two possible hydrogen transfer process is actually occurring in the photoisomerization of ortho-nitrobenzylpyridines.

Laser flash photolysis of 2,2'-NBP and 4,2'-NBP in methanol has revealed that two transients, a short-lived one with the band at 433 nm and a long-lived one with the bands at 588 and 366 nm, were involved in the case of 2,2'-NBP, while three transients, a short-lived one with the band at 431 nm, another short-lived one with the band at 392 nm, and a long-lived one with the bands at 544 and 368 nm, were involved in the case of 4,2'-NBP.

Time-resolved resonance Raman spectra of 2,2'-NBP and 4,2'-NBP in methanol (Fig.2) indicated the following. (1) The 433 nm transient of 2,2'-NBP with the bands at 1513, 1503, 1448 and 1227 cm^{-1}, and the 431 nm transient of 4,2'-NBP, are in the aci-nitro acid structure. Raman bands of the latter transient are not clearly seen in Fig. 2 because of overlapping by the bands of another transient. (2) The 588 nm transient of 2,2'-NBP with the bands at 1640, 1615, 1301 and 1166 cm^{-1}, and the 544 nm transient of 4,2'-NBP with the bands at 1654, 1592 and 1543 cm^{-1} take the N-H quinoid structure. (3) The 392 nm transient of 4,2'-NBP with the bands at 1512, 1440, 1255 and 1104 cm^{-1} is the aci-nitro anion. This transient is identical with that observed in strongly basic solutions of 4,2'-NBP. The

fact that the aci-nitro anion is involved in the photoreaction of 4,2'-NBP but not in that of 2,2'-NBP indicates that the aci-nitro acid of 4,2'-NBP is more strongly acidic than that of 2,2'-NBP.

The spectral changes with time indicate that the hydrogen abstraction of the methylene group occurs in the S_1 state. In the case of 2,2'-NBP a methylene hydrogen atom is abstracted by an oxygen atom of the nitro group generating the aci-nitro acid isomer, and then this hydrogen atom is again abstracted by the nitrogen atom of the 2-pyridyl group to produce the N-H ortho-quinoid isomer. On the other hand, in the case of 4,2'-NBP the firstly generated aci-nitro acid isomer is dissociated into the aci-nitro anion and a proton which is accepted by the nitrogen atom of the 4-pyridyl group to produce the N-H para-quinoid isomer (Fig. 3).

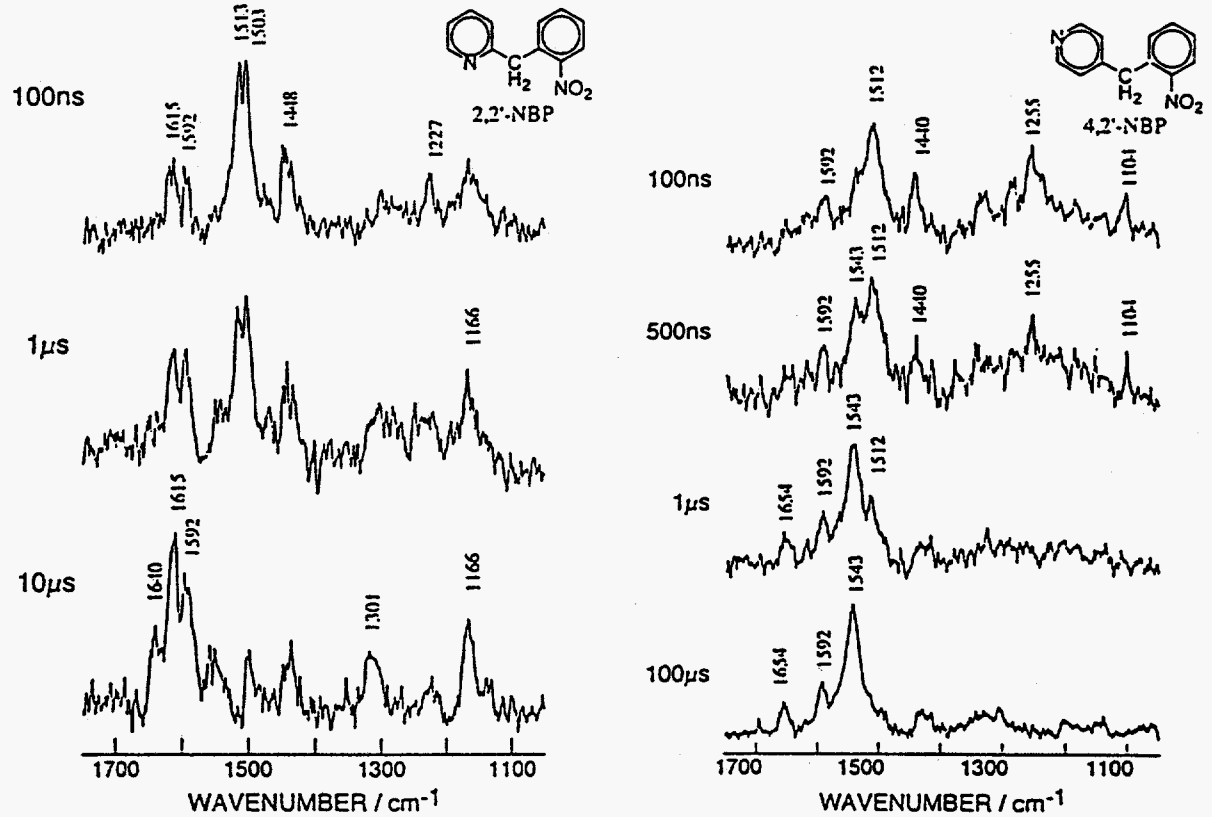

Figure 2: Time-resolved resonance Raman spectra of 2,2'-NBP (left) and 4,2'-NBP(right) in methanol. Concentration, 2.5×10^{-3} mol dm^{-3}. Pump wavelength, 308 nm. Probe wavelength, 390 nm.

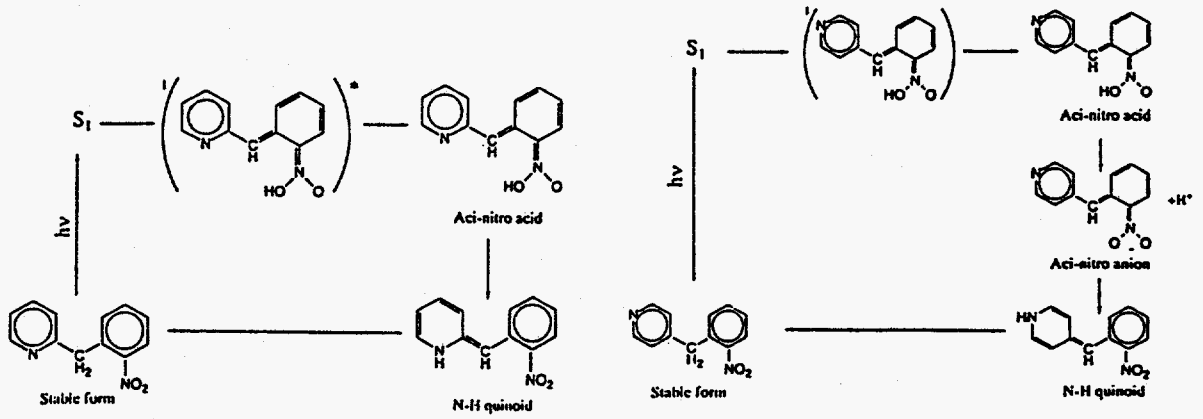

Figure 3: Photochemical reaction scheme of 2,2'- and 4,2'-NBP.

Triplet State Raman Spectra of C_{60} and C_{70}

Sunae Kim[1], Seong Keun Kim[1], Sae Chae Jeoung[2], and Dongho Kim[2]
[1]*Department of Chemistry, Seoul National University, Seoul 151-742, Korea*
[2]*Spectroscopy Laboratory, Korea Research Institute of Standards and Science Taejon 305-600, Korea*

The present study aims to obtain, and identify the features of the triplet state Raman spectra of C_{60} and C_{70} in toluene. Since the increase in cw laser power to populate the excited states often causes the photodegradation as well as the local heating, we employed a nanosecond pump/probe technique to avoid these artifacts.

Fig. 1 presents the time-resolved Raman spectra for the pentagonal pinch mode of C_{60} in toluene with 7 ns delay between pump and probe pulses. The pump pulse at 532 nm and the Raman probe pulse at 416 nm are in resonance with the ground state absorption band and the T_1-T_n absorption band of C_{60} solution, respectively. Since the S_1 state lifetime of C_{60} solution is 1.2 ns at room temperature and the S_1-T_1 intersystem crossing dominates S_1 state decay processes [1], the 7 ns delay was sufficient to probe the triplet state Raman spectrum of C_{60}. The pentagonal pinch mode of the ground state C_{60} in toluene was observed at 1470 cm^{-1} (Fig. 1A). The difference spectrum (Fig. 1C) was obtained by subtracting the ground-state contribution (Fig. 1A) from the pump/probe spectrum (Fig. 1B). A Lorentzian curve fitting of this difference spectrum revealed that the main peak was composed of two Raman bands at 1461 cm^{-1} and 1475 cm^{-1} (Fig. 1C). The intensity at 1475 cm^{-1} was almost five times stronger than that at 1461 cm^{-1}.

Closs et al. [2] reported that the EPR spectrum of $^3C_{60}^*$ has nonvanishing zero-field splitting parameters indicating the loss of spherical symmetry in the triplet state. The symmetry change in the electronically excited molecules usually results in the emergence of silent modes and the splitting of degenerate modes in the ground state. Since the Raman band at 1470 cm^{-1} is totally symmetric and non-degenerate a_g mode, the appearance of the side bands at 1461 cm^{-1} and 1475 cm^{-1} is considered to be the activation of silent modes. Similar results have been obtained in C_{60}^-, substituted C_{60} such as $Pt(PPh_3)_2(\eta^2\text{-}C_{60})$ and $(\eta^5\text{-}C_9H_7)Ir(CO)(\eta^2\text{-}C_{60})$, intercalated C_{60} such as C_{60} · TDAE (tetrakis (dimethylamino) ethylene), and $^{13}C_n{}^{12}C_{60-n}$(n=1,2), in which the symmetry reduction provides more allowed vibrational modes than in the ground state C_{60}.

The intensity ratio of the component bands can possibly be explained in terms of the structural differences between the ground state C_{60} and $^3C_{60}^*$. C_{60} has an icosahedral geometry in the ground state, whereas $^3C_{60}^*$ is thought to have a squashed geometry akin to the ground state C_{70} with D_{5h} symmetry. The pentagons located near the pole of $^3C_{60}^*$ will have a larger surface curvature than those elsewhere. The larger curvature leads to stiffer vibrations along the surface normal and weaker vibrations along the surface tangent. Since the present pentagonal pinch mode is a purely surface tangential mode, we expect the pentagonal pinch motion at the pole area of $^3C_{60}^*$ will be down-shifted, whereas up-shift is observed elsewhere. It is also interesting that the intensity ratio of 1:5 between these two bands may well correlate with the number of polar pentagons and pentagons elsewhere, i.e. 2:10, although the difference in the Raman scattering cross sections between these two classes of pentagons may alter the intensity ratio.

Fig. 2 displays the time-resolved Raman spectra for C_{70} in toluene. Two Raman bands at 1368 cm^{-1} and 1448 cm^{-1} showed 15 cm^{-1} and 16 cm^{-1} down-shifts upon excitation, respectively. Another weak Raman band at 1470 cm^{-1} remained unchanged upon excitation. The overall down-shift in Raman frequencies for C_{70} triplet state is considered to be dominated by the increase in antibonding

character in the electronically excited state as observed in most aromatic molecules.

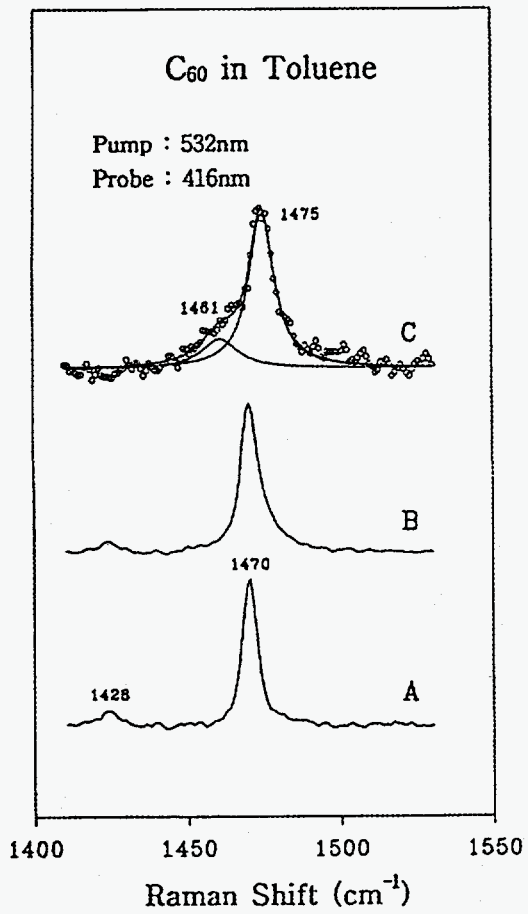

Figure 1. Time-resolved Raman spectra of C_{60} in toluene obtained with 532nm pump and 416nm probe pulses at 7ns time delay; (A) probe only spectrum, (B) pump and probe spectrum, and (C) difference spectrum (B-A) with a subtraction factor. Lorentzian curve fitting is also presented.

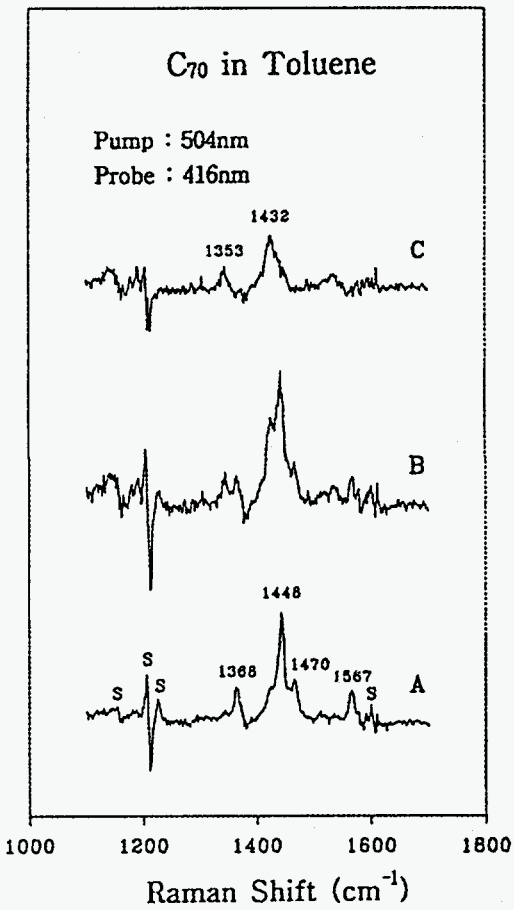

Figure 2. Time-resolved Raman spectra of C_{70} in toluene obtained with 504nm pump and 416nm probe pulses at 7ns time delay; (A) probe only spectrum, (B) pump and probe spectrum, and (C) difference spectrum (B-A) with a subtraction factor. S denotes the peak due to solvent band subtraction.

Acknowledgments

This work was supported by MOST (D.Kim), the Basic Science Research Institute Program (S. K.Kim), and KOSEF through the Center for Molecular Science (D.Kim & S.K.Kim).

References

[1] D. Kim, M. Lee, Y.D. Suh, and S.K. Kim, J. Am, Chem. Soc. 114 (1992) 4429.

[2] G.L. Closs, P. Gautam, D. Zhang, P.J. Krusic, S.A. Hill, and E. Wasserman, J. Phys. Chem. 96 (1992) 5228.

Time-resolved Two-dimensional Vibrational Spectroscopy and its Application to High Explosives

Xiaoyu Hong and Dana D. Dlott
School of Chemical Sciences, University of Illinois, Urbana IL 61801

Vibrational dynamics of polyatomic molecules in condensed phases plays important roles in the fields of biology, chemistry, physics, and materials science. One of the most important practical applications where vibrational energy transfer is thought to play a dominant role is in the initiation and detonation of energetic materials. In this paper we summarize the first direct measurements of molecular vibrational energy transfer in a condensed phase high explosive, nitromethane (NM) [1], and also discuss measurements of intermolecular vibrational energy transfer between various small molecules and NM in polyatomic solutions [2].

A picosecond (ps) time resolved two dimensional vibrational spectroscopy technique [3] is used. A tunable mid-infrared ps laser pulse is used to selectively excite a specific higher frequency vibrational level of a polyatomic molecule. Vibrational energy relaxation from this excited level to lower energy levels is monitored by probing the anti-Stokes-Raman scattering produced by a second, delayed ps laser pulse. The advantages of this technique are excitation selectivity and probe selectivity, which allow one to investigate intramolecular as well as intermolecular processes in polyatomic solutions. These difficult experiments were performed using a high repetition rate Nd:YLF laser and a mid-IR optical parametric amplifier (OPA). The second harmonic (527 nm) of the YLF laser is used to pump the OPA and as the anti-Stokes probe pulse. A synchronously pumped dye laser provides the signal input to the OPA. The system produces > 10 μJ pulses of ~100 ps duration in the 2.5-3.5 μm range using $LiIO_3$ crystals for the OPA process [1].

Figure 1 shows the basic idea of this experiment on neat NM. The mid-IR pulses are used to pump the $\nu(CH_3)$ vibration and the subsequent vibrational cascade is probed with a 527 nm pulse. Some representative data is shown at right. The $\nu_s(NO_2)$ state is first pumped to a high level and then it subsequently decays to a plateau denoting the bulk temperature jump induced by the IR pump pulses. This phenomenon is termed "vibrational overheating" [1] and the overheating of the $\nu_s(NO_2)$ state is direct evidence that the vibrational energy pumped into the $\nu(CH)$ states has been transferred efficiently into the $\nu_s(NO_2)$ state.

In more recent work [2], we studied intermolecular energy transfer in NM solutions. We found pumping the $\nu(OH)$ state of alcohols ($\omega \sim 3700$ cm^{-1}) in low concentration (~5%) results in efficient energy transfer to $\nu_s(NO_2)_{NM}$. Such efficient intramolecular vibrational transfer has not been observed previously in polyatomics. In a series of experiments using deuterated NM and alcohol molecules, we determined that the dominant vibrational energy transfer process has the form,

$$\nu(OH)_{MeOH} \rightarrow \nu(CH)_{MeOH} \rightarrow \delta(CH)_{MeOH} \rightarrow \nu_s(NO_2)_{NM}.$$

The surprising finding of efficient energy transfer to the $\nu(NO_2)_{NM}$ state from impurities in the liquid NM suggests some intriguing possibilities for understanding energy concentration

mechanisms which might lead to accidental detonations, and for understanding why the NO_2 group is ubiquitous in secondary explosives [2].

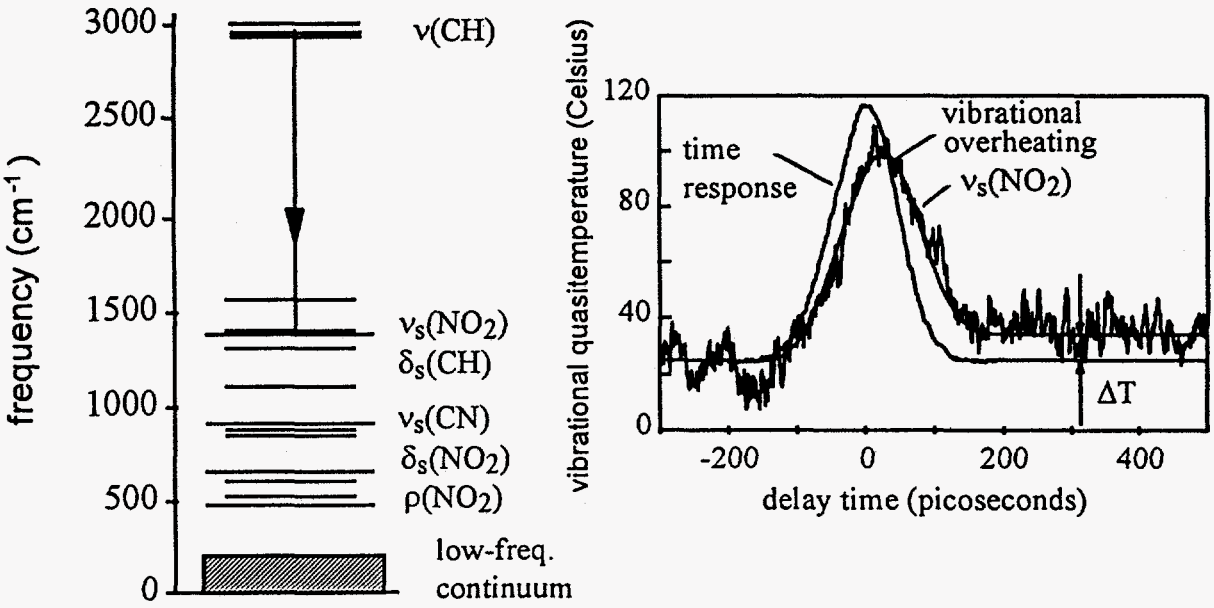

Figure 1. (left) Schematic level diagram for liquid NM. Mid-IR pulses pump the ν(CH) transition. Incoherent anti-Stokes Raman scattering probes lower energy vibrations such as $\nu_s(NO_2)$. (right) The instantaneous anti-Stokes intensity is converted into vibrational quasitemperature. The data show a rapid rise to a peak, indicating rapid efficient energy transfer from ν(CH) to $\nu_s(NO_2)$. The bulk temperature jump induced by the mid-IR pulses is about 10 deg.

In our most recent work, we have developed a diode-pumped mode-locked Nd:YLF laser which is used to seed the high-power YLF system with a much shorter duration 15 ps pulse. We have been able to improve the time resolution of the apparatus by a factor of ~6. In the 2.5-3.5 μm range, we have generated ~10 μJ mid-IR pulses of ~15 ps duration at a repetition rate of >600 pulses per second, using KTA as the OPA material. This greatly improved apparatus will be used to study energy transfer in a wide variety of energetic materials.

Acknowledgments

This work was supported by Army Research Office contract DAAH 04-93-G-0016, Air Force Office of Scientific Research contract F49620-94-1-0108, and National Science Foundation grant DMR 94-04806.

Citations and References

1. S. Chen, X. Hong, J. R. Hill, and D. D. Dlott, J. Phys. Chem., 99 (1995) 4525.

2. X. Hong, S. Chen, and D. D. Dlott, J. Phys. Chem. (in press).

3. T. Elsaesser and W. Kaiser, Annu. Rev. Phys. Chem. 42 (1991) 83.

Picosecond time-resolved coherent Raman temperature-pressure jump spectroscopy.

David E. Hare, Jens Franken and Dana D. Dlott
School of Chemical Sciences, University of Illinois, Urbana IL 61801

High speed mechanical processes involve large stresses and stress rates, and in many cases high heating rates and temperatures. Some important practical processes of this type include the initiation of energetic materials and laser ablation. We have developed a picosecond coherent Raman temperature-pressure jump spectroscopy (T-P jump CARS) to study the detailed dynamical properties of materials under extreme conditions.

In our experiments, a typically 3.5 μm thick polymer film is doped with a near-IR dye. Pumping the dye with a ps-duration pulse from a Nd:YAG laser produces a sizable temperature jump of typically hundreds of degrees. When a sample is heated faster than it can undergo thermal expansion, a pressure jump is also generated. In our samples, the time for expansion is typically a few ns, considerably longer than the ~150 ps duration of our near-IR pulses. The magnitude of the pressure jump in polymers is ~1 MPa/K (10 atm/deg). Even higher pressures are generated if volatile polymer decomposition products are produced by fast heating.

A Q-switched, mode-locked, cavity-dumped Nd:YAG laser synchronously pumps two cavity-dumped dye lasers. The dumped YAG pulse arrives at the sample first, jumping its temperature and pressure. After a variable delay up to 11 ns, two simultaneous pulses from the dye lasers arrive at the center of the heated volume to generate the CARS signal. One dye laser has a narrow bandwidth of < 1 cm^{-1} while the second has a broad bandwidth typically > 200 cm^{-1}. A multiplex CARS spectrum is obtained using a spectrograph and array detector. Often, the pump pulse produces destructive temperatures and stresses. Under such conditions, probing the heated volume sample is strictly a one-shot affair. Our thin film samples have a large surface area, and a precision motorized x-y translation stage continually translates the large area film so a fresh sample volume is pumped and probed with each laser shot.

Polymethylmethacrylate (PMMA) is used for most of our studies. We have investigated the dynamics of the ~808 cm^{-1} vibration, attributed to a pseudosymmetric stretching of the methyl ester. This vibration shifts in a well-characterized way with T and P. Increasing T gives a redshift and increasing P gives a blueshift, which we have measured accurately. Some experimental data are shown in Fig. 1. CARS lineshapes are shown in the upper corner. The time dependent peak shift gives both T and P in a straightforward manner. The fast shift results from combined effects of T and P. After the ns time scale relaxation, the pressure has released back to 1 atm, and T_f can be easily determined from the peak redshift. An iterative method is then used to back-calculate T_i and P_i, which as shown can be on the order of hundreds of degrees and tens of kilobars [1,2].

In recent work, we have studied shock-induced dynamics of crystalline energetic materials by embedding 1 μm diameter crystallites in the PMMA. The pressure jump in PMMA compresses the crystallites very rapidly and their CARS spectra can then be measured. Some results obtained

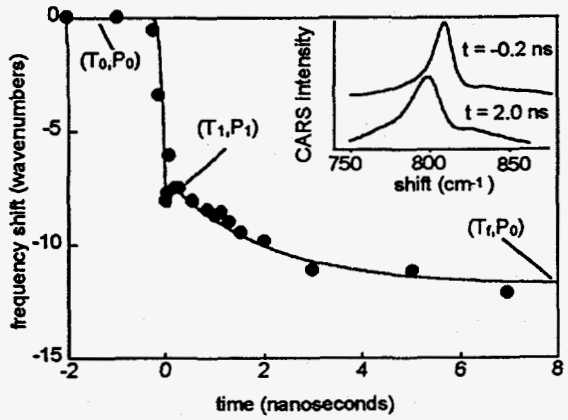

Figure 1. Time-dependent frequency shift of the ~808 cm^{-1} transition in PMMA with ps pulse heating. The *inset* shows representative CARS lineshapes. Analysis of the displayed data at an incident laser fluence J = 1.5 J/cm^2, yields T_f = 440 (±30)°C, T_1 = 625 (±50)°C, and P_1 = 26 (±3) kilobars. The smooth curve through the points is a visual guide.

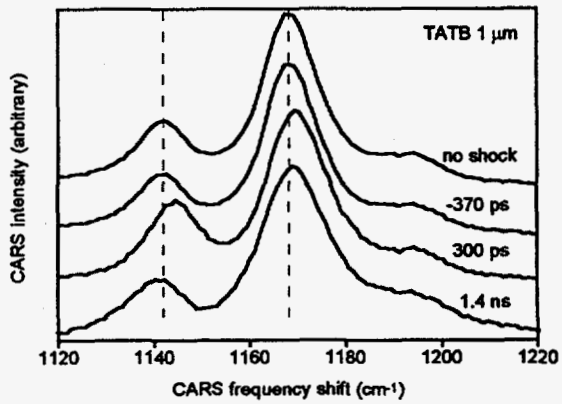

Figure 2. CARS spectra of 1 μm diameter TATB crystals during shock generation by picosecond pulse heating of the surrounding polymer. The vertical lines denote the positions of two TATB vibrational transitions under ambient conditions. At 300 ps, the particle compression is near maximum. At 1.4 ns, most of the shock unloading has already occurred.

on the totally symmetric stretch of the C-NH_2 group at 1168 cm^{-1} and the NH_2 rocking mode at 1142 cm^{-1} of TATB (triamino-trinitro-benzene) are displayed in Fig. 2. Both vibrational transitions show a fast blueshift due to shock compression. As the high pressure unloads, the transitions shift back to the red. At ~ 1.4 ns, the residual shifts are interpreted to arise from shock-induced heating. This method shows great promise for studying the dynamics and chemistry of shock-induced processes occurring in energetic materials. In particular, it is very important to know how much heat is generated in a solid after fast shock compression.

Acknowledgment

This work was supported by Army Research Office contract DAAH 04-93-G-0016, Air Force Office of Scientific Research contract F49620-94-1-0108, and National Science Foundation grant DMR 94-04806. We thank Dr. Randall Simpson of the Energetic Materials Center at LLNL for providing the material samples, and for suggesting the crystallite precipitation method.

References

[1] D. E. Hare, E. L. Chronister, J. Flores, J. Franken and D. D. Dlott, Appl. Phys. Lett. 65, 3051 (1994).

[2] D. E. Hare, J. Franken and D. D. Dlott, J. Appl. Phys. 77, 5950 (1995).

[3] D. E. Hare, J. Franken and D. D. Dlott, submitted to Chem. Phys. Lett. May 1995.

ABSTRACTS FOR POSTERS
BIOLOGY

Time-Resolved Resonance Raman Spectroscopy of Peroxidase Porphyrin π-Cation Radical and Ferryl Intermediates

James Terner and Charles M. Hosten
Dept. of Chemistry, Virginia Commonwealth University, Richmond, VA 23284-2006

J. Matthew Mauro, Mark A. Miller and Joseph Kraut
Dept. of Chemistry, University of California, San Diego, La Jolla CA 92093

A transient state known as compound I is a key physiological intermediate in the mechanism of peroxidases, and has beem implicated in the mechanisms of many other heme enzymes which play important roles in metabolic systems. Though evidence for such states in the cytochrome P-450 enzymes is accumulating [1], compound I intermediates of the peroxidases have been known and investigated for many years.

The oxoferryl porphyrin π-radical cation structures of the compound I-type intermediates have been extensively modelled via chemical synthesis at low temperature, however the biologically occurring species possess attributes that remain unique to the protein environment. The orbital structures of compound I porphyrin π-cation radical intermediates have been longstanding topics [2]. The prevailing symmetry state assignment for enzymes such as horseradish peroxidase has been A(2u). By using excitation in the ultraviolet region we have been able to take advantage of the differing enhancement profiles of porphyrin π-radical cation intermediates and those of other enzymatic forms [3]. Model compound studies have indicated that specific bands of porphyrin π-radical cation intermediates can be expected to exhibit a specific shifting pattern relative to the ferryl forms of the enzymes. The shifting patterns that we have observed in a number of these enzymes have been strongly indicative of the A(1u) rather than the expected A(2u) type. We have in fact found no evidence supportive of the A(2u) porphyrin π-radical cation type in peroxidase heme proteins.

At the present time developments in the field are being derived from X-ray crystal structures that are frequently becoming available. Resonance Raman spectroscopy is ideal as a sensitive probe of the dynamic aspects of these protein structures. A peroxidase for which the most extensive X-ray structure data are available is yeast cytochrome c peroxidase [4]. We have examined resonance Raman data for the ferryl intermediate of this enzyme, and find that the oxoferryl stretching frequency is much lower than has been previously reported. It is in fact 25 cm^{-1} lower than in enzymes such as horseradish peroxidase. Examination of the crystal structures provides a rationale. The cytochrome c peroxidase active site has differences from those of other peroxidases, such as a tryptophan instead of a phenylalanine in the distal pocket. In order to characterize effects arising from differences in heme pocket amino acid configurations we examined oxoferryl structures of unstable ferryl forms of cytochrome c peroxidase with specific mutations on the heme distal side. We observed that the oxoferryl frequency shifts up by approximately 30 cm^{-1} for certain distal substitutions.

Chloroperoxidase is a heme containing glycoprotein secreted by the fungus Caldariomyces fumago. The unique structure and function of chloroperoxidase

relative to other peroxidases, and similarities in magnetic and spectroscopic properties with the cytochrome P-450 enzymes, have been attributed to strong electron donation by a heme-ligated cysteine thiolate. The peroxidase activity of this enzyme includes catalase activity and the ability to catalyze the halogenation of organic substrates by chloride, bromide, and iodide (but not fluoride) using H_2O_2 as the oxidant. The enzyme also catalyzes a number of P-450 type mono-oxygenase reactions.

The X-ray crystal structure of chloroperoxidase has very recently been obtained to 2.0 Å resolution [5]. The active site of this enzyme has the greatest dissimilarities with respect to other peroxidases seen to date. It was known prior to the crystal structure that the heme of chloroperoxidase is ligated by cysteine, similar to cytochrome P-450, as opposed to the histidine found in other peroxidases. However the distal side of the chloroperoxidase was expected to resemble the polar environment of peroxidase active sites as compared to the more nonpolar environment in cytochrome P-450. The crystal structure of chloroperoxidase shows that the distal heme pocket is polar but there are marked differences from the usual peroxidase distal constellation, sometimes termed the "catalytic triad", of phenylalanine (or tryptophan), histidine and arginine [6]. In chloroperoxidase the heme distal position is occupied by a glutamic acid rather than a histidine, and the usual arginine is absent.

Resonance Raman spectra of the ferrous form of chloroperoxidase have been previously shown to display an abnormally low ν_4 frequency. We have found that chloroperoxidase compound II also displays a markedly lowered ν_4 frequency relative to other ferryl hemes. Resonance Raman spectra of chloroperoxidase compound I showed upshifted ν_2, ν_{11} and ν_{37} frequencies relative to compound II, arguing for an A(1u) in preference to A(2u) ground state for the porphyrin π-cation radical [7]. This behavior was similar to that previously observed for horseradish peroxidase compound I, though the magnitude of the shifts were somewhat different. Resonance Raman spectra of chloroperoxidase compound I also displayed a moderately strong anomalously polarized band at 1150 cm^{-1}. A somewhat weaker anomalously polarized band at 1164 cm^{-1} was seen in resonance Raman spectra of horseradish peroxidase compound I [8].

Acknowledgement: This work was supported by NIH Grant GM34443.

References

1. T. Egawa, H. Shimada and Y. Ishimura, Biochem. Biophys. Res. Commun. (1994) 201, 1464-1469
2. P. Du and G. Loew, Biophys. J. (1995) 68, 69-80
3. V. Palaniappan and J. Terner J. Biol. Chem. (1989) 264, 16046-16053
4. T.L. Poulos, S.T. Freer, R.A. Alden, S.L. Edwards, U. Skogland, K. Takio, B. Eriksson, N.H. Xuong, T. Yonetani, and J. Kraut Biochemistry (1980) 255, 575-580
5. M. Sundaramoorthy, J. Terner and T.L. Poulos (1995) submitted for publication
6. A.M. English and G. Tsaprailis Adv. Inorg. Chem. (1995) in press
7. C.M. Hosten, A.M. Sullivan, V. Palaniappan, M.M. Fitzgerald and J. Terner, Time-Resolved Vibrational Spectroscopy VI, Springer Proc. in Physics (1994) 74, 243-246
8. C.M. Hosten, A.M. Sullivan, V. Palaniappan, M.M. Fitzgerald and J. Terner, J. Biol. Chem. (1994) 269, 13966-13978

Ultrafast Dioxygen Recombination in Hemoglobin Measured by Sub-Picosecond Time-Resolved Resonance Raman Spectroscopy

Stefan Franzen, Laurent Kiger, Claude Poyart, Jean-Louis Martin

Laboratoire d'Optique Appliquee
ENSTA-Ecole Polytechnique
91120 Palaiseau, France

One means of understanding differences in the electronic barrier to ligand rebinding to the heme iron for the diatomic ligands CO, NO, and O_2 is to study ultrafast ligand recombination that occurs more rapidly than the decay of photophysical intermediate states. In the hemoproteins myoglobin (Mb) and hemoglobin (Hb), the photolyzed ligands O_2 and NO have a phase of rebinding to the heme iron that is as a rapid as heme photophysical decay (≈3 ps 1/e time) [1-5]. In a comparison of deoxy Hb, HbCO, and HbNO TRRR spectra we have previously demonstrated ultrafast heme iron displacement (0.4 Å in < 1 ps) following ligand photolysis [6] by measuring the intensity and frequency of the Fe-histidine out-of-plane mode at ≈223 cm^{-1} [7]. We have also shown that there is no ultrafast rebinding of CO in photolyzed Hb*CO. Photophysical studies based on transient spectra and TRRR with sub-ps time resolution have shown that a sequential decay of the heme through two excited states Hb^*_I (≈ 300 fs lifetime) and Hb^*_{II} (≈ 3 ps lifetime) [2,8]. The assignments of the electronic states are 1.) Hb^*_I is a charge transfer state that rapidly reactivates the initially formed ^1Q state 2.) Hb^*_{II} is a porphyrin ground state with an excited configuration of d-electrons on the heme iron. The similarity of Hb^*_{II} with the porphyrin ground state indicates that Soret band shift relaxations on the ≈3 ps time scale can appear as ligand rebinding and therefore the true extent of ligand rebinding on this time scale should be reconsidered. Here we report measurement of ultrafast ligand rebinding in photolyzed Hb*NO and Hb^*O_2 measured by time-resolved resonance Raman (TRRR) spectroscopy with sub-picosecond time resolution. The laser experimental apparatus consisted of excitation using 100 fs pulses at 570 nm and Raman probe using 700 fs pulses at 435 nm [6,9].

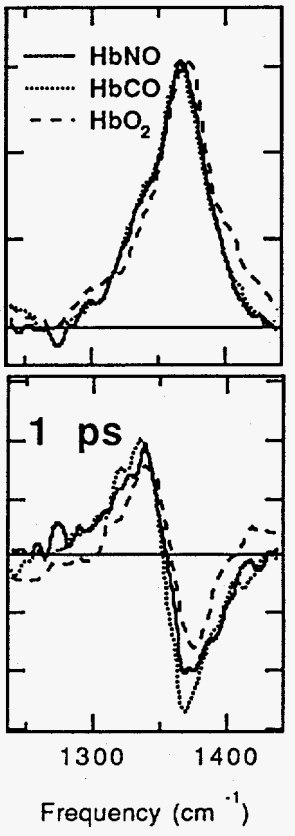

Figure 1: Raman spectrum of oxidation state marker modes and difference Raman spectra at 1 ps.

A comparison of the HbO_2, HbNO, and HbCO equilibrium ligated Raman spectra and difference Raman spectra at 1 ps are shown in Figure 1 for the oxidation state marker band. The shape of difference Raman spectrum shown at 1 ps is attributable to a decrease in intensity of the ligand bound state at ≈1370 cm^{-1} and an increase in intensity of the deoxy Hb state at 1357 cm^{-1}. In TRRR difference spectra the band shifts are larger than the equilibrium frequency difference because there are effects of unrelaxed conformational strain and photophysical relaxations on the time scale of 0-10 ps that further lower the frequency of the oxidation state marker band [6,9]. The relative intensity of the difference Raman feature provides an estimate for the yield dissociated species in the respective species. Relative quantum

yields in Hb*CO were calibrated to an absolute intensity standard of 1 M ammonium sulfate and the change in intensity of the Fe-CO stretch at 505 cm^{-1}. While Hb*NO and Hb*CO have similar Raman difference spectra at 1 ps, the magnitude of the difference Raman feature at 1 ps is significantly smaller for HbO_2 than for either HbCO or HbNO. It is unlikely that this difference is due to an excited heme electronic state in Hb^*O_2. We interpret the difference in the intensity of the oxidation state marker band shown in Figure 1 as a ≈25-30% reduced yield of deoxy photoproduct at 1 ps. The presence of a rapid phase (≈300 fs) in the Hb^*O_2 recombination kinetics suggests that the photolysis yield is unity and that the process observed in the TRRR signal is ultrafast geminate O_2 rebinding that is not present in either Hb*NO or Hb*CO.

The nature of the barrier to recombination of O_2 with the heme iron is significantly different from that of the more frequently studied CO [10-12]. The electronic configuration of CO is a singlet while oxygen has a ground state $^3\Sigma$ configuration. Recombination with the heme iron is spin-allowed for CO only if the heme iron is in a low spin S=0 spin configuration. By contrast, ground state oxygen can recombine with the heme iron in an S=1 state in a spin-allowed process giving rise to an electronic structure in which a bond is formed between the d_{z2} orbital of the iron and an oxygen p orbital and a second bond is formed between the d_{yz} orbital and the three-electron p system of the O_2 ligand. The heme-O_2 complex is diamagnetic and therefore the heme iron must be in an S=1 state that is significantly displaced from the heme plane due to core size effects. Consistent with this hypothesis, the geometry of the heme iron complex in six coordinate MbO_2 consists of a significant ≈0.19 Å out-of-plane distortion of the heme iron unlike the planar geometry in MbCO [13, 14]. These factors suggest that both intermediate spin configurations (S=1) and out-of-plane heme geometries are accessible to O_2, but not CO. Thus, if the excited state Hb^*_I has charateristics of an S=1 state with significant heme out-of-plane displacement, ultrafast ligand recombination is possible for O_2, but not CO.

It is interesting to note that studies of ligand rebinding to myoglobin at cryogenic temperature have noted an apparent smaller quantum yield for oxygen photodissociation [15]. The overall yield of about 0.7 at cryogenic temperature is roughly equivalent to the apparent yield on the ps time scale at room temperature. If the same electronic states are populated at cryogenic temperature, the explanation given here for the differences between CO and O_2 are consistent with this observation as well. These observations suggest that O_2 rebinding to the Hb^*_I state is essentially barrierless, unlike other ligand recombination pathways seen in hemoproteins.

References

1. Chernoff, D. A., Hochstrasser, R. M., Steele, A. W., *Proc. Natl. Acad. Sci.*, **1980**, 77, 5606-5610
2. Petrich, J. W., Poyart, C., Martin, J. L., *Biochemistry*, **1988**, 27, 4049-4060
3. Petrich, J. W., Lambry, J. C., Balasubramanian, S., Lambright, D. G., Boxer, S.G., Martin, J.L., *J. Mol. Biol.*, **1994**, 238, 437-444
4. Walda, K. N., Liu, X. Y., Sharma, V. S., Magde, D., *Biochemistry*, **1994**, 33, 2198-2209
5. Carlson, M. L., Regan, R., Elber, R., Li, H., Phillips, G. N., et al., *Biochemistry*, **1994**, 33, 10597-10606
6. Franzen, S., Bohn, B., Poyart, C., Martin, J.L., *Biochemistry*, **1995**, 34, 1224-1237
7. Franzen, S., Lambry, J. C., Bohn, B., Poyart, C., Martin, J. L., *Nature Struct. Biol.*, **1994**, 1, 230-233
8. Franzen, S., Bohn, B., Poyart, C., Martin, J.L., *J. Phys. Chem.*, **1995** submitted
9. Petrich, J. W., Martin, J.-L., Houde, D., Poyart, C., Orszag, A., *Biochemistry*, **1987**, 26, 7914-7923
10. Zerner, M., Gouterman, M., Kobayashi, H., *Theoret. Chim. Acta*, **1966**, 6, 363-400
11. Olafson, B. D., Goddard, W. A., *Proc. Natl. Acad. Sci. U.S.A.*, **1977**, 74, 1315-1319
12. Waleh, A., Loew, G. H., *J. Am. Chem. Soc.*, **1982**, 104, 2346-2351
13. Phillips, S. E. V., *Nature*, **1978**, 273, 247-251
14. Kuriyan, J., Wilz, S., Karplus, M., Petsko, G. A., *J. Mol. Biol.*, **1986**, 192, 133-154
15. Austin, R. H., Beeson, K. W., Eisenstein, L., Frauenfelder, H., Gunsalus, I. C., *Biochemistry*, **1975**, 14, 5355-5373

Time-Resolved Step-Scan FT-IR Spectroscopy of Halorhodopsin

Susan E. Plunkett, Andrei K. Dioumaev, and Mark S. Braiman
Department of Biochemistry, University of Virginia Health Sciences Center, Charlottesville, VA 22908

INTRODUCTION

Halorhodopsin (hR) is a transmembrane protein found in halophilic bacteria. It functions as an electrogenic chloride pump, transporting anions from the external medium into the cytoplasm. The amino acid sequence is ~30% homologous with bacteriorhodopsin (bR), a transmembrane proton pump found in the same species. The 3-dimensional structures of these 2 proteins are also closely related. A detailed structural understanding of the mechanism of hR should be germane to an array of other ion transport proteins. To this end, the development of sensitive sub-millisecond spectroscopic probes is necessary to obtain detailed structure/function information about the binding and translocation events.

APPROACH

The hR photocycle intermediates have been defined based on changes in the visible absorption maxima of the retinal chromophore. While UV-vis spectroscopy is useful for determining the changes in the retinal chromophore, it provides no direct information regarding the protein itself. FT-IR spectroscopy uses a broadband probe source and an interferometer, and the spectral multiplex advantage inherent to Fourier transform techniques allows the simultaneous detection of a broad range of wavelengths of light. Step-scan FT-IR spectroscopy allows the collection of time-resolved spectra as the moving mirror is kept stationary while the sample is perturbed and the transient changes sampled.[1] This technique has developed to the point where very small changes ($\Delta A = 1\times10^{-5}$) attributable to single amino acids can be followed coherently in time with commercially available instrumentation.

EXPERIMENTAL

A Bruker IFS 66 step-scan FT-IR spectrometer was used with a Quanta-Ray GCR-11 mode-locked Q-switched Nd-YAG laser (532 nm, 5 Hz, 30 mJ/sec), which was used to initiate the photocycle and trigger the spectrometer to begin data collection. The hR sample (prepared from a genetically-engineered overproducing strain of *Halobacterium salinarium*) was a membrane pellet (pH=7, ~1M KCl) squeezed to a thickness of ~10 μm between CaF_2 plates at room temperature. An MCT detector (Belov Technologies, #92503) with an AC-coupled preamplifier board (Nicolet, #9107031) was used to detect the transient IR signal induced by the optical perturbation. The spectrometer's 16 bit internal analog-to-digital converter (ADC) sampled and digitized the detector output at selectable time intervals down to 5 μs. Then the time-resolved transients at each mirror position were re-sorted into a set of interferograms, each at a specific time after the laser perturbation. The interferograms were phase corrected using a modified Mertz routine that limits the phase spectrum to $\pm\pi/2$ radians.[2] Absorbance difference spectra were calculated as $\Delta A = -log(1 + (\Delta I/I_o))$, where ΔI_o is the single-beam intensity difference spectrum and I_o is the reference single-beam

intensity spectrum of the same sample, collected using a normal continuous-scan method. The data collection parameters were: 6 cm^{-1}spectral resolution, 70 laser flashes (coadditions) per mirror position, 50 ms mirror settling time, and 5 μs time resolution. A low-pass optical filter (dielectric on Ge) limited the throughtput to 1974 cm^{-1}, allowing for undersampling at $4\lambda_{HeNe}$. The total data collection time was 2.5 hours. Fourier processing parameters were: 2 orders of zero filling and 64 cm^{-1} resolution for phase spectra.

RESULTS AND DISCUSSION

While time-resolved step-scan FT-IR has previously been used to study bR[3] and carbonmonoxymyoglobin[4], this is the first report of this technique applied to hR. Figure 1 is a representative ΔA spectrum of a single 5 μs time slice corresponding to 10 μs after photolysis. Positive bands are due to photoproduct, while negative bands are due to depletion of hR. The band positions agree well with slower time-resolved FT-IR difference spectra of the photoreaction (measured using a stroboscopic technique).[5] Kinetic analysis of the spectrum, and assignment of vibrational bands to specific amino acids, will provide further information on the structures of the different functional intermediates.

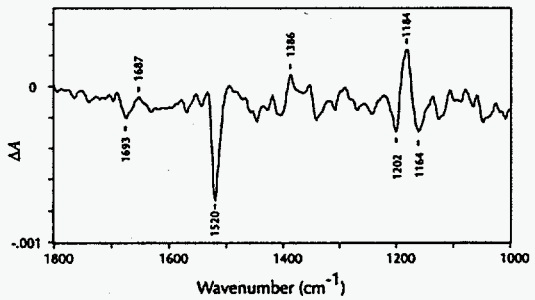

Figure 1. Difference spectrum of hR measured 10 μs after photolysis.

CONCLUSION

Further improvements in sensitivity could be gained by amplifying the signal before digitization to fully utilize the full 16 bit/20 V dynamic range of the ADC, and by further purifying and concentrating the sample. Nevertheless, the signal-to-noise ratio here already indicates that even faster time-resolved spectra could be obtained with useful noise levels. Sub-nanosecond time resolution will require a faster IR detector (photovoltaic HgMnTe), preamplifier, and digitizer. All of these are now in our lab and are currently being implemented.

REFERENCES

1. R.A. Palmer, *Spectroscopy 8(2)* (1993) 26.
2. C.A. McCoy and J.A. deHaseth, *Appl. Spectrosc. 42* (1988) 336.
3. W. Uhmann, A. Becker, C. Taran, and F. Siebert, *Appl. Spectrosc. 45* (1991) 390.
4. S.E. Plunkett, J.L. Chao, T.J. Tague, and R.A. Palmer, *Appl. Spectrosc.* in press (1995).
5. T.J. Walter and M.S. Braiman, *Biochemistry 33* (1994) 1724.

Picosecond Time-Resolved Resonance Coherent Anti-Stokes Raman Spectroscopy of Bacteriorhodopsin: Experimental Challenges and the K-590 Spectrum

L. Ujj, A. Popp, F. Jäger, R. Ligon and G.H. Atkinson

Department of Chemistry and Optical Sciences Center, University of Arizona, Tucson,Az 85721

Elucidating the vibrational degrees of freedom in the reactive intermediates found during chemical and biochemical reactions requires high S/N data that merit quantitative analyses. Although spontaneous resonance Raman (RR) spectroscopy has been used extensively for such measurements, it is limited by low efficiency scattering and background fluorescence.

This paper describes coherent Raman techniques that have been used successfully to obtain high quality vibrational data from the room temperature photo-reaction of the trans-membrane proteins bacteriorhodopsin (BR) and rhodopsin (Rh). Attention is given to the challenging experimental methodologies required to record high S/N resonance coherent anti-Stokes Raman spectra (CARS) from an intact protein in water solution and to the third-order non-linear susceptibility ($\chi^{(3)}$) analysis needed to extract quantitative information from these data.

Multiplex CARS with picosecond time resolution (PTR/CARS[1]) is used to measure the vibrational spectra of BR-570 (ground state) and K-590 (intermediate) in the BR room temperature photocycle. The wavelength of the ω_1 laser pulse (663 nm, 7-ps FWHM) is selected to satisfy

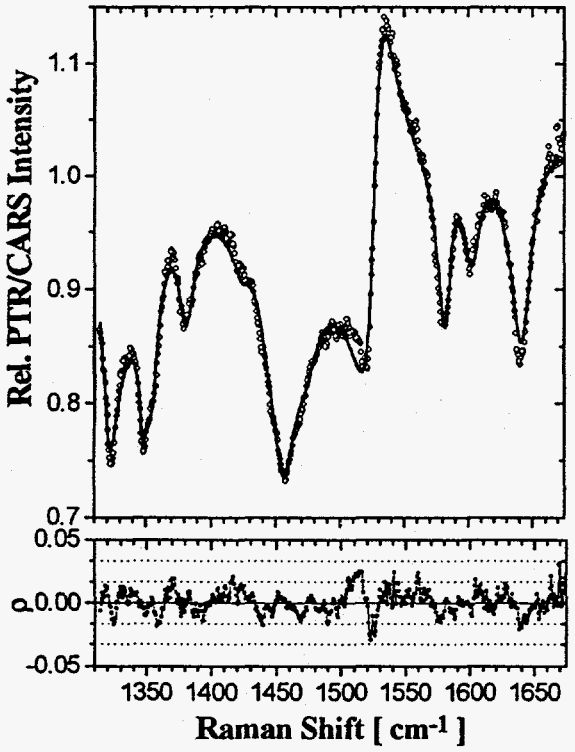

Fig. 1 A. PR/CARS spectrum of BR-570 measured close to the "turn over" point of the 1527-cm^{-1} band (unfilled circles) together with $\chi^{(3)}$ fit (solid line). B. Residual function between the $\chi^{(3)}$ fitting function and the experimental data.

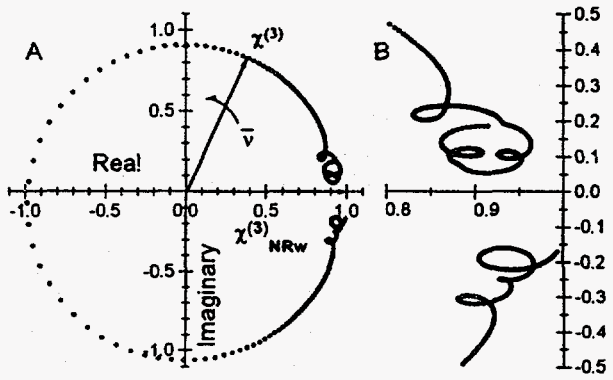

Fig. 2 A. Geometrical interpretation of $\chi^{(3)}$ on the complex plane. The spectrum in Fig.1 is the square modulus of $\chi^{(3)}$ via Raman shift (ν). As the shift increases, the complex susceptibility vector turns counterclockwise and the endpoint runs over the curve. B. Magnified area of A. Each loop represents a vibrational band.

a "negative peak" preresonance condition for BR-570 (the vibrational phase is 93°). In this case, the concentration of BR-570 in water solution (optical density 1.43/cm) can be adjusted to almost cancel the signal of the most intense vibrational band (C=C stretching, 1527 cm^{-1}) using the nonresonant scattering originating from water. Fig. 1 shows the measured picosecond resonance CARS (PR/CARS) spectrum of BR-570 over the 1310 - 1675 cm^{-1} region. The $\chi^{(3)}$ fitting result is also shown (solid line). The third order susceptibility of the sample, obtained by assuming complex Lorentzien vibrational band shapes[2], is drawn on the complex plane (Fig. 2) to illustrate the cancellation of the 1527 cm^{-1} contribution.

The BR photocycle is monitored 50 ps after optical excitation (3-ps pulse at 570 nm) in order to kinetically ensure that only two BR species are present *vida supra*. The concentration of BR-570 and the power of the excitation laser pulse are also adjusted in order to eliminate the C=C stretching vibrational band of BR-570 from the reactive mixture. Picosecond transient absorption (PTA) traces are recorded in order to determine independently the concentrations of the BR intermediates (namely, K-590).

The resulting spectra (i) allow an independent band analysis (with respect to the frequency, bandwidth and amplitude) for BR-570 via a line shape function usually assumed to quantitatively analyze the CARS spectra in terms of $\chi^{(3)}$ relationships[2]. As a consequence of the excellent (<5%) fit, the validity of the theoretical model function can be confirmed. (ii) The K-590 vibrational bands appear clearly in the spectra. The spectra of K-590 are compared to those recorded at different wavelengths and analyzed by the nonlinear fitting procedure which permits a quantitative separation of the contributions from each species[3].

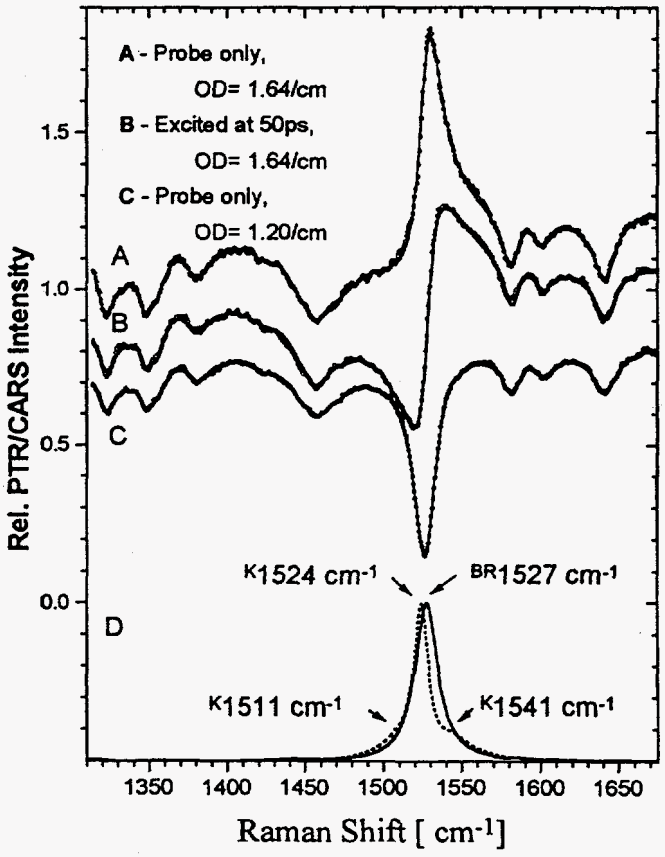

Fig. 3 PTR/CARS spectra of BR sample. **A**,**B**, and **C** are experimental data (unfilled circles) and fitting curves (solid lines), **D** is background free spectra of K-590 and BR-570. The origins of the major bands are indicated by arrows.

References

1.G.H. Atkinson and L. Ujj in: Inst. Phys. Conf. Ser. No 126 Section VIII ed. A. Laubereau (Adam Hilger, IOP Publ., Ltd., England, 1992) p. 599.

2.L. Ujj, B.L. Volodin, A. Popp, J.K. Delaney and G.H. Atkinson *Chem. Phys.* **182** (1994) 291.

3.L. Ujj, A. Popp, and G.H. Atkinson *Chem. Phys.* **188** (1994) 221.

Picosecond Resonance CARS Spectroscopy: Vibrational Spectra of the Deionized Form of Bacteriorhodopsin (Blue Membrane)

R. Ligon, L. Ujj, A. Popp, F. Jäger, and G.H. Atkinson

Department of Chemistry and Optical Science Center University of Arizona, Tucson, Az. 85721

1. INTRODUCTION

Investigations of the deionized or acidified form of bacteriorhodopsin (BR), blue membrane, can significantly advance our understanding of the mechanisms of proton pumping in a trans-membrane protein. Previous studies have shown that the blue membrane undergoes a restricted photocycle attributed to ionization changes at or near the Schiff-base counterion of the retinal chromophore. It has been shown that ground-state blue membrane contains two structurally-distinct retinal chromophores (13-*cis* and all-*trans*) [1,2]. The presence of two retinal isomers has been supported by resonance Raman (RR) spectra recorded from ground-state blue membrane [3,4]. It also has been reported that it is the all-*trans* retinal species that has a restricted photocycle while the *13-cis* has no photocycle [2]. RR spectra recorded from the blue membrane mixture (using cw laser excitation) have been used to identify marker bands for specific intermediates within the restricted all-*trans* photocycle [4].

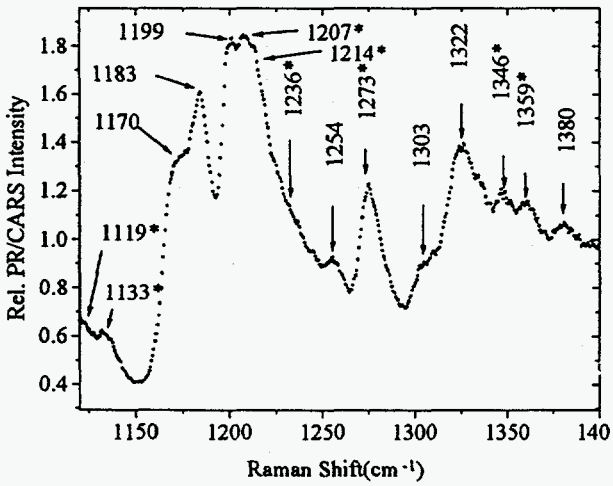

Fig.1 PR/CARS spectrum of the ground state in the C-C stretching region.(*indicates band positions assignable to blue membrane that are previously unreported)

The presence of two structural isomers in the blue membrane creates a variety of experimental and interpretative challenges. Chemical isolation of one of the species from the mixture is the ideal situation for finding the exact contribution of each to vibrational spectra, but this procedure has yet to be successful. Alternatively, a high S/N spectroscopic method such as picosecond resonance coherent anti-Stokes Raman spectroscopy (PR/CARS) provides an opportunity to identify the spectral components assignable to each isomer [5]. The coherent interference of the CARS signals from each isomer creates an unique situation. A 35 nm shift between the maxima of the absorption spectra assignable to the two species causes the electronic phase factor of each to be different. The resultant PR/CARS spectrum can be best fitted via third-order nonlinear susceptibility (χ^3) relationships by assuming two vibrational phase groups for the observed bands.

2.EXPERIMENTAL

Two synchronously-pumped picosecond dye lasers are used to probe the blue membrane sample via the four-wave mixing technique, PR/CARS. The 663-nm (7 ps FWHM) is selected to have a narrow bandwidth (<3 cm^{-1}) while the second laser operates over a broad (10 nm) wavelength range (centered either at 723 nm or 736 nm) to provide access to the C-C stretching (1100-1400 cm^{-1}) and C=C stretching (1350-1650 cm^{-1}) regions respectively. Together, the two beams generate a broadband (≈300 cm^{-1}) PR/CARS signal by arriving simultaneously at the sample. The resulting signal is detected by a multichannel array camera after dispersion in a triple monochromator.

3. RESULTS AND DISCUSSION

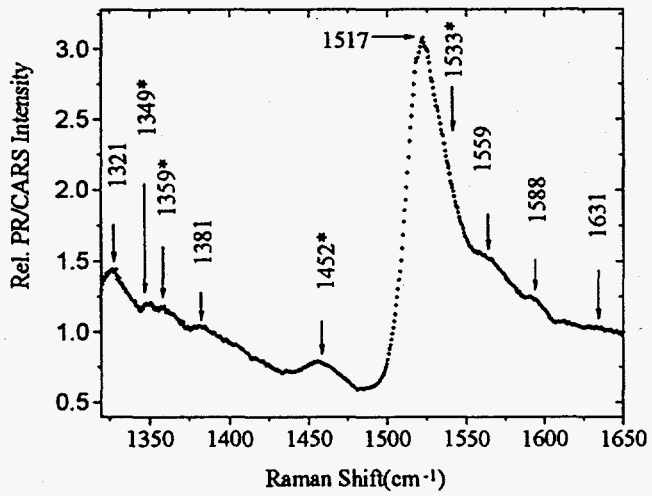

Fig. 2 PR/CARS spectrum of the ground state in the C=C stretching region.(*indicates band positions assignable to blue membrane that are previously unreported)

Previous studies have shown that the 1170-1200 cm^{-1} region of the blue membrane vibrational spectrum is similar to that observed from a dark-adapted, native BR sample [3,4]. In general, the results described here confirm that conclusion, but specifically provide a more complete and detailed characterization. Fig. 1 shows band positions at 1183 cm^{-1} and 1207 cm^{-1} which have C-C counterparts in BR-548 [5]. Similarly, in the C=C region, the 1533 cm^{-1} band position (Fig.2) has its counterpart in the BR-548 spectrum. As importantly, there are several bands in both regions that have not been reported previously , but are evident here due to the high S/N in the PR/CARS data. A χ^3 fit of these features demonstrates that two electronic phase factors are needed. The difference in the phase factors suggests that these bands originate from species with different chromophore structures. A wavelength dependence study should provide a more detailed characterization, by decreasing the contribution of one of the species relative to the other. An accurate fit of the ground state is essential for the next step, determination of the "K" intermediate of blue membrane.

References:

1) P.C. Mowery, R.H. Lozier, Q. Chae, Y.W. Tseng M. Taylor, W. Stoeckenius: Biochemistry, 18, 4100 (1979).

2) H. Ohtani, T. Kobayashi, A. Ikegami:Primary Processes in Photobiology, 193 (Springer, Berlin, 1987).

3) S.O. Smith,R.A. Mathies: Biophysical Journal, 47, 251(1985).

4) E.L. Chronister,M.A. El-Sayed: Photochemistry and Photobiology, 45, 507 (1987)

5) L. Ujj,A. Popp,G.H. Atkinson: Chemical Physics, 188, 221(1994).

A Picosecond Time-Resolved CARS Investigation on the Isotopically-labeled $^{13}C_{14}$-$^{13}C_{15}$ Bacteriorhodopsin

F. Jäger, L. Ujj, A. Popp, J. Popp and G. H. Atkinson
Department of Chemistry and Opt. Sci. Center, The University of Arizona, Tucson, AZ85721, USA
M. Sheves
Department of Chemistry, Weizmann Institute of Science, Rehovot, Israel
M. Ottolenghi
Department of Chemistry, Hebrew University, Jerusalem, Israel

Bacteriorhodopsin (BR), the light driven proton pump, has been intensively under investigation since its discovery by Österhelt 1973 [1].

It is well established that the ground state of BR (BR-570) contains an all-*trans* retinal chromophore which, upon illumination, is believed to undergo isomerization to a 13-*cis* geometry as an early step in the room-temperature (RT) BR photocycle. There has been considerable disagreement among several authors, however, as to whether a 13-14(or 13-15)-di*cis* geometry of the retinal is involved either before or instead of the isomerization from all-*trans* to the 13-*cis* geometry [2,3]. Up to now, isotopic labeling at selected positions of the retinal together with resonance Raman (RR) and Fourier transform infrared (FTIR) spectra recorded from low (77 K) temperature (LT) BR samples have not been able to resolve this issue. LT vibrational data using cw or single pulsed excitation are either not able to detect transient species or may influence the structural properties of the transients. These experiments, therefore, are limited to approximate conclusions. The technique of picosecond time-resolved coherent antistokes Raman spectroscopy (PTR/CARS) has overcome these limitations [5] to provide high signal to noise ratio data which permit the utilization of small quantities of BR e.g., isotopically-labeled samples. As part of a detailed analysis of several isotopically labeled BR samples [10], results are presented here from BR where a ^{13}C-label is located at both the C_{14} and C_{15} position.

It has been shown recently that the PTR/CARS methodology can be successfully applied to BR and rhodopsin [4-7]. The PTR/CARS spectra are recorded here in the spectral region from 1050 cm^{-1} to 1400 cm^{-1} (fingerprint) in H_2O and D_2O solvents in order to investigate changes of the C-C single bond stretching vibrations of the retinal. The C_{14}-C_{15} stretching frequency is especially sensitive to the geometry of the retinal and the magnitude of the shift of the C_{14}-C_{15} band position from BR-570 to the intermediate K-590 is believed to be an indication whether the geometry is 13-*cis* or 13-14-di*cis*. Specifically the C_{14}-C_{15} band position would be expected much lower in the former than in the latter geometry within this model (Table 1). Furthermore, deuteration should increase the C_{14}-C_{15} frequencies only slightly in the C_{14}-*trans*, while in the C_{14}-*cis* configuration it should increase substantially [9].

all-trans	13-cis	13/15-dicis	13/14-dicis
1182	1172	1150	1101

Table 1: C_{14}-C_{15} stretching frequencies according to model compound calculations [9]

The spectral results of the measurements of BR-570 and the excited-state mixture BR-570/K-590 in H_2O (both probed with low energy pulses (<2 nJ)) are presented in Fig. 1. A detailed analysis of these isotopically substituted retinal data based on the $\chi^{(3)}$ third-order nonlinear fitting procedure is described elsewhere [10].

While the BR-570 spectrum is in very good agreement with the published RR data [8], there are significant changes observed in the RT PTR/CARS data of K-590 compared to the LT RR data (Table 2). There are three major bands found in the $\chi^{(3)}$ analysis of the PTR/CARS data, while RR data contain only two bands [8,9]. Furthermore, PTR/CARS data recorded from BR-570 in D_2O show essentially no changes (except for the disappearence of the NH rock at 1345 cm^{-1}) when compared to the BR-570 results in H_2O (data not shown). The absence of changes is in agreement with LT RR data [8,9]. By contrast, a comparison of the respective spectra of the K-590 data (H_2O vs D_2O) reveals substantial changes in the fingerprint region. These changes directly contradict LT RR data [8-10] (data not shown).

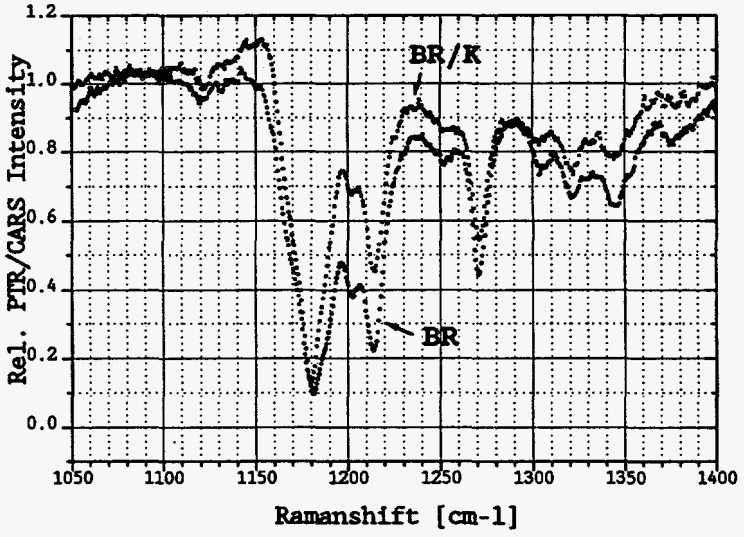

Figure 1: Ground-state (BR) and exited state (BR/K) spectra of the $^{13}C_{14}/^{13}C_{15}$ labeled BR sample.

RR-data [cm-1]	CARS-data [cm-1]
1170	1167
1189	1187
-	1197

Table 2: Selected C-C stretching frequencies of the $^{13}C_{14}/^{13}C_{15}$ BR: RR data from [8] and PTR/CARS data (this work)

References:

1. Oesterhelt, D. & Stoeckenius, W. (1971) Nature New Biol. 233: 149-152.
2. Nonella, M., Windemuth, A. and Schulten, K. (1991) Photochem. Photobiol. 54(6): 937-948; Zhou, F. , Windemuth, A. and Schulten, K. (1993) Biochemistry 32(9): 2291-306.
3. Smith, S.O., Hornung, I., v.d. Steen, R., Pardoen, J.A. , Braiman, M.S., Lugtenburg, J. and Mathies R.A. (1986) Proc. Natl. Acad. Sci. USA 83(4): 967-71; Mathies, R.A., Brito Cruz, C.H., Pollard, W.T. and Shank, C.V. (1988) Science 240(4853): 777-9.
4. Ujj, L. and Atkinson, G.H. (1993) Israel J. of Chem. 33: 207-214
5. Ujj, L., Popp, A. and Atkinson, G.H. (1994) Chemical Physics 188:221-234
6. Popp, A., Ujj, L. and Atkinson, G.H. Biophysics in press
7. Popp, A., Ujj, L. and Atkinson, G.H. Proc. Natl. Acad. Sci. USA submitted
8. Smith, O. S., Myers, A. B., Pardoen, J. A., Winkel, C., Mulder, P. J., Lugtenburg, J. and Mathies R. (1984) Proc. Natl. Acad. Sci. USA (81): 2055-2059.
9. Smith, O. S., (1985) PhD Thesis, University of California, Berkeley
10. Jäger, F., Ujj L. and Atkinson G. H., manuscript in preparation.

Femtosecond Coherence Spectroscopy of Mutant Reaction Centers

Marten H. Vos[1], Michael R. Jones[2], C. Neil Hunter[2], Jacques Breton[3], Jean-Christophe Lambry[1] and Jean-Louis Martin[1]

1. Laboratoire d'Optique Appliquée, INSERM U275, CNRS URA 1406, Ecole Polytechnique-ENSTA, 91120 Palaiseau, France; 2. Krebs Institute for Biomolecular Research and Robert Hill Institute for Photosynthesis, Department of Molecular Biology and Biotechnology, University of Sheffield, Western Bank, Sheffield, S10 2UH, United Kingdom; 3. SBE/DBCM, CEA de Saclay, 91191 Gif-sur-Yvette Cedex, France

INTRODUCTION

Oscillations in the kinetics of stimulated emission in bacterial reaction centers (RC) have previously been shown to reflect coherent nuclear motion in the P^* excited state [1,2], the precursor of physiological electron transfer (ET). The involved vibrational modes, that are activated by the $P \rightarrow P^*$ optical transition, maintain phase correlations on the timescale of primary ET in functional RCs and are candidates for the modes that assist ET. The origin of the observed damping and information about the essentially unknown identity of these low-frequency modes warrants experiments on genetically modified RCs. Here we report experiments on chromatophores containing RCs of *R. sphaeroides* mutated at position M210 and L181, which are known to modify the electronic properties of the chromophore system.

EXPERIMENTAL

Significant technical improvements have been implemented. First, the data were collected with a EG&G OMA4 CCD camera with a readout time fast enough to allow shot-to- shot normalization (at 30 Hz) of the test and reference beam. This allowed determination of the time evolution of the entire stimulated emission band with a high signal to noise. Second, the probe pulse compression was improved and the probe pulse was essentially chirp-free (<20 fs) over a wavelength range of 80 nm. Both developments are especially advantageous for studying series of mutants with *a priori* unknown emission profiles. The experiments were conducted at 10K, but coherence is also maintained for more than 1 ps at room temperature [3].

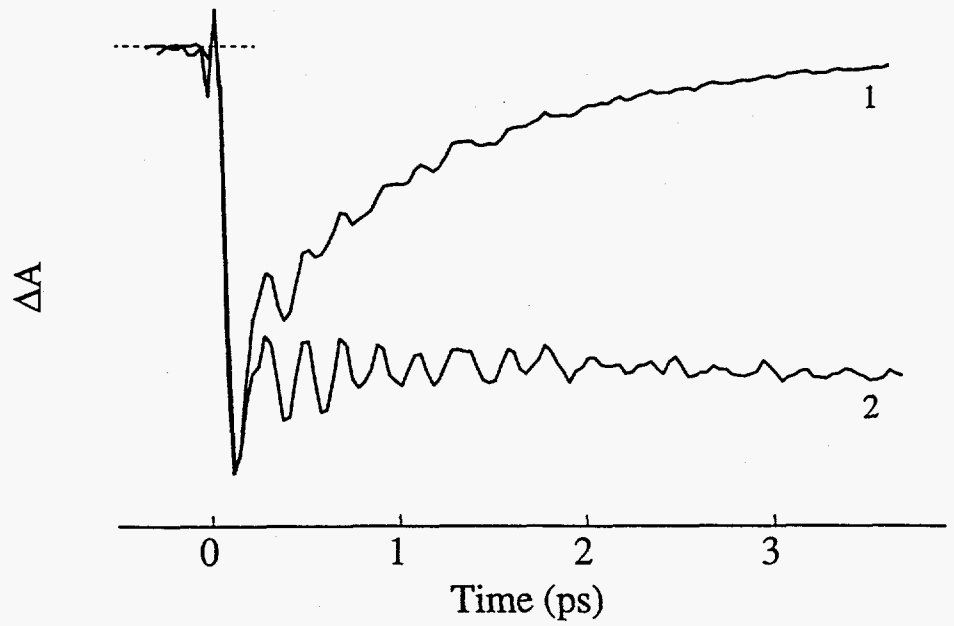

Figure 1: *Transient absorption kinetics at 10K probed at 940 nm after excitation at 880 nm. 1: wild type. 2: Y M210 W mutant.*

RESULTS AND DISCUSSION

A series of single residu-mutants, at position M210 and the symmetry-related position L181 was studied. These mutations change the time scale of primary ET over about two orders of magnitude [4] without major structural changes in the vicinity of P. Figure 1 shows the kinetics of stimulated emission in WT and a mutant in which tyrosine M210 is replaced by tryptophan, where P^* decays in several hundreds of picoseconds. Clearly the dephasing of the oscillations is substantially longer in this mutant and phase correlations are observed up to at least 4 ps. We stress that the observed damping may be (partially) due to the fact that a manifold of vibrational modes is activated. Therefore the observed damping time can only be considerd as a *lower limit* of the molecular vibrational dephasing time. The faster damping in WT RCs is can be ascribed solely to the depletion of the P^* excited state, in which these coherent motions take place. Experiments on three other single-residu mutants, in which tyrosine M210 is replaced by leucine or histidine and where histidine L181 is replaced by tyrosine, displaying both faster and slower ET than WT (not shown) confirm this conclusion. The ensemble of results also confirm the previous assignment of the oscillations to excited state vibrational motion.

Fourier transform analysis of the data in Fig. 1 and corresponding data for other mutants demonstrate that the frequencies of the coupled modes are not strongly modified by the mutations, indicating that these mutants influence merely the electronic parameters of the cofactor system (redox potentials and electronic coupling) but not the light-induced relative motions of the cofactors.

References

1. Vos, M.H., Rappaport, F., Lambry, J.-C., Breton, J. & Martin, J.-L. *Nature* **363** (1993), 320-325
1. Vos, M.H., Jones, M.R., Hunter, C.N., Breton, J., Lambry, J.-C. & Martin, J.-L. *Biochemistry* **33** (1994), 6750-6757
3. Vos, M.H., Jones, M.R., Hunter, C.N., Breton, J. & Martin, J.-L. *Proc. Natl. Acad. Sci. USA* **91** (1994), 12701-12705
4. Chan, C.K., Chen, L.X.Q., DiMagno, T.J., Hanson, D.K., Nance, S.L., Schiffer, M., Norris, J.R. & Fleming, G.R. *Chem. Phys. Lett.* **176** (1991), 366-372

Structure-Function Relationship in Hemoglobin (HbI) from *Lucina pectinata*

J. Lopez-Garriga*, J. Colon, R. Lopez-Mejias, A. Navarro, M. Maldonado.

*Chemistry Department University of Puerto Rico, Mayagüez Campus, Mayagüez, P.R. 00680-5000, USA. E-mail address: J_lopez@rumac.upr.clu.edu

Introduction

Lucina pectinata is a bivalved mollusc that lives in sulfide-rich coastal sediments on the south-west coast of Puerto Rico and houses intracellular chemoautotrophic symbiotic bacteria which provide organic carbon to the clam. *Lucina pectinata* contains three different hemoglobins: Hemoglobins I, II, and III. Hb I, the monomeric sulfide reactive species has, in the ferric state, an extraordinary affinity for sulfide, with fast combination and very slow dissociation dynamics. The other two hemoglobins, Hb II and Hb III, do not bind sulfide and are oxygen transport proteins. Hb I reacts with hydrogen sulfide and oxygen to form the ferric sulfide complex needed to transport the sulfide to the bacteria symbiont of the clam. Hydrogen sulfide is believed to be released to the bacteria upon formation of the ferrous protein by electron transfer from a still unknown reductant. Hb I is probably the only heme protein that carries its function in the hydrogen-sulfide bound ferric state and in the dioxygen bound ferrous state.[1] The X-ray crystal structure of Hb I in the ferric form recently obtained by Rizzi *et al.*[2] *L. pectinata* Hb I has a histidine in the proximal position to the heme. However the distal position E7 has a glutamine residue instead of a histidine, just as in elephant myoglobin. In addition to the Gln64(E7) residue, HbI has the unusual Phe29(B10) and the unique Phe68(E11) residues. Furthermore, HbI has an array of nearly parallel aromatic amino residues around the heme pocket. Thus, the ligand binding properties of Hb I may be influenced by the low distal pocket polarity resulting from the array of phenylalanyl residues surrounding the heme. Studies on monomeric hemoglobins, such as Hb I, with extreme hydrophobic heme pocket environments can provide useful models for heme proteins to answer questions such as: how does ligand selection occur? How do the heme pocket aromatic residues contribute or modulate the association and dissociation ligand rate constants?.

Results and Discussion

The FTIR spectroscopic measurements for the HbI-CO complex at room temperature showed two main heme-CO conformers at 1964 cm^{-1} and 1939 cm^{-1}, respectively. These frequencies are not significantly dependent of the pH and solvent (H_2O/D_2O) exchange. The decomposed FTIR spectrum of the HbICO showed the presence of the A_3 main conformer occurring at 1936cm^{-1} (61%), and a shoulder of A_0 at 1960 cm^{-1} (30%). A minor component, the $A_{1,2}$ conformer occurrs at 1950 cm^{-1} (9%). The high intensity band of the HbI-CO complex is 8 cm^{-1} lower in energy than the 1944 cm^{-1} found in SW-Mb. Since the distal histidine in heme proteins has been assigned the role of modulating the ligand reactivity towards the heme centers, it is not clear

why the natural His64(E7)→Gln substitution in HbI-CO complex showed lower ν_{CO} frequencies. Positive electrostatic potentials, for example hydrogen bond or charged amino acids near the oxygen atom of the heme-carbon monoxide complex, stabilize the resonance structures of the FeCO moiety which mainly contribute to the formation of the $A_{1,2}$ and A_3 conformers.[3] However, these positive fields should be weaker for the glutamine residue in elephant Mb and HbI than for histidine residue and therefore can not explain the much lower ν_{CO} frequencies observed in elephant Mb and HbI. The positive field increase due to a nearby phenyl multipole of a phenylalanine has been proposed to decrease the CO stretching frequency. Both elephant and HbI have a phenylalanine at position 29(B10) and therefore show lower CO frequencies than SW-Mb which has leucine at that position.[4] The single and double mutants with phenylalanine at positions 29(B10) and /or 68 (E11) show low VCO frequencies, but the triple mutant {His64(E7)→Gln64(E7), Leu29(B10)→ Phe29 (B10), Val68(E11)→Phe68(E11)} mimics HbI.

Time resolved infrared spectroscopy was used to follow the 1939 cm^{-1} conformer of the HbICO moiety. The results showed that FeCO recombination time with a half-life of 25 μs. The rate constant for the recombination between HbI and CO was 8.33 $\mu M^{-1}s^{-1}$. This value is higher than the rate constant reported for similar species and mutants. The HbICO association rate constant is in the order of magnitude of the recombination constant reported for the triple mutant of 3.1 $\mu M^{-1}s^{-1}$ using flash photolysis techniques. Nevertheless, a reported value of 0.78 $\mu M^{-1}s^{-1}$ was determined previously for HbI using the same technique. Since time-resolved infrared spectroscopy is a more accurate technique in establishing the precise nature of the CO kinetics, our measurements suggest that a association constant of 8.33 $\mu M^{-1}s^{-1}$ for the HbI and CO reaction is acceptable. This indicates that the triple mutant not only mimics the FeCO vibrational frequency, but also mimics the CO association rate constant. This suggests that the functionality of the Gln64(E7), Phe29 (B10), and Phe68(E11) in HbI increases the CO association rate relative to SM-Mb which lacks this aromatic environment in the heme pocket. This indicates that the synergistic action of both phenylalanines accounts for the observed low CO frequencies of HbI. Therefore, it seems that the aromatic nature of the heme pocket in HbI is the main factor contributing to the observed conformers and ligand dynamics.

Acknowledgments

We would like to express our thanks to Professor J. Olson for providing us with the sperm-whale myoglobin triple mutant. We thanks Professor J. Wittenberg and Professor M. Bolognesi for helpful discussions with us. J.L.G. acknowledges support from the EPSCoR-MBTC Program and MRCE-UPR-NSF. J.L.C. acknowledges the financial of the NSF (CHE-91534 and 91223).

References

1. E.Casale, C. Lionetti, A. Coda, A. Merli, P. Ascenzi, J.B.Wittenberg and M. Bolognesi J. Mol Biol. 222 (1991) 447.
2. M. Rizzi, J.B. Wittenberg, A. Coda, M. Fasano, P.Ascenzi and M. Bolognesi J. Mol. Biol. 244 (1994), 86..
3. T. Li, M.L. Quillin, G.N. Phillips, and J.S. Olson Biochemistry 33, (1994), 1433.
4. J. Ling, T. Li, J.S. Olson, G.N. Phillips, Y. Dou, M. Ikeda-Saito, R. Regan, M. Carlson, Q. Gibson, H. Li and R. Elber. J. Mol. Biol. 245, (1995) 416.

Rebinding and Concomitant Protein Relaxations of CO-Myoglobin Studied by Time-Resolved Infrared Difference Spectroscopy

Christoph Rödig and Friedrich Siebert
Institut fuer Biophysik und Strahlenbiologie der Universität Freiburg
Albertstraße 23, D-79104 Freiburg, Germany

Myoglobin represents an ideal model system for studying protein dynamics, structural changes associated with ligand binding and structure-function relationship. It has been studied extensively by various techniques including UV-vis spectroscopy, resonance Raman spectroscopy and infrared spectroscopy[1-3].

Up to now there is little information available about more general structural changes during the rebinding of the ligand after flash photolysis, i.e. about the structure associoated with the different conformational substates. In order to study this question, we used two techniques of time- resolved FTIR-spectroscopy: the step-scan technique was used to monitor ligand rebinding at ambient temperature with a time resolution of 500 ns, while the rapid-scan technique shows processes in the ms time range at low temperatures.

Measuring FTIR-difference spectra in the whole spectral range between 2220 cm^{-1} and 900 cm^{-1} enables us to obtain simultaneously information on different parts of the protein: there are the well known difference bands monitoring the ligand in free and bound state in the spectral range above 1900 cm^{-1}, bands in the amide-I and amide-II region reflect possible alterations of the protein backbone in addition to those of amino acid side chains; further bands between 1300 cm^{-1} and 1100 cm^{-1} can probably be assigned to the heme ring.

Fig. 1 shows results of our time-resolved measurements. The six difference spectra on the right hand side were obtained with the step-scan technique. They represent the state of the molecule at different times after laser flash photolysis (we used a Nd:YAG-laser with a pulse energy of 5 mJ in a 7 mm diameter spot). One can clearly distinguish the CO-stretching band at 1945 cm^{-1} with a sholder at 1965 cm^{-1}. The slight increase of this band before the decay is probably due to a photoselection effect followed by rotational diffusion. This effect may also cause some alterations of the amide-I difference bands. The bands in the amide-I and amide-II region (1700 cm^{-1} to 1500 cm^{-1}) reflect alterations of the proteine backbone. Other caracteristical bands, assigned to the heme ring, appear in the spectral range between 1300 cm^{-1} and 1100 cm^{-1}.

The rapid-scan measurements were performed at 85 K where the rebinding of the ligand is slowed down by several orders of magnitude in time. The five difference spectra on the left hand side in Fig. 1 reflect the rebinding of CO with a time resolution of 2 ms. In addition to the spectra at room temperature, the band of the photoproduct can be seen at 2130 cm^{-1}. In The spectra shown, the shoulder on the 1954 cm^{-1} -band does not appear. This is probably due to the faster rebinding kinetic of the A_0-band [4], which can't be resolved with the rapid scan technique. Another property of these spectra is the change in the relative intensities of the bands in the amide-I region and the band at 1545 cm^{-1}. The developement with time of all difference bands is caracterized by a decrease that doesn't change relative intensities.

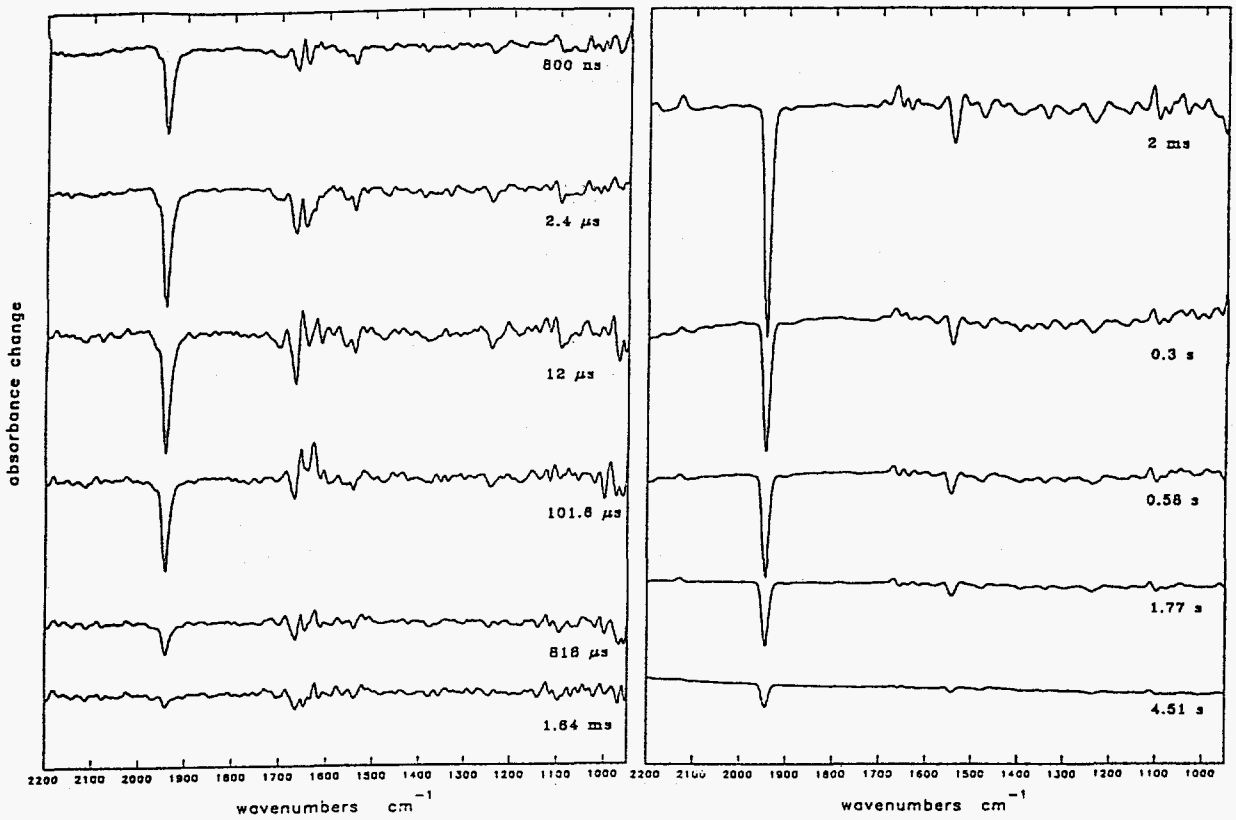

Fig. 1 FTIR-difference spectra of horse MbCO at different times after laser flash photolysis with a spectral resolution of 4 cm^{-1}, measured with the step-scan technique (right, 5 mmol solution of Mb in phosphate buffer, pH 7, at room temperature, on CaF_2 windows with 5μ spacer) and with the rapid-scan technique (left, 7 mmol solution in 3:1 v/v phosphate buffer/glycerol at 85 K)

In order to investigate in more detail the above results and to complete the data, a number of addtitional experiments have to be carried out. Measurements of deuterated samples will help to reduce noise in the amide-I region and could be helpful to assign the observed difference bands. Further step-scan measurements shold clarify spectral differences of the protein in the conformational substates. Also the evaluation of the kinetics of the caracteristical difference bands shold yield information about relations between structure and function of the molecule. Finally, measurements using myoglobin mutants could reveal spectral differences relative to wild type samples and also help band assignment.

References

[1] A.Ansari et al., Bioph. Chem., 26 (1987) 337-355
[2] P.Causgrove and B.Dyer, Biochemistry, 32 (1993) 11985-11991
[3] T.Kitagawa et al., Chem. Phys. Lett., 196 (1992) 150-154
[4] H.Frauenfelder et al:, J. Phys. Chem., 94 (1990) 1024-1037

ABSTRACTS FOR POSTERS
CHEMICAL PHYSICS AND THEORY

A Comparison of Time and Frequency Domain Resonance Raman Spectroscopies in Triiodide

Alan E. Johnson and Anne B. Myers*
Department of Chemistry, University of Rochester, Rochester, NY 14627-0216
Sanford Ruhman
Department of Physical Chemistry, Hebrew University of Jerusalem, 91904, Jerusalem, Israel

Vibrational spectroscopy has traditionally been performed in the frequency domain. While there are many transient vibrational spectroscopies which use a pump pulse to initiate a photochemical reaction prior to the measurement of the transient spectrum, the spectrum is still obtained by frequency resolving the absorbed or emitted radiation. However, with the recent proliferation of lasers with pulses shorter than vibrational periods, true time domain vibrational spectroscopies have been developed. In particular, Resonance Impulsive Stimulated Raman Scattering (RISRS) is a time domain vibrational spectroscopy involving a single pump pulse and a single probe pulse. Both RISRS and spontaneous resonance Raman (RR) spectroscopies can provide information about the structure and dynamics of the resonant excited electronic state. While it is often assumed that RISRS and RR spectra are essentially equivalent, our work [1] and that of others [2] demonstrate otherwise. In this paper, we present experimental and computational comparisons of the RISRS [3] and RR [4] spectra of the triiodide ion, which undergoes ultrafast photodissociation to the diiodide ion and an iodine atom.

Figure 1 compares the experimental RR spectrum [4] (bottom) and the Fourier transform of the experimental degenerate RISRS signal [3] (top) for triiodide in ethanol at nearly identical excitation wavelengths. The RR spectrum is dominated by a progression in the symmetric stretch and also shows some antisymmetric stretch activity. The RISRS spectrum is dominated by the fundamental of the symmetric stretch and does not show overtone or antisymmetric stretch activity. The RR symmetric stretch linewidth also appears to be about a factor of two broader than the linewidths in both the RISRS spectrum and the preresonant spontaneous Raman spectrum. Extensive numerical simulations of RR and RISRS spectra using a common model indicate that the suppression of overtones and combination bands in the RISRS spectra is a general feature of two-pulse RISRS spectra and that it is not due to limited bandwidth or limited time resolution in the experiment.[1] This suggests that the seemingly large vibrational linewidths observed in the RR spectrum could be due to unresolved combination bands with low frequency solvent modes that are excited on resonance. This type of combination band has been resolved in the resonance Raman spectrum of ozonide in water.[5]

Figure 2 shows the dependence of the calculated RR (bottom) and RISRS (top) lineshapes as a function of the number of initial vibrational states populated (solid: ground vibrational state only; dash: assumes a temperature of 150K and includes all states with energy < 261 cm^{-1}) assuming that the solvent contribution to the spectrum can be modeled as a single low frequency (10 cm^{-1}) harmonic oscillator with a linewidth comparable to the frequency. As the number of initial states included in the calculation is increased, the linewidth in the RISRS spectrum stays

almost constant, but the linewidth in the RR spectrum is seen to increase dramatically, due to contributions from the solvent mode.

Upon initial inspection, the resonance Raman spectrum seems to contain much more information, especially about the higher overtones of the triiodide symmetric stretch. In contrast, the RISRS spectrum is dominated by the symmetric stretch fundamental. At other laser wavelengths, the resonance Raman spectra look similar to the spectrum shown here,[4] but the calculated RISRS spectrum can show overtone activity, sometimes even in the absence of fundamental activity.[1] In general, the spontaneous resonance Raman spectrum contains all of the possible vibronic transitions, weighted by the appropriated Franck-Condon and thermal factors. The RISRS spectrum is a subset of this spectrum that has been projected out by the spectral and temporal properties of the pump and probe pulses. In the current case (60 fs pulses at 308 nm) the RISRS spectrum is dominated by the fundamental of the symmetric stretch at 112 cm^{-1}. The same vibronic information is potentially available in both experiments. However, interpretation of the frequency domain data may be clouded by the presence of many overlapping transitions, while in the time domain, high overtones may be difficult to excite in a simple two pulse experiment.

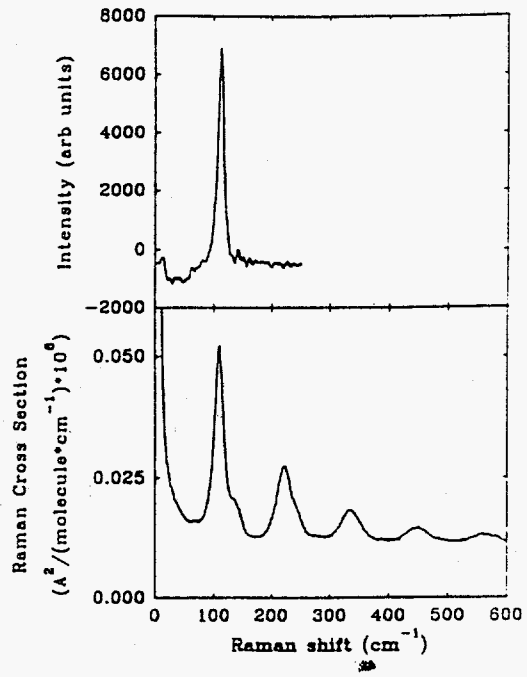

Figure 1

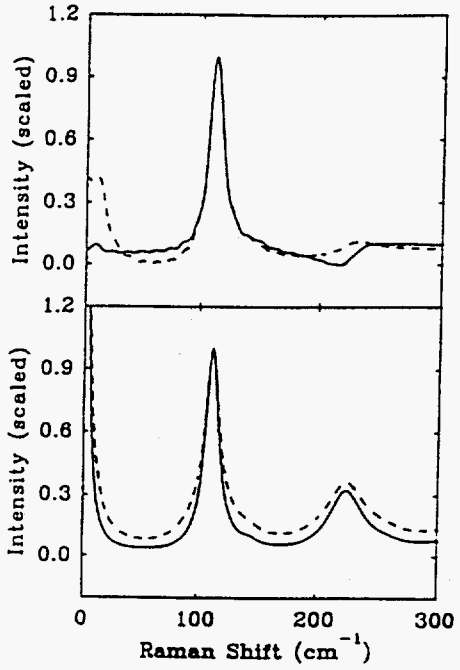

Figure 2

References

1. A.E. Johnson and A.B. Myers, in preparation
2. W.T. Pollard, S.L. Dexheimer, Q. Wang, L.A. Peteanu, C.V. Shank and R.A. Mathies, J.Phys.Chem. 96 (1992) 6147.
3. U. Banin, R. Kosloff and S. Ruhman, Isr.J.Chem. 33 (1993) 141.
4. A.E. Johnson and A.B. Myers, J.Chem.Phys. 102 (1995) 3519.
5. Y. Su and G.N.R. Tripathi, Chem.Phys.Lett. 188 (1992) 388.

Optical-Heterodyne-Detection of Polarization-Selective Impulsive Stimulated Raman Scattering Responses by Liquids

Yong Joon Chang, Peijun Cong and John D. Simon
Department of Chemistry and Biochemistry & Institute for Nonlinear Science
University of California, San Diego
9500 Gilman Drive, La Jolla, CA 92093-0341, U.S.A.

The study of intermolecular interactions in the condensed phase is important for determining the medium's role in affecting the dynamics of a chemical reaction. In this regard, the use of time-resolved third-order nonlinear spectroscopic techniques such as polarization-selective transient grating impulsive stimulated Raman scattering (TG-ISRS) [1] and optical-heterodyne-detected Raman-induced Kerr effect (OHD-RIKES) [2] have been quite fruitful in studying the intermolecular dynamics in liquids.

An important advantage of OHD-RIKES is that the heterodyne-detection allows the measurement of the optical signal that is linearly proportional to the material nonlinear susceptibility response, $\chi^{(3)}(t)$; TG-ISRS measures the signal that is proportional to $|\chi^{(3)}(t)|^2$. The linear signal detection allows the separate measurement of the real (dispersive) and imaginary (absorptive) parts of $\chi^{(3)}(t)$. The distinct advantage of TG-ISRS technique over OHD-RIKES is that the former is able to probe different $\chi^{(3)}$ tensor elements by the choice of polarization combinations of the pump and probe fields (i.e., $|\chi^{(3)}_{1111}(t)|^2$, $|\chi^{(3)}_{1122}(t)|^2$ or $|\chi^{(3)}_{1212}(t)|^2$ in isotropic medium); OHD-RIKES can only measure the depolarized component (i.e., $\chi^{(3)}_{1212}(t)$) because of the cross-polarization geometry used for this experiment.

The advantages of the two techniques have been brought together by the implementation of OHD in the TG-ISRS experiment [3]. This was achieved by introducing a Mach-Zehnder interferometer [3(b)] to the standard TG-ISRS experimental set-up to provide a local oscillator field, E_{lo}, that can interact coherently with the ISRS signal field, E_s. Using phase-sensitive detection, the intensity linear in the signal field, $Re(E_s \cdot E^*_{lo})$, and therefore linear in $\chi^{(3)}$ is measured. By controlling the relative phase relationship between E_s and E_{lo} using a piezoelectric transducer, it is possible to selectively measure the real and imaginary parts of an *arbitrary* $\chi^{(3)}$ tensor element in either the time- or frequency domain. By coherently interfering the diffracted TG-ISRS signal with either the in-phase or 180° out-of-phase local oscillator, the real part of $\chi^{(3)}(t)$ is selectively measured; the imaginary part is measured through interfering with the 90° out-of phase local oscillator.

The in-phase heterodyne-detected and homodyne-detected $\chi^{(3)}_{1111}(t)$ are compared for the liquids CS_2 and benzene in Figures 1 and 2, respectively. As expected from the linearization of the ISRS signal, the relaxation times obtained from the single exponential decay fit of the long time rotational diffusion response differ by a factor of two between the heterodyne- and homodyne-detected ISRS responses. We are currently investigating the relationship between the polarized and depolarized components of $\chi^{(3)}$ responses to obtain a more complete picture of the molecular interaction potential that governs the ultrafast motions observed in these liquids.

By being able to independently measure the compiementary polarized and depolarized

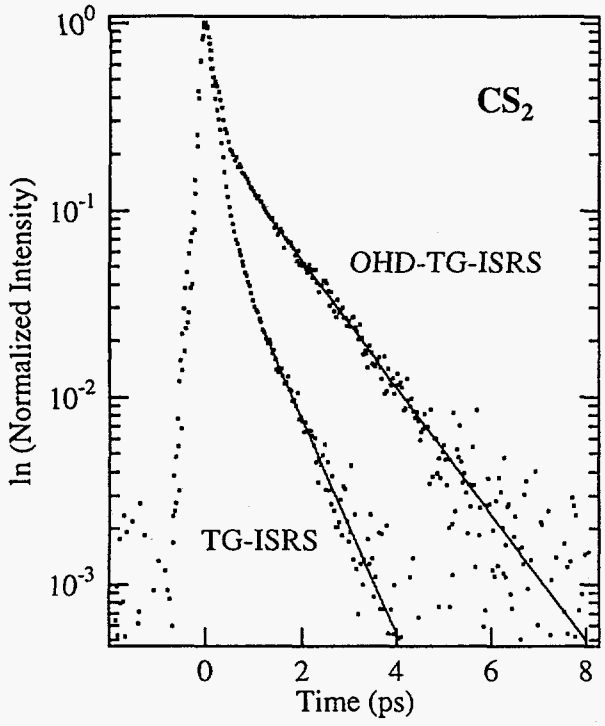

Figure 1. Comparison of heterodyne- and homodyne-detected TG-ISRS responses for CS_2. The solid lines are single exp. decay fits to the long time rotational diffusion response. The calculated time constants are 1.3+/-0.1 ps and 0.7+/-0.1 ps for heterodyne- and homodyne-detected responses, respectively.

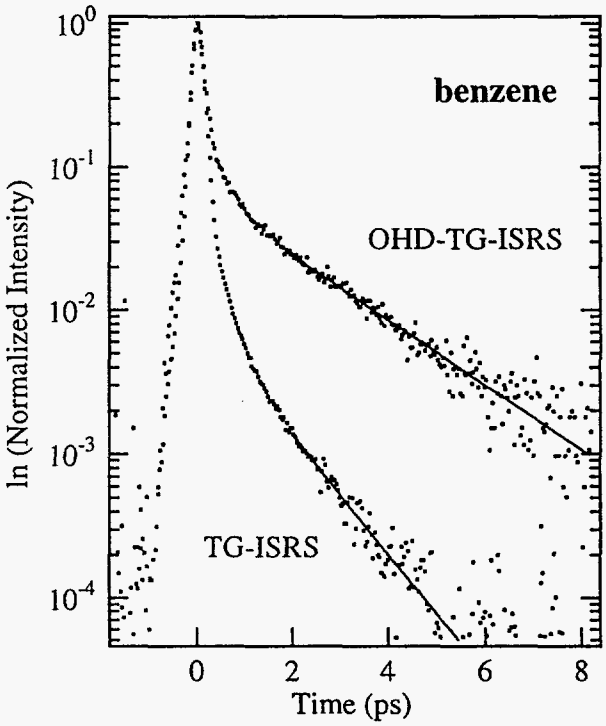

Figure 2. Comparison of heterodyne- and homodyne-detected TG-ISRS responses for benzene. The solid lines are single exp. decay fits to the long time rotational diffusion response. The calculated time constants are 1.9+/-0.1 ps and 1.0+/-0.1 ps for heterodyne- and homodyne-detected responses, respectively.

components of the linearized material nonlinear optical response using OHD-TG-ISRS, a more comprehensive picture of molecular motions that occur in liquids and their effects on chemical reactivity should be attainable. The technique OHD-TG-ISRS promises to be an important spectroscopic tool for studying the details of molecular interactions that shape the overall condensed phase solution dynamics.

Acknowledgment

The support of this work from the National Science Foundation is gratefully acknowledged.

References

1. (a) S. Ruhman, A. G. Joly, B. Kohler, L. R. Williams and K. A. Nelson, Rev. Phys. Appl. **22** (1987), 1717; (b) J. Etchepare, G. Grillon and J. Arabat, J. Appl. Phys B **49** (1989), 425; (c) F. W. Deeg and M. D. Fayer, J. Chem. Phys. **91** (1989), 2269.
2. (a) D. McMorrow, W. T. Lotshaw and G. A. Kenney-Wallace, IEEE J. Quantum Electron. **QE-24** (1988), 443; (b) M. Cho, M. Du, N. F. Scherer, G. R. Fleming and S. Mukamel, J. Chem. Phys. **99** (1993), 2410; (c) Y. J. Chang and E. W. Castner Jr., J. Phys. Chem. **98** (1994), 9712; (d) H. P. Deuel, P. Cong and J. D. Simon, J. Phys. Chem. **98** (1994), 12600.
3. (a) P. Vöhlinger and N. F. Scherer, J. Phys. Chem. **99** (1995), 2684; (b) Y. J. Chang, P. Cong and J. D. Simon, J. Phys. Chem. **99** (1995), 7857.

Direct Measurement of Polarized and Depolarized Raman Spectral Densities of Liquids using Femtosecond Stimulated Raman Gain Spectroscopy

Yong Joon Chang, Peijun Cong and John D. Simon
Department of Chemistry and Biochemistry and Institute for Nonlinear Science
University of California, San Diego
9500 Gilman Drive, La Jolla, CA 92093-0341 U.S.A.

Intermolecular interactions in the condensed phase give rise to collisional as well as dielectric friction that directly affect phenomena such as electronic/vibrational dephasing, energy flow, molecular diffusion, and chemical transformation. Traditionally, the low-frequency intermolecular motions in liquids have been studied using frequency-domain spectroscopic techniques such as spontaneous Raman scattering, far-infrared absorption, and microwave absorption. Recently, techniques such as femtosecond optical-heterodyne-detected Raman-induced Kerr effect (OHD-RIKE) [1] and frequency-resolved stimulated Raman gain (SRG)[2] have provided additional means to directly obtain highly accurate depolarized or anisotropic component of the low-frequency spectral density.

In addition to the depolarized part of the intermolecular spectral density, it is desirable to be able to also accurately measure the complementary polarized spectral density. The critical comparison of these two spectral densities will give detailed insight into the nature of the intermolecular motions in terms of the underlying liquid structure and symmetry. Unfortunately, very little attention has been given to making these comparisons mainly because of the difficulty in accurately measuring the polarized part of the intermolecular spectrum.

We demonstrate the ability to directly obtain both the polarized and depolarized intermolecular Raman spectral densities using the electronically off-resonant, time-resolved stimulated Raman gain (TR-SRG) spectroscopy. The two-pulse TR-SRG measures the transient response of the imaginary part of molecular third-order nonlinear susceptibility, $\mathrm{Im}[\chi^{(3)}(t)]$, following the impulsive stimulated excitation of the low-frequency Raman modes by a broadband, femtosecond pump pulse. By setting the polarization of the pump and probe beams to be parallel or perpendicular, the polarized ($\mathrm{Im}[\chi^{(3)}_{1111}(t)]$) or depolarized ($\mathrm{Im}[\chi^{(3)}_{1122}(t)]$) TR-SRG response can be selectively measured. A related technique, transient grating impulsive stimulated Raman scattering (TG-ISRS) [3], can also measure the different third-order susceptibility tensor element responses. Because TG-ISRS measures the squared modulus of $\chi^{(3)}(t)$, the real and imaginary parts cannot be separated and the spectral densities cannot be routinely obtained. Recently, we have implemented optical heterodyne detection in the TG-ISRS experiment [4]. This enables the selective measurement of either the real or imaginary part of the $\chi^{(3)}(t)$ molecular response. The attraction for TR-SRG in comparison to OHD-TG-ISRS is the simplicity of the former experiment.

The polarized ($\mathrm{Im}[\chi^{(3)}_{1111}(t)]$) and depolarized ($\mathrm{Im}[\chi^{(3)}_{1122}(t)]$) TR-SRG responses for the liquids CS_2 and benzene are shown in Figures 1 and 2, respectively. In Figure 1, the inertial lag of the nuclear responses with respect to the instantaneous electronic response (limited by the pump-probe cross-correlation full-width, half maximum of ~30 fs) is clearly observable. It is also interesting to note that the sign of the nuclear response reverses with respect to the electronic response in going from the polarized to the depolarized $\mathrm{Im}[\chi^{(3)}(t)]$. This sign relationship was also observed previously by Minoshima *et al.* [5] in liquid CS_2 using a femtosecond interferometric method. Using the data presented in Figures 1 and 2, the polarized and

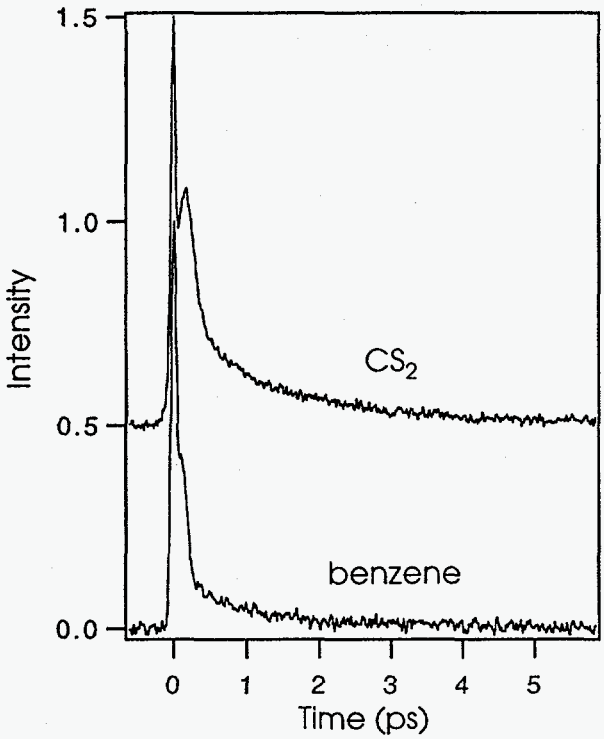

Figure 1. Polarized TR-SRG data shown in a stacked plot. Electronic response is normalized to unity.

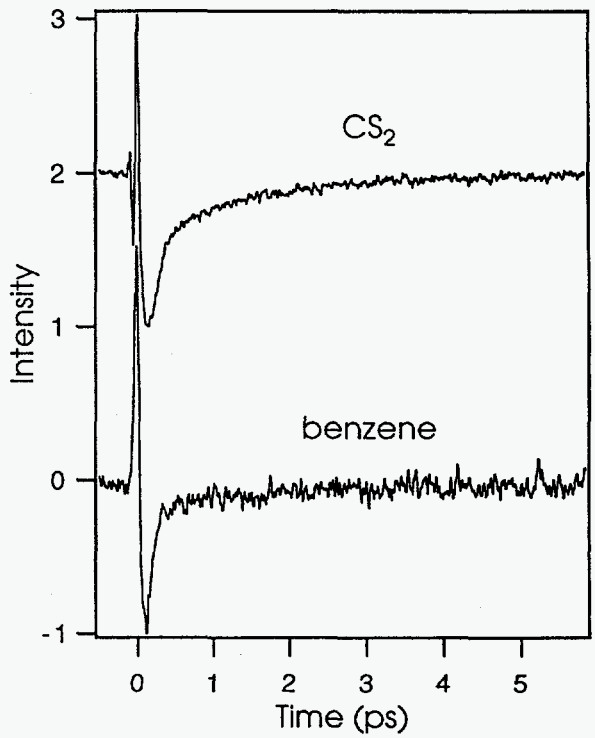

Figure 2. Depolarized TR-SRG data shown in a stacked plot. Nuclear response is normalized to unity.

depolarized intermolecular spectral densities can be directly obtained through a Fourier-transformation/deconvolution procedure. Preliminary results indicate that the profiles of the polarized and depolarized spectral densities are very similar if not identical within our experimental error for the liquids CS_2 and benzene. This indicates that the intermolecular modes probed in these liquids are mostly anisotropic in nature. Similar experiments are being carried out for a class of more structured, hydrogen-bonding liquids to compare the complementary intermolecular spectral densities.

Acknowledgment

The support of this work from the National Science Foundation is gratefully acknowledged.

References

1. (a) D. McMorrow, W. T. Lotshaw and G. A. Kenney-Wallace, IEEE J. Quantum Electron., **QE-24** (1988), 443; (b) M. Cho, M. Du, N. F. Scherer, G. R. Fleming and S. Mukamel, J. Chem. Phys., **99** (1993), 2410; (c) Y. J. Chang and E. W. Castner Jr., J. Phys. Chem., **98** (1994), 9712; (d) H. P. Deuel, P. Cong and J. D. Simon, J. Phys. Chem., **98** (1994), 12600.
2. J. S. Friedman and C. Y. She, J. Chem. Phys., **99** (1993), 4960.
3. (a) S. Ruhman, A. G. Joly, B. Kohler, L. R. Williams and K. A. Nelson, Rev. Phys. Appl., **22** (1987), 1717; (b) F. W. Deeg and M. D. Fayer, J. Chem. Phys., **91** (1989), 2269.
4. Y. J. Chang, P. Cong and J. D. Simon, J. Phys. Chem., **99** (1995), 7857.
5. K. Minoshima, M. Taiji and T. Kobayashi, Opt. Lett., **21** (1991), 1683.

The Intermolecular Vibrational Dynamics of Substituted Benzene and Cyclohexane Liquids, Studied by Femtosecond OHD-RIKES

Edward W. Castner, Jr. and Yong Joon Chang†
Brookhaven National Laboratory, Chemistry Department, Building 555A
Upton, NY 11973-5000 U.S.A. Internet: castner1@bnl.gov
†present address: Dept. of Chemistry, Univ. of California, San Diego, CA 92093-0341

With femtosecond laser pulses, it is now possible to impulsively excite all of Raman-active intermolecular dynamics in a liquid sample. By using the femtosecond optical-heterodyne detected, Raman-induced Kerr effect spectroscopy (fs-OHD-RIKES) experiment, we have studied the intermolecular dynamics of toluene, benzyl alcohol, benzonitrile, cyclohexane, and methylcyclohexane in both the time and frequency domains [1]. The intermolecular dynamics may be broadly categorized as inertial, or underdamped motions, or diffusive, or overdamped motions. The underdamped motions include the intermolecular collisions, inertial rotations, and libration caging motions arising from torques caused by strong intermolecular electrostatic interactions. The slower diffusive motions that we observe are reorientational motions with the characteristics of Brownian motion. Because of the high signal-to-noise inherent with all OHD techniques, and because the OHD-RIKES signal is linear in the molecular response, we can analyze the third-order molecular response in both the time and frequency domains via Fourier transformation. The measured fs-OHD-RIKES birefringence transients for the five liquids are shown in Figure 1 over a four picosecond time window.

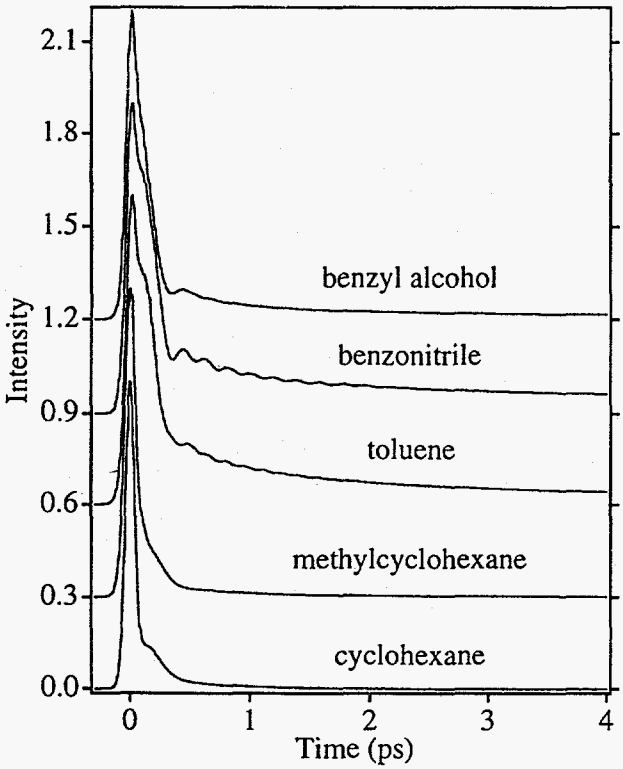

Figure 1. OHD-RIKES time-domain data, normalized to unity, are shown in a stacked plot.

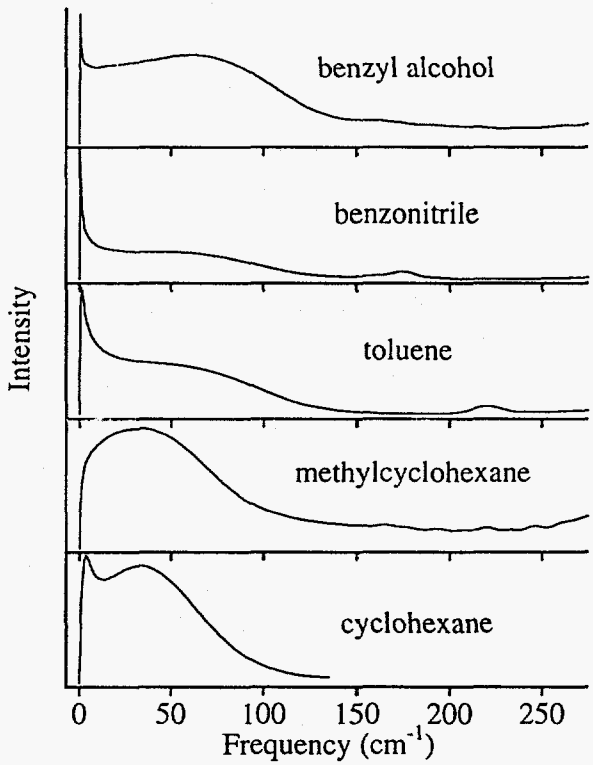

Figure 2. Frequency-domain representation of data in Fig. 1 obtained through Fourier-transformation/deconvolution.

In all of the five liquids, a slower diffusive relaxation is observed on time scales ranging from 1.5 ps in cyclohexane to 63 ps in benzyl alcohol. Though the five solvent molecules are similar in shape and volume, their diffusive reorientation times are related not only to symmetry, but are more strongly correlated with the intermolecular electrostatic interactions. Though methylcyclohexane and toluene have the same molecular symmetry and are of a similar volume, the longest time constants for diffusive relaxation are 2.64 ps and 5.90 ps, respectively.

The frequency domain representation of the time domain OHD-RIKES data are shown in Figure 2. In the aromatic liquids, we observe intramolecular bending modes at about 200 cm^{-1}, and a librational feature at about 70 cm^{-1} arising from strong intermolecular dipolar and quadrupolar interactions. The librational feature is absent in the cyclohexanes, as there are no strong intermolecular forces present in these non-polar liquids. Instead, a collision-induced band is clearly observed in cyclohexane and methylcyclohexane, peaked at about 40 cm^{-1}. The sharp Lorentzian peak near 0 cm^{-1} observed for the aromatic liquids corresponds to the long rotational diffusion dynamics. This same feature is significantly broadened in the cyclohexanes because of the much shorter rotational diffusion time constants.

To further understand the isolated molecule structure and electrostatic properties of these five liquids, *ab initio* molecular orbital calculations were carried out at the restricted Hartree-Fock level of theory, followed by a density functional correction for electron-correlation and electron-exchange, using the 6-31G** basis set. To briefly summarize the results, we find that even in the most strongly dipolar liquid studied, benzonitrile (μ~4.0 D), that the electrostatic interactions are dominated by quadrupole-quadrupole interactions. Thus, the similarities in the librational lineshapes fitted for toluene, benzyl alcohol, and benzonitrile, should not be surprising.

The polarizability autocorrelation function, $<\alpha(t)\alpha(0)>$, was also generated for each liquid from the OHD-RIKES data. Utilizing the relationship between the dipole and polarizability correlation functions provided by the Gaussian Librational Caging model [2] and the connection between the reorientational dynamics of solvent molecules to solvation dynamics provided by the theoretical treatment of Maroncelli *et al.* [3], the solvation time correlation function, $C_v(t)$, was generated from OHD-RIKES data for liquids toluene, benzonitrile and benzyl alcohol. In all three cases, we observe a bimodal $C_v(t)$ response that contains the fast, inertial Gaussian-like relaxation and the slower, diffusive exponential response. For more than 100 relevant citations, and a much more detailed presentation, please see reference [1].

Acknowledgments

This research was carried out at Brookhaven National Laboratory under contract DE-AC02-76CH00016 with the U.S. Department of Energy and supported by its Division of Chemical Sciences, Office of Basic Energy Sciences.

Reference:

1. Y. J. Chang and E. W. Castner, Jr., J. Phys. Chem., submitted.
2. R. M. Lynden-Bell and W. A. Steele, J. Phys. Chem., **88** (1984), 6514-6518.
3. M. Maroncelli, V. P. Kumar and A. Papazyan, J. Phys. Chem., **97** (1993), 13-18.

Effect of photoisomerization on electronic and vibrational dephasing

A. Kummrow, A. Lau, L. Dähne
(Max-Born-Institut für Nichtlineare Optik und Kurzzeitspektroskopie, Rudower Chaussee 6, D-12474 Berlin, Germany)

1. INTRODUCTION

In this paper we study optical dephasing of excited states by incoherent light techniques. Polymethine dyes like all-*trans*-bis-dimethylamino-heptamethinium are well known to isomerize upon photoexcitation into the lowest excited electronic level of the parent molecule leading to metastable photoisomers (most likely 2,3 mono-cis-heptamethine is formed [1]). Photoexcitation was performed on the short wavelength side of the absorption band of the parent molecule to avoid back-transformation of the photoisomer. The time interval between dephasing measurement and the photoisomerization pulse was varied from 4ns (i.e. partial temporal overlap) up to 20µs.

2. EXPERIMENT AND DISCUSSION

Electronic dephasing was studied by *forced light scattering* (FLS) [2,3]. The wavelength of the broadband laser used in FLS was varied between 508 nm and 585 nm on the long wavelength side of the absorption band of the parent molecule (Fig. 1). For the relatively low dynamic range of measurement available for experiments in the wings of the absorption bands, the formal description with a Gaussian lineshaping function $g(t)=\exp(-\Delta_G^2 t^2/2)$ suffice, were Δ_G is the modulation strength. From time-resolved decay curves of the diffracted intensity, Δ_G was deduced by deconvolution (results given in Fig. 1). Decreasing modulation strength is found for increasing wavelength of the broadband laser, for the parent molecule as well as for the photoisomer. There was no influence of delay after the photoisomerization pulse within error bars of ±2THz, indicating that a photoisomer, which is stable for microseconds, behaves much like stable molecule.

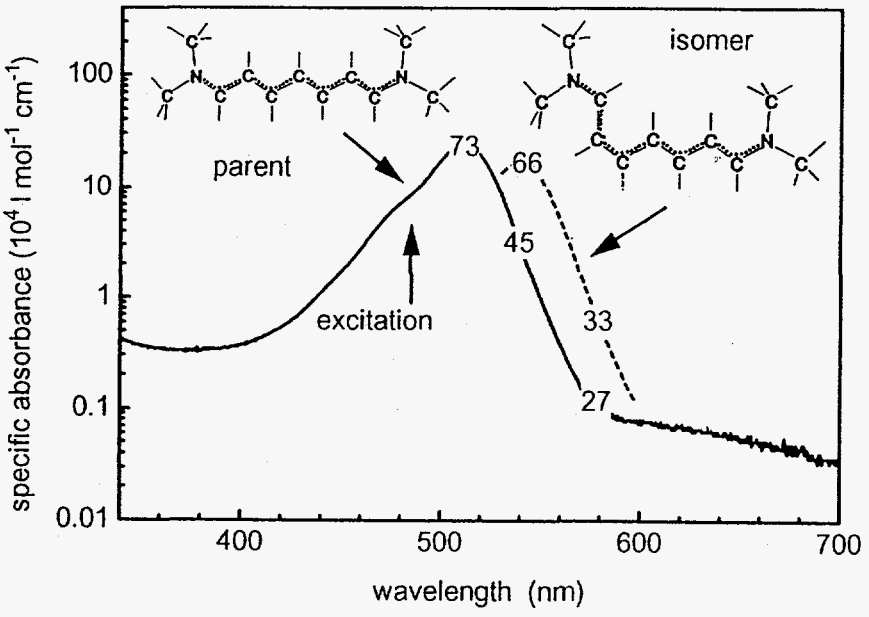

Figure 1:
Absorption spectra of all-*trans*-heptamethine (parent molecule) and its photoisomer (chemical structure shown as inset). The numbers plotted on the absorption curves give the measured Δ_G (modulation strength) in THz measured at that pump laser wavelength.

The same behaviour is observed in vibrational dephasing. A characteristic vibration of the photoisomer is the 1072 cm^{-1} mode, which is formed immediately after photoexcitation of the parent molecule [1]. Vibrational dephasing was studied by *interferometric coherent anti-Stokes Raman scattering* (I-CARS, [4]). We were able to fit the time-resolved dephasing of the vibration, measured by I-CARS, with the same molecular parameters (complex susceptibilities) as used for frequency-resolved scanning CARS, taking exponentially damped functions for I-CARS and Lorentzian line shapes for scanning CARS (Fig. 2); the dephasing time was T_2=0.7 ps for ν_v = 1072 cm^{-1} and T_2=0.9 ps for ν_v = 1122 cm^{-1}. This indicates a homogeneously broadening of the Raman lines.

It can be concluded that the photoproduced isomer behaves similarly as the parent molecule. The increased modulation strength at the same wavelength can be explained with the redshift of the absorption band. The new vibrational mode at 1072 cm^{-1} is the result of the modified molecular structure, but its Raman line seems to be homogeneously broadened as are the lines of the parent molecule [5].

Acknowledgements

This work was supported by the Deutsche Forschungsgemeinschaft. We thank R. Goleschny for her assistance.

References

[1] W. Wernicke, A. Lau, M. Pfeiffer, H. J. Weigmann, W. Freyer, J. T. Tschö and M. B. Kim, Chem. Phys. 118 (1978) 133.
[2] A. Kummrow, S. Woggon and A. Lau, Phys. Rev. A 50 (1994) 4264.
[3] A. Kummrow, Chem. Phys. Lett. 236 (1995) 362.
[4] M. A. Dugan and A. C. Albrecht, Phys. Rev. A 43 (1991) 3877; ibid p. 3922.
[5] A. Lau, A. Kummrow, M. Pfeiffer and S. Woggon, J. Raman Spectrosc. 25 (1994) 607.

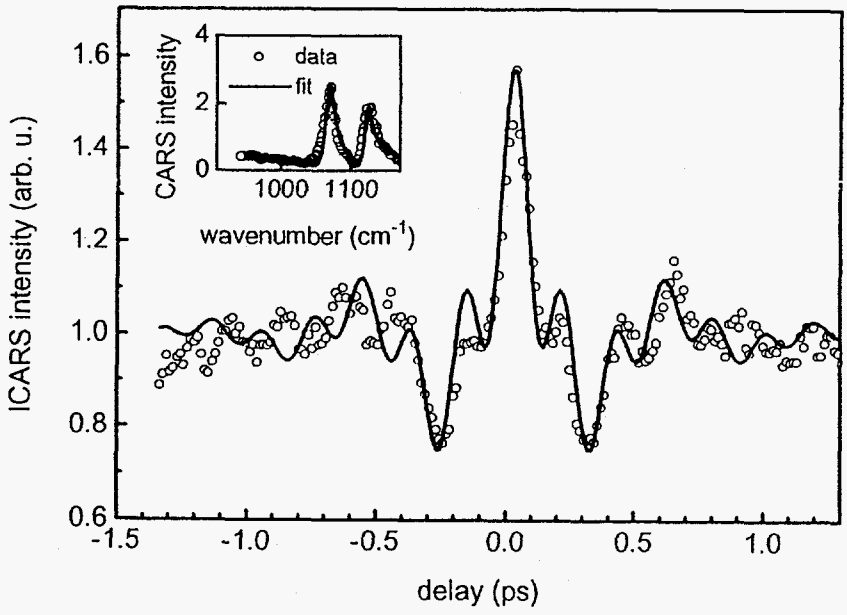

Figure 2:
I-CARS detuning oscillation of the photoisomer for vibrational modes between 850 cm^{-1} and 1140 cm^{-1} (scanning CARS spectrum shown as inset for comparison): pump laser: 585 nm (FWHM 10.2 nm); Stokes: 621 nm; narrowband detection wavelength 550.57 nm; by 50 ns advanced isomerizing pulse: 480 nm. Solid lines are fits to the I-CARS and the scanning CARS experiment using identical molecular parameters.

Time-Resolved Higher Order Nonlinear Spectroscopy in Liquids: Overtone Vibrational Dephasing

Keisuke Tominaga, Gary P. Keogh*, Jangseok Ma, and Keitaro Yoshihara

Institute for Molecular Science, Myodaiji, Okazaki, 444 JAPAN

INTRODUCTION

Vibrational spectra in solution are sensitive probes for intermolecular interactions and microscopic dynamics in liquids [1,2]. Dependences of vibrational band widths and peak frequency shifts on physical parameters such as density and temperature have been investigated to study microscopic details of liquids [2]. A vibrational quantum number is another important degree of freedom to investigate solvent effects on vibrational transition and dephasing [3-7]. Although analysis of spectral profile of the overtone would give more detailed information, such approach has been rather limited and the alteration of the spectral width has been a subject of discussion because of a relatively low signal level of the overtone signal, non-negligible contribution of the slit width to the spectral shape, so on.

In this work we have developed a technique to observe time-profiles of vibrational dephasing of overtone (v=2) as well as fundamental in liquids with a good signal-to-noise ratio under non-resonant condition using femtosecond pulses. This method allows one to compare experimental results and theoretical predictions of the vibrational dephasing in a quantitative level.

RESULTS AND DISCUSSION

Figure 1 (a) shows a dephasing of the overtone mode of the C-D stretching of CD_3I together with that of the fundamental. Two femtosecond pulses centered at 592 nm, $\mathbf{k}_I$ and $\mathbf{k}_p$, and one picosecond pulse at 679 nm, $\mathbf{k}_S$, are focused into the sample to generate fifth order response from the liquid, which corresponds to the overtone dephasing signal, $\mathbf{k}_{v=2}$. This signal appears at an angle which satisfies the following phase-matching condition;

$$\mathbf{k}_{v=2} = 2(\mathbf{k}_I - \mathbf{k}_S) + \mathbf{k}_p. \qquad (1)$$

The signal is identified as an overtone signal from its right power dependences on the femtosecond

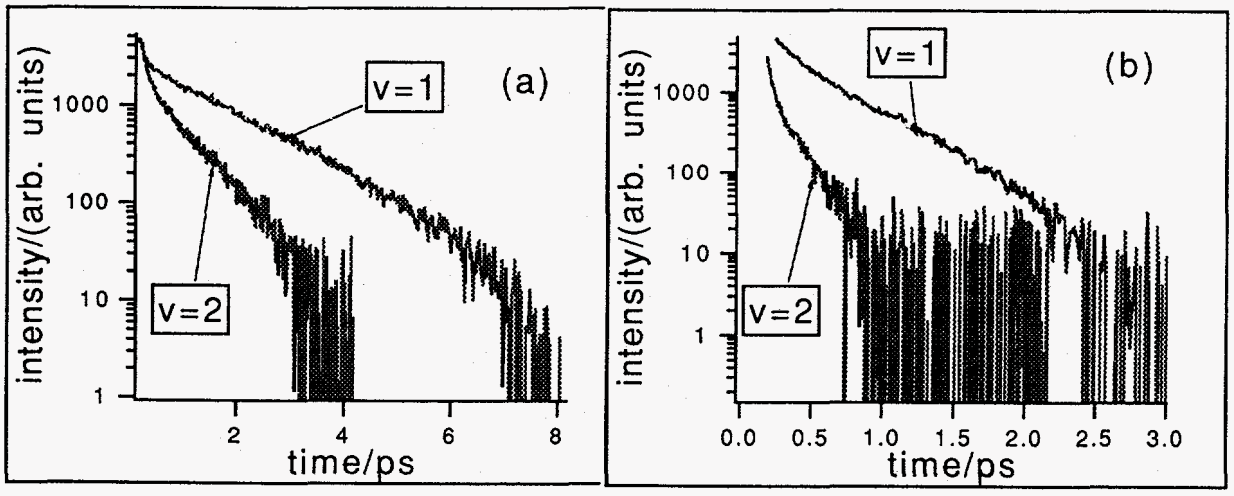

Figure 1. Time-profiles of vibrational dephasing of overtone and fundamental bands of (a) the C-D stretching of CD_3I and (b) C=C stretching of $Cl_2C{=}CCl_2$.

(third order) and picosecond (second order) pulses and its right wavelength at the maximum intensity of the scattered light. Since the spectral width of the femtosecond pulse is enough broad (~200 cm^{-1}), the v=2 level can be coherently excited by this method even there is an anharmonicity. The polarization condition of the pulses and the signal is chosen so that the fundamental signal is rotational free. The intensity of the overtone dephasing is three to four-orders of magnitude weaker than that of the fundamental. Another examples for the overtone dephasing is shown in Figure 1(b) for the C=C stretching of $Cl_2C=CCl_2$. These vibrational modes are carefully chosen so that any combination bands do not contribute to the signal. Possible quantum path ways to generate the overtone signal based on the fifth-order nonlinear process are shown in Figure 2.

The time profiles of both the fundamental and overtone dephasing are analyzed in terms of a couple theoretical models based on the stochastic theory developed by Kubo [9]. For example, one of them is a one-stochastic-mode model which assumes that the time correlation function of the deviation of the vibrational frequency from the average value, $\Delta(t)$, can be expressed by an exponential function,

$$<\Delta(0)\Delta(t)> = D^2 exp(-t/\tau). \quad (2)$$

Then, the time profile of the n-th overtone is given by [5]

$$I(t;n) \propto exp\{-2n^2D^2\tau t[1 - \tau/t[1 - exp(-t/\tau)]]\}. \quad (3)$$

This expression predicts that a vibrational band width of n-th overtone is proportional to n^2 in rapid modulation limit ($D\tau \ll 1$) and to n in the static limit ($D\tau \gg 1$), and has been used to interpret dependences of vibrational band widths on the quantum number [4,5,7,8]. However, we have found that there is no set of parameters, D and τ, which simultaneously reproduces the observed time-profiles of both the fundamental and overtone dephasing. This result indicates that to describe the vibrational dephasing accurately we may need to consider more complicated effects such as anharmonicity, population relaxation, so on.

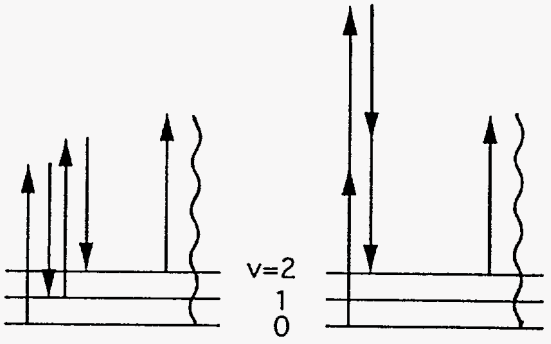

Figure 2. Possible quantum pathways for the overtone signal.

References;

*Permanent address; Department of Chemistry, Imperial College of Science, Technology, and Medicine, London, SW7 2AY, UK.
1. D.W. Oxtoby, Adv. Chem. Phys., 40 (1979) 1.
2. J. Jonas, Acc. Chem. Res., 17 (1984) 74.
3. A.B. Myers and F. Markel, Chem. Phys., 149 (1990) 21.
4. W. Kiefer and H.J. Bernstein, J. Raman Spec., 1 (1973) 417.
5. M.R. Battaglia and P.A. Madden, Mol. Phys., 36 (1978) 1601.
6. R. Arndt and J. Yarwood, Chem. Phys. Lett., 45 (1977) 155.
7. J. Yarwood, R. Arndt, and G. Doge, Chem. Phys., 25 (1977) 387.
8. J. Soussen-Jacob, C. Breuillard, J. Bessiere, J. Tskiris, and J. Vincent-Geisse, Mol. Phys., 46 (1982) 545.
9. R. Kubo, in Fluctuations, Relaxation, and Resonance in Magnetic Systems, Ed. D. ter Haar, (Plenum, New York, 1962).

Picosecond Anti-Stokes Studies of Intramolecular Vibrational Redistribution in Solution

Sandra L. Schultz, Jun Qian, and John M. Jean*
Department of Chemistry, Washington University, St. Louis, MO 63118

INTRODUCTION

Time-resolved emission studies of trans-stilbene(tS) and several of its derivatives have provided insight into the dynamics of intramolecular vibrational redistribution (IVR) in the S_1 state under isolated conditions [1]. At sufficiently high vibrational energy, the IVR process is dissipative with the microcanonical rate given by the Golden Rule expression, $k(E)=2\pi<V^2>\rho(E)$, where $<V^2>$ is the average anharmonic coupling between the initially populated level and the "dark" continuum and $\rho(E)$ the density of vibrational levels that are effectively coupled to the "bright" state. In solution, solute-solvent interactions result in the eventual loss of excess energy to the solvent [2]. Several recent picosecond Stokes studies of vibrational cooling of tS have shown that the S_1 state thermally equilibrates with the solvent on the 10-15 ps timescale [3-6]. In addition to its usefulness as a probe of the longer timescale cooling process, time-resolved resonance Raman scattering also provides a mode-specific probe of the IVR process. Here we present anti-Stokes studies of S_1 tS and its torsionally-constrained derivative, 2-phenylindene (2-PI), which address the role of solute molecular structure, specifically large amplitude torsional motion, on the rate of IVR in solution.

EXPERIMENTAL

The resonance Raman spectrometer used in our studies has been described previously [3]. The pump and probe pulses (1-2 ps duration) are the second harmonic and fundamental of a modelocked dye laser amplified at 1 kHz in a multi-pass dye cell pumped by a diode-pumped, Q-switched Nd:YLF laser. The samples (5mM) were contained in a rotating cell at 295 K.

RESULTS AND DISCUSSION

The S_1 states of tS and 2-PI were prepared by pumping either ~1600 cm^{-1} or ~3200 cm^{-1} above the electronic origin, which is near resonant with the v'=1 or v'=2 level of the strongly Franck-Condon active C=C mode seen in both the absorption spectrum and S_1 Stokes spectrum of both molecules [7]. In the case of tS, this mode is primarily ethylenic stretching motion (ν_7). Fig.1.a.-b. shows anti-Stokes spectra of tS and 2-PI in hexane as a function of delay time after pumping with 3200 cm^{-1} of excess vibrational energy. In the spectra of tS, we see substantial changes in the intensity of the C=C band at 1570 cm^{-1} during the first few ps. An intensity analysis has shown that these changes are inconsistent with the cooling of a thermalized molecule, strongly suggesting the short time spectra reflect the IVR process [8]. The absence of anti-Stokes scattering in the C=C region of 2-PI suggests that IVR in this system is considerably faster than in tS, even though constraining the C=C and C-phenyl torsional motion substantially reduces $\rho(E)$ at a given energy. Anti-Stokes spectra of tS obtained by pumping with 1600 cm^{-1} of excess energy are shown in Fig.1.c. The relative intensities and timescale of IVR are similar to the those obtained by pumping 3200 cm^{-1} above the origin, providing further evidence that the spectra at short times reflect nonthermal vibrational dynamics.

It is interesting to compare our results with those of Zewail and co-workers [1,9]. The IVR rate in tS at 1600 cm^{-1} in solution, ~$(4\ ps)^{-1}$, is an order of magnitude faster than that observed under isolated conditions when pumped in a similar energy range. In addition, the effect of solute structural rigidity on the IVR rate in solution is opposite to that seen in the gas phase. Banares, et.al.[9] found that IVR in 2-PI pumped 1193 cm^{-1} above the origin was complete in 280 ps compared to 33 ps for tS pumped with only slightly higher energy (1241 cm^{-1}). Though the modes pumped in these two studies are different, we expect, based on previous studies [1], that the gas phase results would be qualitatively similar at higher energies. The faster IVR rate for 2-PI compared to tS in solution may be the result of increased anharmonic coupling as a result of constrained torsional motion. Alternatively, this effect may be the result of solute-solvent interactions. Fluctuations of solute energy levels induced by solvent collisions may be more efficiently transferred through the more rigid structure resulting in faster dephasing of the initially localized excitation. We are currently carrying out similar studies on a series of substituted napthalenes in various solvent environments to test this latter hypothesis.

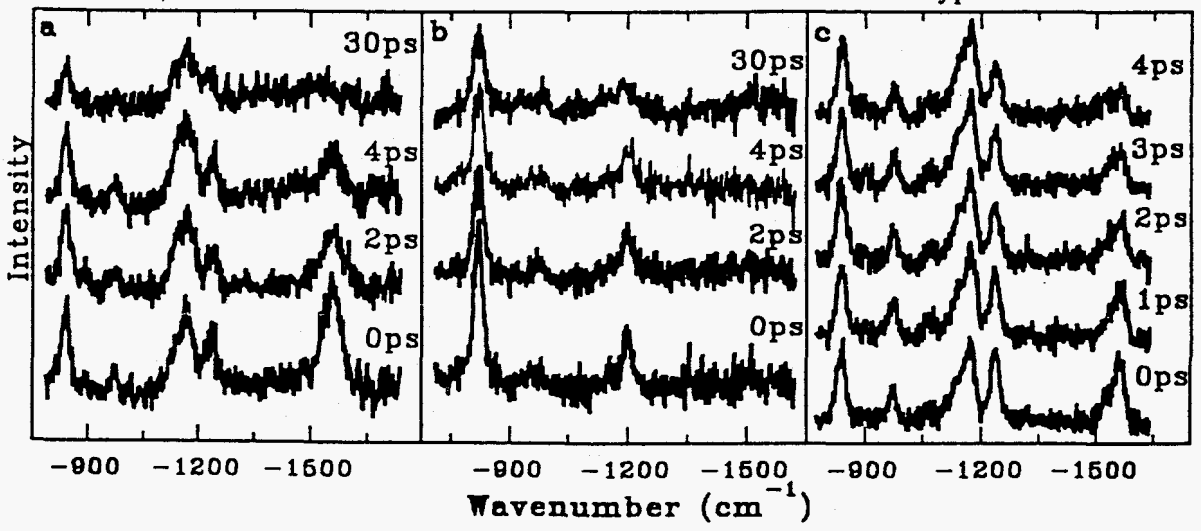

Fig. 1. Anti-Stokes spectra at the indicated delay times. **a.** tS in hexane; 292 nm pump, 584 nm probe. **b.** 2-PI in hexane; 296 nm pump, 592 nm probe. **c.** tS in methanol; 305 nm pump, 610 nm probe.

ACKNOWLEDGEMENTS

S.L.S. acknowledges support from a G.A.A.N.N. fellowship from the Department of Education. Acknowledgement is made to the donors of the Petroleum Research Fund, administered by the ACS, for support of this research.

REFERENCES

1. P.M. Felker and A.H. Zewail, Adv. Chem. Phys., 70 (1988) 265.
2. J.C. Owrutsky and R.M. Hochstrasser, Annu. Rev. Phys. Chem., 45 (1994) 519.
3. J. Qian, S.L. Schultz, G.R. Bradburn and J.M. Jean, J. Phys. Chem., 97 (1993) 10638.
4. W. Weaver, L. Huston, K. Iwata and T.L. Gustafson, J. Phys. Chem., 96 (1992) 8956.
5. K. Iwata and H. Hamaguchi, Chem. Phys. Lett., 196 (1992) 462.
6. R.E. Hester, P. Matousek, J.N. Moore, A.W. Parker, W.T. Toner and M.Towrie, Chem. Phys. Lett., 208 (1993) 471.
7. S.L. Schultz, J. Qian and J.M. Jean, submitted to J. Phys. Chem.
8. J. Qian, S.L. Schultz and J.M. Jean, Chem. Phys. Lett., 233 (1995) 9.
9. L. Banares, A.A. Heikal and A.H. Zewail, J. Phys. Chem., 96 (1992) 4127.

Mode-Selective Vibrational Energy Redistribution in Model Fe Porphyrins

C. M. Cheatum[1], M. R. Ondrias[1], M. C. Simpson[1,2]

[1] Department of Chemistry, University of New Mexico, Albuquerque, NM 87131.
[2] Fuel Sciences Department, Sandia National Laboratories, Albuquerque, NM 87185-0710.

Vibrational energy redistribution may be important in regulating the function of hemes and related macrocycles. Recently, vibrational coherences have been observed in biological systems, including bacterial photosynthetic reaction centers [1], rhodopsin [2], and heme proteins [3]. These observations lend credence to the idea that the initial vibrational energy dynamics may affect the outcomes of biologically relevant reactions.

Iron porphyrins are good subjects for study of intra- and intermolecular energy relaxation. These molecules are the active sites of enzymes with a variety of functions, and often their catalytic behavior can be photoinitiated. In addition, their large optical cross-sections make analysis by absorbance and resonance Raman scattering feasible. In these experiments, a steady-state approach is used to generate and detect a non-thermal vibrational energy distribution in the electronic ground state of Fe^{II} octaethyl porphyrin - (2-methyl imidazole) (FeOEP-2MeIm) by exposing molecules to fairly intense nanosecond laser pulses in resonance with the Soret electronic transition. Interpretation relies upon a rapid (< 5 ps) recovery of the electronic ground state. Considerable evidence indicates that five-coordinate, high-spin iron porphyrins return to the ground state via non-radiative decay processes with appropriate rapidity [4]. The ratio of anti-Stokes to Stokes scattering intensities is used to probes the populations of porphyrin modes. If the 'temperature' is not the same for all modes, then the system is not at thermal equilibrium.

Transient resonance Raman experiments previously revealed a non-Boltzmann vibrational energy distribution among heme normal modes in deoxyhemoglobin and protoporphyrin IX-(2MeIm) [5]. Our studies on five-coordinate iron porphyrin model compounds have been extended to Fe^{II}OEP-2MeIm in CH_2Cl_2. Flux-dependent anti-Stokes peak positions, Stokes and anti-Stokes linewidths, and anti-Stokes:Stokes area ratios are found for some modes (ν_4, ν_3, 1259 cm^{-1}) but not others (ν_7) (Figure 1; Table 1). Under our incident flux conditions the solvent band (704 cm^{-1}) is unaffected by increasing laser flux, and we observe no evidence of ground state saturation. We interpret these data to indicate that we are indeed monitoring vibrational energy relaxation on the ground electronic surface, and that this non-Boltzmann vibrational energy distribution persists for > 5 ps in this system.

We previously reported that six-coordinate, low-spin iron porphyrins (PPIX-$(Im)_2$) respond in the same manner to laser flux as do five-coordinate, high-spin species. However, in studies of Fe^{II}OEP-$(Im)_2$ we observe that the response of the spin-state marker band ν_3 to increased laser flux suggests photolysis of one ligand. As the flux is increased, the intensity of a ~1465 cm^{-1} component grows relative to that of a ~1490 cm^{-1} band. Also, ν_4 broadens to lower frequency. These results suggest that our previous conclusions were in error. We now conclude that our results are most consistent with efficient photolysis of the six-coordinate species, and generation and detection of a non-Boltzmann vibrational energy distribution within the newly created five-coordinate, high-spin species.

Acknowledgements
Funded by NIH (GM33330, to MRO), a DOE Distinguished Postdoctoral Research Fellowship (MCS), and a Minority Engineering and Mathematics Scholarship (CMC). M.C. Simpson was previously M.C. Schneebeck.

References

1. M.H. Vos, et al., Proc. Nat. Acad. Sci. (USA), 91 (1994) 12701. M.H. Vos et al., Nature, 363 (1993) 320. M.H. Vos et al., Biochemistry, 33 (1994) 6750. R.J. Stanley and S.G. Boxer, J. Phys. Chem., 99 (1995) 859.
2. Q. Wang et al., Science, 226 (1994) 422.
3. L. Zhu, et al., Phys. Rev. Lett, 72 (1994) 301. L. Zhu, et al., Science 266 (1994) 629.
4. D. Huppert, K.D. Straub, P.M. Rentzepis, Proc. Nat. Acad. Sci. (USA) 74 (1977) 4139; M.Lim, T.A. Jackson, P.A. Anfinrud, J. Phys. Chem. (1995) manuscript in preparation.
5. M.C. Schneebeck et al., Chem. Phys. Lett., 215 (1993) 251. R.G. Alden, et al., J. Raman Spec., 23 (1992) 259. M. C. Schneebeck et al., Proc. XIV[th] International Conference on Raman Spectroscopy, (1994) p 488; M.C. Simpson, et al., J. Am. Chem. Soc. (1995) manuscript in preparation.
6. M.C. Simpson, Ph.D. Dissertation, U. of New Mexico, (1994).

Figure 1 & Table 1: TRR Studies of Fe^{II}OEP-2MeIm: Flux-Dependence of Stokes and anti-Stokes Scattering

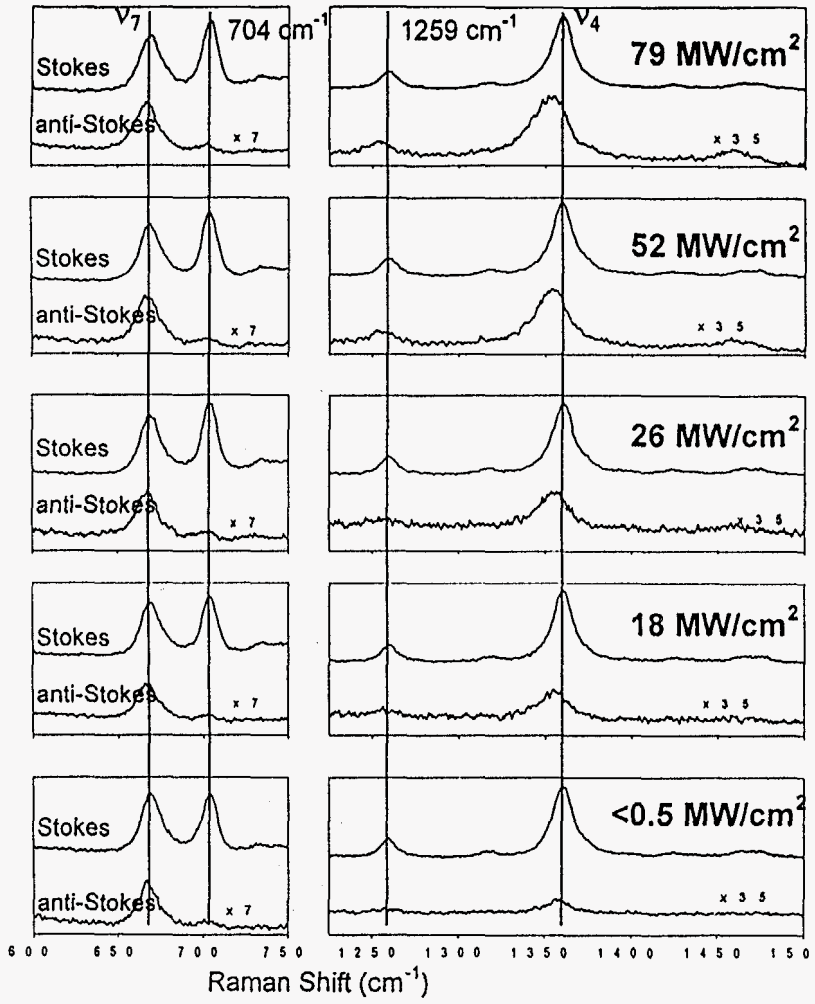

Flux (W/cm^2)	ω_S	ω_{aS}	Γ_S	Γ_{aS}	aS:S ratio	T_B (K)	T_C (K)
ν_4 $7.9x10^7$	1360	1352	15.1	24.7	0.0401	607	824
$5.2x10^7$	1360	1353	14.9	22.1	0.0342	578	772
$2.6x10^7$	1360	1355	14.8	20.0	0.0198	497	634
$1.8x10^7$	1360	1355	13.6	18.2	0.0145	461	576
$<5x10^5$	1360	1358	14.4	16.9	0.00606	382	458
ν_3 $7.9x10^7$	1474	1459	15.0	27.9	0.189	1268	>1400
$3.2x10^6$	1474	1459	9.2	33.5	0.212	1364	>1400
$2.6x10^7$	1475	1460	10.5	22.4	0.0901	878	1308
$1.8x10^7$	1476	----	10.4	---	----	----	----
$<5x10^5$	1474	----	14.8	---	----	----	----
1259 cm^{-1}							
$7.9x10^7$	1259	1254	11.6	15.3	0.0264	686	658
$3.2x10^6$	1259	1255	11.7	15.5	0.0249	670	644
$2.6x10^7$	1259	1256	10.7	17.7	0.0133	544	526
$1.8x10^7$	1259	1256	10.6	19.5	0.0167	584	564
$<5x10^5$	1259	1259	10.5	12.2	0.00524	425	415
705 cm^{-1}							
$7.9x10^7$	704	702	11.6	15.0	0.0171	249	309
$3.2x10^6$	704	701	11.4	15.3	0.0184	254	316
$2.6x10^7$	704	701	11.0	14.1	0.0191	256	320
$1.8x10^7$	704	702	11.1	13.1	0.0168	248	308
$<5x10^5$	704	702	11.6	17.3	0.0159	245	303
ν_7 $7.9x10^7$	669	667	17.1	15.0	0.102	422	607
$3.2x10^6$	669	667	16.3	14.9	0.113	442	650
$2.6x10^7$	669	667	15.7	15.5	0.108	431	629
$1.8x10^7$	669	667	15.1	14.6	0.0924	404	573
$<5x10^5$	669	667	14.9	11.8	0.0819	385	535

Figure 1 & Table 1: TRR spectra were obtained as described elsewhere [5,6]. Samples were run anaerobically in CH_2Cl_2 under a layer of ~0.5 M Na dithionite in water. λ_{ex} = 436 nm; 10 or 15 Hz; spot size was measured by exposing Polaroid photographic film to single laser shots at the sample face, which yields comparable results to translation of a razor blade through the beam. Flux was attenuated with neutral density filters and/or focusing optics. Curvefitting was carried out using a program based upon the Levenberg-Marquardt non-linear least squares method [6]. No parameters were fixed. Lorentzian line shapes were used. A linear baseline was included in the fit for the high frequency region; a quadratic function for the low frequency region.

The Structure of Psoralen Triplet States: Time-Resolved Infrared Spectra and Quantum Chemical Calculations

John P. Toscano, Christopher M. Hadad, Matthew S. Platz, and Terry L. Gustafson
Department of Chemistry, The Ohio State University, 120 West 18th Avenue, Columbus, OH 43210

Tetsuro Yuzawa and Hiro-o Hamaguchi
Molecular Spectroscopy Laboratory, Kanagawa Academy of Science and Technology,
KSP East 301, 3-2-1 Sakato, Kawasaki 213, Japan

Psoralens have been widely used as photosensitizers in photochemotherapy of a variety of skin diseases, including psoriasis and vitiligo. Unfortunately, such treatment often results in harmful side effects, such as erythema, edema, and hyperpigmentation.[1] The photochemotherapeutic action of these molecules is thought to arise from the formation of cyclobutane type adducts with pyrimidine bases of DNA and/or from the formation of singlet oxygen.[2] For this study we have focussed on the structure of the triplet states of two psoralens, khellin and visnagin. Of particular interest is the role of the solvent on the photophysics of these systems. The photobiological activity of the psoralens may vary considerably depending on the local environment. In order to address this issue we have obtained the time-resolved infrared spectra of the triplet states of khellin and visnagin in benzene, CD_3CN, and CD_3OD.

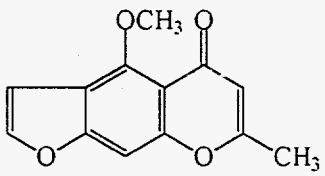

Visnagin

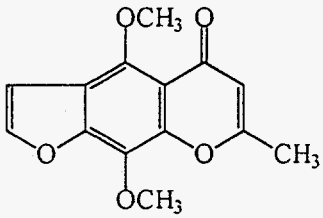

Khellin

The experimental approach that we have taken is to obtain the structure of the triplet states using the time-resolved infrared apparatus developed by Yuzawa *et al.*[3] For these experiments we used an excitation wavelength of 262 nm (20 μJ/pulse, 190 Hz). The sample concentrations were ca. 10 mM. The spectra were obtained over the region from 1800 to 1100 cm^{-1}. We kept the sample free from oxygen by bubbling the sample with Ar gas in a sealed flowing sample cell. The ground state and triplet state spectra of visnagin in CD_3CN are shown in Figure 1. The triplet spectrum was obtained by adding a fraction of the ground state spectrum to the raw difference

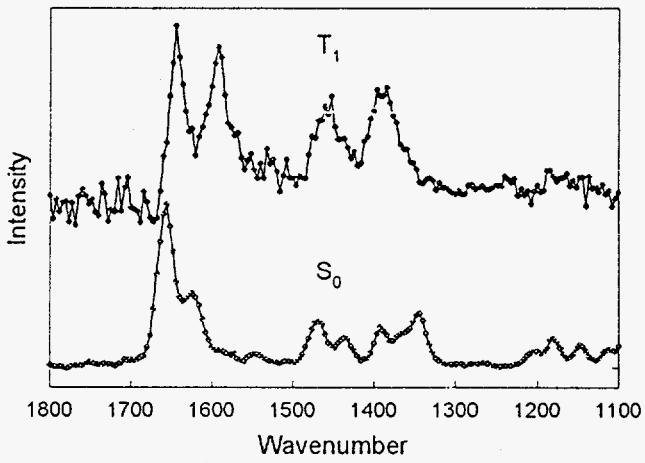

Figure 1: The infrared spectra of the ground and triplet states of visnagin.

spectrum that is obtained in the measurement. All of the triplet state bands exhibited the same time dependence, with a lifetime of ca. 1 μs. We verified that the spectrum was the triplet by observing a reduction in the lifetime when the solution was saturated with oxygen. In Figure 2 we show the ground state and triplet state spectra of khellin in CD_3CN. The ground state spectra vary only slightly in the different solvents. The triplet state spectra of khellin and visnagin in benzene and CD_3CN are nearly identical, but the triplet state spectra exhibit large band shifts in CD_3OD.

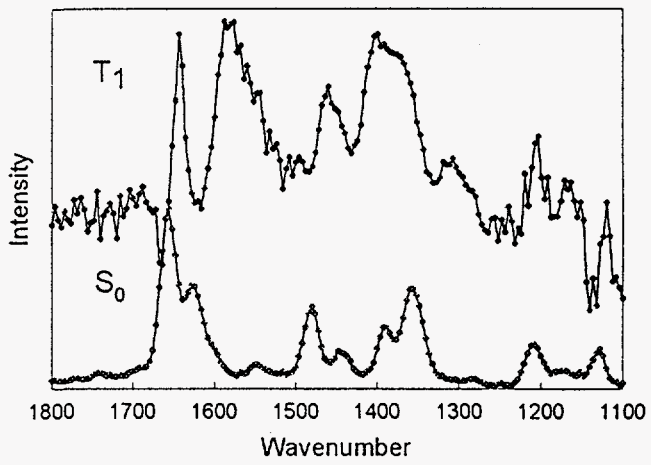

Figure 2: The infrared spectra of the ground and triplet states of khellin.

We have utilized semi-empirical and *ab initio* molecular orbital calculations to rationalize some of the experimental results for visnagin. We have calculated the ground state geometries of the different rotamers of visnagin with the AM1, PM3, and restricted Hartree-Fock (HF) levels using the STO-3G and 6-31G* basis sets. The AM1 and PM3 calculations are inconsistent with our *ab initio* results for the most stable ground state conformation of visnagin. The experimental ground state vibrational frequencies of visnagin are satisfactorily reproduced at the RHF/6-31G* level after application of the usual scaling factors. We have begun to examine the triplet states of visnagin at the unrestricted HF (UHF) and restricted open-shell HF (ROHF) levels using both the STO-3G and 6-31G* basis sets. Our preliminary results thus far indicate that the carbon skeleton of visnagin is non-planar in the triplet state. This asymmetric distortion will have important ramifications in the TRIR experiments. We are also beginning to probe the unusual solvent effects on the ground state vibrational frequencies via *ab initio* calculations with the self-consistent reaction field (SCRF) method. These calculations are now in progress.

References

1. Y. H. Paik and S. C. Shim, *J. Photochem. Photobiol. A*, 56 (1991) 349.
2. C. N. Knox, E. J. Land, and T. G. Truscott, *Photochem. Photobiol.*, 43 (1986) 359.
3. T. Yuzawa, C. Kato, M. W. George, and H. Hamaguchi, *Appl. Spectrosc.*, 48, (1994) 684.

A Computational Study of Many-Dimensional Quantum Energy Flow and Localization: Spectra and Dynamics

Sarah A. Schofield and Robert E. Wyatt
Department of Chemistry and Biochemistry and Institute for Theoretical Chemistry
University of Texas, Austin
Austin, Tx. 78712
and
Peter G. Wolynes
Department of Chemistry
University of Illinois, Urbana-Champaign
Urbana, Il. 61801

Knowledge of intramolecular energy flow is central to a comprehensive understanding of rates and microscopic mechanisms of chemical reactions [1]. Here, quantum calculations of intramolecular molecular vibrational energy flow and localization in a model system of $s = 6$ nonlinearly coupled anharmonic oscillators are presented. The harmonic frequencies of the oscillators were chosen from a random distribution. Both spectra and survival probabilities, the probabilities for the wavefunctions to overlap their initial conditions, were computed for all initial conditions having five quanta shared among the oscillators. Previously, results showing that at a critical coupling strength the eigenstates localize in this system were presented [2]. The localization occurs with respect to the normal modes of the zeroth order anharmonic oscillators. The averaged survival probability, obtained by first computing individual survival probabilities and then averaging over initial conditions, shows a power law decay in time with an exponent that varies with the degree of localization of the eigenstates, in agreement with theoretical prediction. This behavior results from the locality of the coupling and the homogeneity of the state space. In the strongly delocalized limit, the theory uses a semiclassical picture of diffusion on the constant energy surface in the space of the quantum numbers which describe the degree of excitation in the individual oscillators. Here it is shown that a predicted linear variation of the rate of energy flow with coupling strength, in the limit of strongly delocalized eigenstates [3], is reflected in the average spectrum, as well in the average survival probability [2], as depicted in Figure 1. It is also found that in this quantum system the procedures of averaging over initial conditions and of computing a survival probability from a spectrum using the usual Fourier transform techniques are *not* interchangable, as regards the detailed dynamics. This effect is weak in the strongly delocalized limit, when the semiclassical picture pertains. However, it increases with decreasing coupling strength and is pronounced near the transition to localized eigenstates, as Figure 2 demonstrates. This means that in this regime it is crucial to distinguish, when making comparison to theoretical calculation, which dynamical quantity is obtained by experiment.

1. T. Uzer, Phys. Rep. **199**, 73 (1991); J. I Steinfeld, J. S. Francisco, and W. L. Hase, *Chemical Kinetics and Dynamics* (Prentice Hall, Engelwood Cliffs, 1989); R. E. Wyatt and J. Z. Zhang, ed. *Dynamics of Molecules and Chemical Reactions* (Marcel Dekker, Inc., New York, in press).

2. S. A. Schofield, P. G. Wolynes, and R. E. Wyatt, Phys. Rev. Lett. **74**, 3720 (1995).

3. D. E. Logan and P. G. Wolynes, J. Chem. Phys. **93**, 4994 (1990); R. Bigwood and M. Gruebele, Chem. Phys. Lett. **235**, 604 (1995).

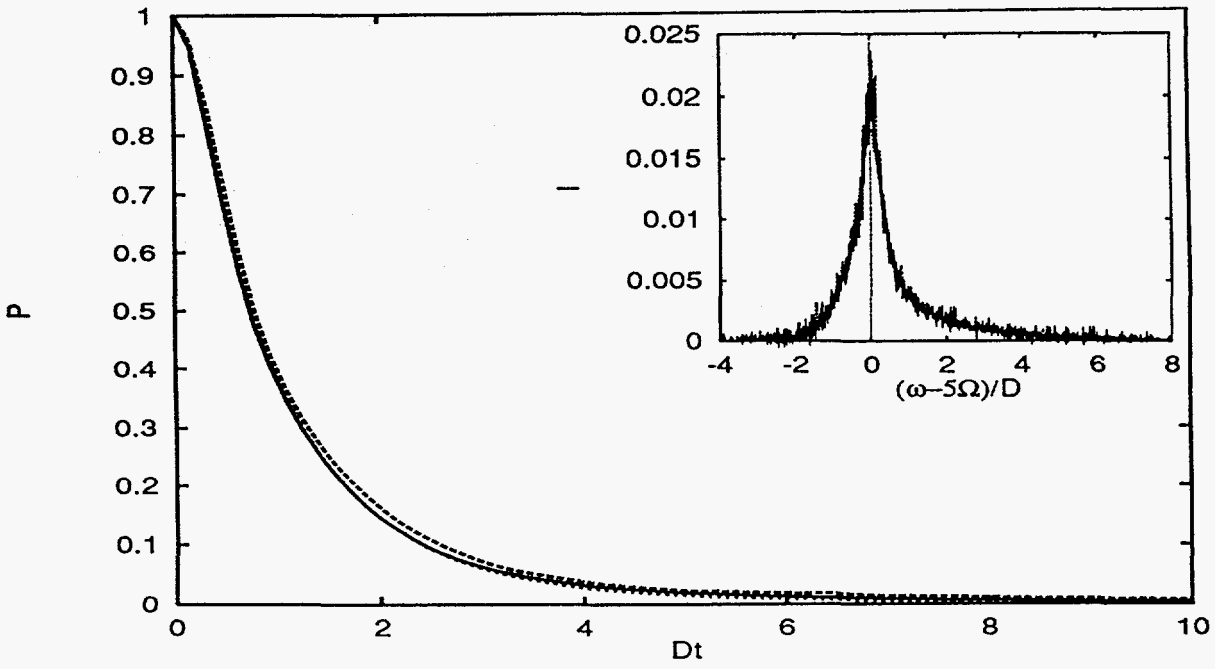

Figure 1: Average survival probability and average spectrum (inset) in the strongly delocalized limit. The ratio of coupling strength, ϕ, to predicted critical value is: $10^{3.8}$ (solid); $10^{3.3}$ (long dashed); $10^{2.8}$ (short dashed), and $D = 11\phi$ [2]. Ω is the average harmonic frequency.

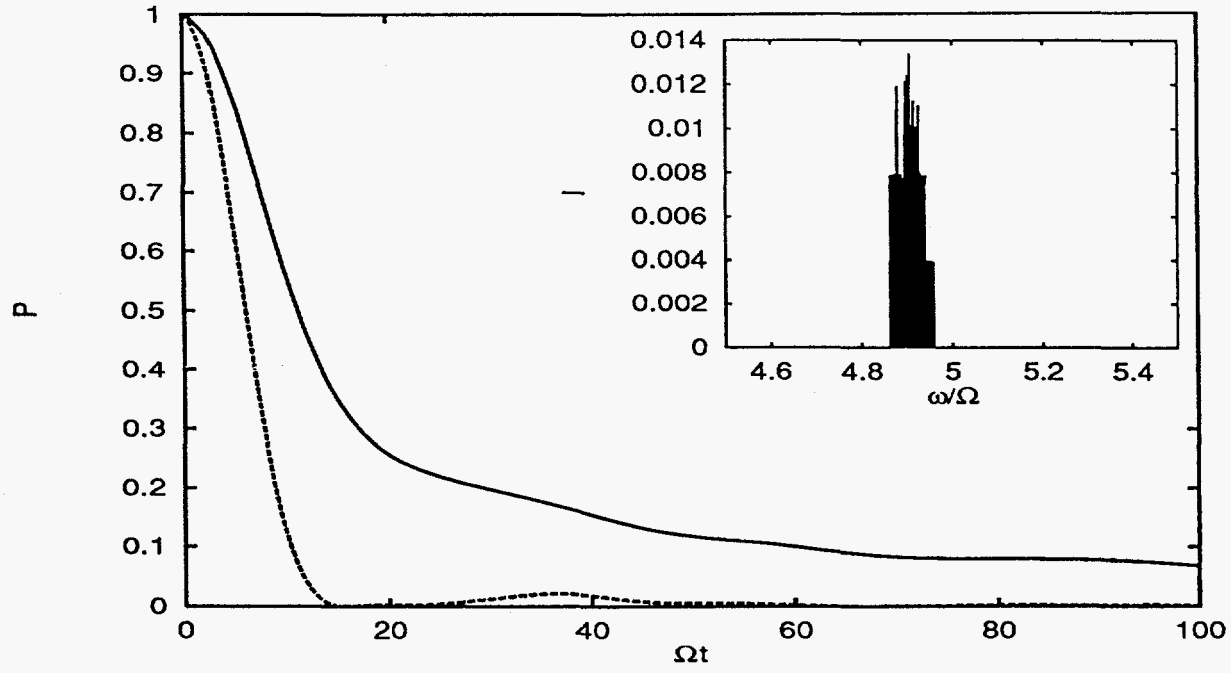

Figure 2: Average survival probability (solid) and the survival probability (dashed) as inferred from the average spectrum (inset), near to the localization transition. Ω is the average harmonic frequency.

Picosecond Time-Resolved Fourier-Transform Raman Spectroscopy of the Excited Singlet State of Anthracene

Gouri S. Jas, Krzysztof Kuczera, Chaozhi Wan, and Carey K. Johnson
Department of Chemistry, University of Kansas, Lawrence, KS 66045

INTRODUCTION

Time-resolved Fourier-transform Raman spectra of the first singlet excited state of anthracene and deuterated anthracene have been measured following photoexcitation at 355 nm. This method [1,2] utilizes Raman excitation in the near-infrared region to allow spectral separation of Raman scattering in the near-IR from fluorescence in the visible or UV regions. An *ab initio* calculation for the excited state at the CIS/6-31G level was carried out to generate a complete normal mode analysis of the ground and excited singlet states [3]. Good agreement between the computational and experimentally measured Raman frequencies is observed for both anthracene and anthracene *d*-10.

EXPERIMENTAL METHOD

A detailed description of the time-resolved Fourier-transform (FT) Raman system has been published elsewhere [1,2]. Pump and probe pulses at 355 nm (35μJ, 1 kHz) and 1064 nm (175 μJ, 2 kHz) were generated by a mode-locked, Q-switched Nd:YAG laser (Coherent Antares). Picosecond time-resolved FT Raman spectra of anthracene and deuterated anthracene were measured with a step-scan interferometer (Bio-Rad FTS 60A). The interferometer signal was processed by a lock-in amplifier referenced at 1 kHz to generate the difference interferogram induced by the pump pulses. The step rate of the Bio-Rad FTS-60A interferometer was 100 Hz. The spectral resolution was 8 cm^{-1}. The ground-state concentration of the sample was 10-12 mM.

RESULTS AND DISCUSSION

Picosecond time-resolved FT Raman spectra of anthracene in cyclohexane are shown in Figure 1. Similar results have been obtained for anthracene in hexane, ethanol, and propanol. The 1064-nm probe wavelength (9395 cm^{-1}) is resonant with the S_3-S_1 transition of anthracene [4]. Strong positive and negative bands appearing in the spectrum decay with the excited-state lifetime for anthracene in cyclohexane. The observed and Raman frequencies are compared with calculated frequencies in the Table. The anthracene modes observed in the excited-state FT Raman spectra can be assigned to totally symmetric vibrations. The negative bands at 800 cm^{-1}, 1027 cm^{-1}, 1265 cm^{-1}, and 1443 cm^{-1} are solvent bands depleted as a result of excited-state absorption of the 1064-nm pulses following excitation of anthracene at 355 nm. The intensities of these bands recover with the same lifetime as the decay of the excited-state Raman bands. Picosecond time-resolved FT Raman spectra of deuterated anthracene in cyclohexane have also been generated (see Table).

Acknowledgments

This work was supported by NSF under EPSCoR grant No. 9255223 and received matching support from the State of Kansas EPSCoR program. The FT-Raman instrumentation was funded by the NSF Chemical Instrumentation Program.

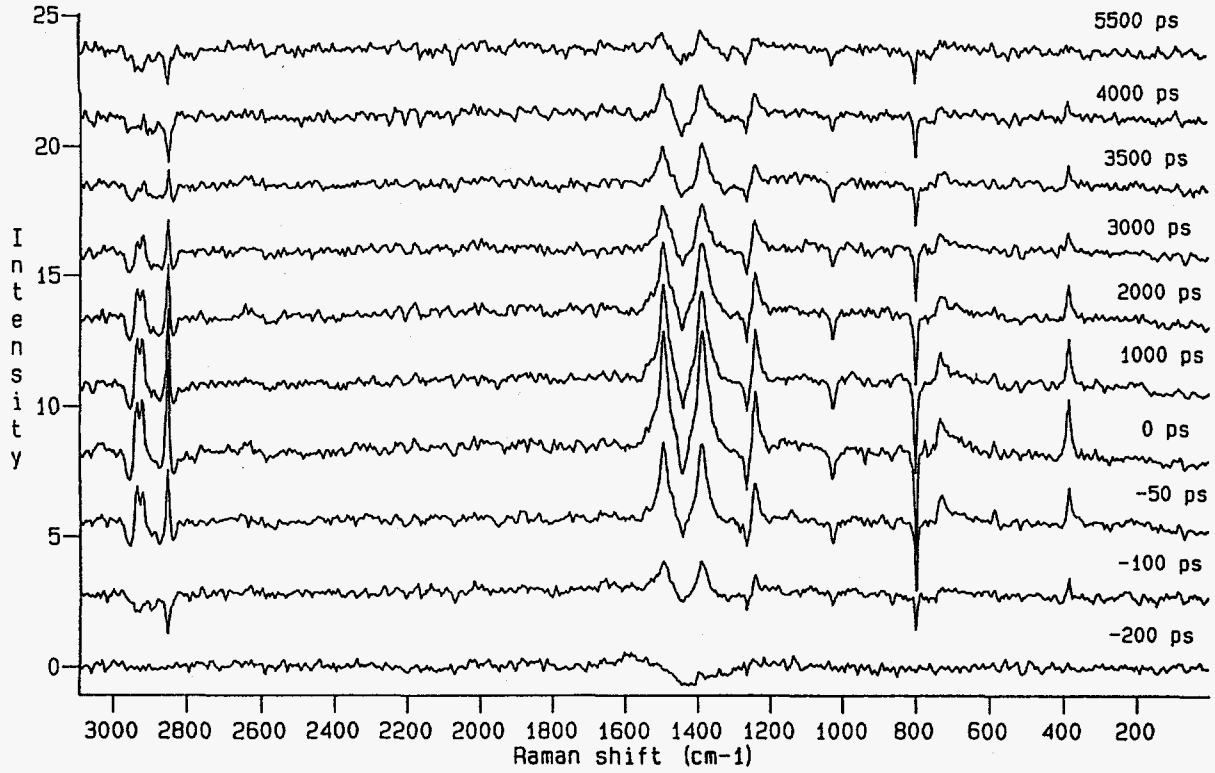

Figure 1: Time-resolved Fourier-transform Raman spectra of anthracene in cyclohexane. The interferometer was stepped at 100 steps/s. A total of 170 scans were summed at each time delay.

Table. Excited Singlet State Anthracene Raman Frequencies (cm^{-1}).

$\underline{S}_1(-h_{10})$		$\underline{S}_1(-h_{10})$ (CIS/6-31G[b])		Normal modes s = stretching d = deformation
Raman	Assignment[a]	Unscaled	Scaled	
386	12	426	384	sC-C (52) + dCCC (47)
587	11	680	612	dCCC (96)
730	10	805	725	sC-C (73) + dCCC (26)
1242	7	1372	1235	sC-C (65) + dCCH (33)
1389	6	1493	1344	sC-C (88)
1497	5	1663	1497	sC-C (49) + dCCH (44)

[a] a_g mode number. [b] G.S. Jas and K. Kuczera, companion paper in this volume.

References

1. G. S. Jas, C. W. Wan, and C. K. Johnson, *Spectrochim. Acta*, **50A** (1994) 1825.
2. G. S. Jas, C. Z. Wan, and C. K. Johnson, *Appl. Spectrosc.*, **49** (1995) 645.
3. G.S. Jas and K. Kuczera, companion paper in this volume.
4. P. R. Salvi, G. Marconi, *J. Chem. Phys.*, **84** (1986) 2542.

Normal Mode Analysis of S_1 Excited States of Benzene, Naphthalene, and Anthracene from *ab initio* Quantum Chemical Calculatons

Gouri S. Jas and Krzysztof Kuczera
Department of Chemistry, University of Kansas, Lawrence, KS 66045

In this paper we present normal mode calculations for the lowest singlet excited states S_1 of benzene ($^1B_{2u}$), naphthalene ($^1B_{1u}$), and anthracene (^1B_u). The chosen molecules are of fundamental spectroscopic importance, and understanding their excited state vibrations is of significant experimental and theoretical interest. As the method of calculation we choose the Hartree-Fock CI Singles (CIS) approach [1,2] as implemented in the GAUSSIAN92 [3] program. The availability of the CIS energy gradient allows for geometry optimization by standard methods, while harmonic force constants are obtained by numerical differentiation of the gradient. The calculated vibrational frequencies are scaled by 0.9, the same factor used to correct for symmetric errors of Hartree-Fock ground-state frequencies.

Optimized geometries and cartesian harmonic force constants of the excited states were obtained from *ab initio* calculations at the CIS/6-31G, CIS/6-31G*, CIS/6-311G, CIS/6-311G* levels for benzene, and CIS/6-31G and CIS/6-31G* levels for naphthalene and anthracene. Normal mode analysis was performed in internal coordinates, using the program MOLVIB [4], yielding vibrational frequencies and normal modes for the parent molecules and their perdeuterated derivatives. The normal modes were analyzed by calculating the Potential Energy Distribution (PED) and displaying diagrams of atomic displacements. The results are compared with corresponding properties of the ground state S_0 calculated at the Hartree-Fock level. To test the quality of the calculated results we compare the S_1 frequencies, $S_0 \rightarrow S_1$ frequency shifts and hydrogen-deuterium shifts within the S_1 state with the available experimental data. The calculation results are accurate enough to augument the sparse experimental data on excited state vibrations of these molecules.

The overall changes in molecular geometry and vibrational spectra upon $S_0 \rightarrow S_1$ excitation of benzene, naphthalene, and anthracene are small. Most vibrational frequencies decrease upon electronic excitation, in agreement with intuition and experimental results. For benzene we find excellent agreement of the entire calculated S1 vibrational spectrum with experimental results [5,6]. The rms deviations between the calculated and observed frequencies are 67, 55, 59, 52 cm^{-1} for the CIS/6-31G, CIS/6-31G*, CIS/6-311G, CIS/6-311G* methods, respectively. Our calculations confirm the reassignments of the a_{2g} mode *v3* from 1246 to 1320 cm^{-1} and e_{2g} mode *v8* from 1454 to 1520 cm^{-1} based on empirical force field determination [5,6].

For naphthalene and anthracene our calculation provide predictions of S_1 frequencies and normal modes for the complete vibratonal spectra of these molecules. For naphthalene, we present the first theoretical calculation of the S_1 state vibrations. Our results are in good agreement with the 7 observed a_g and 4 of the 5 observed b_{3g} excited state frequencies (Table 1; rms deviation is 26 cm^{-1} for CIS/6-31G* method [7]. The relatively large deviation for the b_{3g} mode *v6* (calculated: 993 cm^{-1}, experimental 1166 cm^{-1}) suggests that this frequency has been erroneously assigned in [7]. For anthracene our results are at the highest level of theory reported so far; two previous theoretical calculations of the S_1 state vibrations have been performed, using the semiempirical QCFF/PI method [8] and the *ab initio* approach with a small basis set [9]. Our results are in good agreement with all the 9 observed a_g and 6 of the 7 observed b_{3g} excited state frequencies (rms deviation is 49 cm^{-1} for the CIS/6-31G* method) [10,11]. Comparison with the reported experimental spectra suggests a reassignment of the b_{3g} mode *v11* and reassignments of several bands previously considered to be combinations of fundamentals.

Normal Mode Analysis for the S_1 state of Naphthalene with PED, all frequencies are in cm^{-1}

	CIS/6-31G	CIS/6-31G*	Obs.	$\Delta(cal.)_{6\text{-}31G^*}$	Δ(obs.)	PED
a_{1g}	497	485	501	-11	-11	dCCC(65) +sC-C(34)
	721	715	700	-33	-63	sC-C(86) + dCCC(11)
	1027	1020	984	15	-41	sC-C(74) + dCCH(24)
	1164	1137	1143	-21	-1	dCCH(76) + sC-C(24)
	1321	1302	1388	9	-36	sC-C(90)
	1453	1444	1432	-28	-19	dCCH(61) + sC-C(34)
	1532	1533	1495	-72	-84	sC-C(57) + dCCH(27) + dCCC(16)
	3027	3031		7		sC-H(100)
	3058	3058		10		sC-H(99)
b_{3g}	469	454	435	-45	-71	dCCC(80) + sC-C(20)
	915	890	910	-30	-26	dCCC(80) + sC-C(17)
	1055	993	1166	-153	-2	sC-C(76) + dCCH(22)
	1220	1197	1196	-38	-44	sC-C(42) + dCCH(34) + dCCC(24)
	1374	1370	1376	-91	-60	dCCH(70) + sC-C(19) + dCCC(11)
	1430	1415		-245		dCCH(70) + sC-C(26)
	3019	3022		7		sC-H(100)
	3037	3040		6		sC-H(100)

s = stretching, d = deformation, $\Delta(cal.) = Cal.(S_1\text{-}S_0)$, $\Delta(obs.) = Obs.(S_1\text{-}S_0)$, PED = Potential Energy Distribution obs. frequencies from Ref. 7

References

1. J. B. Foresman, M. Head-Gordon, J. A. Pople, and M. Frisch, *J. Phys. Chem.*, **96** (1992) 135.
2. J. B. Foresman, H. B. Schlegel, Recent Experimental and computational Advances, Ed. R. Fausto, NATO-ASI Series C, (Kluwer Academic: The Netherlands, 1993) p. 11.
3. Gaussian 92, Revision C, M .J. Frisch, G. W. Trucks, M. Head-Gordon, P. M. W. Gill, M.W. Wong, J. B. Foresman, B. G. Johnson, H. B. Schlegel, M. A. Robb, E. S. Replogle, R. Gomperts, J. L. Andres, K. Raghavachari, J.S. Binkley, C. Gonzales, R. L. Martin, D. S. Fox, D. J. Defrees, J. Baker, J. J. P. Stewart, and J. A. Pople, Gaussian Inc., Pittsburg PA, 1992.
4. K. Kuczera, and Wiorkiewicz-Kuczera, MOLVIB, a Program for Analysis of Molecular Vibrational Spectra.
5. L. D. Ziegler, B. S. Hudson, *Excited States*, Ed. E.C. Lim (Academic Press: New York, 1982) vol. 5, p 62.
6. K. Krogh-Jespersen, R. P. Rava, L. Goodman, *J. Phys. Chem.*, **88** (1984) 5503.
7. S. M. Beck, J. B. Hopkins, D. E. Powers, R. E. Smalley, *J. Chem. Phys.*, **74** (1981) 43.
8. D. Gruner, A. Nguyen, P. Brumer, *J. Chem. Phys.*, **101** (1994) 10365.
9. S. Zilberg, V. Samuni, R. Fraenkel, Y. Haas, *Chem. Phys.*, **186** (1994) 303.
10. W. R. Lambert, P. M. Felker, J. A. Syage, A. H. Zewail, *J. Chem. Phys.*, **81** (1984) 2195.
11. G. S. Jas and C. K. Johnson companion paper.

Unimolecular Reaction Dynamics of Methyl Isocyanide: Consistent Comparison of Classical Dynamical and Statistical Rate Coefficients Computed on the Same Potential-Energy Surface

Thomas D. Sewell,[a] Harold W. Schranz,[b] and Sture Nordholm[c]
a. Theoretical Division, Los Alamos National Laboratory, Los Alamos, New Mexico, USA
b. Research School of Chemistry, Australian National University, Canberra, Australia
c. Department of Physical Chemistry, University of Gothenburg, Gothenburg, Sweden

INTRODUCTION

A longstanding question in the field of chemical dynamics is that of whether the unimolecular dynamics of methyl isocyanide (CH_3NC) can be reconciled with the assumptions of statistical theories of unimolecular decay [1-6]. The reaction that has attracted the greatest interest is the isomerization of CH_3NC to yield CH_3CN. There have been several theoretical studies of the problem. They consist primarily of RRKM calculations and classical trajectory simulations. Most of the results have focused on "apparent" nonstatistical behavior, i.e., mode specificity, and were performed for energies far beyond those accessible in the laboratory.

What is missing from the studies performed in the past is the means of comparing the results of two independent theoretical methods, one explicitly dynamical and the other statistical, that employ the same mechanics (i.e., classical or quantum), in order to investigate intrinsic nonstatistical behavior. Such a comparison is not possible if, for example, the results of classical trajectory calculations are compared to quantum mechanical RRKM calculations. The desired comparison can be accomplished, however, if the results of classical trajectory calculations are compared to those obtained using Monte Carlo variational transition-state theory (MCVTST); and we have recently completed such a study for CH_3NC, using a new potential-energy surface which provides a qualitatively realistic description of the forces along the CH_3NC-->CH_3CN isomerization pathway as well as the effects of C--H and CH_3--NC bond fission on the relevant bending potentials (one of which is the isomerization coordinate). Ours are the first dynamical calculations to yield rate coefficients for energies extending down into the experimental regime.

Additionally, apparent mode-specific effects were considered by studying the effects of selective excitation of various modes of the system subject to the constraint of constant total energy. Changes in the total rate coefficient or shifts in the branching ratios for chemically distinct reaction channels will be observed if the system is exhibiting mode-specific behavior.

COMPUTATIONAL METHODS

The computational methods used here (classical trajectory calculations and MCVTST) have been described previously [7]. Ensembles of 500-1000 trajectories were used for each set of conditions considered. Typical MCVTST runs employed chains comprised of 2.5×10^7 states. Total energies of 75, 100, 125, 150, and 175 kcal/mol were studied using both trajectories and MCVTST. Energies down to 50 kcal/mol and up to 250 kcal/mol were studied using MCVTST.

RESULTS

A plot containing a comparison between the isomerization rate coefficients obtained using classical trajectory methods and MCVTST is shown in Fig. 1. Also included in the plot are the experimental results reported by Reddy and Berry [1] and Snavely et al. [2]. There is roughly a factor of ten discrepancy in the rate coefficients computed using classical trajectories and

MCVTST; this is an indication of bottlenecks to intramolecular vibrational energy transfer. The factor becomes smaller at higher energies and larger at lower ones. Figure 2 contains the results

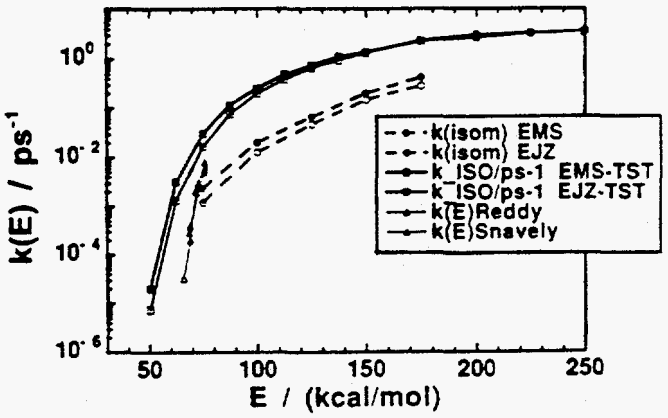

Figure 1. Comparison among statistical, dynamical, and experimental rate coefficients for CH_3NC isomerization. "EMS" denotes microcanonical sampling. "EJZ" indicates sampling only over the J=0 subspace. "-TST" suffix indicates MCVTST calculations. "Reddy" and "Snavely" are experimental data.

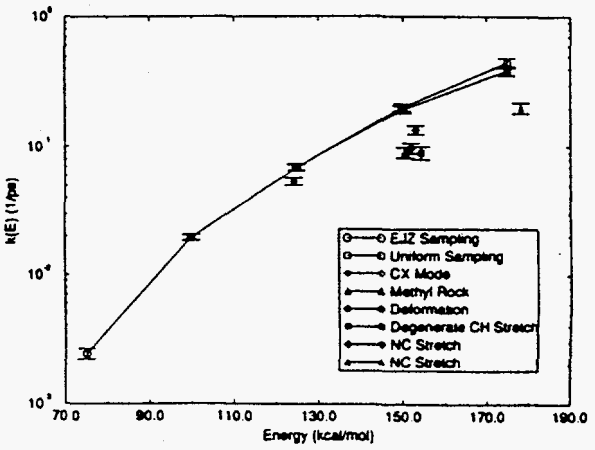

Figure 2. Plot demonstrating mode specificity in the isomerization of CH_3NC. Zero-point energy was assigned to each mode afterwhich the difference between the total energy and the ZPE was added to the mode indicated in the legend of the Figure.

of calculations designed to probe for mode specificity at several total energies. In these calculations, zero-point energy (ZPE) was first added the molecule using normal modes, then the difference between the ZPE and the total energy was added to the mode indicated in the legend. There is clear evidence for mode-specific behavior, as the rate coefficients depend fairly sensitively on the initial partitioning of the available energy.

CONCLUSIONS

Classical trajectory calculations and Monte Carlo variational transition-state theory (MCVTST) calculations have been used in a study of the unimolecular reaction dynamics of CH_3NC. Both isomerization and bond fission channels have been considered. The calculations reported here are the first to provide the basis for a consistent comparison of the dynamical and statistical rate coefficients in this system. The results indicate that CH_3NC does behave nonstatistically, in both the apparent and intrinsic senses. There is roughly a factor of ten difference in the statistical and dynamical rate coefficients, indicating the existence of (possibly weak) bottlenecks to IVR. Mode-specific excitations of the molecule lead to rate coefficients which vary significantly for a fixed total energy. The calculated results are in reasonable agreement with experimental values, giving us increased confidence about the validity of the potential-energy surface used. A full description of this work, including many more aspects of the dynamics of this system, will be presented in forthcoming publications.

References

[1] K.V. Reddy and M.J. Berry, Faraday Disc. Chem. Soc., 67 (1979) 188.
[2] S. Hassoon, N. Rajapakse, and D.L. Snavely, J. Phys. Chem., 96 (1992) 2576.
[3] D.L. Bunker and W.L. Hase, J. Chem. Phys., 59 (1973) 4621.
[4] B.G. Sumpter and D.L. Thompson, J. Chem. Phys., 87 (1987) 5809.
[5] A.J. Marks, J. Chem. Phys., 100 (1994) 8096.
[6] D. Shen and H.O. Pritchard, Int. J. Chem. Kinet., 62 (1994) 729.
[7] T. Sewell, H. Schranz, D.L. Thompson, and L.M. Raff, J. Chem. Phys., 95 (1991) 8089.

Theoretical Study on the Time and Frequency-Resolved Nonlinear Absorption in Molecular Aggregates

T. Kato and Y. Fujimura
Department of Chemistry, Graduate School of Science, Tohoku University, Sendai 980, Japan

INTRODUCTION The excited state dynamics of molecular aggregates is a subject of current interest [1-3]. Time and frequency-resolved nonlinear absorption spectra of molecular aggregates have recently been measured to observe one-exciton to two-exciton transitions and one-exciton state dynamics [4-7]. In this paper, we formulate the time and frequency-resolved nonlinear absorption spectrum on the basis of the perturbative density matrix method. We clarify the effects of exciton-phonon interactions on the nonlinear absorption spectra by using the expression derived.

EXCITON-PHONON INTERACTION Consider an aggregate system described by a 1 D homogeneous Frenkel exciton system, which is composed of N two-level molecules, phonons and their interactions. The exciton-phonon interaction is modeled by first derivatives of both intermolecular interaction energy ($G_\lambda^{(2)}$) and molecular transition energy ($G_\lambda^{(1)}$) with respect to lattice distortion in the adiabatic approximation. In our model, exciton-phonon interaction parameters are given by ratio $G_\lambda^{(1)} / G_\lambda^{(2)}$ and Huang-Rhys factor S that is defined by the renolmalization adiabatic potential energy of one-exciton state3.

We determine the vibronic states of the aggregate of N=100 by diagonalizing the total Hamiltonian matrix represented by our bases that are composed by a direct product of several hundred phonon states and three one-exciton states (k=1,2 and 3) or four two-exciton (kk'=12,13,14,23 and 24) states. These exciton states are taken to ensure proper dipole transitions between the ground and one-exciton, and those between one-exciton and two-exciton states, and to fill the lower energy edge of one- and two-exciton bands.

TIME AND FREQUENCY-RESOLVED NONLINEAR ABSORPTION SPECTRUM When the probe light absorption is measured by using time-integrated intensity of transmitted light pulse, the time and frequency-resolved nonlinear absorption spectrum is expressed as,

$$A_{nl}(\Omega_2,\Omega_1,\tau) = -\int_{-\infty}^{\infty} dt\, I(t,\Omega_2,\Omega_1,\tau). \qquad (1)$$

In Eq.(2), $I(t,\Omega_2,\Omega_1,\tau)$ is the probe light intensity at time t, which is derived by the 4th-order solution of the density operator for the whole system (aggregate and light pulses) with respect to the aggregate-light pulse interaction. $\Omega_1(\Omega_2)$ is the central frequency of the pump (probe) light pulse and τ is the separation between two pulses.

RESULTS Figure 1 shows calculated nonlinear absorption spectra (a) of molecular aggregates (N=100) together with induced absorption component (b) and induced emission component (c) at T=20K. A dipole intermolecular interaction model is used and the magnitude of the nearest interaction is set to $J = -600cm^{-1}$. The maximum frequency of the acoustic phonon (λ=100) is

$100cm^{-1}$, $G_\lambda^{(1)} / G_\lambda^{(2)} = -10^{-4}$ and mean value of S=0.01. The pulse duration is 10ps and the central frequency of the pump pulse is taken to be resonant k=1 one-exciton state (left column) and to k=3 one-exciton state transition (right column). In Table 1, we summarize the effective number defined by

$$N_{eff} = N(\text{radiative damping rate}) / (\text{super radiative damping rate}). \quad (2)$$

We can see how i) the shape of nonlinear absorption spectrum depends on excitation wavelength, and ii) the effective number decreases as temperature, Huang-Rhys factor (S) and pump pulse frequency increase. This dependence on the excitation wavelength is due to mixing of k=1, k=2 and k=3 one-exciton states by the exciton-phonon coupling.

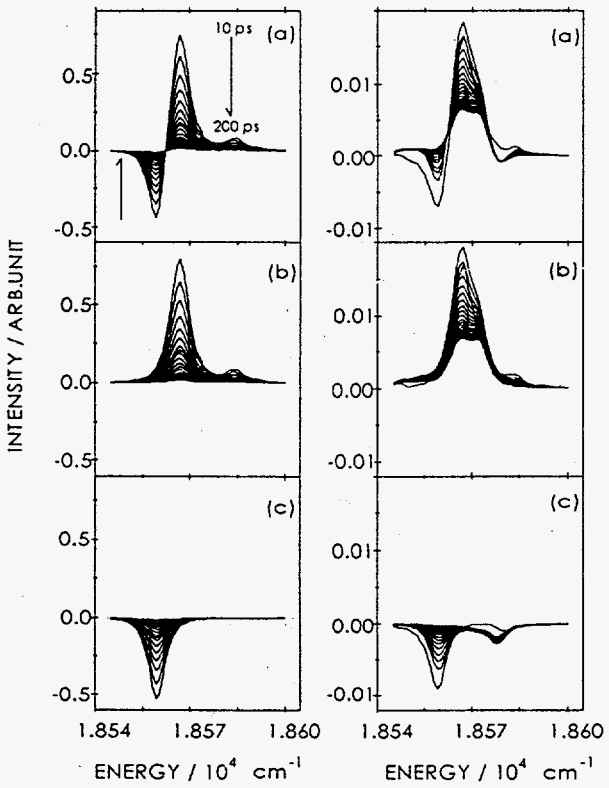

Figure 1:

one-exciton state	temp /K	Huang-Rhys factor (S) 0.0	0.01	0.05
k1	0.0	100	99.8	—
	10	—	97.1	85.9
	20	—	96.6	83.3
	30	—	96.4	82.3
k2	0.0	100	99.8	72.3
	10	—	97.1	67.4
	20	—	96.6	65.3
	30	—	96.4	64.5
k3	0.0	100	93.7	63.3
	10	—	80.3	53.0
	20	—	79.8	52.9
	30	—	80.0	52.8

Table 1:

References

1. F. C. Spano, J. R. Kuklinski and S. Mukamel, Phys. Rev. Lett. , 65 (1990) 211
2. S. De Boer and D. A. Wiersma, Chem. Phys. Lett. , 165 (1990) 45
3. T. Kobayashi, in *Adv.in Multi-photon Processes and Spectroscopy* vol.8 , Ed. S. H. Lin, A. A. Villaeys and Y. Fujimura (World Scientific Publishing, Singapore, 1993) 345
4. M. van Burgel, D. A. Wiersma and K. Duppen, J.Chem. Phys. , 102 (1995) 20
5. H. Fidder, J. Knoester and D. A. Wiersma, J. Chem. Phys. , 98 (1993) 6564
6. S. Kobayashi and F. Sasaki, J.Lumin. , 58 (1994) 113
7. H. Fidder, J. Terpstra and D. A. Wiersma, J. Chem. Phys. , 94 (1991) 6895

List of Conference Participants

Seventh International Conference on Time-Resolved Vibrational Spectroscopy

June 11 - 16, 1995

La Fonda Hotel
Santa Fe, New Mexico, USA

Participant List (157)

1. Andreas Albrecht
Cornell University
Department of Chemistry
Ithaca, NY 14853-1301
USA

Ph: 607/255-3990
Fax: 607/255-4137
E-mail: acaf@cornell.edu

2. Philip A. Anfinrud
Harvard University
Department of Chemistry
12 Oxford Street
Cambridge, MA 02138
USA

Ph: 617/495-5634
Fax: 617/495-5634
E-mail: anfinrud@chemistry.harvard.edu

3. Savina Angel
Coherent, Inc.
8203 South St. Paul Way
Littleton, CO 80122
USA

Ph: 303/796-0025
Fax: 303/796-0026
E-mail:

4. David Arnett
University of Pennsylvania
Department of Chemistry
Philadelphia, PA 19104-6323
USA

Ph: 215/898-8424
Fax: 215/573-2112
E-mail: arnett@a.chem.upenn.edu

5. Caroline J. Arnold
University of York
Department of Chemistry
Helsington York Y01 5DD UK
UK

Ph: 44-1904-432603
Fax: 44-1904-432562
E-mail: cja4@york.ac.uk

6. Sanford A. Asher
University of Pittsburgh
Department of Chemistry
Pittsburgh, PA 15260
USA

Ph: 412/624-8570
Fax: 412/624-0588
E-mail: asher@vms.cis.pitt.edu

7. George H. Atkinson
University of Arizona
Department of Chemistry
Tucson, Arizona 85721
USA

Ph: 602/621-6293
Fax: 602/621-4858
E-mail:

8. Gerald T. Babcock
Michigan State University
Department of Chemistry
East Lansing, MI 48824
USA

Ph: 517/355-9715
Fax: 517/353-1793
E-mail:

9. James Bailey
Los Alamos National Laboratory
CST-4, MS J586
Los Alamos, NM 87545
USA

Ph: 505/667-5551
Fax: 505/667-0851
E-mail:

10. Ashfaq Bengali
Los Alamos National Laboratory
CST-6, MS J567
Los Alamos, NM 87545
USA

Ph: 505/665-9265
Fax: 505/665-4817
E-mail: ashfaq_bengali@cls.lanl.gov

11. Joel Berendzen
Los Alamos National Laboratory
P-21, MS M715
Los Alamos, NM 87545
USA

Ph: 505/665-2552
Fax: 505/665-4507
E-mail: joelb@lanl.gov

12. Mark A. Berg
University of South Carolina
Chemistry Department
Columbia, SC 29208
USA

Ph: 803/777-1514
Fax: 803/777-5263
E-mail: berg@psc.scarolina.edu

13. Carlo A. Bignozzi
University of Ferrara
Dipartimento di Chimica
Via L. Borsari 46
Ferrara 44100
Italy

Ph: 532-291163
Fax:
E-mail: g4Sfedg1@iciueca.bitnet

14. Milton E. Blackwood Jr.
Princeton University
Department of Chemistry
Princeton, NJ 08544
USA

Ph: 609/258-3908
Fax: 609/258-6746
E-mail: blackwood@chemvax.princeton.edu

15. Marco J. P. Brugmans
FOM Institute AMOLF
Kruislaan 407

1098 SJ Amsterdam
The Netherlands

Ph: 31-30-6081234
Fax: 31-30-6684106
E-mail: brugmans@amolf.amolf.nl

16. Robert Callender
Albert Einstein College of Medicine
Department of Biochemistry
1300 Morris Park Ave.
Bronx, NY 10461
USA

Ph: 212/650-6872
Fax: 212/650-5503
E-mail: call@scisun.sci.ccny.suny.edu

17. Edward W. Castner Jr.
Brookhaven National Laboratory
Department of Chemistry
PO Box 5000
Upton, NY 11973-5000
USA

Ph: 516/282-4362
Fax: 516/282-5815
E-mail: castner1@bnl.gov

18. Timothy P. Causgrove
Mississippi University for Women
Box W-100
Columbus, Mississippi 39701
USA

Ph: 619/329-7244
Fax: 619/329-7238
E-mail: tcaus@sunmuw1.muw.edu

19. Paul M. Champion
Northeastern University
Physics Department
360 Huntington Avenue
Boston, MaA 02115
USA

Ph: 617/373-3918
Fax: 617/373-2943
E-mail: champ@neu.edu

20. Yong Joon Chang
University of California at San Diego
Department of Chemistry, MC 0341
7500 Gilman Drive
La Jolla, CA 92093-0341
USA

Ph: 619/534-5975
Fax: 619/534-7042
E-mail: yjchang@chem.ucsd.edu

21. Xingguo Chen
University of Pittsburgh
Chemistry Department
4910 Centre Avenue, #F-3
Pittsburgh, PA 15213
USA

Ph: 412/624-8875
Fax: 412/624-0588
E-mail: xgchen@vms.cis.pitt.edu

22. Dae Won Cho
Chungnam National University
Department of Chemistry
Taejon 305-764
Korea

Ph: 42-821-6346
Fax:
E-mail:

23. Eric L. Chronister
University of California at Riverside
Department of Chemistry
Riverside, CA 92521
USA

Ph: 909/787-3288
Fax: 909/787-4713
E-mail: eric.chronister@ucr.edu

24. Kelvin Chu
Los Alamos National Laboratory
P-21, MS M715
Los Alamos, NM 87545
USA

Ph: 505/665-1983
Fax: 505/665-4507
E-mail: kelvin@lanl.gov

25. William G. Clark
Clark-MXR, Inc.
7300 W. Huron River Drive
Dexter, MI 48130
USA

Ph: 313/426-2803
Fax: 313/426-6288
E-mail: clark@cmxr.com

26. Peijun Cong
University of California at San Diego
9500 Gilman Drive
La Jolla, CA 92093-0341
USA

Ph: 619/534-5975
Fax: 619/534-7042
E-mail: pcong@grove.ucsd.edu

27. Nancy A. David
Environmental Research Institute of
1701 Old Pecos Trail
Santa Fe, NM 87505
USA

Ph: 505/982-9180
Fax: 505/982-0322
E-mail: ndavid@erim.org

28. Geurt Deinum
Michigan State University
Department of Chemistry
East Lansing, MI 48824
USA

Ph: 517/355-9715
Fax: 517/355-1793
E-mail: deinum@cemvax.cem.msu.edu

29. Susan Dexheimer
Washington State University
Department of Physics
P.O. Box 642814

Pullman, WA 99164-2814
USA

Ph: 509/335-6389
Fax:
E-mail: dexheimer@wsu.edu

30. Rolf Diller
Freie Universitat
Inst. f. Exp. Physik
FU Berlin, Arnimallee 14
Berlin 14195
Germany

Ph: 49-30-838-6107
Fax: 49-30-838-6081
E-mail: diller@omega.physik.fu-berlin.de

31. Brian Dyer
Los Alamos National Laboratory
CST-4, MS J586
Los Alamos, NM 87545
USA

Ph: 505/667-4194
Fax: 505/665-4817
E-mail: bdyer@lanl.gov

32. Reiner Dziewior
Freie University of Berlin
Inst. f. Exp. Physik
Arnimallee 14
Berlin 14195
Germany

Ph: 49-30-838-6107
Fax: 49-30-838-6081
E-mail:

33. Mostafa A. El-Sayed
Georgia Institute of Technology
School of Chemistry and Biochemistry
Boggs Building
Atlanta, GA 30332-0400
USA

Ph: 404/894-0292
Fax: 404/894-0294
E-mail: mostafa.el-sayed@chemistry.gatech.edu

34. Baochen Fan
University of New Mexico
Department of Chemistry
Albuquerque, NM 87131
USA

Ph: 505/277-5129
Fax: 505/277-2609
E-mail:

35. Michael D. Fayer
Stanford University
Chemistry Department
Stanford, CA 94305
USA

Ph: 415/723-4446
Fax: 415/723-4817
E-mail: fayer@d31mf0.stanford.edu

36. John T Fourkas
Boston College
Department of Chemistry
Chesnut Hill, MA 02167
USA

Ph: 617/552-3611
Fax: 617/552-2705
E-mail: fourkas@hermes.bc.edu

37. Stefan Franzen
Los Alamos National Laboratory
CST-4, MS J586
Los Alamos, NM 87545
USA

Ph: 505/665-9284
Fax: 505/667-8021
E-mail: sfranzen@mst.lanl.gov

38. Hans Frauenfelder
Los Alamos National Laboratory
P-21, MS M715
Los Alamos, NM 87545
USA

Ph: 505/665-2547
Fax: 505/665-4507
E-mail: hf@lanl.gov

39. Yukio Furukawa
The University of Tokyo
Department of Chemistry
School of Science
Bunkyo-ku, Tokyo 113
Japan

Ph: 81-3-3812-2111 Ext. 4328
Fax: 81-3-3814-2627
E-mail:

40. Alexander J. Gancarz
Los Alamos National Laboratory
DDCST, MS J514
Los Alamos, NM 87545
USA

Ph: 505/667-4457
Fax: 505/665-4355
E-mail: gancarz_alexander@lanl.gov

41. Feng Gao
University of New Mexico
Department of Chemistry
Albuquerque, NM 87131
USA

Ph: 505/277-5129
Fax:
E-mail: fgao@unm.edu

42. Suzanne Garney
Environmental Research Institute of Michigan (ERIM)
1701 Old Pecos Trail
Santa Fe, NM 87505
USA

Ph: 505/982-9180
Fax: 505/982-0322
E-mail:

43. Holger Georg
Universitat Freiburg
Institute fuer Biophysik
Albertstrasse 23
79104 Freiburg
Germany

Ph: 761-203-5370
Fax: 761-203-5016
E-mail: hiob@sun2.ruf.uni-freiburg.de

44. Michael W. George
University of Nottingham
Department of Chemistry
Nottingham NG7 2RD
UK

Ph: 44-115-9513512
Fax: 44-115-9513563
E-mail: dczmwg@unicorn.nott.ac.uk

45. Terry L. Gustafson
The Ohio State University
Department of Chemistry
120 West 18th Avenue
Columbus, OH 43210
USA

Ph: 614/292-1832
Fax: 614/292-1685
E-mail: gustafson.5@osu.edu

46. David E. Hare
University of Illinois at Urbana-Champaign
34-1 RAL
School of Chem. Sci.

Urbana, Illinois 61801
USA

Ph: 217/333-8382
Fax: 217/244-3186
E-mail: hare@c.scs.uiuc.edu

47. Gary Hastings
Los Alamos National Laboratory
CST-4, MS J586
Los Alamos, NM 87545
USA

Ph: 505/665-1128
Fax: 505/667-0851
E-mail: hastings@lanl.gov

48. Edwin J. Heilweil
National Institute of Standards and
2268 Building 221
Gaithersburg, Maryland 20899
USA

Ph: 301/975-2370
Fax: 301/975-3038
E-mail: ejh@tiber.nist.gov

49. Ronald E. Hester
University of York
Chemistry Department
York Y01 5DD
England

Ph: 44-904-432557
Fax: 44-904-432562
E-mail: reh1@york.ac.uk

50. Robin M. Hochstrasser
University of Pennsylvania
Department of Chemistry
Philadelphia, PA 19104-6323
USA

Ph: 215/898-8410
Fax: 215/898-0590
E-mail: hochstras@a.chem.upenn.edu

51. Xiaoyu Hong
University of Illinois at Urbana-Champaign
Department of Chemistry
Box 28-1
Urbana, Illinois 61801
USA

Ph: 217/333-8382
Fax: 217/333-3186
E-mail: hong@aries.scs.uiuc.edu

52. John Hopkins
Louisiana State University
Department of Chemistry
Baton Rouge, Louisiana 70803
USA

Ph: 504/388-3458
Fax: 504/388-3458
E-mail:

53. Yixiang Huang
Louisiana State University
B-10 Chemistry Department
Baton Rouge, LA 70853
Baton Rouge, Louisiana 70803
USA

Ph: 504/388-3460
Fax:
E-mail: huangy@unix1.lsu.scnn.edu

54. Frank Jäger
University of Arizona
Department of Chemistry
Tucson, Arizona 87521
USA

Ph: 602/621-6693
Fax: 602/621-4858
E-mail: fjager@ccit.arizona.edu

55. Gouri S. Jas
The University of Kansas
Department of Chemistry
Malott Hall 2010
Lawrence, Kansas 66045
USA

Ph: 913/864-3249
Fax: 913/864-5396
E-mail: gouri@tedybr.chem.ukans.edu

56. John M. Jean
Washington University
Department of Chemistry
One Brooking Drive
St. Louis, Missouri 63130
USA

Ph: 314/935-8534
Fax: 314/935-4431
E-mail: jean@wuchem.wush.edu

57. Alan E. Johnson
University of Rochester
Chemistry Department
Hutchinson Hall, River Campus
Rochester, New York 14627
USA

Ph: 716/275-6979
Fax: 716/473-6889
E-mail: anjn@db1.cc.rocheser.edu

58. Valey Kamalov
Georgia Institute of Technology
School of Chemistry and Biochemistry
Boggs Building
Atlanta, GA30332-0400
USA

Ph: 404/894-0292
Fax:
E-mail:

59. Gary S. Kanner
Los Alamos National Laboratory
MST-6, MS G755
Los Alamos, NM 87545
USA

Ph: 505/667-0082
Fax: 505/667-8021
E-mail: gsk@lanl.gov

60. Norihisa Katayama
Kitasato University
School of Science
Kitasato 1-15-1
Sagamihara, Kanagawa 228
Japan

Ph: 81-427-78-8692
Fax: 81-427-78-9369
E-mail: nory@medcc.kitasato-u.ac.jp

61. Tsuoshi Kato
Tohoku University
Department of Chemistry
Graduate School of Science
Kawauchi, Aobaku, Sendai 980-77
Japan

Ph: 22-217-7715/7725
Fax: 22-217-7715
E-mail: kato@mcl.chem.tohoku.ac.jp

62. Tamas Keszthelyi
Risoe National Laboratory
Environmental Science and Technology
MIL-313
DK-4000 Roskilde
Denmark

Ph: 45-46-774242
Fax: 45-41-370403
E-mail: tamas@risoe.dk

63. Dongho Kim
Korea Research Institute of Standards &
Science, Spectroscopy Laboratory
Taejon
Korea

Ph: 82-42-868-5210
Fax: 82-42-868-5027
E-mail: dongho@krisso1.kriss.re.kr

64. Teizo Kitagawa
Institute for Molecular Science
Okazaki National Research Institute
Myodaiji
Okazaki 444
Japan

Ph: 81-564-55-7340
Fax: 81-564-55-4639
E-mail: teizo@ims.ac.jp

65. Yasushi Koyama
Kwansei Gakuin University
Faculty of Science
Wegahara
Nishinomiya 662
Japan

Ph: 81-798-54-6389
Fax: 81-798-51-0914
E-mail:

66. Andreas Kummrow
Max-Born-Institut
Rudower Chaussee 6
Berlin 12474
Germany

Ph: 49-30-6392-1431
Fax: 49-30-6392-1429
E-mail:

67. Jaan Laane
Texas A&M University
Department of Chemistry
College Station, TX 77843-3255
USA

Ph: 409/845-3352
Fax: 409/845-3154
E-mail: laane@chemvx.tamu.edu

68. Albrecht Lau
Max-Born-Institute
MBJ, Rudower Chaussec 6
Berlin
Germany

Ph:
Fax:
E-mail:

69. Alfred Laubereau
Technical University Munich
Physik-Department E11
James-Frank-Strassee

D-85748 Garching
Germany

Ph: 49-89-3209-2840
Fax: 49-89-3209-2842
E-mail:

70. Pusheng Li
University of Pittsburgh
Chemistry Department
University of Pittsburgh
Pittsburgh, PA 15213
USA

Ph: 412/624-8669
Fax: 412/624-0588
E-mail: psli@vms.cis.pitt.edu

71. Tianquan Lian
University of California at Berkeley
Department of Chemistry
Berkeley, CA 94720
USA

Ph: 510/642-6389
Fax: 510/642-6794
E-mail: lian@xenon.cchem.berkeley.edu

72. Edgar R. Ligon
University of Arizona
#138 Optical Science Center
Tucson, Arizona 85721
USA

Ph: 602/621-6693
Fax: 602/621-4858
E-mail: eligon@ccit.arizona.edu

73. Qiang Liu
Louisiana State University
Department of Chemistry
E-9
Baton Rouge, Louisiana 70803
USA

Ph: 504/388-3460
Fax:
E-mail: gliu@unix1.lsu.edu

74. Juan Lopez-Garriga
University of Puerto Rico-Mayaguez
Chemistry Department
P.O. Box 5000, College Station
Mayaguez, Puerto Rico 00681-5000
Puerto Rico

Ph: 809/832-4040 Ext. 3762
Fax: 809/832-4680
E-mail: m_schwarz@rumac.upr.clu.edu

75. Raul A. Lopez-Mejia
University of Puerto Rico-Mayaquez
College Station, Box 5050
Mayaguez, Puerto-Rico 00681
USA

Ph: 809/832-4040, Ext. 3762
Fax: 809/265-3849
E-mail:

76. Robert M. Lougheed
ERIM
1975 Green Road
Ann Arbor, MI, 48105
USA

Ph: 313/994-1200
Fax:
E-mail: lougheed@erim.org

77. Gina MacDonald
James Madison University
Department of Chemistry
Harrisonburg, VA 22807
USA

Ph: 540/568-6852
Fax:
E-mail: handalgm@jmu.edu

78. Christopher Manning
Manning Applied Technology
121 Sweet Avenue
Moscow, Idaho 83843
USA

Ph: 208/885-3800
Fax: 208/885-3803
E-mail: manning@peterhouse.chem.uidaho.edu

79. Werner G. Mantele
Universitat Erlangen
Inst. fur Physikalische Chemie
Egerland Strasse 3
Erlangen 91058
Germany

Ph: 49-9131-85-7317
Fax: 49-9131-85-8307
E-mail: maentele@pctc.chemie.uni-erlangen.de

80. Andrea G. Markelz
Quantum Institute
University of California
Santa Barbara, CA 93106
USA

Ph: 805/893-8118
Fax: 805/893-4170
E-mail: andrea@physics.ucsb.edu

81. Jean-Louis Martin
INSERM, Ecole Polytechnique
Palaiseau
France

Ph:
Fax:
E-mail:

82. Mary Ann D. Martinez
Los Alamos National Laboratory
TRVS-7 Conference Secretariat
CST-4, MS G758
Los Alamos, NM 87545
USA

Ph: 505/667-5324
Fax: 505/667-0110
E-mail: trvs@lanl.gov

83. Richard A. Mathies
University of California at Berkeley
Chemistry Department
Berkeley, CA 94720
USA

Ph: 510/642-4192
Fax: 510/642-3599
E-mail: rich@zinc.cchem.berkeley.edu

84. Pavel Matousek
Rutherford Appleton Laboratory
Central Laser Facility Chilton
Didcot, Oxfordshire OX11 OQX
England

Ph: 44-1235-446141
Fax: 44-1235-445888
E-mail: pm3@rl.ac.uk

85. Duncan McBranch
Los Alamos National Laboratory
CST-6, MS J567
Los Alamos, NM 87545
USA

Ph: 505/665-4836
Fax: 505/665-4817
E-mail: mcbranch@lanl.gov

86. Micah J. McCauley
Colorado State University
Biochemistry Department
Fort Collins, CO 80523
USA

Ph: 970/491-0576
Fax:
E-mail: micah@lamar.colostate.edu

87. Sandra Mecklenburg
Los Alamos National Laboratory
CST-4, MS J586

Los Alamos, NM 87545
USA

Ph: 505/665-7182
Fax: 505/667-0851
E-mail: meck@lanl.gov

88. R. Dwayne Miller
University of Toronto
Department of Chemistry
Toronto, Ontario M5S 1A1
Canada

Ph:
Fax:
E-mail:

89. John N. Moore
University of York
Chemistry Department
Helsington York Y01 5DD
UK

Ph: 44-1904-432548
Fax: 44-1904-432562
E-mail: jnm2@york.ac.uk

90. Jay Moskovic
Princeton Instruments, Inc.
C/O 3660 Quakerbridge Road
Trenton, NJ 08619
USA

Ph: 609/587-9797
Fax: 609/587-1970
E-mail:

91. Shaul Mukamel
University of Rochester
Chemistry Department
468 Hutchinston Hall
Rochester, NY 14627-0216
USA

Ph: 716/275-3080
Fax: 716/473-6889
E-mail: samu@dbl.cc.rochester.edu

92. Ishita Mukerji
Wesleyan University
Molecular Biology & Biochemistry
Hall-Atwater Labs
Middletown, CT 06459-0175
USA

Ph: 203/685-2422
Fax: 203/685-2141
E-mail: imukerji@wesleyan.edu

93. Anne B. Myers
University of Rochester
Department of Chemistry
Rochester, NY 14627-0216
USA

Ph: 716/275-2415
Fax: 716/473-6889
E-mail: amye@db2.cc.rochester.edu

94. Laurence A. Nafie
Syracuse University
Department of Chemistry
Syracuse, NY 13244-4100
USA

Ph: 315/443-4109
Fax: 315/443-4070
E-mail: lanafie@summon.syr.edu

95. Kristin M. Omberg
University of North Carolina
Department of Chemistry
CB# 3290, Venable Hall
Chapel Hill, NC 27599-3290
USA

Ph: 919/962-7531
Fax: 919/962-2388
E-mail: kristino@email.enc.edu

96. Mark Ondrias
University of New Mexico
Department of Chemistry
Albuquerque, NM 87131
USA

Ph: 505/277-0479
Fax:
E-mail:

97. Anthony W. Parker
Rutherford Appleton Laboratory
Central Laser Facility
Chilton Didcot, Oxfordshire OX1 0QX
England

Ph: 44-1235-445109
Fax: 44-1235-445888
E-mail: awp@rl.ac.uk

98. Linda A. Peteanu
Carnegie Mellon University
4400 Fifth Avenue #139
Pittsburgh, PA 15213
USA

Ph: 412/268-1327
Fax: 412/268-6397
E-mail: peteanu@andrew.cmu.edu

99. Eric S. Peterson
Albert Einstein College of Medicine
1300 Morris Park, Ave.
Department of Physiology
Bronx, NY 10461
USA

Ph: 718/430-3215
Fax: 718/430-8819
E-mail: peterson@aecom.yu.edu

100. Kristen A. Peterson
New Mexico State University
Chemistry Department
Box 30001, Department 3C
Las Cruces, NM 88003
USA

Ph: 505/646-1547
Fax: 505/646-2649
E-mail: krpeters@praseo.nmsu.edu

101. Lauren M. Peterson
Environmental Research Institute of
P.O. Box 134001
Ann Arbor, MI 48113
USA

Ph: 313/994-1200
Fax: 313/994-5704
E-mail: peterson@erim.org

102. Michael Pfeiffer
Max-Born-Institute
Nonlinear Optics and Short Time
MBJ, Rudower Chaussec 6
Berlin D 124 89
Germany

Ph: 49-30-63971414
Fax: 49-30-63921429
E-mail: pfeiffer@mbi.fta-berlin.de

103. David Lee Phillips
University of Hong Kong
Department of Chemistry
Pokfulam Road
Hong Kong
Hong Kong

Ph: 852-2859-2160
Fax: 852-2857-1586
E-mail: phillips@hkucc.hku.hk

104. Susan E. Plunkett
University of Virginia
Department of Biochemistry
440 Jordan Hall
Charlottesville, Virginia 22908
USA

Ph: 804/924-1943
Fax: 804/924-5069
E-mail: sep4n@virginia.edu

105. Stephen E. Ralph
Emory University
Department of Physics
1510 Clifton Road
Atlanta, GA 30322
USA

Ph: 404/727-4294
Fax: 404/727-0873
E-mail: seralph@physics.emory.edu

106. Philip J. Reid
University of Washington
Department of Chemistry
Mail Stop: 351700

Seattle, WA 98195
USA

Ph: 206/543-6147
Fax: 206/685-8665
E-mail: preid@macmail.chem.washington.edu

107. George Rodriguez
Los Alamos National Laboratory
Materials Science and Technology
MS E525
Los Alamos, NM 87545
USA

Ph: 505/665-3408
Fax: 505/665-4632
E-mail: rodrigeo@lanl.gov

108. Christoph Roedig
University Freiburg
Institut fuer Biophysik
Albertstrasse 23
Freiburg 89104
Germany

Ph: 761-203-5380
Fax: 761-203-5016
E-mail: roedig@sun2.ruf.uui-freiburg.de

109. Daniele Romanini
Universite J. Fourier Grenoble
Laboratoire De Spectrometrie Physique
B.P. 87
St. Martin D'Meres Cedex 38902
France

Ph: 33-76-51-4319
Fax: 33-76-51-4544
E-mail: romanini@grenet.fr

110. Denis Rousseau
Albert Einstein College of Medicine
Department of Physiology and Biophysics
1300 Morris Park Ave.
Bronx, NY 10461
USA

Ph: 718/430-4264
Fax: 718/430-8819
E-mail: rousseau@aecom.yu.edu

111. Craig Schenck
Colorado State University
Department of Biochemistry
Fort Collins, CO 80523
USA

Ph: 970/491-6899
Fax:
E-mail:

112. Norbert F. Scherer
University of Pennsylvania
Department of Chemistry
Philadelphia, PA 19104-6323
USA

Ph: 215/898-6137
Fax: 215/573-2112
E-mail: scherer@a.chem.upenn.edu

113. Vincenzo Schettino
University of Florence
Dipartmento di Chimica
via G. Capponi 9
Firenze 50121
Italy

Ph: 39-55-2757586
Fax: 39-55-2476961
E-mail: schettini@vm.chim.unifi.it

114. Sarah A. Schofield
University of Texas, Austin
Department of Chemistry
Austin, TX78712
USA

Ph: 512/471-1023
Fax: 512/471-8696
E-mail: scho@quantum.cm.utexas.edu

115. Jon R. Schoonover
Los Alamos National Laboratory
CST-4, MS J586
Los Alamos, NM 87545
USA

Ph: 505/667-9628
Fax: 505/667-0851
E-mail: schoons@lanl.gov

116. Sonya Scott
University of Otago
Chemistry Department
P.O. Box 56
Dunedin, 006403
New Zealand

Ph: 006-403-4797599
Fax: 006-403-4797906
E-mail: kgordon@alkali.otago.ac.nz

117. Thomas D. Sewell
Los Alamos National Laboratory
T-14, MS B214
Los Alamos, NM 87545
USA

Ph: 505/667-8205
Fax: 505/665-4055
E-mail: sewell@lanl.gov

118. John A. Shelnutt
Sandia National Laboratory
Fuel Science Department 6211
MS 0810, PO Box 5800
Albuquerque, NM 87185-0710
USA

Ph: 505/844-8856
Fax: 505/845-9500
E-mail: jasheln@sandia.gov

119. Lenian Shen
Bruker Instruments
19 Fortune Drive
Billerica, MA 01821
USA

Ph: 508/667-9580
Fax: 508/667-3954
E-mail:

120. Andrew P. Shreve
Los Alamos National Laboratory
CST-4, MS G755
Los Alamos, NM 87545
USA

Ph: 505/667-6933
Fax: 505/667-0110
E-mail: shreve@lanl.gov

121. JeNell B. Sibbald
Iowa State University
Department of Chemistry
0211 Gilman Hall
Ames, Iowa 50011
USA

Ph: 515/294-4276
Fax: 515/294-0105
E-mail: pederson@iastate.edu

122. Morgan S. Sibbald
Iowa State University
Department of Chemistry
1109 Gilman Hall
Ames, Iowa 50011
USA

Ph: 515/294-7552
Fax: 515/294-0105
E-mail: msibbald@iastate.edu

123. Friedrich Siebert
Universitat Freiburg
Institut fuer Biophysic
Albertstrasse 23

Freiburg D-79104
Germany

Ph: 49-761-2035396
Fax: 49-761-2035016
E-mail: frisi@sun2.ruf.uni-freiburg.de

124. Carlos Silva
University of Minnesota
207 Pleasant St. SE
Department of Chemistry
Minneapolis, MN 55455
USA

Ph: 612/624-7335
Fax: 612/624-7541
E-mail: silva@chemsun.chem.umn.edu

125. M. Cather Simpson
Case Western Reserve University
Department of Chemistry
10900 Euclid Avenue
Cleveland, OH 44106
USA

Ph:
Fax:
E-mail: mcs9@pop.cwru.edu

126. Timothy J. Simpson
University of Otago
Chemistry Department
P.O. Box 56
Dunedin
New Zealand

Ph: 0064-03-4797599
Fax: 0064-03-4797906
E-mail: tsimpson@alkali.otago.ac.nz

127. Laura Smilowitz
Boston University
Physics Department
590 Commonwealth Avenue
Boston, MA 02215
USA

Ph: 617/353-2600
Fax:
E-mail: smilo@buphy.bu.edu

128. Thomas G. Spiro
Princeton University
Department of Chemistry
Princeton, NJ 08544
USA

Ph: 609/258-3907
Fax: 609/258-6746
E-mail: spiro@princeton.edu

129. Jean Stark
Los Alamos National Laboratory
PA-1, P366

Los Alamos, NM 87545
USA

Ph: 505/667-5225
Fax: 505/667-7530
E-mail: jstark@lanl.gov

130. Page O. Stoutland
Los Alamos National Laboratory
CST-6, MS J567
Los Alamos, NM 87545
USA

Ph: 505/665-4692
Fax: 505/667-0440
E-mail: pos@lanl.gov

131. Geoffrey F. Strouse
Los Alamos National Laboratory
CST-1, MS G755
Los Alamos, NM 87545
USA

Ph: 505/667-1547
Fax: 505/667-8021
E-mail: strouse@lanl.gov

132. Basil I. Swanson
Los Alamos National Laboratory
CST-DO, MS J565
Los Alamos, NM 87545
USA

Ph: 505/667-5814
Fax: 505/665-4631
E-mail: basil@lanl.gov

133. Hiroaki Takahashi
Waseda University
Department of Chemistry
School of Science and Engineering
Tokyo, 169
Japan

Ph: 81-3-3208-0850
Fax: 81-3-3208-2735
E-mail:

134. Shoou-yu Tang
Colorado State University
Department of Chemistry
Fort Collins, CO 80523
USA

Ph: 303/491-6442
Fax: 303/491-0494
E-mail: sytang@lamar.colostate.edu

135. Mitsuo Tasumi
The University of Tokyo
Department of Chemistry
School of Science
Bunkyo-ku, Tokyo 113
Japan

Ph: 81-3-3815-8684
Fax: 81-3-3815-8684
E-mail: tasumi@tansei.cc.u-tokyo.ac.jp

136. James Terner
Virginia Commonwealth University
Department of Chemistry, Box 842006
1001 West Main Street
Richmond, Virginia 23284-2006
USA

Ph: 804/828-7500
Fax: 804/828-8599
E-mail: jterner@cabell.vcu.edu

137. Buranda Tione
University of New Mexico
103 Clark Hall
Chemistry Department
Albuquerque, NM 87131
USA

Ph: 505/277-5129
Fax: 505/277-2609
E-mail: buranda@carina.unm.edu

138. Keisuke Tominaga
Institute for Molecular Science
Okazaki National Research Institute
Myodaiji, Okazaki, 444
Japan

Ph: 82-564-55-7352
Fax: 82-564-54-2254
E-mail: tominaga@ims.ac.jp

139. William T. Toner
Rutherford Appleton Laboratory
Central Laser Facility
Chilton Didcot, Oxfordshire, OX11 OQX
England

Ph: 01235-445582
Fax: 01235-445888
E-mail: w.t.toner@rutherford.ac.uk

140. Virginia Triant
Los Alamos National Laboratory
CST-4, MS J586
Los Alamos, NM 87545
USA

Ph:
Fax:
E-mail:

141. James J. Turner
University of Nottingham
Department of Chemistry
Nottingham, NG7 2RD
UK

Ph: 44-115-9513490
Fax: 44-115-9513563
E-mail: james.turner@nott.ac.uk

142. Laszlo Ujj
University of Arizona
3401 N. Columbus Blvd. 24P
Tucson, Arizona 85712
USA

Ph: 602/621-6693
Fax: 602/621-4858
E-mail: ujj@ccit.arizona.edu

143. Siva Umapathy
Indian Institute of Science
Department of Inorganic and Physical Chemistry
Bangalore, 560012
India

Ph: 80-3092595
Fax: 80-3341683
E-mail: umapathy@ipc.iisc.ernet.in

144. Clifford J. Unkefer
Los Alamos National Laboratory
National Stable Isotope Resource Director
CST-4, MS G758
Los Alamos, NM 87545
USA

Ph: 505/667-5324
Fax: 505/667-0110
E-mail: cju@lanl.gov

145. Constantinos Varotsis
Michigan State University
East Lansing, MI 48824
USA

Ph:
Fax:
E-mail:

146. Sondra E. Vitols
Los Alamos National Laboratory
CST-4, MS J586
Los Alamos, NM 87545
USA

Ph: 505/665-5591
Fax: 505/667-0851
E-mail: vitols@lanl.gov

147. Marten H. Vos
Ecole Polytechnique
Inserm U275
Palaiseau 91120
France

Ph: 331-6010-0318
Fax: 331-6010-6025
E-mail: vos@enstay.ensta.fr

148. Gilbert C. Walker
University of Pittsburgh
G-12 Chevron Science Center
Chemistry Department
Pittsburgh, PA 15260
USA

Ph: 412/383-9650
Fax: 412/383-9646
E-mail: gilbertw@vm.cis.pih.edu

149. Ben Wampler
Los Alamos National Laboratory
CST-DO, MS J515
Los Alamos, NM 87545
USA

Ph: 505/667-4457
Fax: 505/665-4355
E-mail: wampler_fred_b@lanl.gov

150. Marc M. Wefers
Massachusetts Institute of Technology
77 Massachusetts Avenue
Room 2-052
Cambridge, MA 02139
USA

Ph: 617/253-1956
Fax: 617/253-7030
E-mail: mwefers@athena.mit.edu

151. Douwe A. Wiersma
University of Groningen
Chemistry/Physics Department
Nijenborgh 4
9747 AG Groningen
The Netherlands

Ph: 50-634440
Fax: 50-634441
E-mail: wiersma@chem.rug.nl

152. Robert Wilbrandt
Risoe National Laboratory
Department of Environmental Science and
MIL/313
Roskilde 4000
Denmark

Ph: 45-4677-4248
Fax: 45-4237-0403
E-mail: wilbrandt@risoe.dk

153. Skip Williams
Phillips Laboratory/GPOS
29 Randolph Road
Hanscom AFB, MA 01731-3010
USA

Ph: 617/377-2076
Fax: 617/377-8202
E-mail: skipw@plh.af.mil

154. Stacie E. Williams
AmberGen, Inc.
1106 Commonwealth Ave.
Boston, MA 02215
USA

Ph: 617/277-2547
Fax: 617/277-2434
E-mail: staciew@buphy.bu.edu

155. William H. Woodruff
Los Alamos National Laboratory
CST-4, MS G758
Los Alamos, NM 87545
USA

Ph: 505/665-2557
Fax: 505/667-0110
E-mail: woody@lanl.gov

156. Klaas Wynne
University of Pennsylvania
Department of Chemistry
231 South 34th Street
Philadelphia, PA 19104
USA

Ph: 215/898-5136
Fax: 215/898-0590
E-mail: wynne@d.chem.upenn.edu

157. Keitaro Yoshihara
Institute for Molecular Science
Okazaki National Research Institute
Myodaiji, Okazaki, 444
Japan

Ph: 81-564-55-7350
Fax: 81-564-54-2254
E-mail: yosihara@ims.ac.jp

• U.S. GOVERNMENT PRINTING OFFICE 1997-0-573-028/27039